AGC-2 Graphite Preirradiation Data Analysis Report

INL/EXT-13-28612
Revision 2

Advanced Reactor Technologies

DECEMBER 2025

William E. Windes
W. David Swank
David T. Rohrbaugh
Joseph R. Lord

Idaho National Laboratory

Idaho National Laboratory

Battelle Energy Alliance manages INL for the U.S. Department of Energy's Office of Nuclear Energy

DISCLAIMER

This information was prepared as an account of work sponsored by an agency of the U.S. Government. Neither the U.S. Government nor any agency thereof, nor any of their employees, makes any warranty, expressed or implied, or assumes any legal liability or responsibility for the accuracy, completeness, or usefulness, of any information, apparatus, product, or process disclosed, or represents that its use would not infringe privately owned rights. References herein to any specific commercial product, process, or service by trade name, trade mark, manufacturer, or otherwise, does not necessarily constitute or imply its endorsement, recommendation, or favoring by the U.S. Government or any agency thereof. The views and opinions of authors expressed herein do not necessarily state or reflect those of the U.S. Government or any agency thereof.

INL/EXT-13-28612
Revision 2

AGC-2 Graphite Preirradiation Data Analysis Report

William E. Windes
W. David Swank
David T. Rohrbaugh
Joseph R. Lord
Idaho National Laboratory]

December 2025

Idaho National Laboratory
Advanced Reactor Technologies
Idaho Falls, Idaho 83415

http://www.art.inl.gov

Prepared for the
U.S. Department of Energy
Office of Nuclear Energy
Under DOE Idaho Operations Office
Contract DE-AC07-05ID14517

Page intentionally left blank

REVISION LOG

Rev.	Date	Affected Pages	Revision Description
0	04//2013		New document.
1	08/2013		
2	12/02/2025	pp. 16, 32, 33, 35, 36, 38, 39. pp. 44, 49, 50, 55, 60, 61, 66, 71, 72, 77, 82, 83, 92-96, 100, 103, 106, 109, 159-163. pp. 176-197.	Changed grain orientation discussions and tables. Replotted Figures A-4, A-5, A-15, A-16, A-26, A-27, A-37, A-38, A-48, A-49, A-59, A-60, A-70, A-71, A-81, A-82, A-101, A-102, A-103, A-104, A-105, A-106, A-107, A-108, A-116, A-117, A-122, A-123, A-128, A-129, A-134, A-135, A-235, A-236, A-237, A-238, A-239, A-240, A-241, A-242. Recalculated statistics in all Tables in appendix B.

Page intentionally left blank

INL ART Program

AGC-2 Graphite Preirradiation Data Analysis Report

INL/EXT-13-28612
Revision 2

December 2025

Technical Reviewer: (Confirmation of mathematical accuracy, and correctness of data and appropriateness of assumptions.)

AUSTIN MATTHEWS (Affiliate) Digitally signed by AUSTIN MATTHEWS (Affiliate) Date: 2025.12.02 14:22:28 -07'00'

Austin C. Matthews
Mechanical Engineer — Date

Approved by:

WILLIAM WINDES (Affiliate) Digitally signed by WILLIAM WINDES (Affiliate) Date: 2025.12.04 14:26:21 -07'00'

William E. Windes
ART Graphite Technical Lead — Date

KIP KLEIMENHAGEN (Affiliate) Digitally signed by KIP KLEIMENHAGEN (Affiliate) Date: 2025.12.03 12:22:08 -07'00'

Kip Kleimenhagen
ART Project Manager — Date

MICHELLE SHARP (Affiliate) Digitally signed by MICHELLE SHARP (Affiliate) Date: 2025.12.03 14:22:54 -07'00'

Michelle T. Sharp
INL Quality Assurance — Date

Page intentionally left blank

SUMMARY

This report describes the specimen loading order and documents all preirradiation examination material property measurement data for graphite specimens contained within the Second Advanced Graphite Capsule (AGC 2) irradiation capsule. The AGC 2 capsule is the second in six planned irradiation capsules comprising the Advanced Graphite Creep (AGC) test series. The AGC test series is used to irradiate graphite specimens in order to garner quantitative data necessary for predicting the irradiation behavior and operating performance of new nuclear grade graphites. This testing will ascertain the in service behavior of the graphite for pebble bed and prismatic very high temperature reactor designs. Similar to the First Advanced Graphite Capsule (AGC 1) preirradiation examination report, material property tests were conducted on specimens from 18 nuclear grade graphite types. However, AGC 2 tested an increased number of specimens (i.e., 512) prior to loading them into the AGC 2 irradiation assembly. All AGC 2 specimen testing was conducted at Idaho National Laboratory from July 2009 to August 2010.

This report also details the specimen loading methodology for graphite specimens inside the AGC 2 irradiation capsule. The AGC 2 capsule design requires “matched pair” creep specimens that have similar dose levels above and below the neutron flux profile mid plane. This provides similar specimens with and without an applied load. Analysis in this document utilizes the neutron flux profile calculated for the AGC 2 capsule design, the capsule dimensions, and the size (i.e., length) of the selected graphite specimens to create a stacking order that produces “matched pairs” of graphite specimens above and below the AGC 2 capsule elevation mid point, thus providing specimens with similar neutron dose levels.

Page intentionally left blank

CONTENTS

1. INTRODUCTION 1
2. DESCRIPTION OF THE ADVANCED GRAPHITE CREEP EXPERIMENT 2
   2.1. Background Information for the Advanced Graphite Creep Experiment 2
   2.2. Description of AGC-2 Test Series 4
      2.2.1. Establishing the Capsule's Physical Centerline to the Core Neutron Flux Mid-Plane 5
      2.2.2. Establishing the Dose Levels as a Function of Position within the Capsule 7
      2.2.3. Determining the Physical Positions of Irradiation Creep Specimens in the Stacks 9
      2.2.4. Determining the Physical Positions of Piggyback Specimens in the Central Stack 17
3. GENERAL TESTING PROVISIONS 17
   3.1. Characterization Plans and Work Procedures 17
   3.2. Specimen Description and Preparation 18
   3.3. Personnel and Training 18
   3.4. Variations, Exceptions, and Discrepancies 19
   3.5. Calibration and Functional Validation 19
4. GRAPHITE STANDARDS AND METHODS 19
5. DETAILED DESCRIPTION OF TEST METHODS 21
   5.1. Mass, Dimensions, and Bulk Density 22
   5.2. Electrical Resistivity 22
   5.3. Approximation of Elastic Modulus from the Measurement of Sonic Velocity 23
   5.4. Modulus of Elasticity by Measurement of Fundamental Frequency 26
   5.5. Thermal Expansion 27
   5.6. Thermal Diffusivity 28
6. DATA ANALYSIS 30
   6.1. Analysis of Mass, Dimensions, and Density Data 30
   6.2. Electrical Resistivity 33
   6.3. Approximation of Elastic Modulus from the Measurement of Sonic Velocity 34
   6.4. Modulus of Elasticity by Measurement of Fundamental Frequency 35
   6.5. Thermal Expansion 36
   6.6. Thermal Diffusivity 38
7. REFERENCES 40

Appendix A AGC-2 Pre-irradiation Data 42

Appendix B Statistical Tables 176

FIGURES

Figure 1. Irradiation dose and temperature parameters of the AGC test series. 3
Figure 2. Revised irradiation dose and temperature parameters of the AGC test series. 5
Figure 3. Elevation sketch of the Advanced Graphite Creep capsule. 6
Figure 4. Calculated dose levels for AGC-2 after 140 effective full-power days. 7
Figure 5. Advanced Test Reactor flux profile, as a function of core mid-plane position. 8
Figure 6. Typical AGC-2 dose profile for creep-graphite specimens utilizing similar applied stress levels in matched stacks 11
Figure 7a. Estimated creep-specimen dose profiles for each major graphite grade. 12
Figure 7b. Estimated creep-specimen dose profiles for each major graphite grade. 13
Figure 7c. Estimated creep-specimen dose profiles for each major graphite type. 14
Figure 8. Electrical resistivity measurement station. 23
Figure 9. Sonic velocity measurement station. 24
Figure 10. Sonic velocity measurement user interface. 25
Figure 11. Fundamental frequency measurement station. 26
Figure 12. Commercial push rod dilatometer for measuring the coefficient of thermal expansion. 28
Figure 13. Laser flash apparatus measurement station for determining thermal diffusivity. 29
Figure 14. Schematic showing location and dimensional details of NBG-17 billet density investigation 31
Figure 15. Density of NBG-17 as a function of depth in the billet. 31
Figure 16. Resistivity of NBG-17 as a function of density. 32
Figure 17. Electrical resistivity for several nuclear-grade graphite types. 33
Figure 18. Measured longitudinal velocity as a function of density for NBG-17 creep specimens. 34
Figure 19. Mean coefficient of thermal expansion for several types of nuclear-grade graphite as a function of temperature. 37
Figure 20. Coefficient of thermal expansion anisotropy ratio for several types of nuclear-grade graphite as a function of temperature. 38
Figure 21. Thermal diffusivity for various with-grain graphite types. Error bars are 1 standard deviation in the data and in some cases smaller than the data symbol. 39
Figure 22. Thermal diffusivity anisotropy ratio for several types of nuclear-grade graphite as a function of temperature. 39
Figure A-1. H-451 Creep Pre Thermal Measurement Density. 42
Figure A-2. IG-110 Creep Pre Thermal Measurement Density. 43
Figure A-3. IG-430 Creep Pre Thermal Measurement Density. 43
Figure A-4. NBG-17 Creep Pre Thermal Measurement Density. 44

Figure A-5. NBG-18 Creep Pre Thermal Measurement Density. 44
Figure A-6. PCEA Creep Pre Thermal Measurement Density. 45
Figure A-7. 2114 Piggyback Pre Thermal Measurement Density. 45
Figure A-8. A3 Matrix Piggyback Pre Thermal Measurement Density. 46
Figure A-9. BAN Piggyback Pre Thermal Measurement Density. 46
Figure A-10. H-451 Piggyback Pre Thermal Measurement Density. 47
Figure A-11. HLM Piggyback Pre Thermal Measurement Density. 47
Figure A-12. IG-110 Piggyback Pre Thermal Measurement Density 48
Figure A-13. IG-430 Piggyback Pre Thermal Measurement Density 48
Figure A-14. NBG-10 Piggyback Pre Thermal Measurement Density. 49
Figure A-15. NBG-17 Piggyback Pre Thermal Measurement Density. 49
Figure A-16. NBG-18 Piggyback Pre Thermal Measurement Density. 50
Figure A-17. NBG-25 Piggyback Pre Thermal Measurement Density. 50
Figure A-18. New Matrix Piggyback Pre Thermal Measurement Density. 51
Figure A-19. PCEA Piggyback Pre Thermal Measurement Density. 51
Figure A-20. PCIB Piggyback Pre Thermal Measurement Density. 52
Figure A-21. PGX Piggyback Pre Thermal Measurement Density. 52
Figure A-22. PPEA Piggyback Pre Thermal Measurement Density. 53
Figure A-23. H-451 Creep Pre Thermal Measurement Length. 53
Figure A-24. IG-110 Creep Pre Thermal Measurement Length. 54
Figure A-25. IG-430 Creep Pre Thermal Measurement Length. 54
Figure A-26. NBG-17 Creep Pre Thermal Measurement Length. 55
Figure A-27. NBG-18 Creep Pre Thermal Measurement Length. 55
Figure A-28. PCEA Creep Pre Thermal Measurement Length. 56
Figure A-29. 2114 Piggyback Pre Thermal Measurement Length. 56
Figure A-30. A3 Matrix Piggyback Pre Thermal Measurement Length 57
Figure A-31. BAN Piggyback Pre Thermal Measurement Length. 57
Figure A-32. H-451 Piggyback Pre Thermal Measurement Length. 58
Figure A-33. HLM Piggyback Pre Thermal Measurement Length. 58
Figure A-34. IG-110 Piggyback Pre Thermal Measurement Length. 59
Figure A-35. IG-430 Piggyback Pre Thermal Measurement Length. 59
Figure A-36. NBG-10 Piggyback Pre Thermal Measurement Length 60
Figure A-37. NBG-17 Piggyback Pre Thermal Measurement Length 60
Figure A-38. NBG-18 Piggyback Pre Thermal Measurement Length 61
Figure A-39. NBG-25 Piggyback Pre Thermal Measurement Length 61

Figure A-40. New Matrix Piggyback Pre Thermal Measurement Length. 62
Figure A-41. PCEA Piggyback Pre Thermal Measurement Length. 62
Figure A-42. PCIB Piggyback Pre Thermal Measurement Length. 63
Figure A-43. PGX Piggyback Pre Thermal Measurement Length. 63
Figure A-44. PPEA Piggyback Pre Thermal Measurement Length. 64
Figure A-45. H-451 Creep Pre Thermal Measurement Diameter. 64
Figure A-46. IG-110 Creep Pre Thermal Measurement Diameter. 65
Figure A-47. IG-430 Creep Pre Thermal Measurement Diameter. 65
Figure A-48. NBG-17 Creep Pre Thermal Measurement Diameter. 66
Figure A-49. NBG-18 Creep Pre Thermal Measurement Diameter. 66
Figure A-50. PCEA Creep Pre Thermal Measurement Diameter. 67
Figure A-51. 2114 Piggyback Pre Thermal Measurement Diameter. 67
Figure A-52. A3 Matrix Piggyback Pre Thermal Measurement Diameter. 68
Figure A-53. BAN Piggyback Pre Thermal Measurement Diameter. 68
Figure A-54. H-451 Piggyback Pre Thermal Measurement Diameter 69
Figure A-55. HLM Piggyback Pre Thermal Measurement Diameter. 69
Figure A-56. IG-110 Piggyback Pre Thermal Measurement Diameter. 70
Figure A-57. IG-430 Piggyback Pre Thermal Measurement Diameter. 70
Figure A-58. NBG-10 Piggyback Pre Thermal Measurement Diameter. 71
Figure A-59. NBG-17 Piggyback Pre Thermal Measurement Diameter. 71
Figure A-60. NBG-18 Piggyback Pre Thermal Measurement Diameter. 72
Figure A-61. NBG-25 Piggyback Pre Thermal Measurement Diameter. 72
Figure A-62. New Matrix Piggyback Pre Thermal Measurement Diameter. 73
Figure A-63. PCEA Piggyback Pre Thermal Measurement Diameter 73
Figure A-64. PCIB Piggyback Pre Thermal Measurement Diameter. 74
Figure A-65. PGX Piggyback Pre Thermal Measurement Diameter. 74
Figure A-66. PPEA Piggyback Pre Thermal Measurement Diameter. 75
Figure A-67. H-451 Creep Pre Thermal Measurement Mass. 75
Figure A-68. IG-110 Creep Pre Thermal Measurement Mass. 76
Figure A-69. IG-430 Creep Pre Thermal Measurement Mass. 76
Figure A-70. NBG-17 Creep Pre Thermal Measurement Mass. 77
Figure A-71. NBG-18 Creep Pre Thermal Measurement Mass. 77
Figure A-72. PCEA Creep Pre Thermal Measurement Mass. 78
Figure A-73. 2114 Piggyback Pre Thermal Measurement Mass. 78
Figure A-74. A3 Matrix Piggyback Pre Thermal Measurement Mass. 79

Figure A-75. BAN Piggyback Pre Thermal Measurement Mass. 79
Figure A-76. H-451 Piggyback Pre Thermal Measurement Mass. 80
Figure A-77. HLM Piggyback Pre Thermal Measurement Mass. 80
Figure A-78. IG-110 Piggyback Pre Thermal Measurement Mass. 81
Figure A-79. IG-430 Piggyback Pre Thermal Measurement Mass. 81
Figure A-80. NBG-10 Piggyback Pre Thermal Measurement Mass. 82
Figure A-81. NBG-17 Piggyback Pre Thermal Measurement Mass. 82
Figure A-82. NBG-18 Piggyback Pre Thermal Measurement Mass. 83
Figure A-83. NBG-25 Piggyback Pre Thermal Measurement Mass. 83
Figure A-84. New Matrix Piggyback Pre Thermal Measurement Mass. 84
Figure A-85. PCEA Piggyback Pre Thermal Measurement Mass. 84
Figure A-86. PCIB Piggyback Pre Thermal Measurement Mass. 85
Figure A-87. PGX Piggyback Pre Thermal Measurement Mass. 85
Figure A-88. PPEA Piggyback Pre Thermal Measurement Mass. 86
Figure A-89. H-451 Creep Coefficient of Thermal Expansion. 86
Figure A-90. H-451 Creep Coefficient of Thermal Expansion @ 100°C. 87
Figure A-91. H-451 Creep Coefficient of Thermal Expansion @ 500°C. 87
Figure A-92. H-451 Creep Coefficient of Thermal Expansion @ 900°C. 88
Figure A-93. IG-110 Creep Coefficient of Thermal Expansion. 88
Figure A-94. IG-110 Creep Coefficient of Thermal Expansion @ 100°C. 89
Figure A-95. IG-110 Creep Coefficient of Thermal Expansion @ 500°C. 89
Figure A-96. IG-110 Creep Coefficient of Thermal Expansion @ 900°C. 90
Figure A-97. IG-430 Creep Coefficient of Thermal Expansion. 90
Figure A-98. IG-430 Creep Coefficient of Thermal Expansion @ 100°C. 91
Figure A-99. IG-430 Creep Coefficient of Thermal Expansion @ 500°C. 91
Figure A-100. IG-430 Creep Coefficient of Thermal Expansion @ 900°C. 92
Figure A-101. NBG-17 Creep Coefficient of Thermal Expansion. 92
Figure A-102. NBG-17 Creep Coefficient of Thermal Expansion @ 100°C. 93
Figure A-103. NBG-17 Creep Coefficient of Thermal Expansion @ 500°C. 93
Figure A-104. NBG-17 Creep Coefficient of Thermal Expansion @ 900°C. 94
Figure A-105. NBG-18 Creep Coefficient of Thermal Expansion. 94
Figure A-106. NBG-18 Creep Coefficient of Thermal Expansion @ 100°C. 95
Figure A-107. NBG-18 Creep Coefficient of Thermal Expansion @ 500°C. 95
Figure A-108. NBG-18 Creep Coefficient of Thermal Expansion @ 900°C. 96
Figure A-109. PCEA Creep Coefficient of Thermal Expansion. 96

Figure A-110. PCEA Creep Coefficient of Thermal Expansion @ 100°C. 97
Figure A-111. PCEA Creep Coefficient of Thermal Expansion @ 500°C. 97
Figure A-112. PCEA Creep Coefficient of Thermal Expansion @ 900°C. 98
Figure A-113. H-451 Creep Modulus by Sonic Resonance. 98
Figure A-114. IG-110 Creep Modulus by Sonic Resonance. 99
Figure A-115. IG-430 Creep Modulus by Sonic Resonance. 99
Figure A-116. NBG-17 Creep Modulus by Sonic Resonance. 100
Figure A-117. NBG-18 Creep Modulus by Sonic Resonance. 100
Figure A-118. PCEA Creep Modulus by Sonic Resonance. 101
Figure A-119. H-451 Creep Resistivity. 101
Figure A-120. IG-110 Creep Resistivity. 102
Figure A-121. IG-430 Creep Resistivity. 102
Figure A-122. NBG-17 Creep Resistivity 103
Figure A-123. NBG-18 Creep Resistivity 103
Figure A-124. PCEA Creep Resistivity. 104
Figure A-125. H-451 Creep Young's Modulus by Sonic Velocity. 104
Figure A-126. IG-110 Creep Young's Modulus by Sonic Velocity. 105
Figure A-127. IG-430 Creep Young's Modulus by Sonic Velocity. 105
Figure A-128. NBG-17 Creep Young's Modulus by Sonic Velocity. 106
Figure A-129. NBG-18 Creep Young's Modulus by Sonic Velocity. 106
Figure A-130. PCEA Creep Young's Modulus by Sonic Velocity. 107
Figure A-131. H-451 Creep Shear Modulus by Sonic Velocity. 107
Figure A-132. IG-110 Creep Shear Modulus by Sonic Velocity. 108
Figure A-133. IG-430 Creep Shear Modulus by Sonic Velocity. 108
Figure A-134. NBG-17 Creep Shear Modulus by Sonic Velocity 109
Figure A-135. NBG-18 Creep Shear Modulus by Sonic Velocity 109
Figure A-136. PCEA Creep Shear Modulus by Sonic Velocity. 110
Figure A-137. H-451 Creep Pre vs. Post Thermal Measurement Length Comparison. 110
Figure A-138. IG-110 Creep Pre vs. Post Thermal Measurement Length Comparison. 111
Figure A-139. IG-430 Creep Pre vs. Post Thermal Measurement Length Comparison. 111
Figure A-140. NBG-17 Creep Pre vs. Post Thermal Measurement Length Comparison. 112
Figure A-141. NBG-18 Creep Pre vs. Post Thermal Measurement Length Comparison. 112
Figure A-142. PCEA Creep Pre vs. Post Thermal Measurement Length Comparison. 113
Figure A-143. 2114 Piggyback Pre vs. Post Thermal Measurement Length Comparison. 113
Figure A-144. A3 Matrix Piggyback Pre vs. Post Thermal Measurement Length Comparison. 114

Figure A-145. BAN Piggyback Pre vs. Post Thermal Measurement Length Comparison. 114
Figure A-146. H-451 Piggyback Pre vs. Post Thermal Measurement Length Comparison. 115
Figure A-147. HLM Piggyback Pre vs. Post Thermal Measurement Length Comparison. 115
Figure A-148. IG-110 Piggyback Pre vs. Post Thermal Measurement Length Comparison. 116
Figure A-149. IG-430 Piggyback Pre vs. Post Thermal Measurement Length Comparison. 116
Figure A-150. NBG-10 Piggyback Pre vs. Post Thermal Measurement Length Comparison. 117
Figure A-151. NBG-17 Piggyback Pre vs. Post Thermal Measurement Length Comparison. 117
Figure A-152. NBG-18 Piggyback Pre vs. Post Thermal Measurement Length Comparison. 118
Figure A-153. NBG-25 Piggyback Pre vs. Post Thermal Measurement Length Comparison. 118
Figure A-154. New Matrix Piggyback Pre vs. Post Thermal Measurement Length Comparison. 119
Figure A-155. PCEA Piggyback Pre vs. Post Thermal Measurement Length Comparison. 119
Figure A-156. PCIB Piggyback Pre vs. Post Thermal Measurement Length Comparison. 120
Figure A-157. PGX Piggyback Pre vs. Post Thermal Measurement Length Comparison. 120
Figure A-158. PPEA Piggyback Pre vs. Post Thermal Measurement Length Comparison. 121
Figure A-159. H-451 Creep Pre vs. Post Thermal Measurement Diameter Comparison. 121
Figure A-160. IG-110 Creep Pre vs. Post Thermal Measurement Diameter Comparison. 122
Figure A-161. IG-430 Creep Pre vs. Post Thermal Measurement Diameter Comparison. 122
Figure A-162. NBG-17 Creep Pre vs. Post Thermal Measurement Diameter Comparison. 123
Figure A-163. NBG-18 Creep Pre vs. Post Thermal Measurement Diameter Comparison. 123
Figure A-164. PCEA Creep Pre vs. Post Thermal Measurement Diameter Comparison. 124
Figure A-165. 2114 Piggyback Pre vs. Post Thermal Measurement Diameter Comparison. 124
Figure A-166. A3 Matrix Piggyback Pre vs. Post Thermal Measurement Diameter Comparison. 125
Figure A-167. BAN Piggyback Pre vs. Post Thermal Measurement Diameter Comparison. 125
Figure A-168. H-451 Piggyback Pre vs. Post Thermal Measurement Diameter Comparison. 126
Figure A-169. HLM Piggyback Pre vs. Post Thermal Measurement Diameter Comparison. 126
Figure A-170. IG-110 Piggyback Pre vs. Post Thermal Measurement Diameter Comparison. 127
Figure A-171. IG-430 Piggyback Pre vs. Post Thermal Measurement Diameter Comparison. 127
Figure A-172. NBG-10 Piggyback Pre vs. Post Thermal Measurement Diameter Comparison. 128
Figure A-173. NBG-17 Piggyback Pre vs. Post Thermal Measurement Diameter Comparison. 128
Figure A-174. NBG-18 Piggyback Pre vs. Post Thermal Measurement Diameter Comparison. 129
Figure A-175. NBG-25 Piggyback Pre vs. Post Thermal Measurement Diameter Comparison. 129
Figure A-176. New Matrix Piggyback Pre vs. Post Thermal Measurement Diameter Comparison. 130
Figure A-177. PCEA Piggyback Pre vs. Post Thermal Measurement Diameter Comparison. 130
Figure A-178. PCIB Piggyback Pre vs. Post Thermal Measurement Diameter Comparison. 131
Figure A-179. PGX Piggyback Pre vs. Post Thermal Measurement Diameter Comparison. 131

Figure A-180. PPEA Piggyback Pre vs. Post Thermal Measurement Diameter Comparison. 132
Figure A-181. H-451 Creep Pre vs. Post Thermal Measurement Mass Comparison. 132
Figure A-182. IG-110 Creep Pre vs. Post Thermal Measurement Mass Comparison. 133
Figure A-183. IG-430 Creep Pre vs. Post Thermal Measurement Mass Comparison. 133
Figure A-184. NBG-17 Creep Pre vs. Post Thermal Measurement Mass Comparison. 134
Figure A-185. NBG-18 Creep Pre vs. Post Thermal Measurement Mass Comparison. 134
Figure A-186. PCEA Creep Pre vs. Post Thermal Measurement Mass Comparison. 135
Figure A-187. 2114 Piggyback Pre vs. Post Thermal Measurement Mass Comparison. 135
Figure A-188. A3 Matrix Piggyback Pre vs. Post Thermal Measurement Mass Comparison..... 136
Figure A-189. BAN Piggyback Pre vs. Post Thermal Measurement Mass Comparison. 136
Figure A-190. H-451 Piggyback Pre vs. Post Thermal Measurement Mass Comparison. 137
Figure A-191. HLM Piggyback Pre vs. Post Thermal Measurement Mass Comparison. 137
Figure A-192. IG-110 Piggyback Pre vs. Post Thermal Measurement Mass Comparison. 138
Figure A-193. IG-430 Piggyback Pre vs. Post Thermal Measurement Mass Comparison. 138
Figure A-194. NBG-10 Piggyback Pre vs. Post Thermal Measurement Mass Comparison..... 139
Figure A-195. NBG-17 Piggyback Pre vs. Post Thermal Measurement Mass Comparison..... 139
Figure A-196. NBG-18 Piggyback Pre vs. Post Thermal Measurement Mass Comparison..... 140
Figure A-197. NBG-25 Piggyback Pre vs. Post Thermal Measurement Mass Comparison..... 140
Figure A-198. New Matrix Piggyback Pre vs. Post Thermal Measurement Mass Comparison. 141
Figure A-199. PCEA Piggyback Pre vs. Post Thermal Measurement Mass Comparison. 141
Figure A-200. PCIB Piggyback Pre vs. Post Thermal Measurement Mass Comparison. 142
Figure A-201. PGX Piggyback Pre vs. Post Thermal Measurement Mass Comparison. 142
Figure A-202. PPEA Piggyback Pre vs. Post Thermal Measurement Mass Comparison. 143
Figure A-203. 2114 Piggyback Diffusivity..... 143
Figure A-204. 2114 Piggyback Diffusivity @ 100°C..... 144
Figure A-205. 2114 Piggyback Diffusivity @ 500°C..... 144
Figure A-206. 2114 Piggyback Diffusivity @ 900°C..... 145
Figure A-207. A3 Matrix Piggyback Diffusivity. 145
Figure A-208. A3 Matrix Piggyback Diffusivity @ 100°C. 146
Figure A-209. A3 Matrix Piggyback Diffusivity @ 500°C. 146
Figure A-210. A3 Matrix Piggyback Diffusivity @ 900°C. 147
Figure A-211. BAN Piggyback Diffusivity. 147
Figure A-212. BAN Piggyback Diffusivity @ 100°C. 148
Figure A-213. BAN Piggyback Diffusivity @ 500°C. 148
Figure A-214. BAN Piggyback Diffusivity @ 900°C. 149

Figure A-215. H-451 Piggyback Diffusivity. 149
Figure A-216. H-451 Piggyback Diffusivity @ 100°C. 150
Figure A-217. H-451 Piggyback Diffusivity @ 500°C. 150
Figure A-218. H-451 Piggyback Diffusivity @ 900°C. 151
Figure A-219. HLM Piggyback Diffusivity. 151
Figure A-220. HLM Piggyback Diffusivity @ 100°C. 152
Figure A-221. HLM Piggyback Diffusivity @ 500°C. 152
Figure A-222. HLM Piggyback Diffusivity @ 900°C. 153
Figure A-223. IG-110 Piggyback Diffusivity. 153
Figure A-224. IG-110 Piggyback Diffusivity @ 100°C. 154
Figure A-225. IG-110 Piggyback Diffusivity @ 500°C. 154
Figure A-226. IG-110 Piggyback Diffusivity @ 900°C. 155
Figure A-227. IG-430 Piggyback Diffusivity. 155
Figure A-228. IG-430 Piggyback Diffusivity @ 100°C. 156
Figure A-229. IG-430 Piggyback Diffusivity @ 500°C. 156
Figure A-230. IG-430 Piggyback Diffusivity @ 900°C. 157
Figure A-231. NBG-10 Piggyback Diffusivity. 157
Figure A-232. NBG-10 Piggyback Diffusivity @ 100°C. 158
Figure A-233. NBG-10 Piggyback Diffusivity @ 500°C. 158
Figure A-234. NBG-10 Piggyback Diffusivity @ 900°C. 159
Figure A-235. NBG-17 Piggyback Diffusivity. 159
Figure A-236. NBG-17 Piggyback Diffusivity @ 100°C. 160
Figure A-237. NBG-17 Piggyback Diffusivity @ 500°C. 160
Figure A-238. NBG-17 Piggyback Diffusivity @ 900°C. 161
Figure A-239. NBG-18 Piggyback Diffusivity. 161
Figure A-240. NBG-18 Piggyback Diffusivity @ 100°C. 162
Figure A-241. NBG-18 Piggyback Diffusivity @ 500°C. 162
Figure A-242. NBG-18 Diffusivity @ 900°C. 163
Figure A-243. NBG-25 Piggyback Diffusivity. 163
Figure A-244. NBG-25 Piggyback Diffusivity @ 100°C. 164
Figure A-245. NBG-25 Piggyback Diffusivity @ 500°C. 164
Figure A-246. NBG-25 Piggyback Diffusivity @ 900°C. 165
Figure A-247. New Matrix Piggyback Diffusivity. 165
Figure A-248. New Matrix Piggyback Diffusivity @ 100°C. 166
Figure A-249. New Matrix Piggyback Diffusivity @ 500°C. 166

Figure A-250. New Matrix Piggyback Diffusivity @ 900°C. 167
Figure A-251. PCEA Piggyback Diffusivity. 167
Figure A-252. PCEA Piggyback Diffusivity @ 100°C. 168
Figure A-253. PCEA Piggyback Diffusivity @ 500°C. 168
Figure A-254. PCEA Piggyback Diffusivity @ 900°C. 169
Figure A-255. PCIB Piggyback Diffusivity. 169
Figure A-256. PCIB Piggyback Diffusivity @ 100°C. 170
Figure A-257. PCIB Piggyback Diffusivity @ 500°C. 170
Figure A-258. PCIB Piggyback Diffusivity @ 900°C. 171
Figure A-259. PGX Piggyback Diffusivity. 171
Figure A-260. PGX Piggyback Diffusivity @ 100°C. 172
Figure A-261. PGX Piggyback Diffusivity @ 500°C. 172
Figure A-262. PGX Piggyback Diffusivity @ 900°C. 173
Figure A-263. PPEA Piggyback Diffusivity. 173
Figure A-264. PPEA Piggyback Diffusivity @ 100°C. 174
Figure A-265. PPEA Piggyback Diffusivity @ 500°C. 174
Figure A-266. PPEA Piggyback Diffusivity @ 900°C. 175

TABLES

Table 1. Typical dose differences between matched pairs in the AGC-1 test-series capsule. 9
Table 2. Total number of irradiated creep specimens in the AGC-2 test-series capsule. 10
Table 3. Final loading configuration for AGC-2 creep specimens in outer stacks. 15
Table 4. NGNP graphite specimen measurement and test equipment. 20
Table 5. Young's modulus by measurement of sonic velocity. 35
Table 6. Young's modulus by measurement of fundamental frequency. 36
Table B-1. Creep Pre Thermal Measurement Length (mm) Summary Statistics. 176
Table B-2. Creep Pre Thermal Measurement Diameter (mm) Summary Statistics. 177
Table B-3. Creep Pre Thermal Measurement Mass (g) Summary Statistics. 178
Table B-4 Creep Pre Thermal Measurement Density (g/cm^3, Summary Statistics. 179
Table B-5. Creep Coefficient of Thermal Expansion (1/K) at 100°C Summary Statistics. 180
Table B-6. Creep Coefficient of Thermal Expansion (1/K) at 500°C Summary Statistics. 181
Table B-7. Creep Coefficient of Thermal Expansion (1/K) at 900°C Summary Statistics. 182
Table B-8. Creep Modulus (GPa) by Sonic Resonance Summary Statistics. 183
Table B-9. Creep Resistivity (Lt0-m) Summary Statistics. 184
Table B-10. Creep Young's Modulus (GPa) by Sonic Velocity. 185

Table B-11. Creep Shear Modulus (GPa) by Sonic Velocity. 186
Table B-12a. Piggyback Pre Thermal Measurement Length (mm) Summary Statistics..... 187
Table B-12b. Piggyback Pre Thermal Measurement Length I mm) Summary Statistics..... 187
Table B-12c. Piggyback Pre Thermal Measurement Length (mm) Summary Statistics..... 188
Table B-13a. Piggyback Pre Thermal Measurement Diameter (mm) Summary Statistics..... 188
Table B-13b. Piggyback Pre Thermal Measurement Diameter (mm) Summary Statistics..... 189
Table B-13c Piggyback Pre Thermal Measurement Diameter (mm) Summary Statistics. 189
Table B-14a. Piggyback Pre Thermal Measurement Mass (g) Summary Statistics. 190
Table B-14b. Piggyback Pre Thermal Measurement Mass (gl Summary Statistics..... 190
Table B-14c. Piggyback Pre Thermal Measurement Mass (g) Summary Statistics. 191
Table B-15a. Piggyback Pre Thermal Measurement Density (g/cm^3) Summary Statistics. 191
Table B-15b. Piggyback Pre Thermal Measurement Density (g/cm^3) Summary Statistics. 192
Table B-15c. Piggyback Pre Thermal Measurement Density (g/cm3) Summary Statistics. 192
Table B-16a. Piggyback Diffusivity (mm^2/sec) at 100°C Summary Statistics. 193
Table B-16b. Piggyback Diffusivity (mm^2/sec) at 100°C Summary Statistics..... 193
Table B-16c. Piggyback Diffusivity (mm^2/sec) at 100°C Summary Statistics. 194
Table B-17a. Piggyback Diffusivity (mm^2/sec) at 500°C Summary Statistics. 194
Table B-17b. Piggyback Diffusivity (mm^2/sec) at 500°C Summary Statistics. 195
Table B-17c Piggyback Diffusivity (mm^2/sec) at 500°C Summary Statistics 195
Table B-18a. Piggyback Diffusivity (mm^2/sec) at 900°C Summary Statistics. 196
Table B-18b. Piggyback Diffusivity (mm^2/sec) at 900°C Summary Statistics. 196
Table B-18c. Piggyback Diffusivity (mm^2/sec) at 900°C Summary Statistics. 197

Page intentionally left blank

ACRONYMS

AG	against-grain
AGC	Advanced Graphite Creep
AGC-1	First Advanced Graphite Capsule
AGC-2	Second Advanced Graphite Capsule
ASTM	American Society for Testing and Materials
ATR	Advanced Test Reactor
COV	coefficient of variation
CTE	coefficient of thermal expansion
dpa	displacements per atom
EFPD	effective full-power days
GPa	gigapascals
HTGR	high-temperature gas-cooled reactor
INL	Idaho National Laboratory
IQR	interquartile range
LFA	laser flash apparatus
MCNP	Monte Carlo N-Particle Transport Code
NGNP	Next Generation Nuclear Plant
PB	piggy-back specimen
PIE	post-irradiation examination
Pre-IE	preirradiation examination
R&D	research and development
TC	thermocouple
TDP	Technology Development Plan
VHTR	very high temperature reactor
WG	with-grain

Page intentionally left blank

AGC-2 Graphite Preirradiation Data Analysis Report

1. INTRODUCTION

The Next Generation Nuclear Plant (NGNP) will be a helium-cooled, very high temperature reactor (VHTR) with a large graphite core. In past applications, graphite has been used effectively as a structural and moderator material in both research and commercial high temperature gas-cooled reactor (HTGR) designs.[1,2] Nuclear graphite H-451, used previously in the United States for nuclear reactor graphite components, is no longer available. New nuclear graphites have been developed and are considered suitable candidates for the new NGNP reactor design. To support the design and licensing of NGNP core components within a commercial reactor, a complete properties database must be developed for these current grades of graphite. Quantitative data on in-service material performance is required for the physical, mechanical, and thermal properties of each graphite grade with a specific emphasis on data accounting for the life-limiting effects of irradiation creep on key physical properties of the NGNP candidate graphites. Further details on the research and development activities and associated rationale required to qualify nuclear-grade graphite for use within the NGNP are documented in the NGNP graphite technology research and development plan.[3,4]

Based on experience with previous graphite-core components, the phenomenon of irradiation-induced creep within the graphite has been shown to be critical to the total useful lifetime of graphite components. Irradiation-induced creep occurs under the simultaneous application of high temperatures, neutron irradiation, *and* applied stresses within the graphite components. Significant internal stresses within the graphite components can result from a second phenomenon—irradiation-induced dimensional change—where the graphite physically changes (i.e., first shrinking and then expanding with increasing neutron dose). This disparity in material-volume change can induce significant internal stresses within graphite components. Irradiation-induced creep relaxes these large internal stresses, thus reducing the risk of crack formation and component failure. Obviously, higher irradiation-creep levels tend to relieve more internal stress, thus allowing the components longer useful lifetimes within the core. Determining the irradiation-creep rates of nuclear-grade graphites is critical for determining the useful lifetime of graphite components and is a major component of the Advanced Graphite Creep (AGC) experiment.

The AGC experiment is currently underway to determine the in-service behavior of these new graphites for both pebble-bed and prismatic reactor designs. This experiment will examine properties and behavior of nuclear-grade graphites over a large spectrum of temperatures, irradiation fluencies, and applied stress levels that are expected to induce irradiation creep strains within a VHTR graphite component. Irradiation data are provided through the AGC test series, which comprises six planned capsules irradiated in the Advanced Test Reactor (ATR) in a large flux trap[3] at the Idaho National Laboratory (INL) Site. This test series exposes the selected graphite specimens to temperatures and a range of doses that are expected within a VHTR design. Each irradiation capsule consists of over 400 graphite specimens that are characterized before and after irradiation.

The First Advanced Graphite Capsule (AGC-1) of the AGC test series was initially characterized, loaded into ATR, irradiated, and is currently undergoing post-irradiation examination (PIE).[5,6,7] Characterization of the graphite specimens for the Second Advanced Graphite Capsule (AGC-2) was recently completed, and the measurements are reported in this document. Data gathered for the characterization of AGC-2 specimens is contained in Appendixes A, B, and C of this report. The original design called for AGC-1 and -2 capsule irradiations to be as similar as possible—similar graphites, irradiation temperatures, and loads applied to the creep specimens with the only difference being total received dose to the specimens. Consequently, material property tests were conducted on specimens of similar graphites as tested in the AGC-1 capsule, but on an increased number of specimens (i.e., 512) due

to a change in the stacking order of the specimens within the capsule. All AGC-2 specimen testing was conducted from July 2009 to August 2010.[8]

To achieve the proper irradiation conditions and applied loads to the creep specimens, an exact specimen loading order is critical. Because irradiation creep is usually determined by the difference in dimensional change occurring within specimens that have an applied load and those that do not, these "matched pair" specimens are assumed to have the same irradiation dose and irradiation temperature values. To achieve these similar irradiation conditions for "matched pairs," a careful map of where each specimen resides within the irradiation capsule is required. A detailed analysis of the reactor flux profile is required to ascertain the dose levels for each specimen, as well as the designed loading configurations within the capsule, in order to guarantee that the matched pairs experience the same temperature and dose levels. This document discusses details of the specimen loading order, the capsule loading design, the flux profile within ATR, and the resulting estimated dose profiles for each graphite specimen for the AGC-2 irradiation capsule.

2. DESCRIPTION OF THE ADVANCED GRAPHITE CREEP EXPERIMENT

The AGC experiment is designed to establish the data necessary to determine the safe operating envelope of graphite core components for a VHTR by measuring the irradiated material property changes and behavior of several new nuclear grade graphites over a large range of temperatures, neutron fluencies, and mechanical compressive loads. The experiment consists of three interrelated stages: preirradiation characterization of the graphite specimens, the irradiation test series (designated as six separate irradiation capsules), and PIE of the graphite specimens after irradiation. Separate reports for each distinct stage are prepared after the activity is completed. The preirradiation examination (pre-IE) reports detail the total number of graphites and specimens, the specimen loading configuration to expose all specimens to the entire range of irradiation conditions, and the preirradiation material property testing results. The irradiation test series reports detail the irradiation history of each capsule while in reactor, noting any changes from the technical and functional specifications for each specific test series capsule, and identifying the possible improvements to the next test series capsule design. The PIE reports detail the changes in the specimen material property measurements, compare the results to the pre-IE material property measurements, and analyze the data to assist in determining a credible safe operating envelope for graphite core components in a VHTR design and licensing application.

2.1. Background Information for the Advanced Graphite Creep Experiment

The AGC experiments will provide data on irradiated material properties for current graphites available for use within a VHTR design. Due to volume limitations within typical material test reactors (i.e. ATR), only a limited number of specimens can be irradiated, which are far fewer than can be used in an accurate statistical specimen population analysis. Therefore, the AGC only measures the changes in irradiated material properties and the behavior of relatively few specimens of new nuclear-grade graphites over the anticipated range of operating temperatures, neutron fluence, and mechanical loads. The experiment does generate quantitative material property change data (and limited irradiation creep data), which will be used in conjunction with the as-fabricated material property to predict the in-service behavior and operating performance of these new nuclear-grade graphites for pebble-bed and prismatic reactor designs. Changes to key thermal, physical, and mechanical material properties are determined by comparing the material properties of each specimen before and after irradiation. Differences measured from the irradiation conditions will provide irradiation-behavior data for graphite, with a specific emphasis on those data that account for the life-limiting effects of irradiation creep on key physical properties of several candidate graphites for use in NGNP.

The critical component of the AGC experiment is the irradiation test series, which irradiates the graphite specimens after pre-IE characterization has been completed. The AGC test series comprises six planned irradiation capsules, which are irradiated in ATR in a large flux trap, as described in the Graphite Technology Development Plan.[3] The test series exposes test specimens of the selected nuclear-grade graphites to temperatures and the range of doses that are expected within an VHTR design. Specifically, graphite specimens will be exposed to fast neutron dose ranging from 1 to 7 displacements per atom (dpa) and temperatures of 600, 900, and 1200°C, as shown in Figure 1. Similar to the AGC-1 irradiation capsule, AGC-2 was designed to be irradiated within the ATR's South Flux Trap.[9] Generally, irradiations within the South Flux Trap require approximately 175 effective full-power days to provide a nominal fast-neutron-dose range (in graphite) of 1–3.5 dpa. For those capsules requiring a 3.5–7.0-dpa dose range, the irradiation capsule (containing the graphite specimens) is irradiated for twice as long inside the ATR, for approximately 350 effective full-power days.

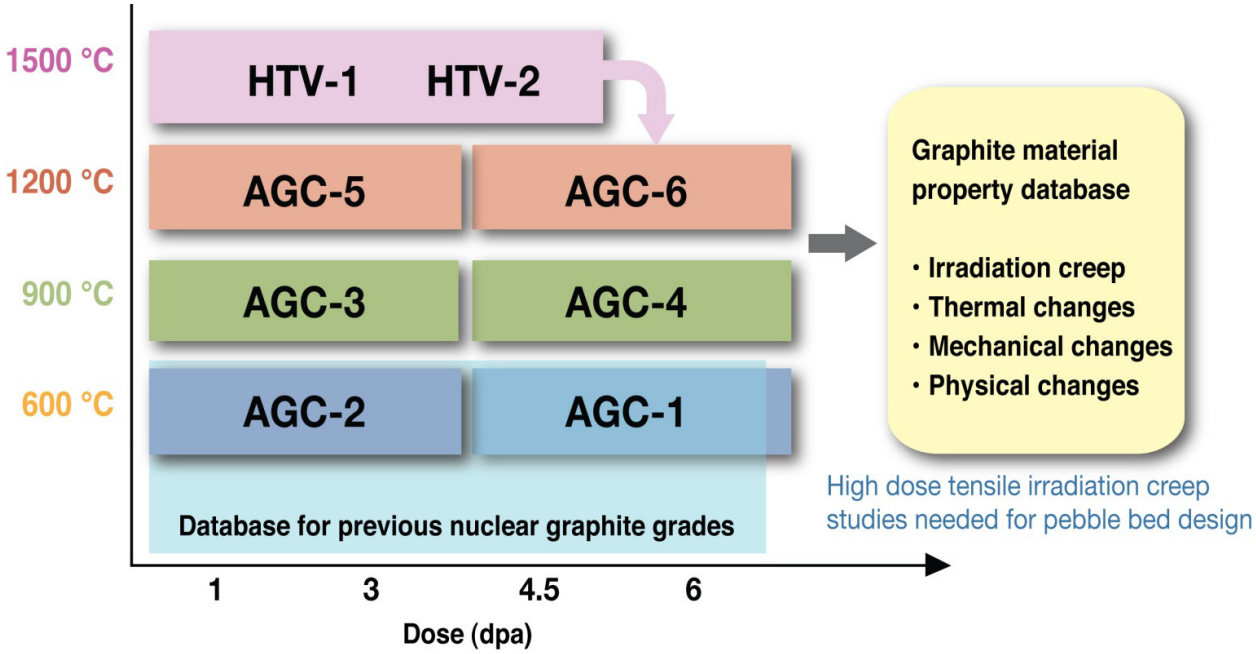

Figure 1. Irradiation dose and temperature parameters of the AGC test series.

The AGC test series dedicates a significant amount of scope to determining rates of irradiation-induced creep for different nuclear-grade graphite. The traditional method for measuring irradiation-induced creep is to apply a significant load to half the specimens during irradiation while leaving the remaining half of the specimens unloaded. The resulting difference in dimensional change between the loaded and unloaded specimens (assuming that temperature and dose levels are the same) provides the amount of irradiation-induced strain for each "matched pair" of graphite specimens. From this strain level, a creep rate for each graphite grade can be calculated as a function of dose if both specimens were irradiated at the same constant temperature. Thus, each capsule is designed to be irradiated at a constant temperature, allowing only the dose and applied mechanical load to vary within the test train of each test-series capsule. With all graphite specimens at a constant temperature, only the applied load and dose will affect the calculated creep rate of each graphite grade within a test series capsule.

To ascertain the temperature dependency of irradiation-induced material property changes, the creep rates of similar graphite specimens, at similar dose and load levels, must be compared between capsules. This implies that similar graphite grades must be in the same locations in every capsule to receive similar dose and load levels at different temperatures.

To provide all necessary material property tests in the AGC experiments, each test-series capsule contains two primary specimens: (1) creep specimens, providing irradiation creep-rate values as well as mechanical properties, and (2) "piggyback" specimens, providing thermal material property changes to the graphite. Generally, the creep specimens are larger (25.4 mm tall) and are irradiated in the mechanically loaded outer stack positions of the capsule body where an applied load can be imposed upon half of the specimens. Piggyback specimens are short (i.e., 6 mm tall) button specimens that reside in the axial spine of the capsule or the lower half of the outer stack positions—receiving no applied load and subjected only to neutron irradiation at high operating temperatures—to assess the effects of a reactor environment on the specific graphite grade. Together, both types of specimens provide the changes in material properties for stressed and unstressed graphite grades. The physical dimensions for both "Creep" and "Piggy-back" specimens are shown in INL Drawing 600786, Rev. 2.[10]

2.2. Description of AGC-2 Test Series

AGC-2 was originally designed to be the longer duration irradiation capsule providing specimens irradiated at the 3.5–7.0-dpa dose level (see Figure 1) at the 600°C temperature conditions. However, due to issues with temperature control within the first AGC-1 capsule,[6] it was decided during AGC-1 irradiation to hold the capsule inside ATR as long as possible to ascertain the viability of the capsule design at high dose levels. Therefore, the irradiation dose levels for AGC-1 were changed to the longer duration irradiation (i.e., 3.5–7.0 dpa) at the 600°C temperature conditions.

Because the AGC-1 specimen temperature limits exceeded the technical specifications, determining material property changes and creep rates at a constant temperature proved to be difficult. Therefore, an intermediate, 1.5–5-dpa dose level, irradiated at 600°C, was selected as the final irradiation condition for the AGC-2 test series to bridge between the two original 600°C test-series capsules, Figure 2. It was assumed that some of the specimens from AGC-1 could be utilized in conjunction with the AGC-2 graphite specimens to produce more reliable material property changes at the constant 600°C-temperature condition. While not optimal, it was determined that providing graphite specimens, irradiated over this overlapping dose level at a more consistent temperature condition, would be sufficient to ascertain the irradiation creep and material property changes for the selected graphites.

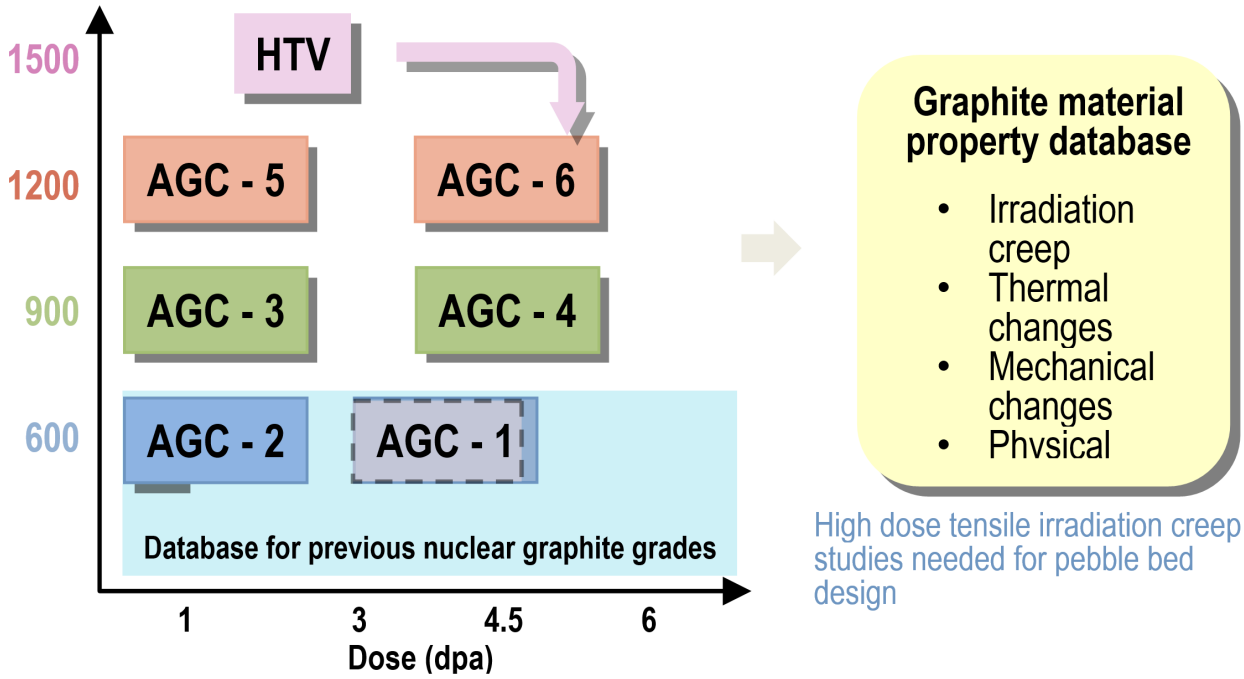

Figure 2. Revised irradiation dose and temperature parameters of the AGC test series. Note the gray area between AGC-1 and AGC-2 is the expected dose overlap between capsule irradiation.

Additionally, one of the graphite grades was changed by request of the graphite vendor (Mersen, USA). Piggy-back specimens of graphite grade 2114 were directly substituted for graphite grade 2020 and irradiated within the AGC-2 central stack (axial spine of capsule). All other graphites irradiated within AGC-2 were similar to the graphites in AGC-1. To duplicate the specimen stacking order as in the AGC-1 test series capsule, the AGC-2 capsule contained the following major graphite grades NBG-17, NBG-18, PCEA, IG-430, H-451, and IG-110. The minor grades of graphite (i.e., "piggyback" specimens) included NBG-25, PCIB, PPEA, NBG-10, BAN, HLM, PGX, 2114, HOPG, and A3 Matrix.

2.2.1. Establishing the Capsule's Physical Centerline to the Core Neutron Flux Mid-Plane

The capsule elevation sketch provided in Figure 3 was generated from a number of AGC-2 capsule and ATR core drawings and used to determine the position of each specimen in the capsule as a function of height above and below the mid-plane of the core neutron flux profile.[11,12] Other considerations included the size of each creep specimen, the need for periodically placed spacers containing flux wires, and the space requirements in the top of the stacks for the push rods. The core flux mid-plane, in relation to the capsule arrangement, was established so that the reactor neutron flux field could be correlated to the physical elevations and positions in the capsule.

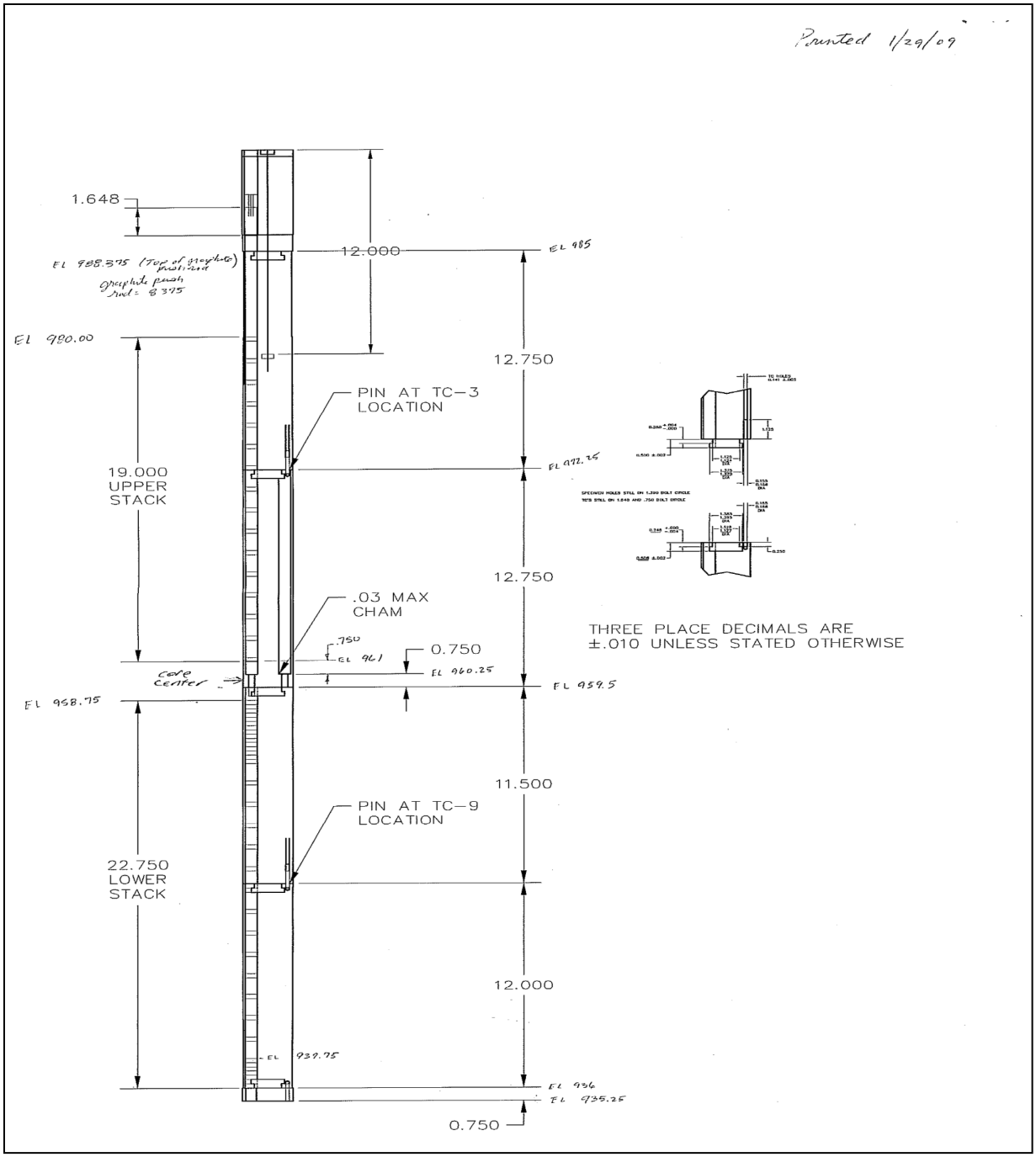

Figure 3. Elevation sketch of the Advanced Graphite Creep capsule.

2.2.2. Establishing the Dose Levels as a Function of Position within the Capsule

Once the physical elevation dimensions were established and correlated to the reactor core centerline, the dose as a function of distance from the core centerline needed to be determined. The estimated AGC-2 experiment fluence profiles were calculated by Reactor Engineering utilizing a Monte Carlo Neutral Particle (transport code) model based on the known neutron flux profile of ATR, the position of the experiment in the South Flux Trap, and the number of effective full-power days planned for the test-series capsule.

Irradiation dose values, as a function of distance from the reactor core centerline, were calculated from the total estimated fluence, using standard conversion factors for carbon in a fast neutron irradiation field (E > 0.1 MeV).[13] There is a neutron flux gradient across the capsule thickness requiring the capsule to be rotated 180 degrees at the irradiation mid-point. This rotation results in a uniform neutron-fluence profile for all stacks, regardless of their position within the capsule, as shown in Figure 4. Because all stacks within the capsule are estimated to have similar dose profiles after complete irradiation, the dose profile for the center stack within the capsule was used to determine the proper stacking order and specimen offset position in the lower half of the irradiation capsule.

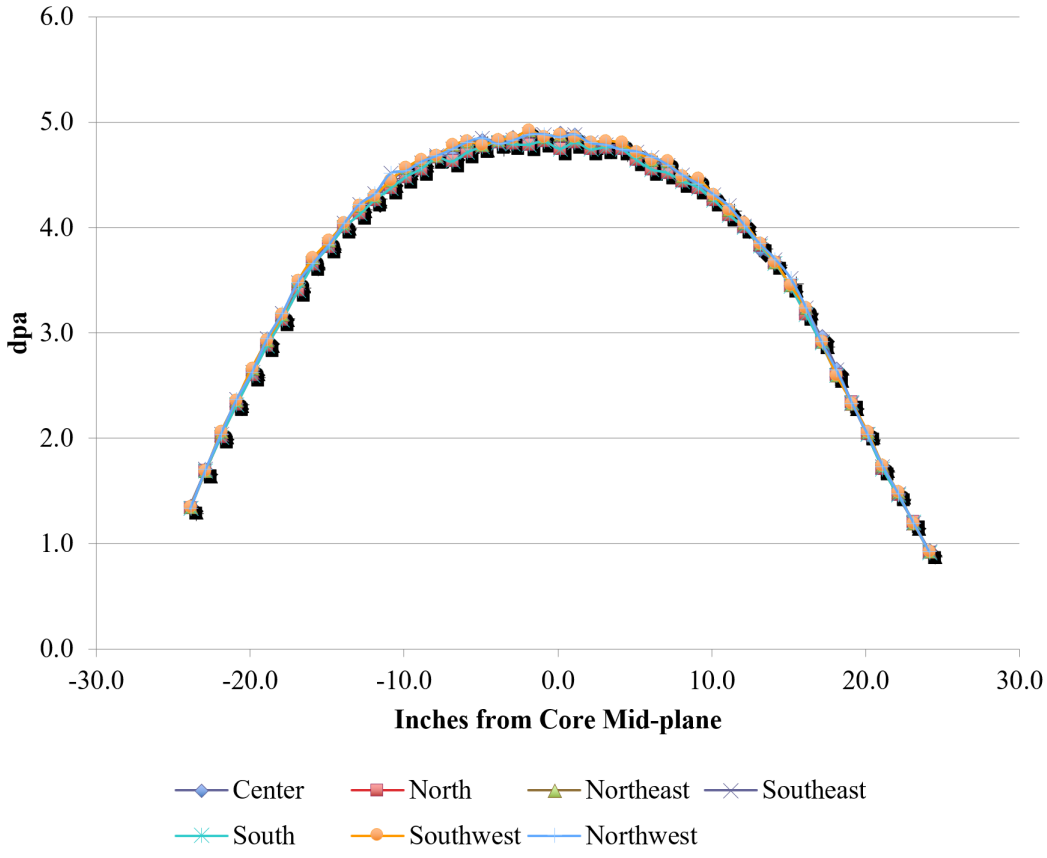

Figure 4. Calculated dose levels for AGC-2 after 140 effective full-power days.

As described in Section 1, Introduction, of this report and as shown in Figure 4, the ATR neutron flux profile is not completely symmetrical along the vertical axis. Thus, to produce matched-pair specimens that have similar dose profiles both above and below the core mid-plane, an offset from the mid-plane is required. This offset adjusts the specimen positions and to matches the dose levels for "matched pair" specimen. For AGC-2, the offset spacing was determined using the accumulated dose levels from the central stack profile, both below and above the core mid-plane. Average dose values at 0.25-in. increments (i.e. height of a piggyback specimen) were calculated along both top and bottom curves allowing for direct comparison between matched positions within each stack.

The dose profiles for the lower and upper core were superimposed upon each other, as shown in Figure 5. To determine the length of the offset space, the dose values above and below the core mid-plane were compared, and the specimens in the bottom half of the AGC capsule were moved farther away from the mid-plane, Figure 5. An offset of 1.25 inches from the core mid-plane for the bottom creep specimens produced the closest dose matches between specimens.

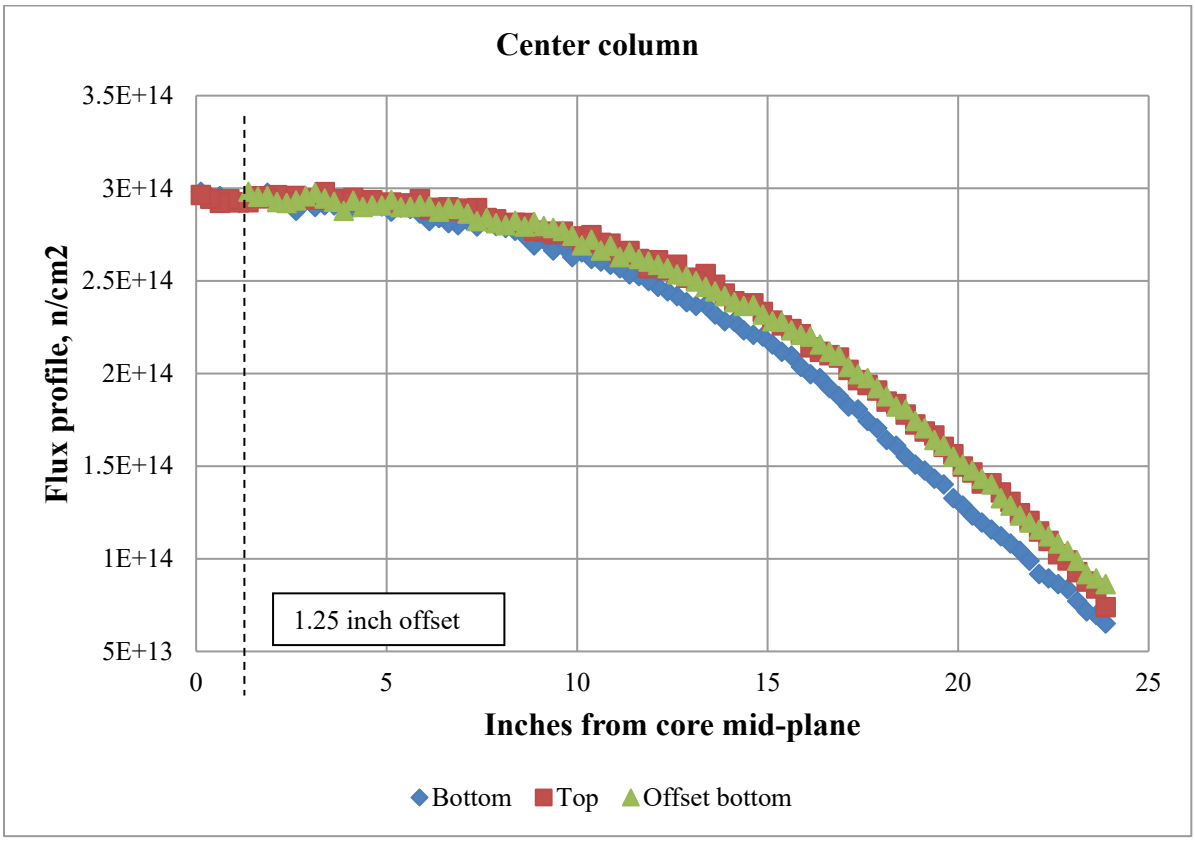

Figure 5. Advanced Test Reactor flux profile, as a function of core mid-plane position.

While it was impossible to exactly match both the upper and lower specimens, the dose levels for each specimen pair were fairly close, ranging from 0–11%. In addition, over time, the specimens in the top stacks should dimensionally shrink more than the bottom specimens (during irradiation) due to the compressive load applied. This effectively moves the top specimens closer to the centerline, thus creating a closer dose match to the specimens in the bottom stack. While this irradiation-induced shrinkage of the top stack of specimens is anticipated to be relatively small at the end of irradiation (i.e., <6 mm for the total stack of specimens), the dose levels do slightly converge rather than diverge.

It should be noted here that the specimen offset distance/position in the lower half of the AGC-1 capsule is significantly different from these offset calculations for the AGC-2 capsule.[14,15] AGC-1 used an older ATR flux profile that did not accurately reflect the current flux profiles within the South Flux Trap. Consequently, the offset was approximately 3.75 in. (i.e., 15 piggyback specimen heights), leading to slightly larger differences between the upper and lower matched-specimen pairs than expected for AGC-2, as shown in Table 1. This will need to be addressed in detail in the AGC-1 PIE report to be issued after PIE is complete.

Table 1. Typical dose differences between matched pairs in the AGC-1 test-series capsule.

Representative Stack (Stack No. 1)	
Matched Pairs	AGC-1 Estimated Dose Difference (%)
1S1/1U1	0.34
1S2/1U2	0.69
1S3/1U3	2.11
1S4/1U4	1.81
1S5/1U5	2.57
1S6/1U6	3.01
1S7/1U7	1.54
1S8/1U8	5.76
1S9/1U9	6.55
1S10/1U10	9.43
1S11/1U11	13.40
1S12/1U11	3.09
1S13/1U12	5.23
1S14/1U13	3.33
1S15/1U14	1.53

2.2.3. Determining the Physical Positions of Irradiation Creep Specimens in the Stacks

Once the specimen-position offset was established for the bottom half of the specimens, the number of total creep specimens for each grade of graphite was determined. To increase the number of creep specimens in the AGC-2 test-series capsule, the 0.25-in.-tall NBG-25 graphite spacers between creep specimens were eliminated. This decision to eliminate the spacers increased the total number of specimens by over 20 in the entire capsule. This allowed more specimens per graphite grade to be irradiated within the AGC-2 capsule.

A further decision was made to increase the creep specimen number population for the newer graphite grades because little-to-no irradiation data are available on these grades. Specifically, more specimens of graphite grades NBG-18 and PCEA were chosen to be irradiated than the IG-110, IG-430, and NBG-17 graphite grades. NBG-18 and PCEA were determined to have 16 specimens per applied stress level, for a total of 48 specimens within AGC-2. Graphite grades IG-110 and IG-430 were represented by only 12 specimens per applied stress level, for a total of 36 specimens within AGC-2. Table 2 shows the total number of specimens irradiated per graphite grade.

Table 2. Total number of irradiated creep specimens in the AGC-2 test-series capsule.

Graphite Grade	Total Number of Creep Specimens
PCEA	48
NBG-18	48
IG-110	36
IG-430	36
NBG-17	24
H-451	24

Other factors had to be considered before the stacking order for each stack could be finalized. First, three load levels are applied to the specimens in the loaded upper parts of the stacks (i.e., loads of 13.8, 17.2, and 20.7 MPa). The six outer stacks in the capsule allow the specimens in two of the stacks to be loaded at 13.8 MPa, while the other two pairs of stacks are loaded at 17.2 and 20.7 MPa, respectively. Because two stacks are at similar applied stress levels, the specimen loading order can be shifted between the two stacks, allowing the same grade of graphite loaded at the specimen stress levels to be exposed over a broader neutron dose range, as shown in Figure 6. Assuming that both stacks will have the same applied stress level, receive similar dose levels per position, and have a constant temperature allows for this shifting of the specimens, and consequently more uniform, smoother dose profile for each graphite grade.

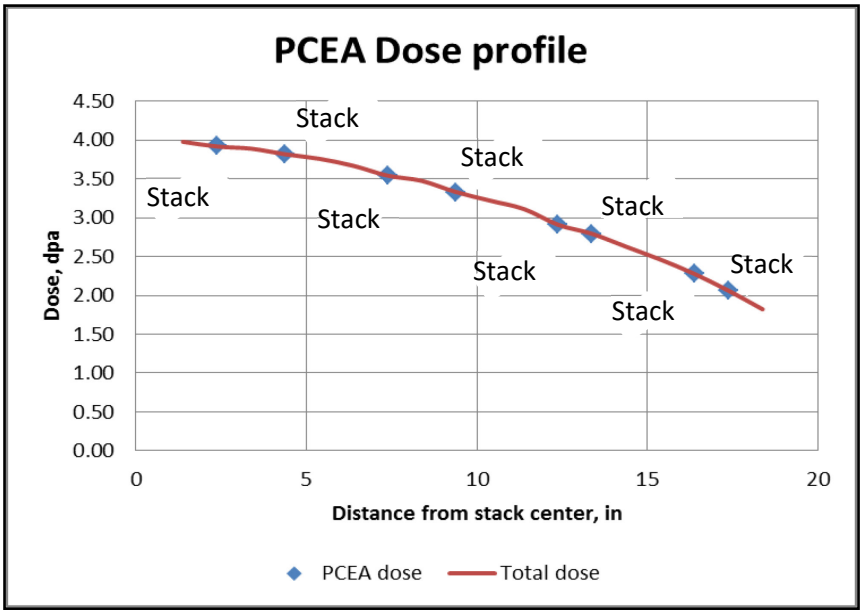

Figure 6. Typical AGC-2 dose profile for creep-graphite specimens utilizing similar applied stress levels in matched stacks.

A further consideration is the grain orientation of the specimens. A decision was made to have approximately 75% of the specimens be orientated in the "with-grain" (WG) direction and 25% of the specimens be "against-grain" (AG). However, in the case of the vibration-molded graphites (i.e., NBG-17 and -18), there are actually two with-grain directions and one against-grain direction as a consequence of the fabrication process. As such, it was logical to split the with-grain and against-grain specimens evenly (i.e., 50/50 ratio) rather than following the 75/25 ratio established for the other specimens.

Once these considerations were accounted for, the dose-level profiles were determined for each graphite grade and within each stack. The estimated creep specimen dose profiles for each graphite grade for each stress level are illustrated in Figure 7a, 7b, and 7c.

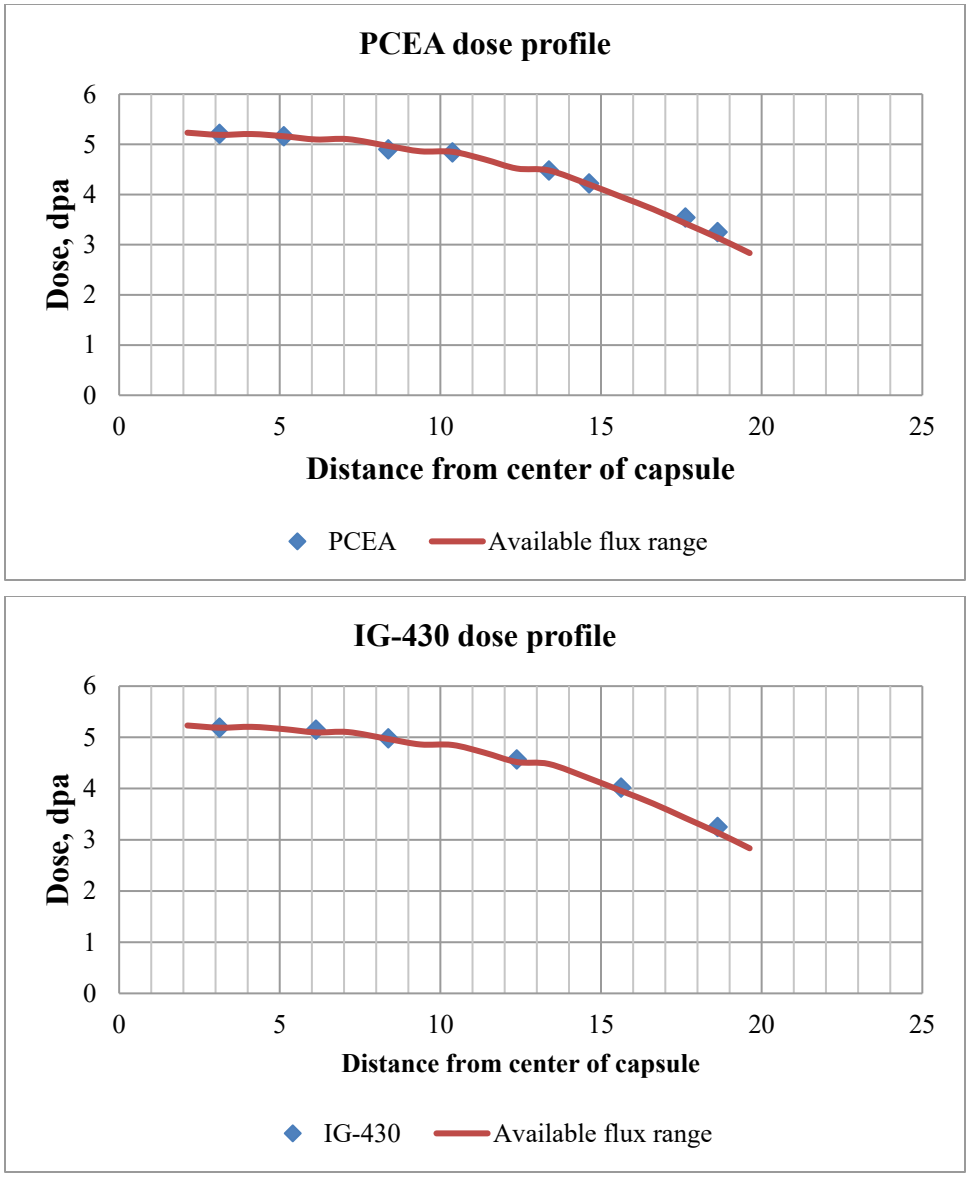

Figure 7a. Estimated creep-specimen dose profiles for each major graphite grade.

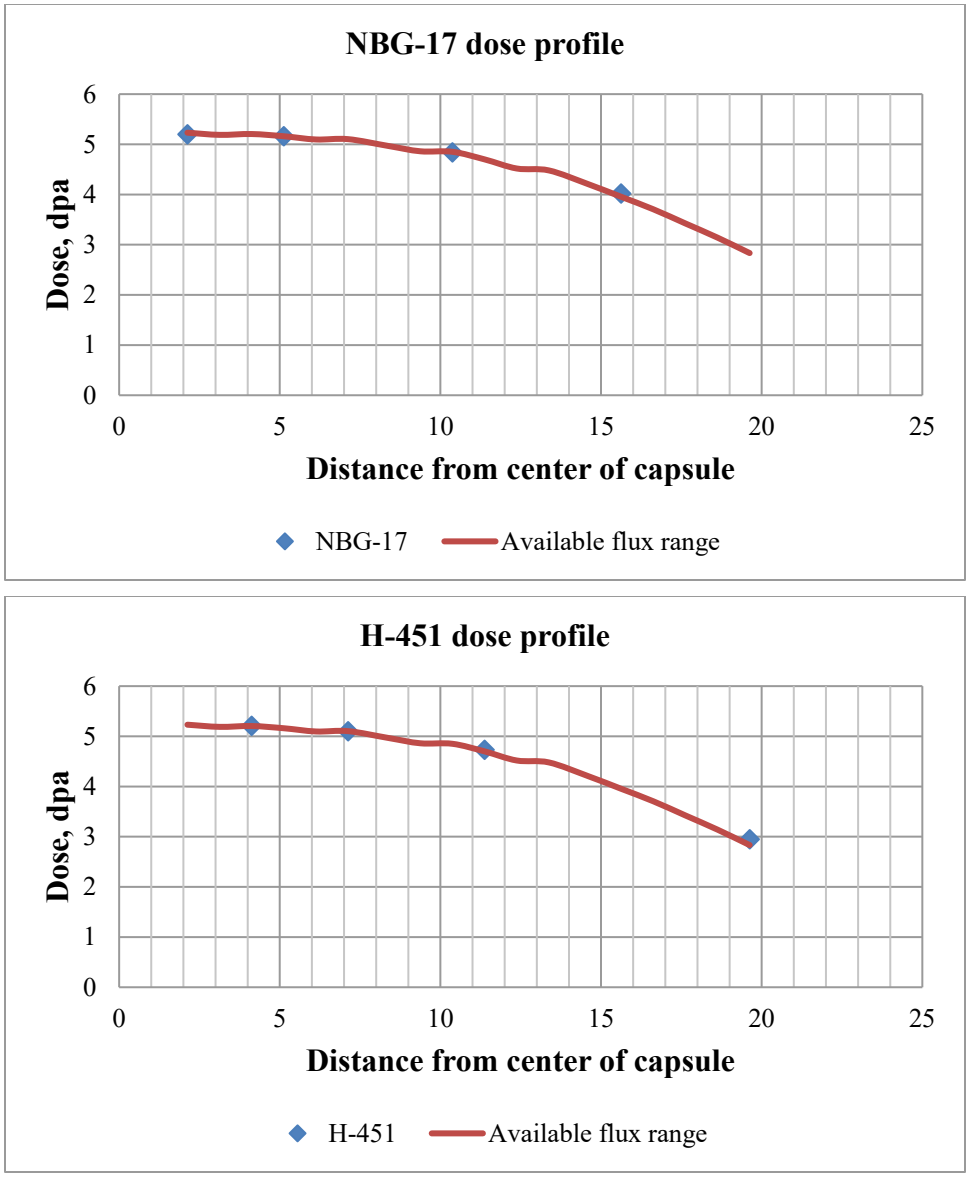

Figure 7b. Estimated creep-specimen dose profiles for each major graphite grade.

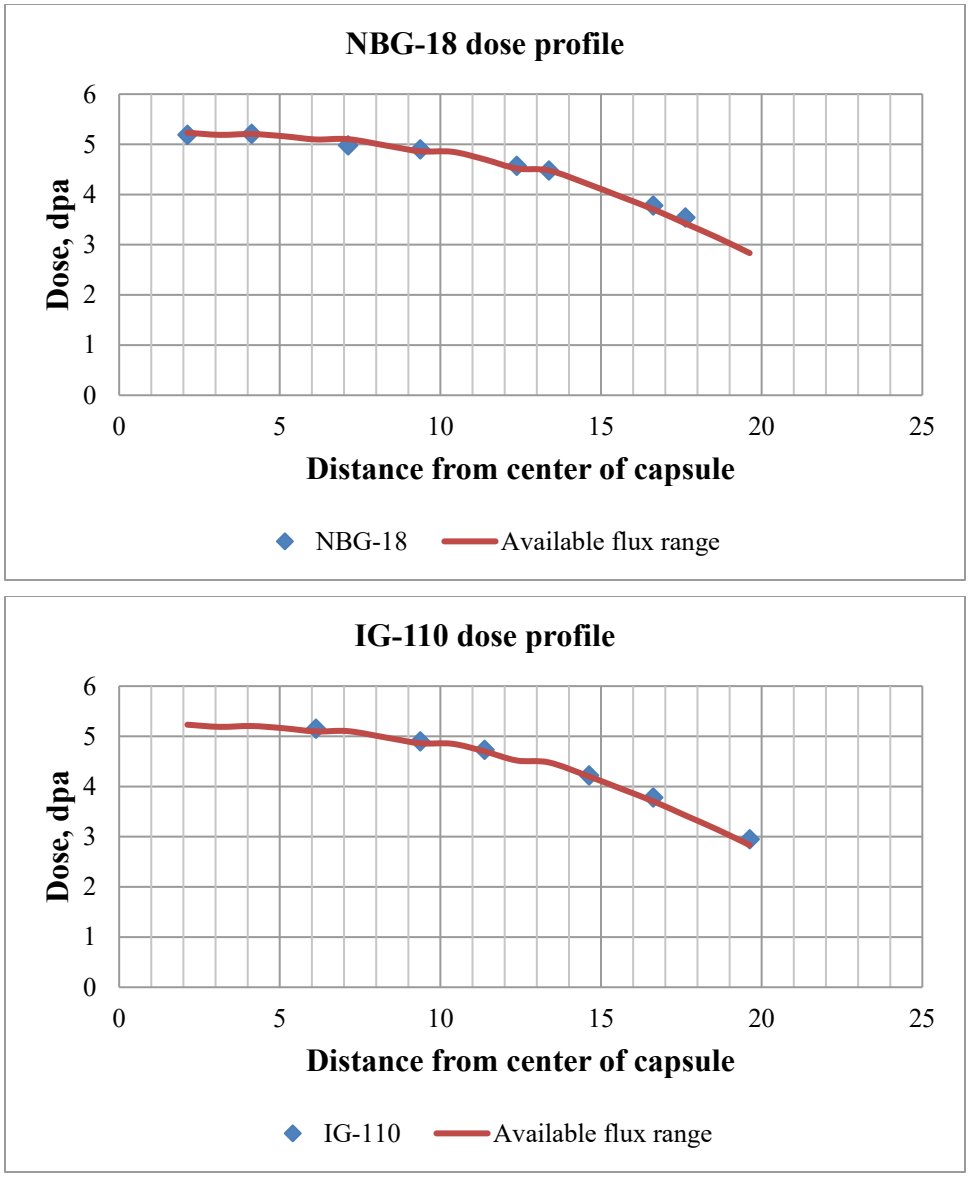

Figure 7c. Estimated creep-specimen dose profiles for each major graphite type.

The final loading configuration for the outer stacks was established once a smooth dose profile was achieved for each graphite grade, Figure 7a, 7b, and 7c. The lower stack offset, the flux wire spacers, creep specimens, and specimen symmetry above and below the capsule mid-plane were mapped for each graphite specimen in Table 3.

Table 3. Final loading configuration for AGC-2 creep specimens in outer stacks.

Stack 1		
ID#	Graphite	Height
CW101	H-451	19.63
	Flux wire	
DW101	PCEA	18.63
BW101	NBG-18	17.63
EW102	IG-110	16.63
FW101	IG-430	15.63
DW102	PCEA	14.63
	Flux wire	
BW102	NBG-18	13.38
FW102	IG-430	12.38
EW104	IG-110	11.38
DW1001	PCEA	10.38
BW103	NBG-18	9.375
FW103	IG-430	8.375
	Flux wire	
CW102	H-451	7.125
EW0201	IG-110	6.125
DW1002	PCEA	5.125
BW1001	NB-18	4.125
FW0104	IG-430	3.125
	Flux wire	
AW101	NBG-17	2.125
Centerline		0
AW102	NBG-17	2.125
	Flux wire	
FW0201	IG-430	3.125
BW1002	NB-18	4.125
DW1003	PCEA	5.125
EW0202	IG-110	6.125
CW103	H-451	7.125
	Flux wire	
FW0202	IG-430	8.375
BW1003	NBG-18	9.375
DW1004	PCEA	10.38
EW0203	IG-110	11.38
FW0203	IG-430	12.38
BW1101	NBG-18	13.38

Stack 2		
ID#	Graphite	Height
EW0301	IG-110	19.63
	Flux wire	
FW0301	IG-430	18.63
DA402	PCEA	17.63
BP402	NBG-18	16.63
AW103	NBG-17	15.63
EW0302	IG-110	14.63
	Flux wire	
DW1103	PCEA	13.38
BW1103	NBG-18	12.38
CW1003	H-451	11.38
AW1001	NBG-17	10.38
EW0303	IG-110	9.375
DA403	PCEA	8.375
	Flux wire	
BP403	NBG-18	7.125
FW0302	IG-430	6.125
AP402	NBG-17	5.125
CW1101	H-451	4.125
DW1104	PCEA	3.125
	Flux wire	
BW1201	NBG-18	2.125
Centerline		0
BW1202	NBG-18	2.125
	Flux wire	
DW1201	PCEA	3.125
CW1102	H-451	4.125
AP403	NBG-17	5.125
FW0303	IG-430	6.125
BP501	NBG-18	7.125
	Flux wire	
DA501	PCEA	8.375
EW0304	IG-110	9.375
AW1002	NBG-17	10.38
CW1103	H-451	11.38
BW1203	NBG-18	12.38
DW1202	PCEA	13.38

Stack 3		
ID#	Graphite	Height
CW1202	H-451	19.63
	Flux wire	
DW1203	PCEA	18.63
BW1301	NBG-18	17.63
EW0403	IG-110	16.63
FW0401	IG-430	15.63
DW1204	PCEA	14.63
	Flux wire	
BW1302	NBG-18	13.38
FW0402	IG-430	12.38
EW0404	IG-110	11.38
DW1301	PCEA	10.38
BW1303	NBG-18	9.375
EW0404	IG-430	8.375
	Flux wire	
CW1203	H-451	7.125
EW0501	IG-110	6.125
DW1302	PCEA	5.125
BW1401	NB-18	4.125
FW0501	IG-430	3.125
	Flux wire	
AW1101	NBG-17	2.125
Centerline		0
AW1102	NBG-17	2.125
	Flux wire	
FW0502	IG-430	3.125
BW1402	NB-18	4.125
DW1303	PCEA	5.125
EW0502	IG-110	6.125
CW1301	H-451	7.125
	Flux wire	
FW0503	IG-430	8.375
BW1403	NBG-18	9.375
DW1304	PCEA	10.38
EW0503	IG-110	11.38
FW0504	IG-430	12.38
BW1501	NBG-18	13.38

Stack 4		
ID#	Graphite	Height
EW0601	IG-110	19.63
	Flux wire	
FW0602	IG-430	18.63
DA503	PCEA	17.63
BP503	NBG-18	16.63
AW1103	NBG-17	15.63
EW0602	IG-110	14.63
	Flux wire	
DW1403	PCEA	13.38
BW1503	NBG-18	12.38
CW1303	H-451	11.38
AW1201	NBG-17	10.38
EW0603	IG-110	9.375
DA601	PCEA	8.375
	Flux wire	
BP601	NBG-18	7.125
FW0603	IG-430	6.125
AP501	NBG-17	5.125
CW201	H-451	4.125
DW1404	PCEA	3.125
	Flux wire	
BW1601	NBG-18	2.125
Centerline		0
BW1602	NBG-18	2.125
	Flux wire	
DW1502	PCEA	3.125
CW202	H-451	4.125
AP502	NBG-17	5.125
FW0604	IG-430	6.125
BP602	NBG-18	7.125
	Flux wire	
DA602	PCEA	8.375
EW604	IG-110	9.375
AW1202	NBG-17	10.38
CW203	H-451	11.38
BW1603	NBG-18	12.38
DW1503	PCEA	13.38

Stack 5		
ID#	Graphite	Height
CW301	H-451	19.63
	Flux wire	
DW1504	PCEA	18.63
BW201	NBG-18	17.63
EW0703	IG-110	16.63
FW0703	IG-430	15.63
DW1601	PCEA	14.63
	Flux wire	
BW202	NBG-18	13.38
FW0704	IG-430	12.38
EW0704	IG-110	11.38
DW1602	PCEA	10.38
BW203	NBG-18	9.375
FW0801	IG-430	8.375
	Flux wire	
CW302	H-451	7.125
EW0801	IG-110	6.125
DW1603	PCEA	5.125
BW301	NB-18	4.125
FW0802	IG-430	3.125
	Flux wire	
AW1301	NBG-17	2.125
Centerline		0
AW1302	NBG-17	2.125
	Flux wire	
FW0803	IG-430	3.125
BW302	NB-18	4.125
DW1604	PCEA	5.125
EW0802	IG-110	6.125
CW303	H-451	7.125
	Flux wire	
FW0804	IG-430	8.375
BW303	NBG-18	9.375
DW1701	PCEA	10.38
EW0803	IG-110	11.38
FW0901	IG-430	12.38
BW401	NBG-18	13.38

Stack 6		
ID#	Graphite	Height
EW0901	IG-110	19.63
	Flux wire	
FW0903	IG-430	18.63
DA303	PCEA	17.63
BP401	NBG-18	16.63
AW1303	NBG-17	15.63
EW0902	IG-110	14.63
	Flux wire	
DW201	PCEA	13.38
BW403	NBG-18	12.38
CW402	H-451	11.38
AW1401	NBG-17	10.38
EW0903	IG-110	9.375
DA302	PCEA	8.375
	Flux wire	
BP303	NBG-18	7.125
FW0904	IG-430	6.125
AP503	NBG-17	5.125
CW403	H-451	4.125
DW202	PCEA	3.125
	Flux wire	
BW501	NBG-18	2.125
Centerline		0
BW502	NBG-18	2.125
	Flux wire	
DW203	PCEA	3.125
CW501	H-451	4.125
AP601	NBG-17	5.125
FW1001	IG-430	6.125
BP302	NBG-18	7.125
	Flux wire	
DA203	PCEA	8.375
EW0904	IG-110	9.375
AW1402	NBG-17	10.38
CW503	H-451	11.38
BW503	NBG-18	12.38
DW204	PCEA	13.38

Stack 1		
ID#	Graphite	Height
	Flux wire	
DW1101	PCEA	14.63
FW0204	IG-430	15.63
EW0204	IG-110	16.63
BW1102	NBG-18	17.63
DW1102	PCEA	18.63
	Flux wire	
CW1002	H-451	19.63

Stack 2		
ID#	Graphite	Height
	Flux wire	
EW0401	IG-110	14.63
AW1003	NBG-17	15.63
BP502	NBG-18	16.63
DA502	PCEA	17.63
FW0304	IG-430	18.63
	Flux wire	
EW0402	IG-110	19.63

Stack 3		
ID#	Graphite	Height
	Flux wire	
DW1401	PCEA	14.63
FW0601	IG-430	15.63
EW0504	IG-110	16.63
BW1502	NBG-18	17.63
DW1402	PCEA	18.63
	Flux wire	
CW1302	H-451	19.63

Stack 4		
ID#	Graphite	Height
	Flux wire	
EW0701	IG-110	14.63
AW1203	NBG-17	15.63
BP603	NBG-18	16.63
DA701	PCEA	17.63
FW0701	IG-430	18.63
	Flux wire	
EW0702	IG-110	19.63

Stack 5		
ID#	Graphite	Height
	Flux wire	
DW1702	PCEA	14.63
FW0902	IG-430	15.63
EW0804	IG-110	16.63
BW402	NBG-18	17.63
DW1704	PCEA	18.63
	Flux wire	
CW401	H-451	19.63

Stack 6		
ID#	Graphite	Height
	Flux wire	
EW1001	IG-110	14.63
AW1403	NBG-17	15.63
BP301	NBG-18	16.63
DA202	PCEA	17.63
FW1002	IG-430	18.63
	Flux wire	
EW1002	IG-110	19.63

NBG-17 specimen - AW### = “against-grain”, AP### = “with-grain”
NBG-18 specimen - BW### = “against-grain”, BP### = “with-grain”
H-451 specimen - CW### = “with-grain”, CA### = “against-grain”
PCEA specimen - DW### = “with-grain”, DA### = “against-grain”
IG-110 specimen - EW#### = “with-grain” (isotropic so no “against grain” direction)
IG-430 specimen - FW#### = “with-grain” (isotropic so no “against grain” direction)

2.2.4. Determining the Physical Positions of Piggyback Specimens in the Central Stack

Similar to the AGC-1 design, the AGC-2 piggyback specimens were contained within the central stack and did not have an applied stress imposed. Because AGC-2 has the same number of major and minor graphite types as the AGC-1 design, the same piggyback stacking order was used.[14,15]

One major change to AGC-2 piggy-back specimens was the elimination of a central hole through each graphite-type specimen. AGC-1 piggyback had a central hole to allow a series of SiC temperature monitors to be placed down the central spine of the experiment to provide independent temperature measurements from the capsule thermocouples (TC). Unfortunately, this central hole in the specimens precluded thermal diffusivity testing on the specimens above room temperature.

A decision was made to not machine a central hole in the AGC-2 piggyback specimens and allow each to be tested for high temperature thermal diffusivity. This eliminated the independent temperature monitoring capability for the AGC-2 capsule, but it was determined that being able to measure the changes to the thermal diffusivity at high temperatures was of more importance.

3. GENERAL TESTING PROVISIONS

A significant level of preparation was needed to meet Nuclear Quality Assurance Level 2 quality requirements prior to actual material property testing. An approved characterization plan was developed that was dependent upon the two graphite specimens' geometry and on the material properties to be measured. In general, all testing was performed through ASTM approved standards; however, due to small size of the graphite specimens some methods required modifications and variations of the testing standards. Details of these testing standard variations along with equipment calibration, personnel training on testing methodology, and data acquisition are provided.

3.1. Characterization Plans and Work Procedures

The AGC-2 specimens have been characterized in accordance with PLN-3267, "AGC-2 Characterization Plan."[16] This plan describes thermal, physical, and mechanical measurement methods used to characterize the graphite specimens and is intended to meet the requirements of MCP-1380, "Research and Development Test Control."[17] Described within the plan are the instruments, fixtures, and methods used for preirradiation material-property measurements of bulk density, thermal diffusivity, coefficient of thermal expansion (CTE), elastic modulus, and electrical resistivity.

All work was performed in accordance with LWP-21220, "Work Management."[18] All records designated in implementing documents as Quality Assurance records were controlled in accordance with PLN-3319, "Records Management Plan for the VHTR Technology Development Office Program."[19]

Data resulting from the preirradiation characterization are plotted in Appendix A and listed in Appendix C. Statistical evaluation has been performed using an inner quartile range analysis to identify levels of uncertainty and outliers in the data. The measured properties and characteristics of different graphite types will be compared along with the effect of grain orientation.

3.2. Specimen Description and Preparation

The major grades of the nuclear graphite to be tested in AGC-2 are NBG17, NBG-18, PCEA, IG-430, H-451, 2114, and IG-110. Minor grades of graphite include NBG-25, PCIB, PPEA, NBG-10, BAN, HLM, PGX, 2114, HOPG, and A3 Matrix. All major grades have been characterized fully in accordance with PLN-3267, and the minor grades have only had dimensional, density, and thermal diffusivity measurements performed on them. The two primary specimen types in the AGC experiments are creep specimens and piggyback specimens. "Creep" specimens from major grade graphite types are shown in INL Drawing 600786, Rev. 1, "ATR Advanced Graphite Capsule (AGC-2) Graphite Specimen Machining Details,"[20] and will be subjected to a mechanical load during irradiation to induce irradiation creep within the specimens. "Piggyback" specimens from both major and minor grade graphite types are shown in INL Drawing 600786, Rev. 1. They are not subjected to a mechanical load and are subjected only to neutron irradiation at high operating temperatures to assess the effects of a reactor environment on the specific graphite grade.

All specimens are 12.7 mm in diameter, with the creep specimens being 25.4 mm long and the piggyback specimens being 6 mm long (INL Drawing 600786, Rev. 2).[10] Details of how specimens were cut from the graphite blocks are contained in INL Drawing 600787, Rev. 3.[21]

Immediately after being machined, each specimen is placed in an individual container that is bar coded with a unique identification number, in accordance with INL Drawing 600787, Rev. 3. Each graphite specimen is then laser-engraved with that same unique identification number around the circumference at one end. Prior to any material property measurement, each specific specimen is identified by its unique identification number, and the data are recorded/stored under this identification number. After the specimens have been laser-engraved, they are ultrasonically cleaned, as follows:

1. Handle the specimens only while wearing cotton or powder-free nitrile gloves
2. Remove all dust and debris using an aerosol pressurized dust-off product
3. Ultrasonically clean specimens for 20 minutes in deionized water
4. Rinse specimens in ethyl alcohol to help displace water
5. Allow to air dry
6. Place specimens in a laboratory oven at 130°C for 2 hours.
7. Allow specimens to cool in a desiccator and retain there in storage until resistivity or bulk density measurements are taken.

It should be noted that irradiated specimens are not washed again prior to characterization measurements. However, for measurements of density and resistivity, Steps 6 and 7 above are followed (i.e., irradiated specimens are dried in a laboratory oven at 130°C for 2 hours and allowed to cool in a desiccators, where they are retained until resistivity and/or bulk density measurements are performed).

3.3. Personnel and Training

Personnel who perform the measurements identified in this report are qualified in accordance with MCP-3052, "VHTR TDO Personnel Qualification and Certification."[22] Their ability to adequately perform measurements described in this report is demonstrated by instrument manufacturers' training and certification and/or performance of an instrument/measurement operational validation. Personnel qualifications are reviewed by the NGNP Graphite Research and Development Technical Lead and documented in the laboratory notebooks.

3.4. Variations, Exceptions, and Discrepancies

Several variations, exceptions, and discrepancies may occur. The first is a known departure from the applicable American Society for Testing and Materials (ASTM) standard. These departures are typically related to geometrical constraints. All currently known departures or exceptions taken to the ASTM standard are described in detail in Section 3 of this plan. Any departure not captured in this plan will be recorded in laboratory notebooks associated with the measurement. In most cases, the effects of the exception or departure from the ASTM method/standard on the measured value are not well understood. When possible, sensitivity studies will be performed and documented in laboratory notebooks to understand the impact of these exceptions and departures.

It is likely that the ASTM standards and/or test methods will be revised and improved during the 10+ year AGC experiment cycle. Each revision or development will be evaluated for how it could impact future measurements and their consistency with measurements made under previous revisions or techniques. A programmatic determination will be made whether to continue with the current version of the ASTM method or use the updated version. This determination will be documented in laboratory notebooks associated with the affected measurement.

While measurements are being made, it is possible that something out of the ordinary may occur. Any unusual event that occurs during a measurement will be documented in the laboratory notebook associated with that specific measurement and duly noted within the database associated with the data generated for this program. The principal investigator will be notified of the event and will determine what impact it has on the data. The significance of the result will be documented in the laboratory notebook by the principal investigator.

3.5. Calibration and Functional Validation

The measurement protocol consists of calibration, functional validation, and data acquisition. Functional validations established for each measurement, in collaboration with the instrument manufacturer, will be performed periodically to ensure that accurate and consistent data are acquired. All validations will be performed on traceable standards and documented in retrievable laboratory notebooks associated with each measurement. In the event that an instrument functional validation fails, the reason for the failure will be investigated and resolved prior to that measurement being used for further characterization. Upon resolution, a determination will be made as to the impact the failure might have had on data taken prior to the failure and back to the last valid measurement. If it is determined the data captured during this interval are suspect, the impacted data will be evaluated for accuracy.

MCP-3066, “VHTR TDO Control of Measuring and Test Equipment,”[23] will be followed for calibration standards, methods, and frequencies that have been established for each measurement. Where it is not possible to use the INL Standards and Calibration Laboratory, calibration by user procedures will be established, based on ASTM standards and manufacturers’ instructions and performed against international standards. These procedures will be documented in laboratory notebooks associated with each measurement.

4. GRAPHITE STANDARDS AND METHODS

A brief summary of the AGC specimen testing methods is included in Table 4 and includes precise dimensional measurements (before and after heating to 1000°C in the dilatometer) and nondestructive characterization of the physical properties. A detailed description of each preirradiation testing method is provided in Section 5, “Detailed Description of Test Methods.”

Table 4. NGNP graphite specimen measurement and test equipment.

Measurement	Standard	Instrumentation	Calibration Method	Result
Physical dimensions and mass	ASTM C559-90 (reapproved 2010)	Mitutoyo Micrometer 121-155 INL ID: 725884 INL ID: 727312 Mitutoyo Caliper CD-6 in CSX INL ID: 725813 INL ID: 726607 INL ID: 727194 Sartorius Scale ME235P INL ID: 412642 INL ID: 415907	INL Standards and Calibration Laboratory	Bulk density
Fundamental frequency	ASTM C747-93[24] (reapproved 2010) ASTM C1259-08[25]	J. W. Lemmens Grindosonic INL ID: 412850	No calibration required per instrument manufacturer	Elastic modulus
Sonic velocity	ASTM C769-09[26]	Olympus NDT Sq. Wave Pulser/Receiver 5077PR INL ID: 728024 National Instruments Digitizer USB 5133 INL ID: 726725 INL ID: 415868	INL Standards and Calibration Laboratory	Young's modulus, Shear modulus, Poisson ratio
Four-point electrical resistivity	ASTM C611-98 (reapproved 2010)	Kiethly 6220 Precision Current Source INL ID: 725865 INL ID: 727290 Kiethly 2182A Nano Voltmeter INL ID: 725866 INL ID: 727289	INL Standards and Calibration Laboratory	Electrical resistivity
Laser flash diffusivity	ASTM E1461-07	Netzsch LFA 457 2 ea. INL ID: 412855 INL ID: 412864	Calibration by user per manufacturer's instructions	Thermal diffusivity
Push rod dilatometry	ASTM E228-06	Netzsch DIL 402 C 2 ea. INL ID: 412860 INL ID: 412861	Calibration by user per manufacturer's instructions	Coefficient of thermal expansion
Environmental monitoring	All	Visala Pressure, Humidity and Temperature PTU301 INL ID: 726912 INL ID: 727884 INL ID: 727502	INL Standards and Calibration Laboratory	Laboratory environmental conditions

The equipment necessary for the measurements listed in Table 4 are segregated into individual stations. Each station has a bar scanner for reading unique specimen identification bar codes, a computer for automated data acquisition, and the test equipment. The bar code of the individual specimen container is read, and the file for that specimen is automatically opened for data input prior to each measurement. Associated with each measurement type/station is a unique laboratory notebook maintained in accordance with MCP-2875, "Maintaining Laboratory Notebooks,"[27] and PLN-2690, "VHTR Technology Development Office Quality Assurance Program Plan,"[28] paragraph 3.3. Accepted data are stored in the NGNP Data Management and Analysis System, a satellite file location for NGNP. Data are transmitted in standardized Excel file format to the NGNP Data Management and Analysis System using Form 435.78, "VHTR Technology Development Office Information Input Sheet,"[29] in accordance with PLN-3319.

In addition to data stored in laboratory notebooks, the specific measuring instruments are networked to a server computer where the measurement data are automatically stored. This has been implemented in the INL Carbon Characterization Laboratory where custom LabVIEW software was written to facilitate automated data acquisition. This software comprises five main programs: Manufacturers Data, Physical and Dimensional Measurements, Electrical Resistivity Measurements, Sonic Resonance (Fundamental Frequency) Measurements, and Sonic Velocity Measurements. These five programs acquire data from instrumentation or user input and record the results in an Excel spreadsheet located on a server computer. In the case of thermal expansion and thermal diffusivity measurements, two other LabVIEW programs have also been written to parse vendor software-acquired data into Excel spreadsheets. MCP-3058, "VHTR TDO Software Quality Assurance,"[30] and FRM-959, "VHTR Software Management Plan,"[31] are currently used to govern the development, accuracy, and configuration control of this software.

Measurements are made in the following sequence:

1. Wash and dry – all specimens
2. Mass and dimensions – all specimens
3. Thermal diffusivity – piggyback specimens
4. Elastic modulus by sonic resonance – creep specimens
5. Electrical resistivity – creep specimens
6. Elastic modulus by measurement of sonic velocity – creep specimens
7. Wash and dry to remove couplant – creep specimens
8. Coefficient of thermal expansion – creep specimens
9. Postcharacterization of mass and dimensions – all specimens.

5. DETAILED DESCRIPTION OF TEST METHODS

Before any measurements are made, specimen numbers and basic information about each type of graphite will be entered into the manufacturer's data program. Once basic information about the graphite type has been recorded, it will be automatically saved to an Excel spreadsheet file, and the individual specimen numbers will be entered using a bar code reader. Following the initial input of general information, individual material property measurements will be made, starting with mass and dimensional measurements for determining bulk density.

5.1. Mass, Dimensions, and Bulk Density

Dimensional change is one of the key parameters affecting the performance of graphite in a neutron environment. Determining volumetric and linear dimension as a function of temperature and radiological dose is necessary to understand critical performance measures (e.g., dimensional change turnaround, irradiation creep, and internal stresses imposed upon graphite components). Dimensional and mass measurements will be performed to ASTM Standard C559-90, "Standard Test Method for Bulk Density by Physical Measurements of Manufactured Carbon and Graphite Articles" (reapproved 2010),[32] which describes in detail the procedure for making dimensional measurements and calculating bulk density.

The accuracy of the dial micrometers used here is stated by the manufacture to be 2 μm. For the larger graphite creep specimens with a 25.4 mm length measurement this corresponds to a 0.008% accuracy for this technique. However, when evaluating the uncertainty of the density determination other factors must be considered, such as, the hardness of the material and the force with which the micrometer blade is engaged with the material, specimen temperature variation, technician skill, etc. These and other factors were considered in a propagation of error analysis to arrive at an uncertainty of 0.08% with the measurement of the specimen diameter being the largest contributor to the error.

5.2. Electrical Resistivity

Electrical resistivity is used as a rapid, simple means to determine grain orientation, structure, and crystallinity of graphite. In conjunction with optical microscopy, it can be used to determine the microstructural texture of graphite components without much specimen preparation work. Resistivity is measured following ASTM C611-98, "Standard Test Method for Electricity Resistivity of Manufactured Carbon and Graphite Articles at Room Temperature" (reapproved 2010).[33] The measurement technique is commonly referred to as "four-point probe." It consists of passing a known current through the specimen and measuring the voltage across the specimen at known locations. Based on Ohms law, the resistance is determined, and the resistivity is calculated from Equation (1):

$$\rho = R \cdot A / L \tag{1}$$

where

ρ = Electrical resistivity

R = Measured resistance

A = Cross sectional area

L = Length over which the voltage is measured.

Figure 8 shows a test fixture fabricated at INL that allows a specimen to be rotated for multiple measurements of voltage around its periphery.

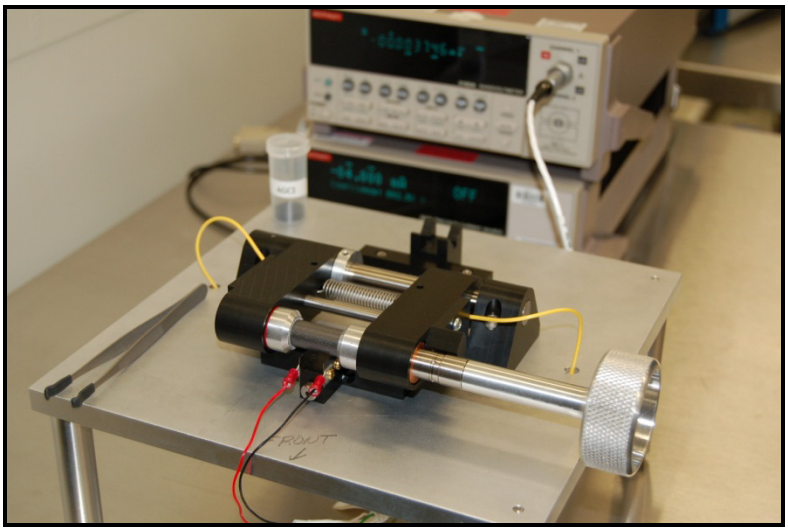

Figure 8. Electrical resistivity measurement station.

Uncertainty in the resistivity measurement is mainly comprised of the contact resistance between the specimen and the contacting blades for the voltage measurement. Specimen temperature and the temperature of other bimetal junctions in the voltage measuring leads are also significant factors. These effects are minimized by passing the current through the sample in two directions and averaging the measured voltage for each direction. In this way any thermoelectric or small differences in junction resistances will cancel. A round robin test series reported in ASTM C 611 precision and bias section states a lab to lab variability of 2.5%. A round robin test series such as this would take into account the variables discussed above and is considered a good estimate of the measurement uncertainty.

5.3. Approximation of Elastic Modulus from the Measurement of Sonic Velocity

The mechanical properties of graphite are necessary to determine the structural integrity of graphite components. These properties are vital to determining the viability of the structural strength and integrity of the reactor core. The as-received and irradiated values are needed for whole-core models, which will be used for the graphite design code. This test is carried out in accordance with ASTM C 769-09, "Standard Test Method for Sonic Velocity in Manufactured Carbon and Graphite Materials for Use in Obtaining Young's Modulus."[26] In this measurement, the transmitting piezoelectric transducer sends a 2.25-MHz sound wave through the specimen. At the opposite end of the specimen, the acoustic wave is received by another piezoelectric transducer. The sonic velocity of the specimen is the ratio of specimen length to the signal time lapse between transducers. An approximate value for Young's modulus, E, can be obtained from Equation (2):

$$E = \rho V^2 \tag{2}$$

where

E = Young's modulus

ρ = Specimen density

V = Sonic velocity.

Figure 9 shows the sonic velocity measurement station. In the foreground are fixtures for clamping the specimen between the transducer and receiver. These fixtures have unique features that improve measurement accuracy, precision, and efficiency. Specimens are easily and rapidly loaded into the fixture using the cam-operated clamp. Measurement precision is improved because the spring-loaded clamp applies consistent pressure between the transducers and specimen, resulting in repeatable couplant thickness.

As specified in paragraphs 8.1 and 8.5.1 of ASTM C 769-09, a suitable coupling medium should be used and reported with the data. Here, "Shear Gel," manufactured by Sonotech, Inc., is used for a shear wave couplant, and "Ultra Gel II," also manufactured by Sonotech, Inc., is used for the transverse wave couplant.

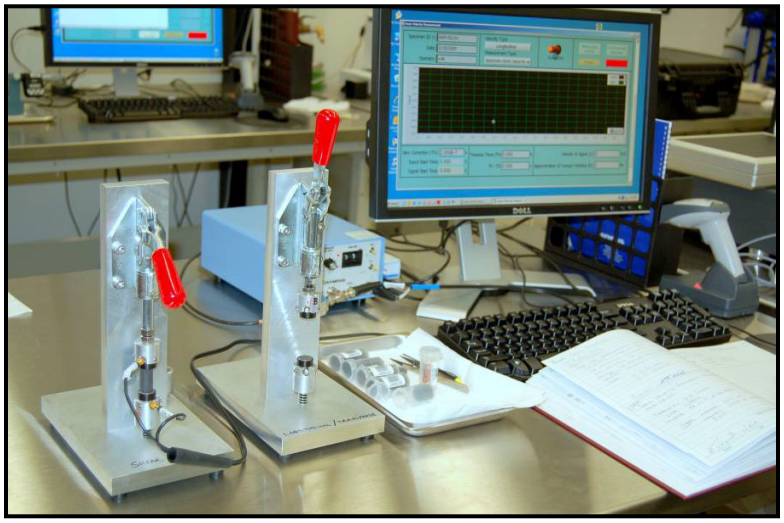

Figure 9. Sonic velocity measurement station.

Figure 9 shows the LabVIEW software user interface display for sonic velocity measurements after scanning the bar code of the specimen to be tested. This screen is used to acquire sonic velocity measurements of a specimen in both the longitudinal and shear directions. Operating much like an oscilloscope, the cursors automatically mark the time between the transmitted wave and the received wave. Also shown in Figure 10 are two examples of the shear wave and transverse wave timing locations for properly coupled specimens. The specimen length divided by this transit time yields the sonic velocity.

The uncertainty in determining of elastic moduli from the measurement of sonic velocity comes from several sources. First there is the effect of material and geometry related dispersion of the transmitted wave. ASTM C-769 provides guidance on how to minimize this problem by choosing the correct frequency. This technique also assumes linear elastic behavior and graphite is not completely linearly elastic. And finally, the operator's judgment on the positions of the timing cursors is somewhat objective. Clean wave forms to base these judgments on are highly dependent on the quality of the transducer-material coupling. These sources of error are difficult to quantify and therefore difficult to combine in a propagation of error analysis. However, ASTM C769 describes in some detail a round robin test series between different labs. Using round robin test data to determine a coefficient of variation (COV) is a good means of estimating the measurement uncertainty. With caution, the COV of 3.8% (reported in C769) is taken here to be representative of the uncertainty for these measurements. When considering a single material and making comparisons between the pre and post irradiation signal values the precision of these measurements is good enough to consider differences greater than 4% significant. However, one is cautioned to refrain from using the values here as absolute or better than ± 10% accurate.

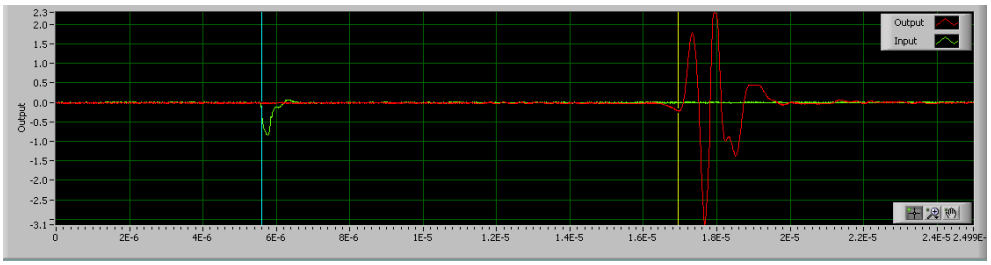

Shear wave timing

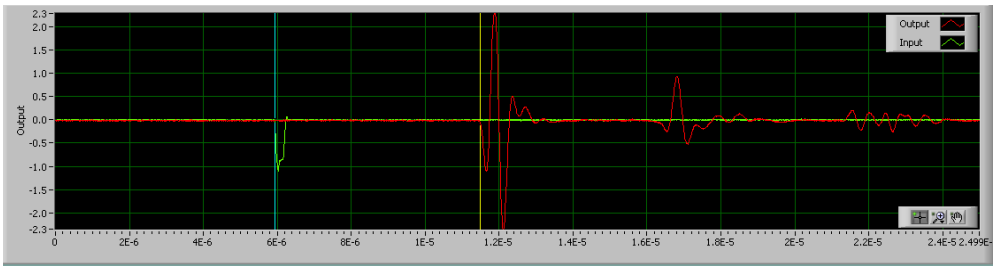

Transverse wave timing

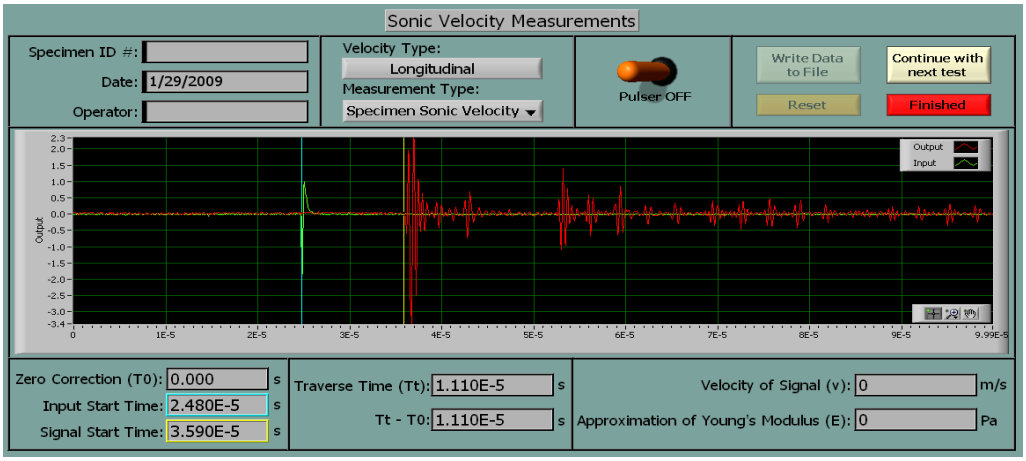

Figure 10. Sonic velocity measurement user interface.

After the longitudinal and shear modulus values have been determined, each specimen Poisson's ratio can be calculated from these results through equation (3):

$$\nu = \left[\frac{E}{2G}\right] - 1 \tag{3}$$

where:

ν = Poisson's ratio

E = Elastic modulus

G = Shear modulus

5.4. Modulus of Elasticity by Measurement of Fundamental Frequency

Understanding the mechanical properties of graphite is necessary to determine the structural integrity of graphitic components. These properties are vital to determining the viability of the structural strength and integrity of the reactor core. This test method measures the fundamental resonant frequency of test specimens of suitable geometry by exciting them mechanically with a singular elastic strike. Specimen supports, impulse locations, and signal pick-up points are selected to induce and measure specific modes of the transient vibration of the specimen. The transient signals are analyzed, and the fundamental resonant frequency is isolated and measured by the signal analyzer. The measured fundamental resonant frequency, specimen dimensions, and mass are used to calculate the dynamic Young's modulus, shear modulus, and Poisson's ratio in accordance with ASTM C747-93, "Standard Test Method for Moduli of Elasticity and Fundamental Frequencies of Carbon and Graphite Materials by Sonic Resonance," (reapproved 2010) in combination with apparatus and calculations described in ASTM C1259-08, "Standard Test Method for Dynamic Young's Modulus, Shear Modulus, and Poisson's Ratio for Advanced Ceramics by Impulse Excitation of Vibration."[25] The fundamental frequency measurement station is shown in Figure 11.

Figure 11. Fundamental frequency measurement station.

After placing a specimen in the test fixture, the user excites it by lightly tapping it with a small mechanical impulse. A consistent impulse is achieved by placing the ball hammer onto a lever that rotates out from under the hammer as it is raised. The specimen is supported in such a way that it vibrates at its natural frequency. A microphone placed underneath one end of the specimen, in combination with the Grindosonic electronics, measures this frequency, which is recorded and displayed by the computer. The modulus of elasticity is calculated and displayed next to the newly acquired frequency. If the results are satisfactory, the user can press the "Save 1st Frequency" button and go on to the next measurement. Following the recommendations of ASTM C-1259-08, 10 readings of the fundamental frequency are measured before the results of the test are written to the applicable Excel spreadsheet.

ASTM C-1259 describes in detail a round robin test series using ceramic materials along with an analysis of the propagation of errors in the calculation of moduli from the measurement of resonant frequency, geometry and mass of the sample. This error analysis shows the major sources of experimental variation are the measurement of the fundamental frequency and the smallest dimension (diameter) of the specimens due to their higher exponent in the modulus calculations. Both the propagation of error analysis and round robin data indicated an uncertainty of less than 2%. However, the creep specimens tested here do not meet the geometry requirements of C-1259. With the current specimen length-to-diameter ratio of only 2 (rather than 5 as specified) the AGC-2 graphite specimens are, at times, difficult to excite consistently and in a single mode of vibration. After significant training, an experienced operator was able to consistently obtain a resonant frequency within 2% uncertainty for the flexural mode of vibration within the specimens.

5.5. Thermal Expansion

Understanding the CTE for graphite components is critical for determining the dimensional changes that occur as a result of temperature cycles. Localized external stresses can be imposed upon mechanically interlocked graphite-core components because the individual pieces suffer differential thermal expansion. Internal stresses can occur within larger graphite components if there is a temperature gradient causing differential expansion within the piece (i.e., one side has a higher temperature than the other). Finally, the thermal expansion is highly dependent upon the graphite microstructure (e.g., orientation/anisotropy, pore size and distribution, and crystallinity). Irradiation damage can significantly alter graphite microstructure and thus CTE values. Determining the extent of the changes as a function of irradiation dose and temperature will be a key parameter for reliable calculation of stress states within graphite components, volumetric changes, and irradiation creep rates.

The CTE measured here follows ASTM E228-06, “Standard Test Method for Linear Thermal Expansion of Solid Materials with a Push-Rod Dilatometer.”[34] This test method uses a push-rod type dilatometer to determine the change in length of a graphite specimen relative to that of the holder as a function of temperature from the specified reference temperature. The temperature is varied over the desired range at a slow, constant heating or cooling rate. The linear thermal expansion and mean CTE, α, are calculated from the recorded data using Equation (4):

$$\alpha = \frac{1}{L_0}\frac{\Delta L}{\Delta T} \tag{4}$$

where

α = Mean CTE

L_0 = Specimen initial length

ΔL = Change in length

ΔT = Temperature difference between a specified reference temperature and the temperature at which the change in length was measured.

The Netzsch DIL 402 C commercial system, shown in Figure 12, currently used at INL does not have the capability to cool the specimen below ambient temperature. Therefore, the initial length at 20°C is linearly extrapolated from expansion data between 100 and 150°C, and the mean CTE is calculated from a 20°C reference temperature.

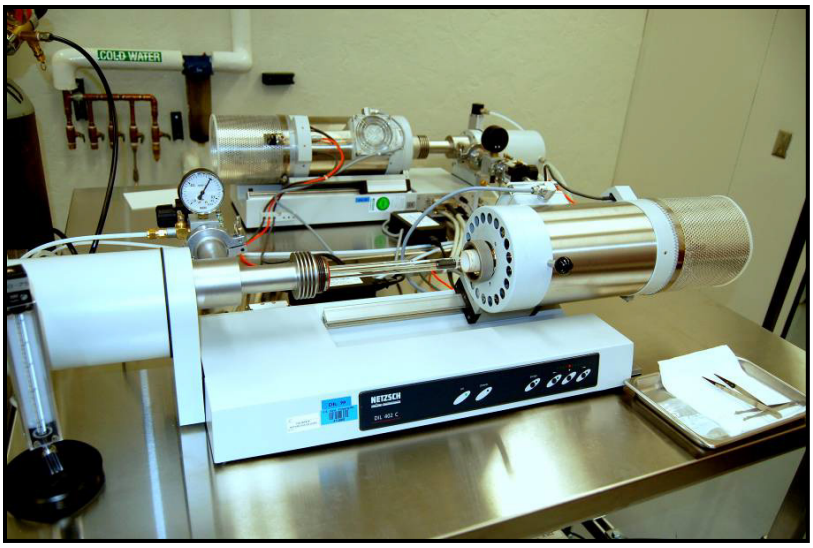

Figure 12. Commercial push rod dilatometer for measuring the coefficient of thermal expansion.

The greatest source of experimental error in the dilatometry method described here is the correction made for the expansion of the specimen holder and push rod/LVDT mechanism. This differential between the specimen and the apparatus must be accounted for in order to isolate the specimen expansion only. Studies reported in the precision and bias section of ASTM E228 have indicated that this type of dilatometry can be accurate to 4% when calibrations are performed carefully.

5.6. Thermal Diffusivity

The ability to conduct heat through the graphite core is critical to the passive removal of decay heat. Reduction of the thermal conductivity within graphite can have a significant effect on the passive heat-removal rate and thus the peak temperature that the core and, subsequently, the fuel particles will experience during off-normal events. Determining changes to the conductivity as a function of irradiation dose and temperature is important for the HTGR safety analysis. Here, ASTM E1461-07, "Standard Test Method for Thermal Diffusivity by the Flash Method," [35] is followed for calculating thermal diffusivity and conductivity. Thermal diffusivity (δ) is measured and defined as the ratio of thermal conductivity to volumetric heat capacity, as shown in Equation (5):

$$\delta = \frac{k}{\rho C_P} \tag{5}$$

where

δ = Thermal diffusivity

k = Thermal conductivity

ρ = Density

C_P = Specific heat.

The measurement is performed on small, thin, disk-shaped specimens. A pulsed laser is used to subject one surface of the specimen to a high-intensity, short-duration energy pulse. The energy of this pulse is absorbed on the front surface of the specimen, and the resulting rise in rear-face temperature is recorded. The thermal diffusivity is calculated from the specimen thickness and the time required for the rear-face temperature to reach 50% of its maximum value. Figure 13 shows a commercially available laser flash apparatus, complete with vendor-developed software for instrument control and data acquisition.

Figure 13. Laser flash apparatus measurement station for determining thermal diffusivity.

Uncertainty in the measurement of thermal diffusivity occurs from specimen heat loss and temperature measurement. Specimen temperature measurement is performed with a calibrated type S thermocouple in the near vicinity of the specimen. Being a relatively straight forward, the specimen temperature measurement is typically a small contribution to the overall measurement error or uncertainty.

The main contributor to the measurement uncertainty is heat loss from the specimen. Because this measurement technique depends on the assumption of one-dimensional heat transfer from the flat face receiving the laser pulse to the flat face radiating to the detector, heat loss errors are mainly attributed to radiative heat loss from the circumference of the specimen at temperatures above 300°C. Typically provided with the instrument software are several correction models to account for this heat loss. As the specimen diameter to thickness ratio decreases the heat loss increases to the point that the correction models no longer can account for the error. A study was performed to gain a fuller understanding of the limits of the models made available with the NETZSCH LFA and the dependence of the diameter to thickness ratio on measurement error. In this study the heat loss models were applied to data taken on specimens with various diameter to thickness ratios and at specimen temperatures between 25°C and 1000°C. It was determined that the Cowan[36] model along with diameter to thickness ratios greater than or equal to 2 resulted in determination of the diffusivity within ASTM E1461 and the manufactures specified uncertainties of 4% and 3%, respectively. This was further verified by instrument functional tests performed monthly on a pure iron validation sample for which the diffusivity was determined to be within 3% of the Touloukian[37] values between 100°C and 700°C.

6. DATA ANALYSIS

Data gathered for the characterization of AGC-2 specimens is contained in the appendixes of this report. Appendix A contains plots of the individual data points for each specimen. Shown by the dashed lines in each plot are the upper and lower limits of the interquartile range (IQR). These limits are established by the lesser of either the least or greatest value in the data or by multiplying the interquartile range by 1.5 and adding or subtracting this value from the third and first quartile. Any datum value outside of these limits is a suspected outlier of the established pattern. However, it is important to note that these outlying values are not only subject to measurement variability but also material variability and, therefore, cannot necessarily be discarded. These outlying values are examined in the context of the entire data set and will be evaluated further following irradiation. Other statistical parameters are calculated and presented in the tables of Appendix B. The mean, standard deviation and coefficient of variance are all calculated for the different measurement data sets and graphite types. Upper and lower limits called out in the tables of Appendix B are the IQR limits described above. Appendix C contains all of the raw data, including parameters specified by the applicable ASTM standard (e.g., dates, performer identifier, and room conditions).

There are many ways to combine and compare the data presented here. In doing so, the validity of the data is exercised and scrutinized. First, the data sets are considered independently with the statistical analysis described above. Additionally, a limited comparison of the absolute property values is performed between different graphite types and grades. The degree of isotropy is also evaluated for a limited number of grades by calculating the anisotropy ratio, as shown in Equation (6).

$$\text{Anisotropy ratio} = \frac{\text{Value of the property in the against - grain direction}}{\text{Value of the property in the with - grain direction}} \tag{6}$$

Note that in the case of isostatically molded graphite “with-grain” and “against-grain” indicate specimens taken from orthogonal planes in the billet.

6.1. Analysis of Mass, Dimensions, and Density Data

Plots of the measured mass, dimensions, and density for all AGC-2 specimens are shown in Figures A-1 through A-88 (see Appendix A). Beginning with graphite grade H-451, the calculated density of with-grain specimens has a higher degree of scatter as compared to the against-grain specimens (see Figure A-1). Both length and mass measurements for the with-grain specimens have relatively high COV (see Figures A-23 and A-67, respectively), but do not compensate for each other in the distribution of density. The higher scatter in density is most likely a result of material variation in the area of the billet from which these specimens were machined; however, it is difficult to completely rule out measurement inaccuracies. Therefore, the with-grain specimen length and mass measurements should be treated with caution. Comparison to the postirradiation measurements should provide more information on this observation.

Similar variations in density were observed in graphite grade NBG-17. In this case, a bimodal distribution in density was observed for both with- and against-grain specimens (see Figure A-4). Dimensional measurements were consistent and well-behaved for all specimens, but the bimodal distribution was observed in the mass measurements. To understand this unusual distribution, a study was completed to investigate the density as a function of depth in the NBG-17 billet. Twenty-three specimens (12 × 12 × 5.5 mm thick) were cut from the top of the billet to a depth of ~125 mm (see Figure 14). Figure 15 shows the density of specimens as a function of depth from the surface. In just 25 mm, the density increases 3%. This low-density area or area of inconsistent properties at the outer surface of the billet is often referred to as the skin effect of the billet.

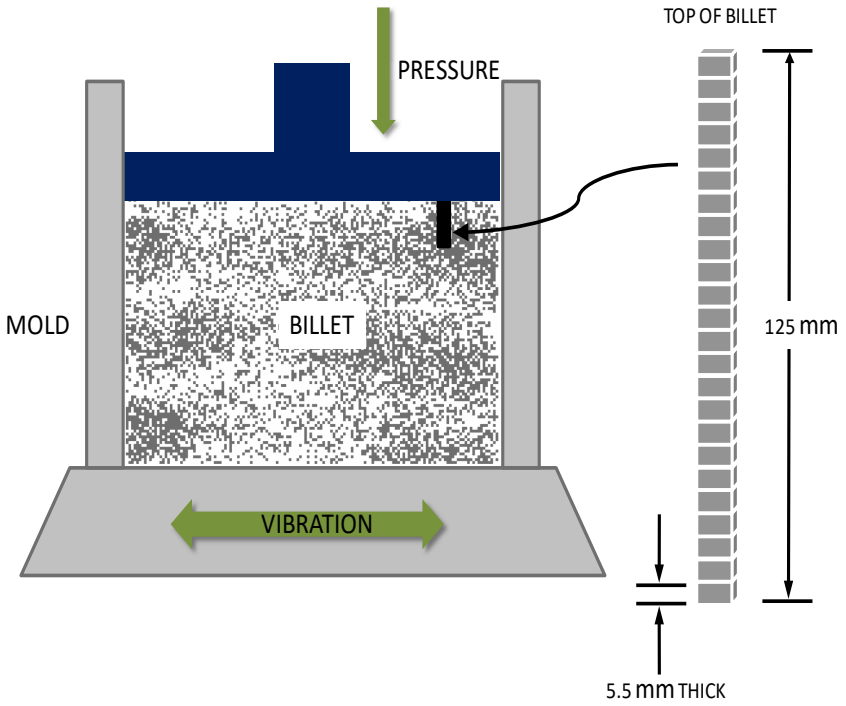

Figure 14. Schematic showing location and dimensional details of NBG-17 billet density investigation.

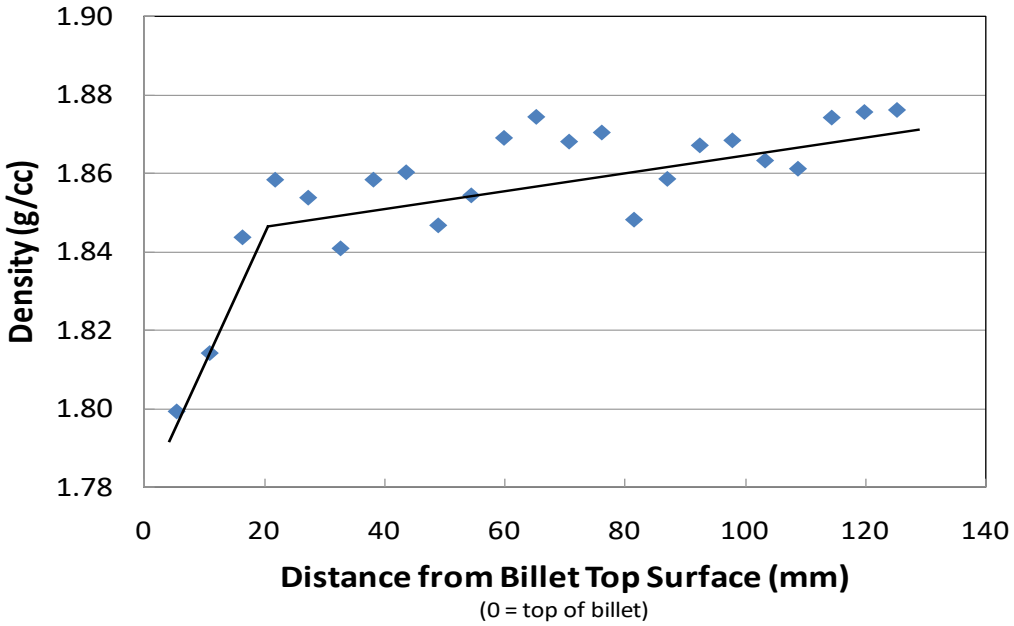

Figure 15. Density of NBG-17 as a function of depth in the billet.

Initially, it appeared unfortunate that specimens were taken from the skin of the billet, but in hindsight, this provided a variation in a significant property. With specimens of the same graphite type (i.e., coke, binder, and particle size) other material variables are held constant. This makes it possible to correlate the effect of density on other intrinsic properties (e.g., resistivity, elastic modulus, and diffusivity). Figure 16 shows an example of this for the resistivity measurements of the NBG-17 specimens. The expected difference in resistivity due to grain orientation is shown for the specimens at a similar density of ~1.864 g/cc. The higher resistivity for low-density against-grain specimens compared to the higher density specimens is most likely a result of higher porosity or micro-crack density inhibiting the flow of electrons. Further discussion of the resistivity data is provided in Section 6.2 of this report.

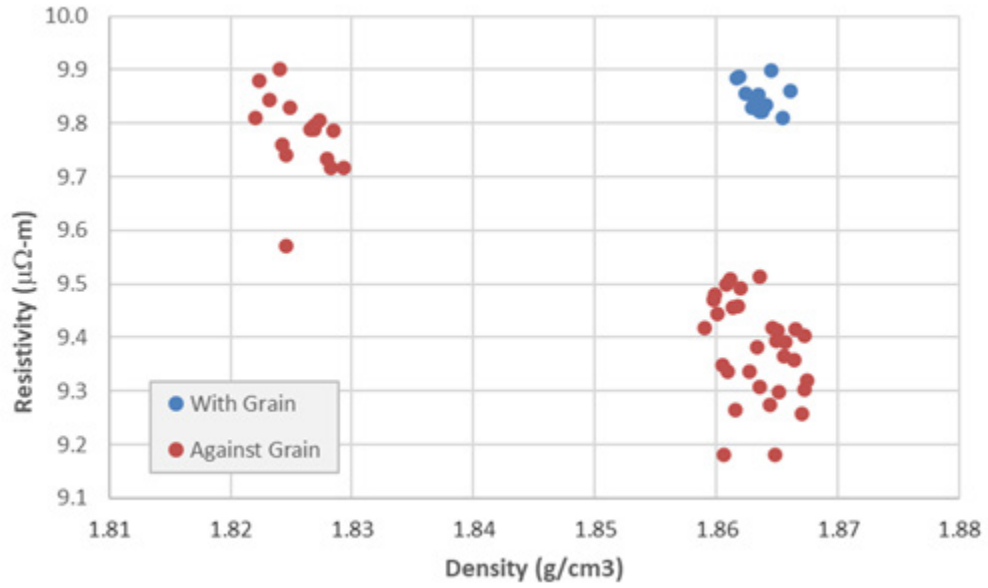

Figure 16. Resistivity of NBG-17 as a function of density.

Occasions arise when the determination of bulk density can be used to evaluate outliers or data that are near the IQR limits in either the dimensional or mass measurements. For example, Figures A-24, A-27, and A-28 show several data values for IG-110, NBG-18 and PCEA dimensional measurements that are near or outside the IQR limits. Evaluation of the corresponding density plots, Figures A-5 and A-16, show that all values fall within the quartile limits, with relatively low COVs. From this, it can be concluded that the dimensional outliers are simply specimens that were machined with different dimensions, resulting in them being outside or near the limit of the quartile analysis.

The density data of all other graphite grades (i.e., 2114, IG-110, NBG-18, NBG-25, BAN, HLM, IG-430, NBG-10, PCIB, PPEA, A3 Matrix, and New Matrix) is well-behaved and consistent with what was expected. The fact that these density data are so well-behaved indicates any outliers found in the associated dimensional or mass data are simply a result of machining tolerances and are valid.

Additionally, the dimensions and mass were measured following the thermal measurement of the CTE and diffusivity. These measurements were performed up to 1000°C, and concerns existed that the specimens maintained some residual stress due to the machining operations and that this stress would relax during the thermal cycle to 1000°C. Figures A-137 through A-202 contain plots of a comparison between the pre and post thermal treatment dimensions and mass. The comparison plots of specimen length show a slight trend of shrinkage of approximately 0.03%. For a 25-mm specimen, the accuracy of the dial micrometers used is 0.01%. Uncertainty in the measurement comprises not only accuracy of the dial micrometer but also other variables (e.g., room temperature, micrometer clutch wear, micrometer blade design, and velocity of blade approach) relative to the specimen hardness. Although there is a

definite trend to the decrease in length measurements after the thermal measurements, it is difficult to draw concrete conclusions, considering that the length change is probably on the order of the measurement uncertainty. Furthermore, the annealing of residual stress would tend to increase the size of the specimen, not decrease it. However, oxidation could decrease the size of the specimen during the thermal measurements if the furnace is not purged of all air; and indeed, the post mass measurements trend to lower values by ~0.03% on average, indicating that a very small amount of oxidation was occurring. Several specimens of graphite type 2114 (specimen numbers TP19 and TP21 were used as filler piggybacks in capsules 2 and 4, respectively, and TP21 was not used in the irradiation experiment) and NBG-18 (specimen number BP502 was not used in the irradiation experiment) displayed mass loss in excess of 0.5% (see Figures A-185 and A-187). This suspected oxidation is corroborated in the relatively large reduction in length and diameter of these specimens. In the analysis of postirradiation dimensional change, these specimens will require careful evaluation, using the post thermal measurement dimensions, if they are used for any calculation of irradiation creep.

6.2. Electrical Resistivity

Plots of electrical resistivity are shown in Figures A-119 through A-124 for graphite grades of PCEA, NBG-18, H-451, IG-110, IG-430, and NBG-17. All of the resistivity measurements were performed on the creep specimens only. Several noteworthy observations resulted from the statistical analysis, and all are related to billet density variations discussed in Section 6.1. Looking at Figure A-122, resistivity measurements for NBG-17 were only performed on the with-grain specimens taken from central locations in the billet where the density is consistent (refer to INL Drawing 600787, Rev. 3). In this case, the resistivity values are extremely consistent, with a coefficient of variance of 0.3%, which is well below the 2.5% uncertainty reported in a round robin test series of ASTM C611-98. The COV of against-grain specimens is much higher than the with-grain specimens at 2.2%. Although this value is relatively high, analysis of the data clearly shows a correlation of specimen density to resistivity (see Figure 15), and therefore, the high COV is a result of material density variation. A similar conclusion can be drawn for the spread of resistivity shown in Figure A-124 for the against-grain specimens of PCEA.

An example of a simple comparison between graphite grades and grain orientation is shown in Figure 17. Here, the resistivity values of several primary grades of graphite are plotted for both grain orientations, and the anisotropy ratio is displayed above the bars. It is interesting to note that all current grades of graphite have improved resistivity isotropy. This plot also shows that there is a 30% difference in resistivity for the current graphite types of interest.

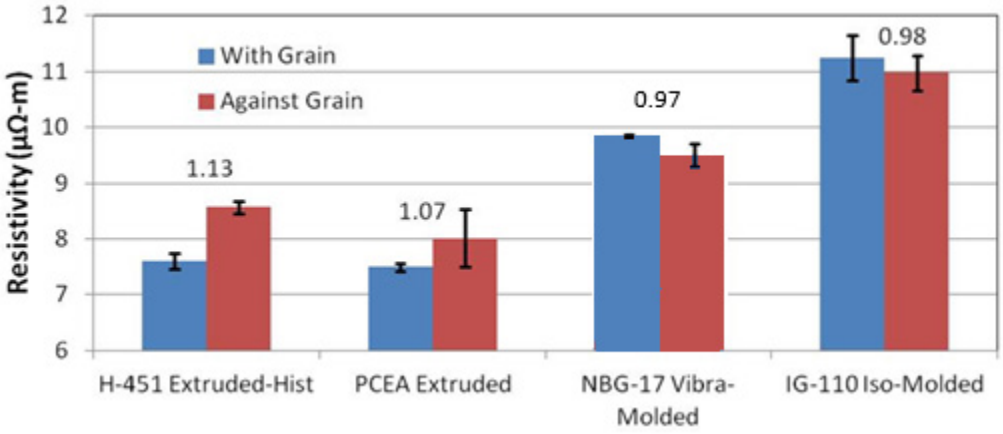

Figure 17. Electrical resistivity for several nuclear-grade graphite types. The anisotropy ratio is called out above each set of data bars.

6.3. Approximation of Elastic Modulus from the Measurement of Sonic Velocity

Figures A-125 through A-136 are plots of Young's and shear moduli determined from the measurement of sonic velocity. Statistical parameters are shown in Tables C-10 and C-11 for Young's and shear moduli, respectively. The IQR analysis does not reveal any inconsistency or outlier problems. As with resistivity, the moduli are easily correlated with the density of the specimens. Figure 18 shows that the sonic velocity increases with density for NBG-17. Therefore, in the calculation of the elastic modulus (i.e., density × the velocity squared), the density effect is compounded. This known behavior results from the fact that material containing more porosity and cracks (lower density) is more compliant and, therefore, will have a lower modulus of elasticity. The bimodal distribution of moduli resulting from density variations in the NBG-17 and PCEA specimens is clearly seen in Figures A-128, A-130, and A-134.

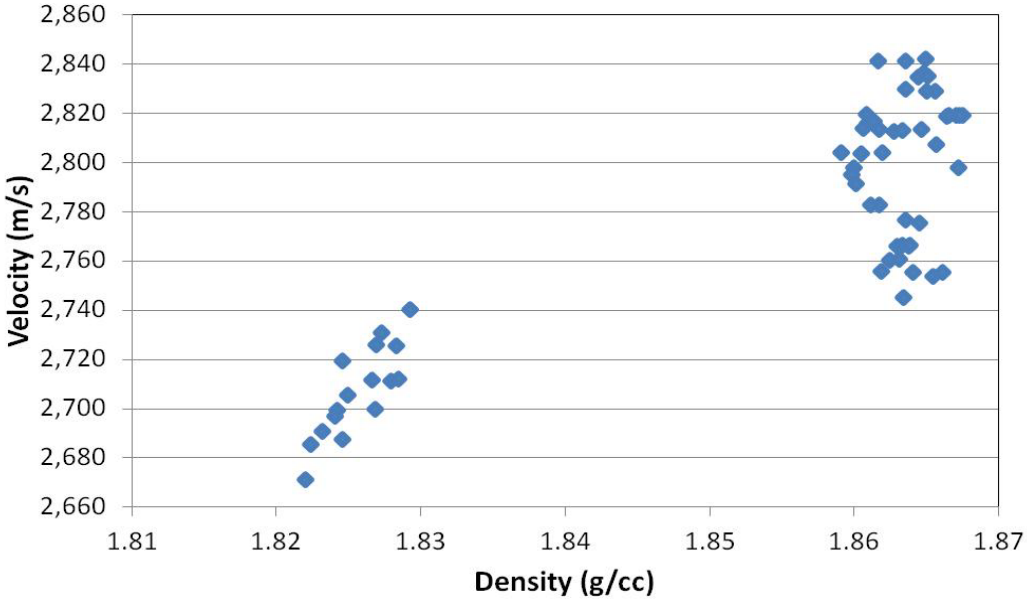

Figure 18. Measured longitudinal velocity as a function of density for NBG-17 creep specimens.

Table 5 shows Young's modulus measured using the sonic velocity technique. Although the COV includes potential material variability, these values compare favorably to a COV of 3.8% reported in the precision and bias section of ASTM C769. Consistent with the discussion of the effects of density here, it is observed that the highest-density graphite (i.e., NBG-17 and -18) produce the highest moduli. With the exception of IG-430, the modulus isotropy of the relevant graphite grades characterized here is better than the historical grade of H-451.

Table 5. Young's modulus by measurement of sonic velocity.

Graphite Type and Process Method	Young's Modulus Against-Grain Mean (GPa)	Against-Grain COV (%)	Young's Modulus With-Grain Mean (GPa)	With-Grain COV (%)	Young's Modulus Anisotropy Ratio
H451 extruded-hist	10.29	0.94	12.06	2.94	0.85
IG-110 iso-molded	11.20	3.97	10.81	3.08	1.04
IG-430 iso-molded	12.01	1.94	10.46	2.54	1.15
NBG-17 vibra-molded	14.31	4.86	14.23	0.72	1.01
NBG-18 vibra-molded	15.46	1.70	16.11	1.08	0.96
PCEA extruded	11.76	0.97	12.47	1.40	0.94

COV = coefficient of variation
GPa = gigapascals

6.4. Modulus of Elasticity by Measurement of Fundamental Frequency

Young's modulus, determined by measurement of fundamental frequency, is plotted in Figures A-113 through A-118, and the statistical data are contained in Table B-8. Statistically, these data are well-behaved, with the IQR analysis showing no problems with outliers. Again, a bimodal effect of density is shown for the against-grain specimens of NBG-17 (see Figure A-116).

Table 6 shows a comparison of Young's modulus from the measurement of fundamental frequency for the primary grades of graphite. The COVs for all except the against-grain specimens of PCEA compare favorably with ~3% uncertainty in the measurement technique. The scatter in modulus values for the against-grain specimens can be seen in Figure A-118. It was noted throughout the resonance testing of PCEA that achieving consistent values for the resonant frequency was difficult. More than 100 strikes were necessary to obtain 10 consistent values, and the average standard deviation of the frequencies measured was an order of magnitude higher than that of the other graphite grades. This can only be explained by the relatively large elongated porosity that existed in the PCEA graphite billet tested. This porosity is termed "wiggler porosity," and based on the testing in this program, the manufacturer has since corrected this problem in their manufacturing process. These elongated pores appear as cracks that run parallel to the grain and extrusion direction. In against-grain specimens, the size of these cracks or flaws can be on the order of the diameter of the specimen and run perpendicular to the direction of the flexural vibration mode, causing very inconsistent damping of the vibrational energy.

Also shown in Table 6 is the consistent fact that the new grades of graphite being tested exhibit better isotropy.

Table 6. Young's modulus by measurement of fundamental frequency.

Graphite Type and Process Method	Young's Modulus Against-Grain Mean (GPa)	Against-Grain COV (%)	Young's Modulus With-Grain Mean (GPa)	With-Grain COV (%)	Young's Modulus Anisotropy Ratio
H451 extruded-hist	8.01	1.64	9.94	3.07	0.80
IG-110 iso-molded	9.99	2.92	9.65	3.16	1.04
IG-430 iso-molded	10.64	2.07	9.39	2.43	1.13
NBG-17 vibra-molded	11.28	4.51	11.16	0.29	1.01
NBG-18 vibra-molded	11.99	1.59	12.42	0.84	0.97
PCEA extruded	8.73	23.35	9.92	2.38	0.87

COV = coefficient of variation
GPa = gigapascals

6.5. Thermal Expansion

Mean CTE data are plotted in Figures A-89 through A-112. A statistical evaluation of the CTE data was performed at three discrete temperatures (i.e., 100, 500, and 900°C) for each graphite type. Again, the dashed lines in these plots indicate the upper and lower IQR limits, and there are no outliers to consider. Tables B-5 through B-7 (see Appendix B) contain the mean, standard deviation, and COV values for data evaluated at the discrete temperatures. With the exception of PCEA, all COVs are below or on the order of the ±3% measurement uncertainty when calculated for the with- and against-grain specimen groups individually.

Figure 19 shows the average of all specimens for several of the primary grades of graphite, with error bars indicating ±1 standard deviation. All increase with temperature in a near-linear fashion between 100 and 1000°C. As an example of how these data may be used in future reactor designs, engineers will need to account for the fact that NBG-18 has a mean CTE that is ~50% higher than the historical grade H-451 if that grade is chosen for the core material.

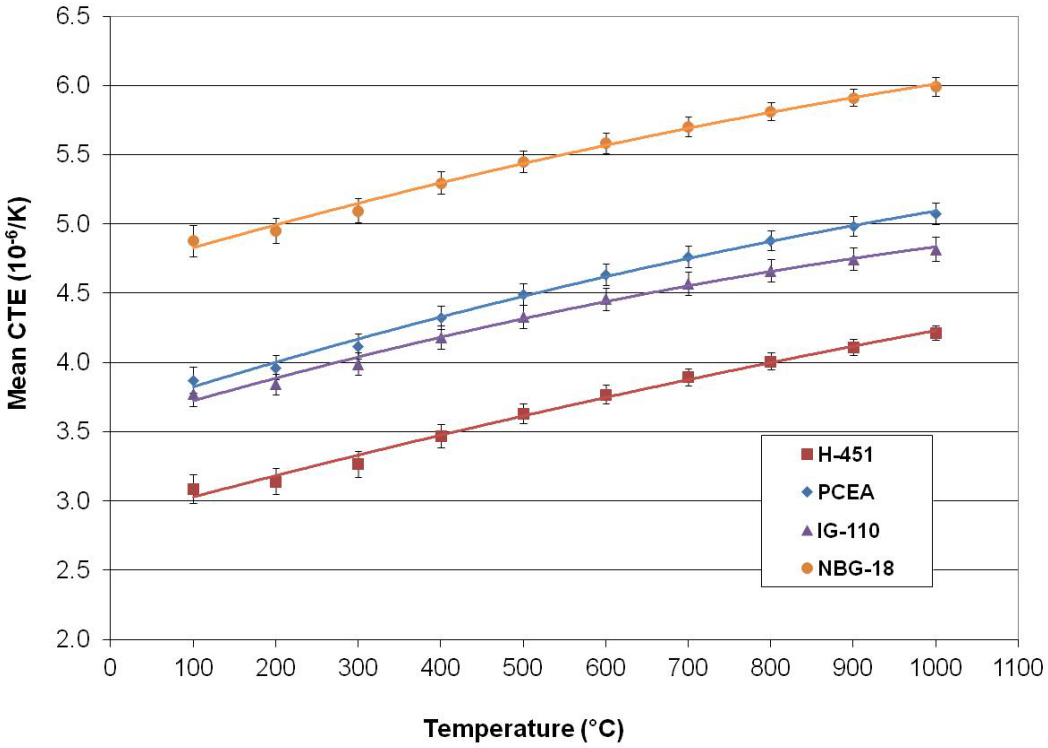

Figure 19. Mean coefficient of thermal expansion for several types of nuclear-grade graphite as a function of temperature. Error bars represent ±1 standard deviation in the data used to obtain the averages plotted.

Measurements of CTE were performed on both with-grain and against-grain specimens. Figure 20 shows the CTE anisotropy ratio for the same primary grades of graphite as a function of temperature. All are relatively constant with temperature. As in other properties, the new grades are more isotropic.

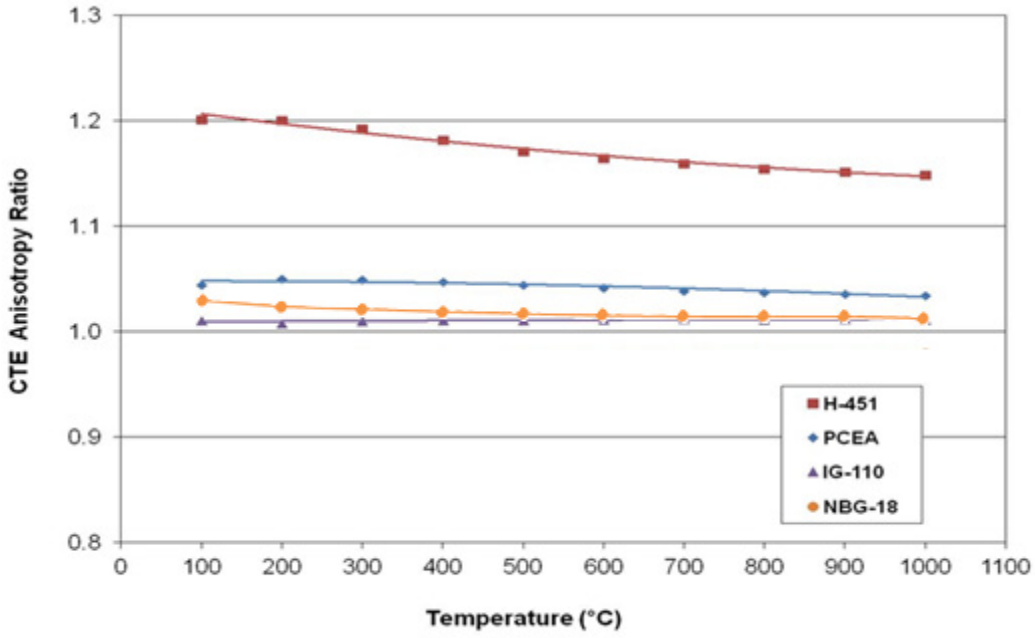

Figure 20. Coefficient of thermal expansion anisotropy ratio for several types of nuclear-grade graphite as a function of temperature.

6.6. Thermal Diffusivity

Plots of thermal diffusivity are shown in Figures A-203 through A-266. As with the CTE data, discrete temperatures of 100, 500, and 1000°C were statistically evaluated. Table B-16a through B-18c contain values of the mean, standard deviation, and COV. Four graphite types show COVs that are higher than the measurement uncertainty of ±3%. Graphite types A3 Matrix and New Matrix are both extremely small-batch graphite specimens, mixed and pressed individually with intentional variations in their composition. Therefore, it is not surprising that these specimens vary in their thermal diffusivity. The variation in diffusivity of PCEA is most likely due to the material variable called wiggler porosity discussed in Section 3.1, and it is speculated that the variation in H-451 is also due to material variability in the billet. For the most part, the diffusivity data are well-behaved, with only a few values that somewhat exceed the IQR limits and again are most likely a result of slight material variability.

Figure 21 shows the average thermal diffusivity for four of the primary graphites of interest. Error bars are ±1 standard deviation and, in most cases, are smaller than the plotted symbol. Also shown on the alternate ordinate is the percent difference between the historical grade of graphite H-451 and the relatively new grade, IG-110. The current grades of graphite all have a lower diffusivity than the historical grade, H-451, with IG-110 being 20–33% lower, depending on the temperature. H-451 is an extruded grade graphite made with relatively large filler coke particle size (0.5 mm). IG-110 is an isomolded graphite and has a filler particle size of 20 microns. This is why H-451 has a high diffusivity in the with-grain orientation. As seen in the CTE measurements, these differences in diffusivity are significant and will need to be considered in future reactor designs.

Figure 22 shows the anisotropy ratio for the same graphite grades. The anisotropy for all grades of graphite are constant with temperature, and as with the other properties, the current grades of graphite show much-improved isotropy of thermal diffusivity.

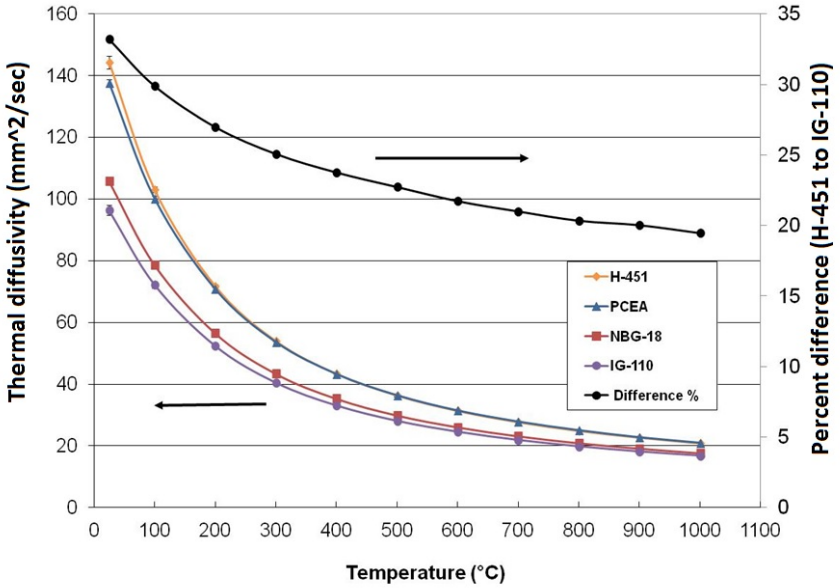

Figure 21. Thermal diffusivity for various with-grain graphite types. Error bars are 1 standard deviation in the data and in some cases smaller than the data symbol. The percent difference between H451 and IG-110 is plotted on the right-hand scale.

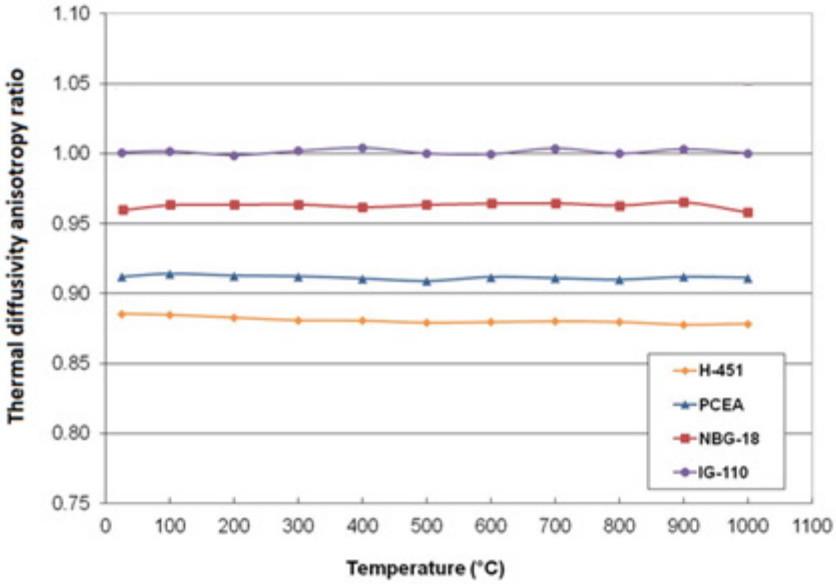

Figure 22. Thermal diffusivity anisotropy ratio for several types of nuclear-grade graphite as a function of temperature.

7. REFERENCES

1. T. Burchell, R. Bratton, W. Windes, NGNP Graphite Selection and Acquisition Strategy, ORNL/TM 2007/153, September 2007.
2. R. L. Bratton and T. D. Burchell, 2005, NGNP Graphite Testing and Qualification Specimen Selection Strategy, INL/EXT 05 00269, Idaho National Laboratory, May 2005.
3. INL/EXT 07 13165, "Graphite Technology Development Plan," Rev. 0, Idaho National Laboratory, September 2007.
4. PLN 2497, 2010, "Graphite Technology Development Plan," Rev. 1, Idaho National Laboratory, October 2010.
5. T. Burchell, J. Strizak, and M. Williams, 2011, AGC 1 Specimen Preirradiation Data Report, ORNL/TM 2010/285, Oak Ridge National Laboratory, August 2011.
6. T. Reed, 2012, "AGC 1 Individual Fluence, Temperature, and Load Calculation and Tabulation," ECAR 1943, Idaho National Laboratory, September 2012
7. T. Reed, 2012, "AGC 1 As Run Thermal Results," ECAR 1944, Idaho National Laboratory, September 2012.
8. D. Swank, 2010, AGC 2 Graphite Preirradiation Data Package, INL/EXT 10 19588, Rev. 0, Idaho National Laboratory, August 2010.
9. TFR 645, 2010, Advanced Graphite Capsule AGC 2 Experiment Test Train, Rev. 0, Idaho National Laboratory, July 2010.
10. INL Drawing 600786, 2012, "ATR Advanced Graphite Capsule (AGC 2) Graphite Specimen Machining Details," Rev. 2, Idaho National Laboratory, July 2012.
11. DWG 601266, 2012, "ATR Advanced Graphite Capsule Number 2 (AGC 2) Capsule Facility Assemblies," Rev. 2, Idaho National Laboratory, July 2012.
12. DWG 601258, 2012, "ATR Advanced Graphite Capsule 2 (AGC 2) Graphite Specimen Holder Assemblies and Details," Rev. 1, Idaho National Laboratory, July 2012.
13. J. R. Parry, 2010, "Engineering Calculations and Analysis Report: Reactor Physics Projections for the AGC 2 Experiment Irradiated in the ATR South Flux Trap," ECAR 1050, Rev. 0, Idaho National Laboratory, October 13, 2010.
14. T. Burchell and R. Bratton, 2005, Graphite Irradiation Creep Capsule AGC 1 Experimental Plan, ORNL/TM 2005/505, Oak Ridge National Laboratory, May 2005.
15. T. Burchell, 2009, A Revised AGC 1 Creep Capsule Layout, ORNL/TM 2009/009, Oak Ridge National Laboratory, January 2009.
16. PLN 3267, 2010, "AGC 2 Characterization Plan," Rev. 0, Idaho National Laboratory, March 19, 2010.
17. MCP 1380, 2012, "Research and Development Test Control," Rev. 3, Idaho National Laboratory, March 2012.
18. LWP 21220, 2012, "Work Management," Rev. 10, Idaho National Laboratory, October 2012.
19. PLN 3319, 2012, "Records Management Plan for the VHTR Technology Development Office Program," Rev. 2, Idaho National Laboratory, May 2012.
20. INL Drawing 600786, 2009, "ATR Advanced Graphite Capsule (AGC 2) Graphite Specimen Machining Details," Rev. 1, Idaho National Laboratory, March 2009.

21. Drawing 600787, 2010, “ATR Advanced Graphite Capsule (AGC 2) Experiment Graphite Specimen Cut Out Diagrams,” Rev. 3, Idaho National Laboratory, July 2010.
22. MCP 3052, 2012, “VHTR TDO Personnel Qualification and Certification,” Rev. 1, Idaho National Laboratory, May 2012.
23. MCP 3066, 2012, “VHTR TDO Control of Measuring and Test Equipment,” Rev. 2, Idaho National Laboratory, May 2012.
24. ASTM C747 93, 2010, “Standard Test Method for Moduli of Elasticity and Fundamental Frequencies of Carbon and Graphite Materials by Sonic Resonance,” American Society for Testing and Materials, 2010.
25. ASTM C1259 08, 2008, “Standard Test Method for Dynamic Young's Modulus, Shear Modulus, and Poisson's Ratio for Advanced Ceramics by Impulse Excitation of Vibration,” American Society for Testing and Materials, 2008.
26. ASTM C769 09, 2009, “Standard Test Method for Sonic Velocity in Manufactured Carbon and Graphite Materials for Use in Obtaining Young’s Modulus,” American Society for Testing and Materials, 2009.
27. MCP 2875, 2012, “Maintaining Laboratory Notebooks,” Rev. 11, Idaho National Laboratory, March 2012.
28. PLN 2690, 2013, “VHTR Technology Development Office Quality Assurance Program Plan,” Rev. 10, Idaho National Laboratory, January 2013.
29. Form 435.78, 2012, “VHTR Technology Development Office Information Input Sheet,” Rev. 2, April 2012.
30. MCP 3058, 2012, “VHTR TDO Software Quality Assurance,” Rev. 2, Idaho National Laboratory, July 2012.
31. FRM 959, 2012, “VHTR Software Management Plan,” Rev. 1, Idaho National Laboratory, 2012.
32. ASTM Standard C559 90, “Standard Test Method for Bulk Density by Physical Measurements of Manufactured Carbon and Graphite Articles,” American Society for Testing and Materials, 2010.
33. ASTM C611 98, 2010, “Standard Test Method for Electricity Resistivity of Manufactured Carbon and Graphite Articles at Room Temperature,” American Society for Testing and Materials, 2010.
34. ASTM E228 06, 2006, “Standard Test Method for Linear Thermal Expansion of Solid Materials with a Push Rod Dialometer,” American Society for Testing and Materials, 2006.
35. ASTM E1461 07, 2007, “Standard Test Method for Thermal Diffusivity by the Flash Method,” American Society for Testing and Materials, 2007.
36. R. D. Cowan, 1963, “Pulse Method of Measuring Thermal Diffusivity at High Temperatures,” Journal of Applied Physics 34 (4): 926.
37. Y. S. Touloukian, “Thermophysical Properties of Matter Thermal Diffusivity,” John Wiley & Sons Ltd (May 6, 1973)

Appendix A

AGC-2 Pre-irradiation Data

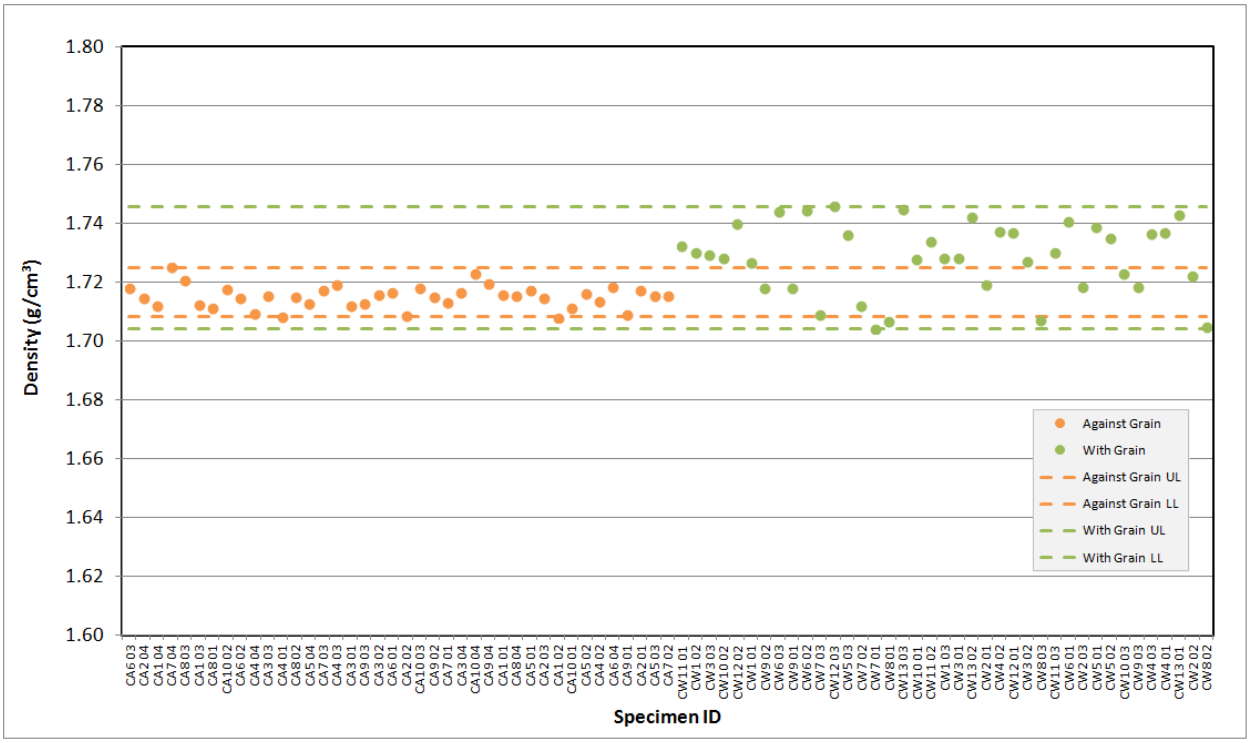

Figure A-1. H-451 Creep Pre Thermal Measurement Density.

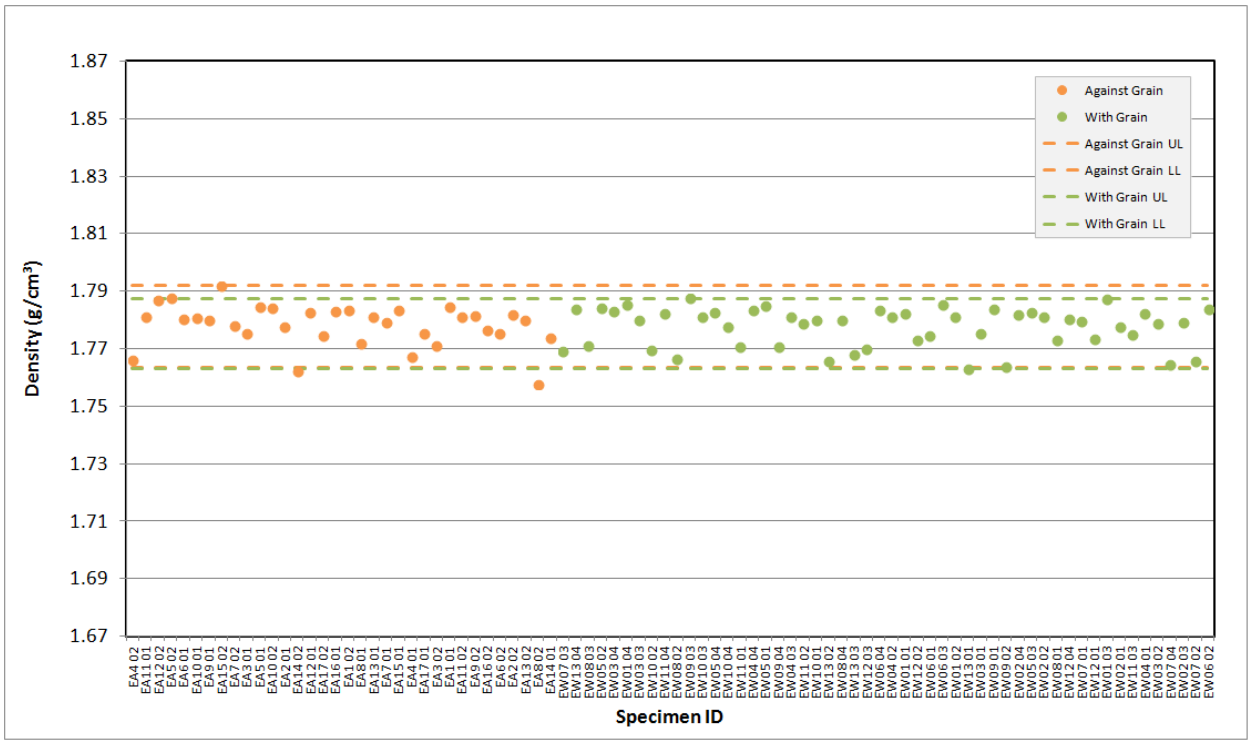

Figure A-2. IG-110 Creep Pre Thermal Measurement Density.

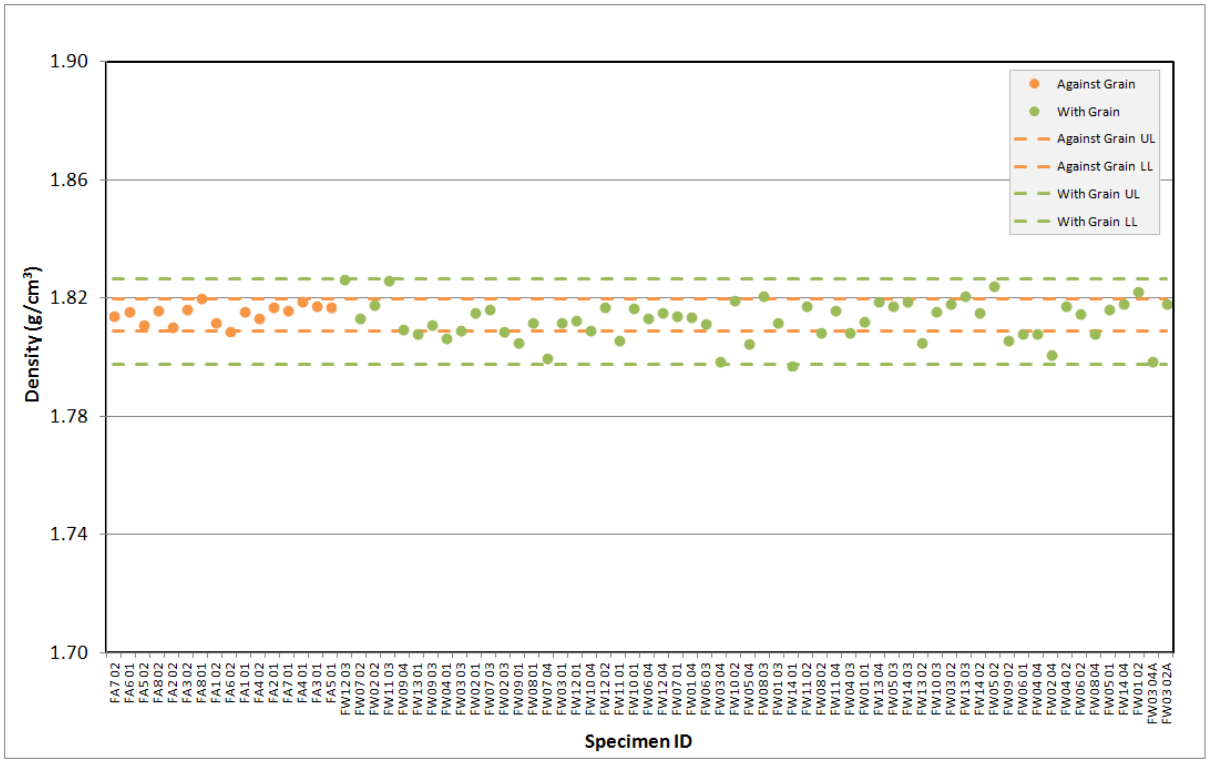

Figure A-3. IG-430 Creep Pre Thermal Measurement Density.

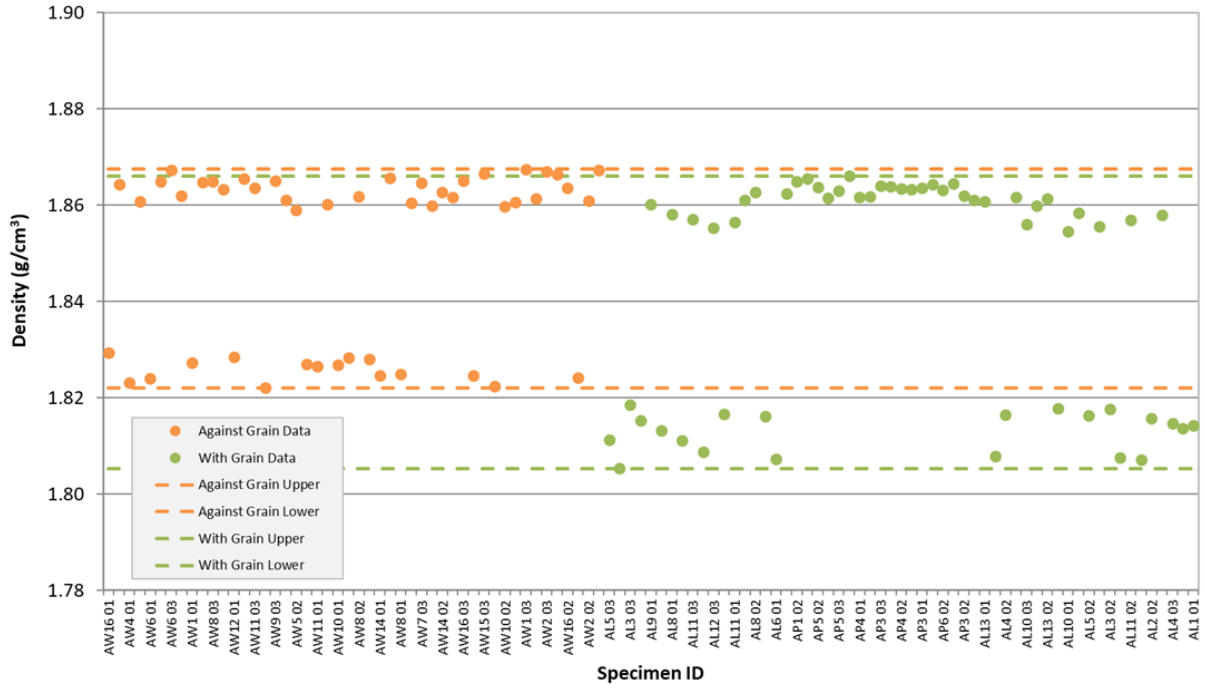

Figure A-4. NBG-17 Creep Pre Thermal Measurement Density.

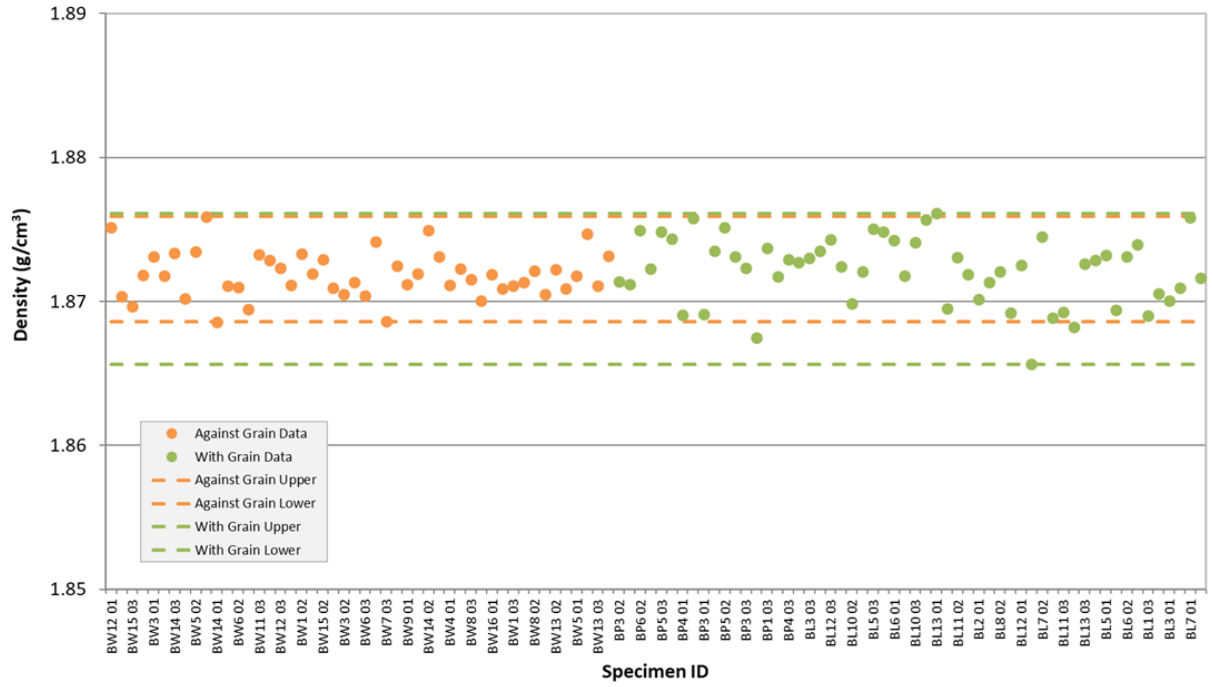

Figure A-5. NBG-18 Creep Pre Thermal Measurement Density.

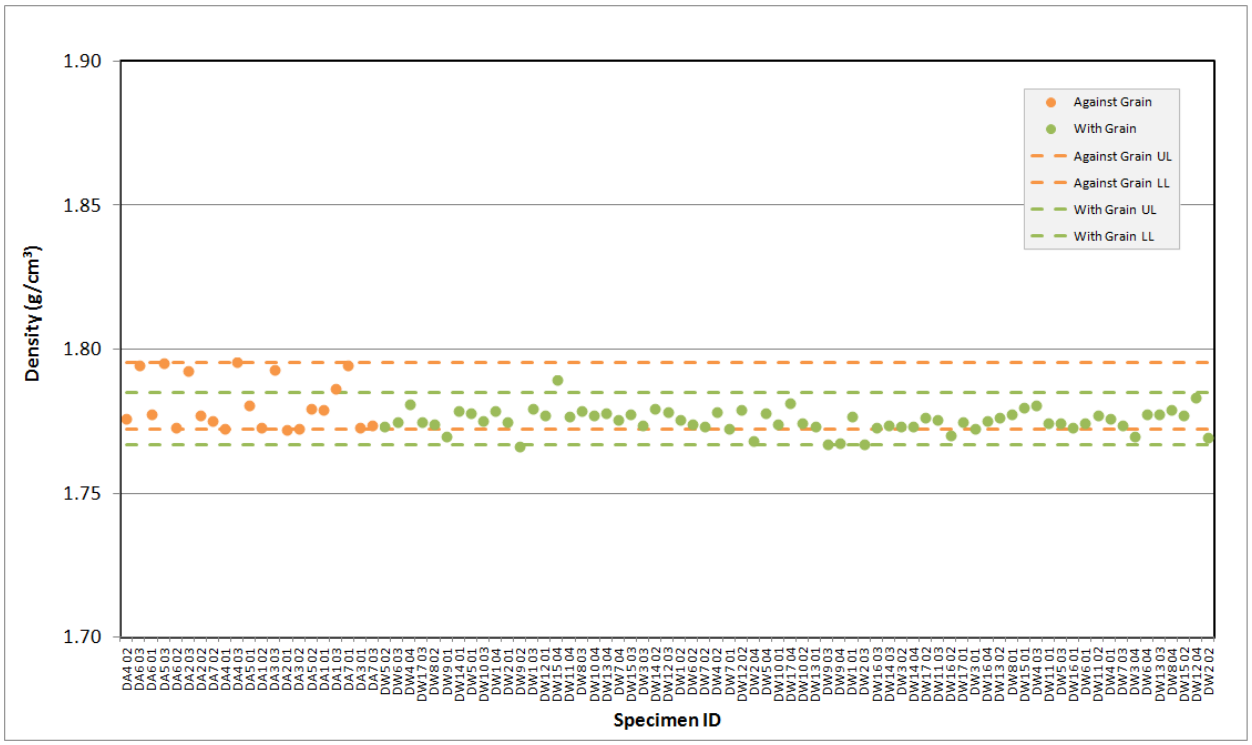

Figure A-6. PCEA Creep Pre Thermal Measurement Density.

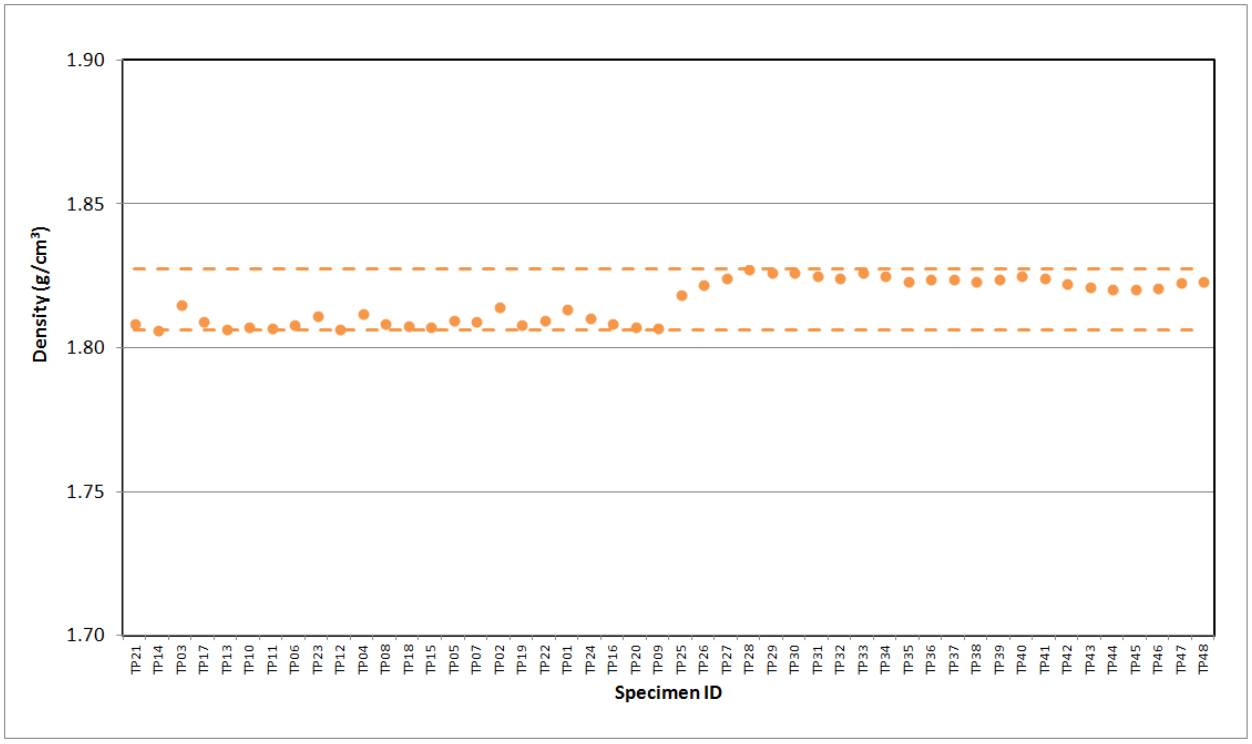

Figure A-7. 2114 Piggyback Pre Thermal Measurement Density.

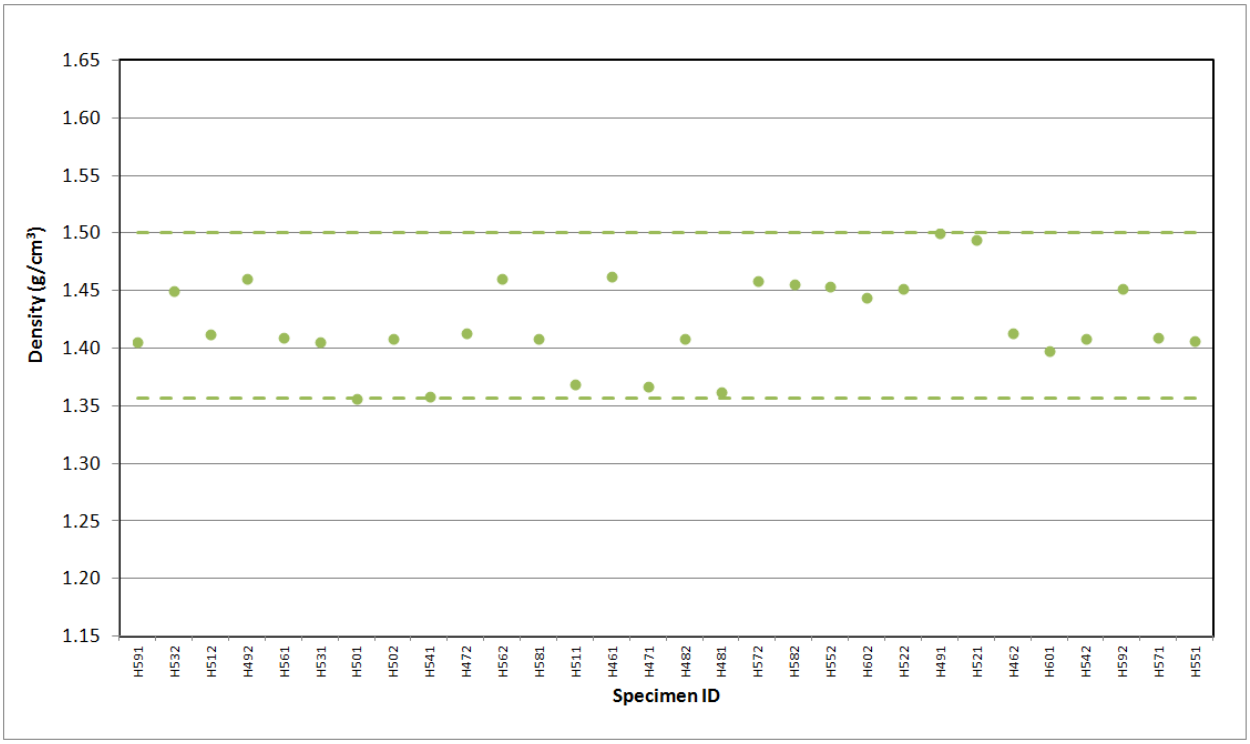

Figure A-8. A3 Matrix Piggyback Pre Thermal Measurement Density.

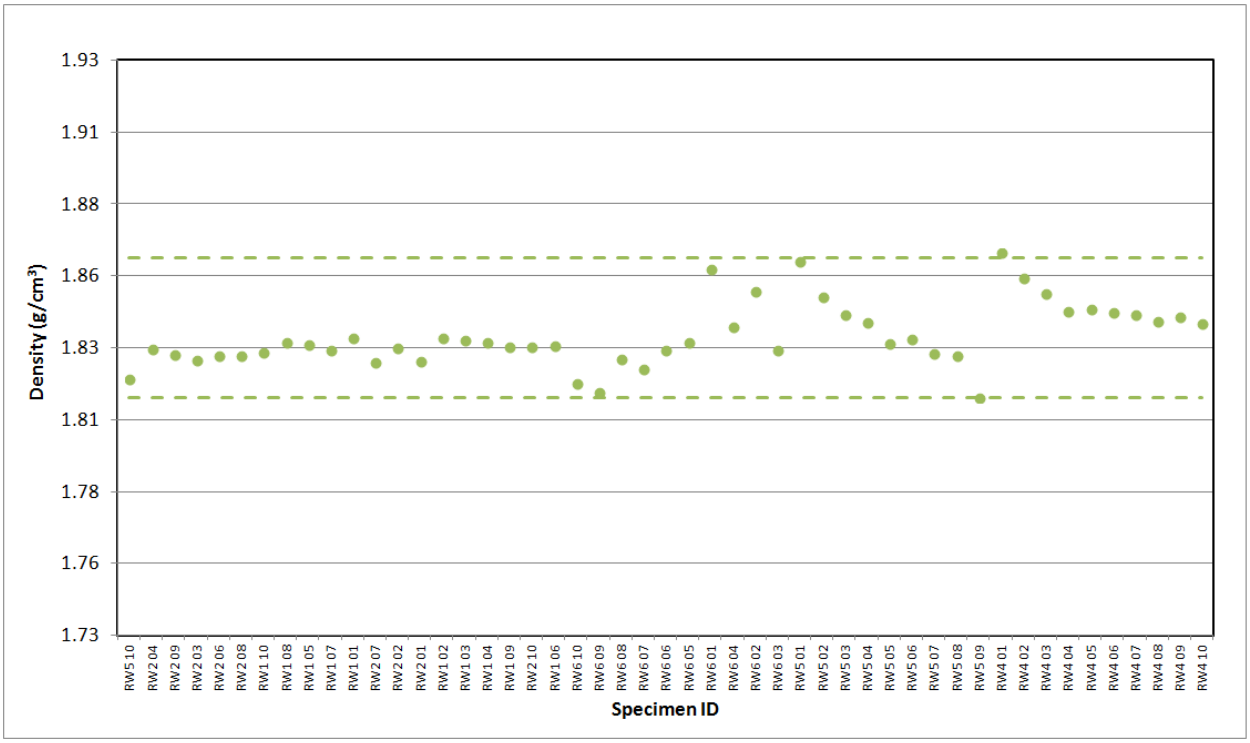

Figure A-9. BAN Piggyback Pre Thermal Measurement Density.

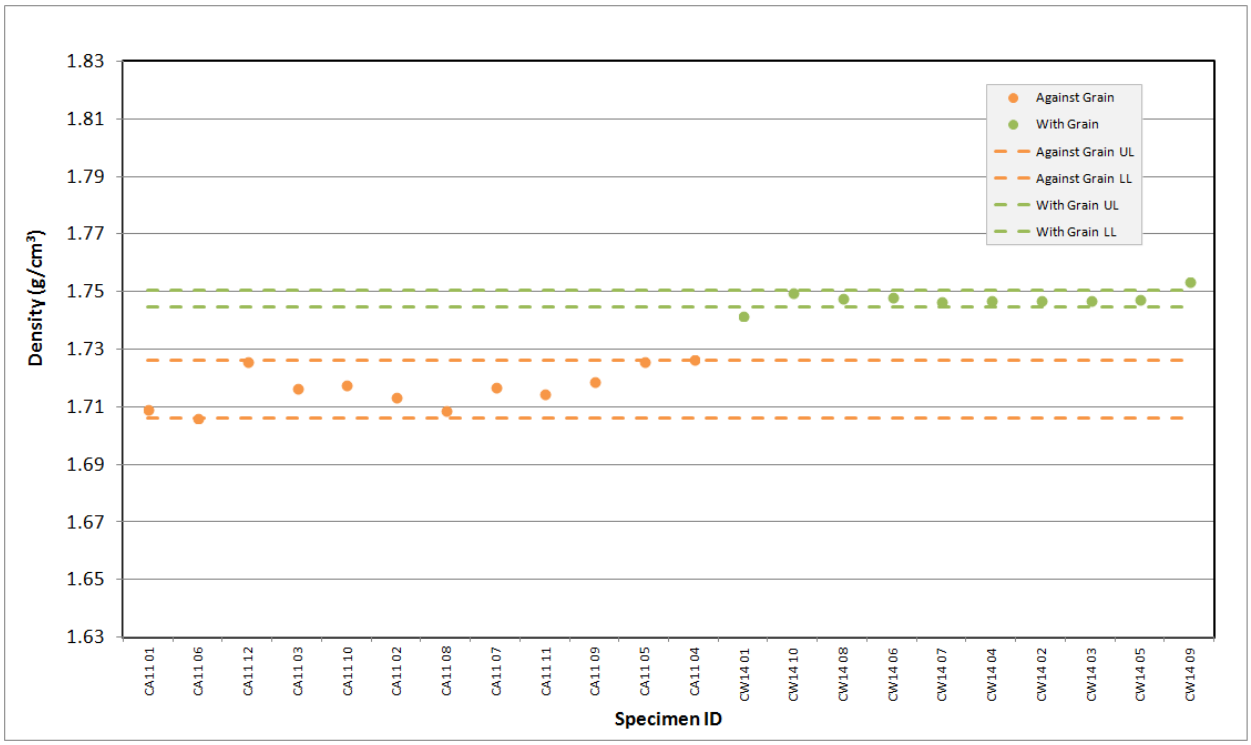

Figure A-10. H-451 Piggyback Pre Thermal Measurement Density.

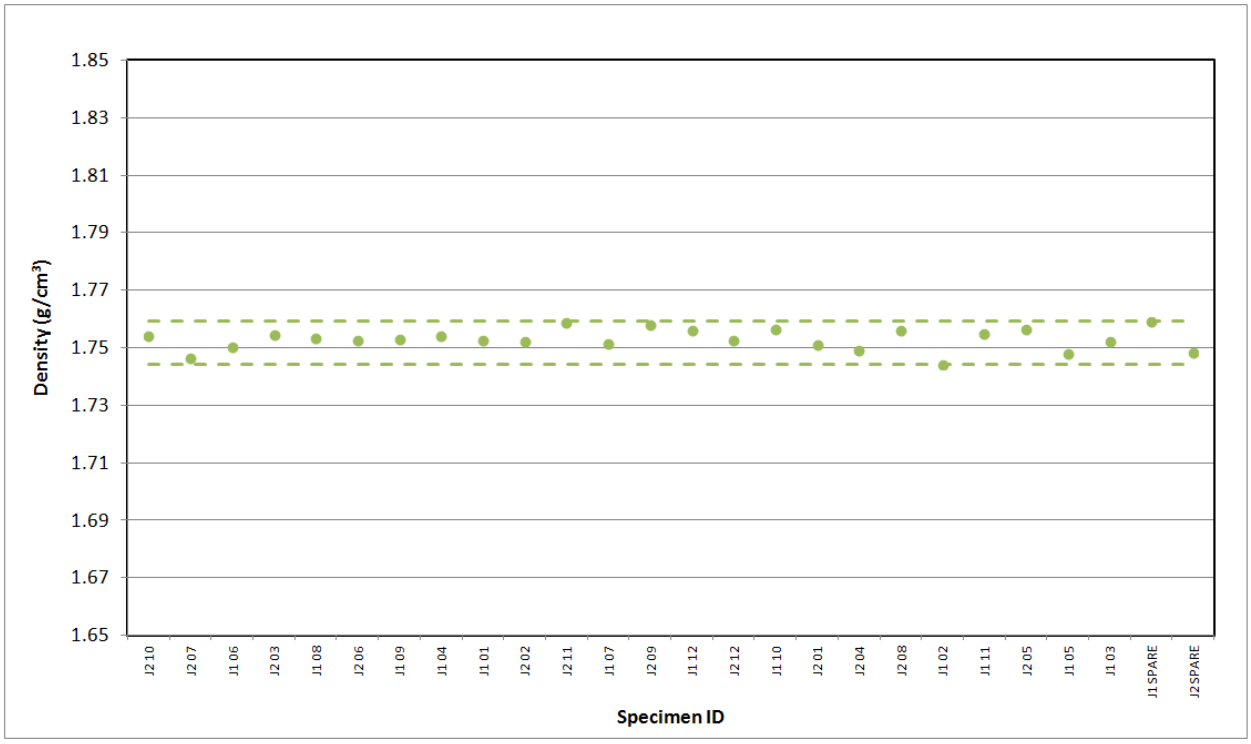

Figure A-11. HLM Piggyback Pre Thermal Measurement Density.

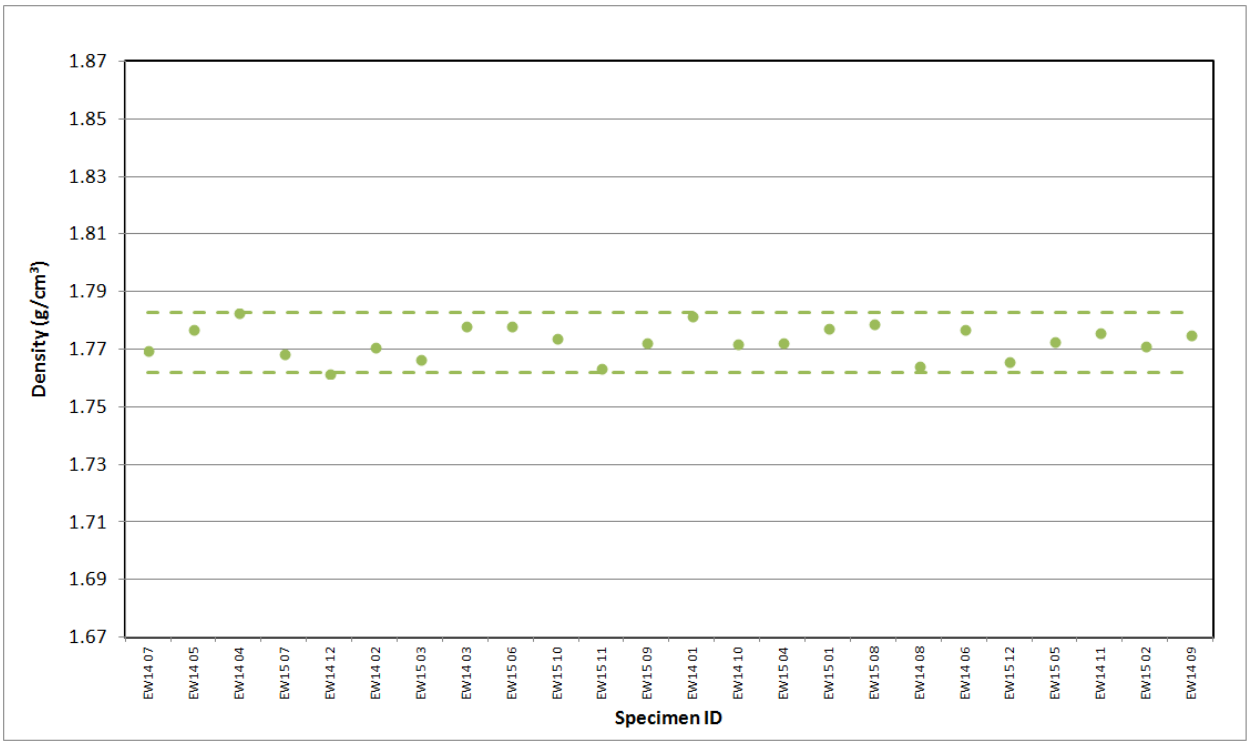

Figure A-12. IG-110 Piggyback Pre Thermal Measurement Density.

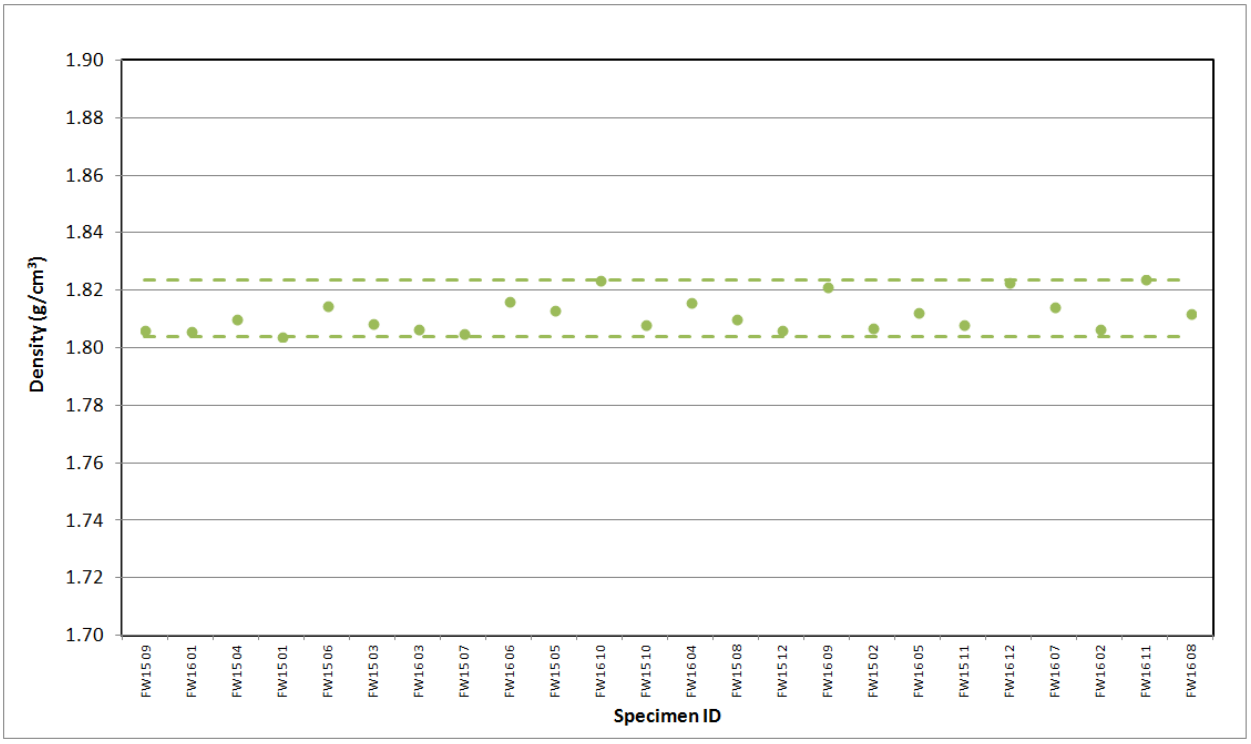

Figure A-13. IG-430 Piggyback Pre Thermal Measurement Density.

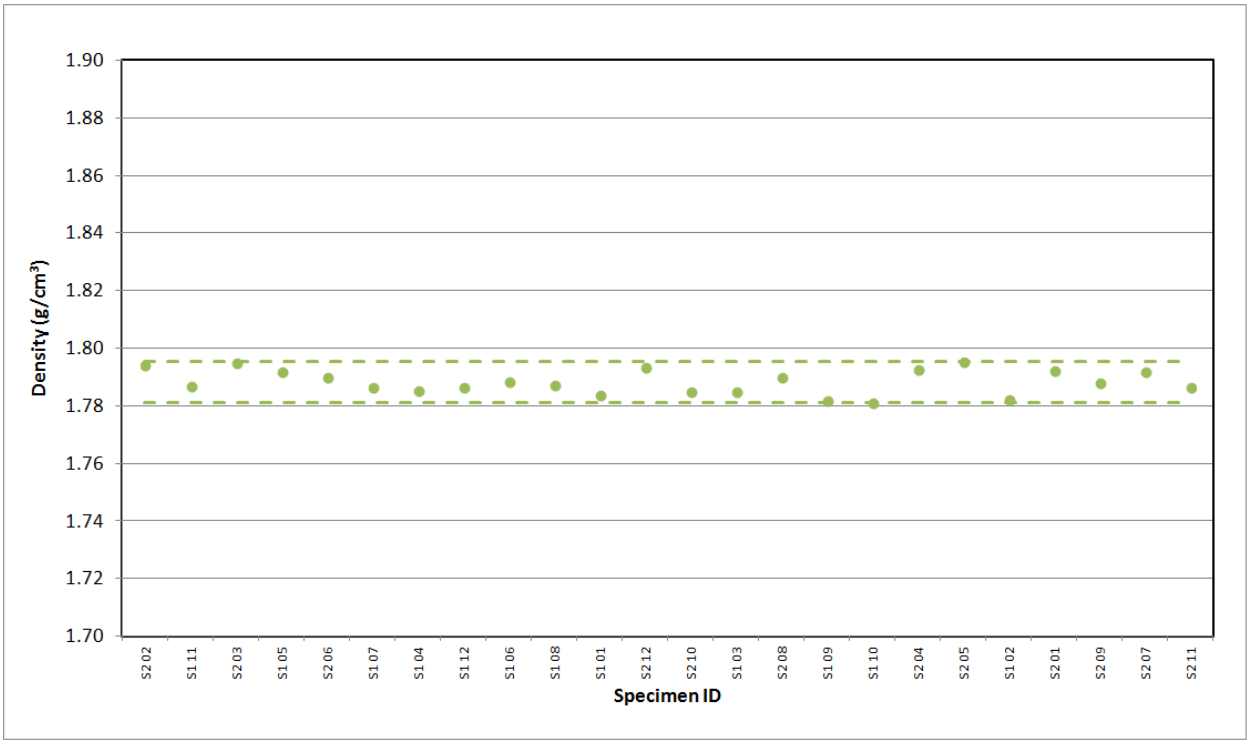

Figure A-14. NBG-10 Piggyback Pre Thermal Measurement Density.

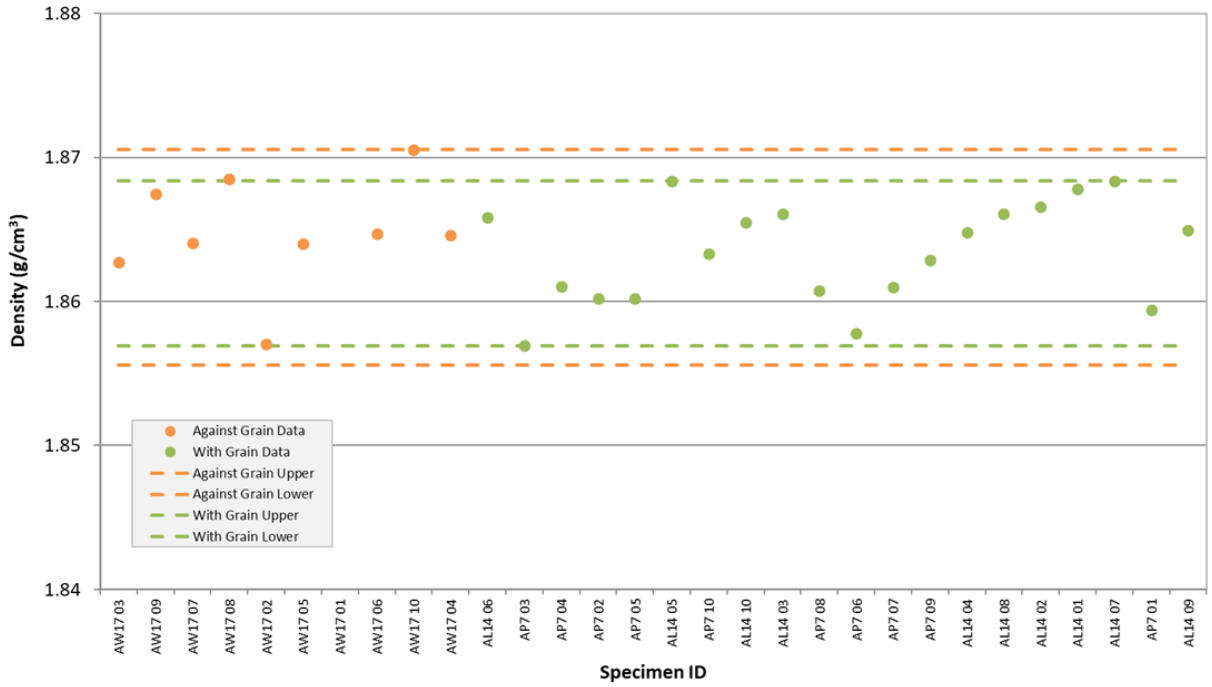

Figure A-15. NBG-17 Piggyback Pre Thermal Measurement Density.

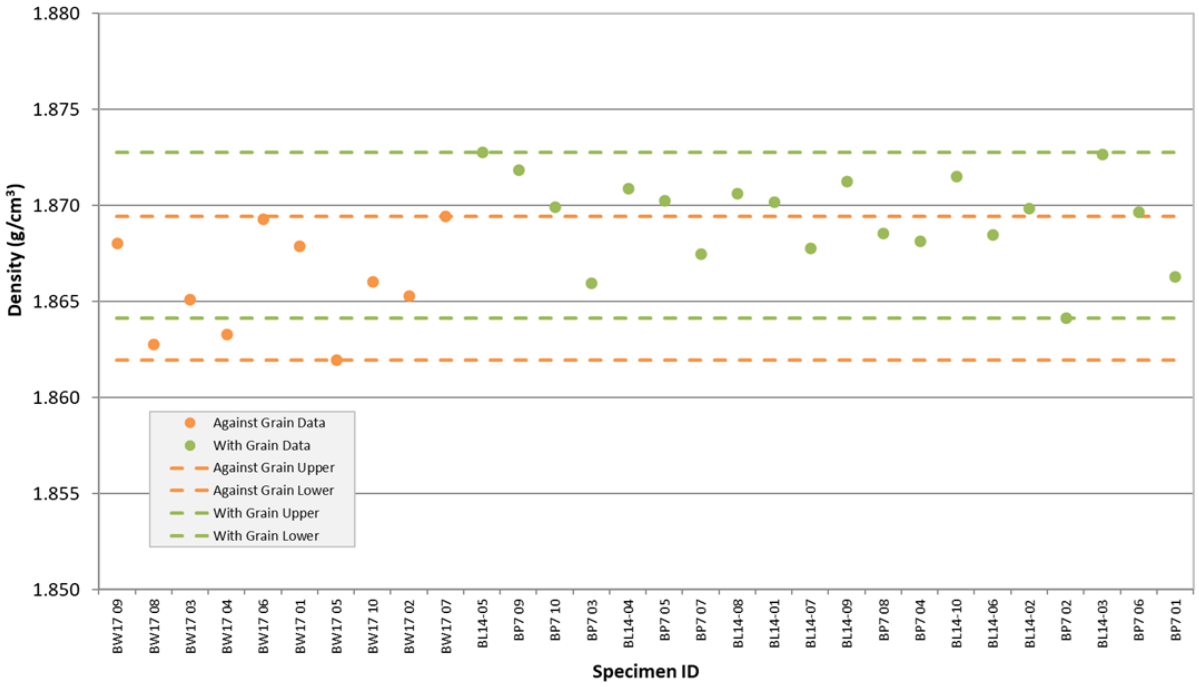

Figure A-16. NBG-18 Piggyback Pre Thermal Measurement Density.

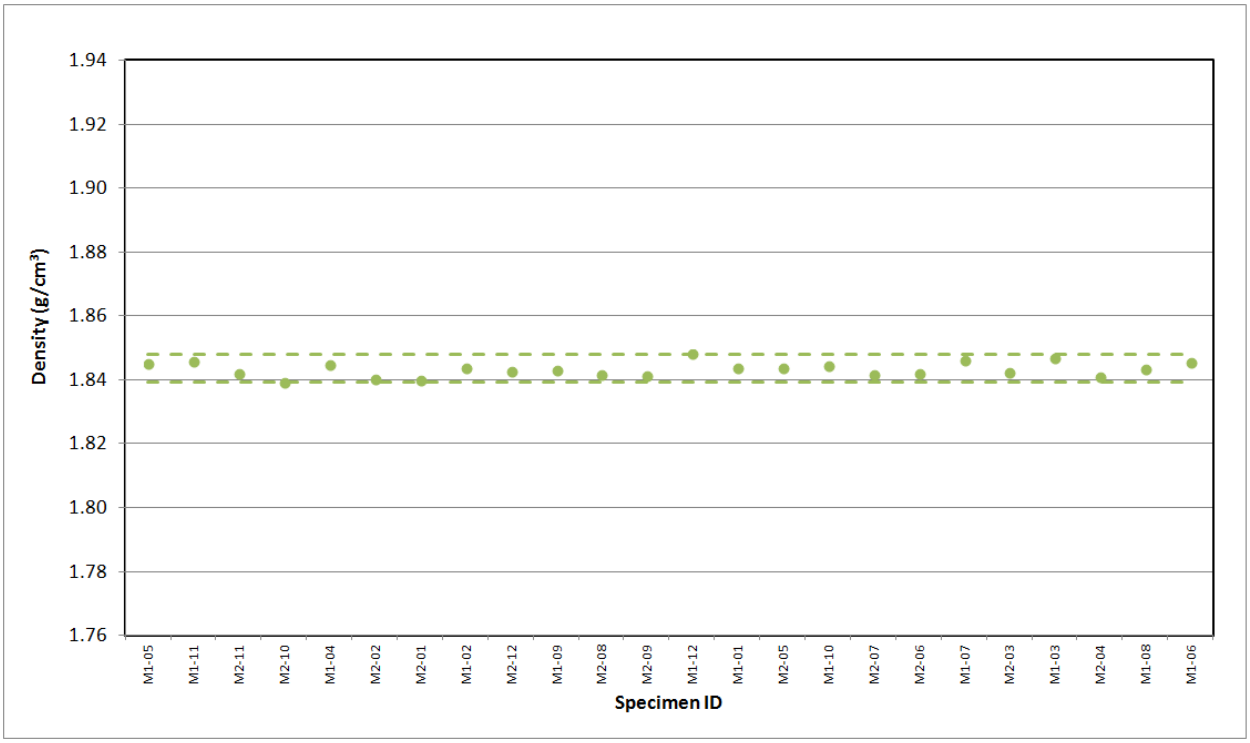

Figure A-17. NBG-25 Piggyback Pre Thermal Measurement Density.

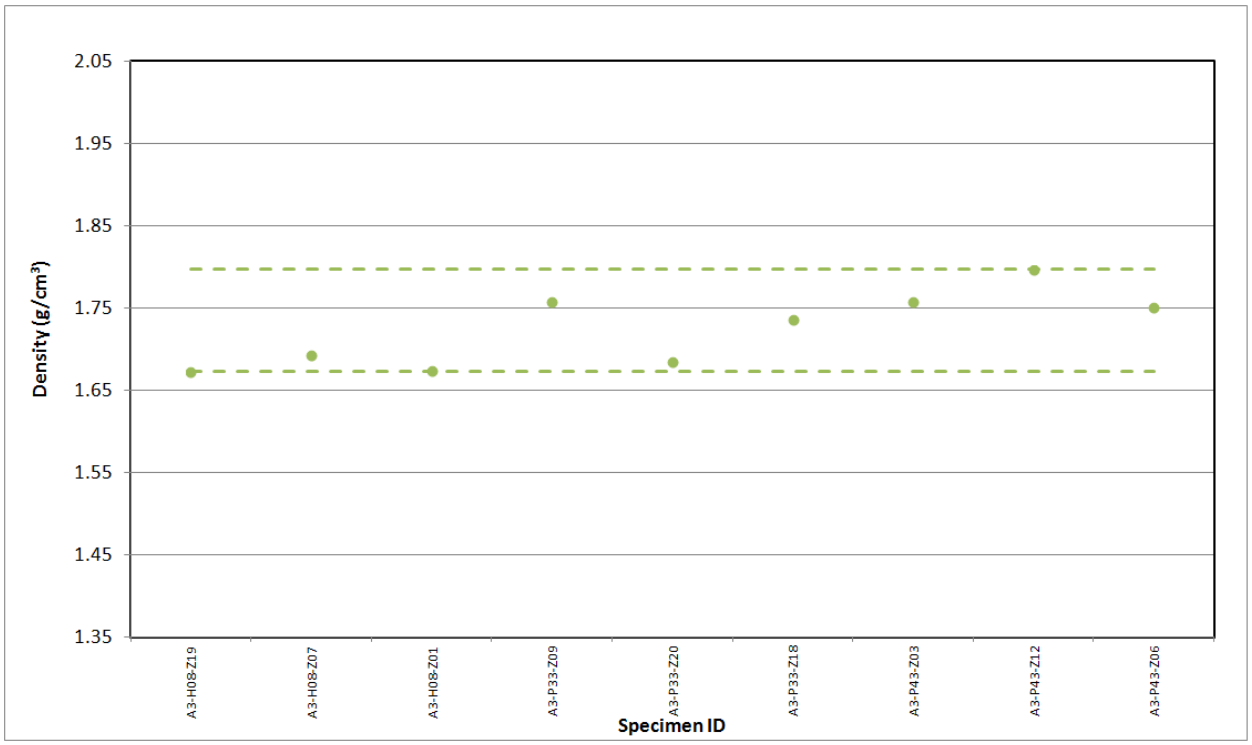

Figure A-18. New Matrix Piggyback Pre Thermal Measurement Density.

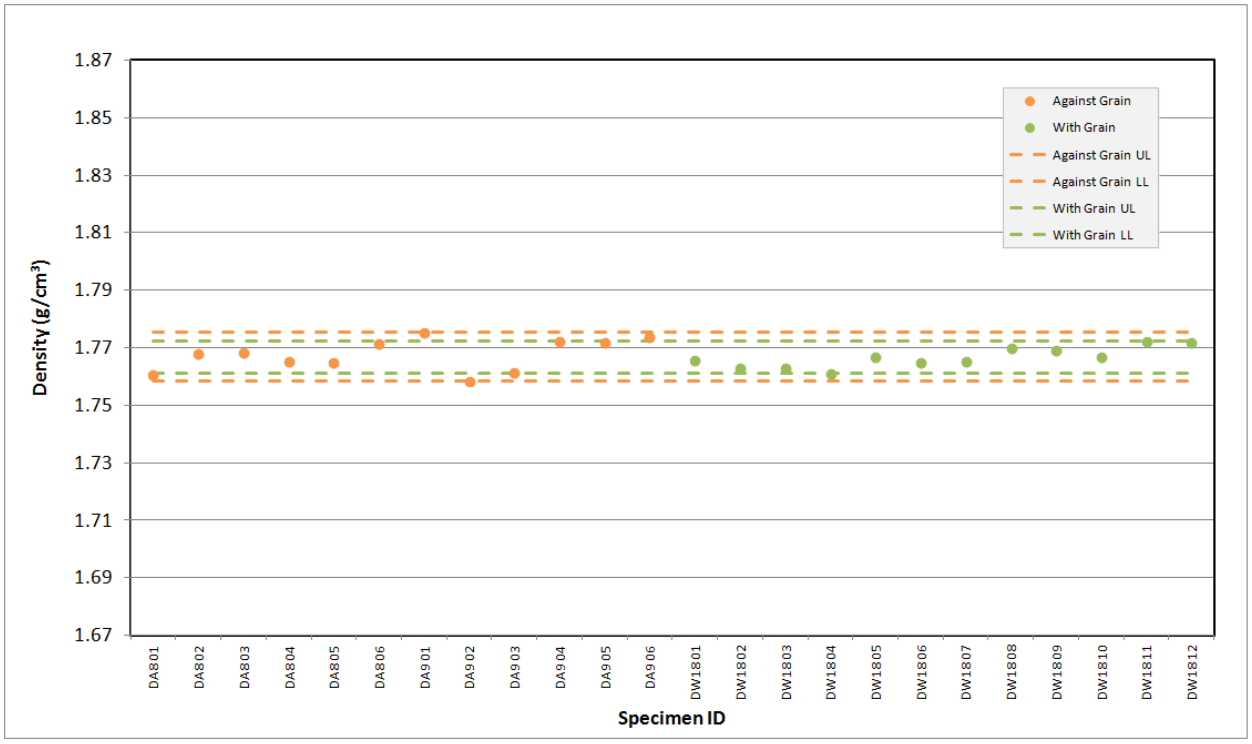

Figure A-19. PCEA Piggyback Pre Thermal Measurement Density.

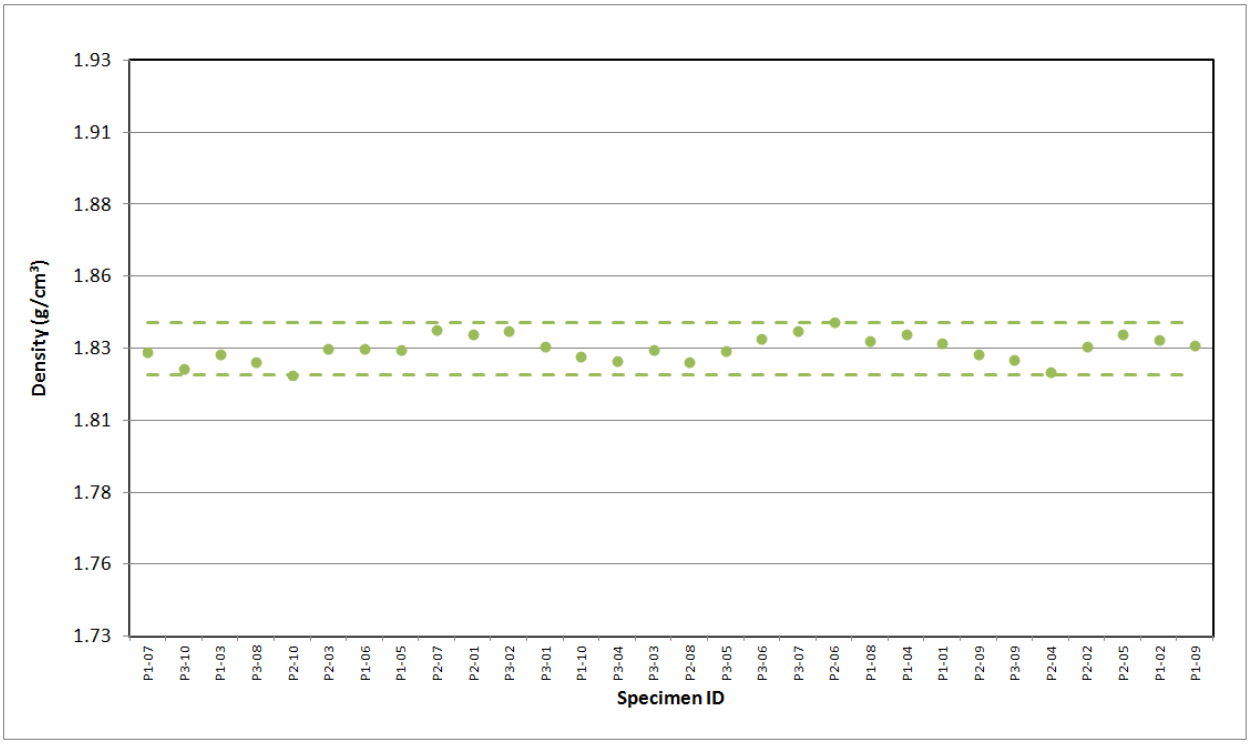

Figure A-20. PCIB Piggyback Pre Thermal Measurement Density.

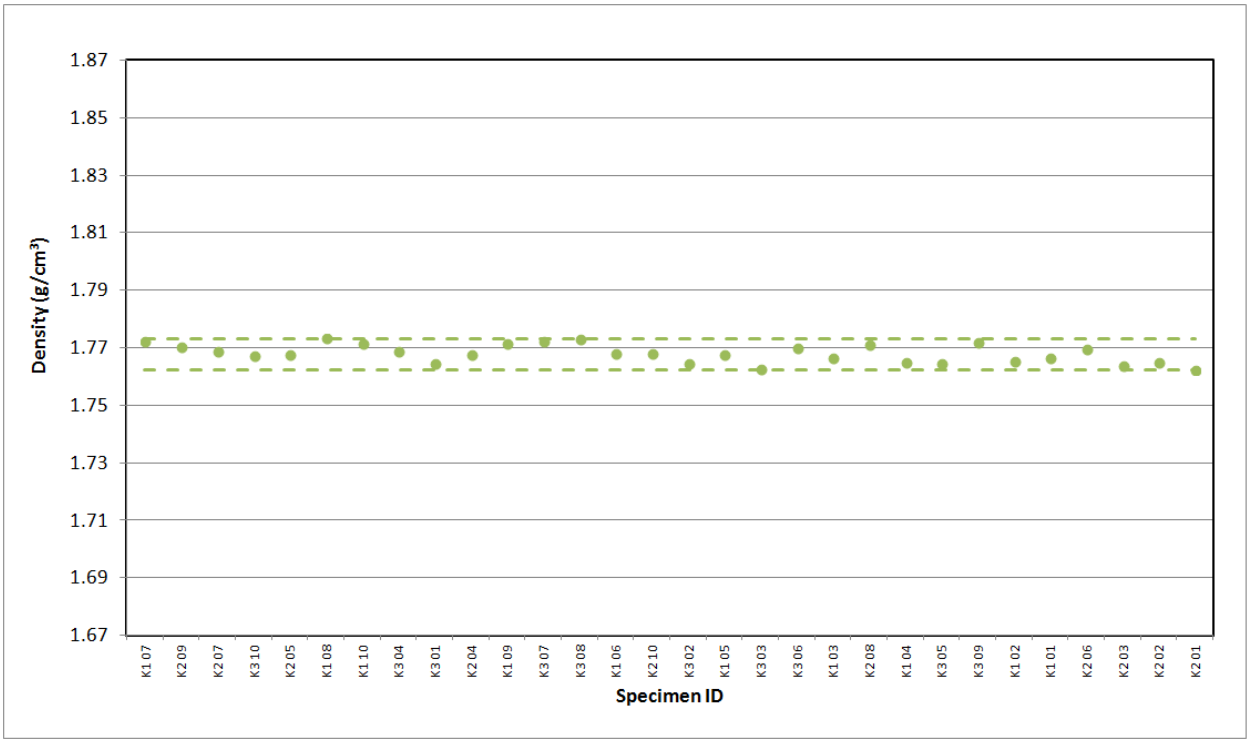

Figure A-21. PGX Piggyback Pre Thermal Measurement Density.

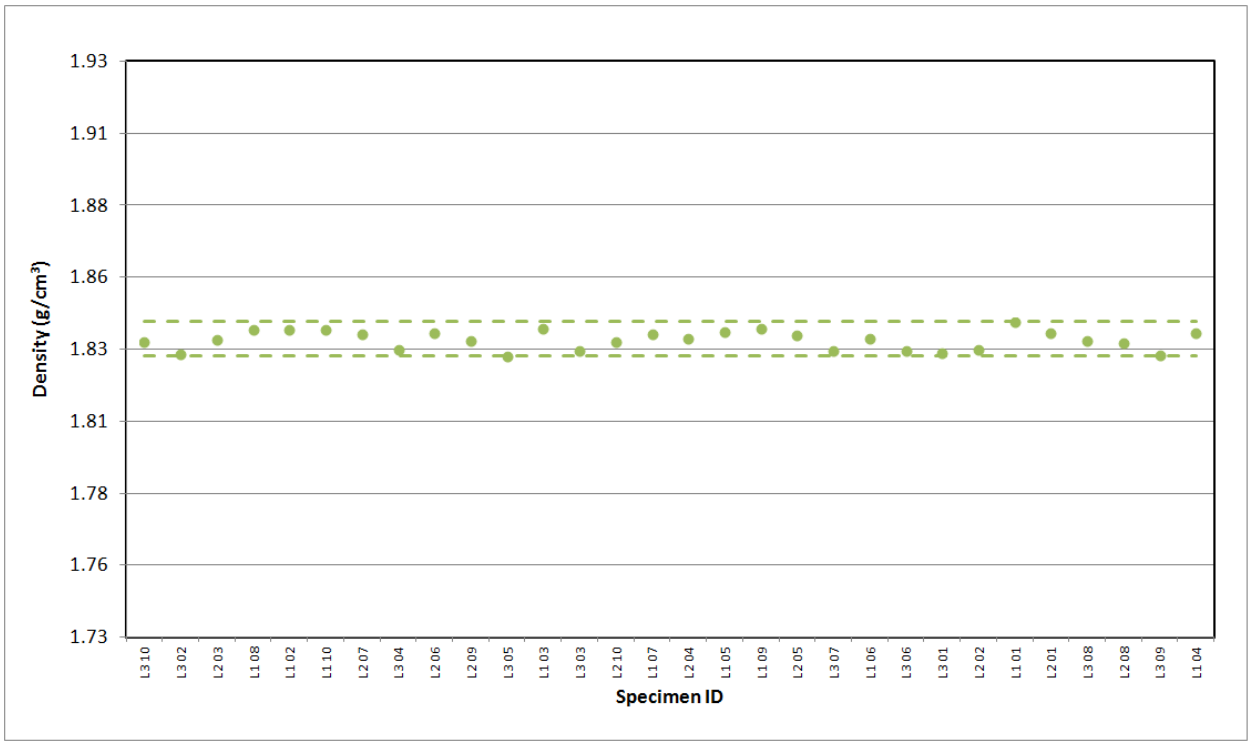

Figure A-22. PPEA Piggyback Pre Thermal Measurement Density.

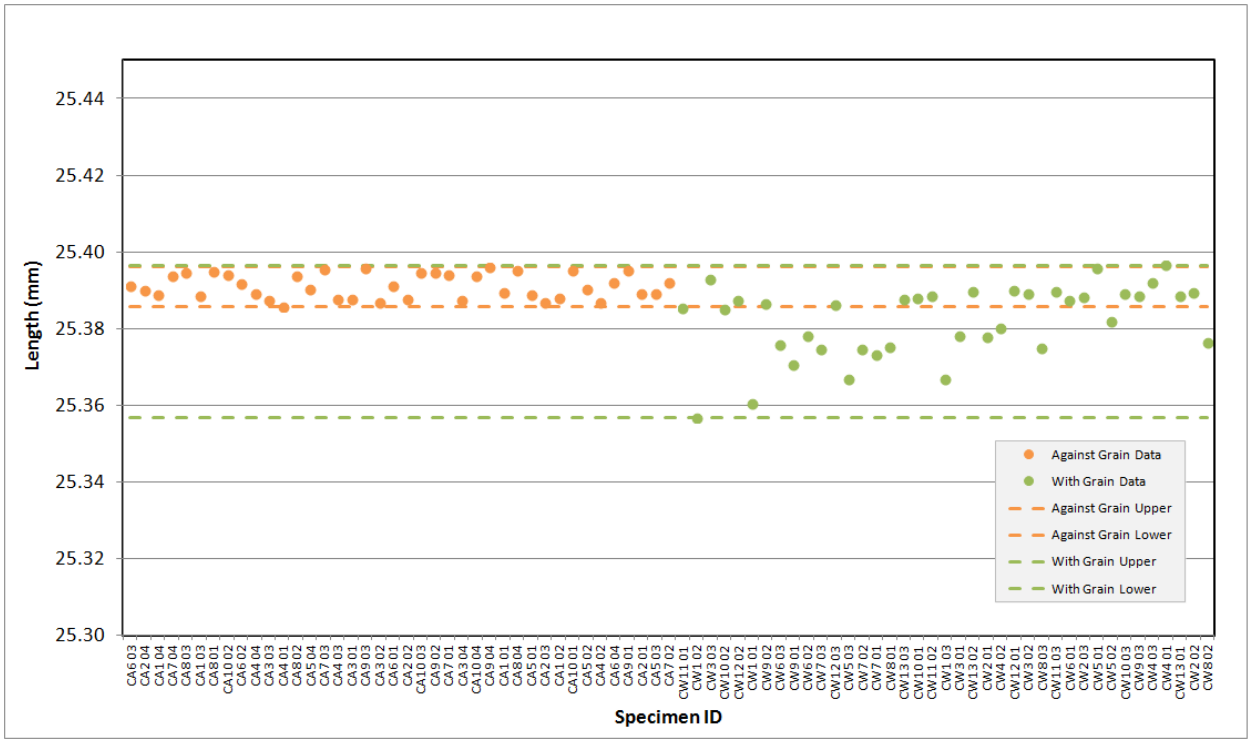

Figure A-23. H-451 Creep Pre Thermal Measurement Length.

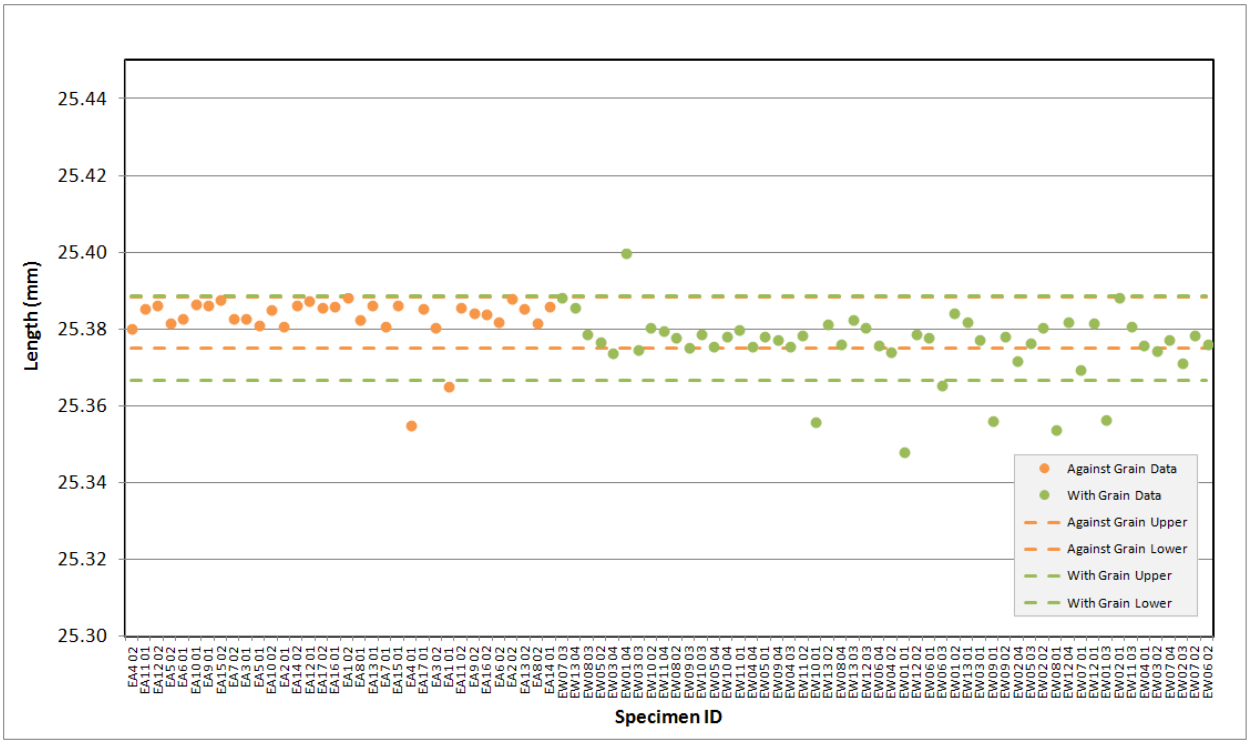

Figure A-24. IG-110 Creep Pre Thermal Measurement Length.

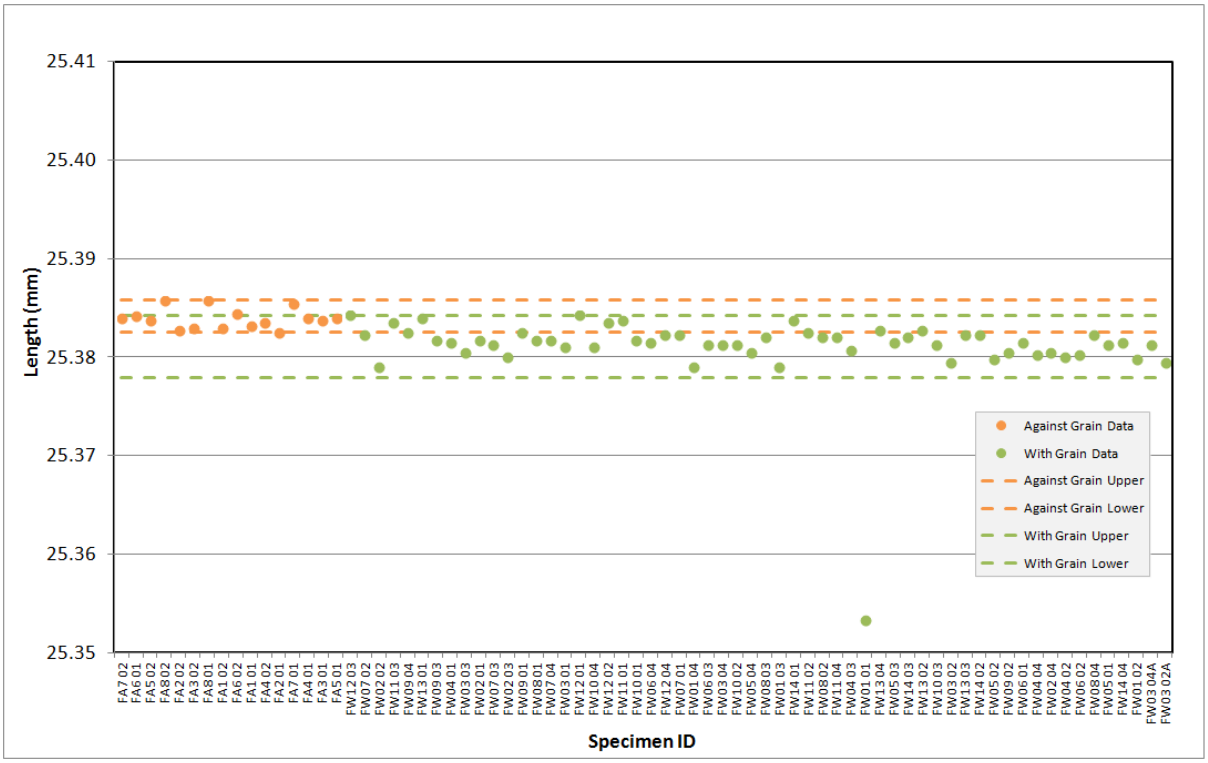

Figure A-25. IG-430 Creep Pre Thermal Measurement Length.

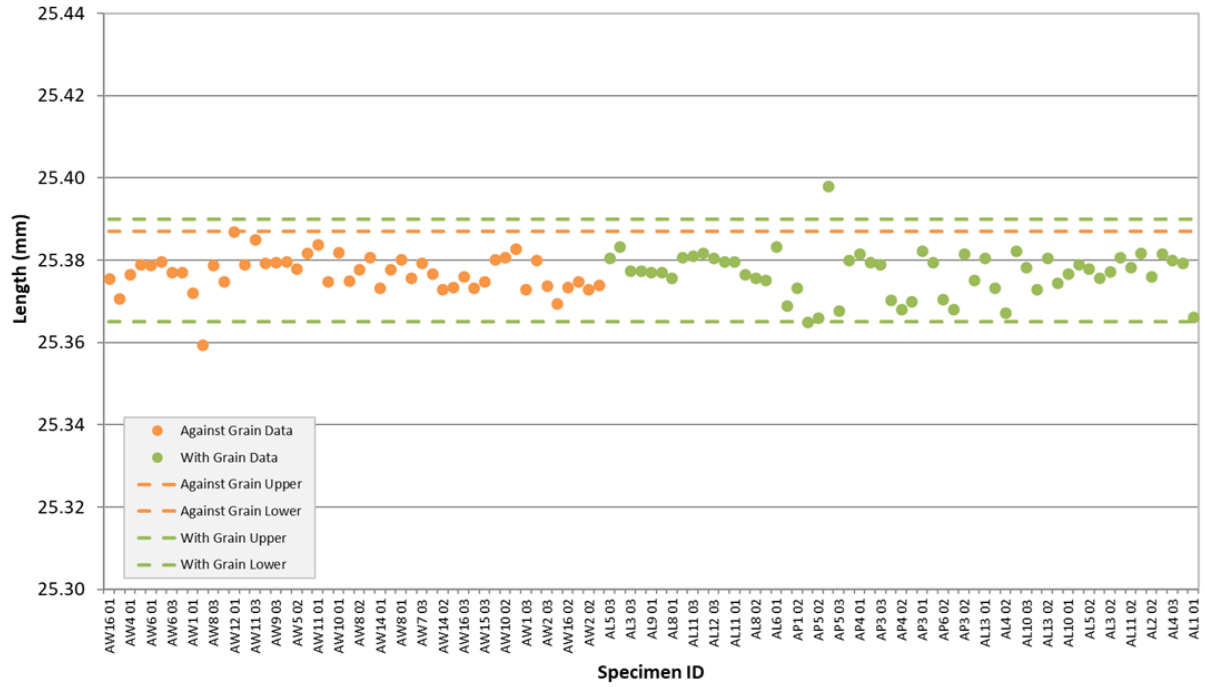

Figure A-26. NBG-17 Creep Pre Thermal Measurement Length.

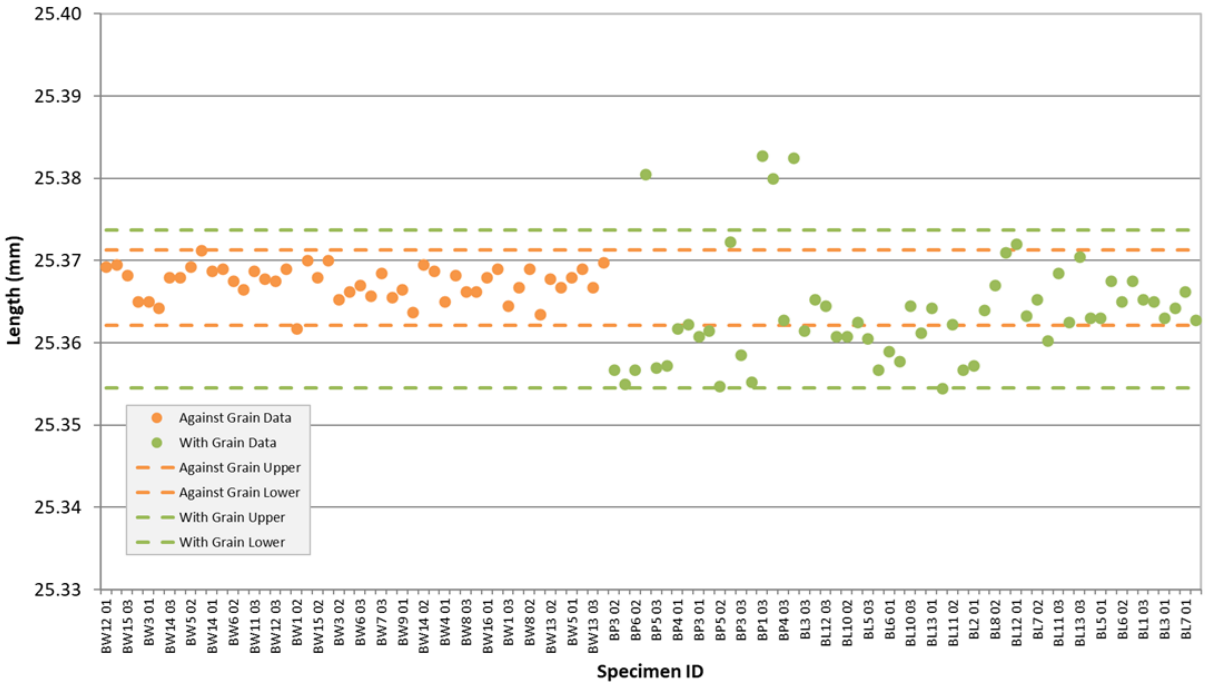

Figure A-27. NBG-18 Creep Pre Thermal Measurement Length.

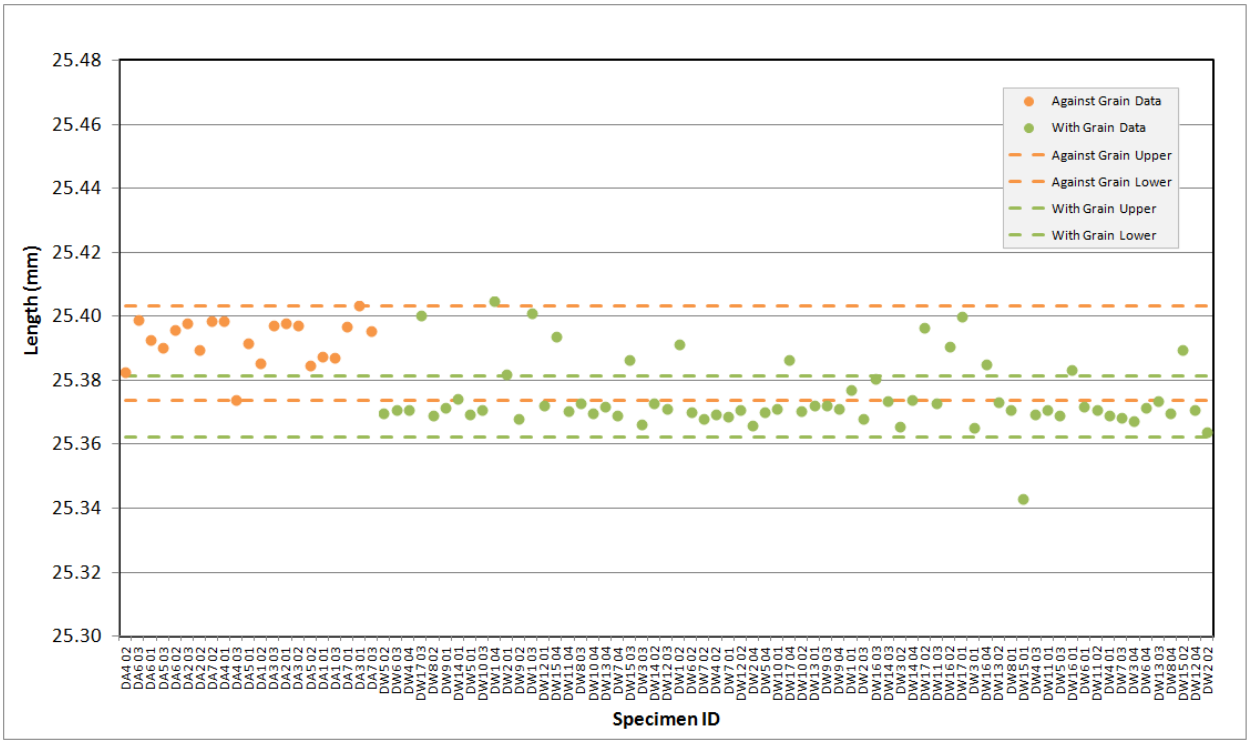

Figure A-28. PCEA Creep Pre Thermal Measurement Length.

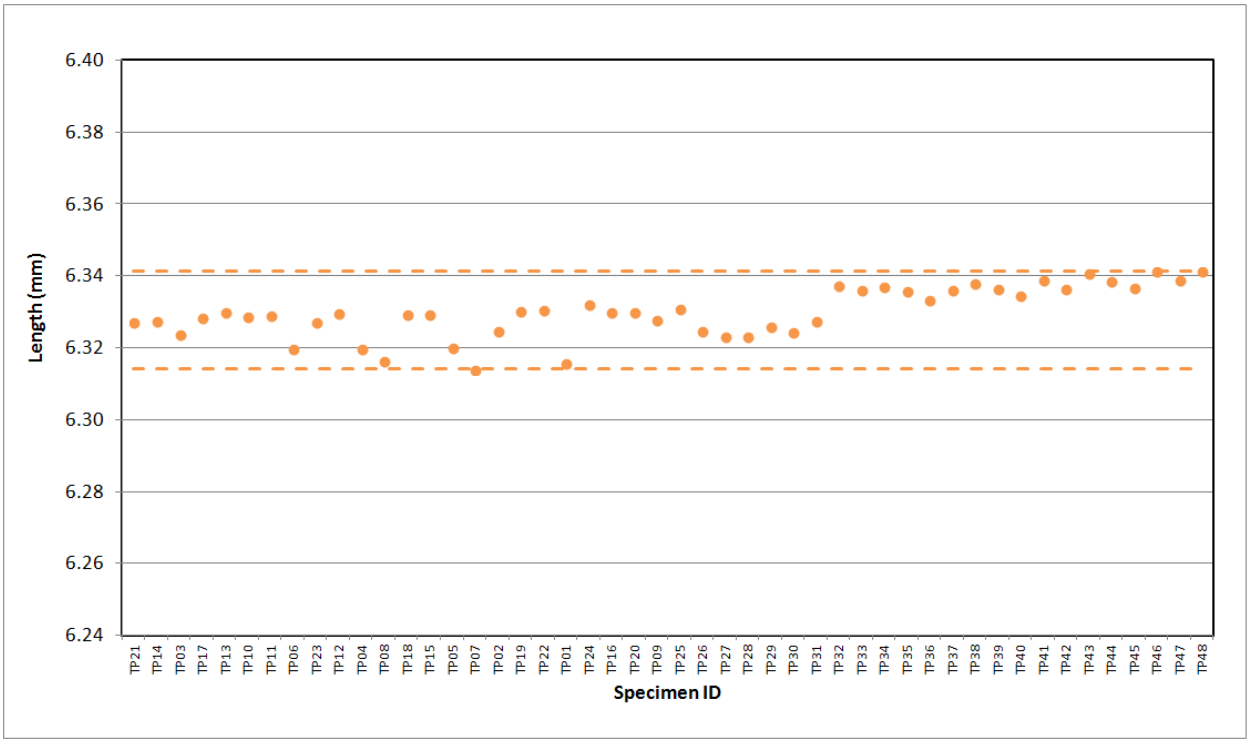

Figure A-29. 2114 Piggyback Pre Thermal Measurement Length.

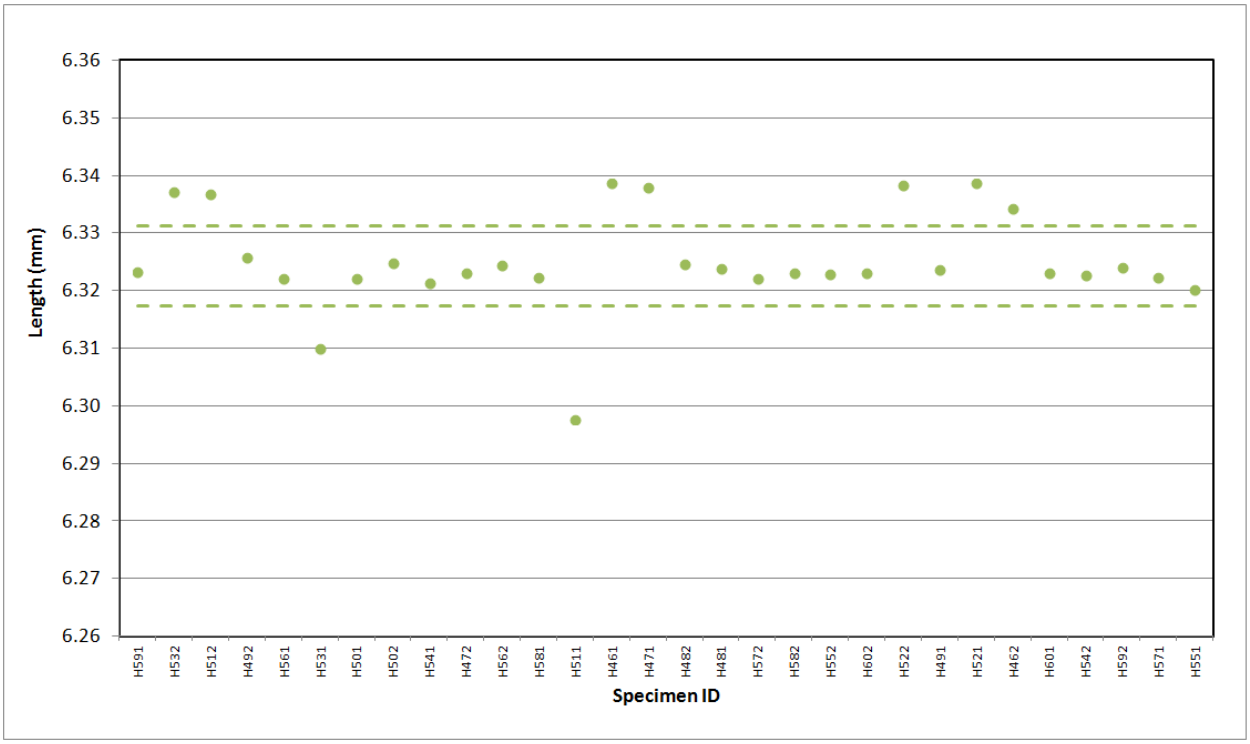

Figure A-30. A3 Matrix Piggyback Pre Thermal Measurement Length.

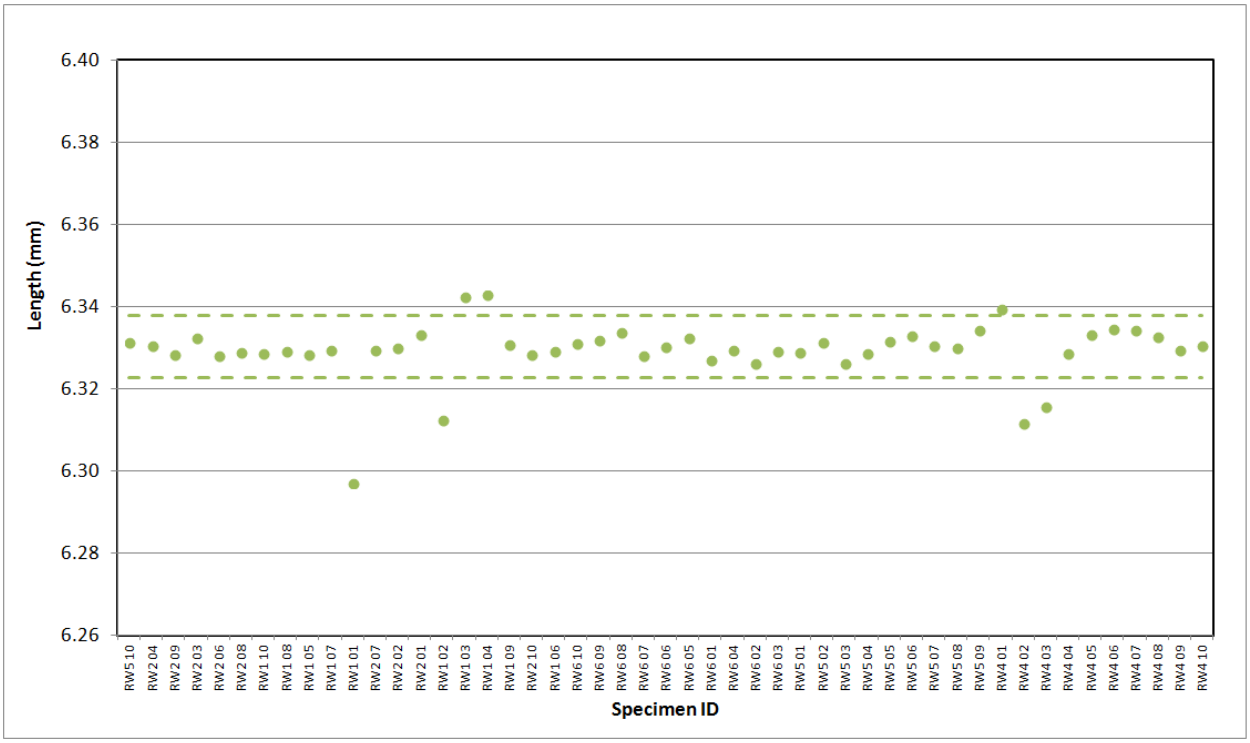

Figure A-31. BAN Piggyback Pre Thermal Measurement Length.

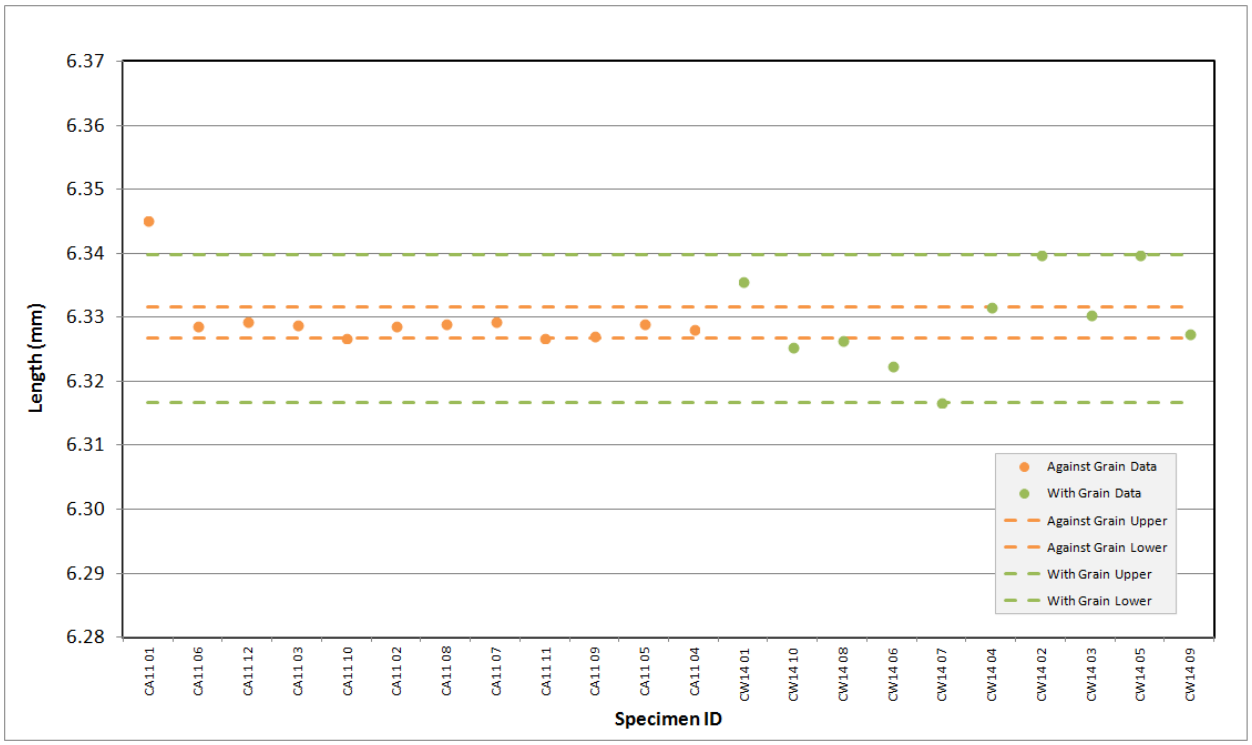

Figure A-32. H-451 Piggyback Pre Thermal Measurement Length.

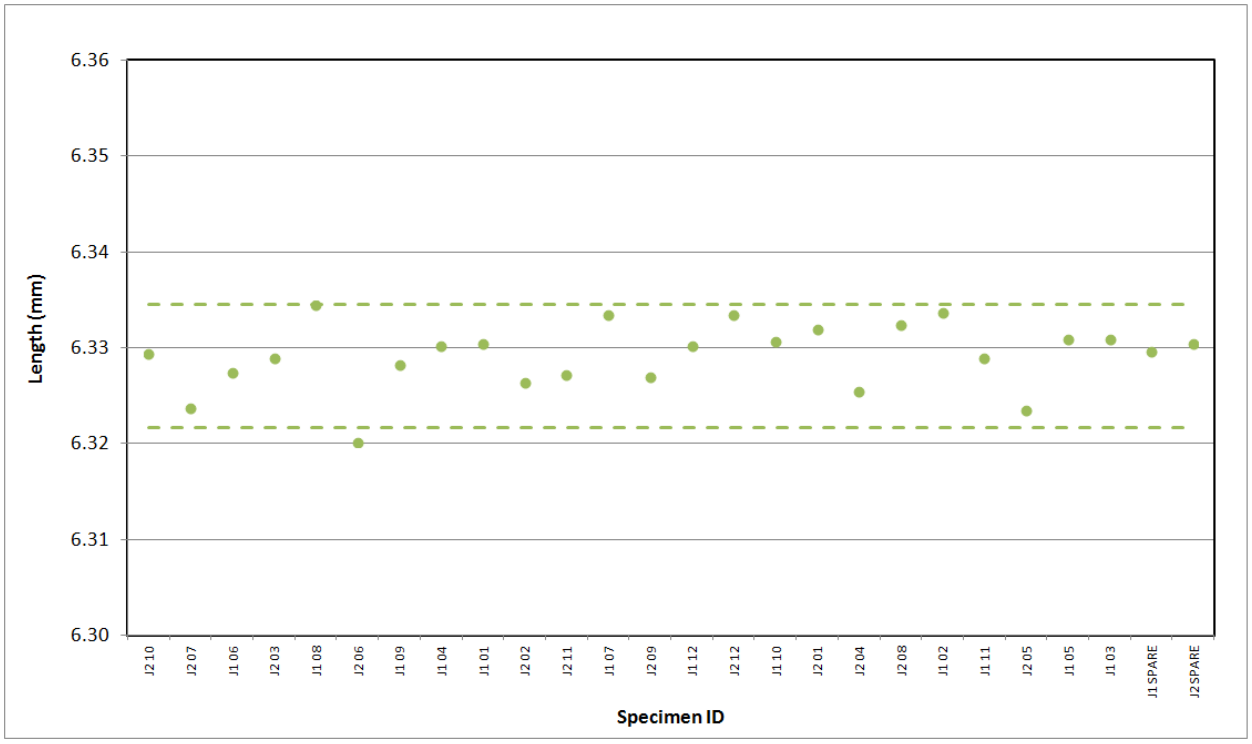

Figure A-33. HLM Piggyback Pre Thermal Measurement Length.

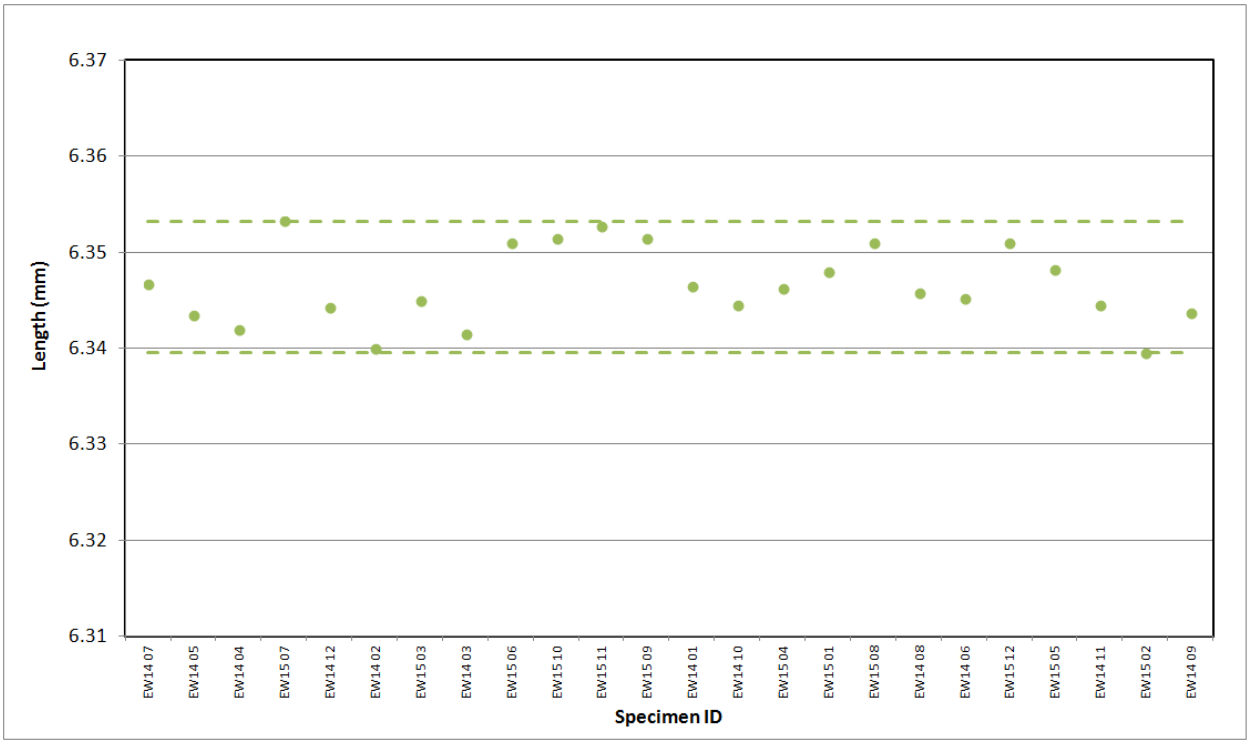

Figure A-34. IG-110 Piggyback Pre Thermal Measurement Length.

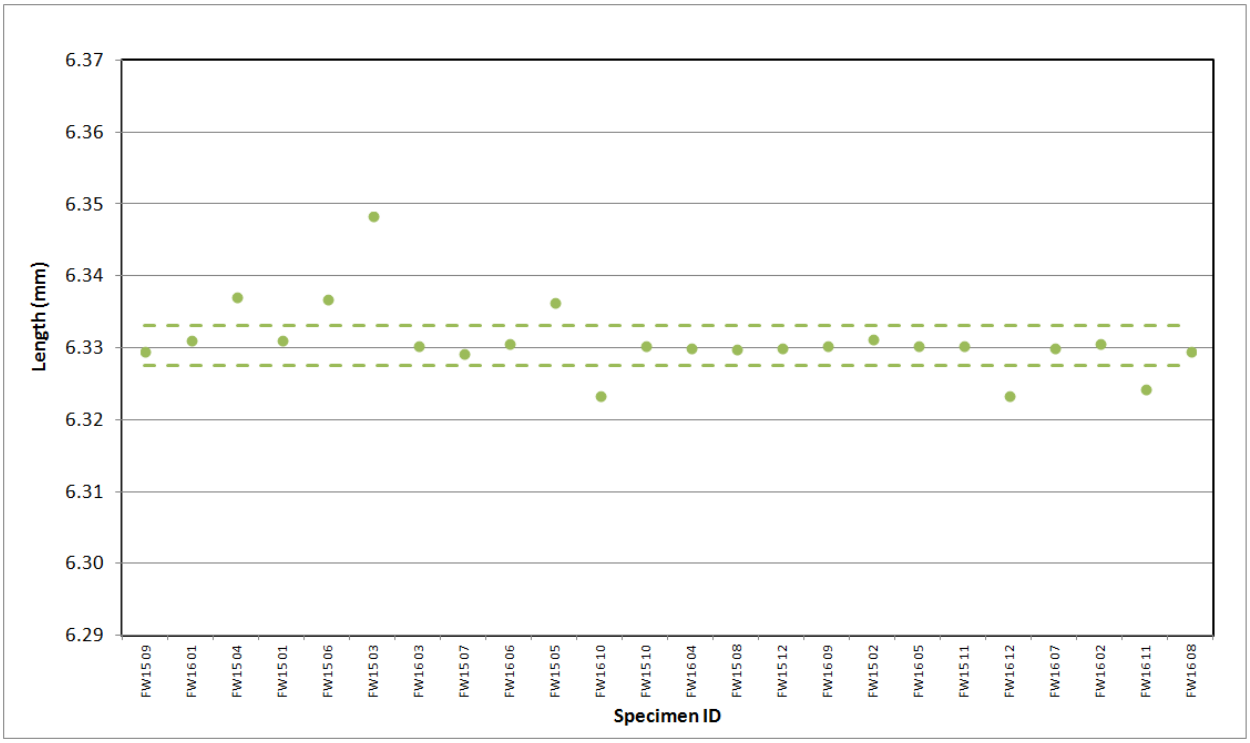

Figure A-35. IG-430 Piggyback Pre Thermal Measurement Length.

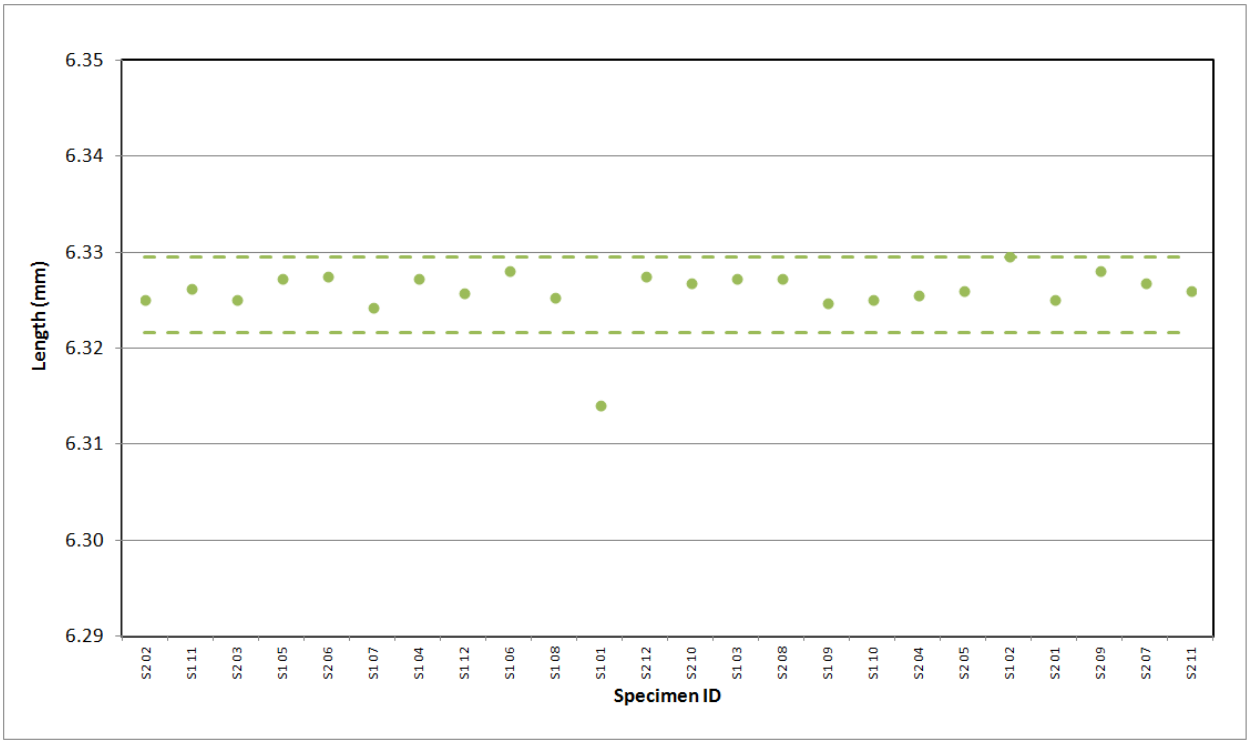

Figure A-36. NBG-10 Piggyback Pre Thermal Measurement Length.

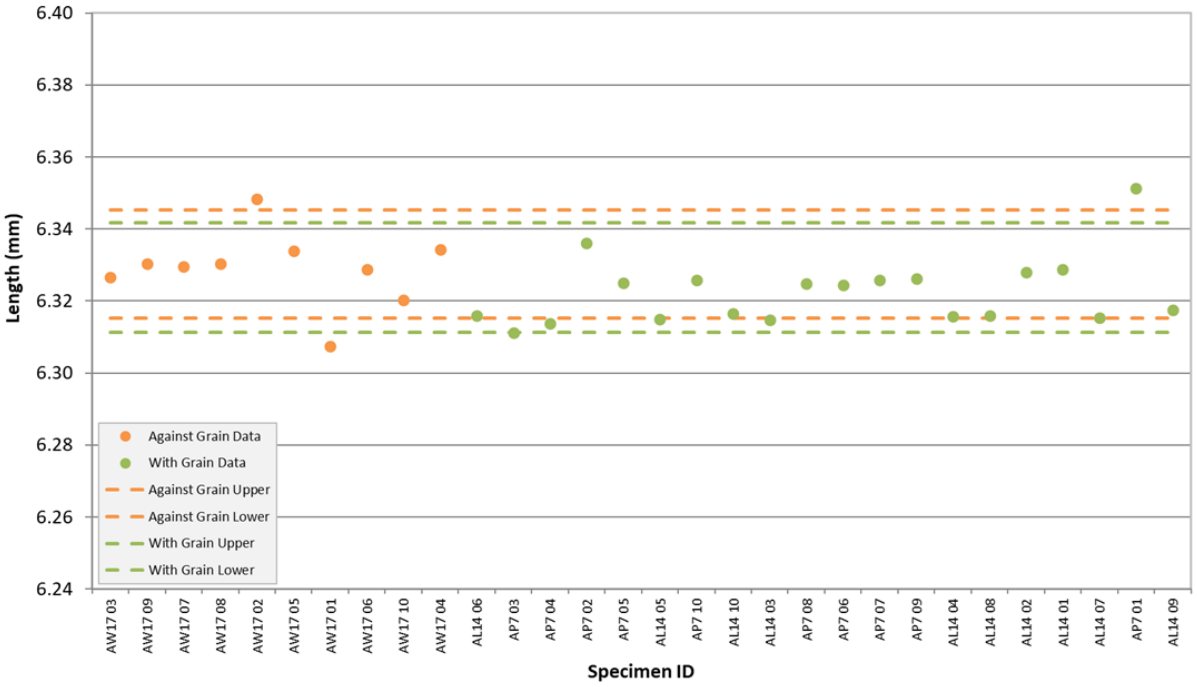

Figure A-37. NBG-17 Piggyback Pre Thermal Measurement Length.

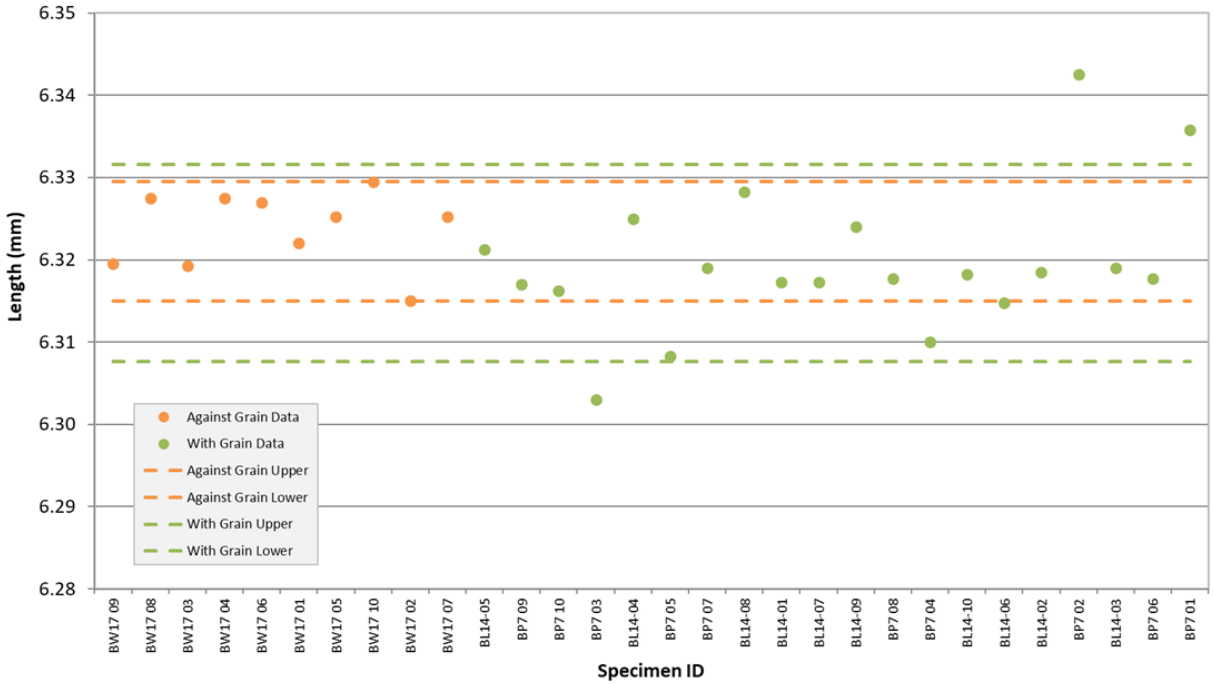

Figure A-38. NBG-18 Piggyback Pre Thermal Measurement Length.

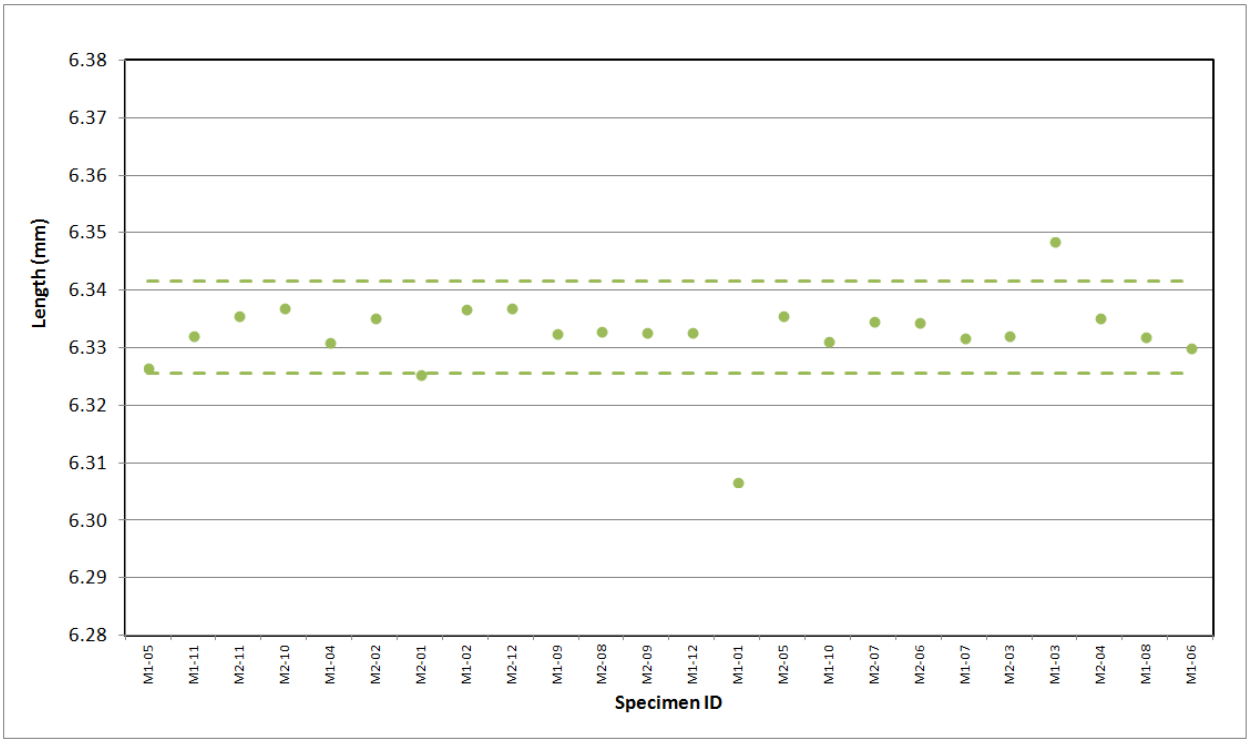

Figure A-39. NBG-25 Piggyback Pre Thermal Measurement Length.

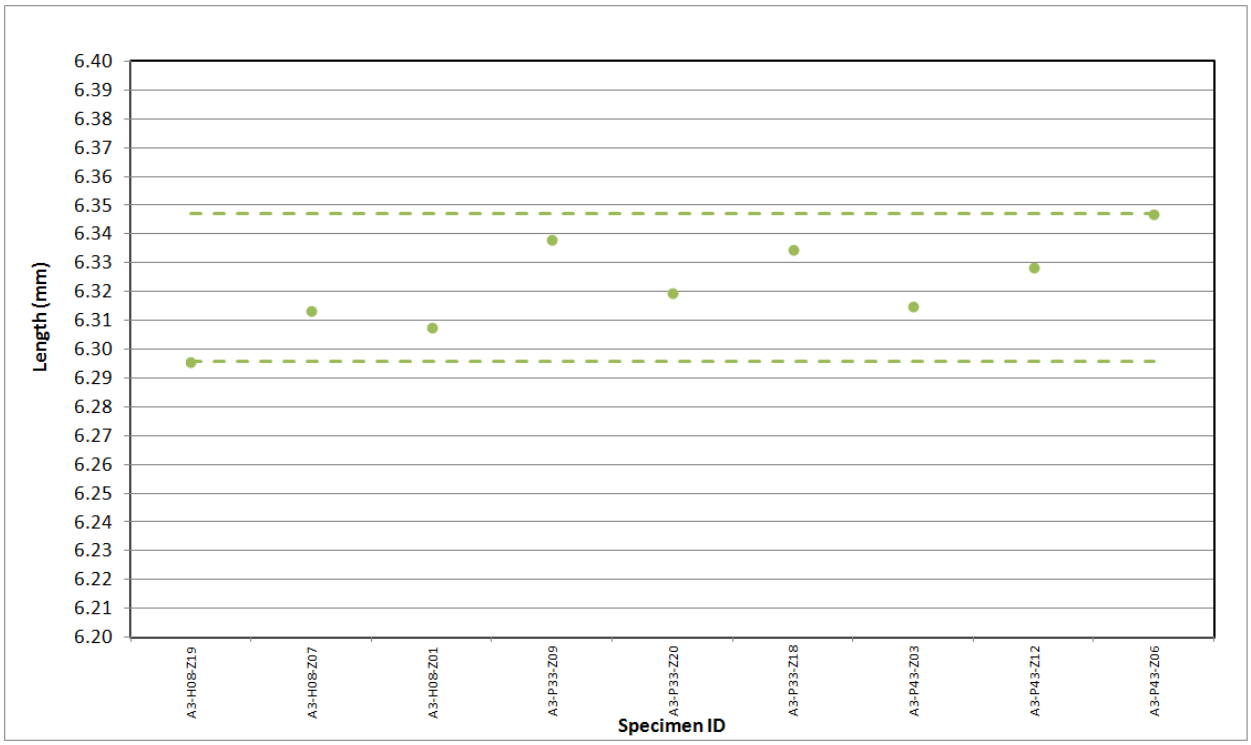

Figure A-40. New Matrix Piggyback Pre Thermal Measurement Length.

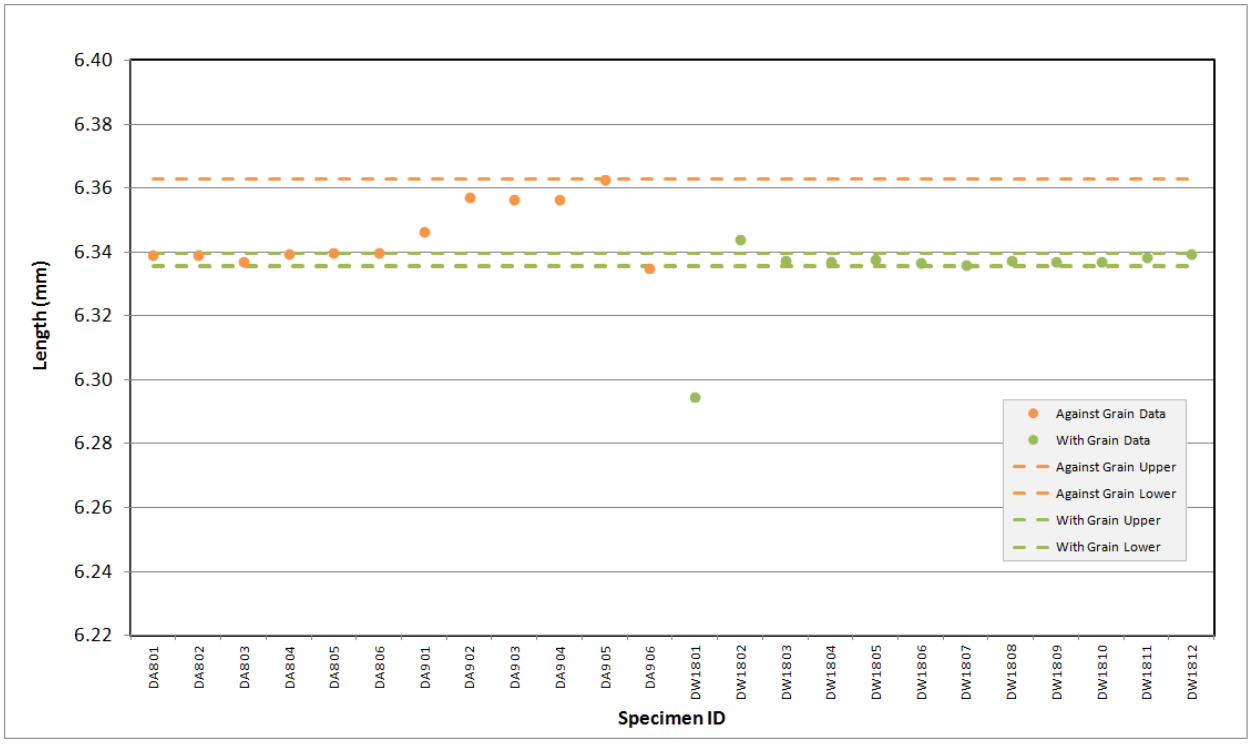

Figure A-41. PCEA Piggyback Pre Thermal Measurement Length.

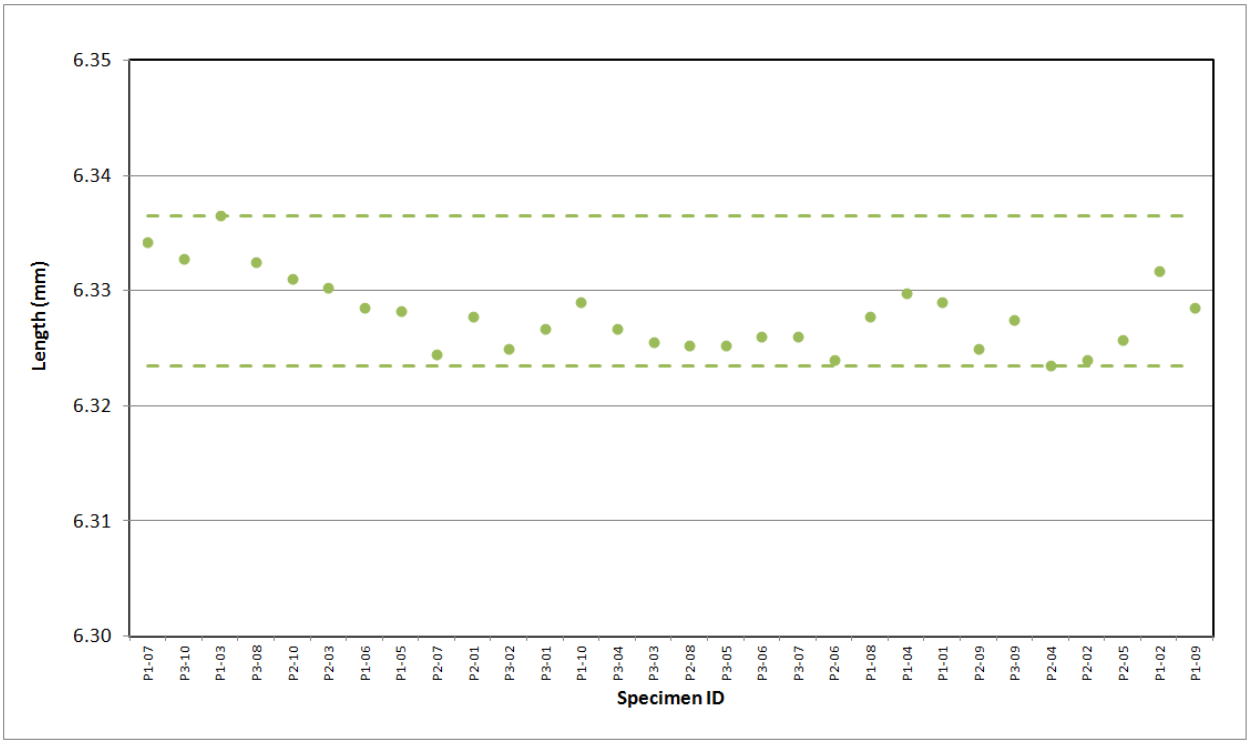

Figure A-42. PCIB Piggyback Pre Thermal Measurement Length.

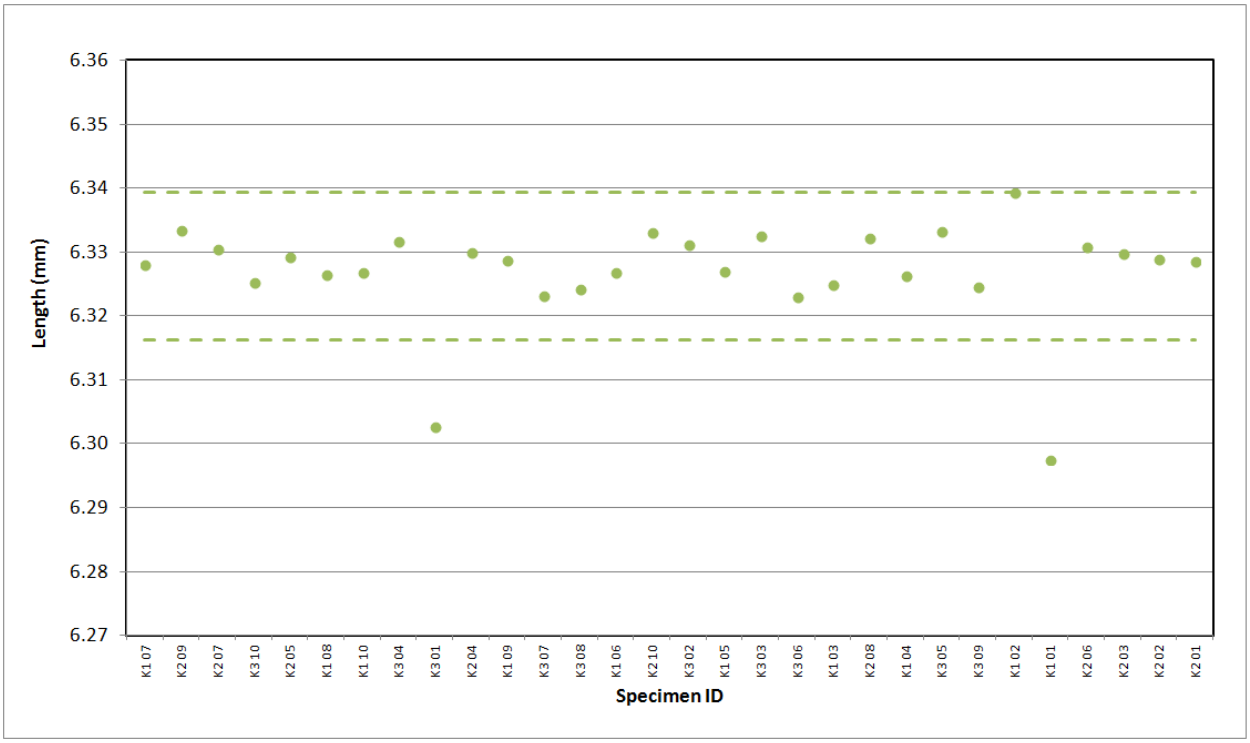

Figure A-43. PGX Piggyback Pre Thermal Measurement Length.

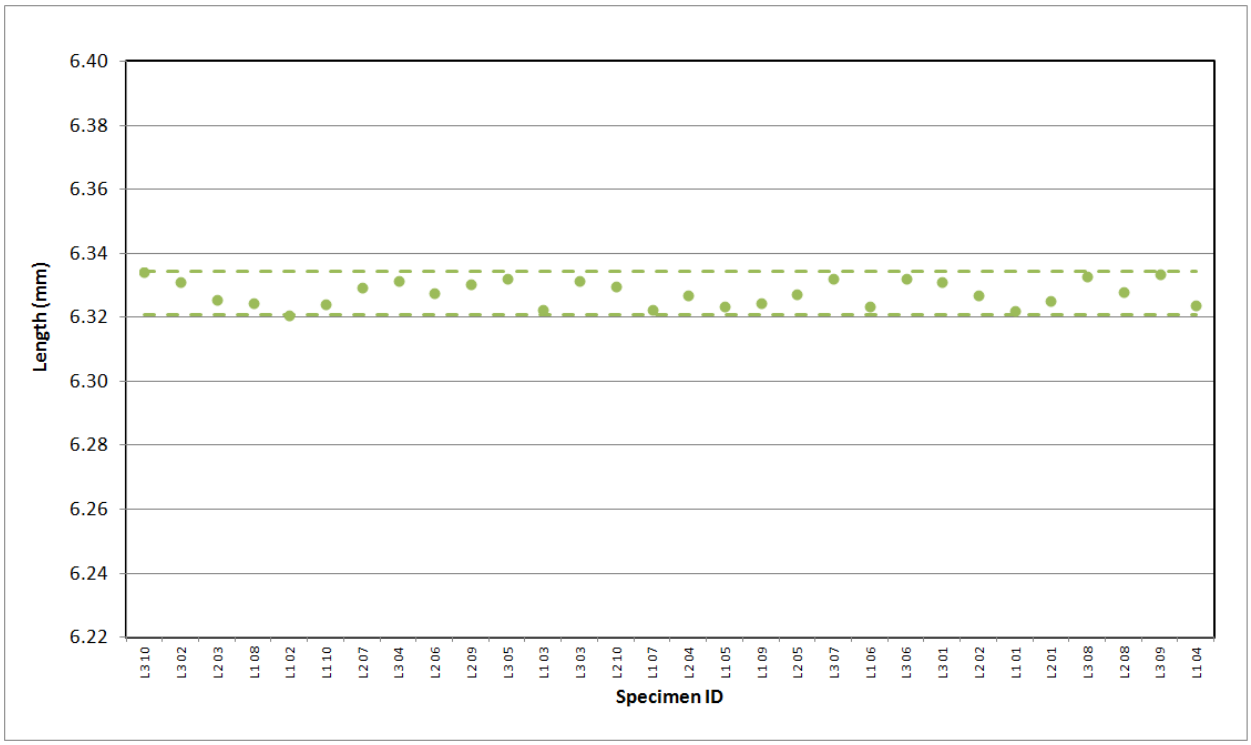

Figure A-44. PPEA Piggyback Pre Thermal Measurement Length.

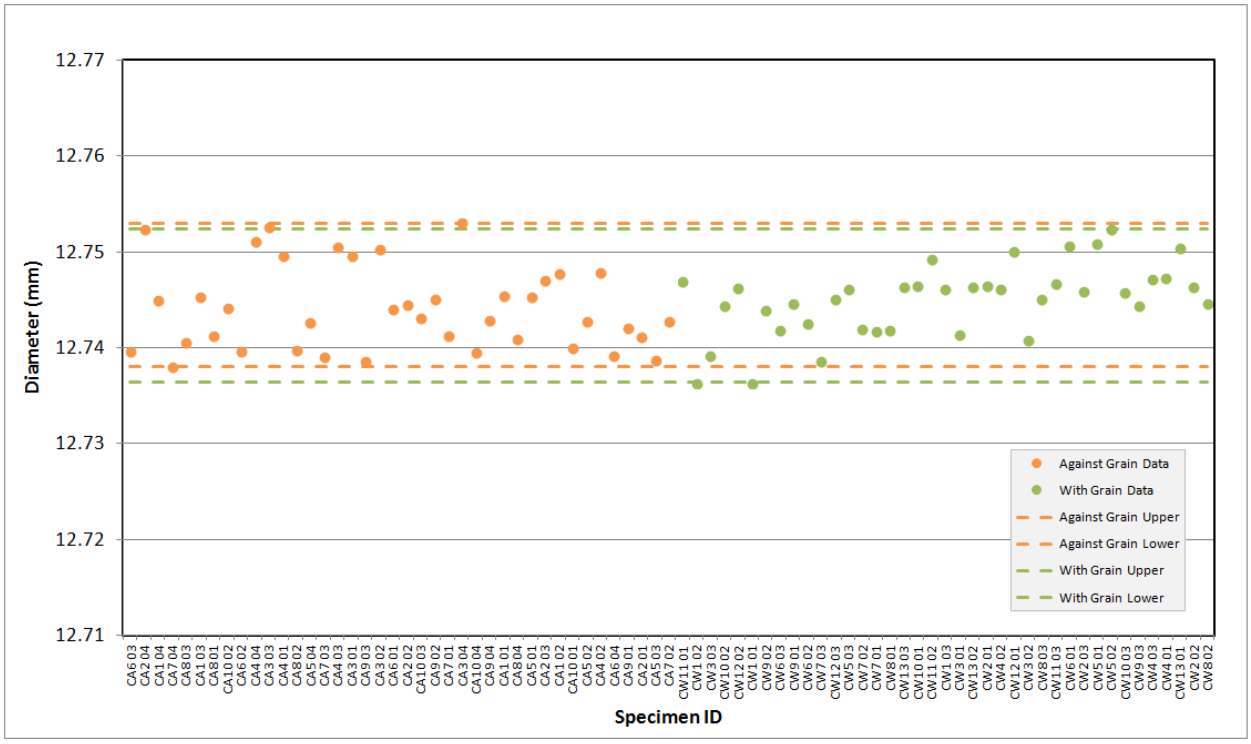

Figure A-45. H-451 Creep Pre Thermal Measurement Diameter.

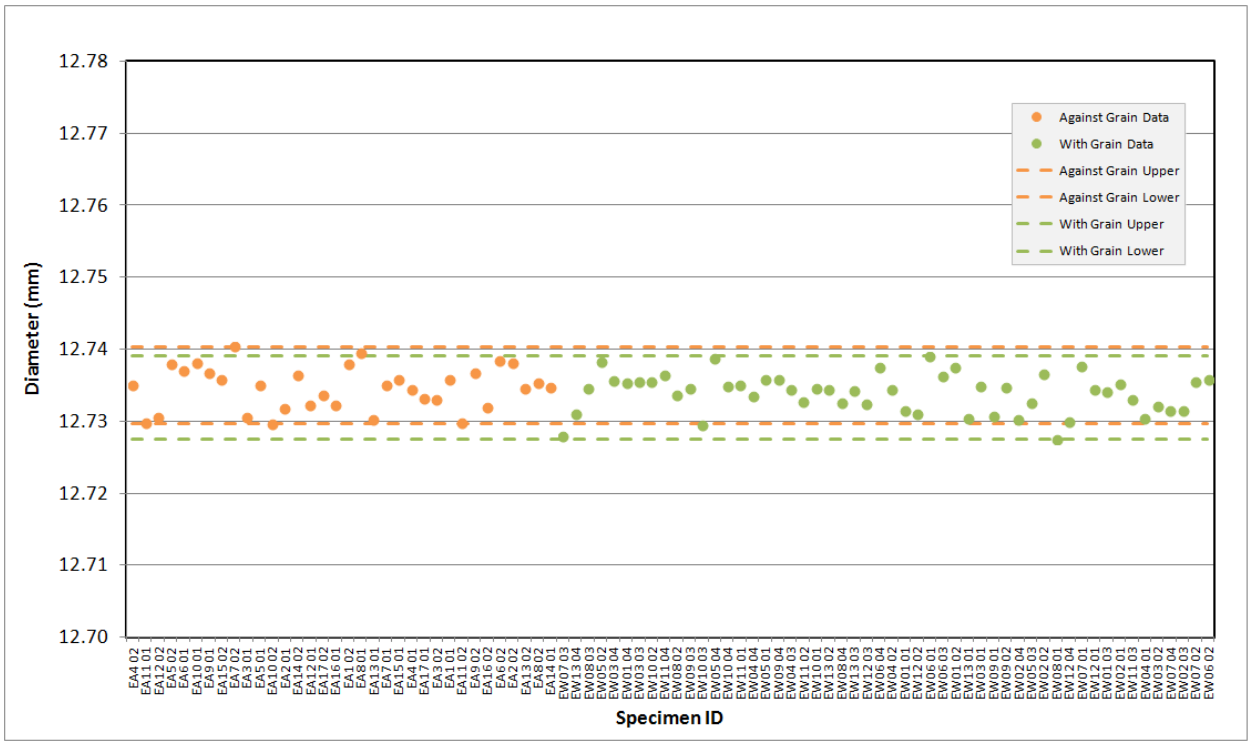

Figure A-46. IG-110 Creep Pre Thermal Measurement Diameter.

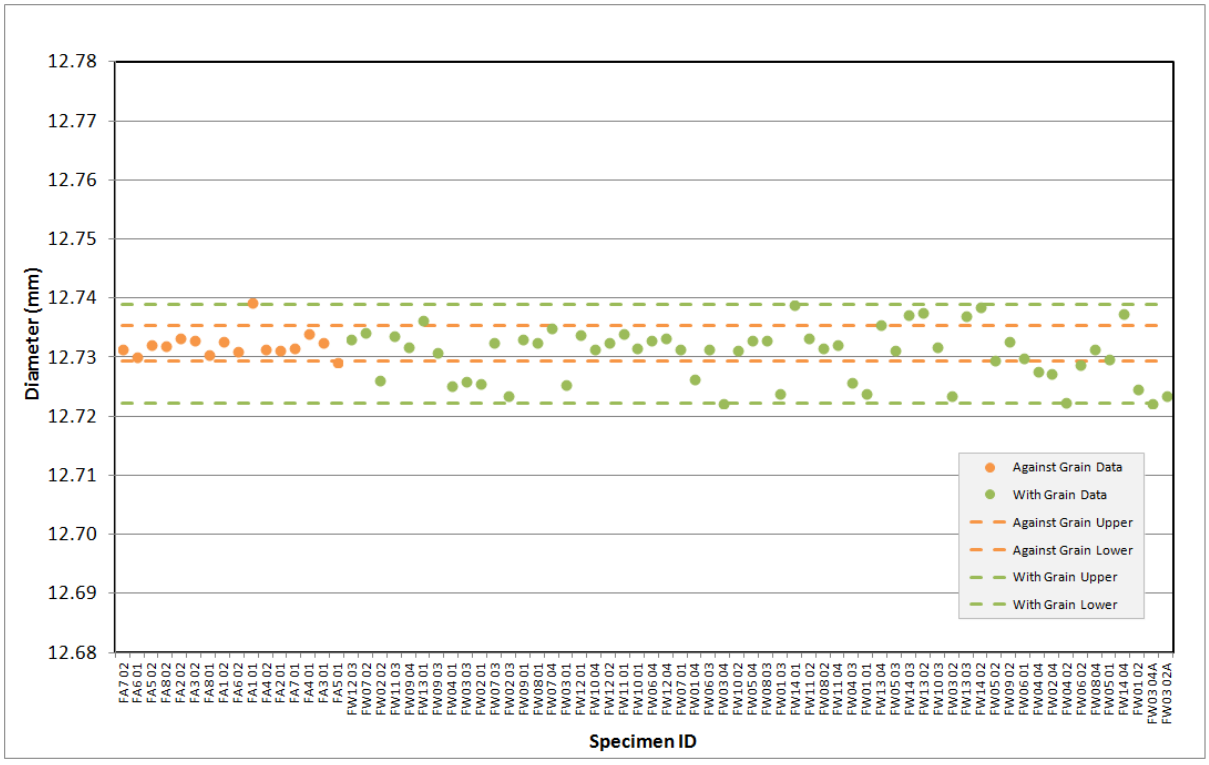

Figure A-47. IG-430 Creep Pre Thermal Measurement Diameter.

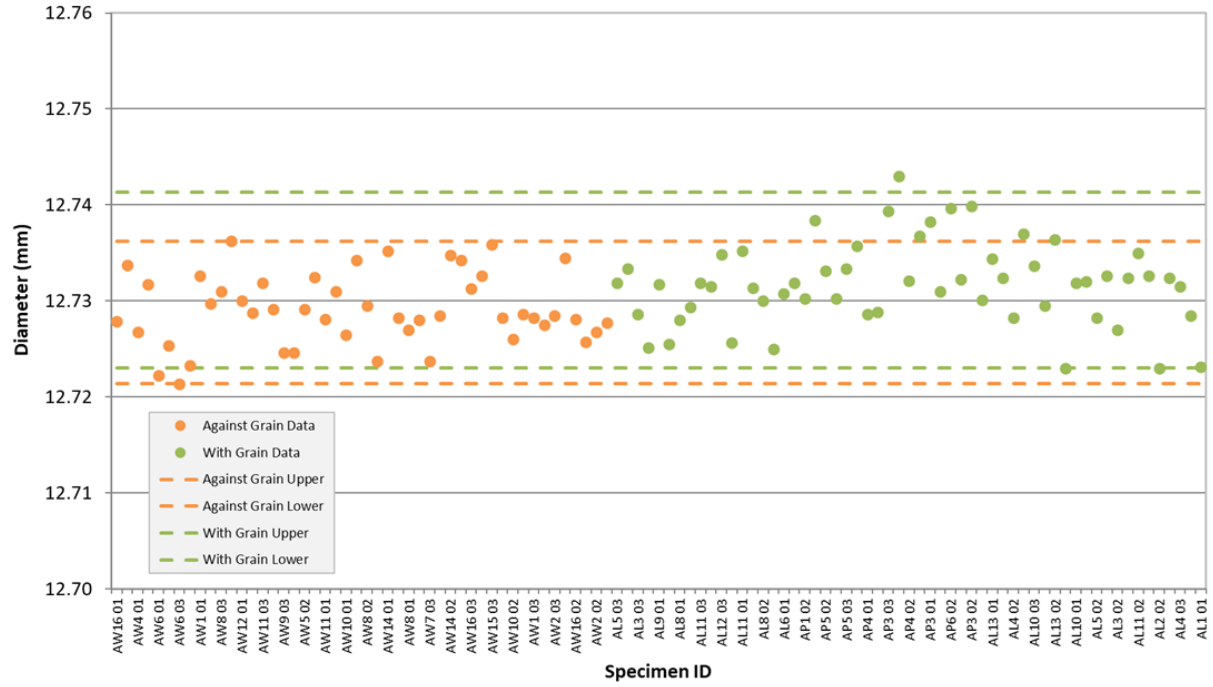

Figure A-48. NBG-17 Creep Pre Thermal Measurement Diameter.

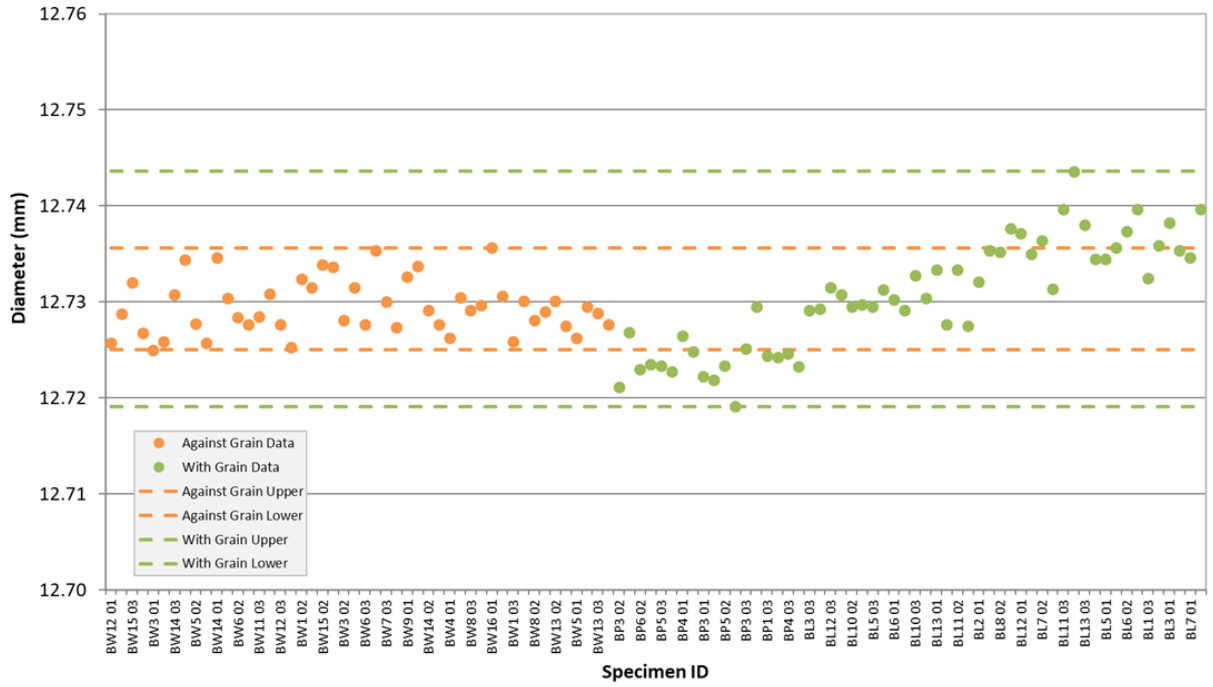

Figure A-49. NBG-18 Creep Pre Thermal Measurement Diameter.

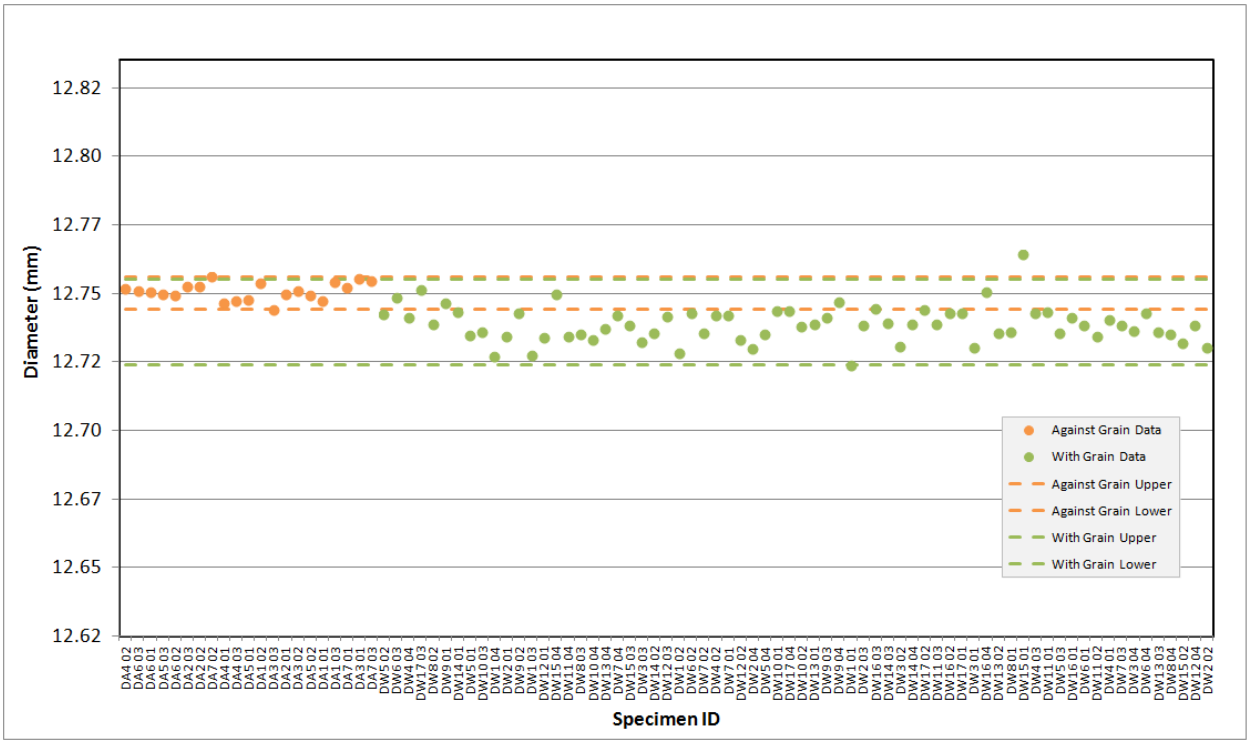

Figure A-50. PCEA Creep Pre Thermal Measurement Diameter.

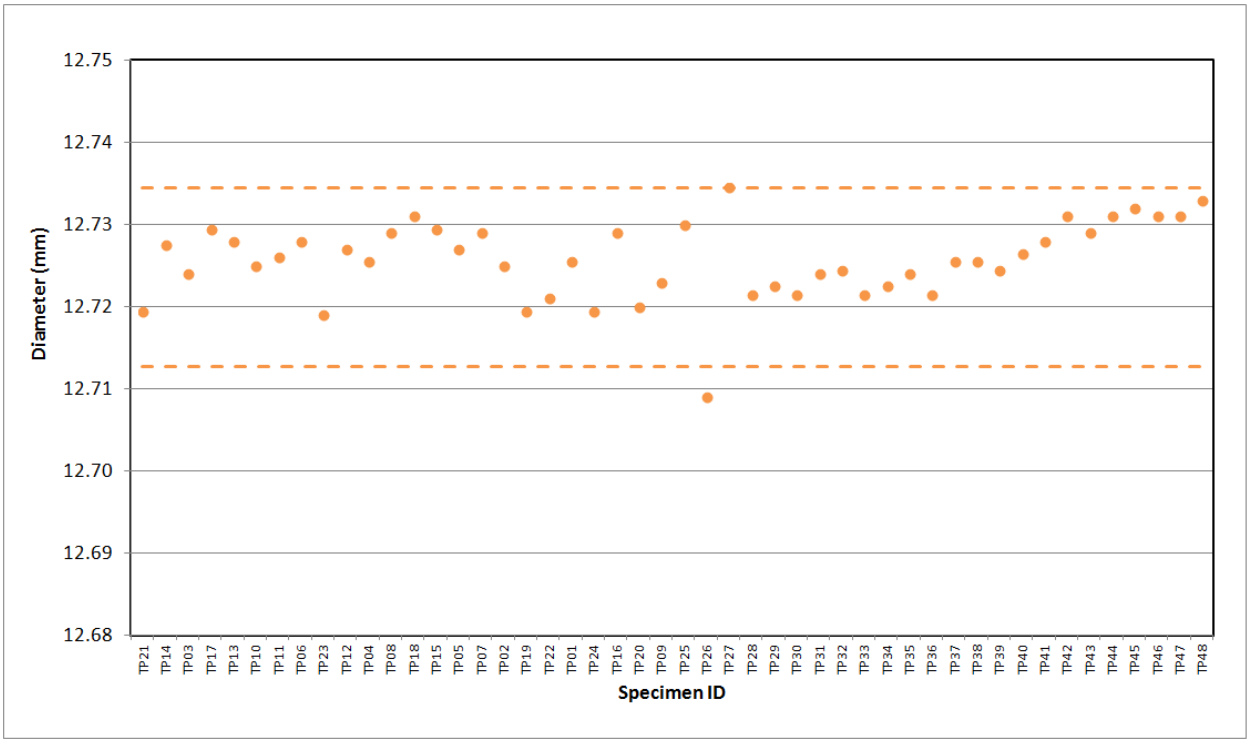

Figure A-51. 2114 Piggyback Pre Thermal Measurement Diameter.

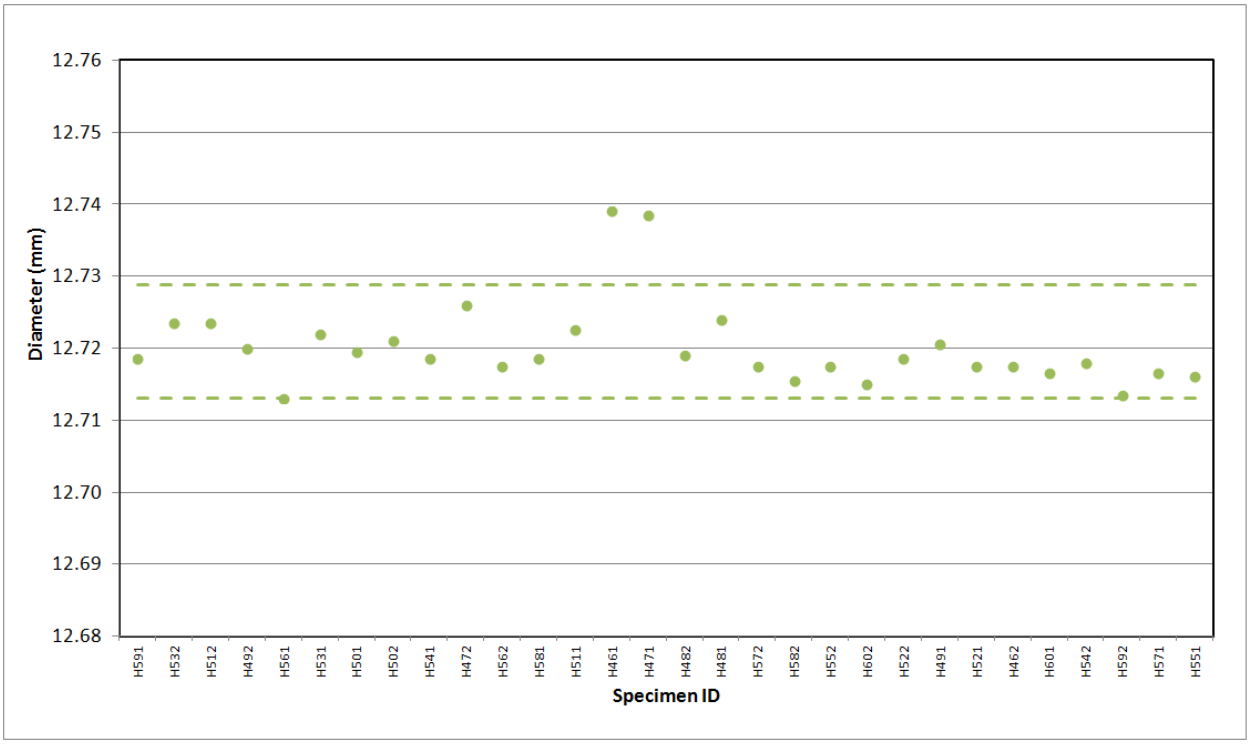

Figure A-52. A3 Matrix Piggyback Pre Thermal Measurement Diameter.

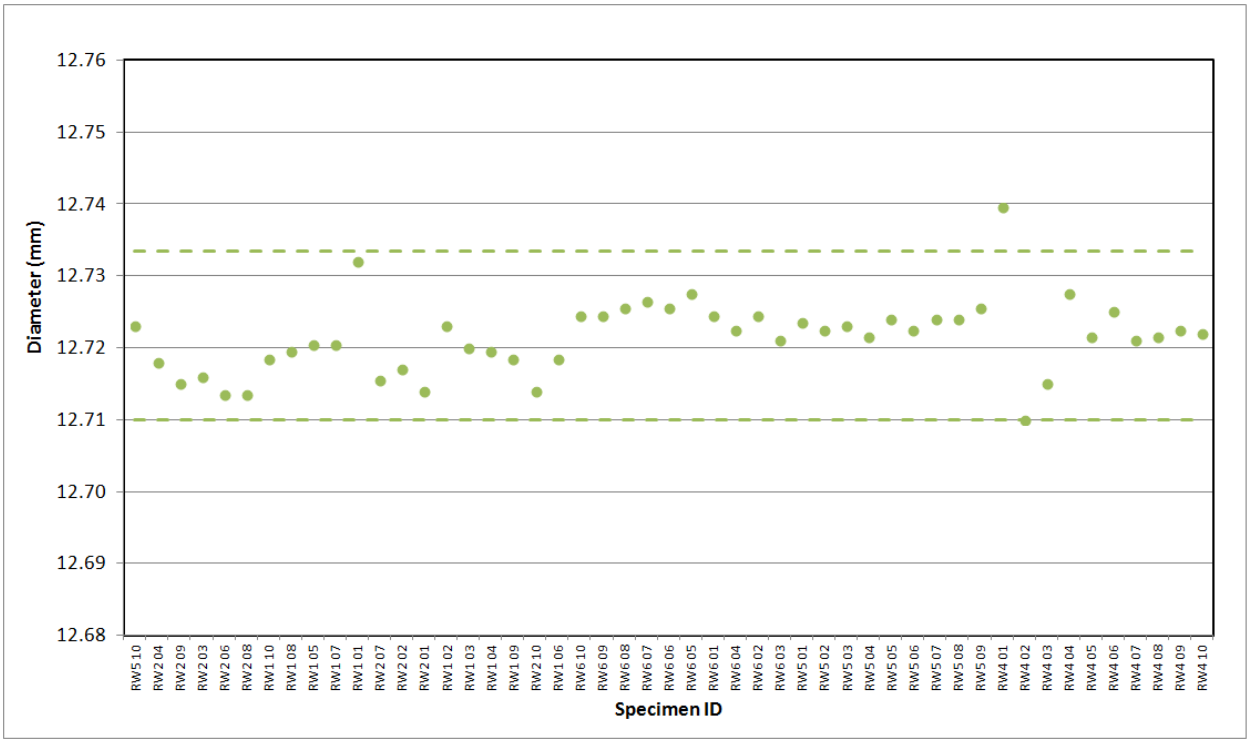

Figure A-53. BAN Piggyback Pre Thermal Measurement Diameter.

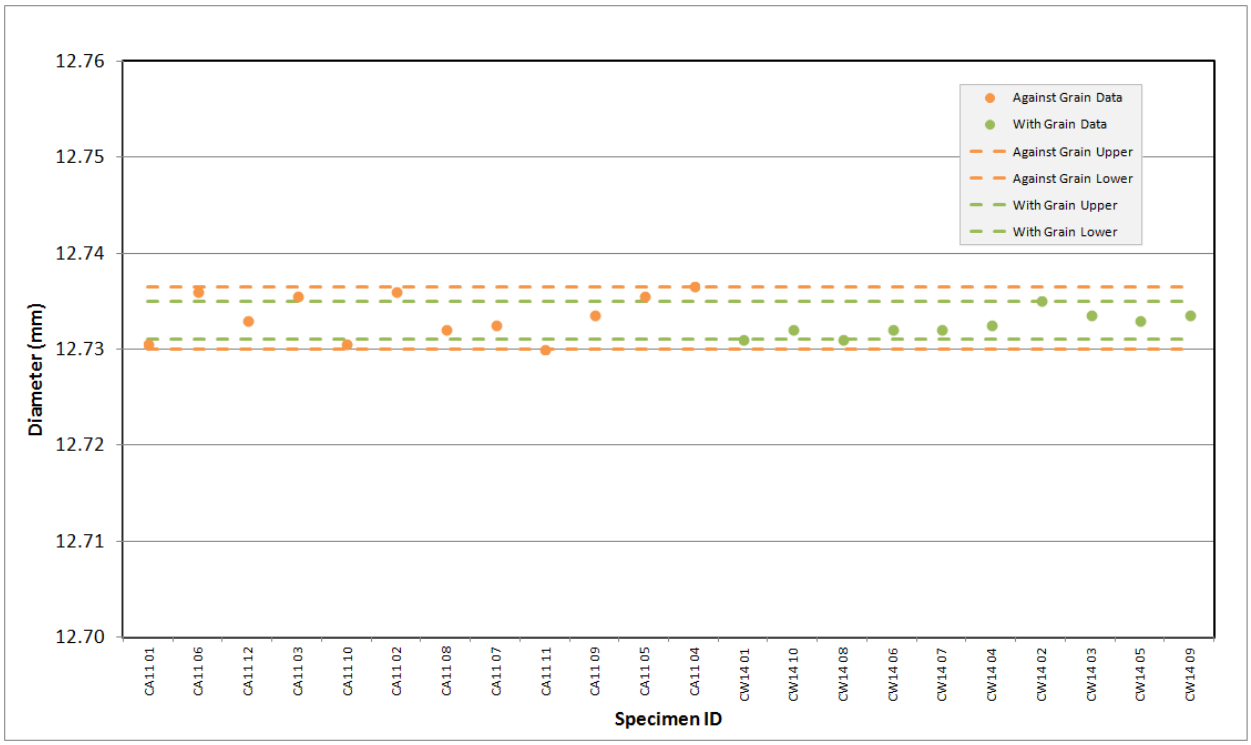

Figure A-54. H-451 Piggyback Pre Thermal Measurement Diameter.

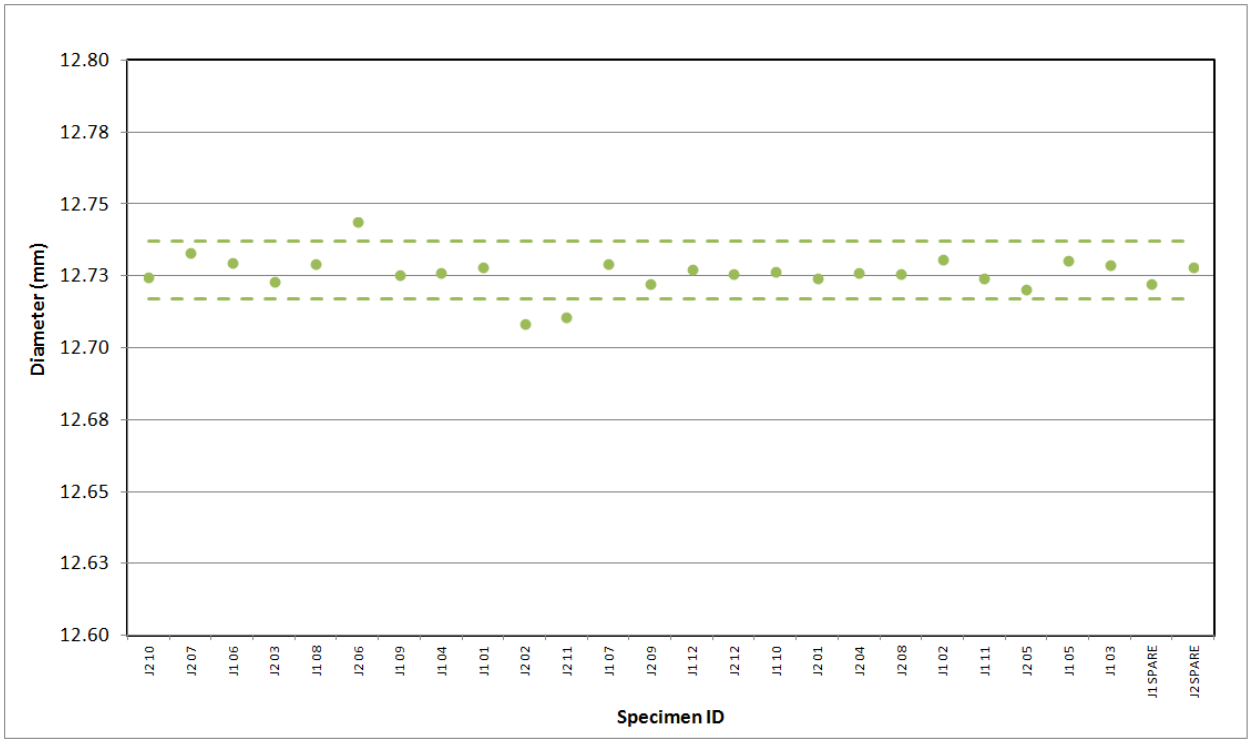

Figure A-55. HLM Piggyback Pre Thermal Measurement Diameter.

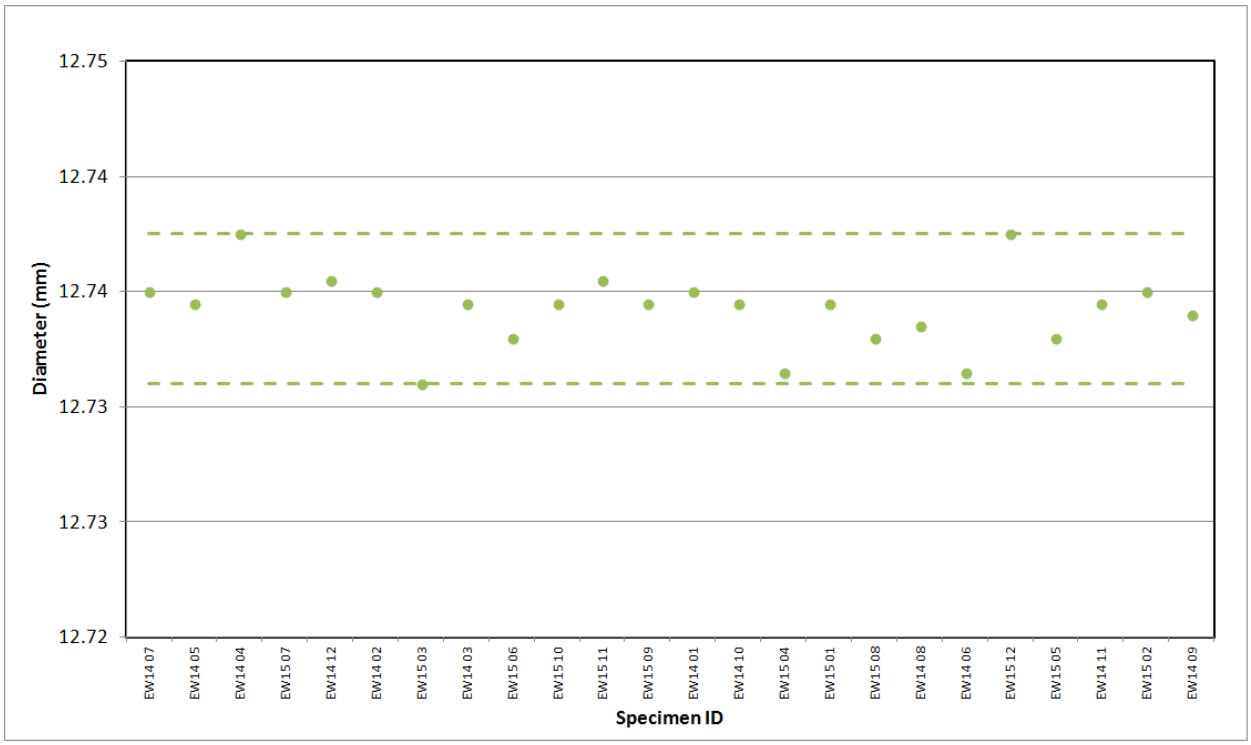

Figure A-56. IG-110 Piggyback Pre Thermal Measurement Diameter.

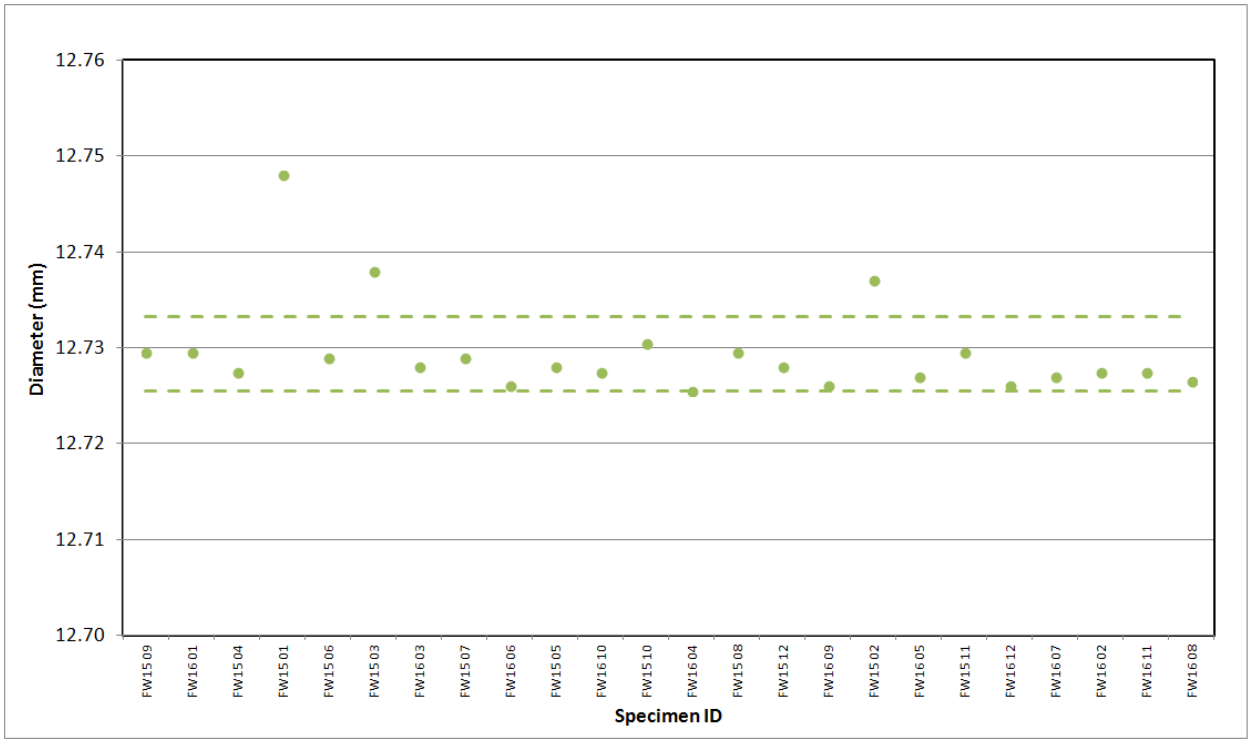

Figure A-57. IG-430 Piggyback Pre Thermal Measurement Diameter.

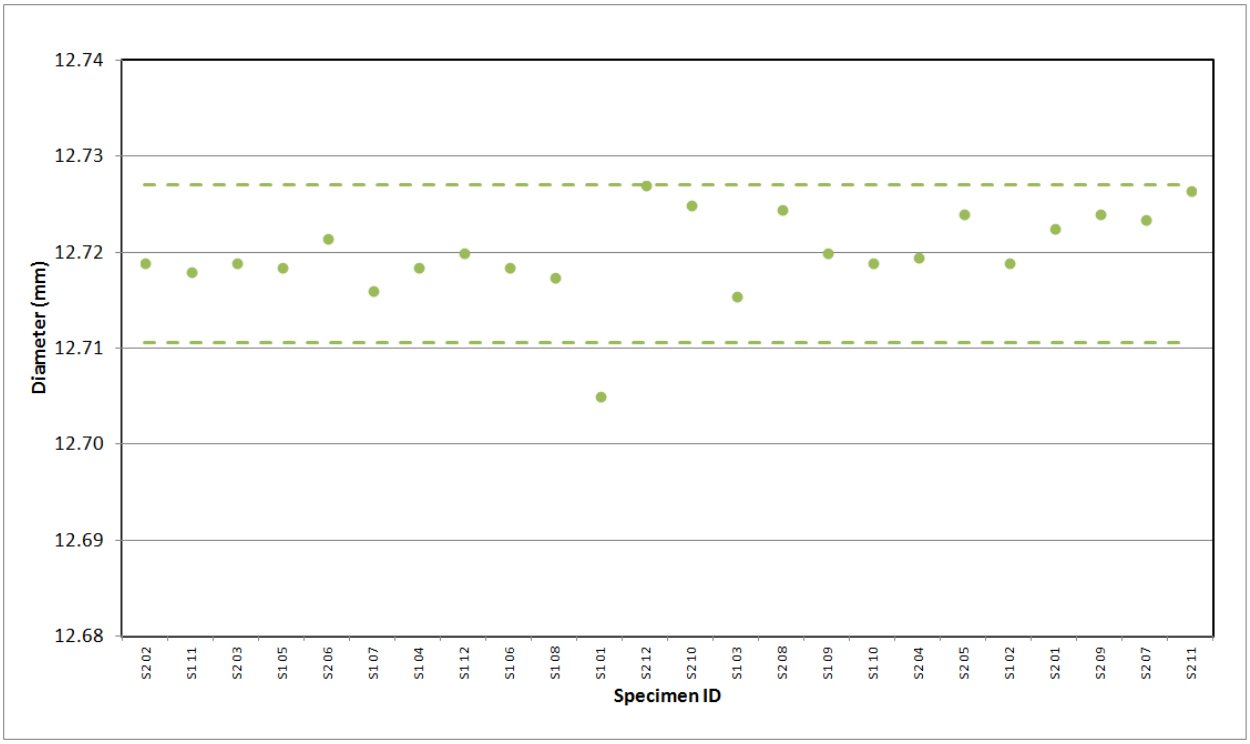

Figure A-58. NBG-10 Piggyback Pre Thermal Measurement Diameter.

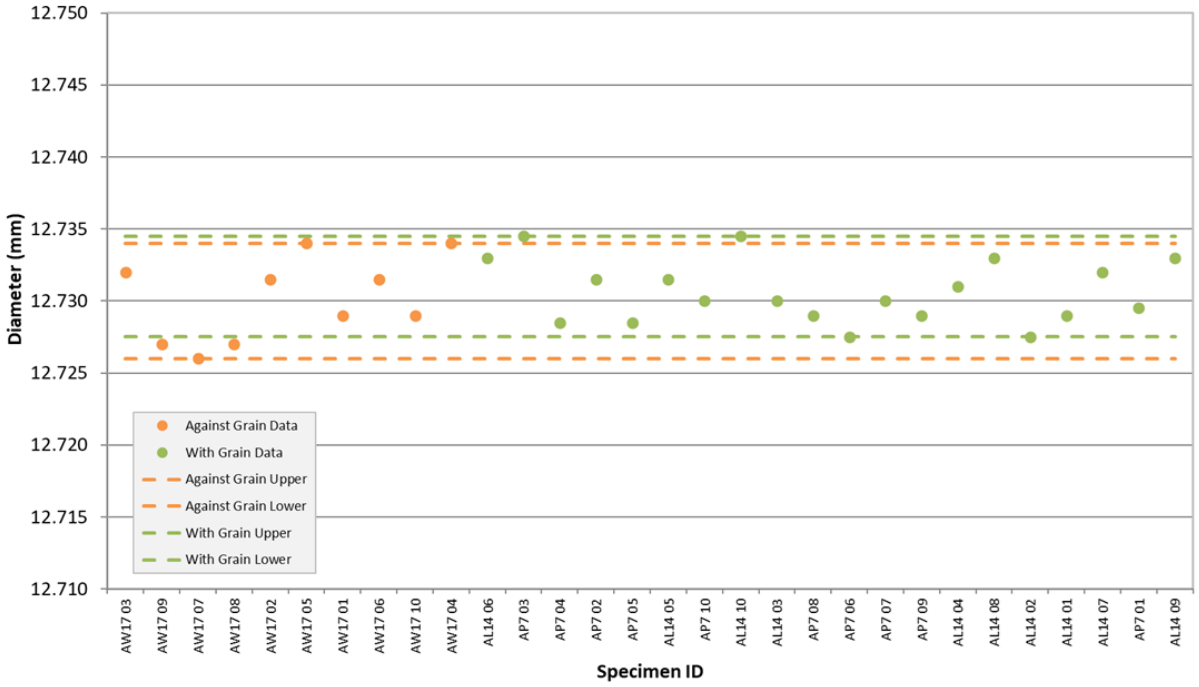

Figure A-59. NBG-17 Piggyback Pre Thermal Measurement Diameter.

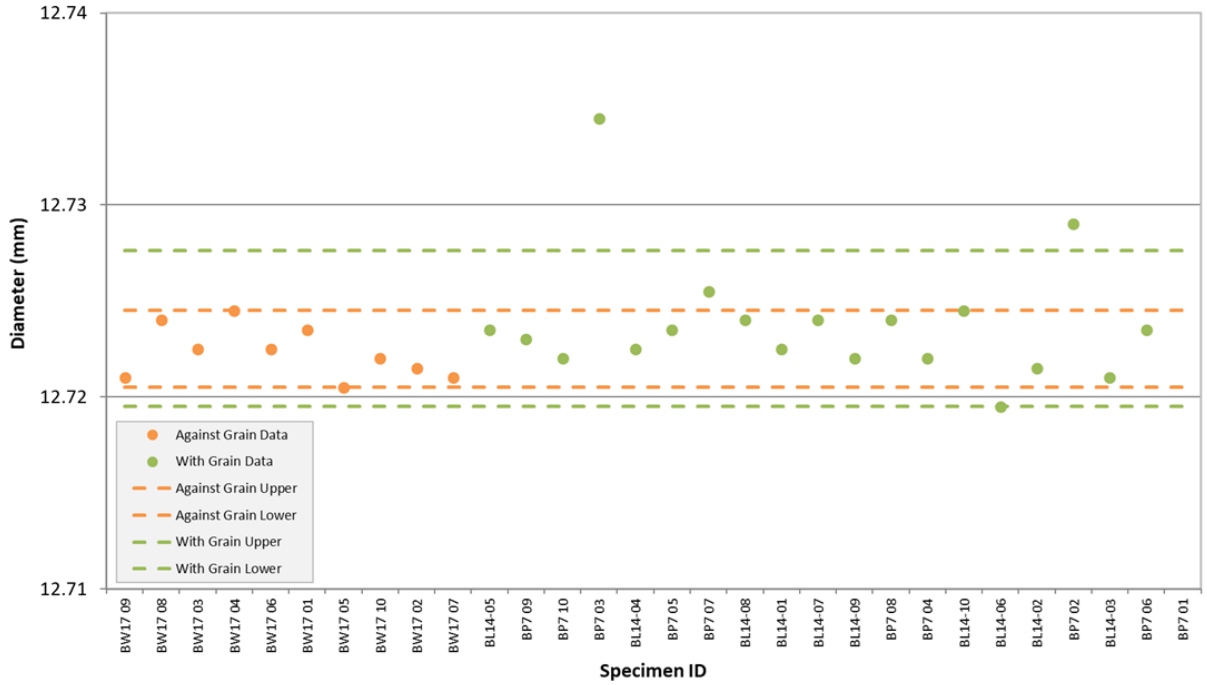

Figure A-60. NBG-18 Piggyback Pre Thermal Measurement Diameter.

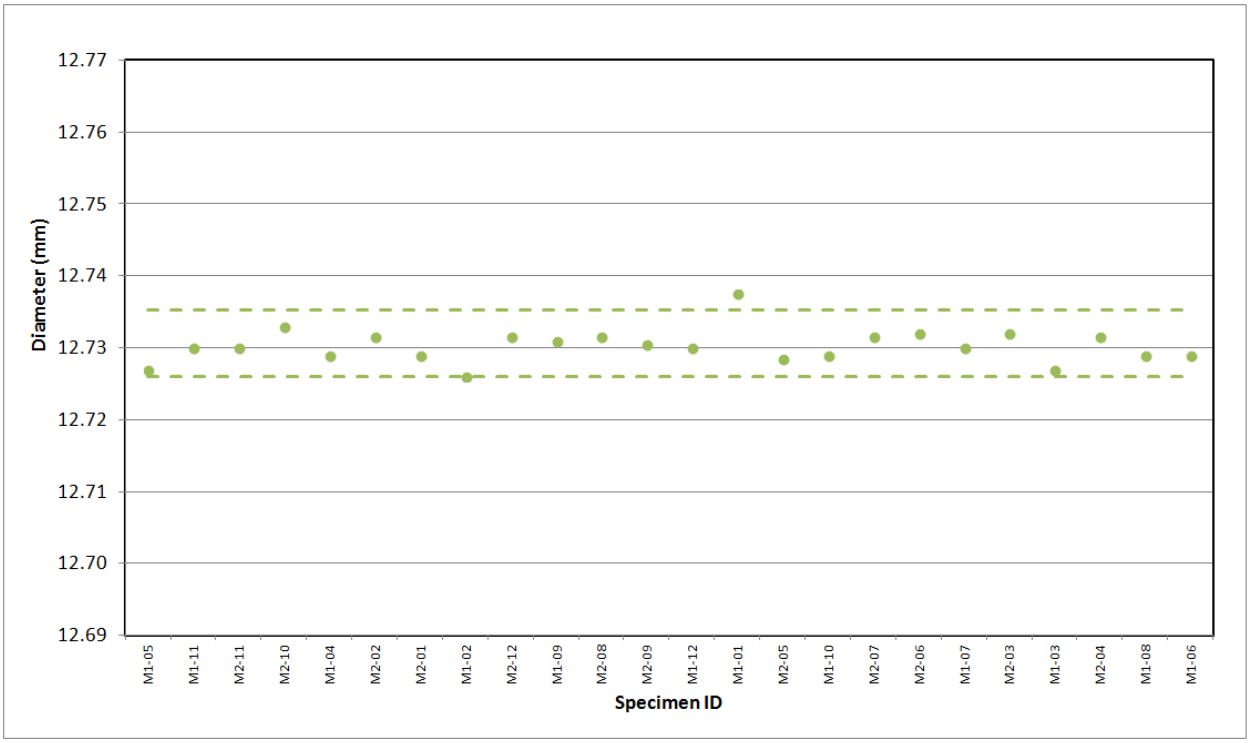

Figure A-61. NBG-25 Piggyback Pre Thermal Measurement Diameter.

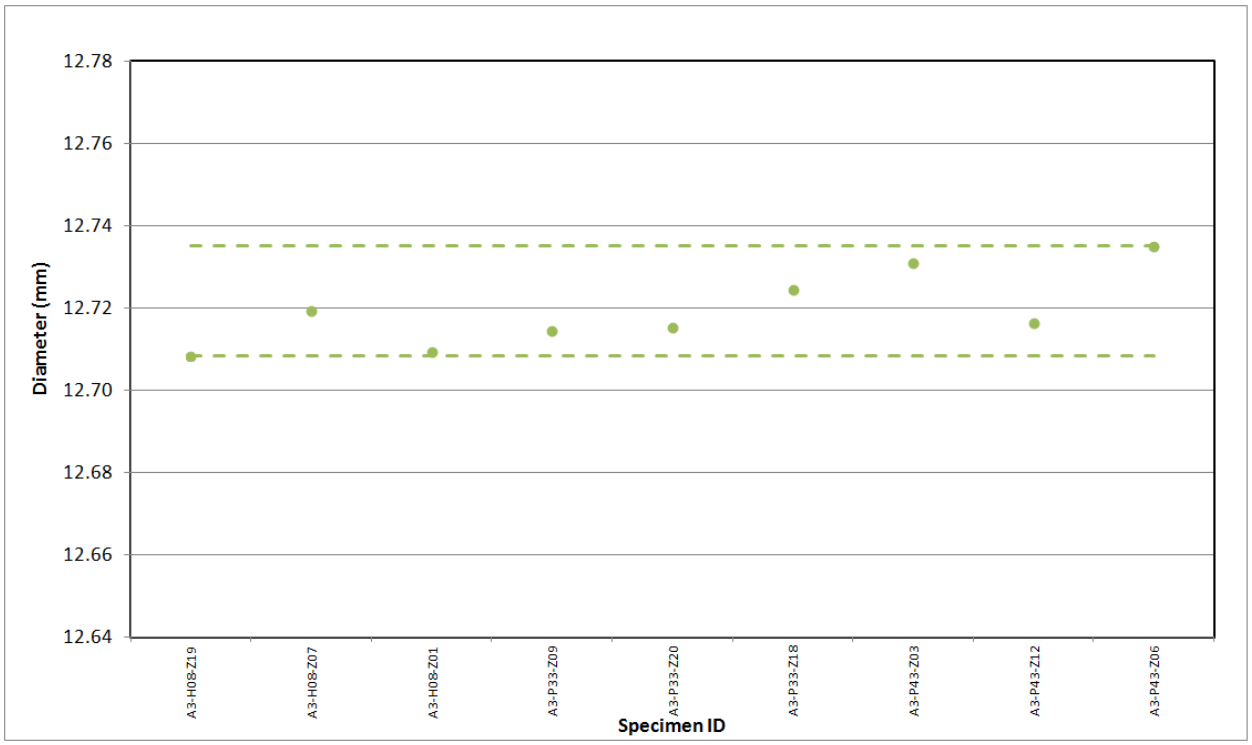

Figure A-62. New Matrix Piggyback Pre Thermal Measurement Diameter.

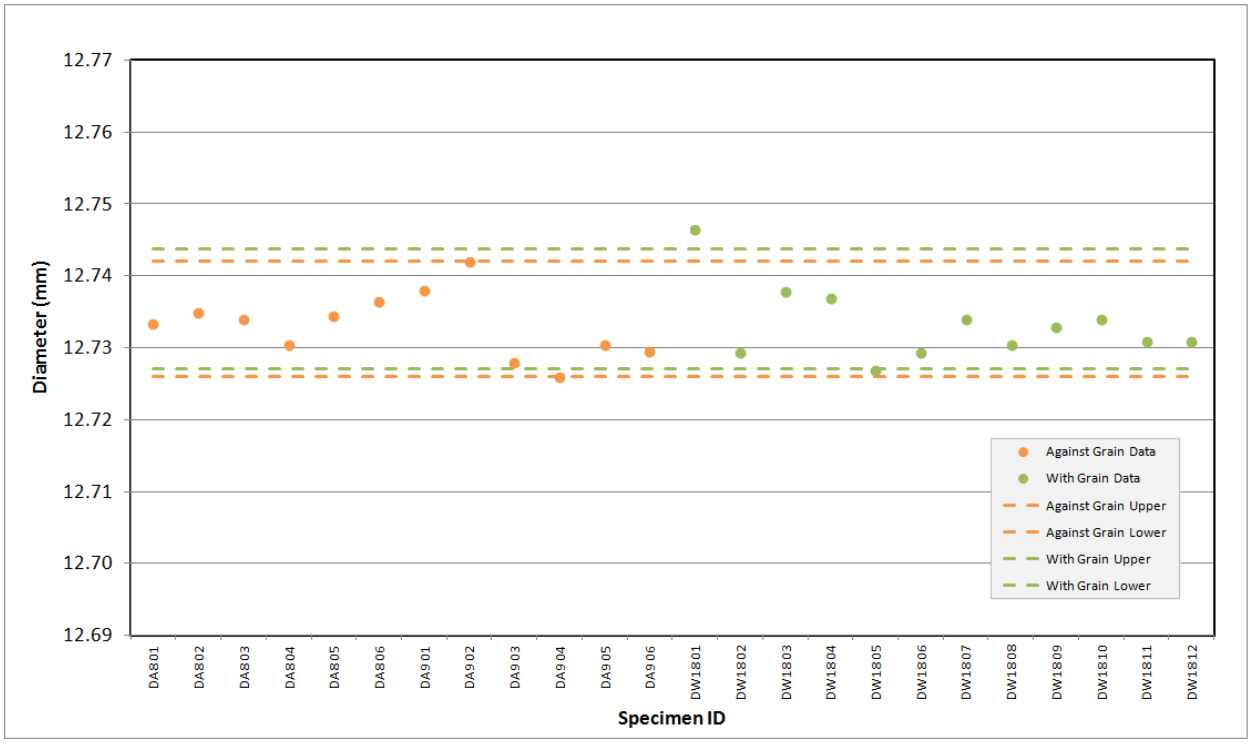

Figure A-63. PCEA Piggyback Pre Thermal Measurement Diameter.

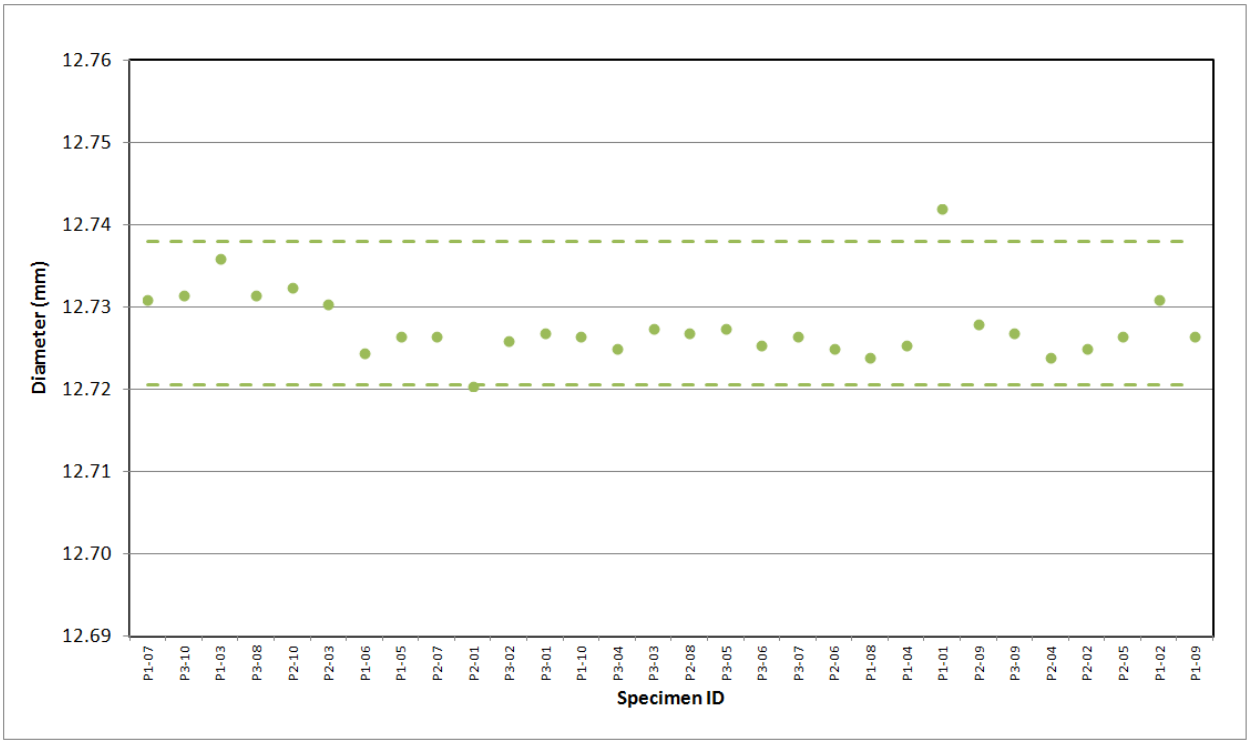

Figure A-64. PCIB Piggyback Pre Thermal Measurement Diameter.

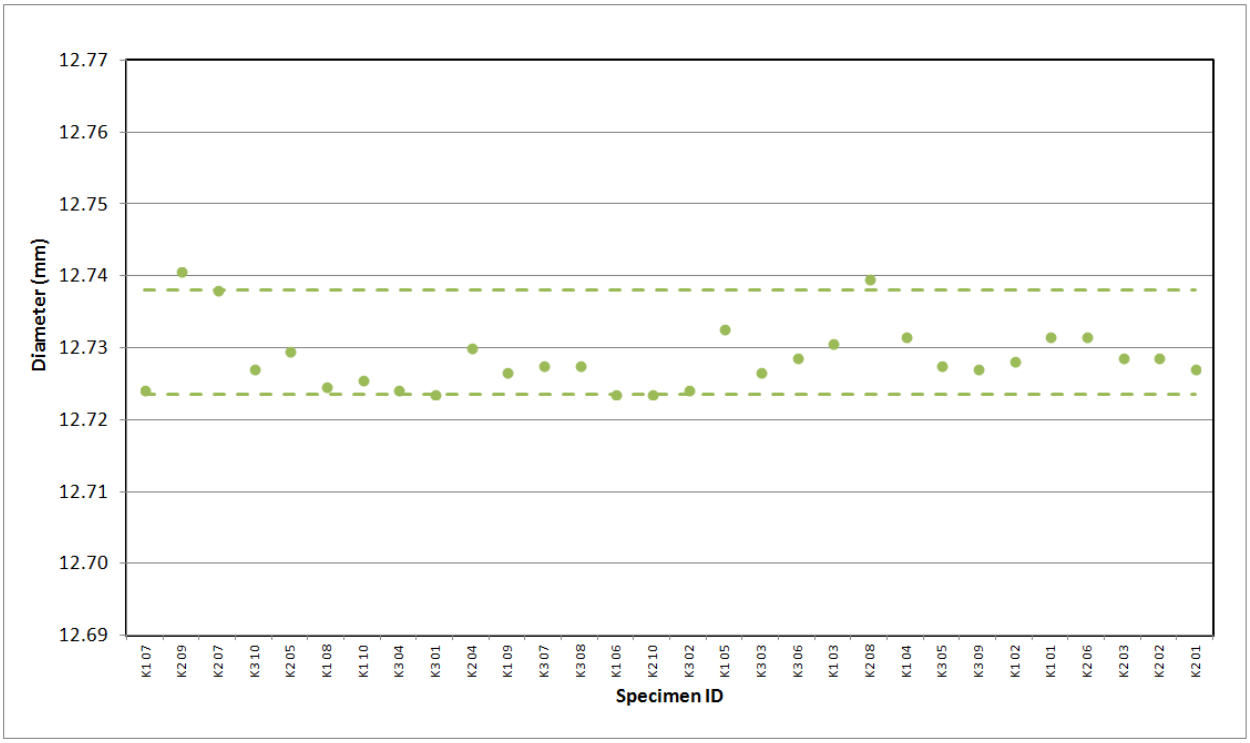

Figure A-65. PGX Piggyback Pre Thermal Measurement Diameter.

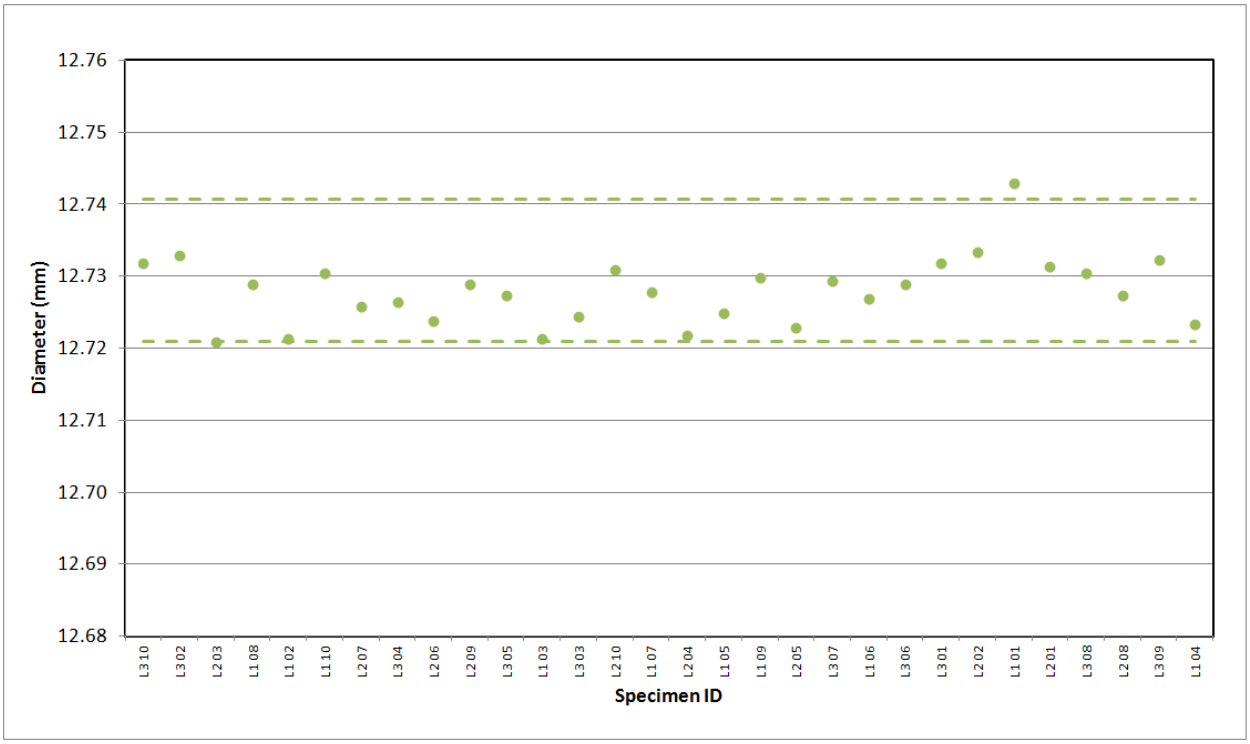

Figure A-66. PPEA Piggyback Pre Thermal Measurement Diameter.

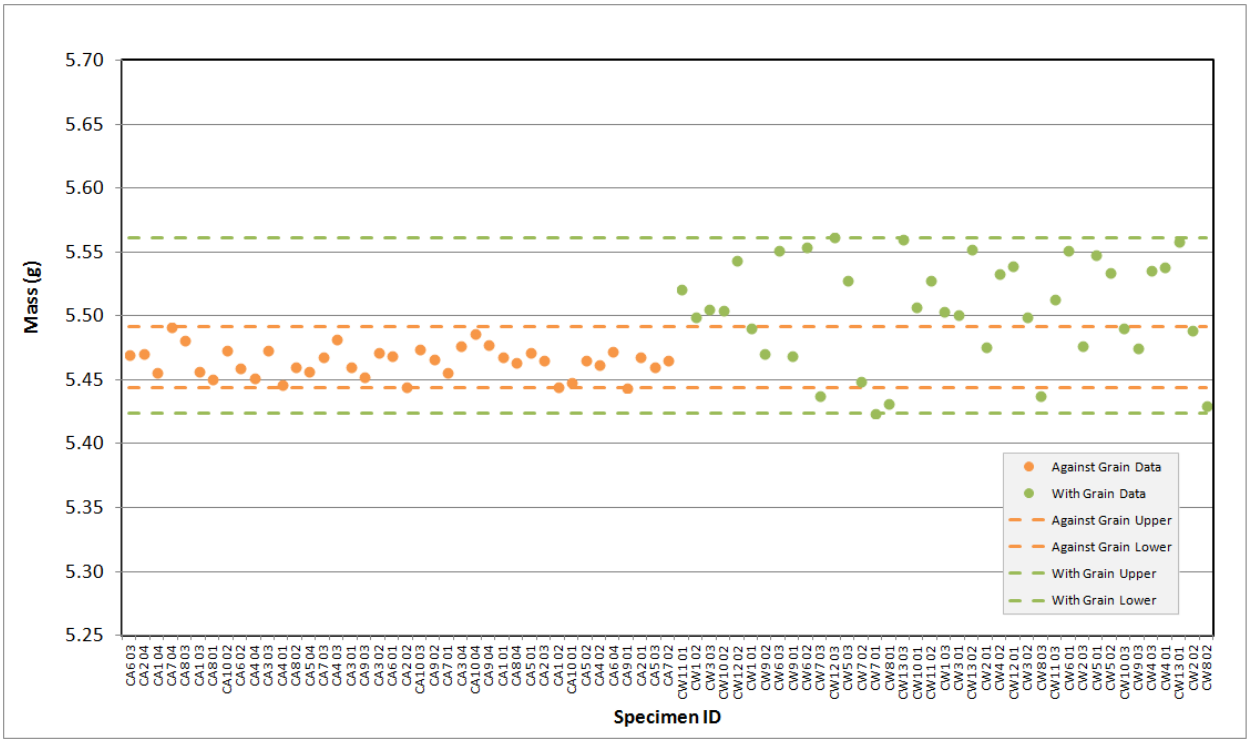

Figure A-67. H-451 Creep Pre Thermal Measurement Mass.

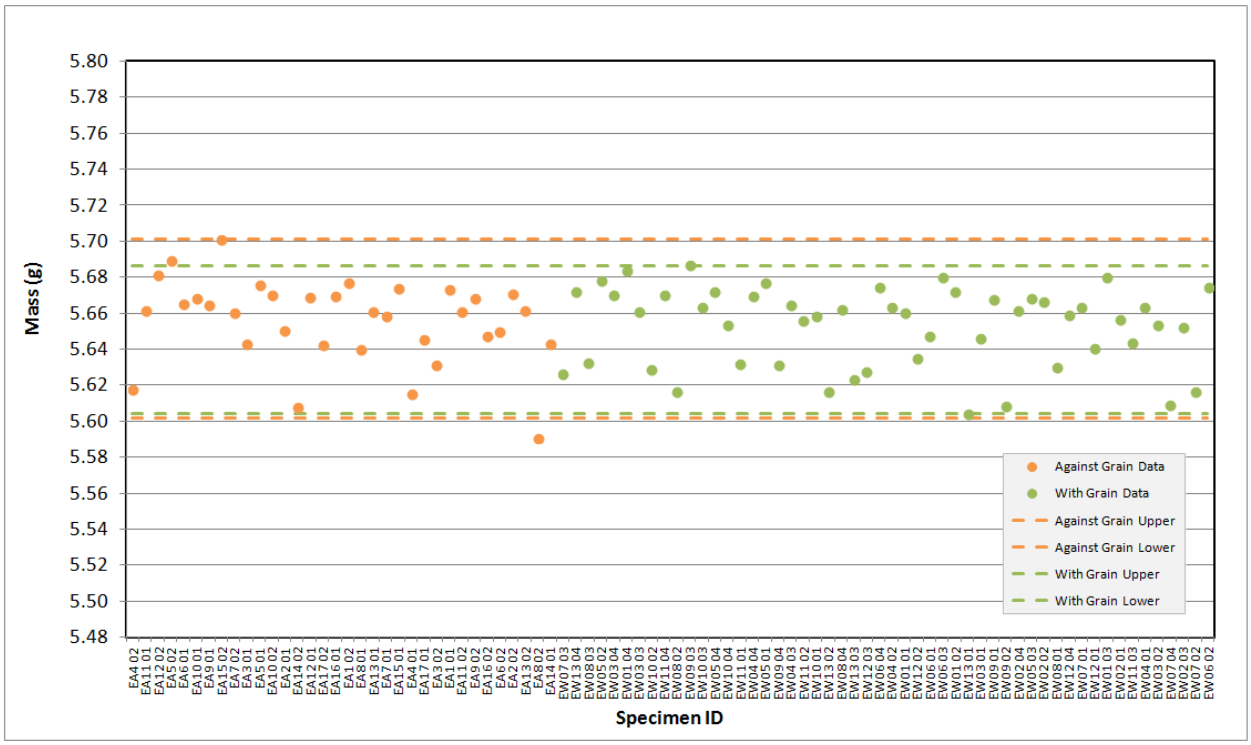

Figure A-68. IG-110 Creep Pre Thermal Measurement Mass.

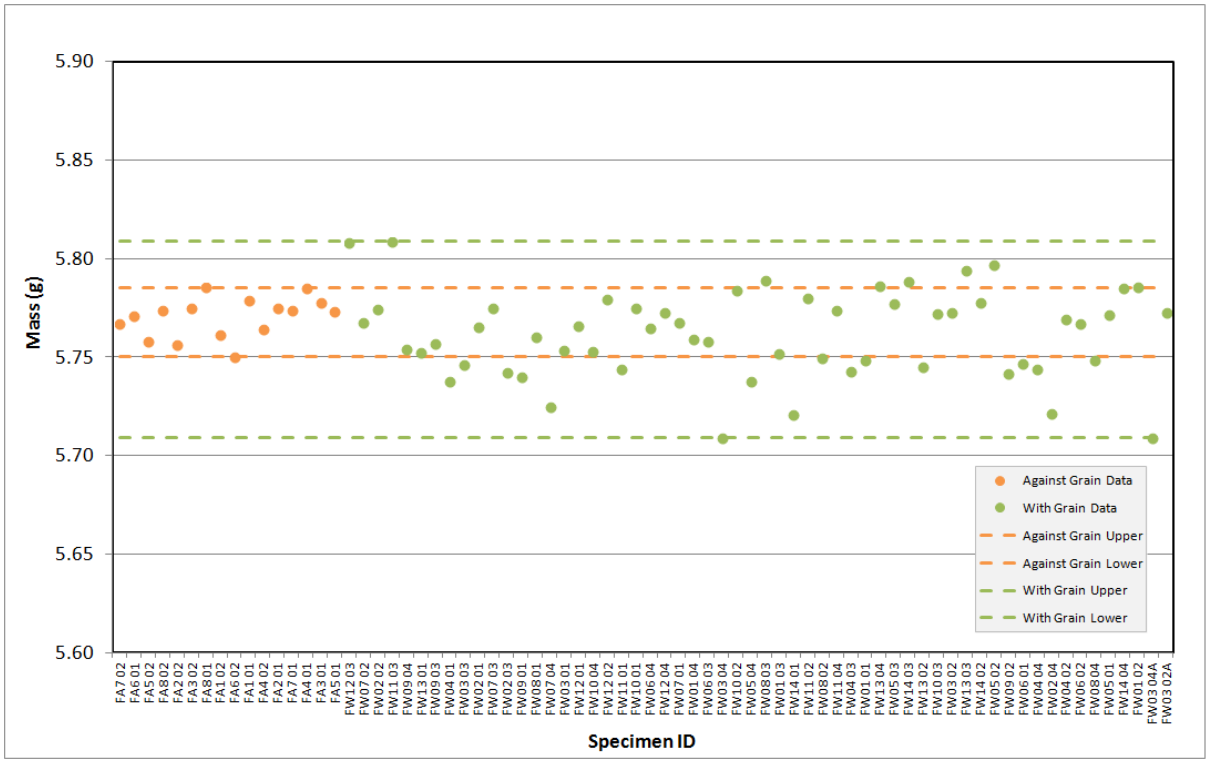

Figure A-69. IG-430 Creep Pre Thermal Measurement Mass.

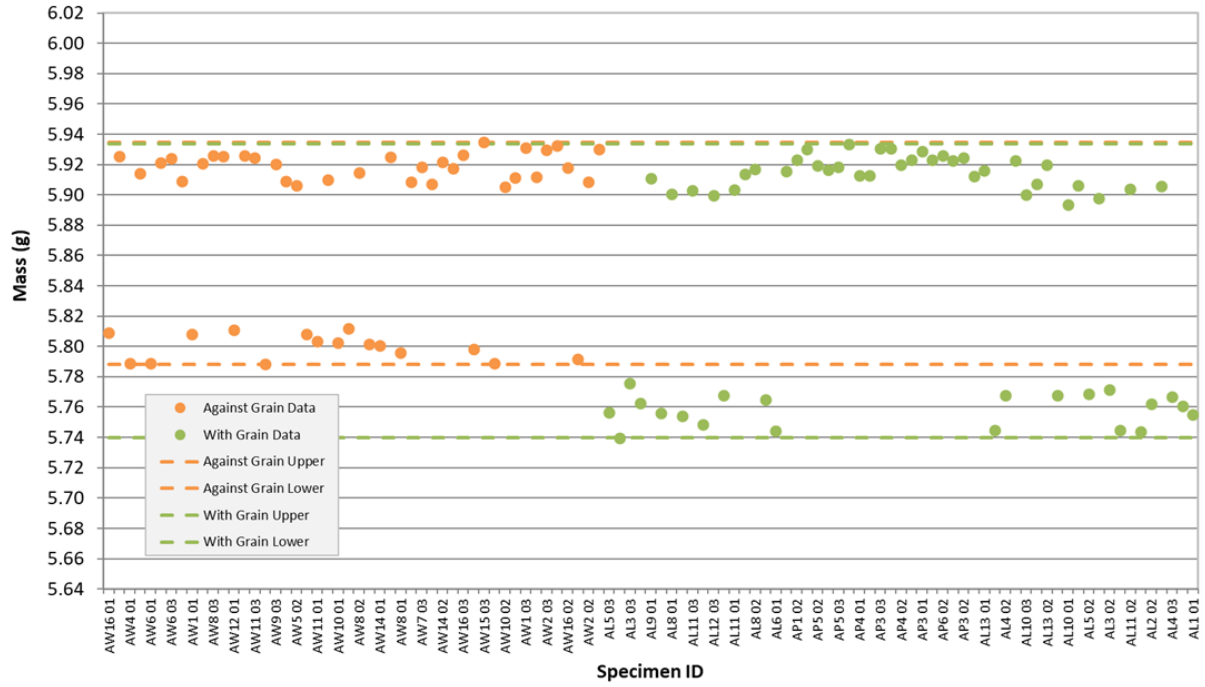

Figure A-70. NBG-17 Creep Pre Thermal Measurement Mass.

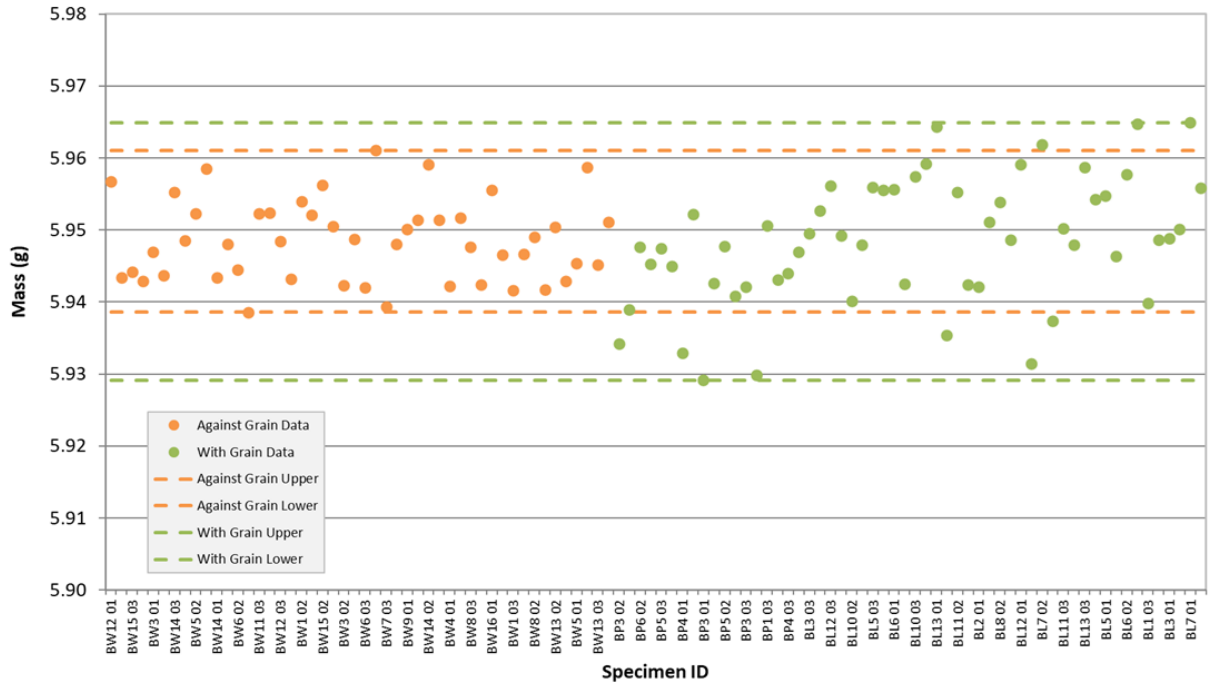

Figure A-71. NBG-18 Creep Pre Thermal Measurement Mass.

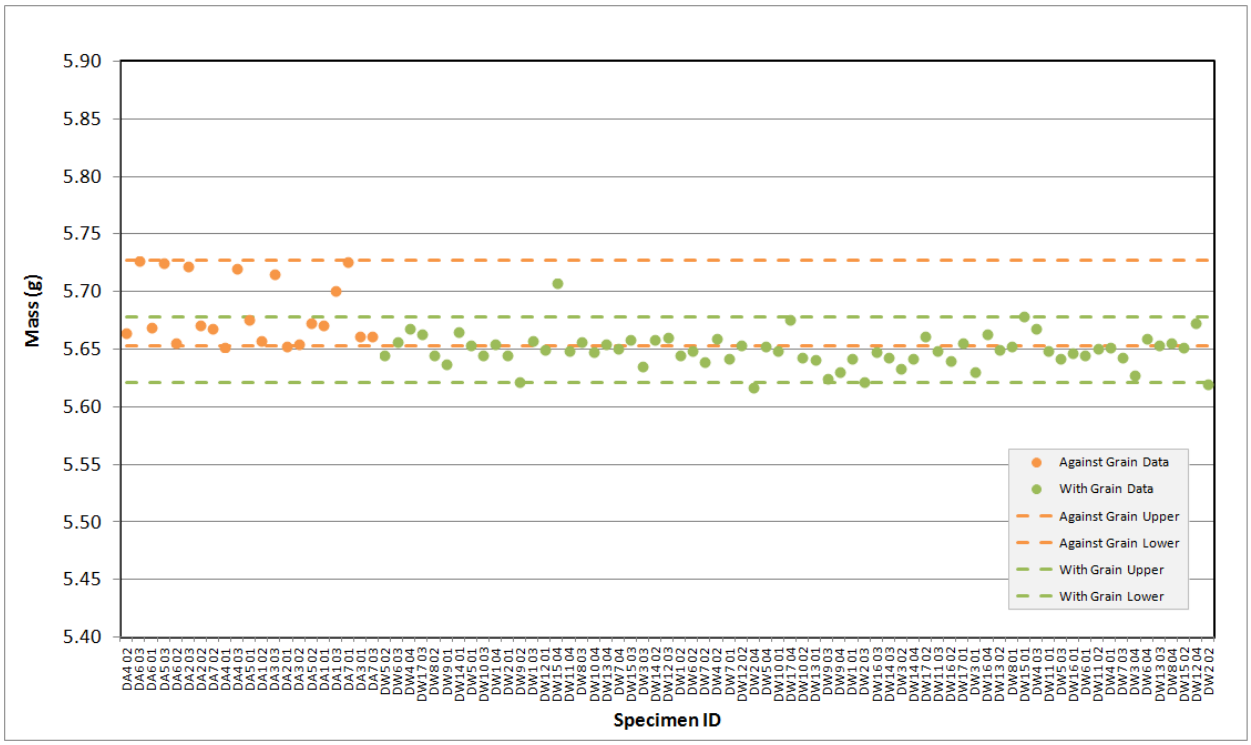

Figure A-72. PCEA Creep Pre Thermal Measurement Mass.

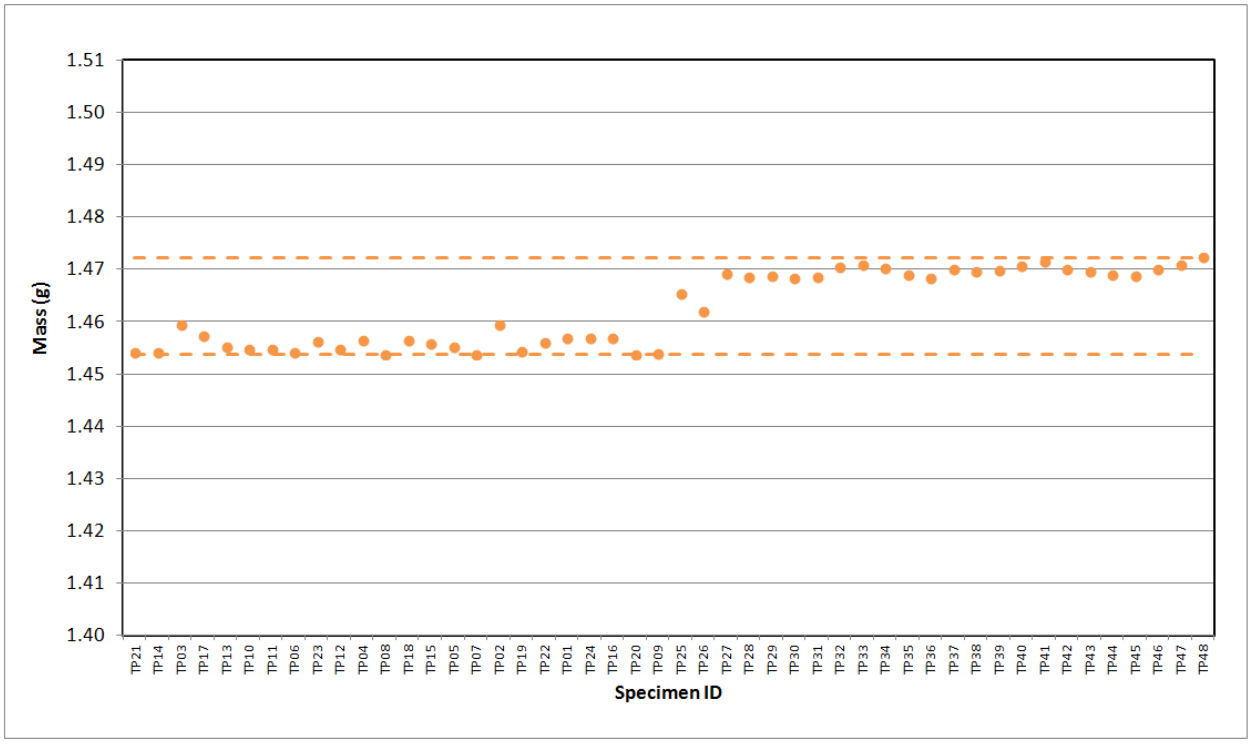

Figure A-73. 2114 Piggyback Pre Thermal Measurement Mass.

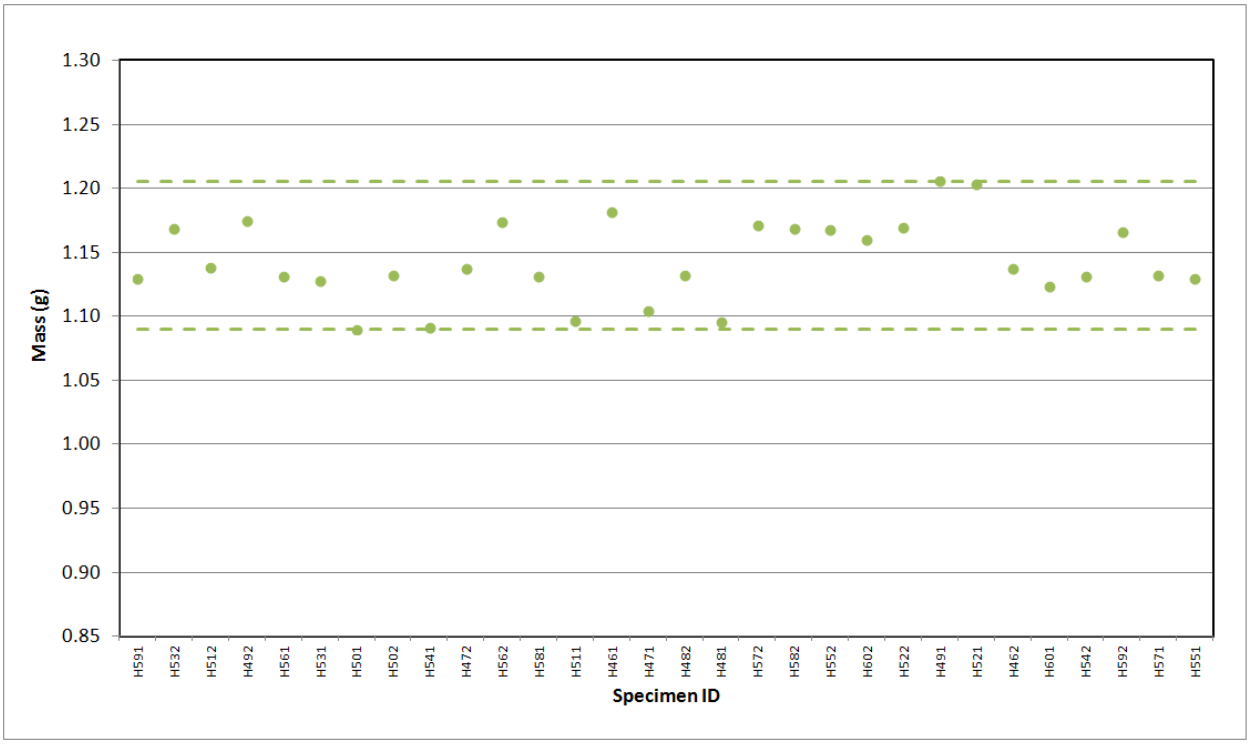

Figure A-74. A3 Matrix Piggyback Pre Thermal Measurement Mass.

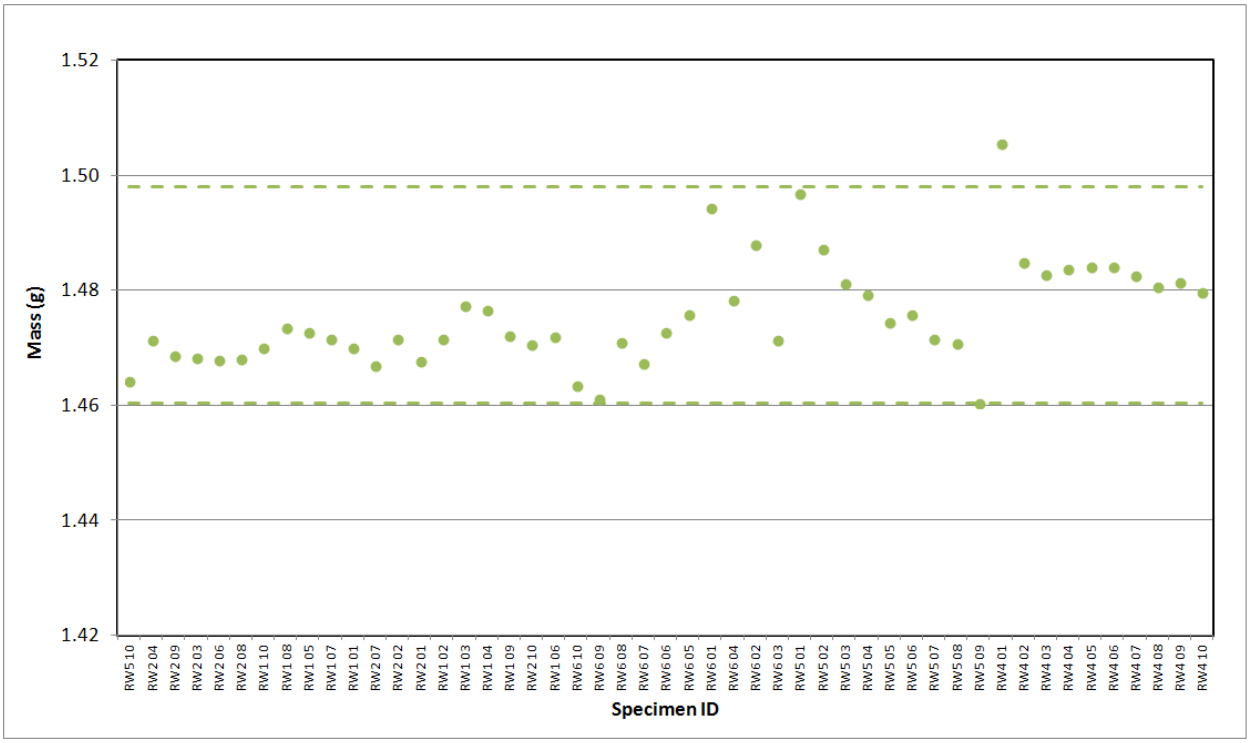

Figure A-75. BAN Piggyback Pre Thermal Measurement Mass.

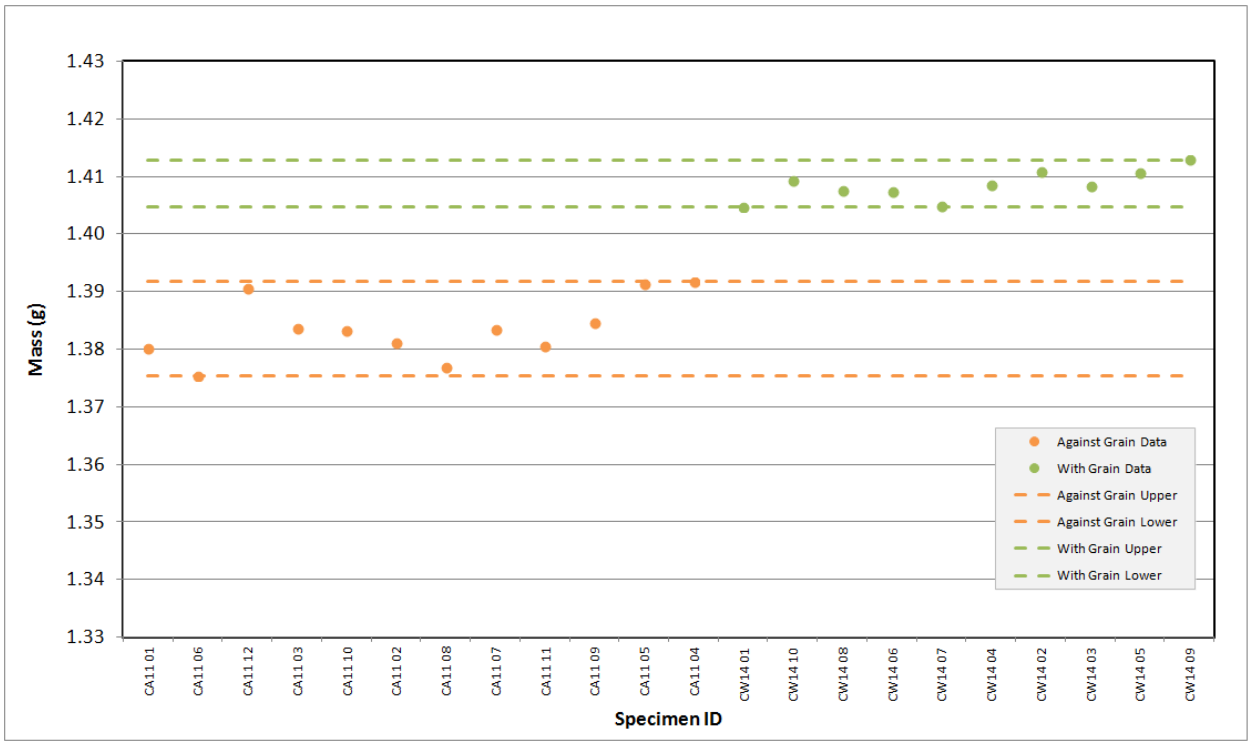

Figure A-76. H-451 Piggyback Pre Thermal Measurement Mass.

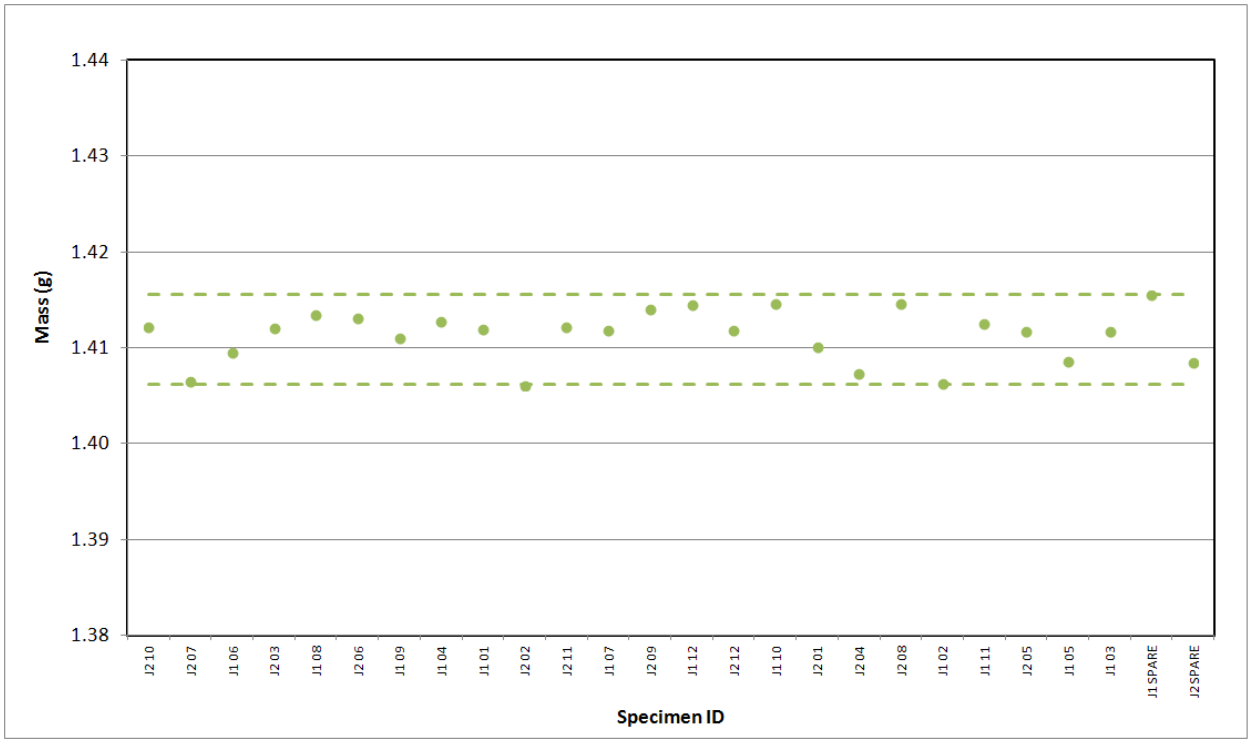

Figure A-77. HLM Piggyback Pre Thermal Measurement Mass.

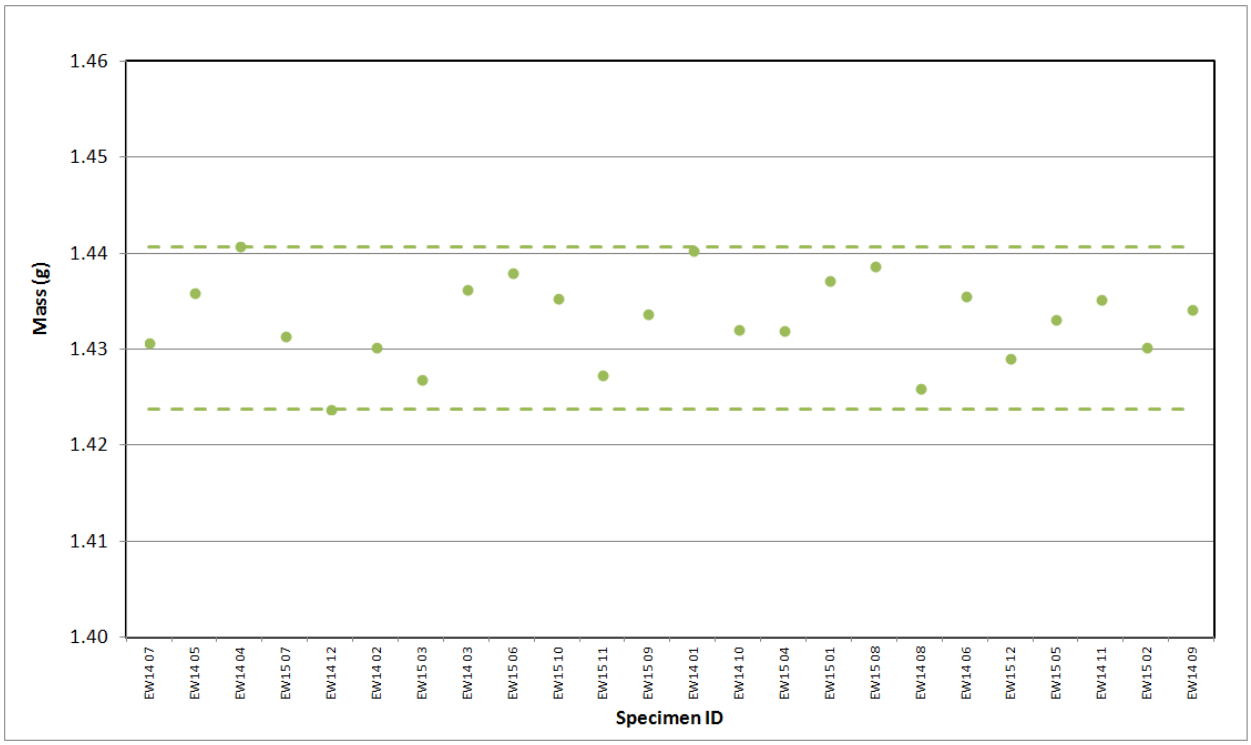

Figure A-78. IG-110 Piggyback Pre Thermal Measurement Mass.

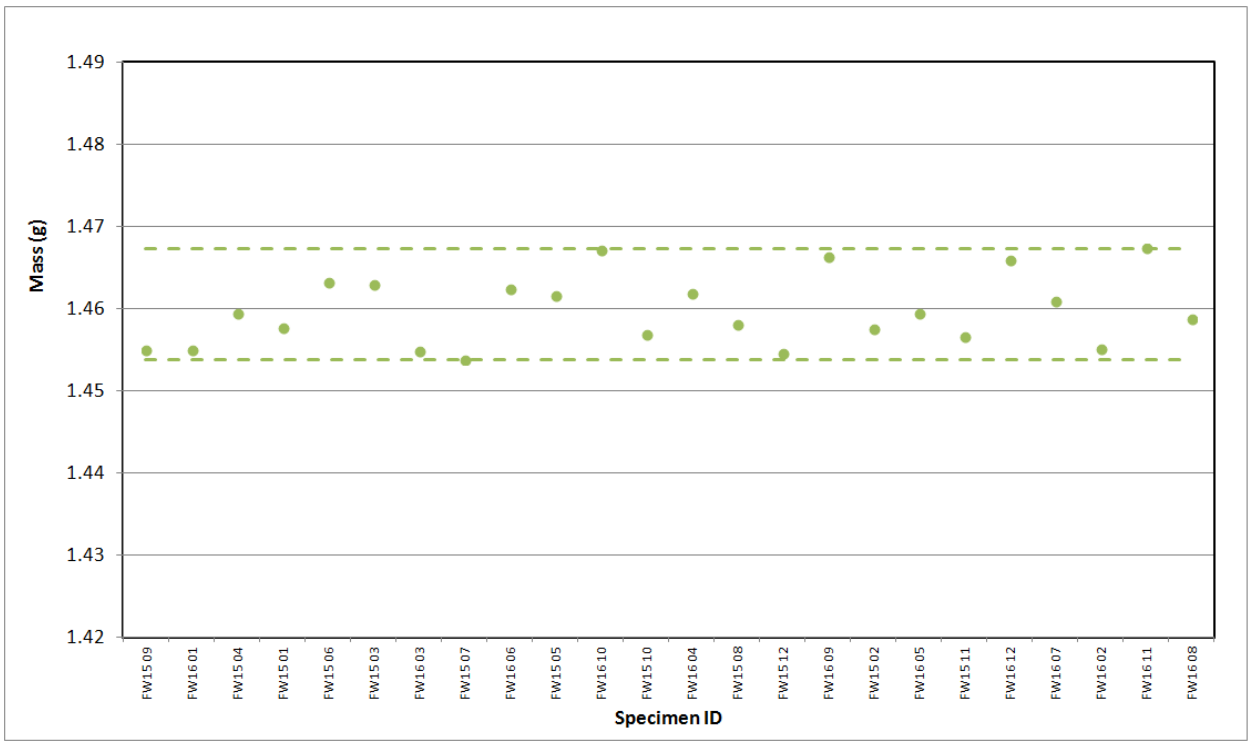

Figure A-79. IG-430 Piggyback Pre Thermal Measurement Mass.

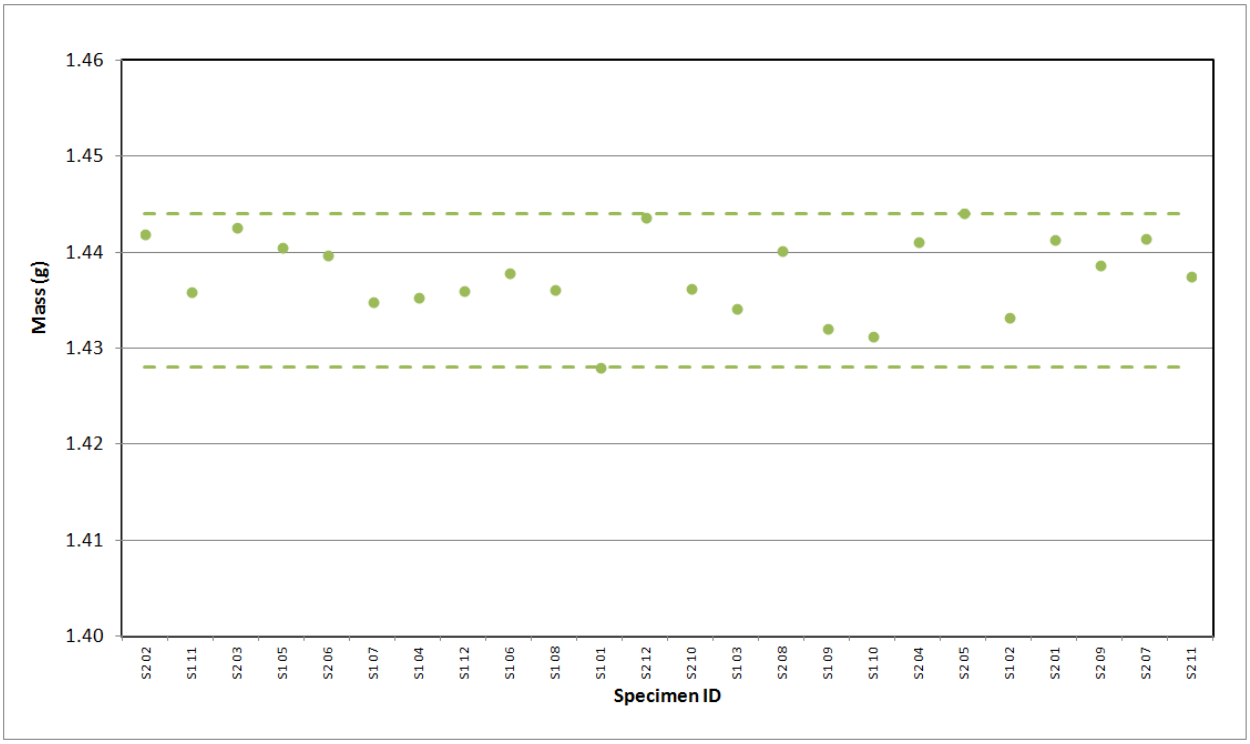

Figure A-80. NBG-10 Piggyback Pre Thermal Measurement Mass.

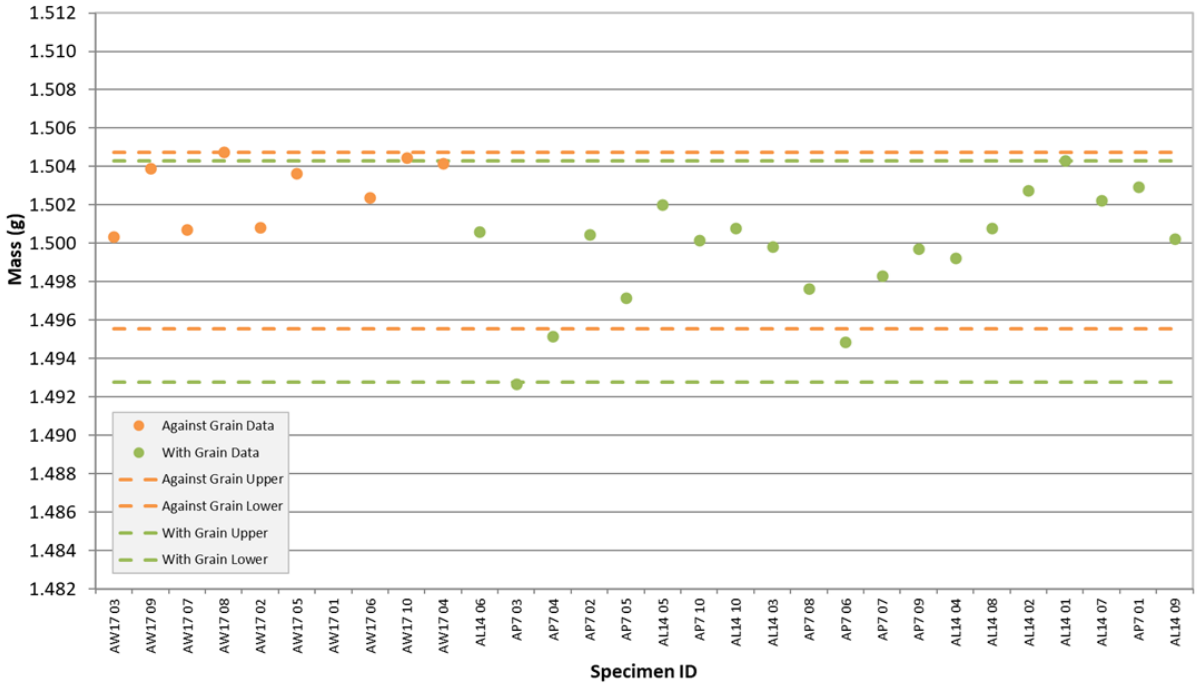

Figure A-81. NBG-17 Piggyback Pre Thermal Measurement Mass.

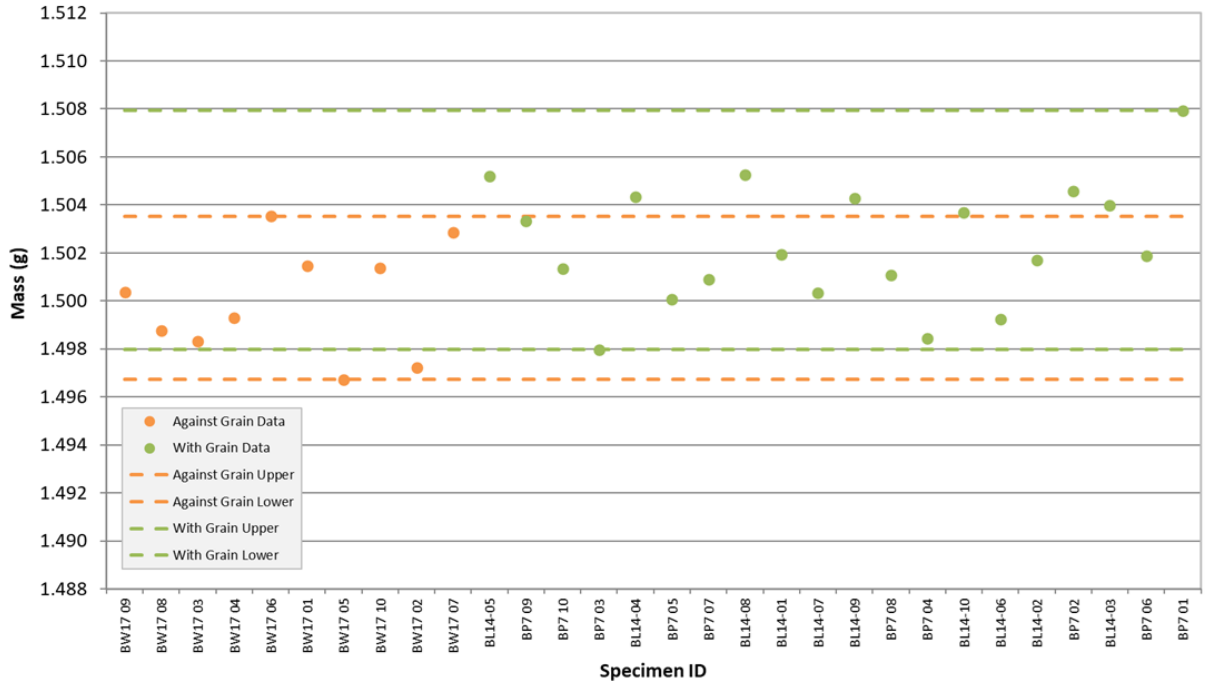

Figure A-82. NBG-18 Piggyback Pre Thermal Measurement Mass.

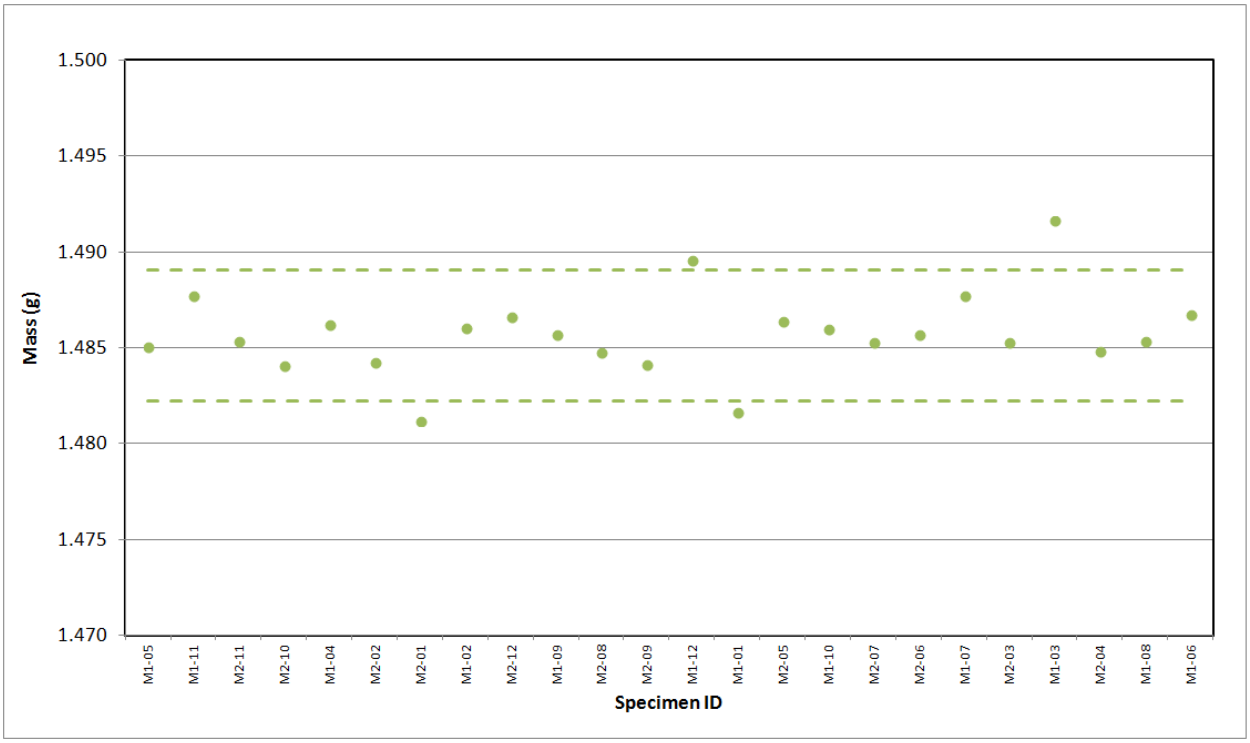

Figure A-83. NBG-25 Piggyback Pre Thermal Measurement Mass.

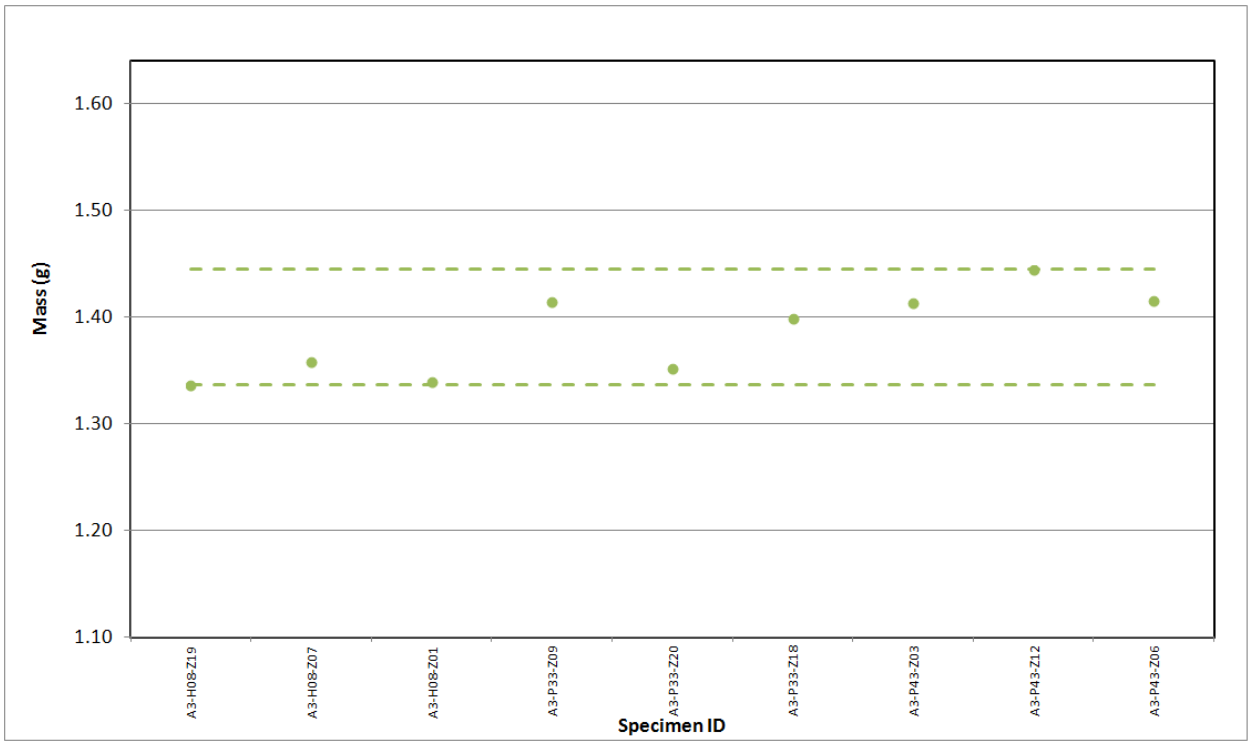

Figure A-84. New Matrix Piggyback Pre Thermal Measurement Mass.

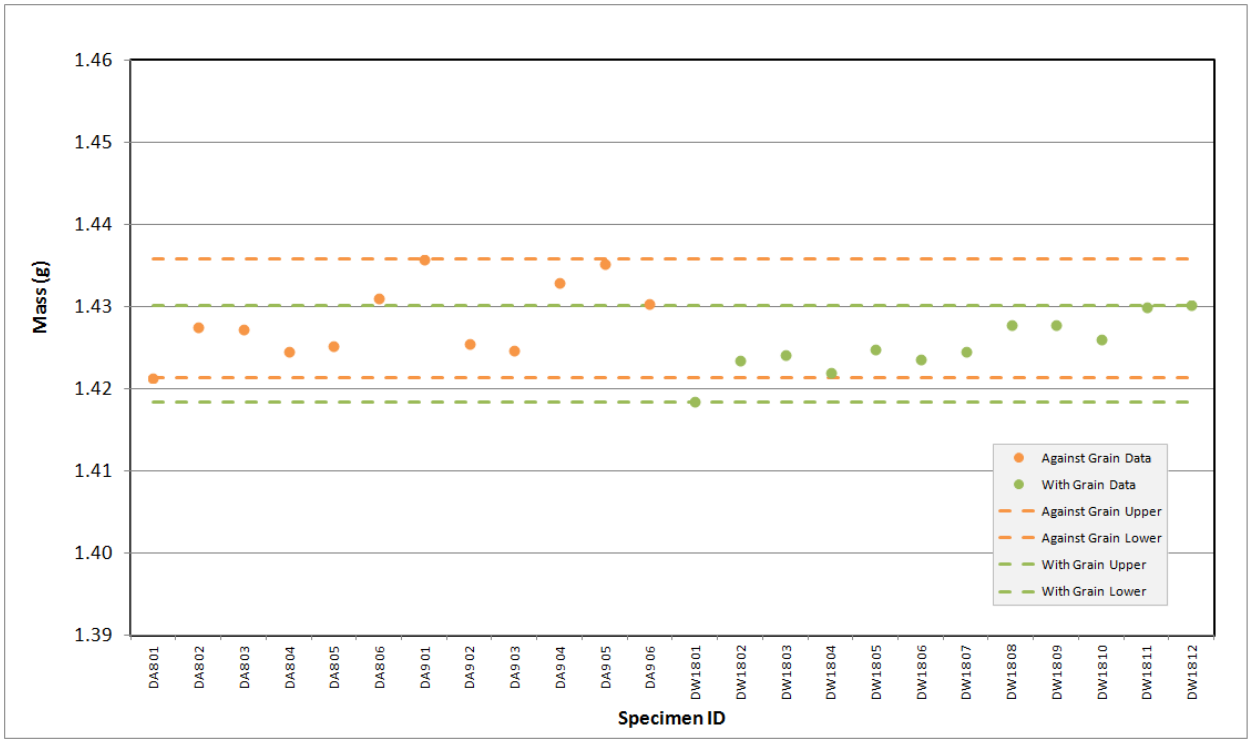

Figure A-85. PCEA Piggyback Pre Thermal Measurement Mass.

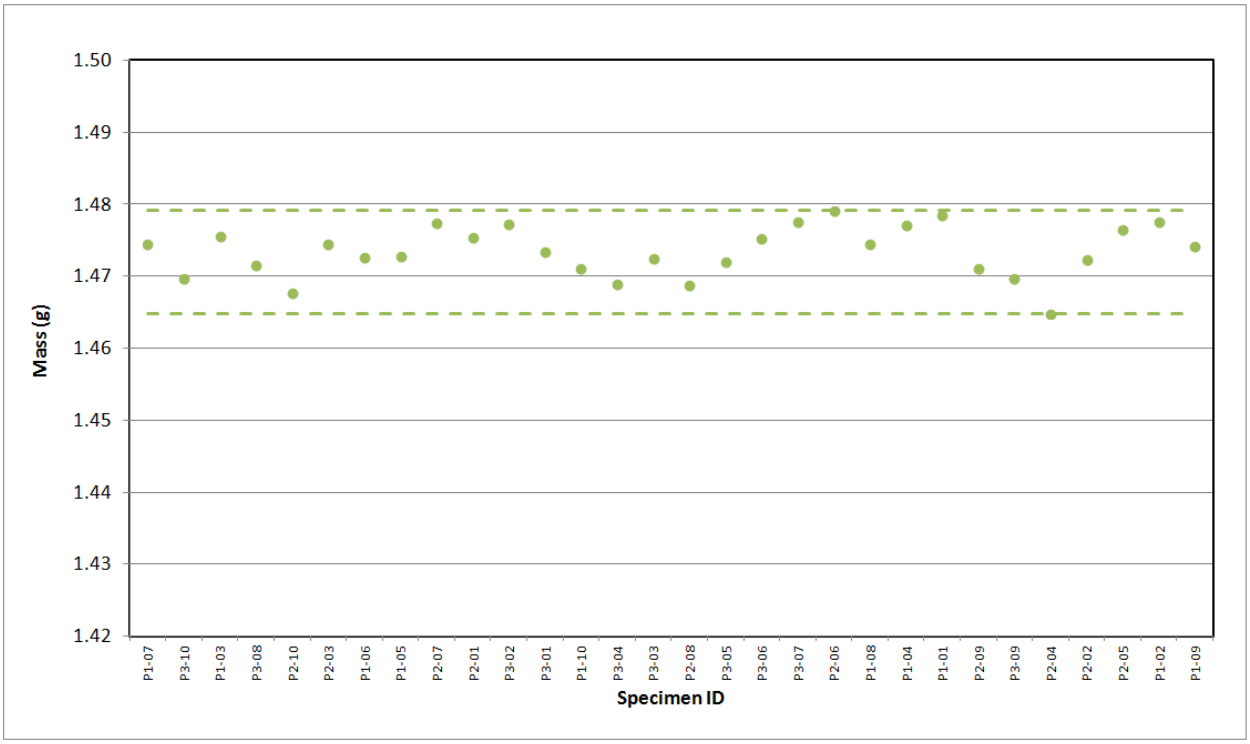

Figure A-86. PCIB Piggyback Pre Thermal Measurement Mass.

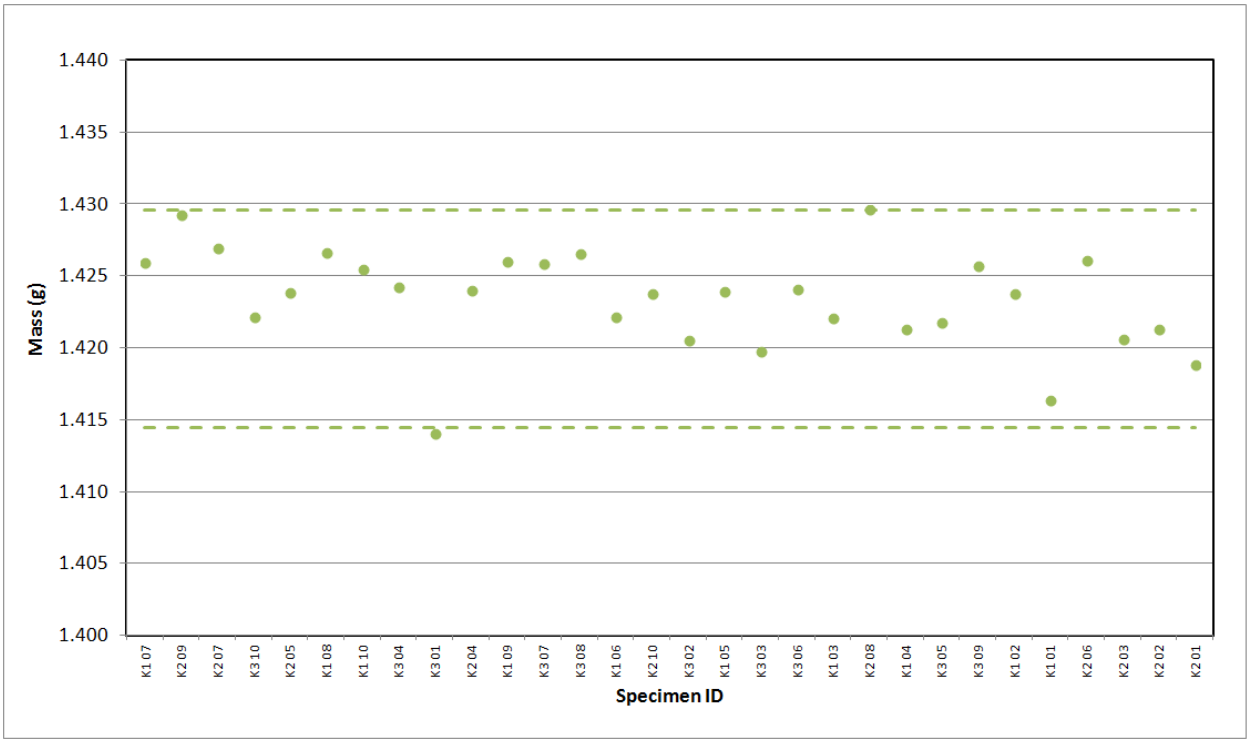

Figure A-87. PGX Piggyback Pre Thermal Measurement Mass.

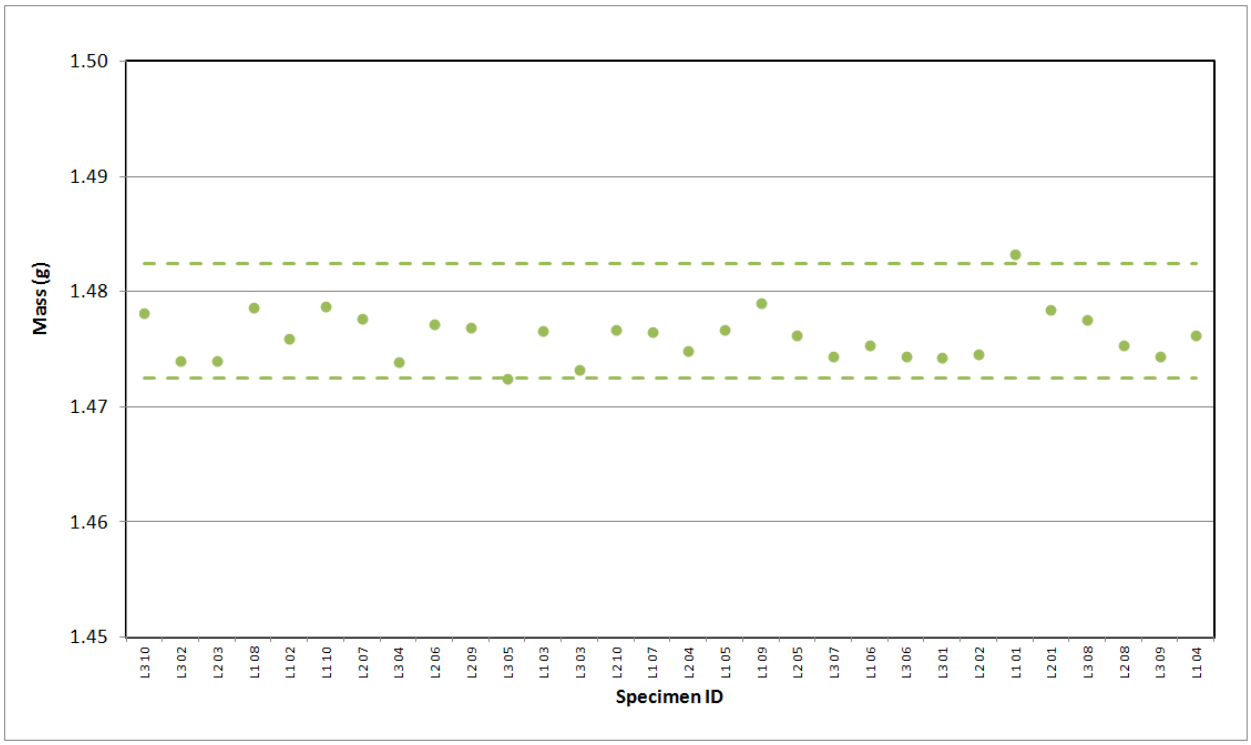

Figure A-88. PPEA Piggyback Pre Thermal Measurement Mass.

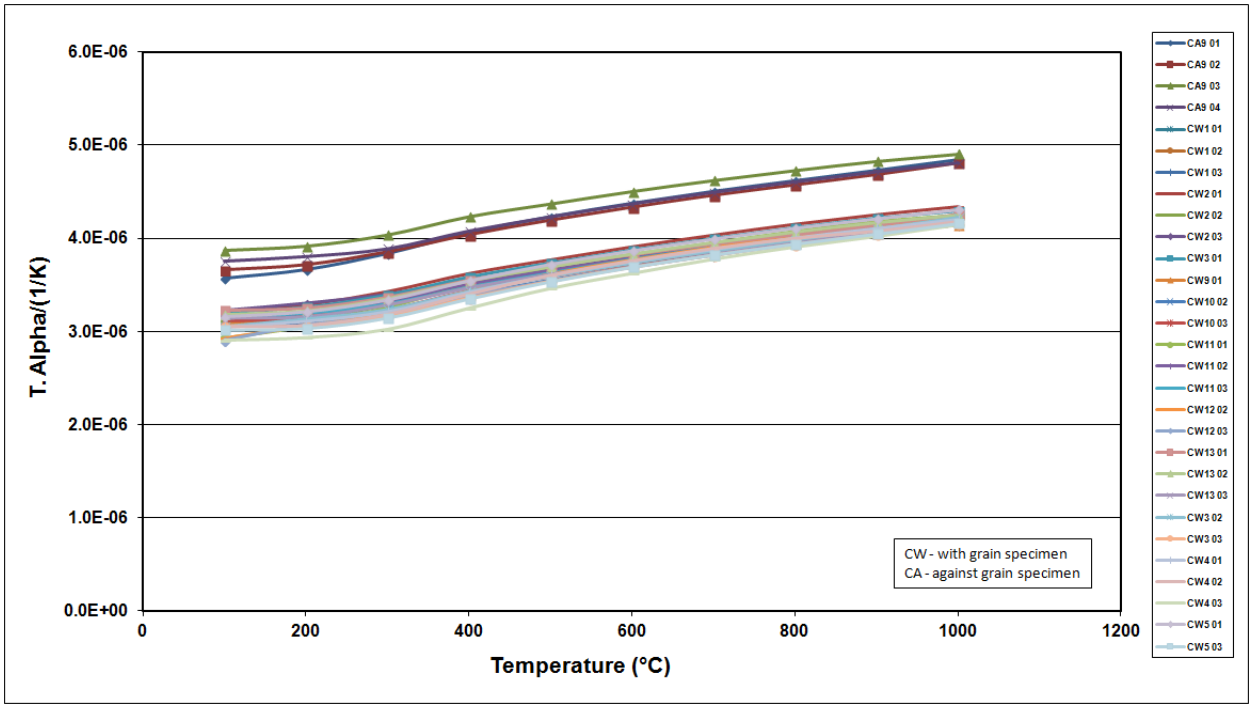

Figure A-89. H-451 Creep Coefficient of Thermal Expansion.

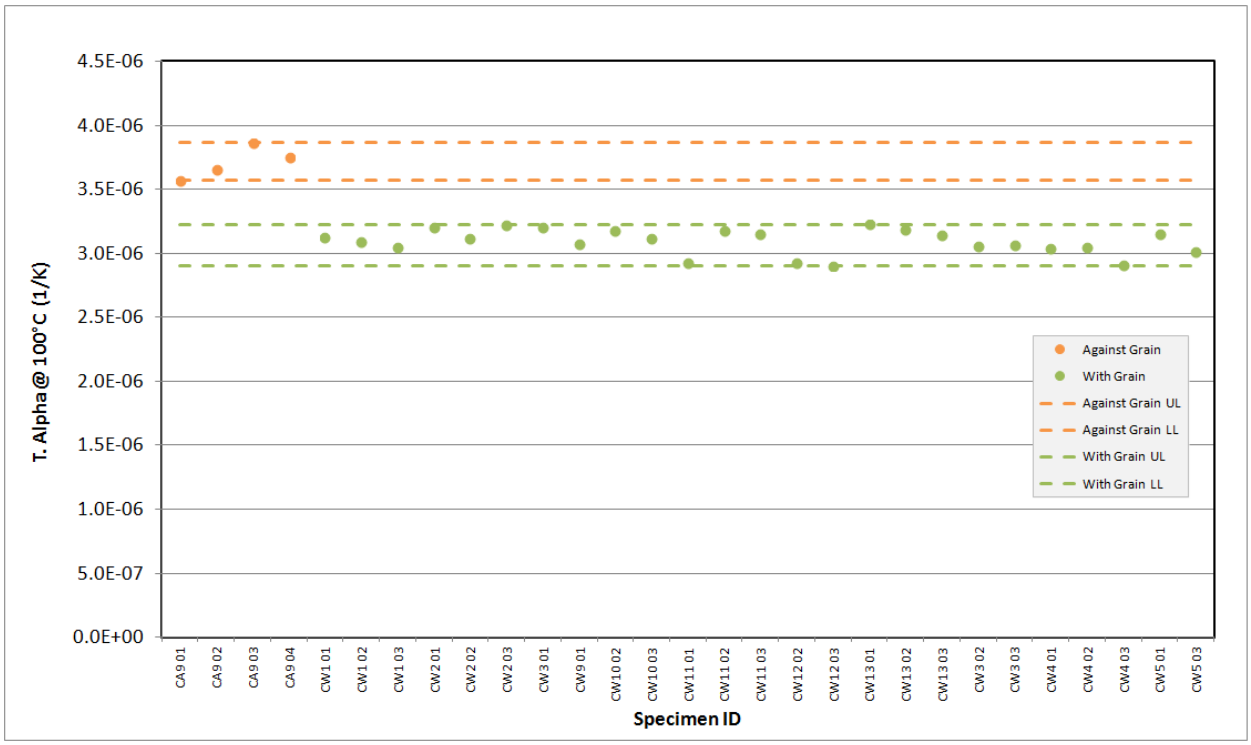

Figure A-90. H-451 Creep Coefficient of Thermal Expansion @ 100°C.

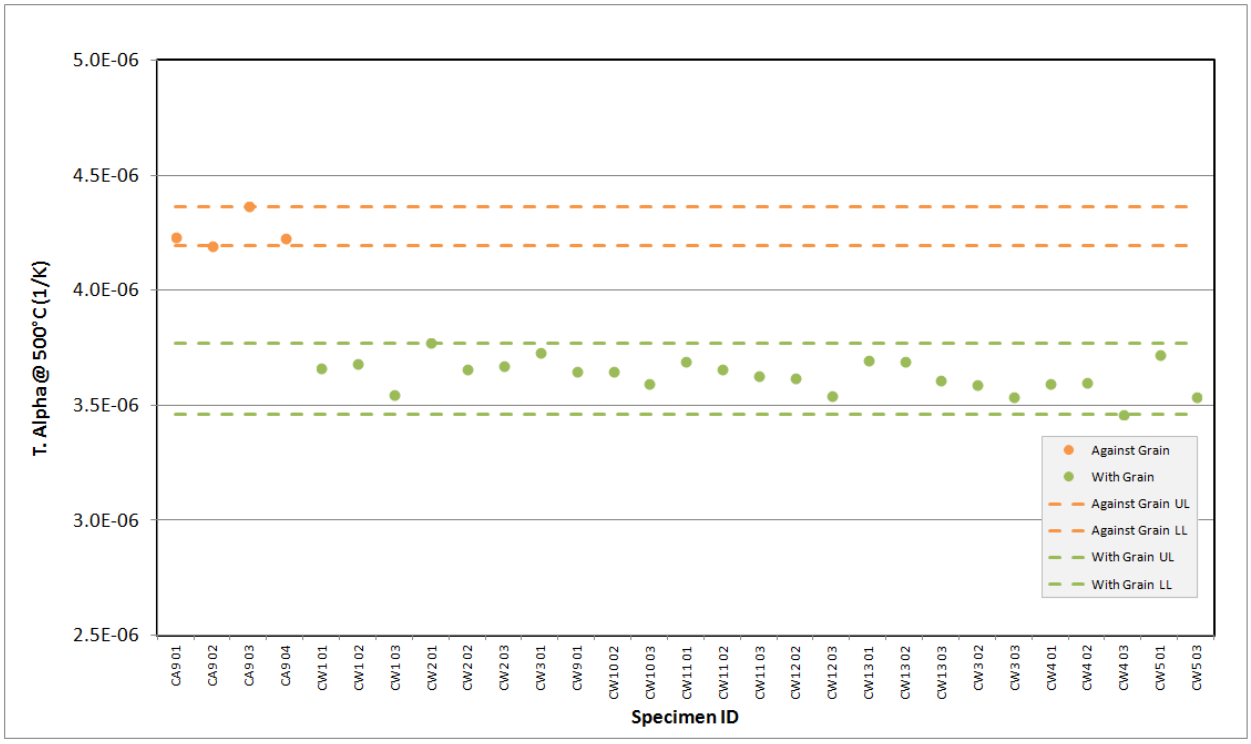

Figure A-91. H-451 Creep Coefficient of Thermal Expansion @ 500°C.

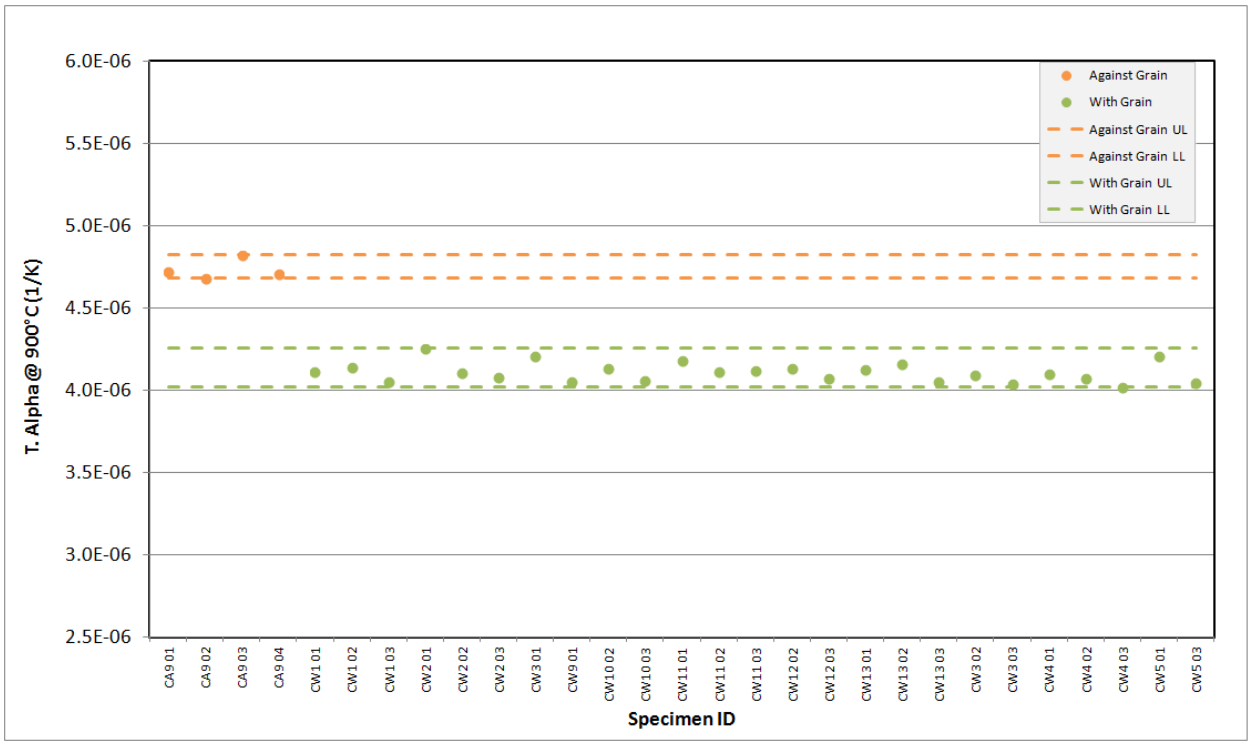

Figure A-92. H-451 Creep Coefficient of Thermal Expansion @ 900°C.

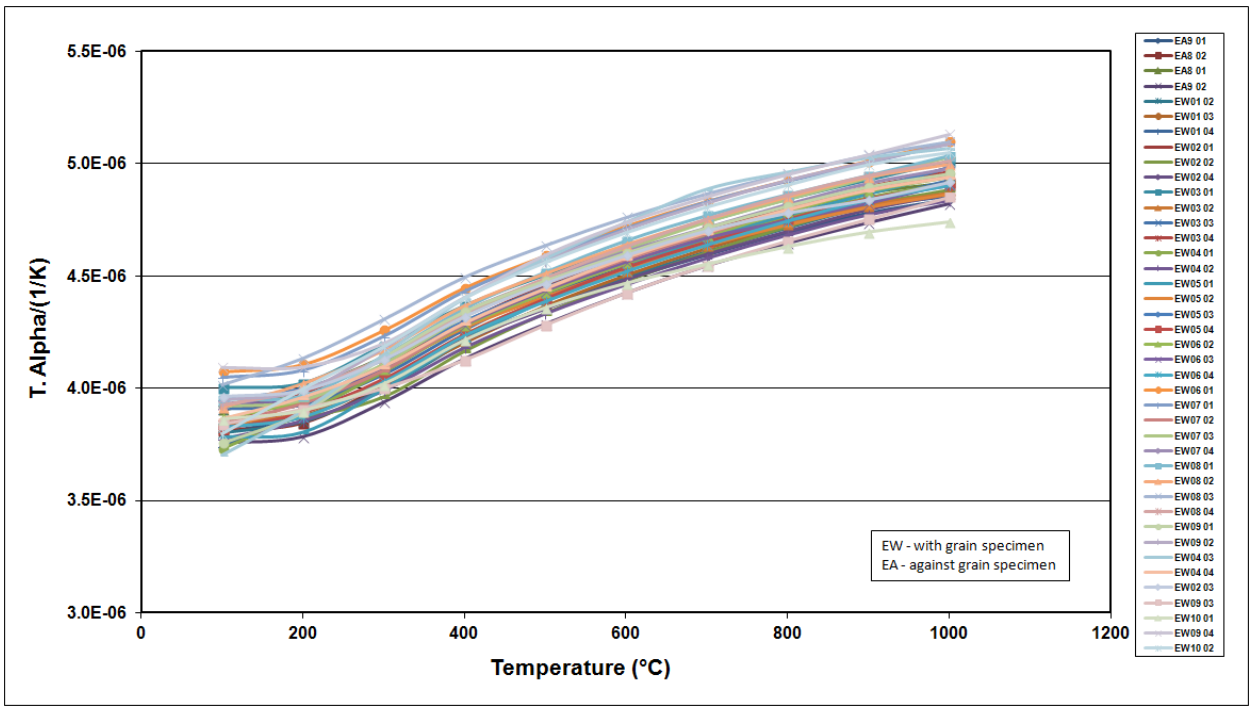

Figure A-93. IG-110 Creep Coefficient of Thermal Expansion.

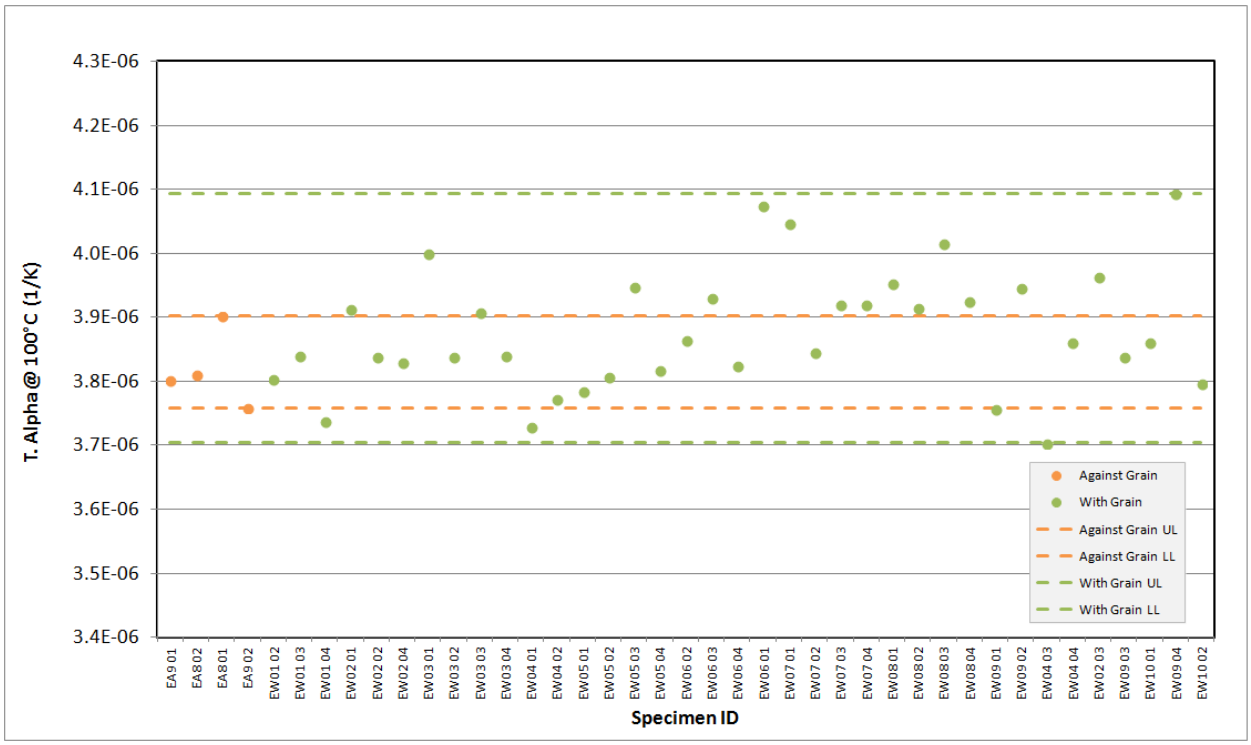

Figure A-94. IG-110 Creep Coefficient of Thermal Expansion @ 100°C.

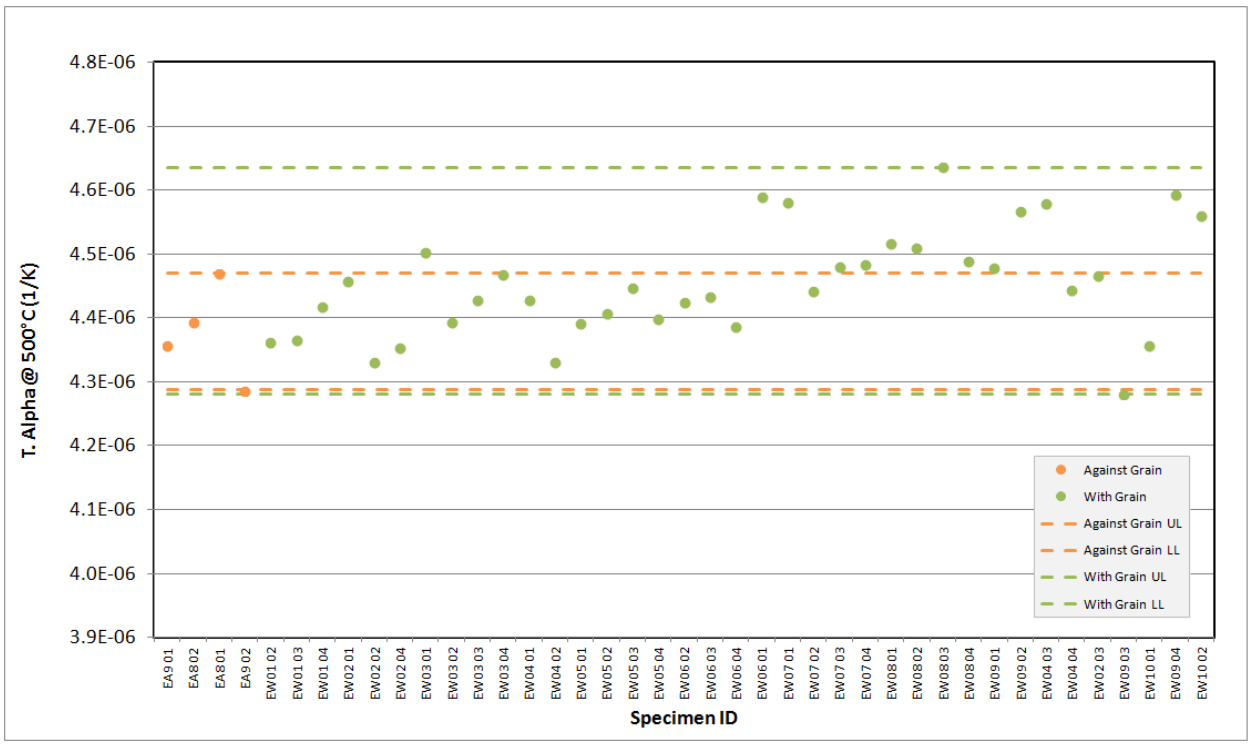

Figure A-95. IG-110 Creep Coefficient of Thermal Expansion @ 500°C.

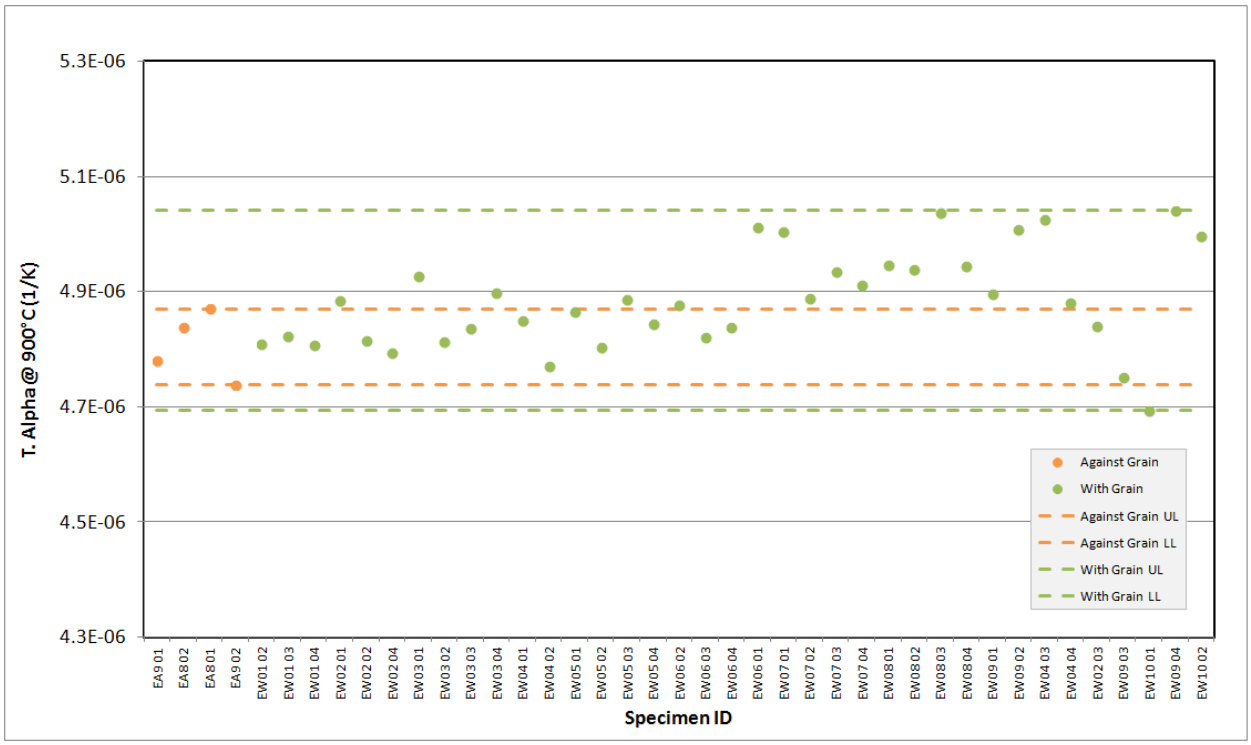

Figure A-96. IG-110 Creep Coefficient of Thermal Expansion @ 900°C.

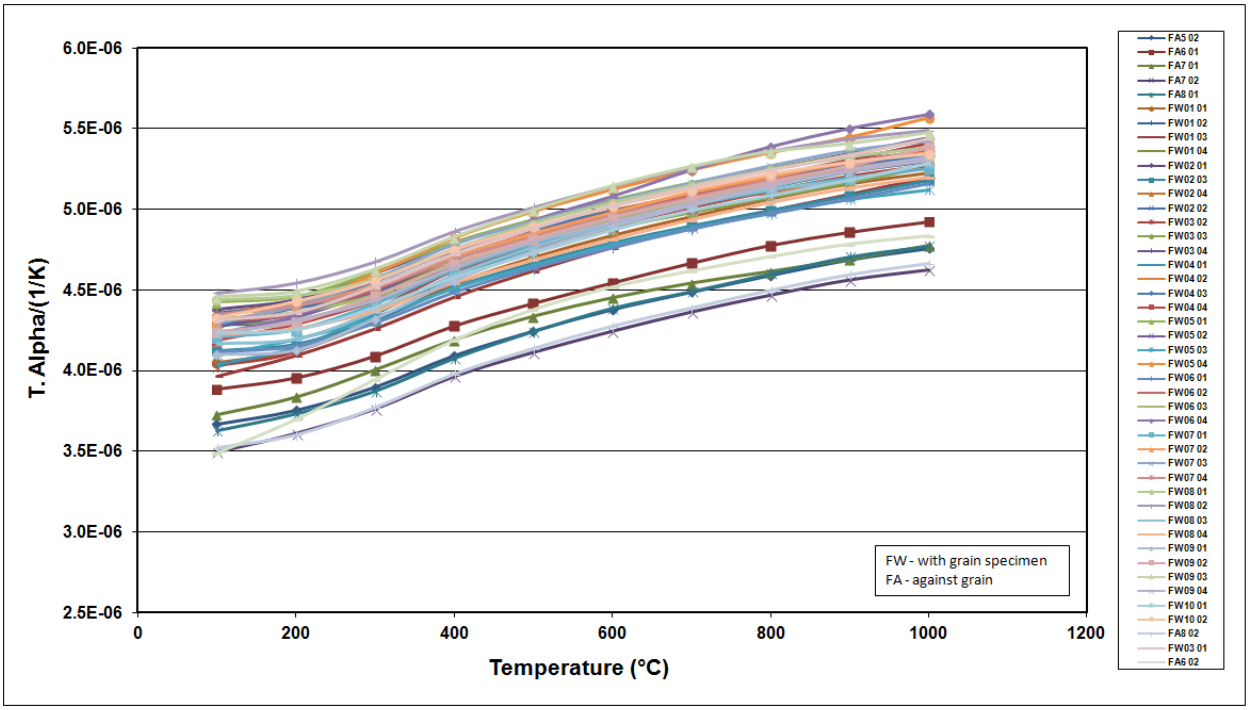

Figure A-97. IG-430 Creep Coefficient of Thermal Expansion.

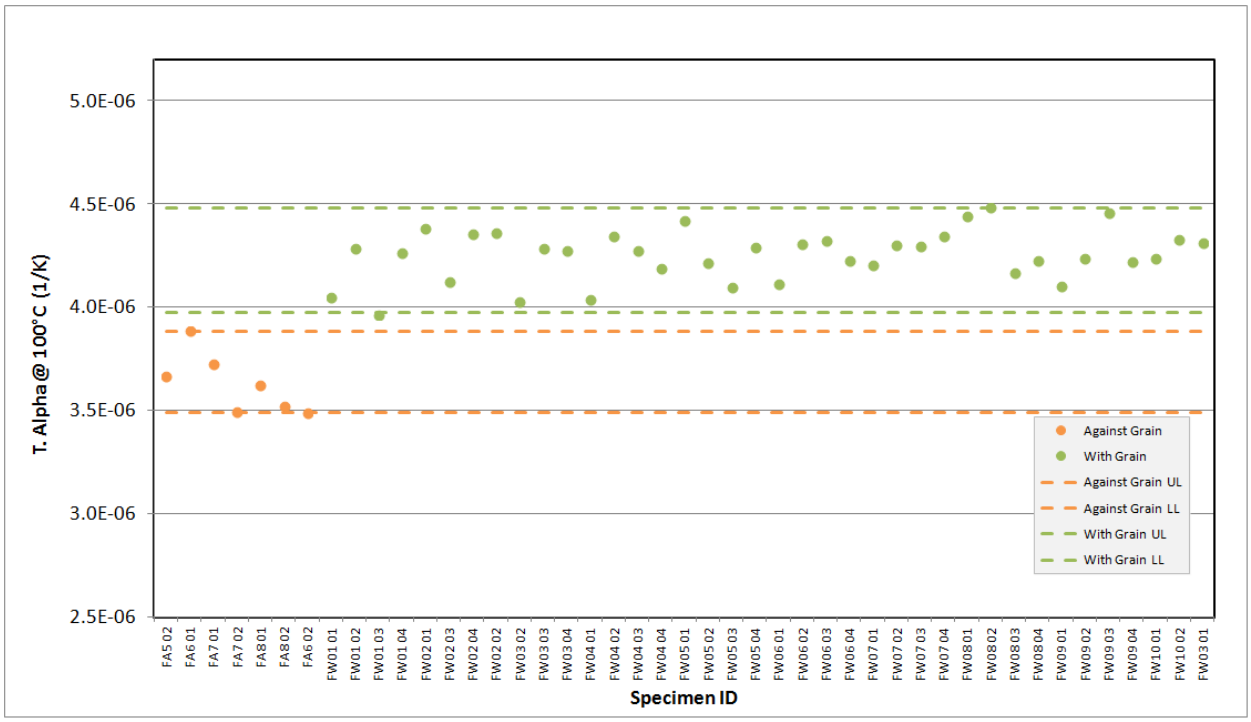

Figure A-98. IG-430 Creep Coefficient of Thermal Expansion @ 100°C.

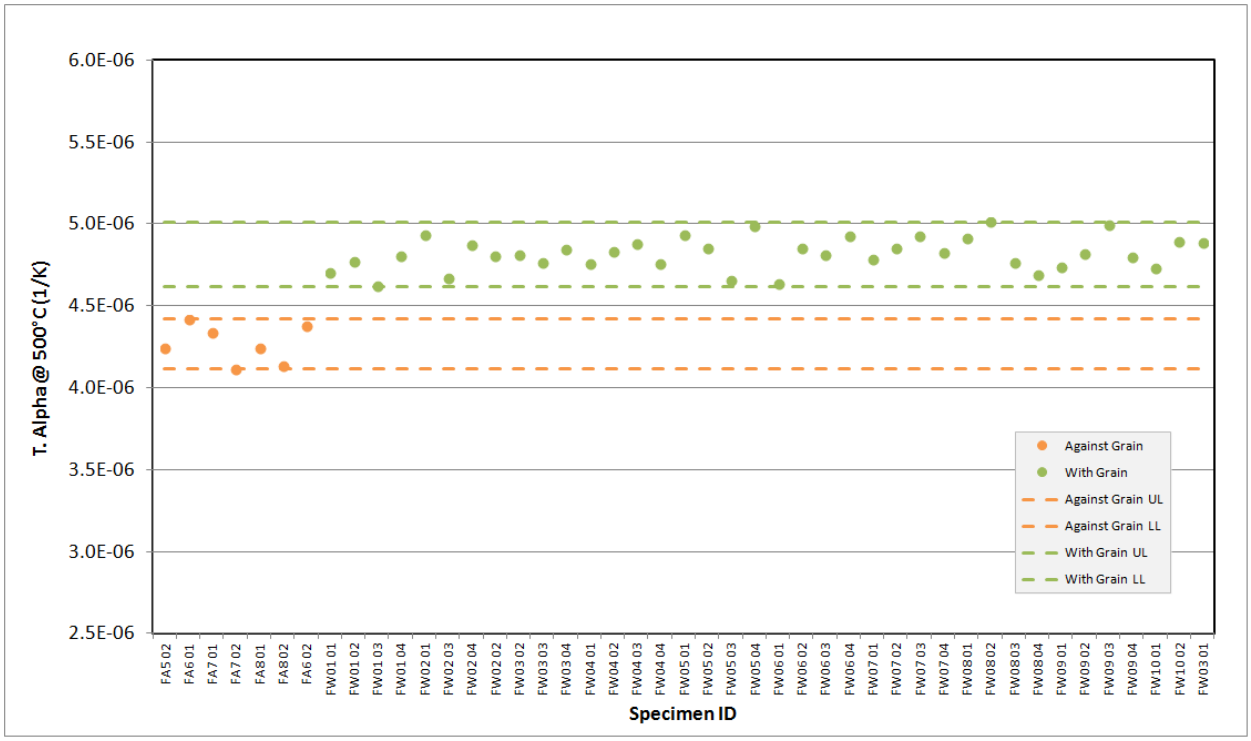

Figure A-99. IG-430 Creep Coefficient of Thermal Expansion @ 500°C.

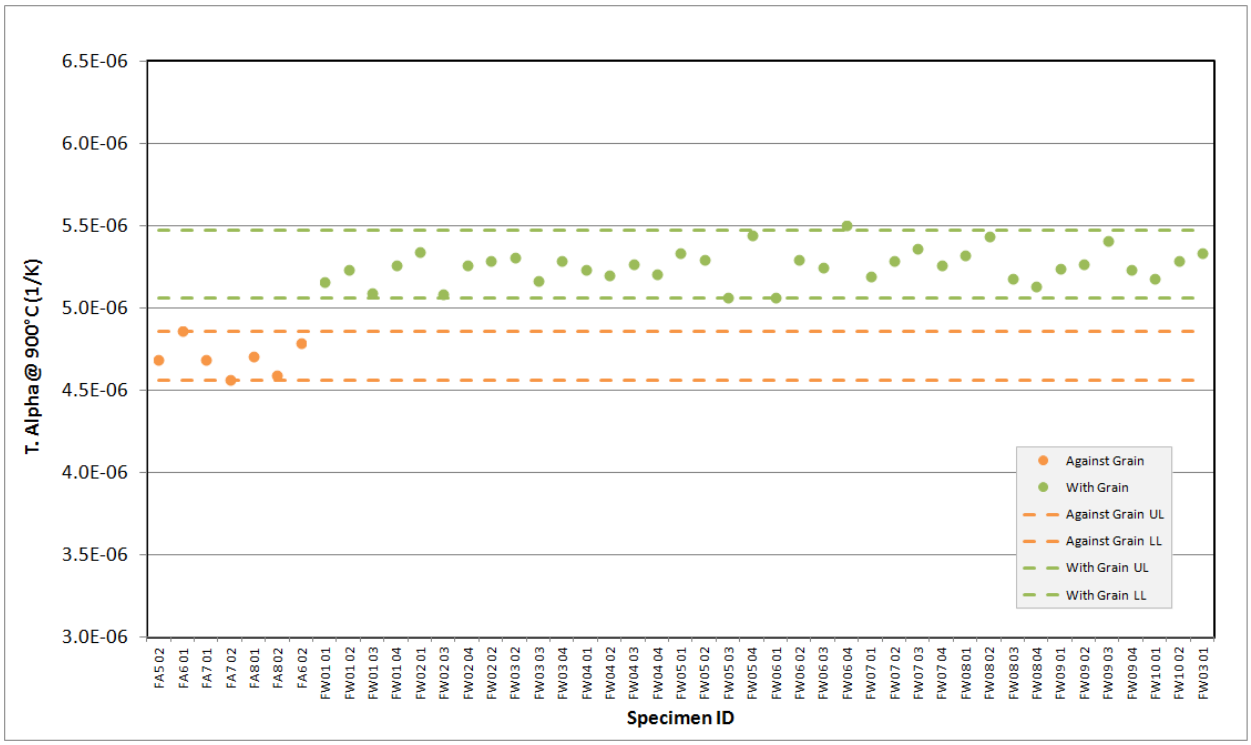

Figure A-100. IG-430 Creep Coefficient of Thermal Expansion @ 900°C.

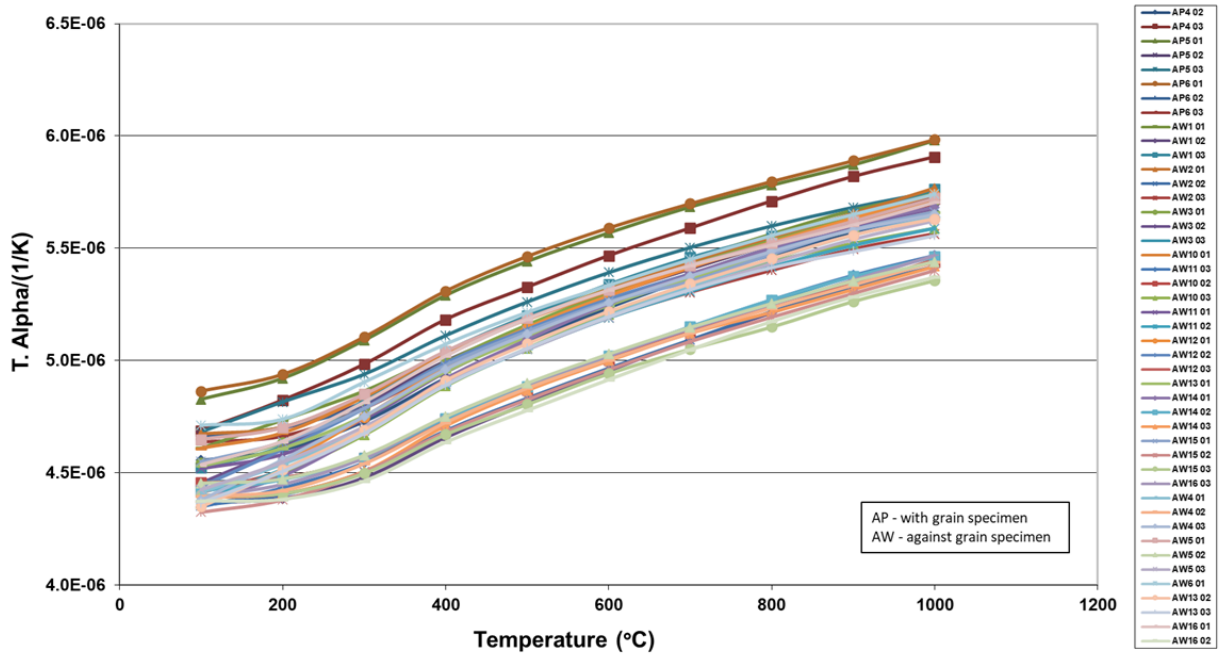

Figure A-101. NBG-17 Creep Coefficient of Thermal Expansion.

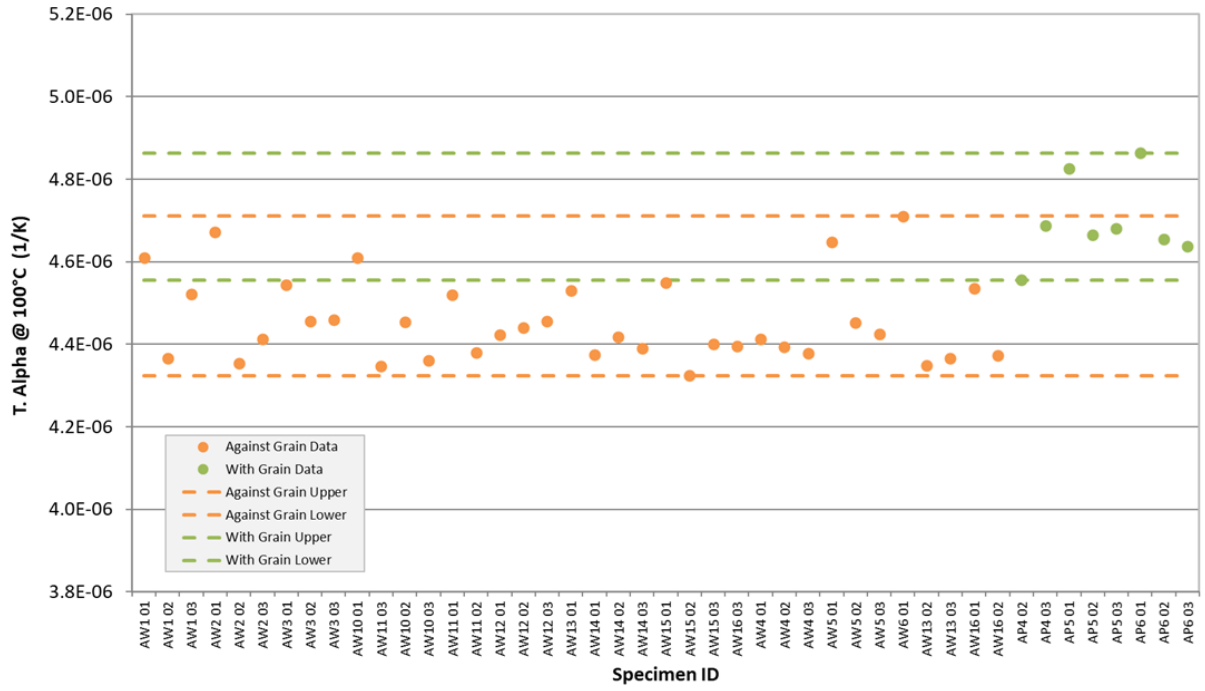

Figure A-102. NBG-17 Creep Coefficient of Thermal Expansion @ 100°C.

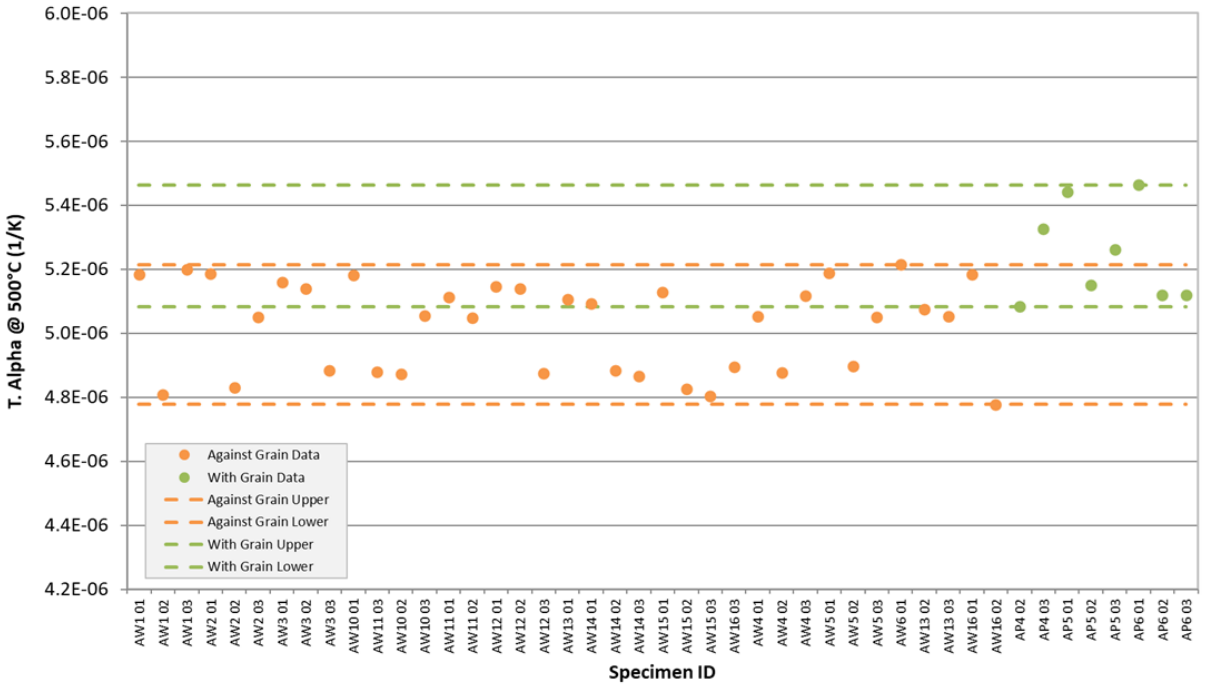

Figure A-103. NBG-17 Creep Coefficient of Thermal Expansion @ 500°C.

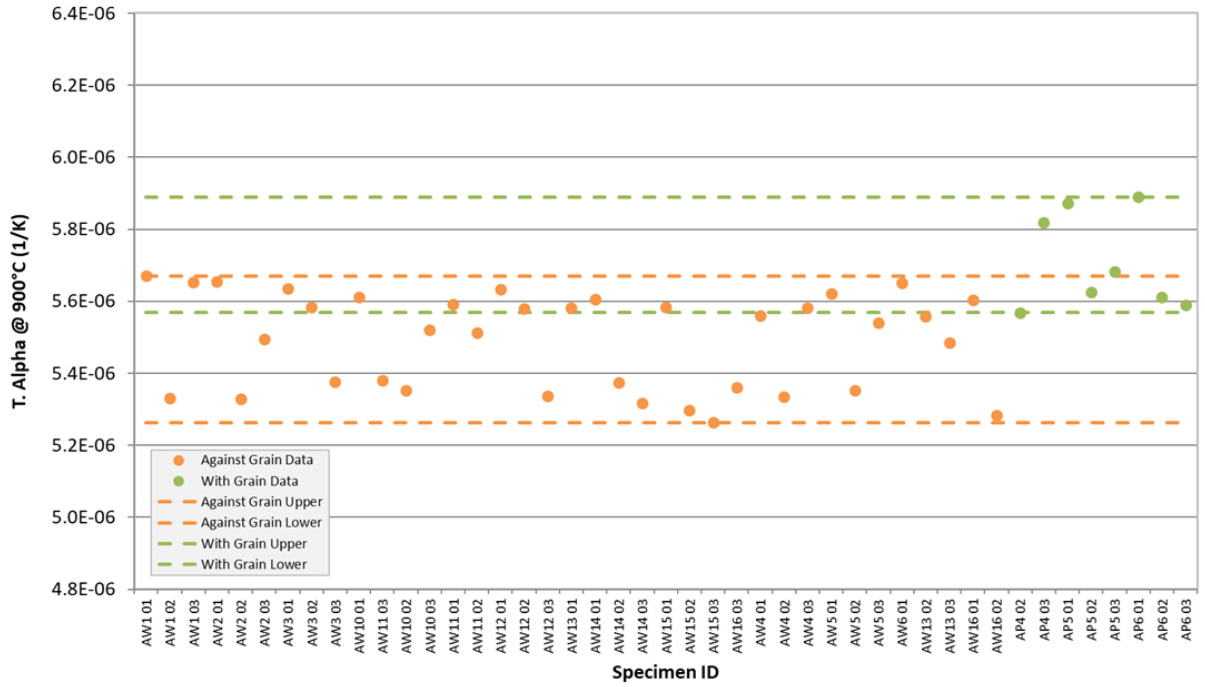

Figure A-104. NBG-17 Creep Coefficient of Thermal Expansion @ 900°C.

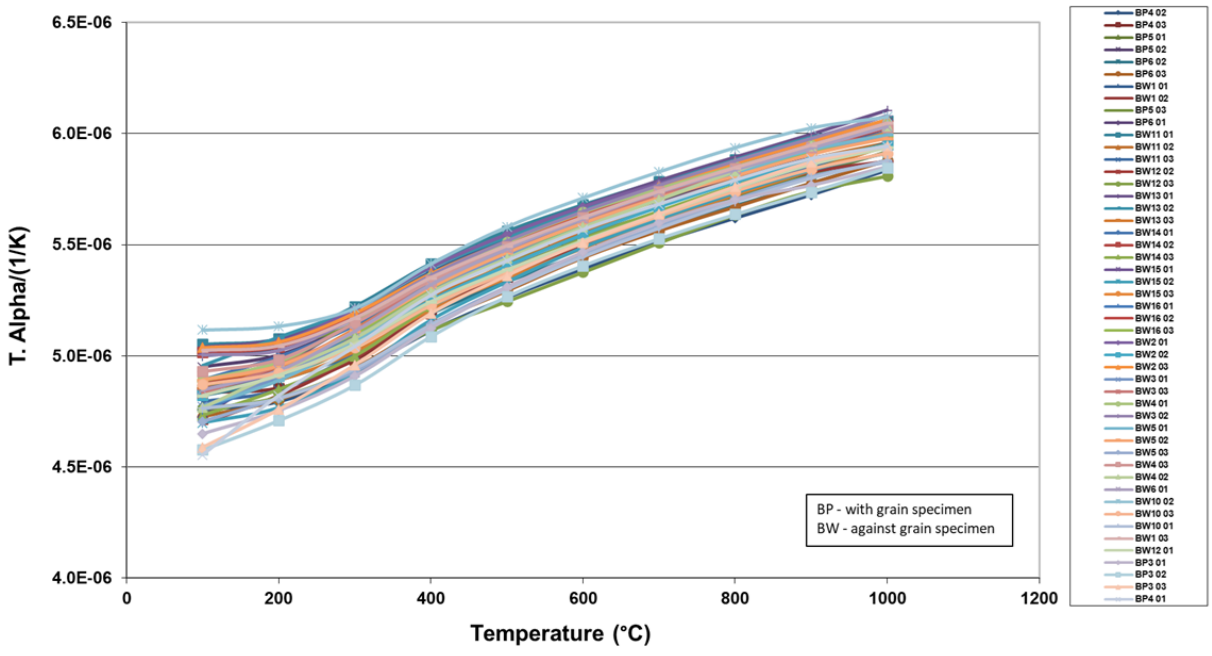

Figure A-105. NBG-18 Creep Coefficient of Thermal Expansion.

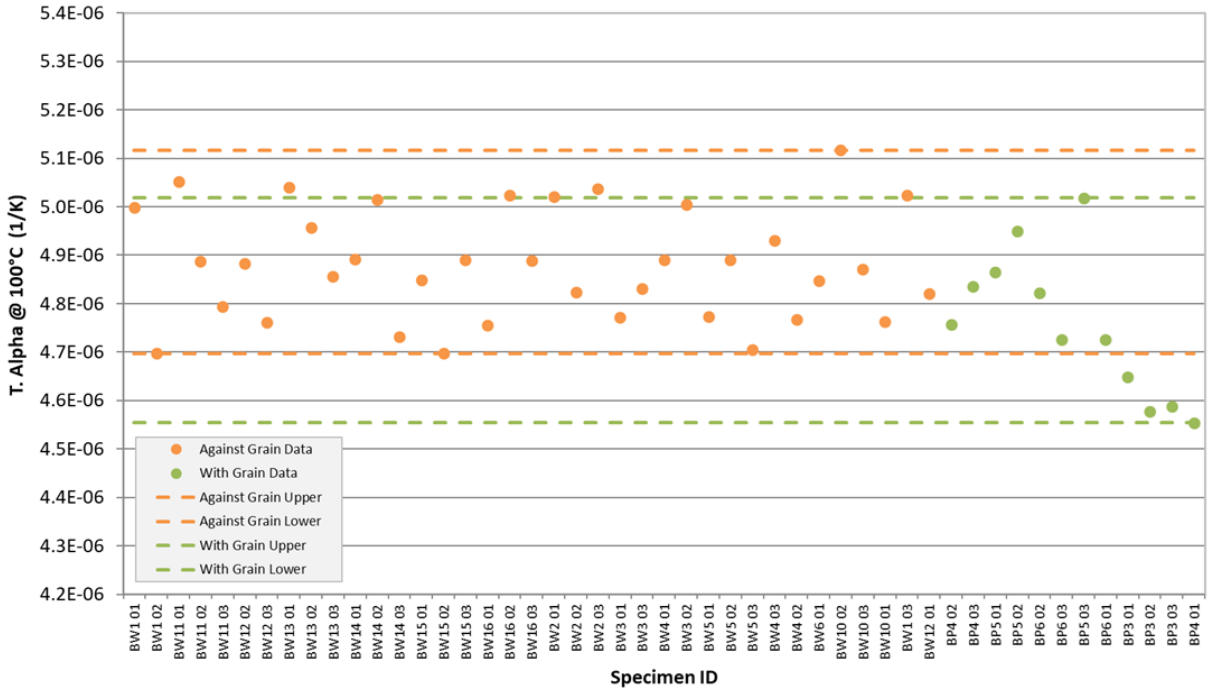

Figure A-106. NBG-18 Creep Coefficient of Thermal Expansion @ 100°C.

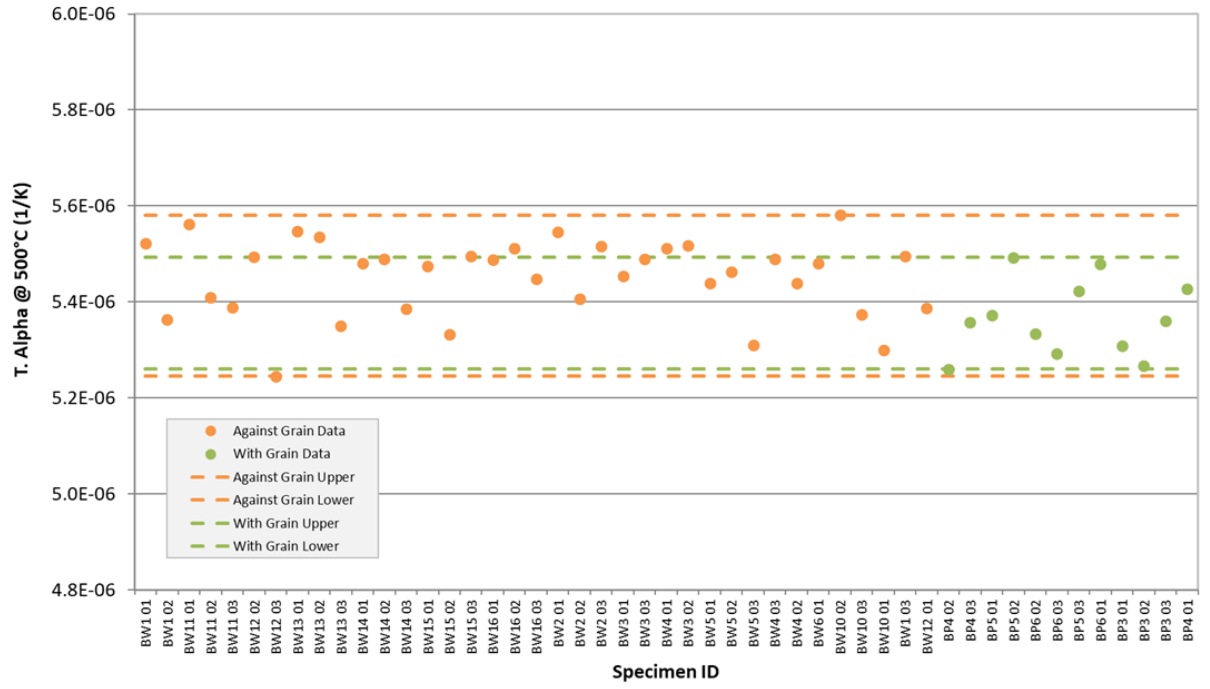

Figure A-107. NBG-18 Creep Coefficient of Thermal Expansion @ 500°C.

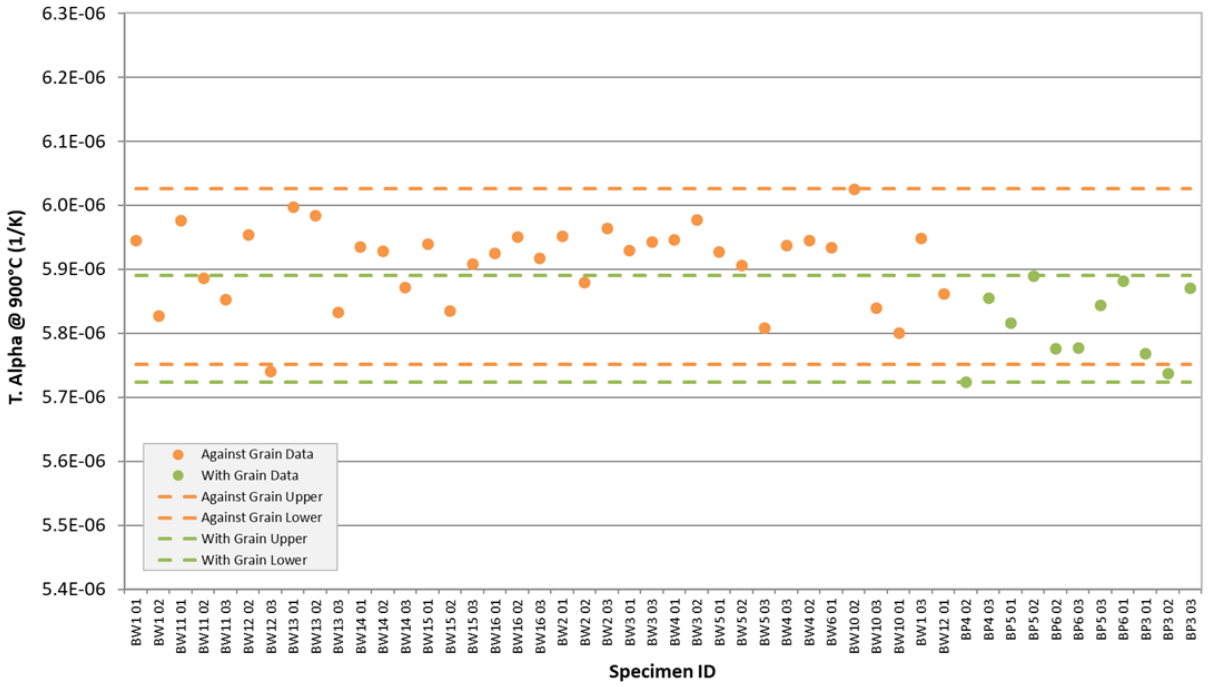

Figure A-108. NBG-18 Creep Coefficient of Thermal Expansion @ 900°C.

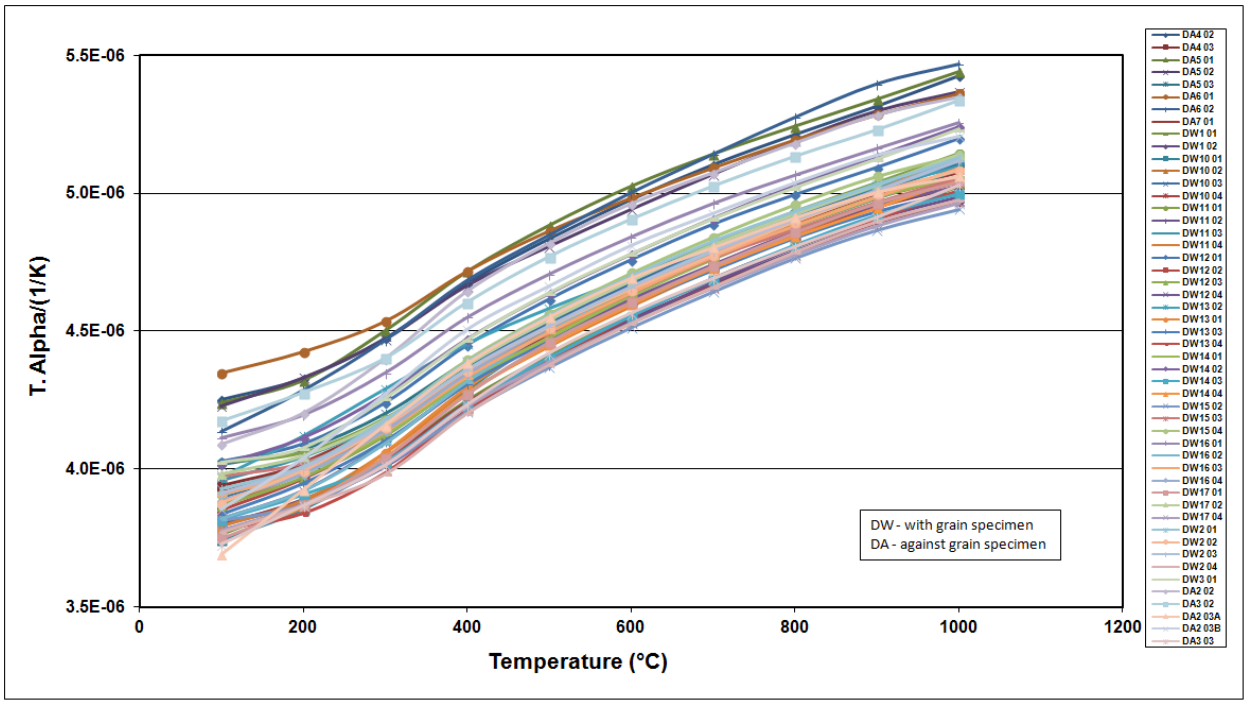

Figure A-109. PCEA Creep Coefficient of Thermal Expansion.

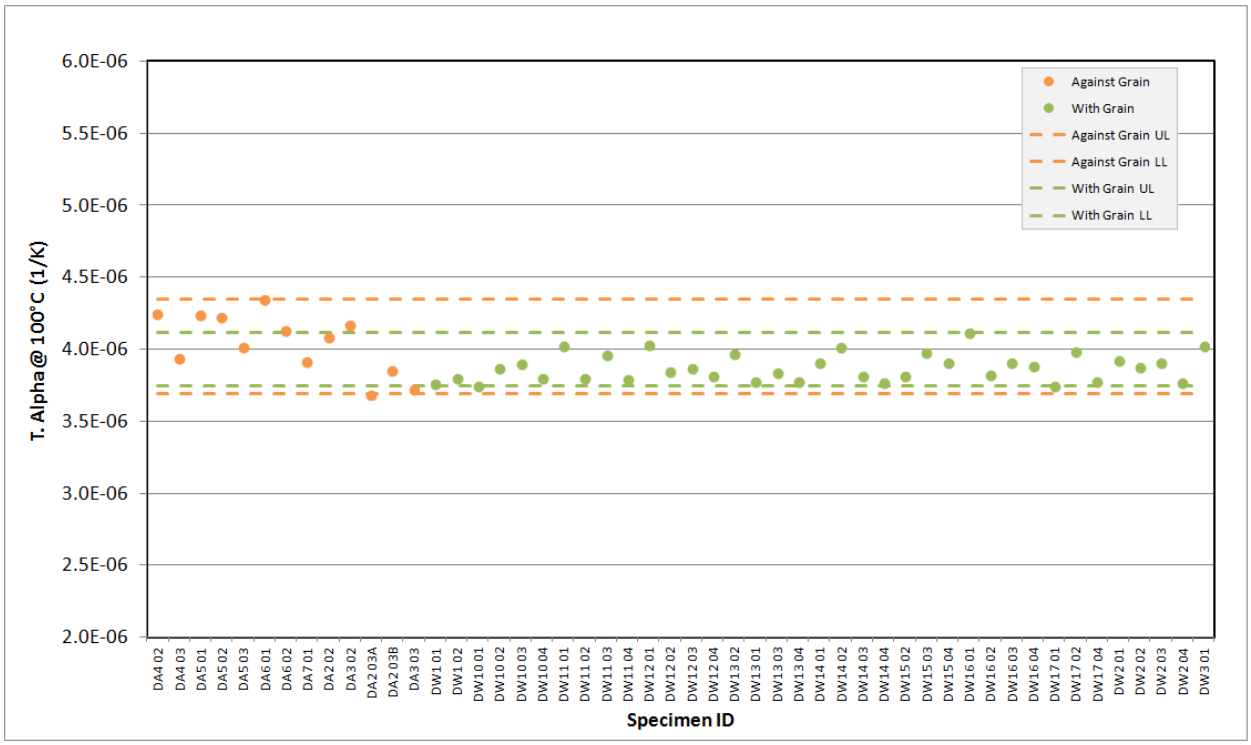

Figure A-110. PCEA Creep Coefficient of Thermal Expansion @ 100°C.

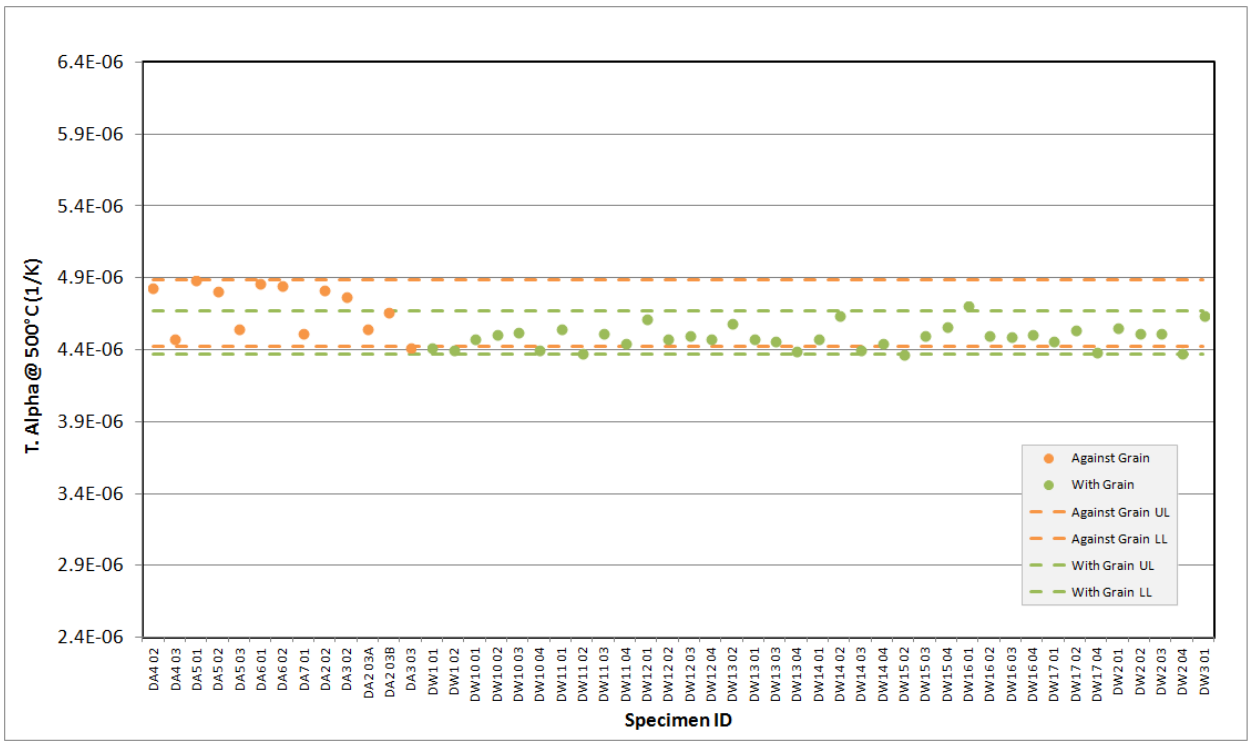

Figure A-111. PCEA Creep Coefficient of Thermal Expansion @ 500°C.

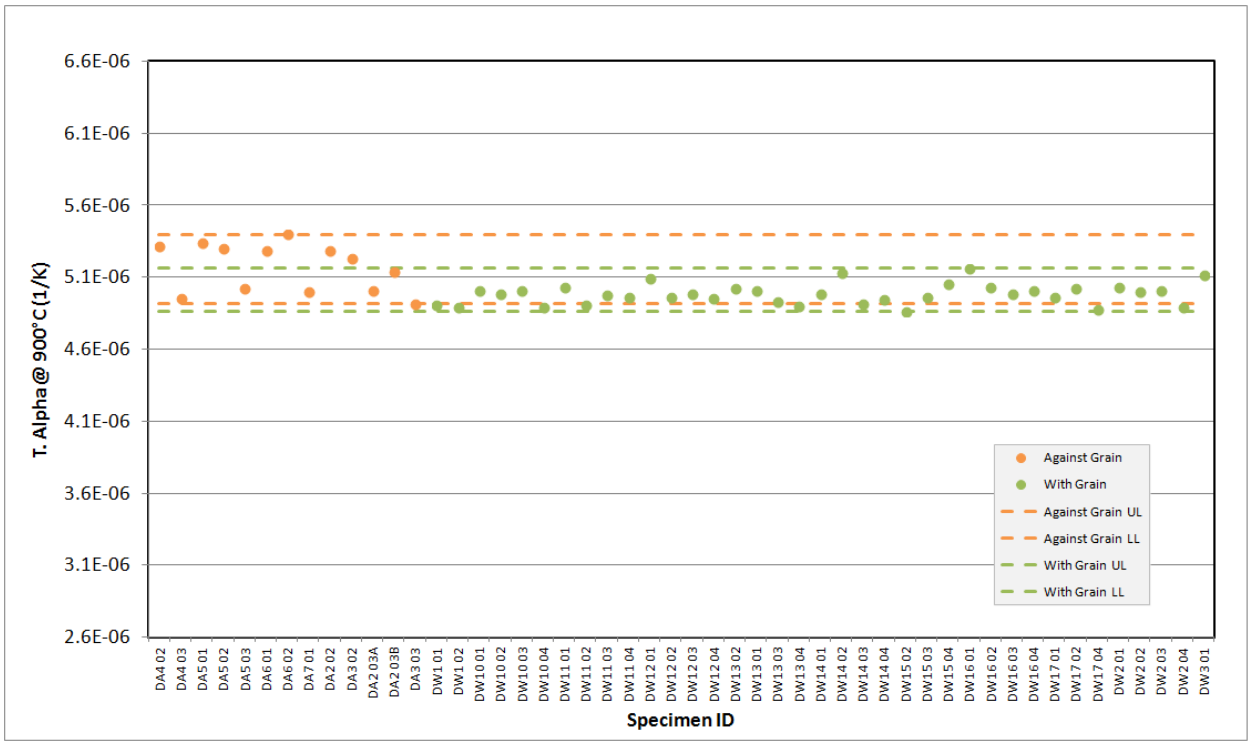

Figure A-112. PCEA Creep Coefficient of Thermal Expansion @ 900°C.

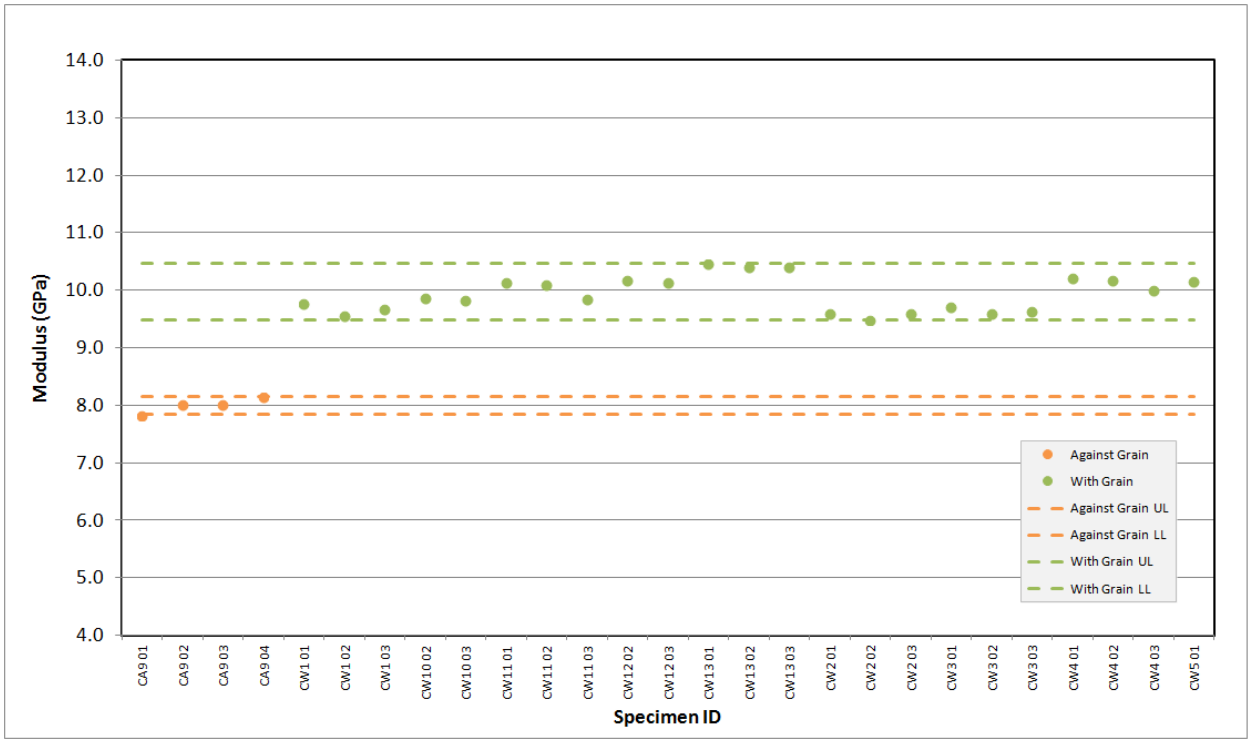

Figure A-113. H-451 Creep Modulus by Sonic Resonance.

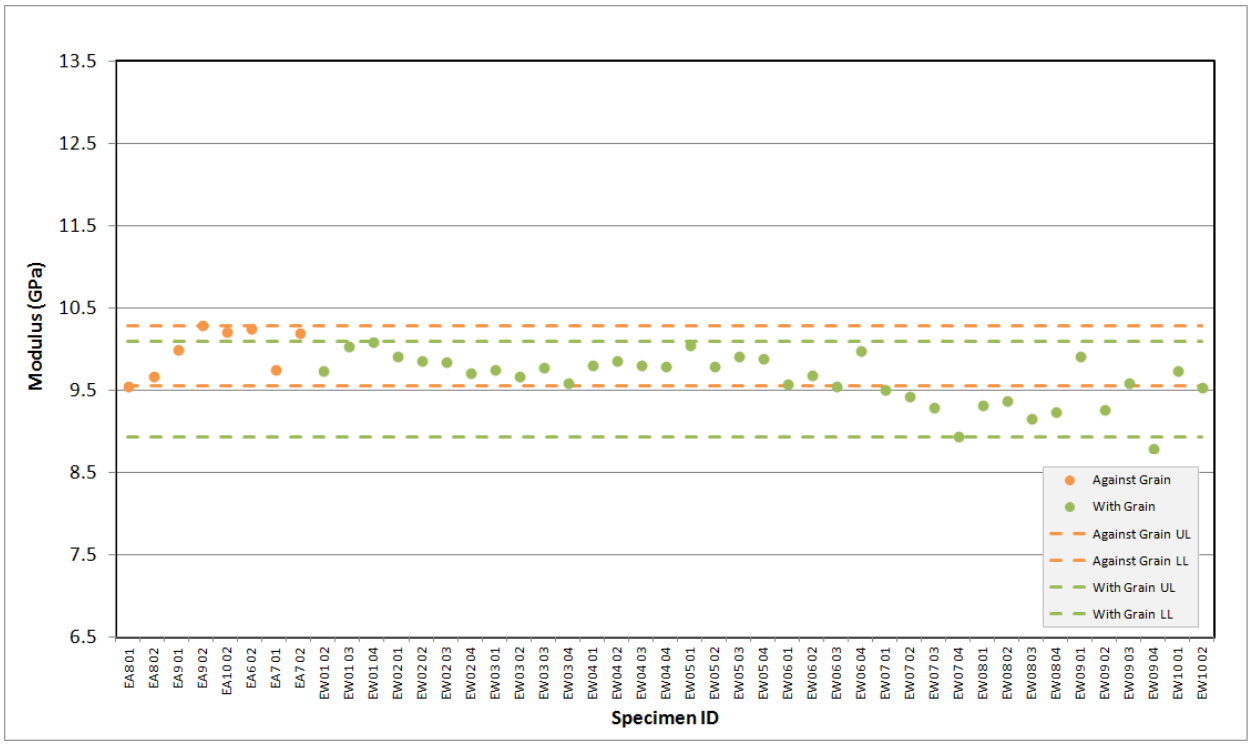

Figure A-114. IG-110 Creep Modulus by Sonic Resonance.

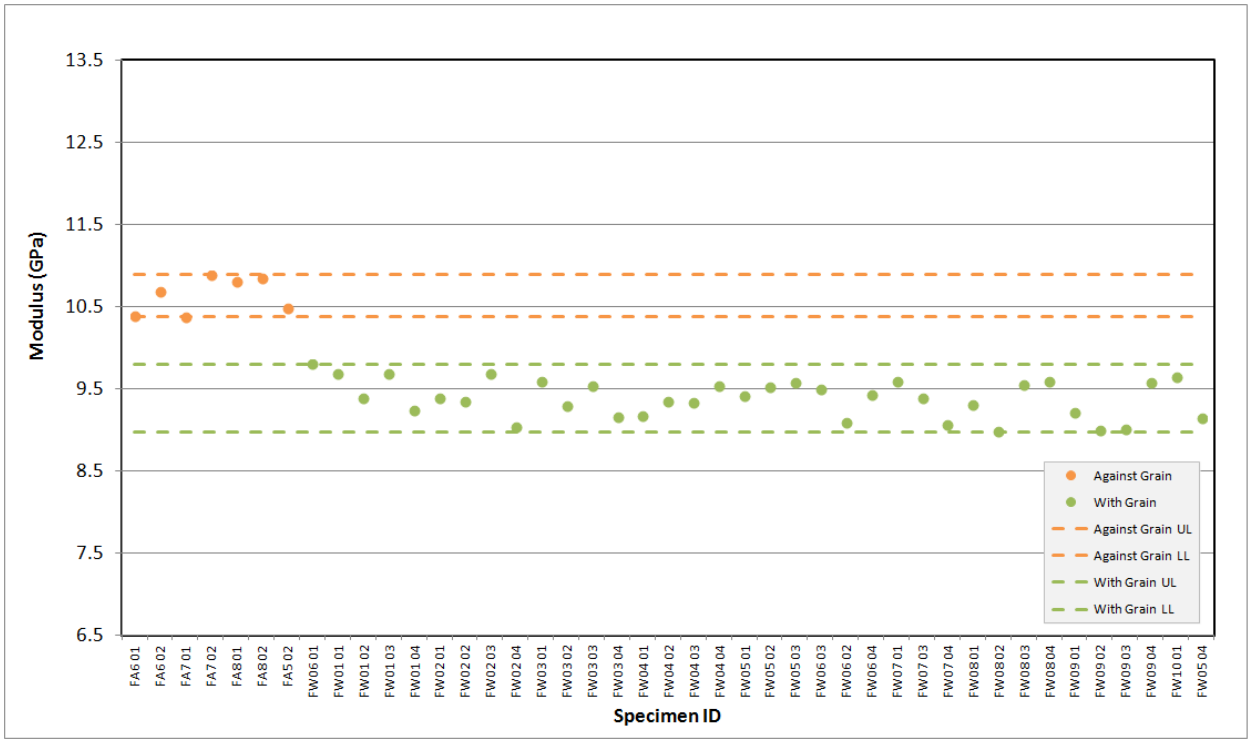

Figure A-115. IG-430 Creep Modulus by Sonic Resonance.

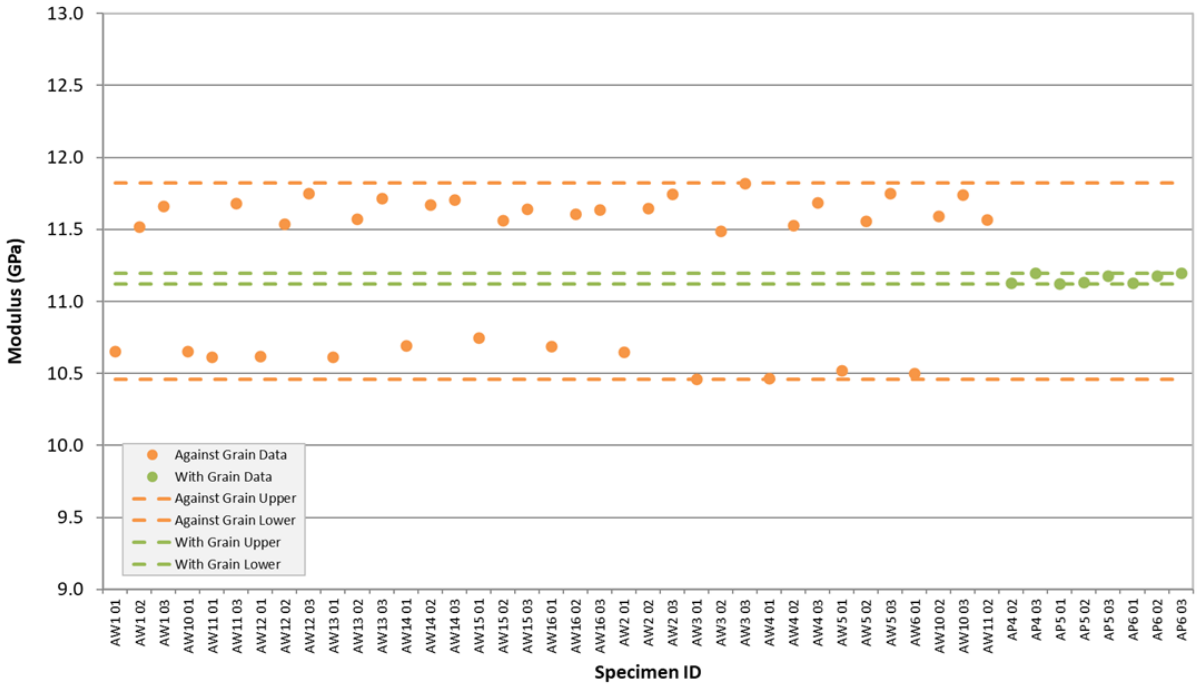

Figure A-116. NBG-17 Creep Modulus by Sonic Resonance.

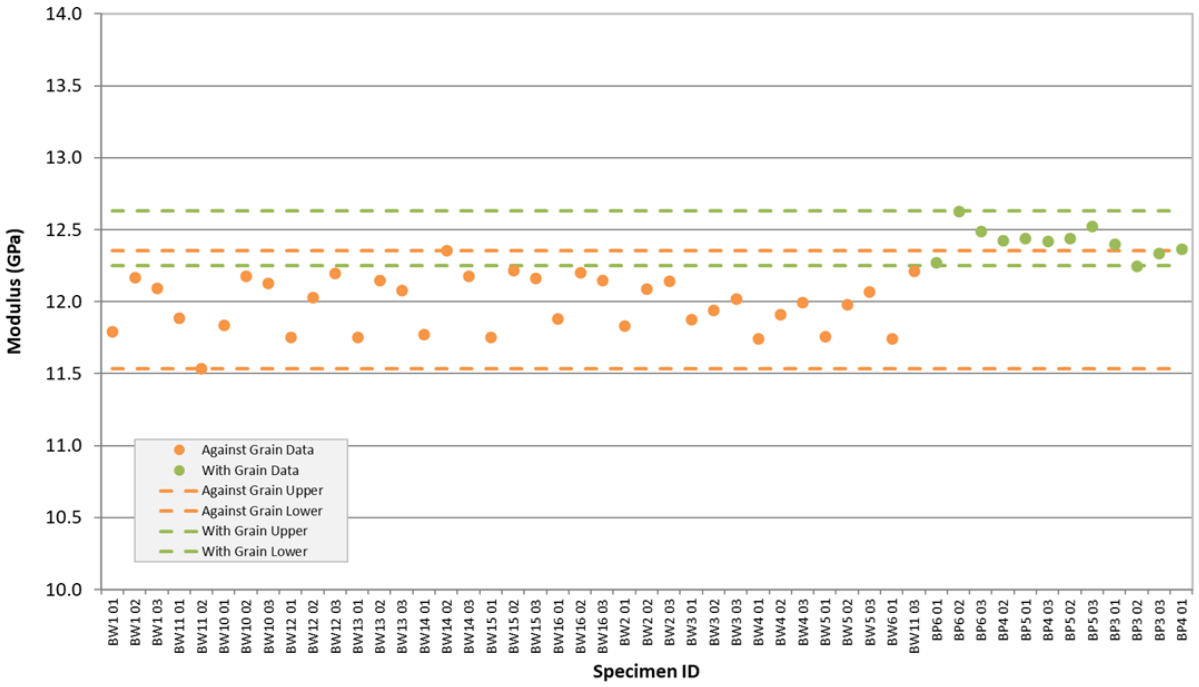

Figure A-117. NBG-18 Creep Modulus by Sonic Resonance.

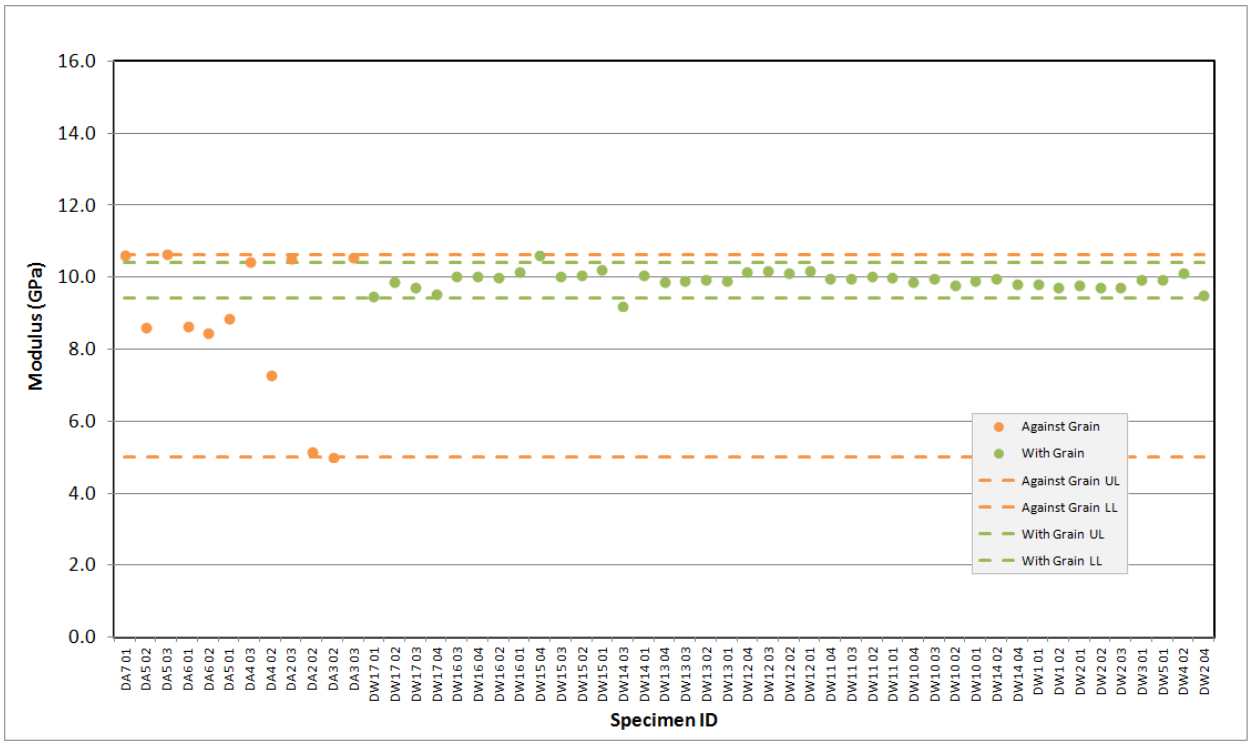

Figure A-118. PCEA Creep Modulus by Sonic Resonance.

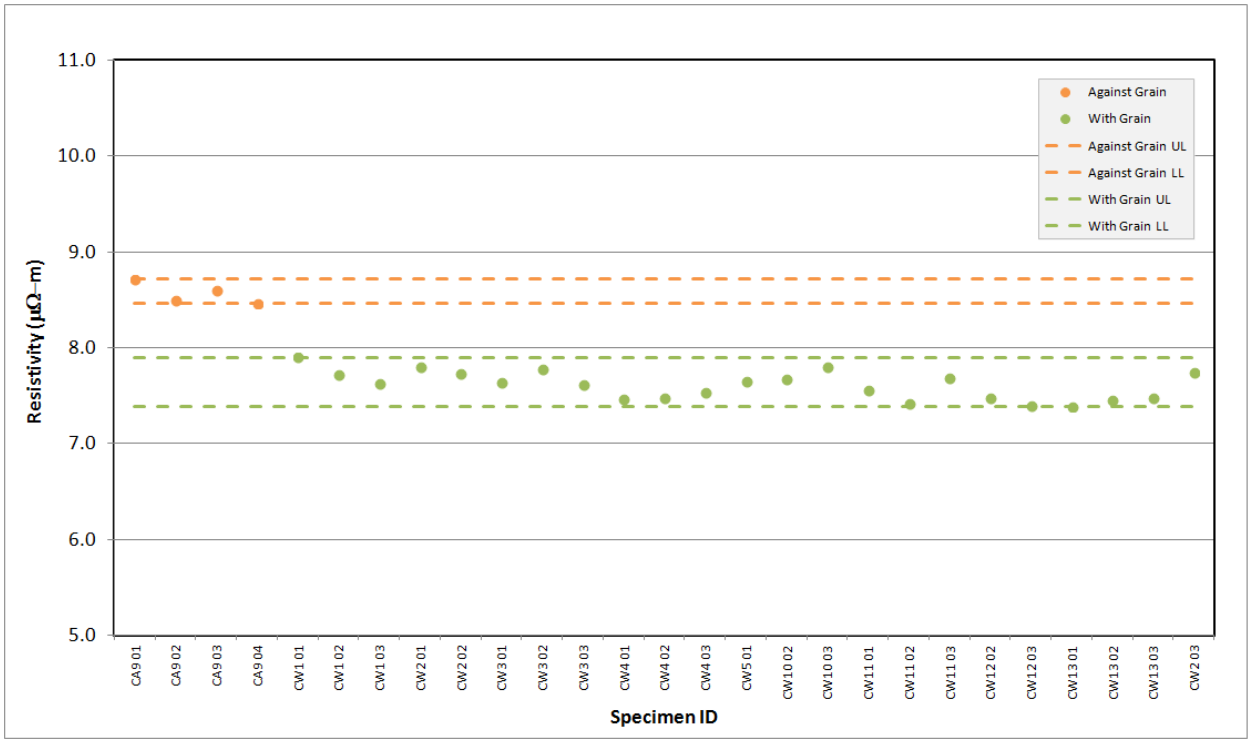

Figure A-119. H-451 Creep Resistivity.

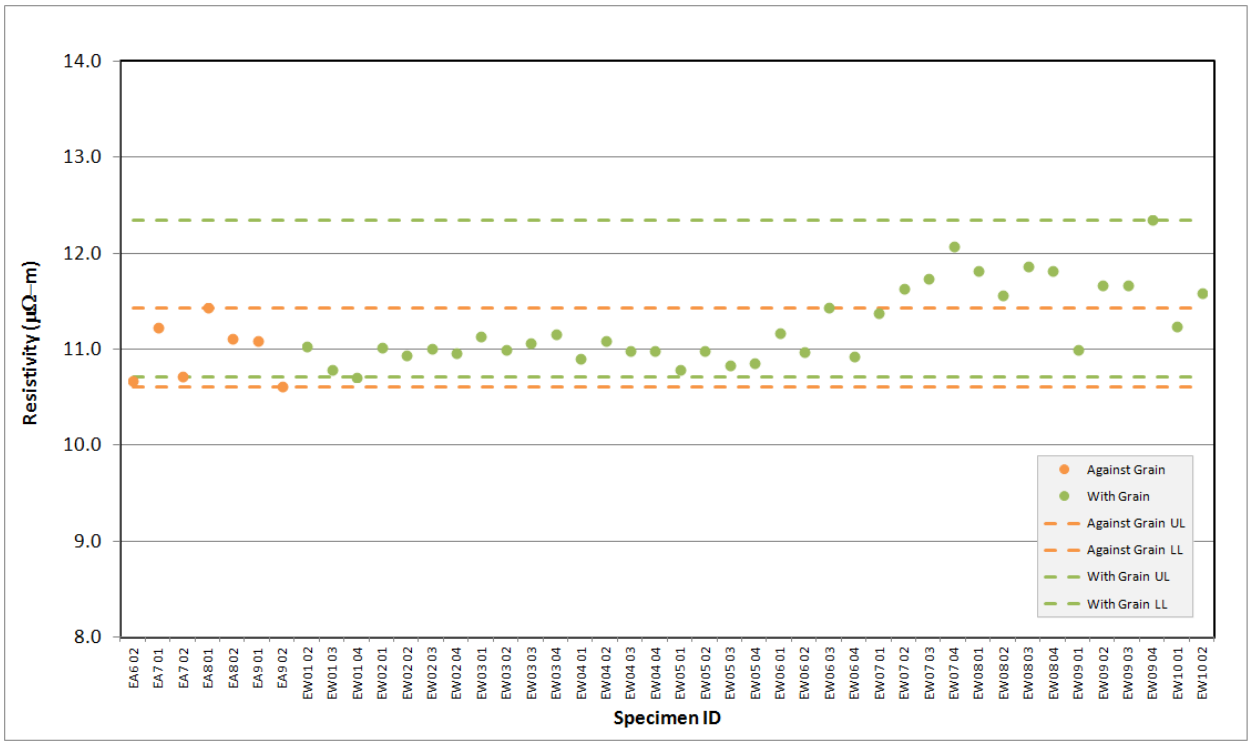

Figure A-120. IG-110 Creep Resistivity.

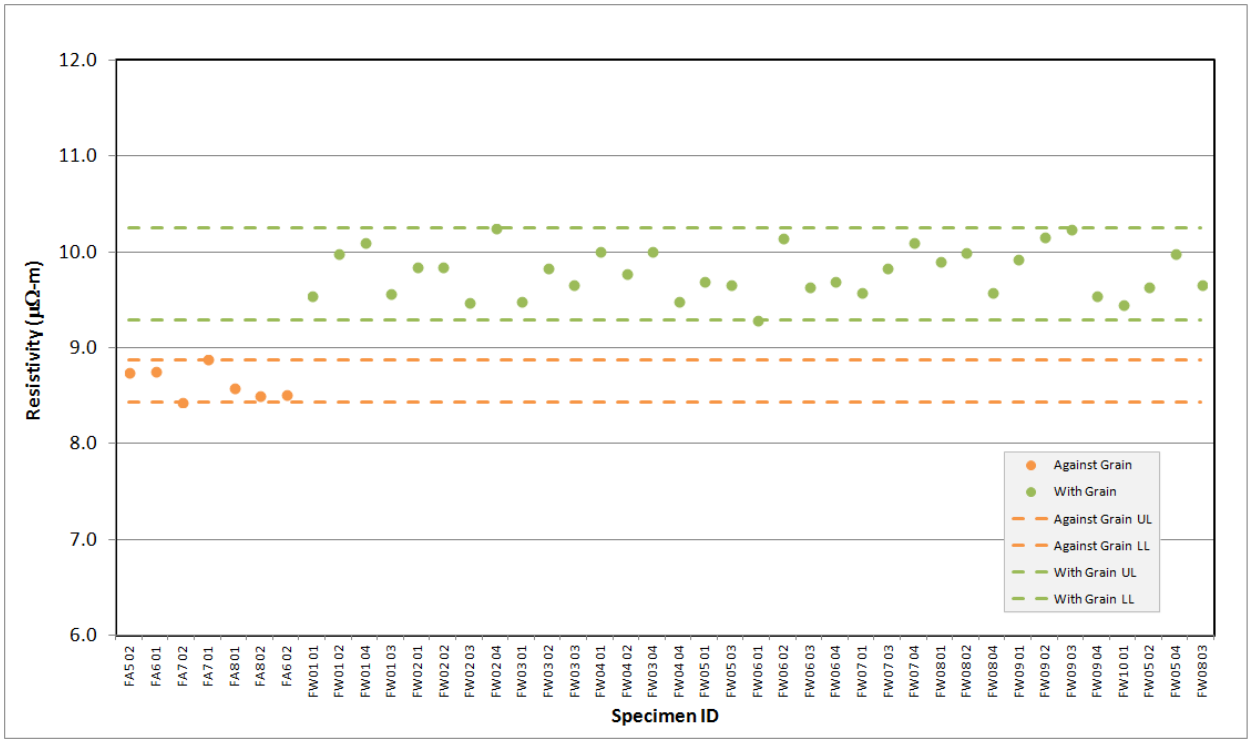

Figure A-121. IG-430 Creep Resistivity.

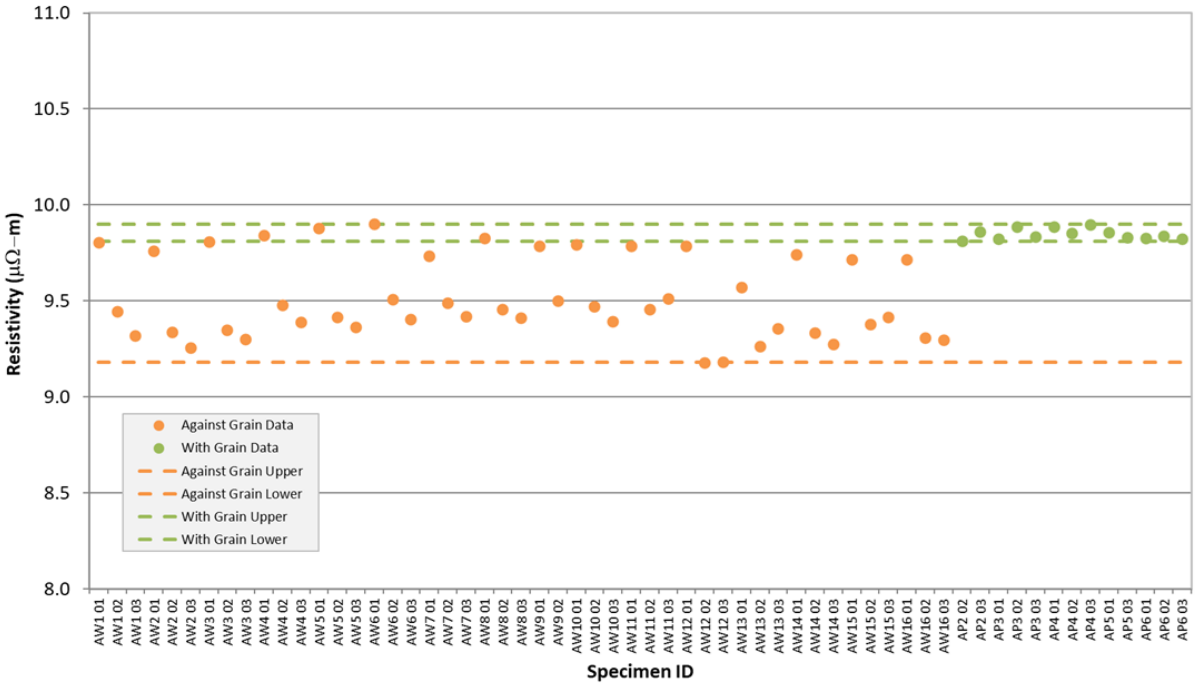

Figure A-122. NBG-17 Creep Resistivity.

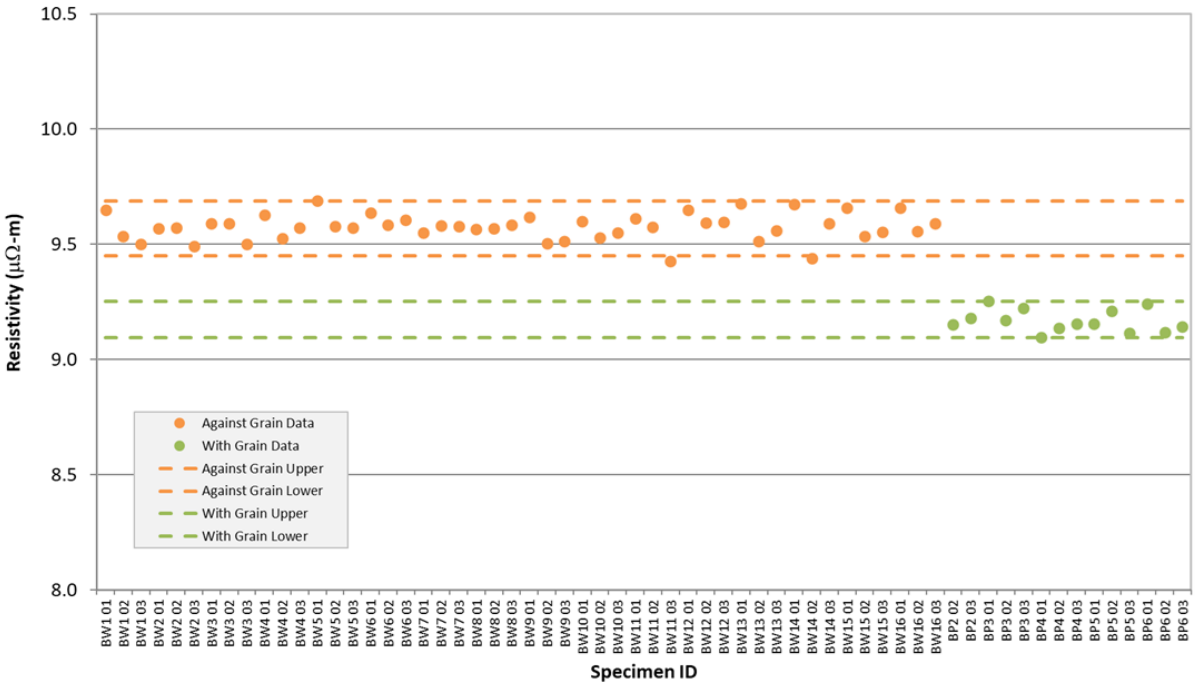

Figure A-123. NBG-18 Creep Resistivity.

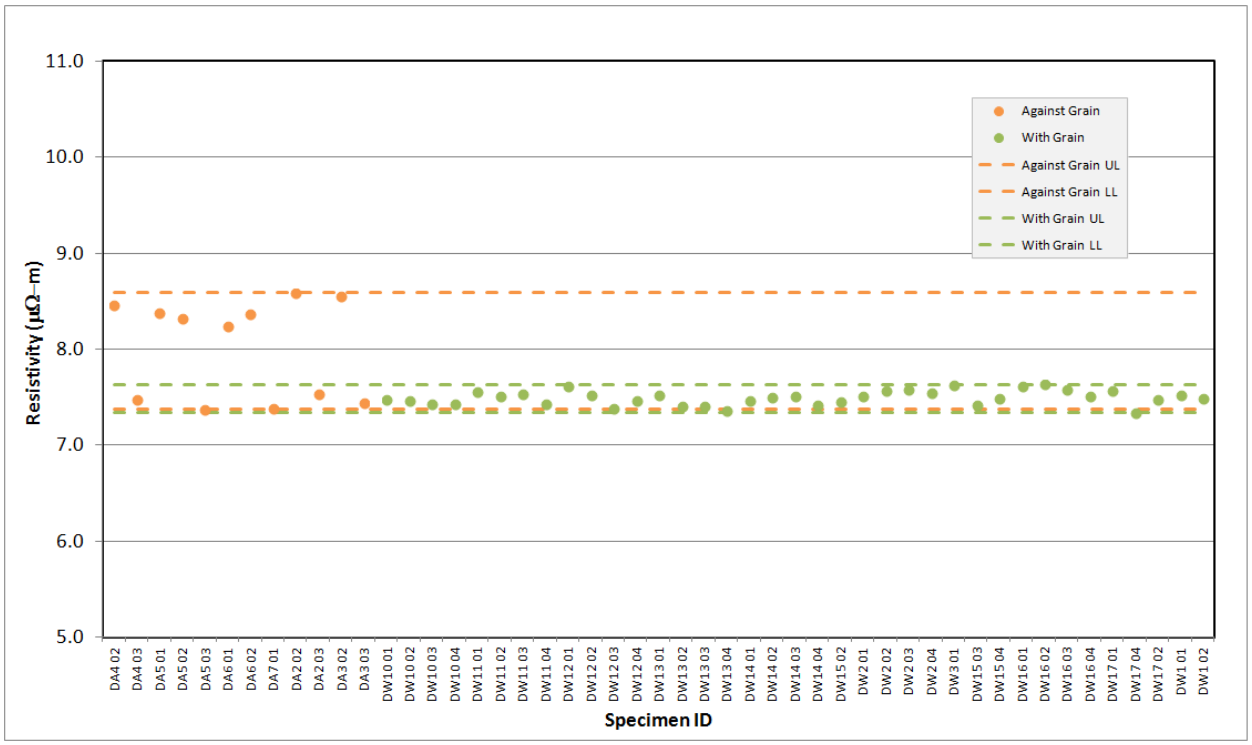

Figure A-124. PCEA Creep Resistivity.

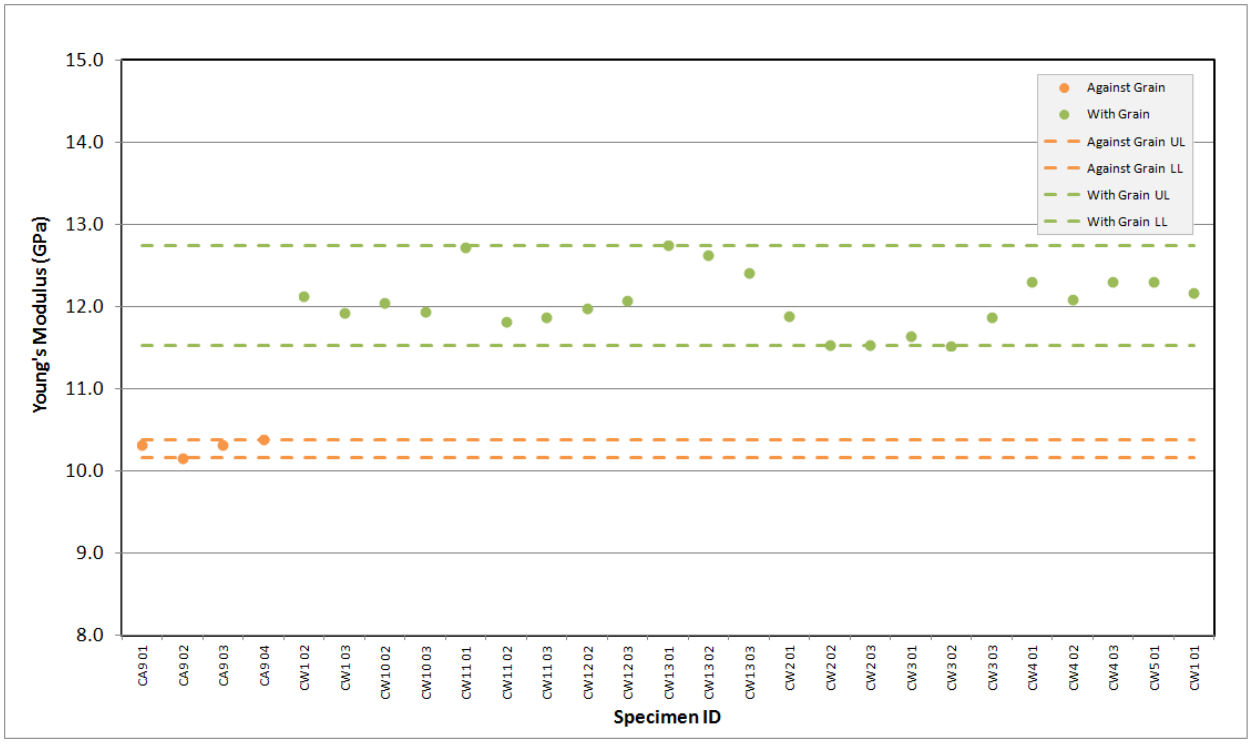

Figure A-125. H-451 Creep Young's Modulus by Sonic Velocity.

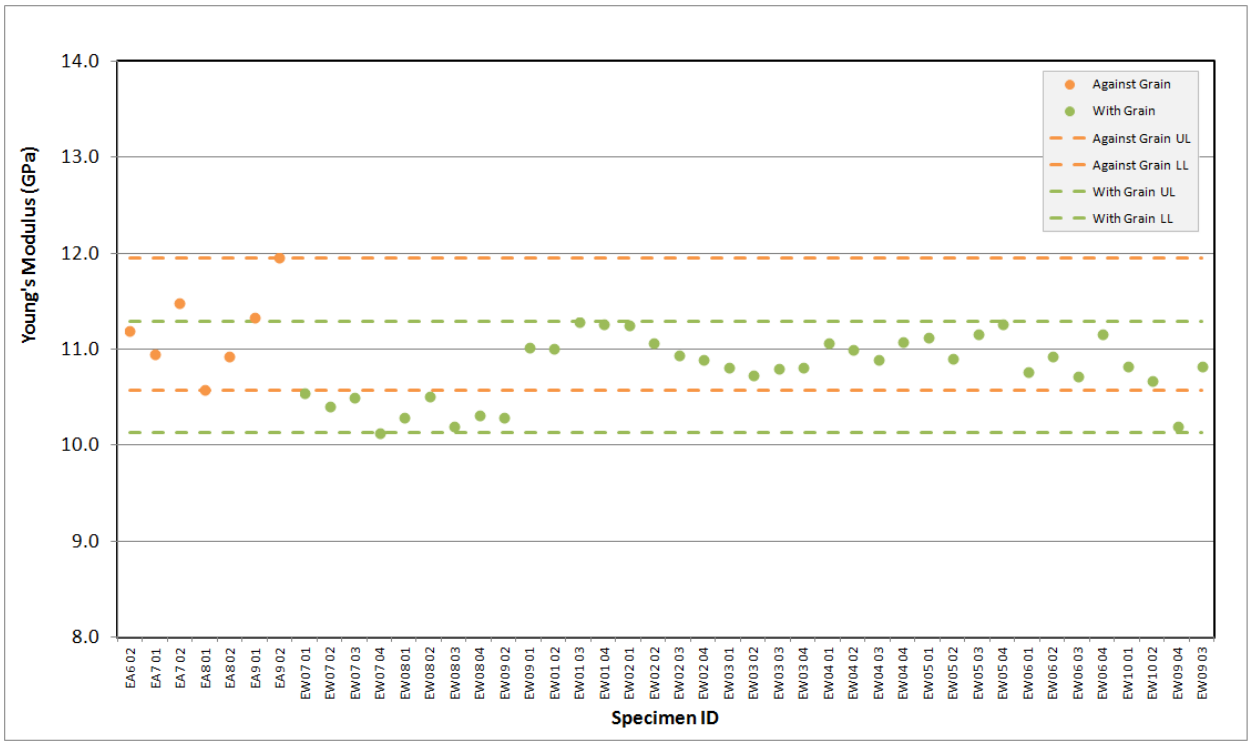

Figure A-126. IG-110 Creep Young's Modulus by Sonic Velocity.

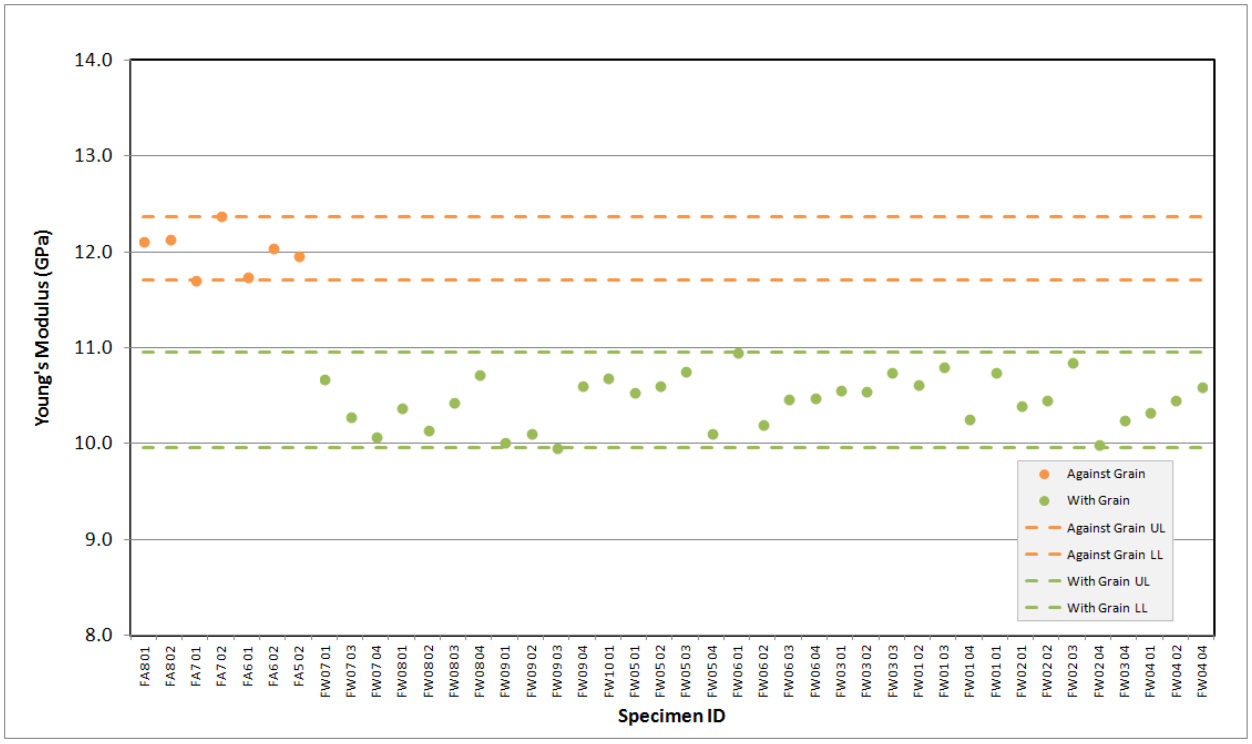

Figure A-127. IG-430 Creep Young's Modulus by Sonic Velocity.

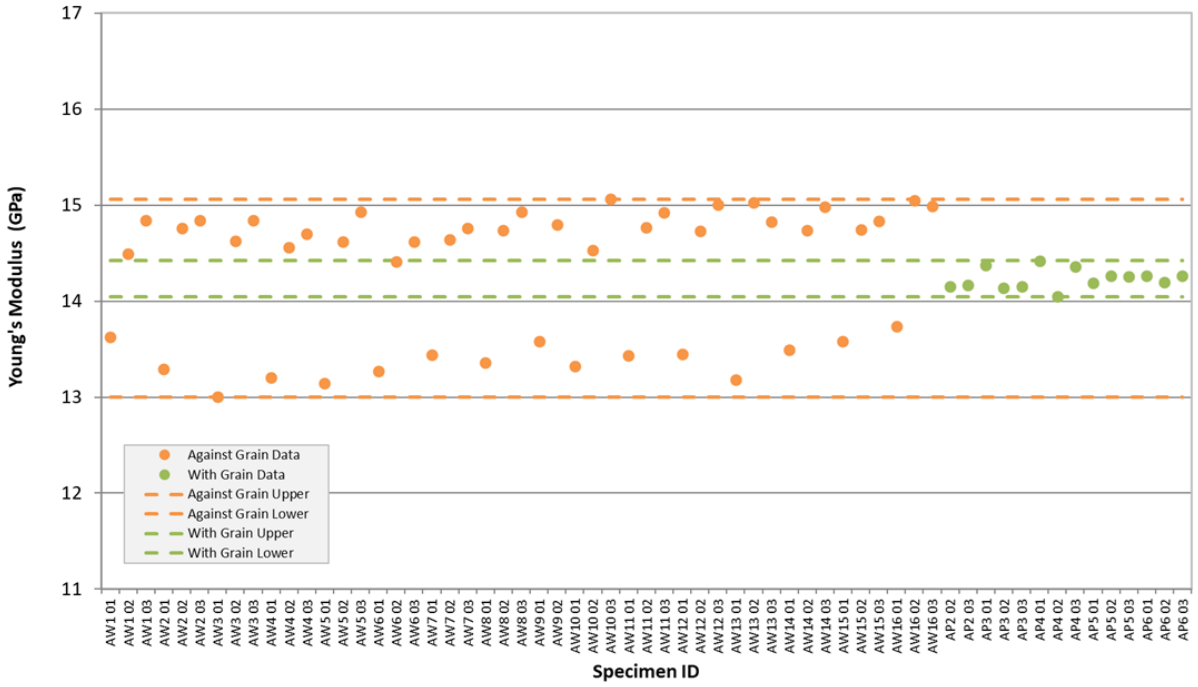

Figure A-128. NBG-17 Creep Young's Modulus by Sonic Velocity.

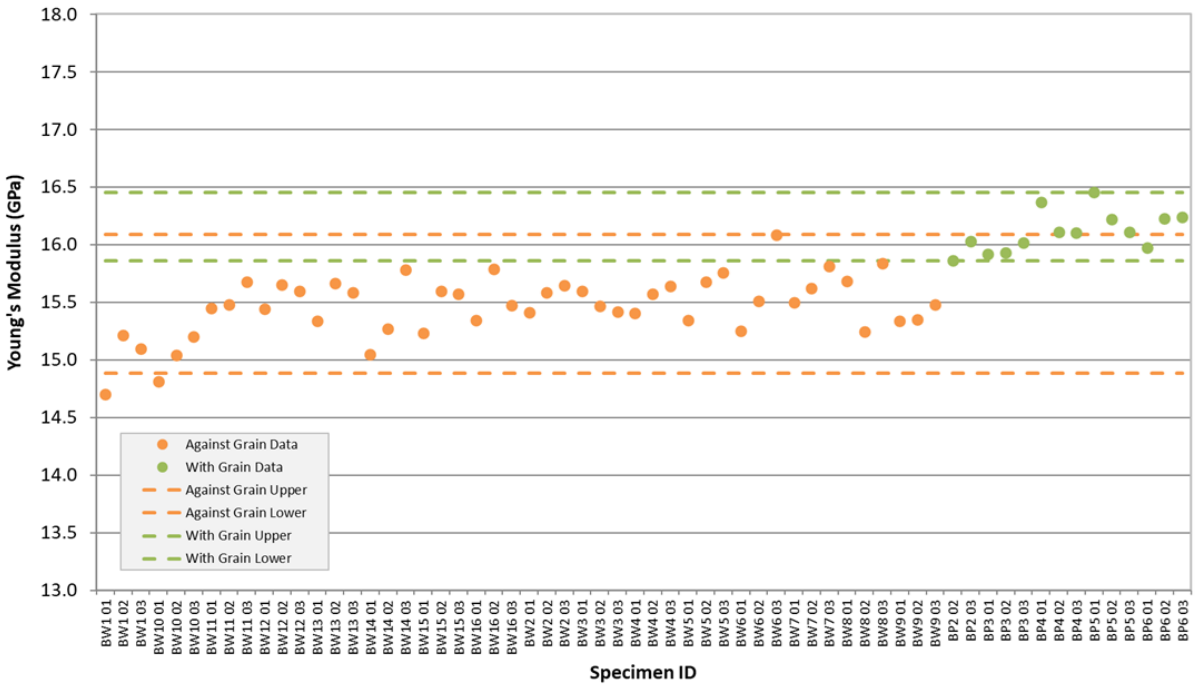

Figure A-129. NBG-18 Creep Young's Modulus by Sonic Velocity.

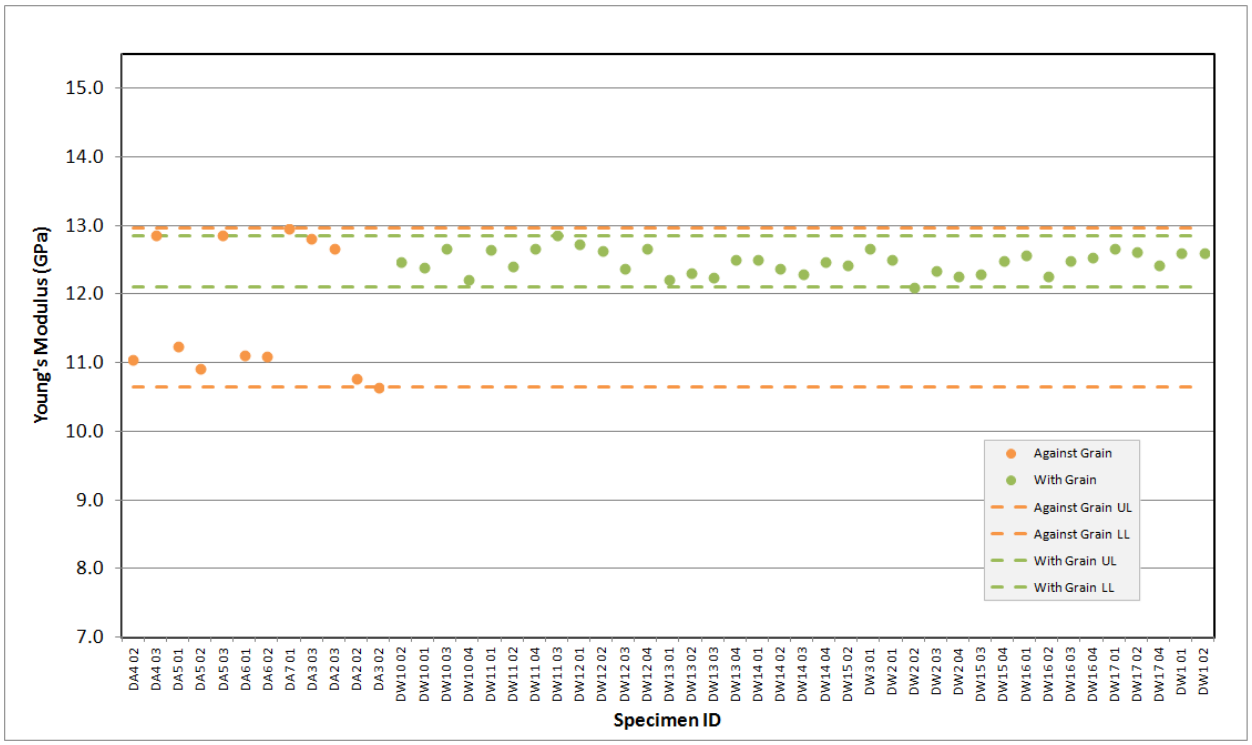

Figure A-130. PCEA Creep Young's Modulus by Sonic Velocity.

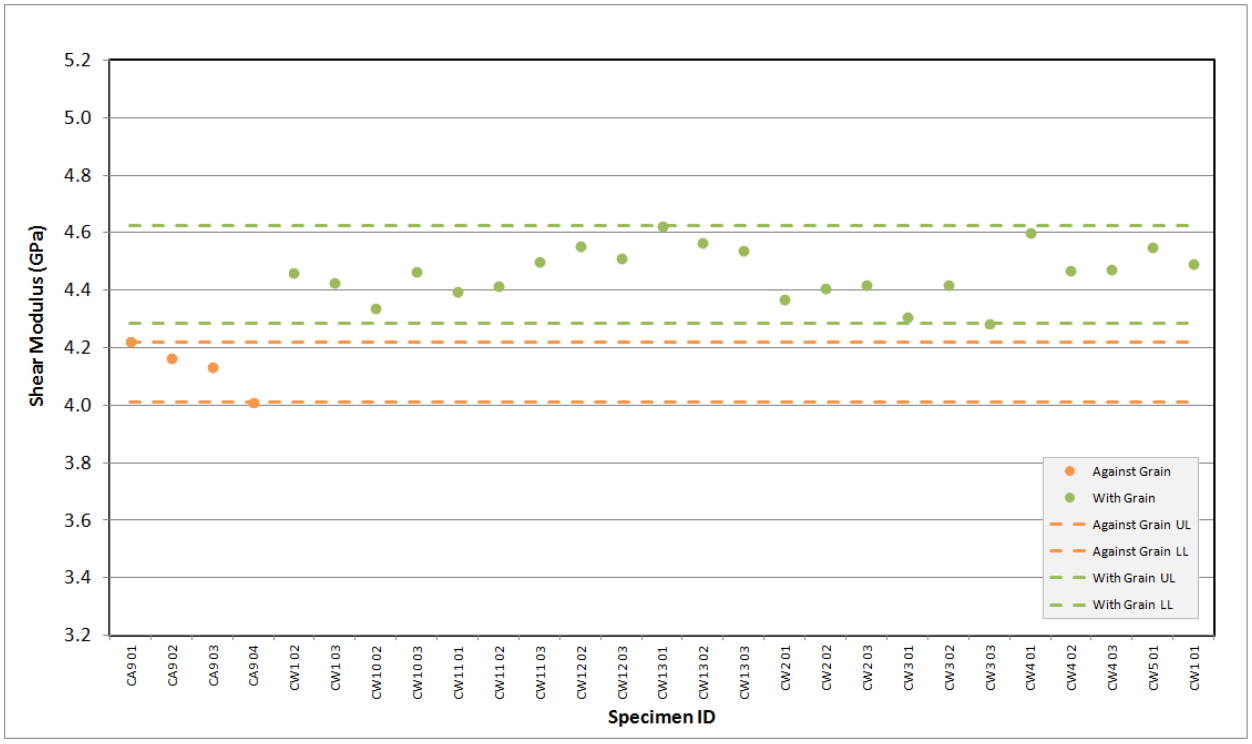

Figure A-131. H-451 Creep Shear Modulus by Sonic Velocity.

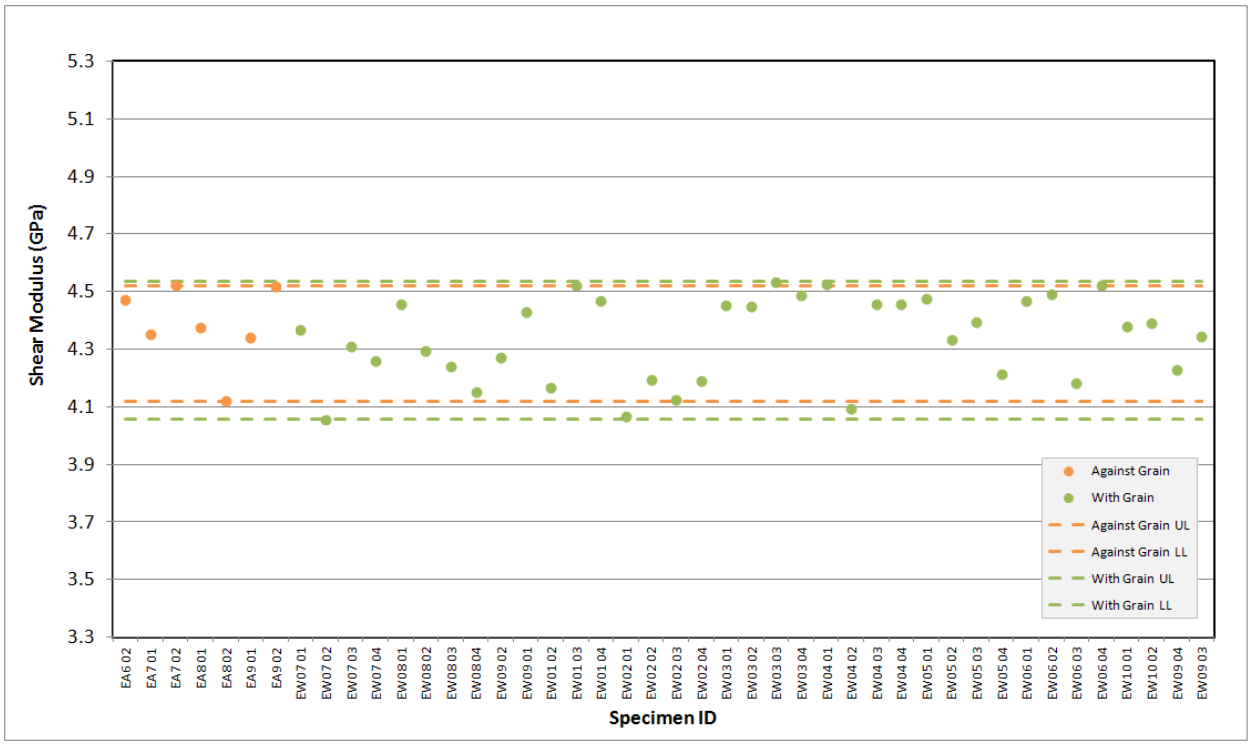

Figure A-132. IG-110 Creep Shear Modulus by Sonic Velocity.

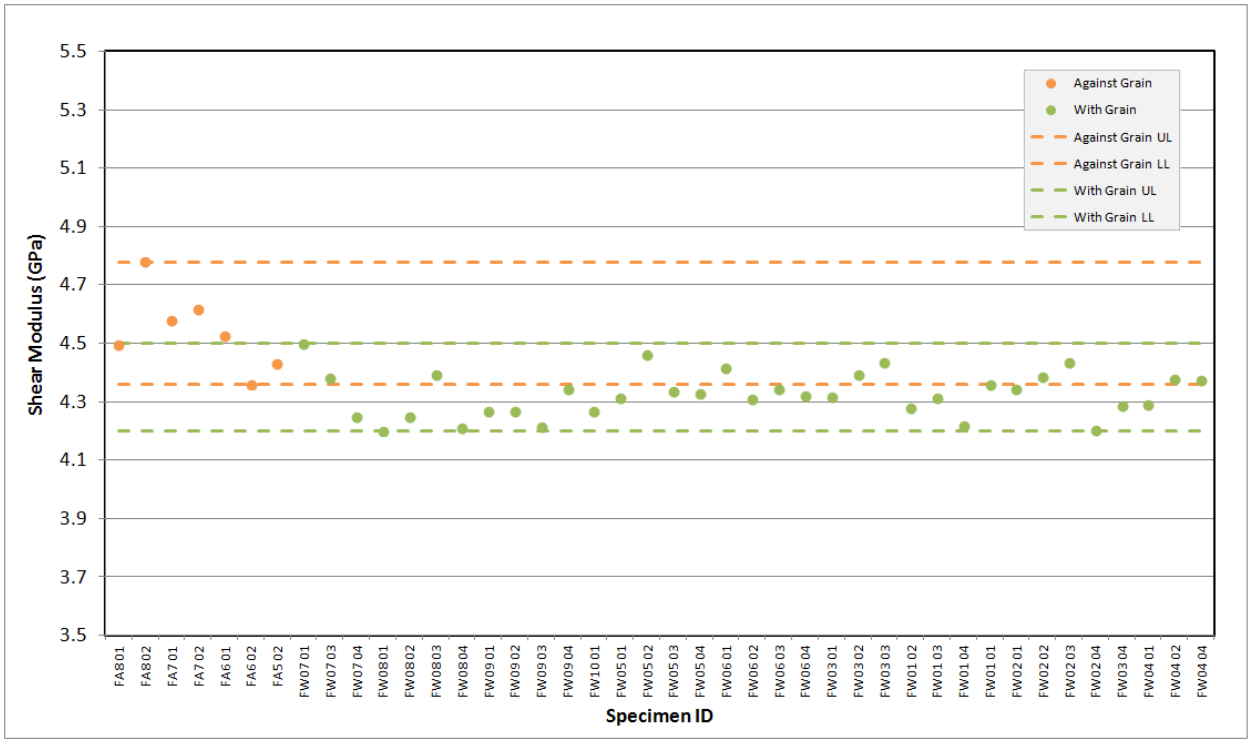

Figure A-133. IG-430 Creep Shear Modulus by Sonic Velocity.

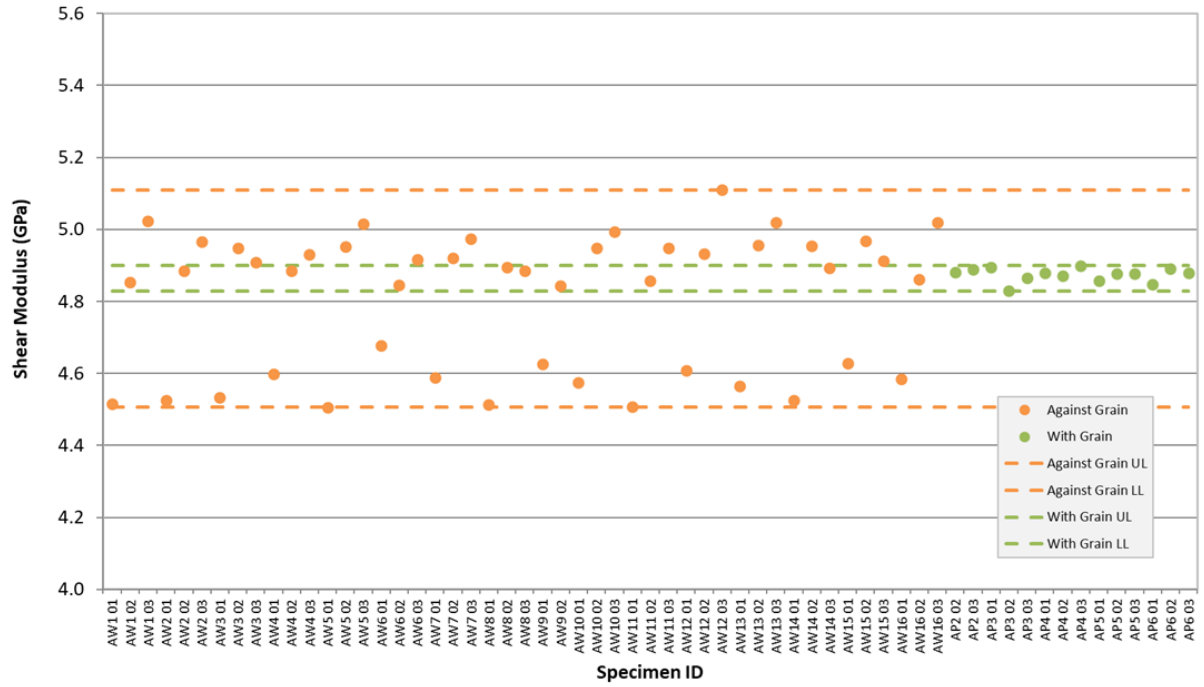

Figure A-134. NBG-17 Creep Shear Modulus by Sonic Velocity.

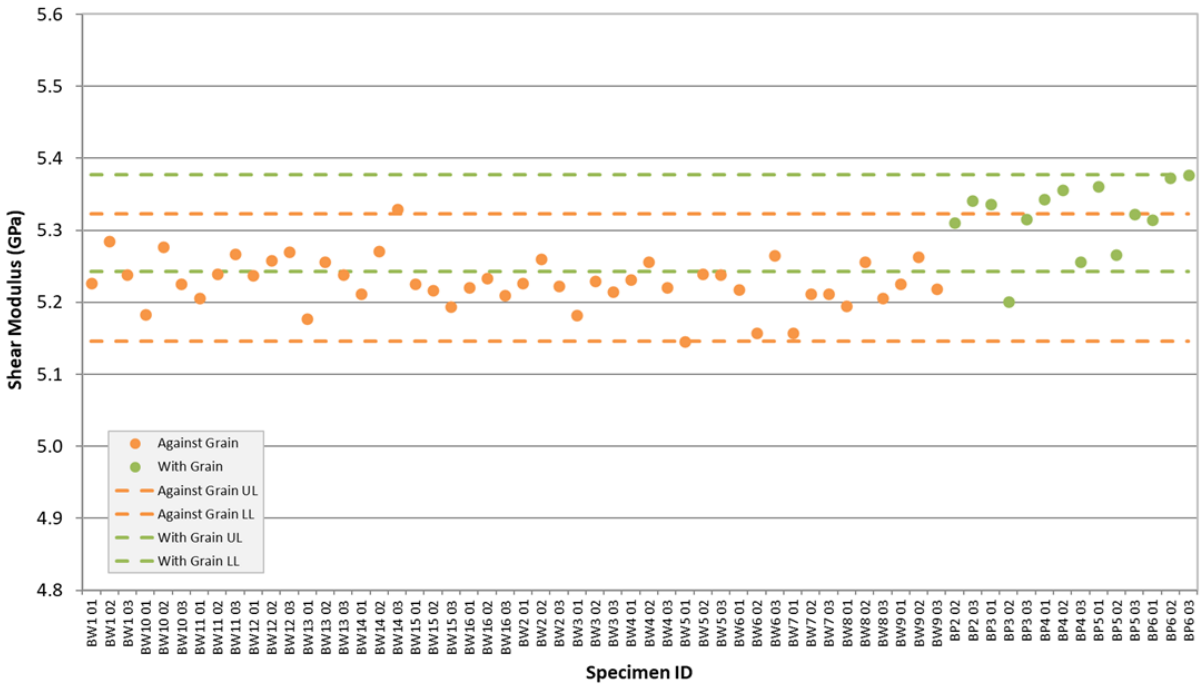

Figure A-135. NBG-18 Creep Shear Modulus by Sonic Velocity.

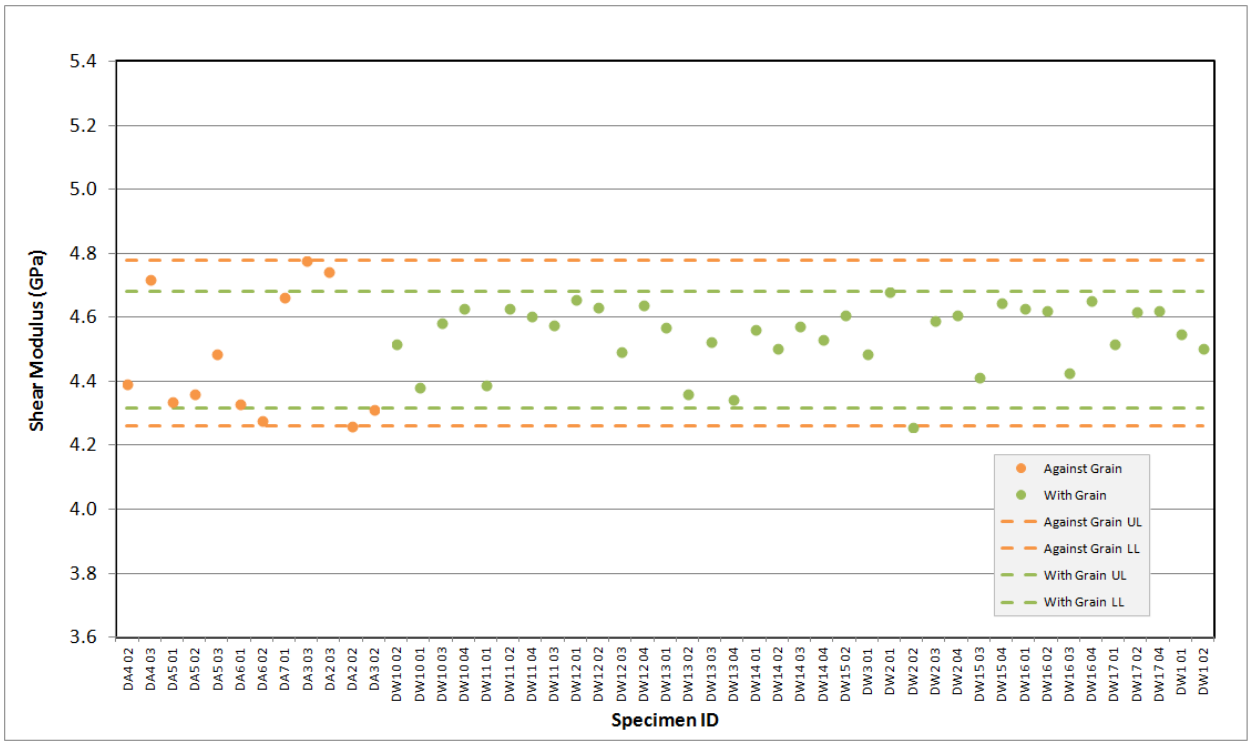

Figure A-136. PCEA Creep Shear Modulus by Sonic Velocity.

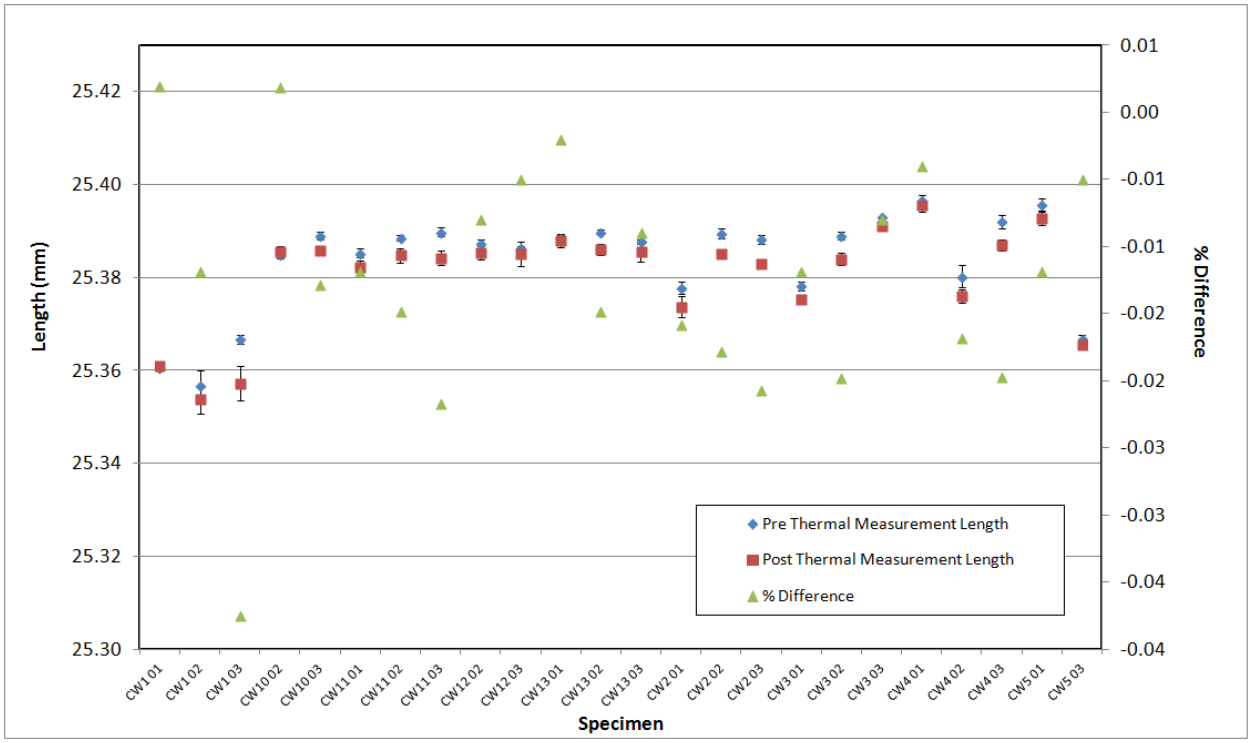

Figure A-137. H-451 Creep Pre vs. Post Thermal Measurement Length Comparison.

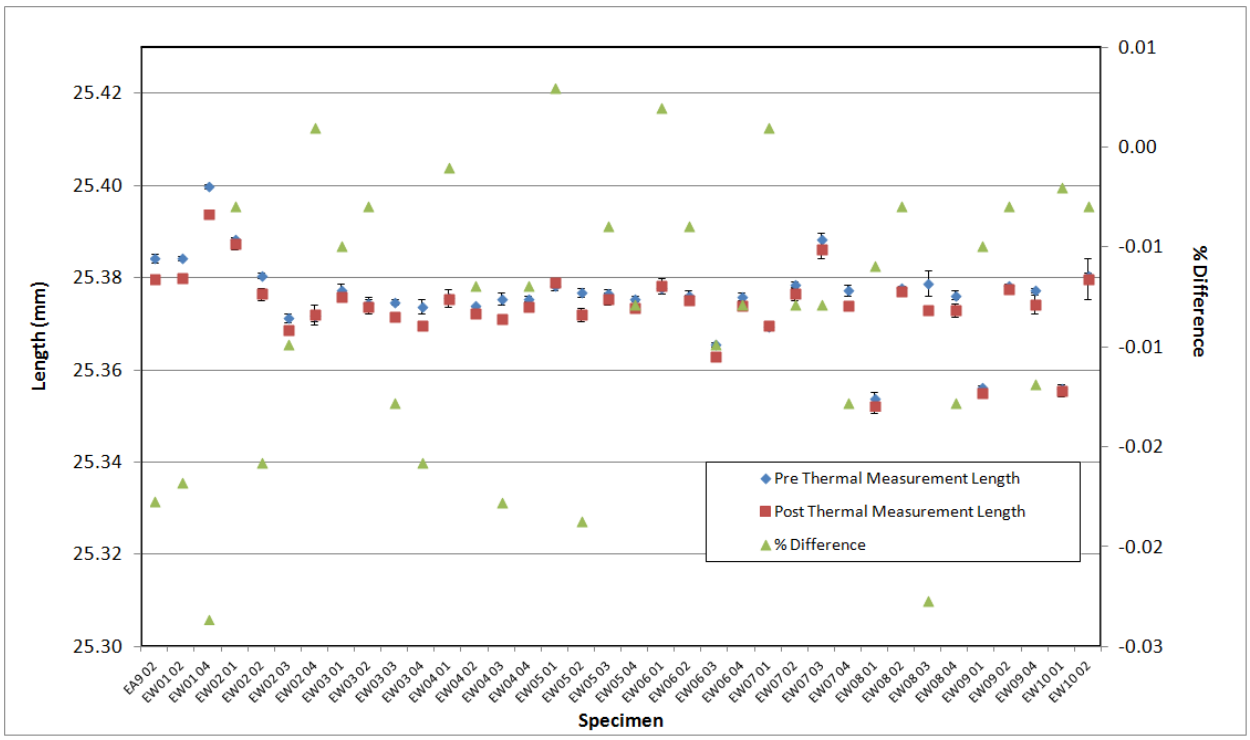

Figure A-138. IG-110 Creep Pre vs. Post Thermal Measurement Length Comparison.

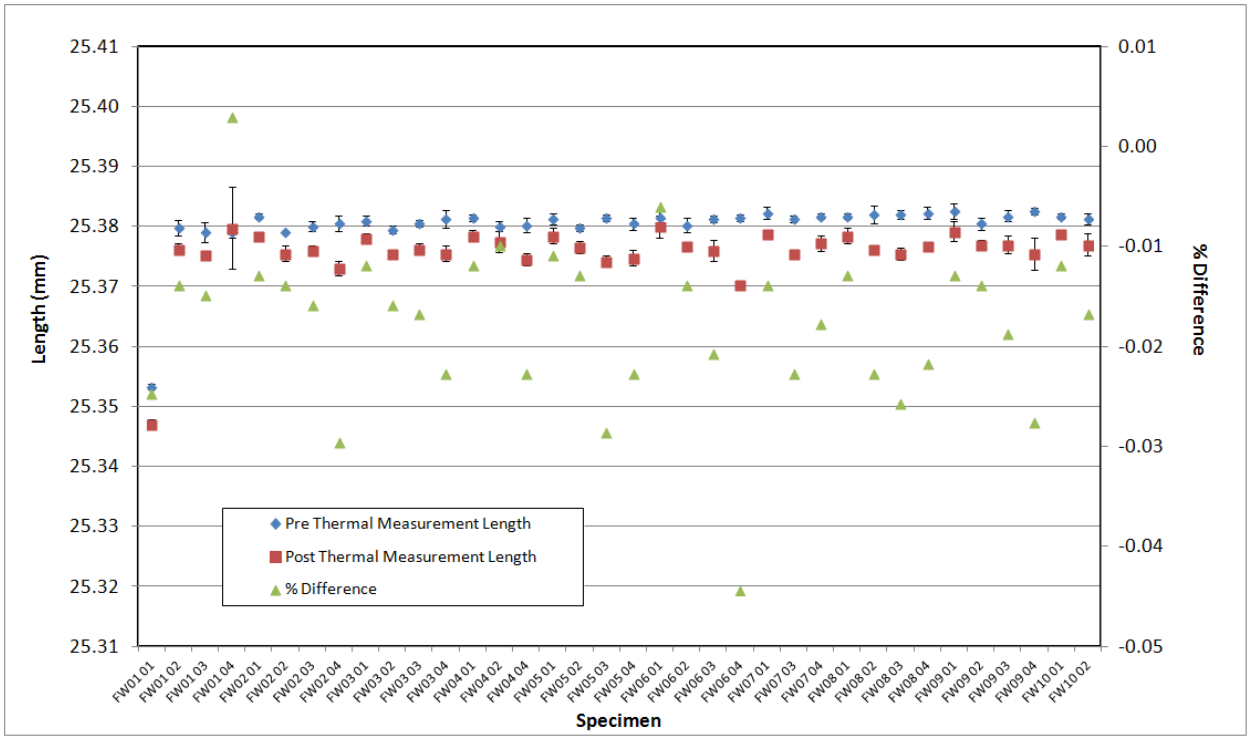

Figure A-139. IG-430 Creep Pre vs. Post Thermal Measurement Length Comparison.

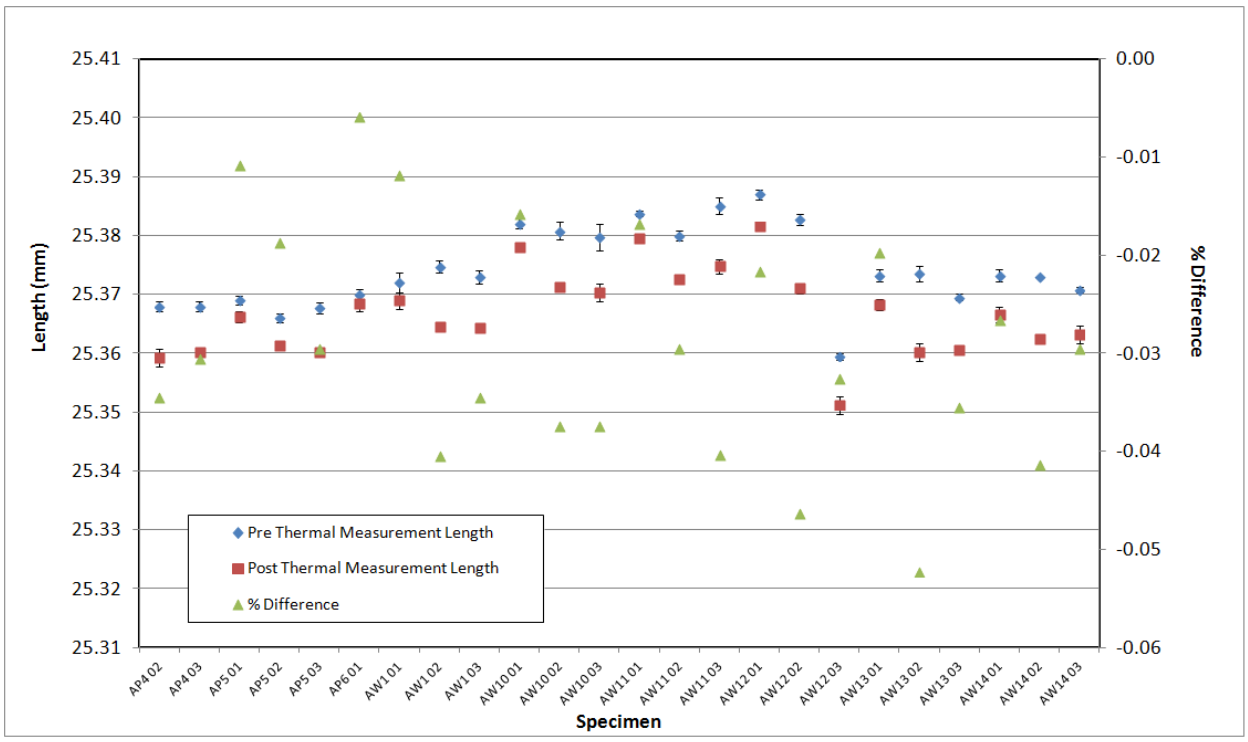

Figure A-140. NBG-17 Creep Pre vs. Post Thermal Measurement Length Comparison.

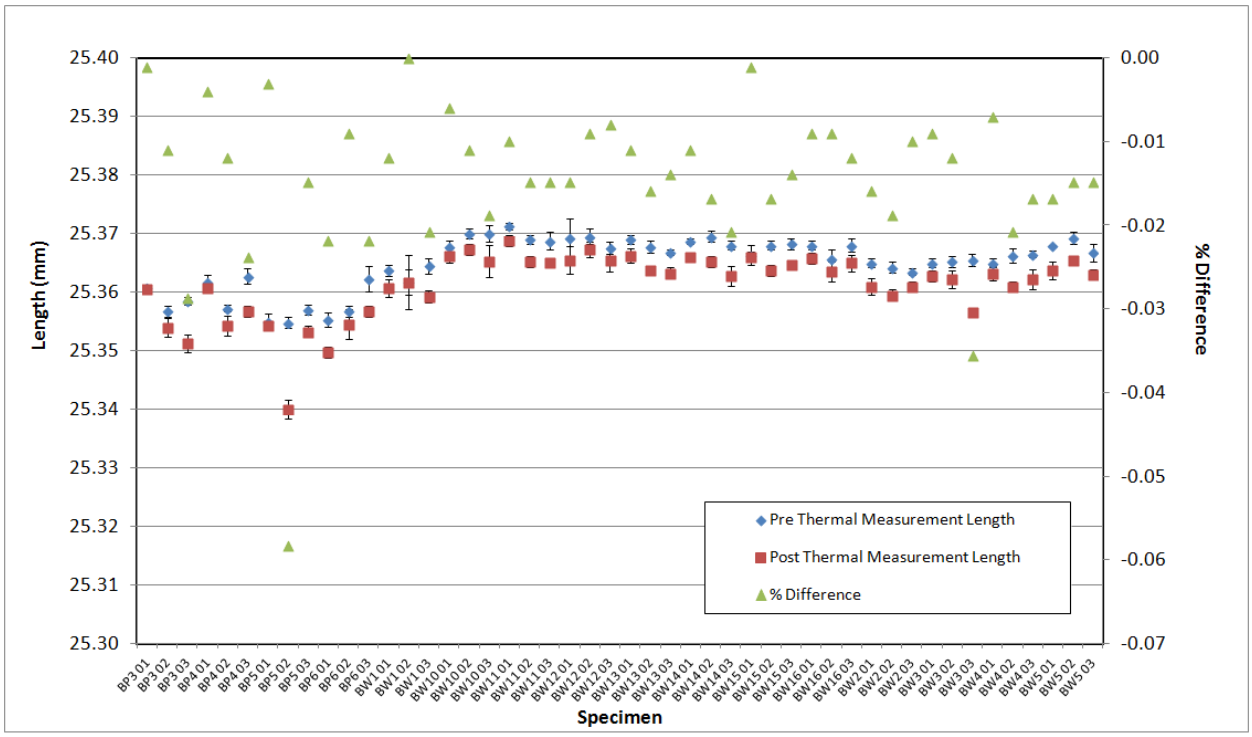

Figure A-141. NBG-18 Creep Pre vs. Post Thermal Measurement Length Comparison.

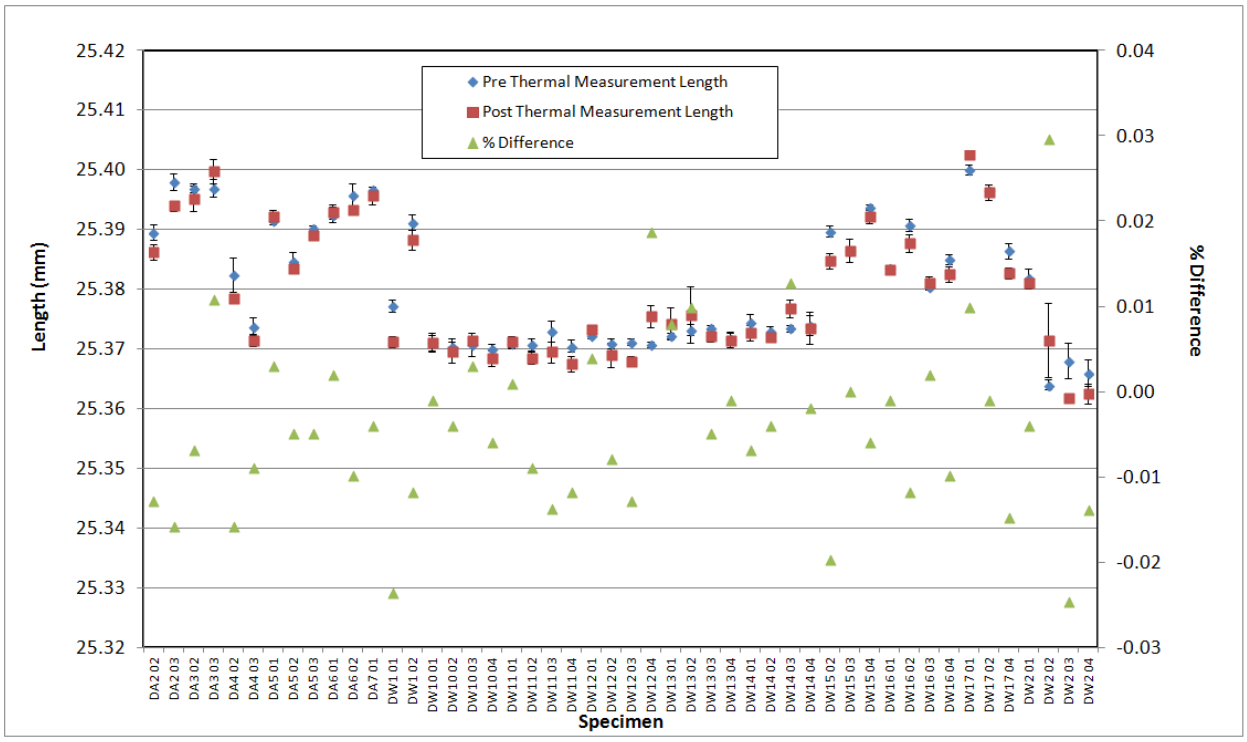

Figure A-142. PCEA Creep Pre vs. Post Thermal Measurement Length Comparison.

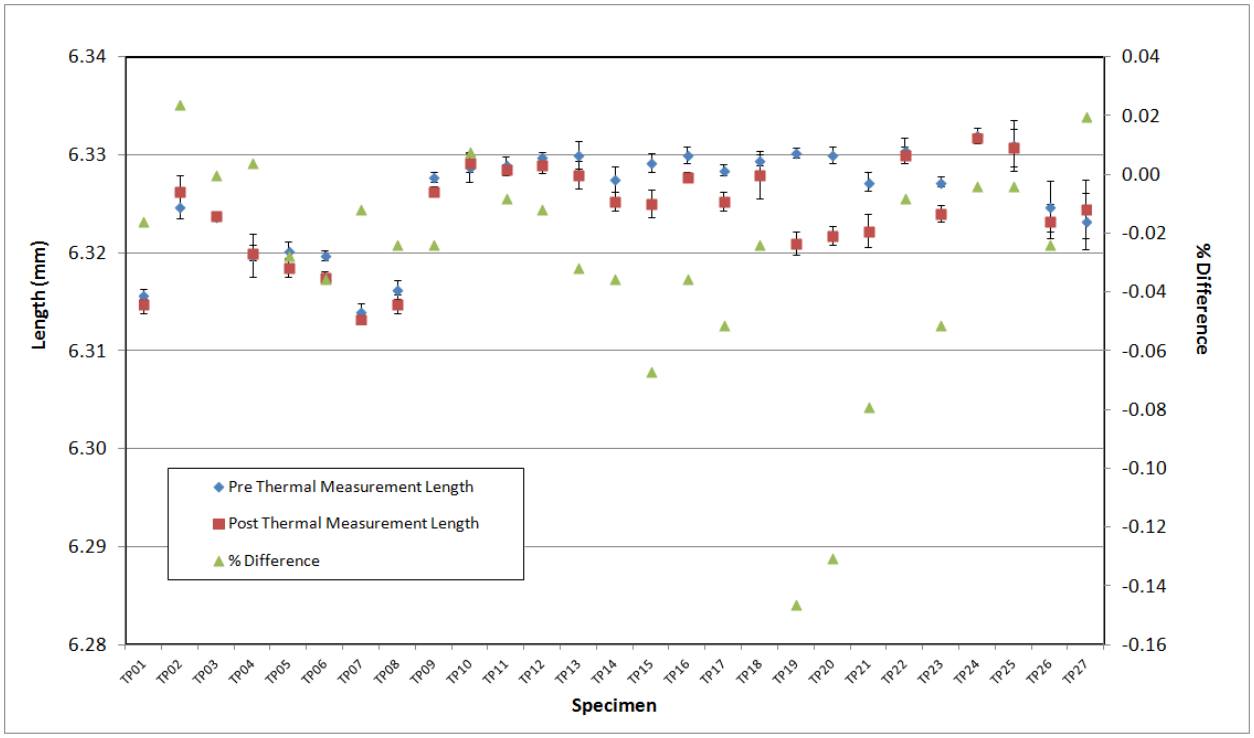

Figure A-143. 2114 Piggyback Pre vs. Post Thermal Measurement Length Comparison.

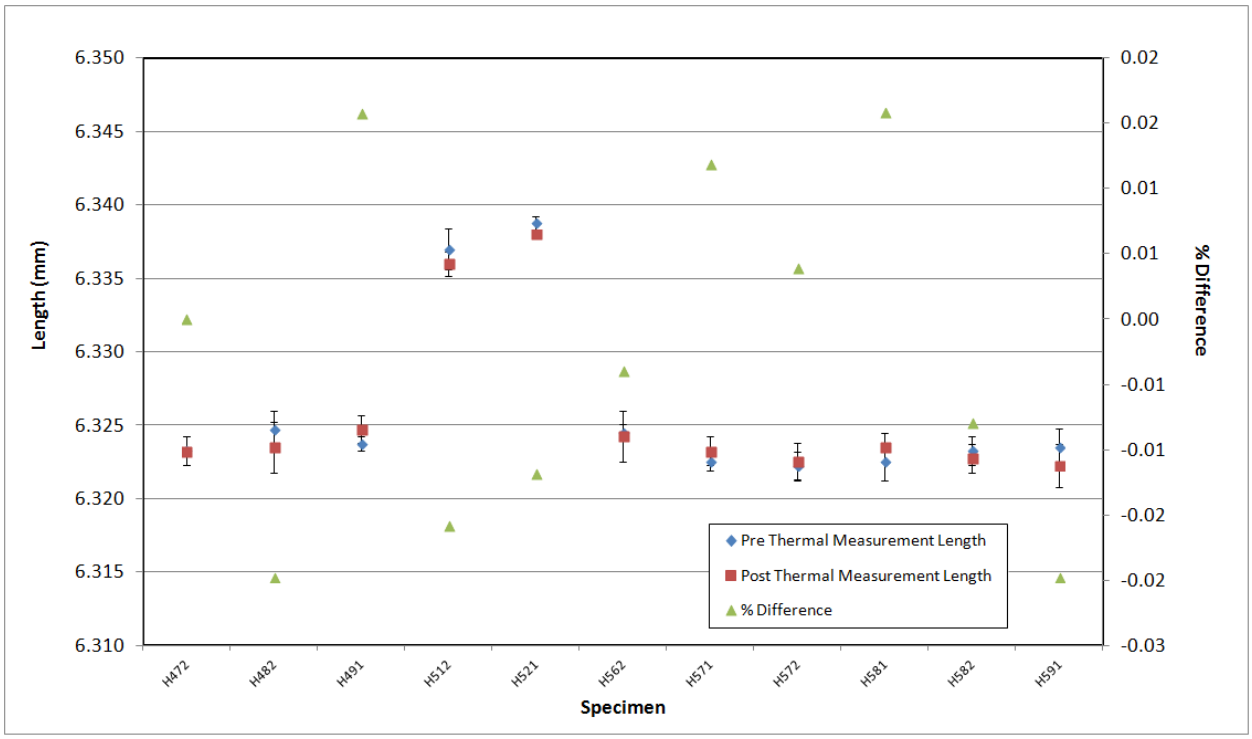

Figure A-144. A3 Matrix Piggyback Pre vs. Post Thermal Measurement Length Comparison.

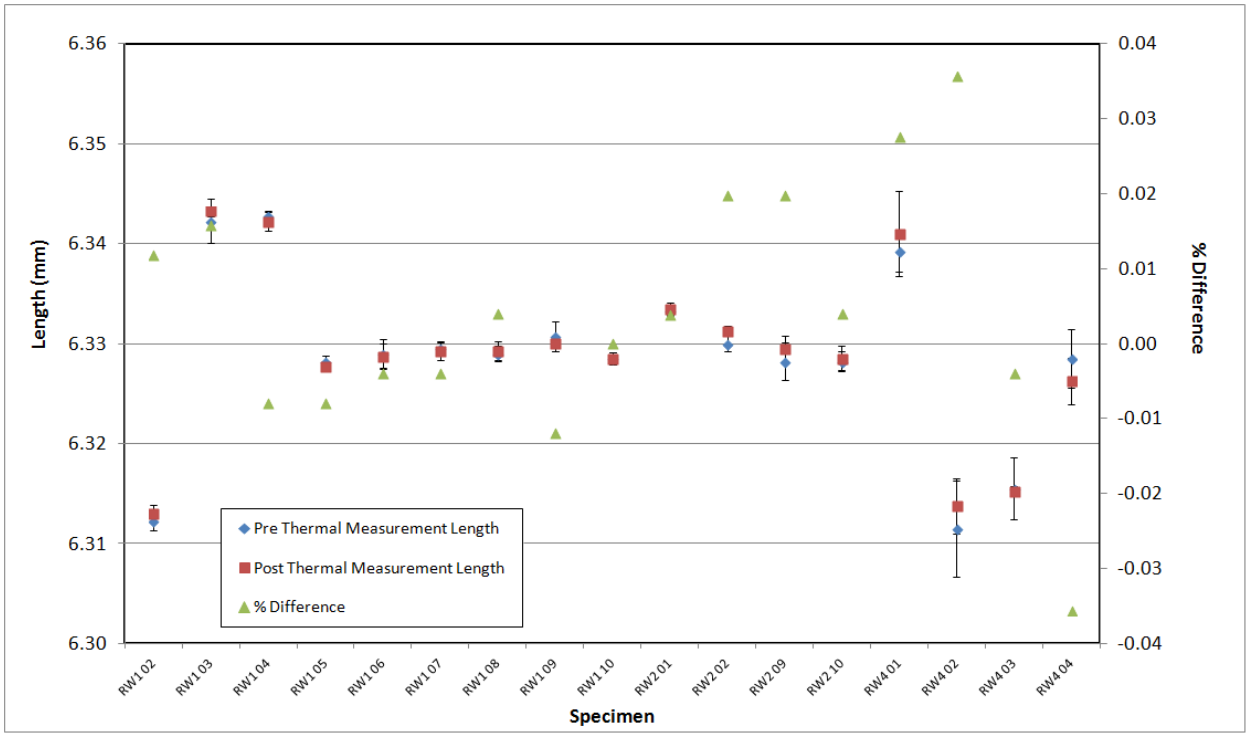

Figure A-145. BAN Piggyback Pre vs. Post Thermal Measurement Length Comparison.

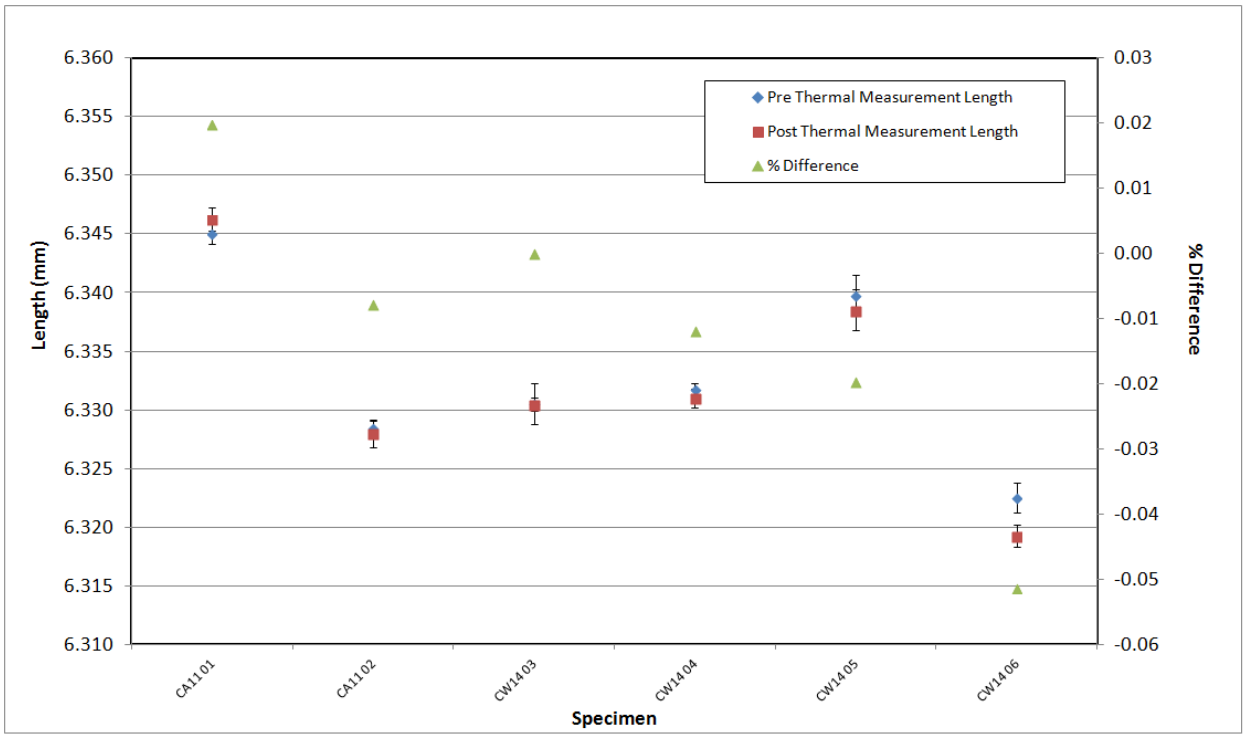

Figure A-146. H-451 Piggyback Pre vs. Post Thermal Measurement Length Comparison.

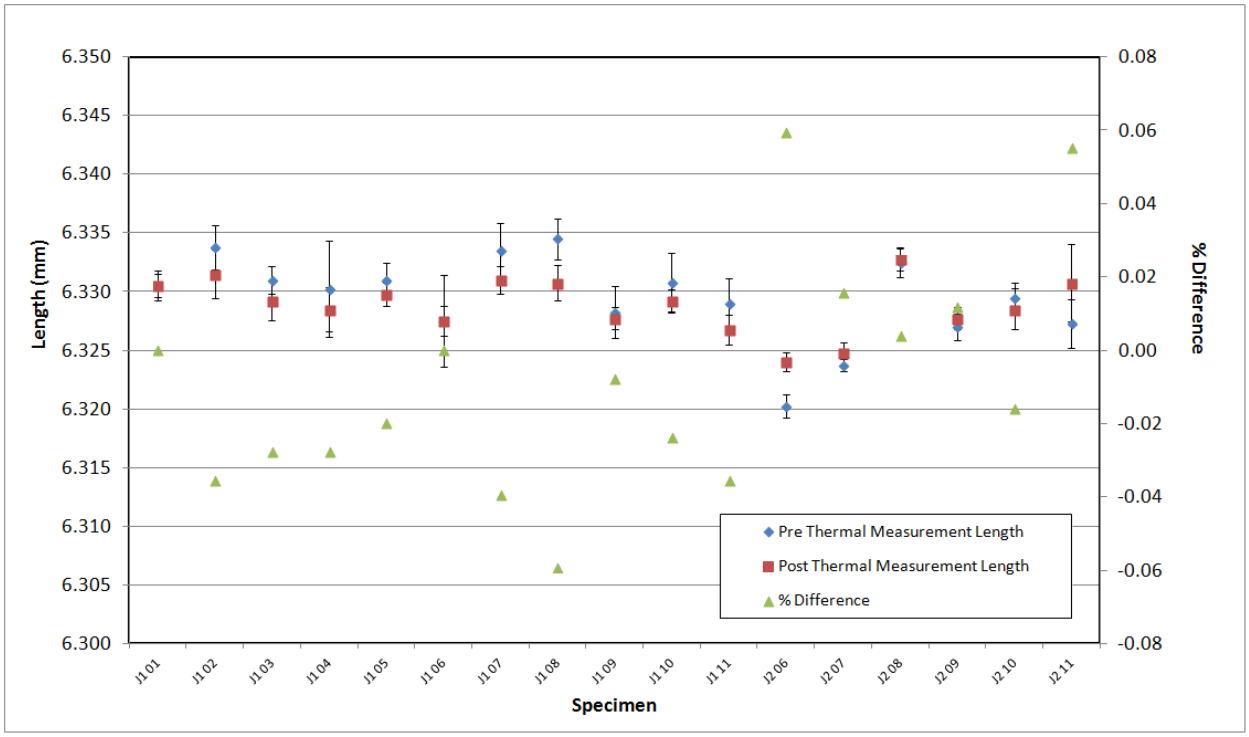

Figure A-147. HLM Piggyback Pre vs. Post Thermal Measurement Length Comparison.

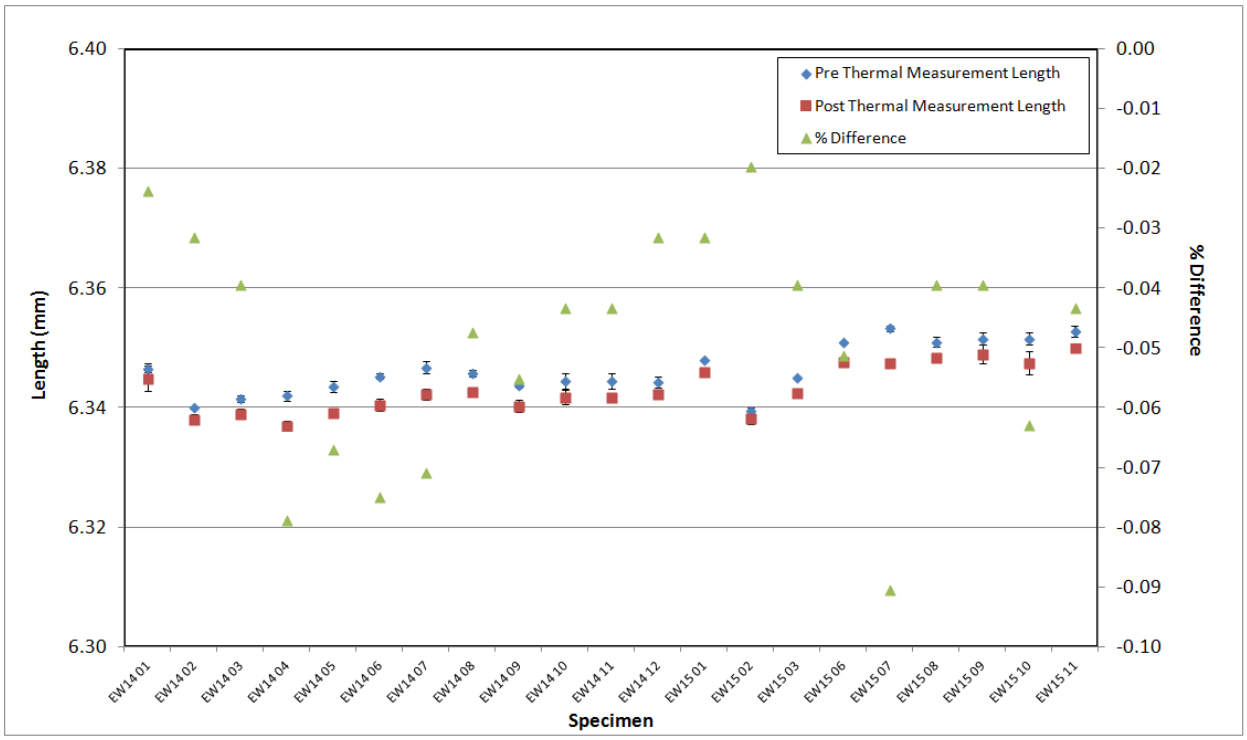

Figure A-148. IG-110 Piggyback Pre vs. Post Thermal Measurement Length Comparison.

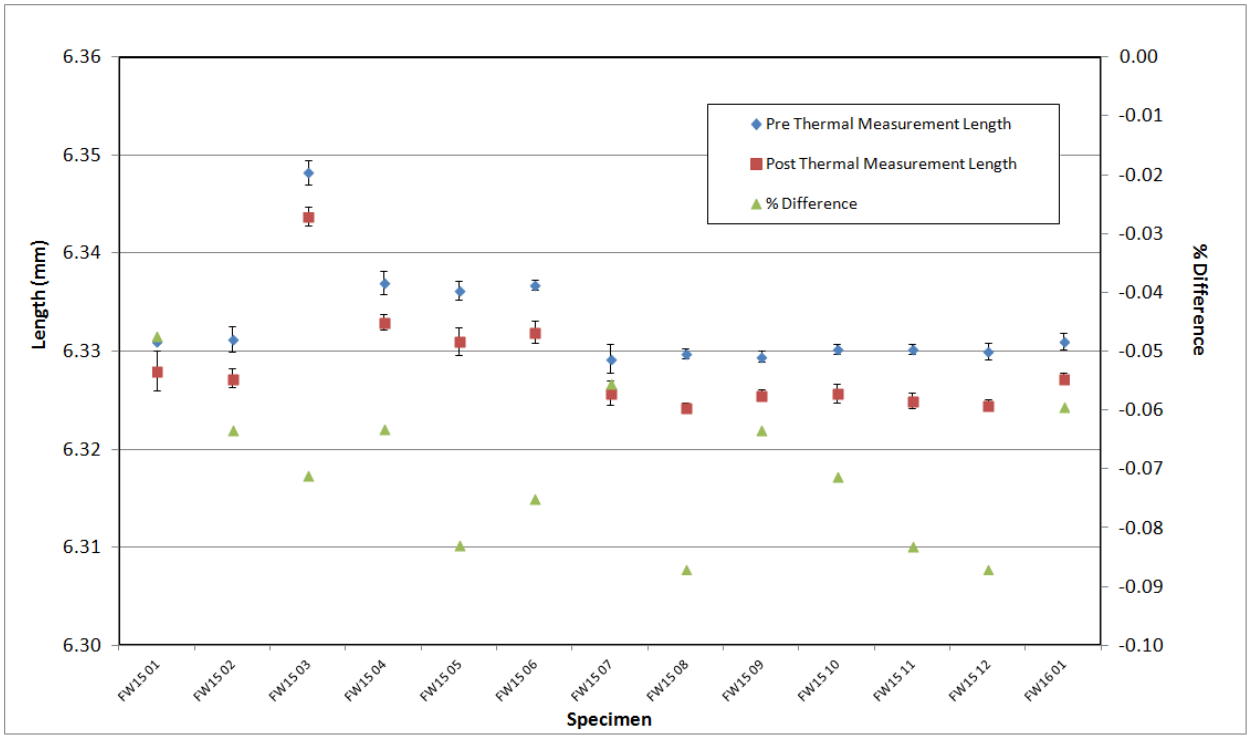

Figure A-149. IG-430 Piggyback Pre vs. Post Thermal Measurement Length Comparison.

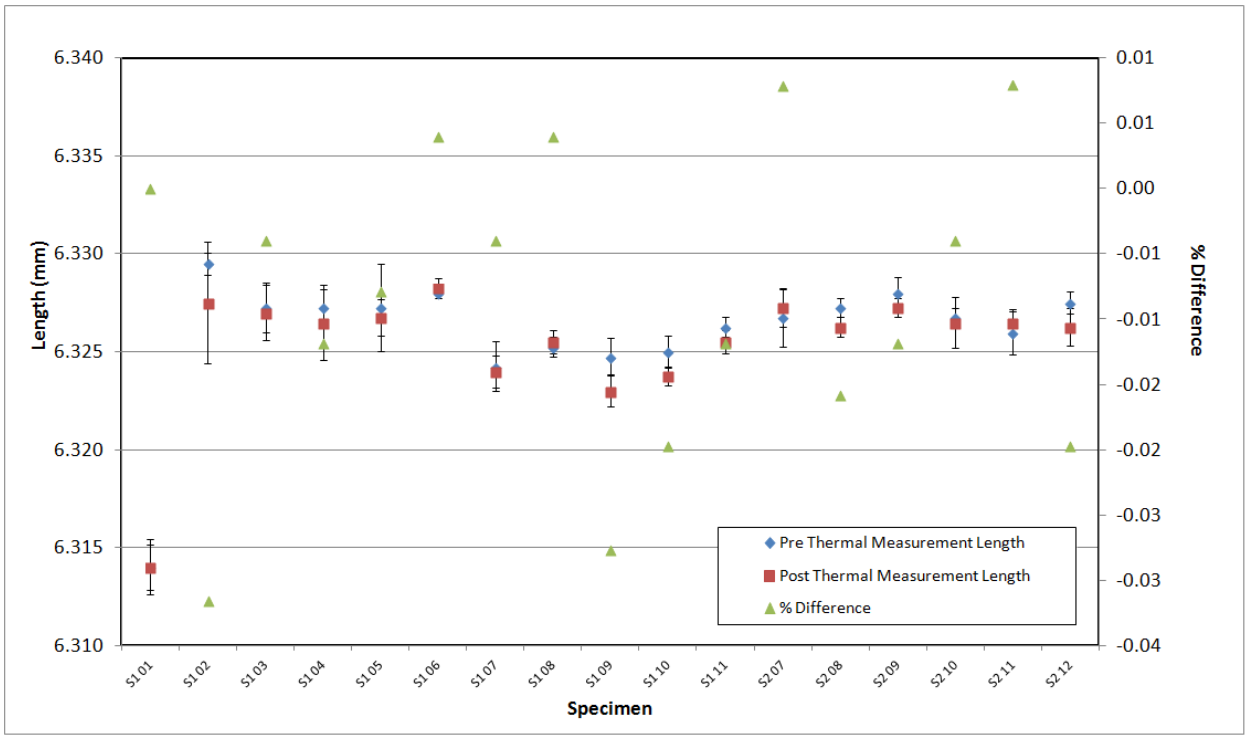

Figure A-150. NBG-10 Piggyback Pre vs. Post Thermal Measurement Length Comparison.

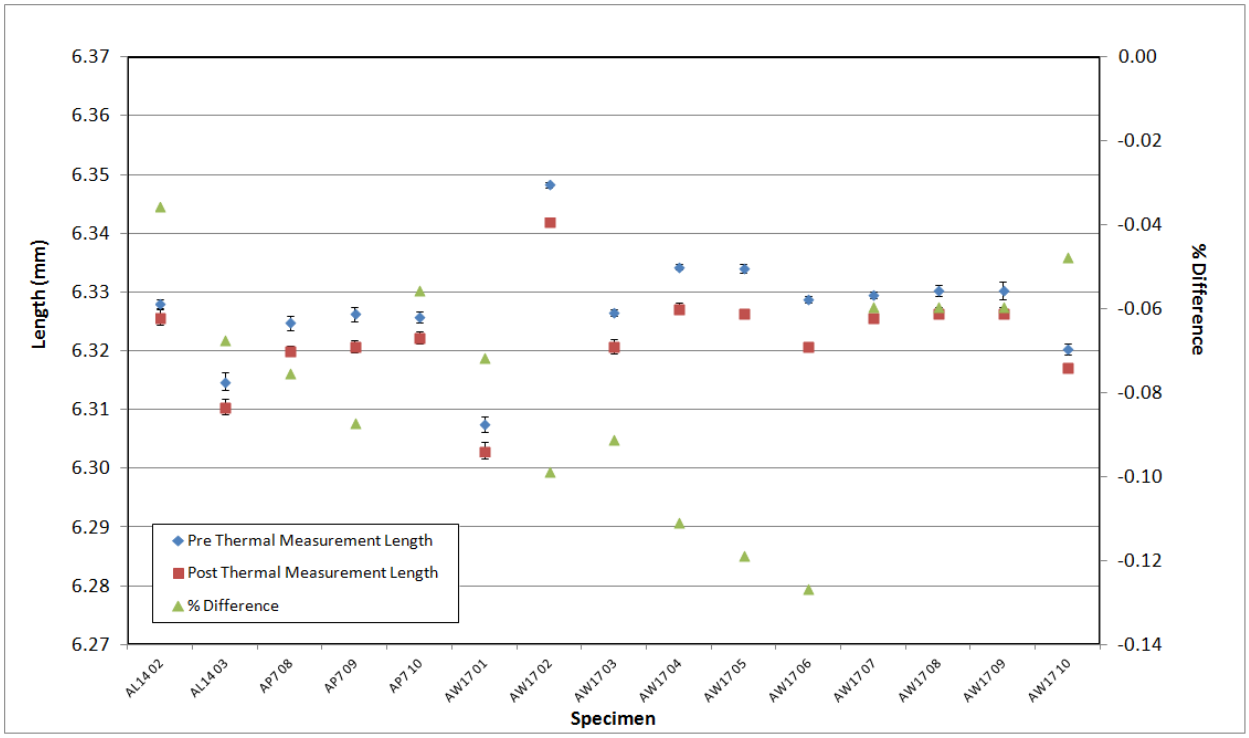

Figure A-151. NBG-17 Piggyback Pre vs. Post Thermal Measurement Length Comparison.

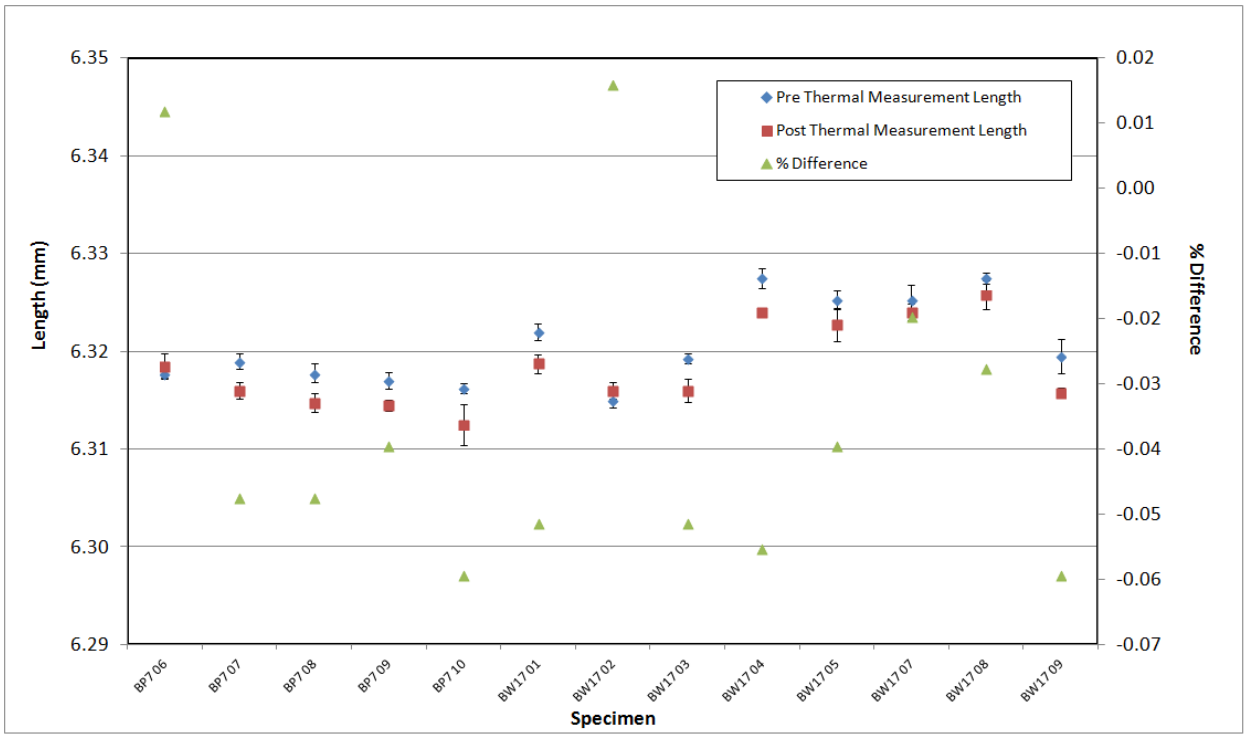

Figure A-152. NBG-18 Piggyback Pre vs. Post Thermal Measurement Length Comparison.

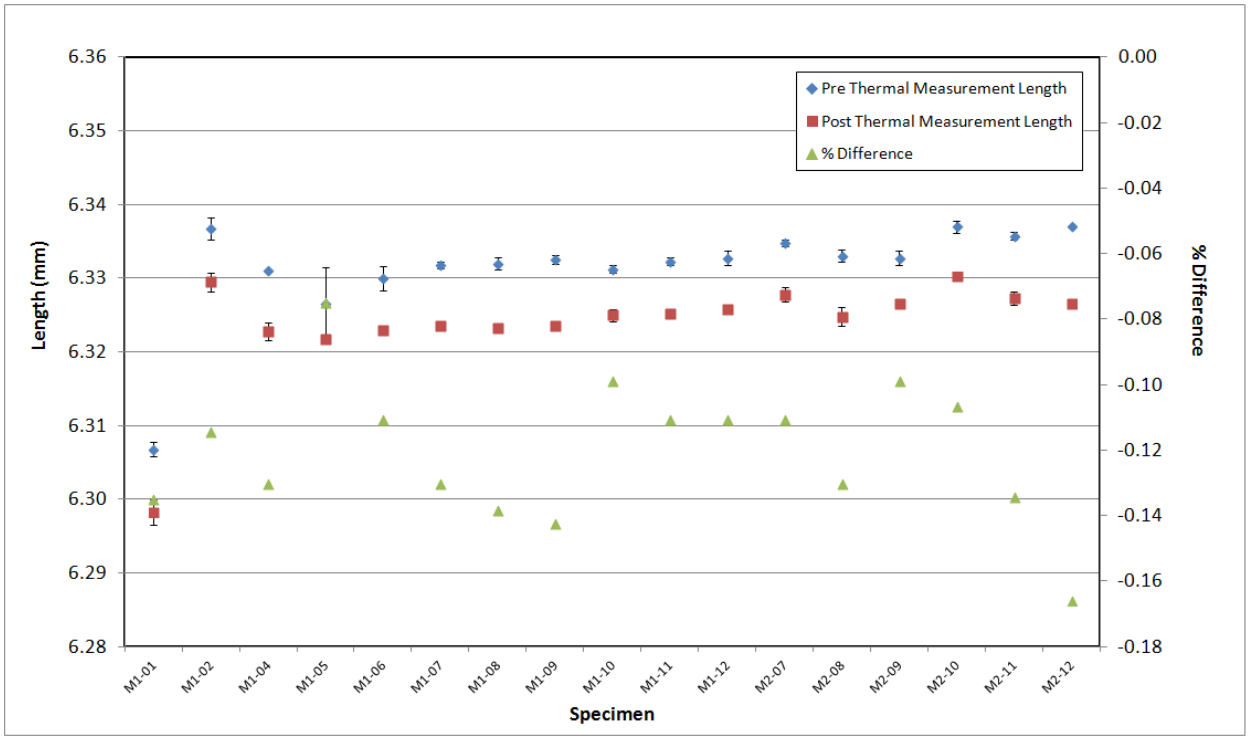

Figure A-153. NBG-25 Piggyback Pre vs. Post Thermal Measurement Length Comparison.

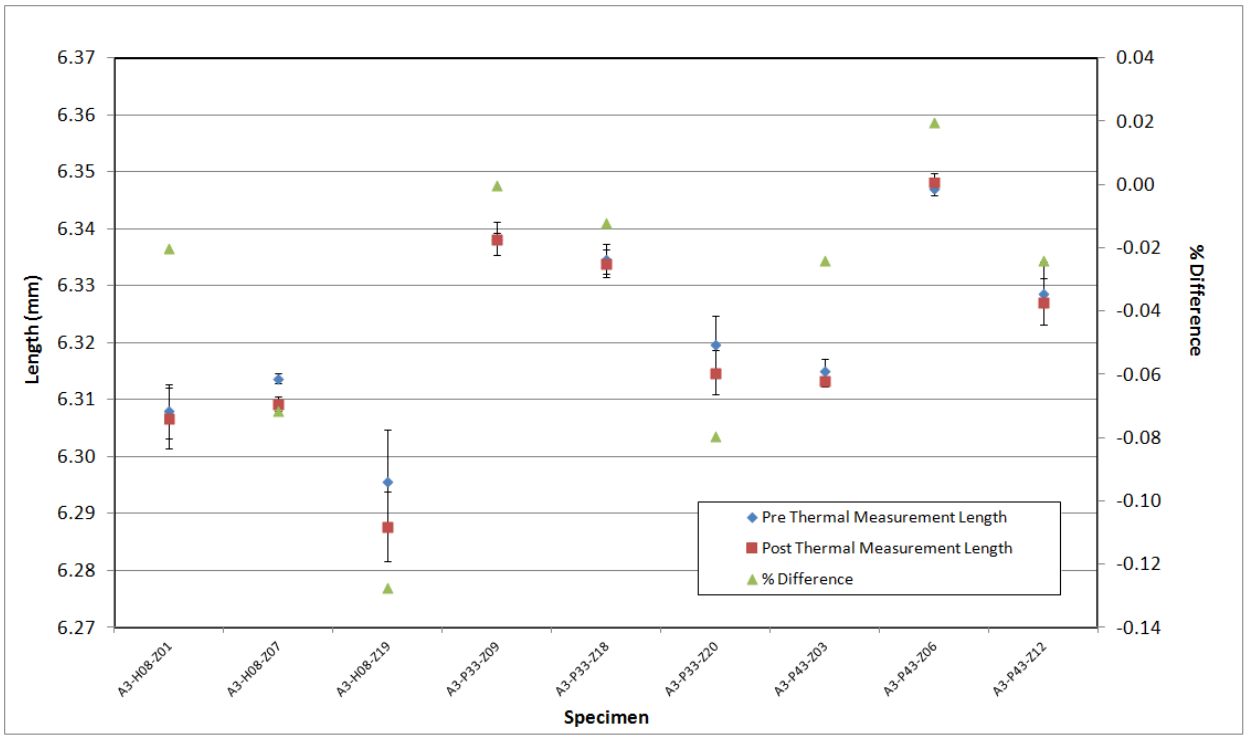

Figure A-154. New Matrix Piggyback Pre vs. Post Thermal Measurement Length Comparison.

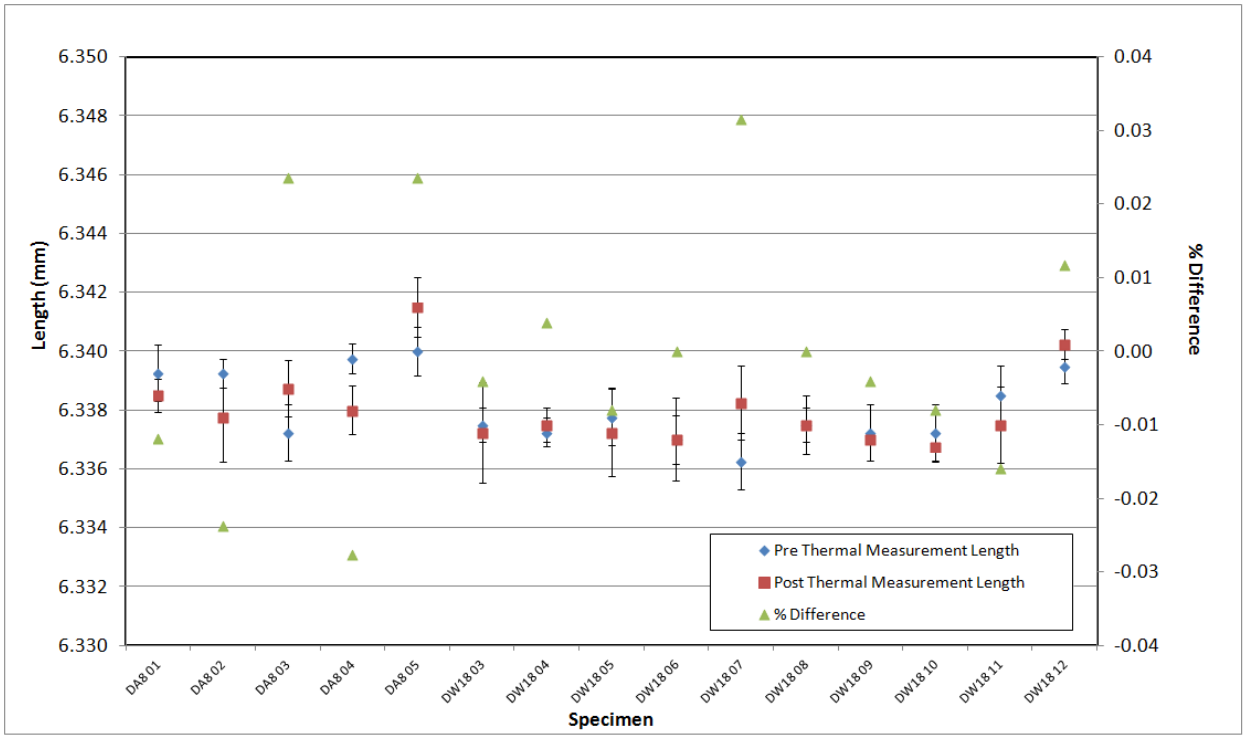

Figure A-155. PCEA Piggyback Pre vs. Post Thermal Measurement Length Comparison.

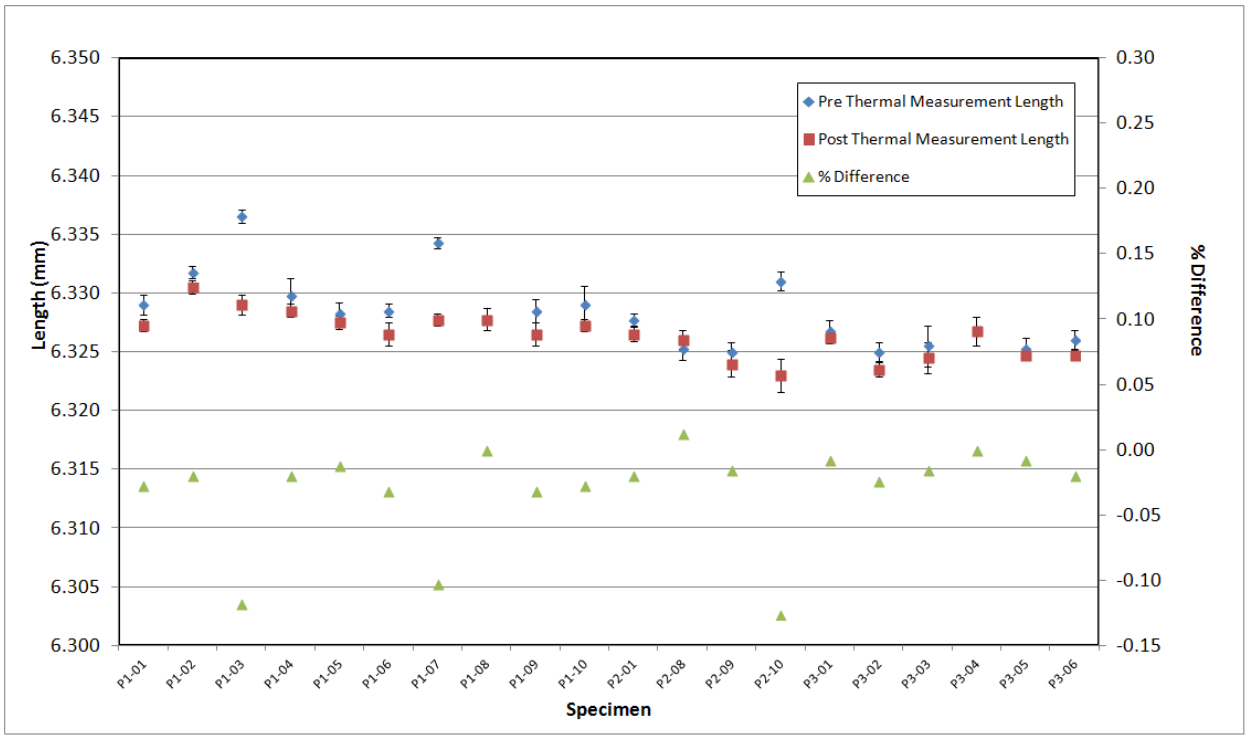

Figure A-156. PCIB Piggyback Pre vs. Post Thermal Measurement Length Comparison.

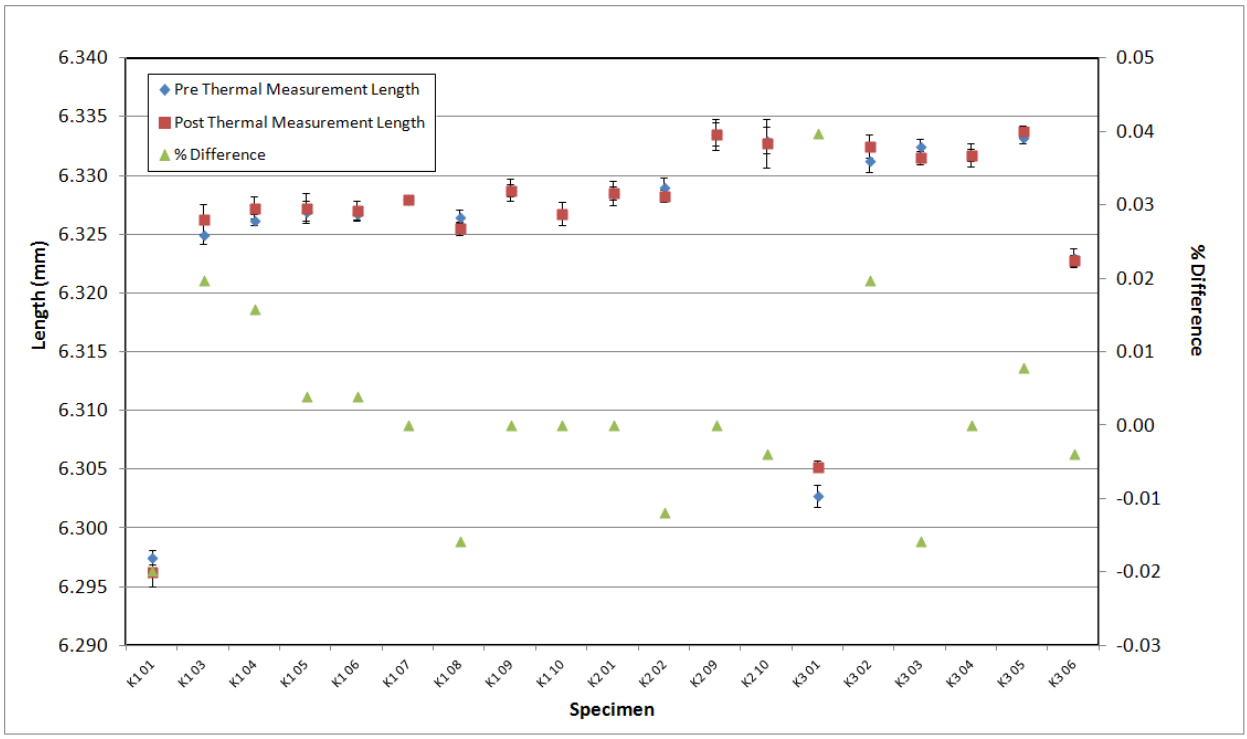

Figure A-157. PGX Piggyback Pre vs. Post Thermal Measurement Length Comparison.

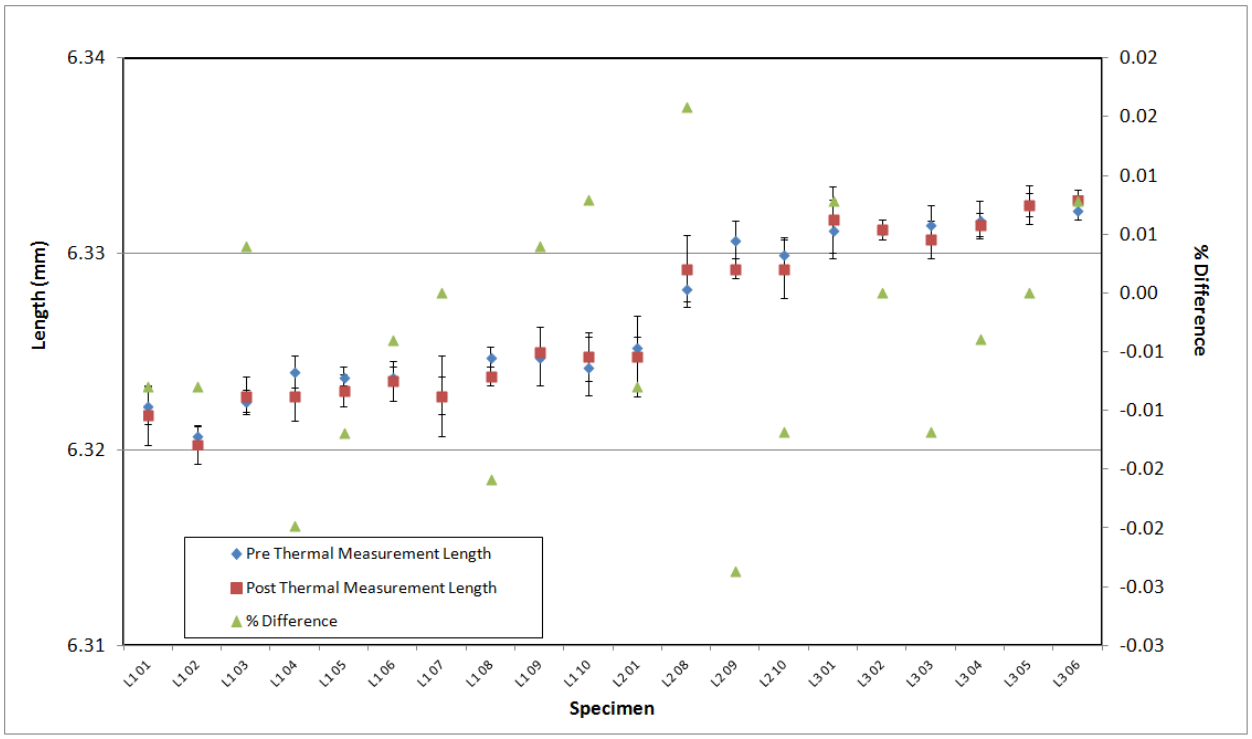

Figure A-158. PPEA Piggyback Pre vs. Post Thermal Measurement Length Comparison.

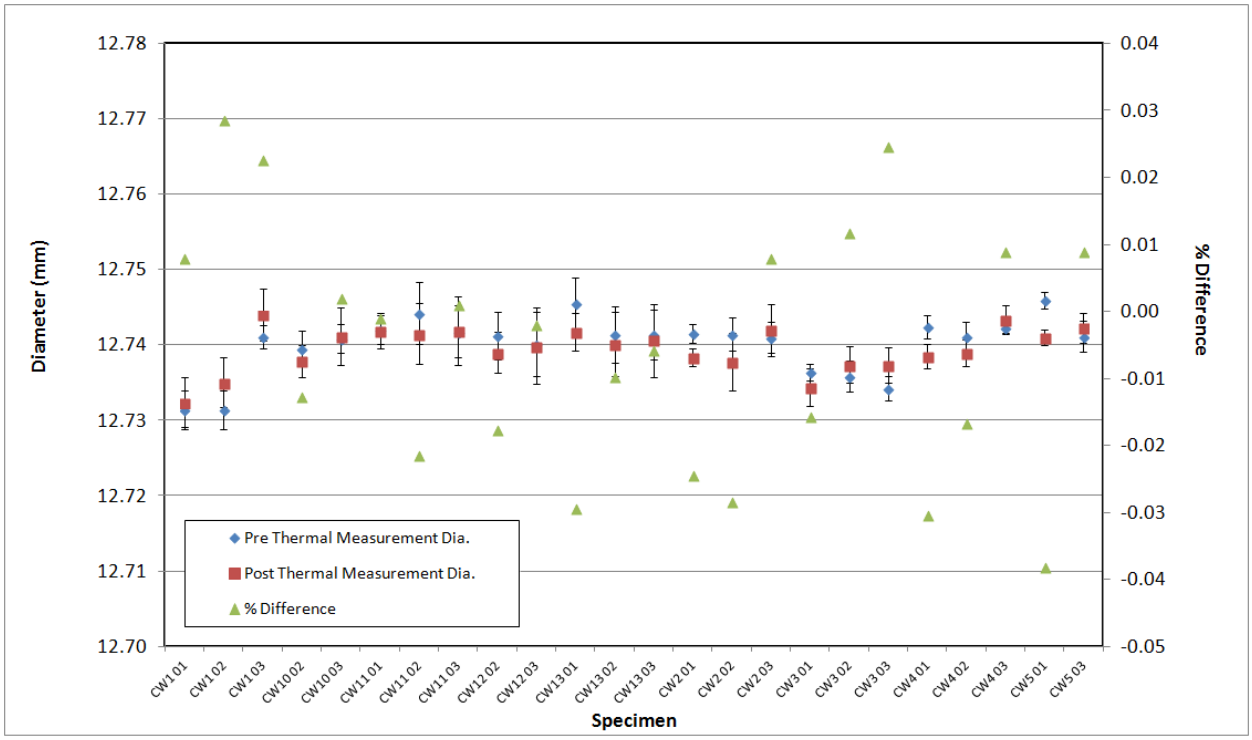

Figure A-159. H-451 Creep Pre vs. Post Thermal Measurement Diameter Comparison.

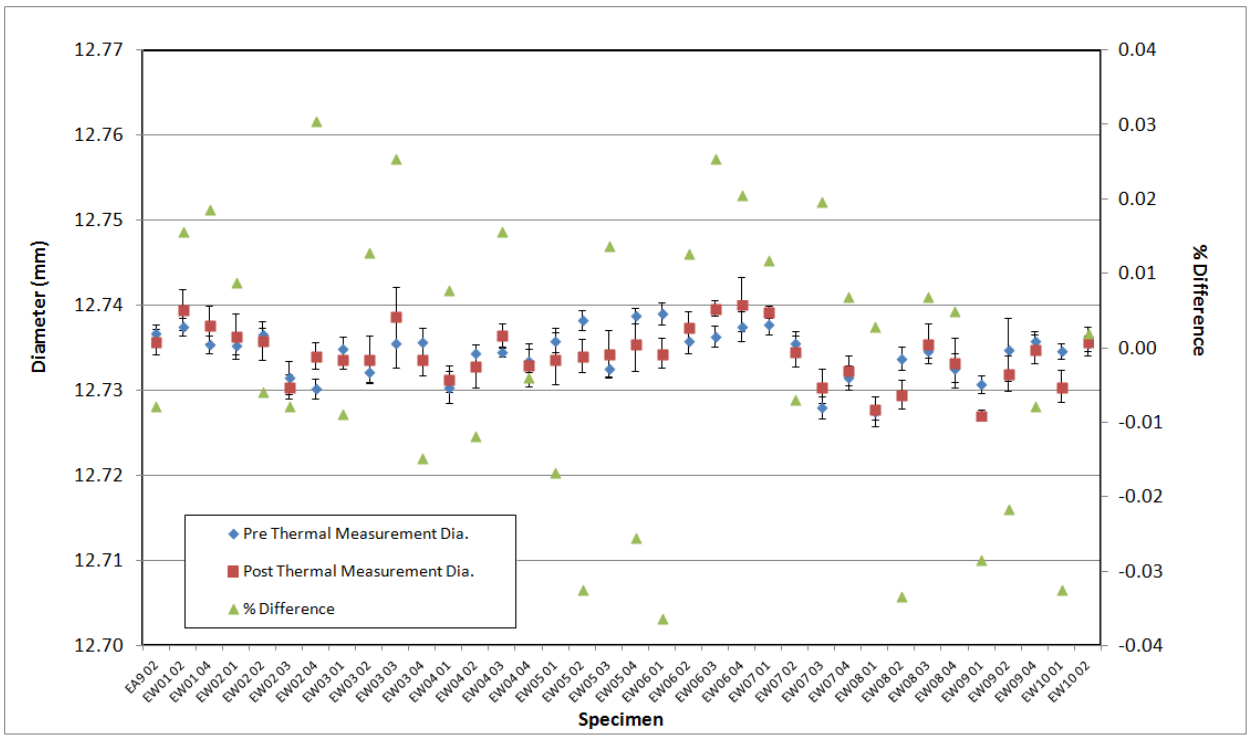

Figure A-160. IG-110 Creep Pre vs. Post Thermal Measurement Diameter Comparison.

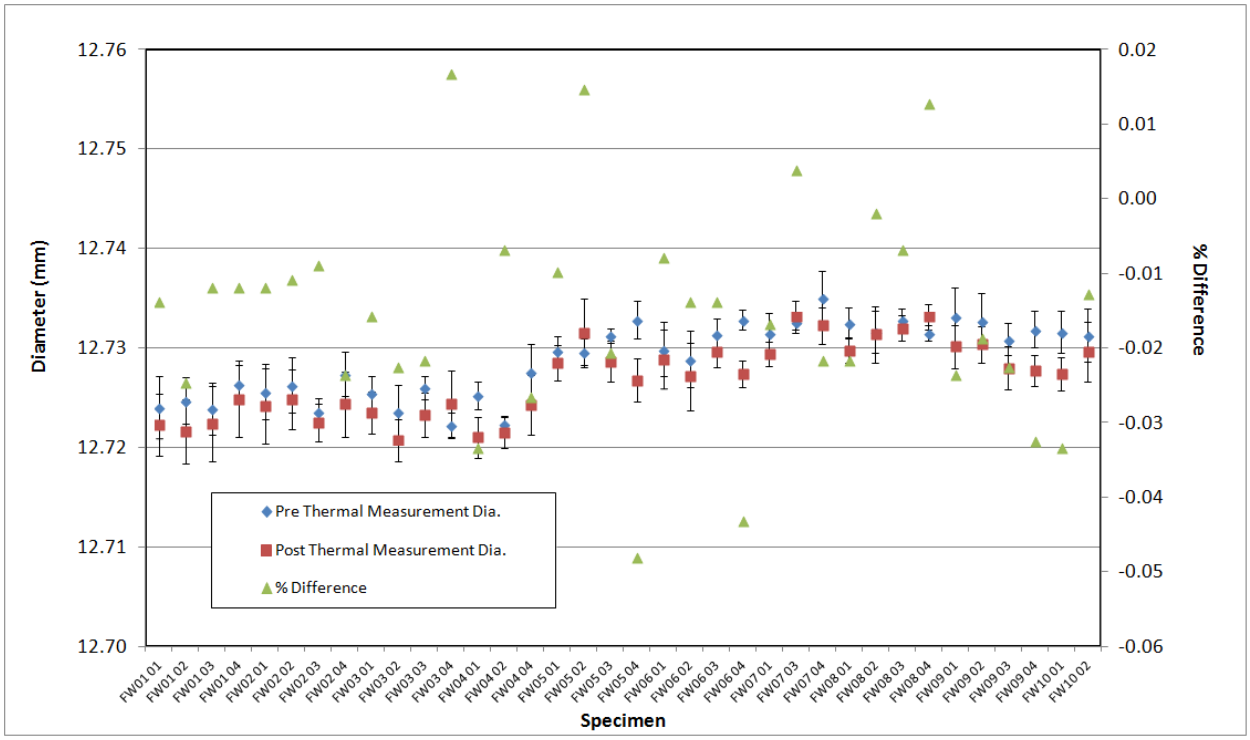

Figure A-161. IG-430 Creep Pre vs. Post Thermal Measurement Diameter Comparison.

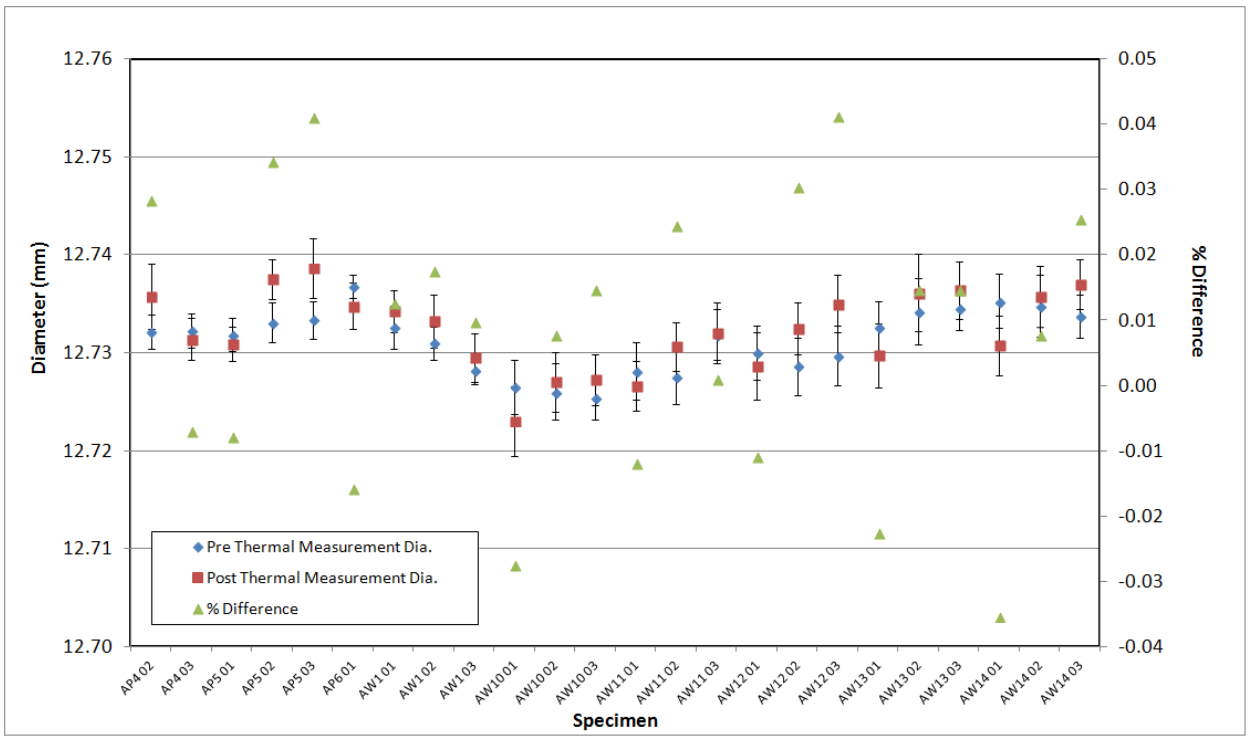

Figure A-162. NBG-17 Creep Pre vs. Post Thermal Measurement Diameter Comparison.

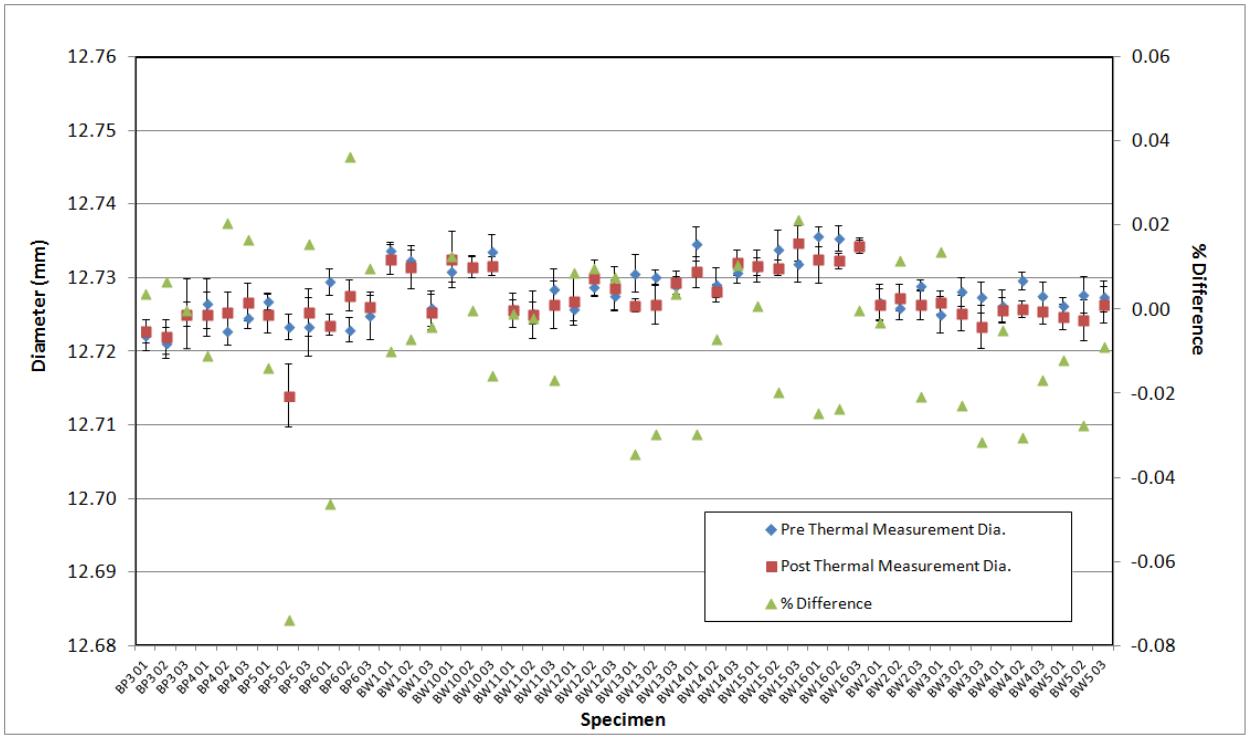

Figure A-163. NBG-18 Creep Pre vs. Post Thermal Measurement Diameter Comparison.

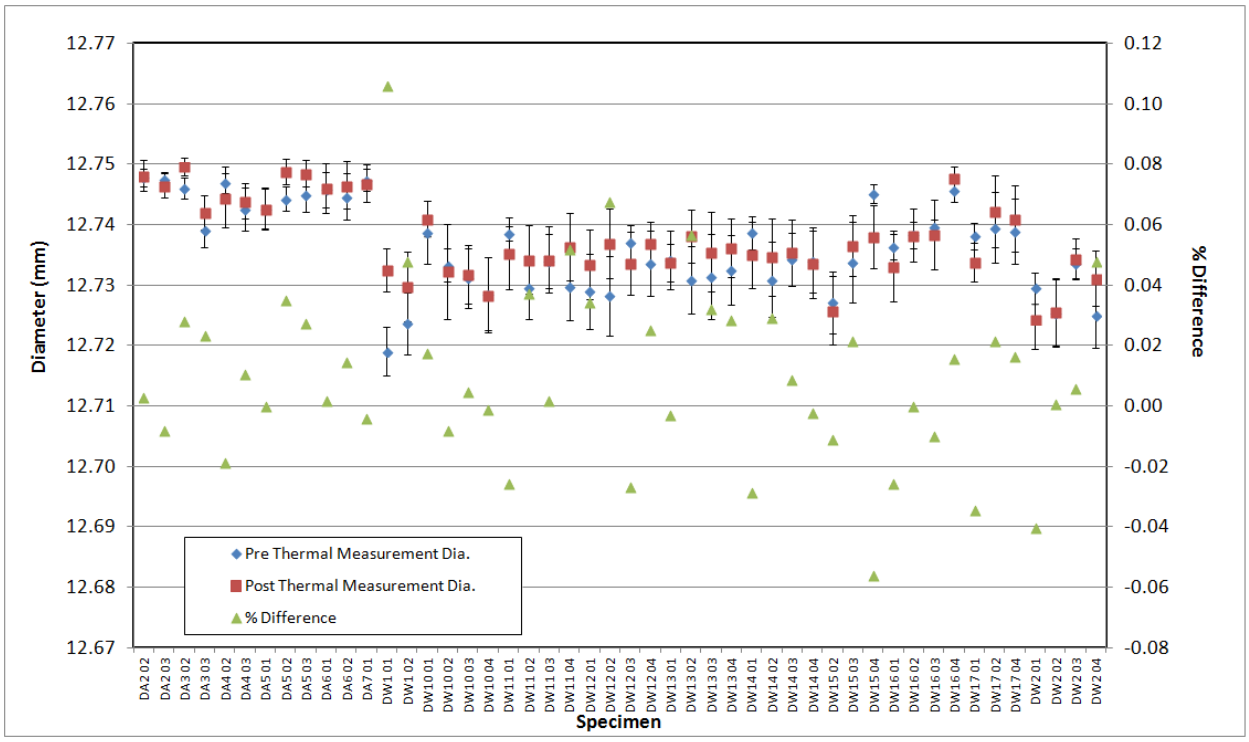

Figure A-164. PCEA Creep Pre vs. Post Thermal Measurement Diameter Comparison.

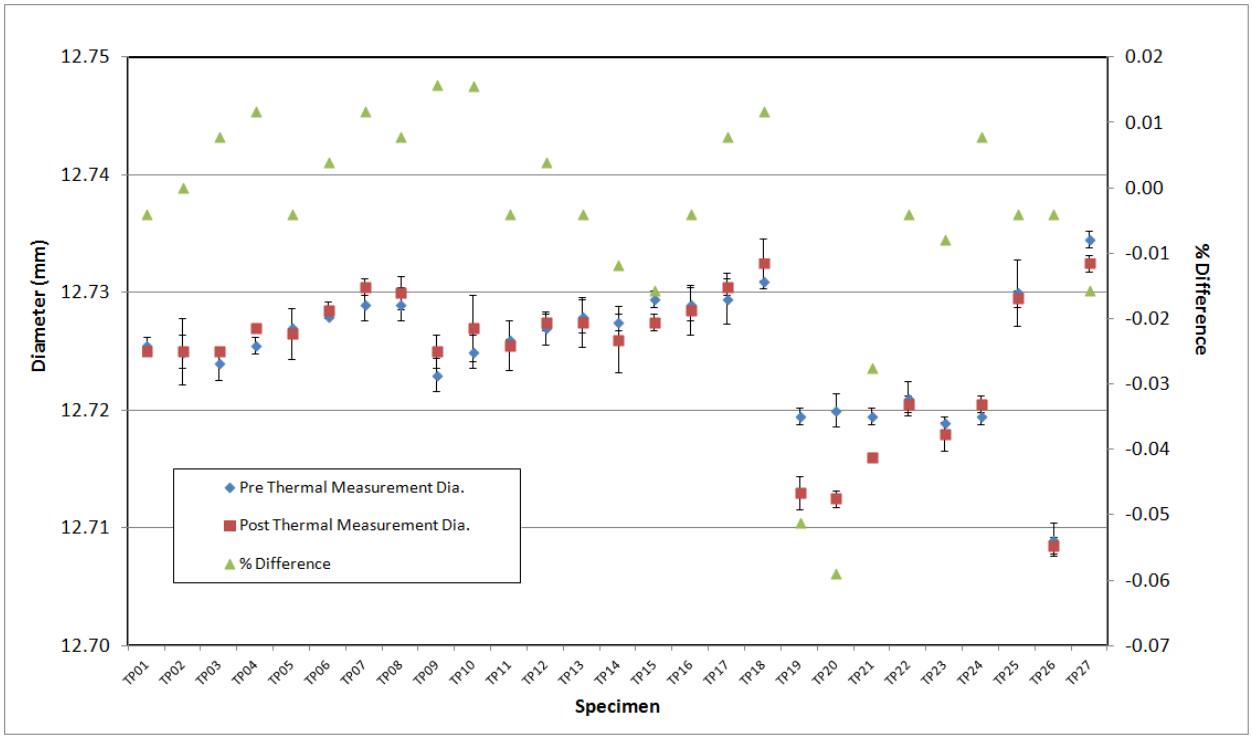

Figure A-165. 2114 Piggyback Pre vs. Post Thermal Measurement Diameter Comparison.

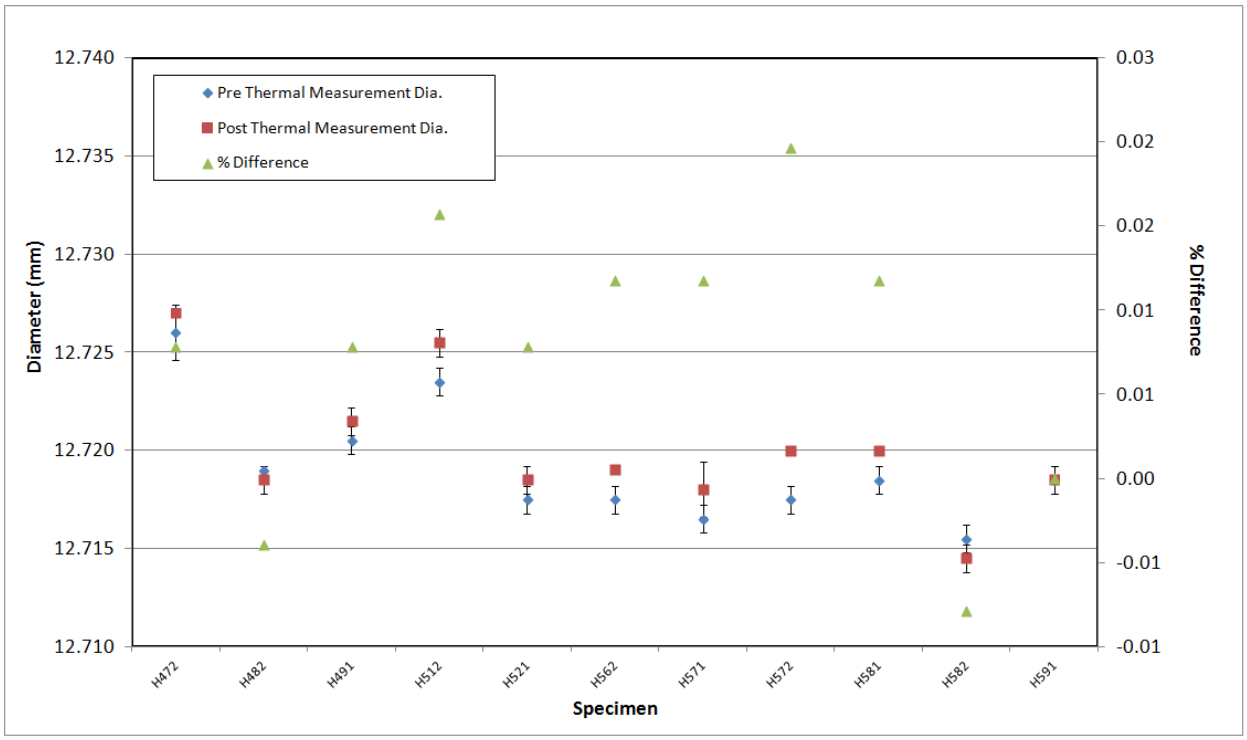

Figure A-166. A3 Matrix Piggyback Pre vs. Post Thermal Measurement Diameter Comparison.

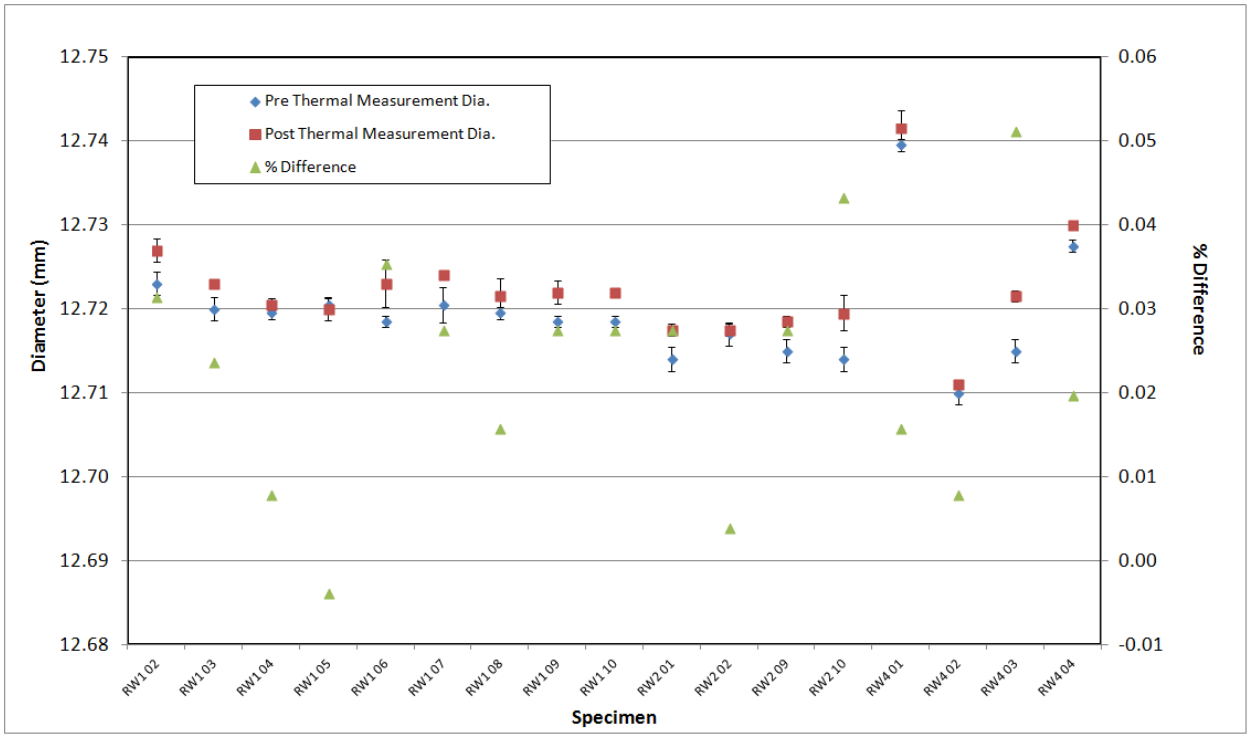

Figure A-167. BAN Piggyback Pre vs. Post Thermal Measurement Diameter Comparison.

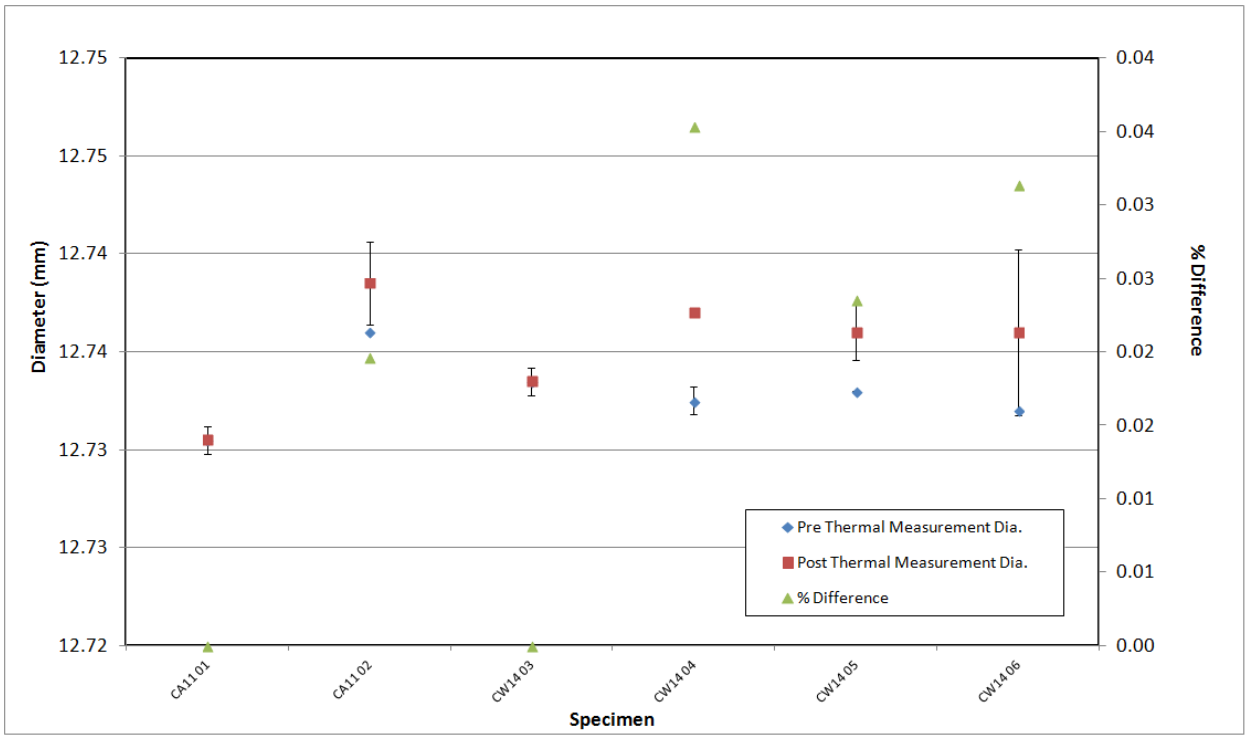

Figure A-168. H-451 Piggyback Pre vs. Post Thermal Measurement Diameter Comparison.

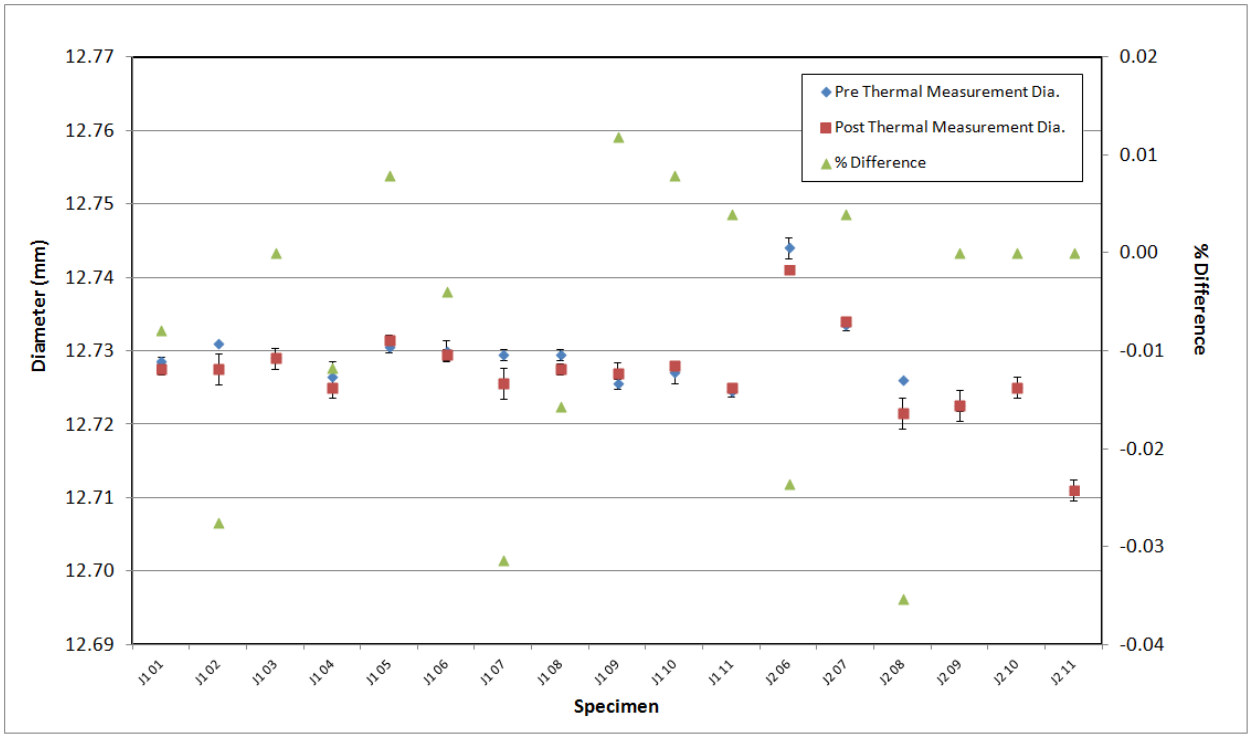

Figure A-169. HLM Piggyback Pre vs. Post Thermal Measurement Diameter Comparison.

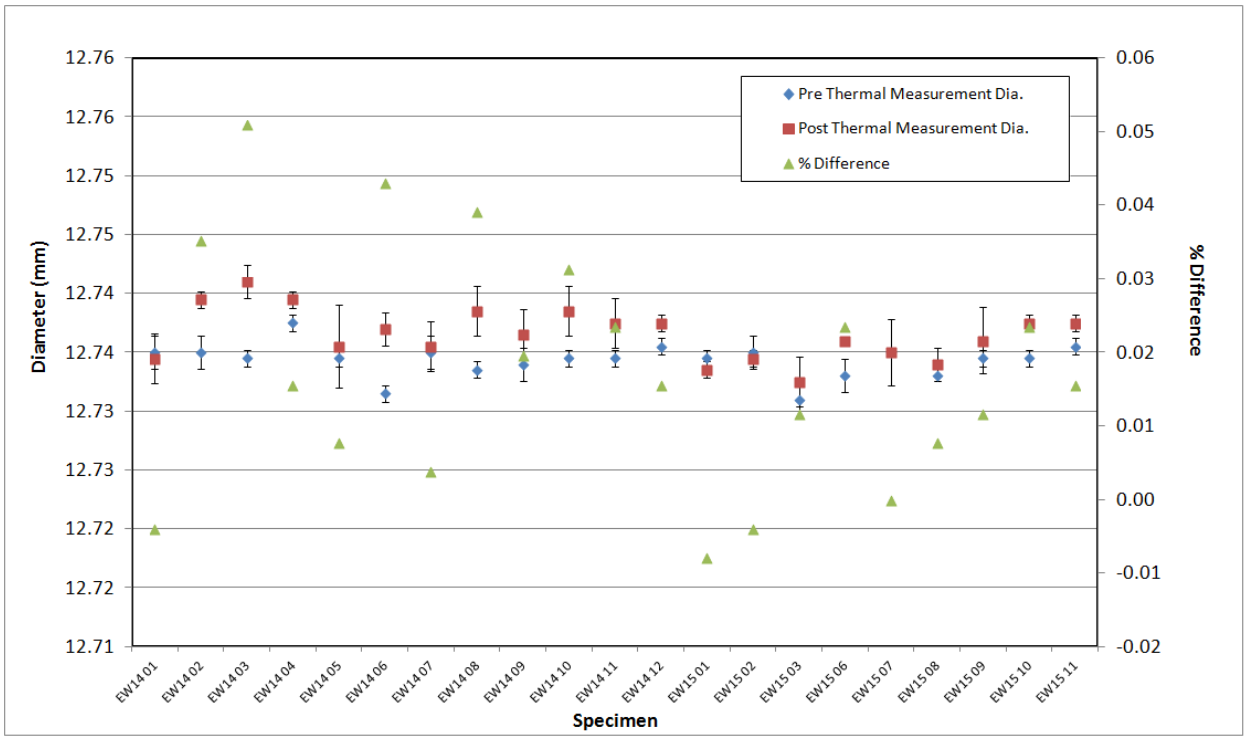

Figure A-170. IG-110 Piggyback Pre vs. Post Thermal Measurement Diameter Comparison.

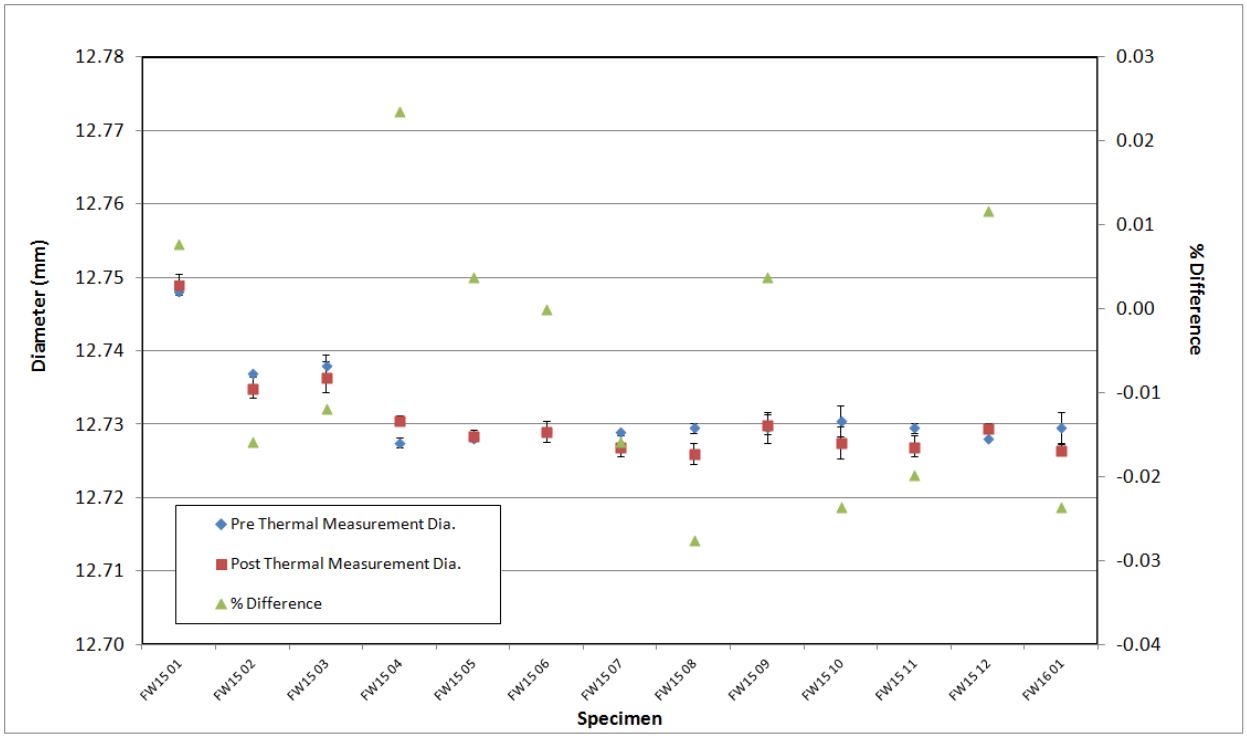

Figure A-171. IG-430 Piggyback Pre vs. Post Thermal Measurement Diameter Comparison.

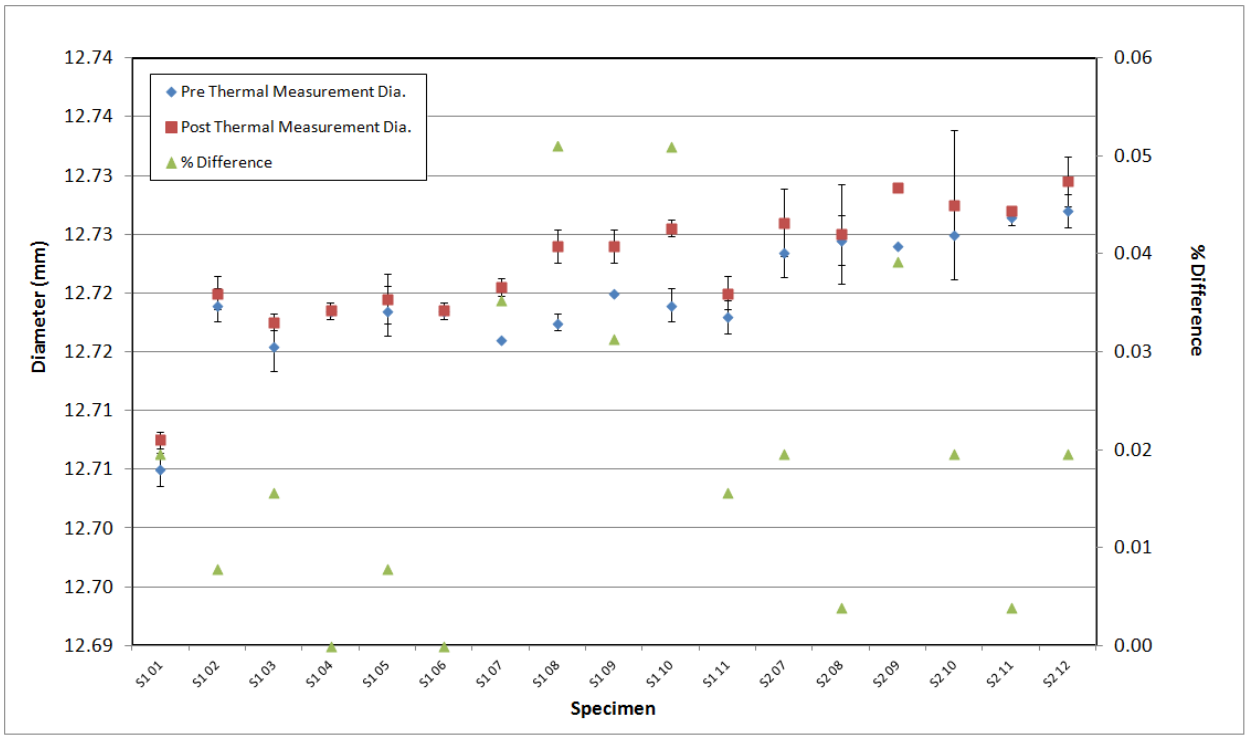

Figure A-172. NBG-10 Piggyback Pre vs. Post Thermal Measurement Diameter Comparison.

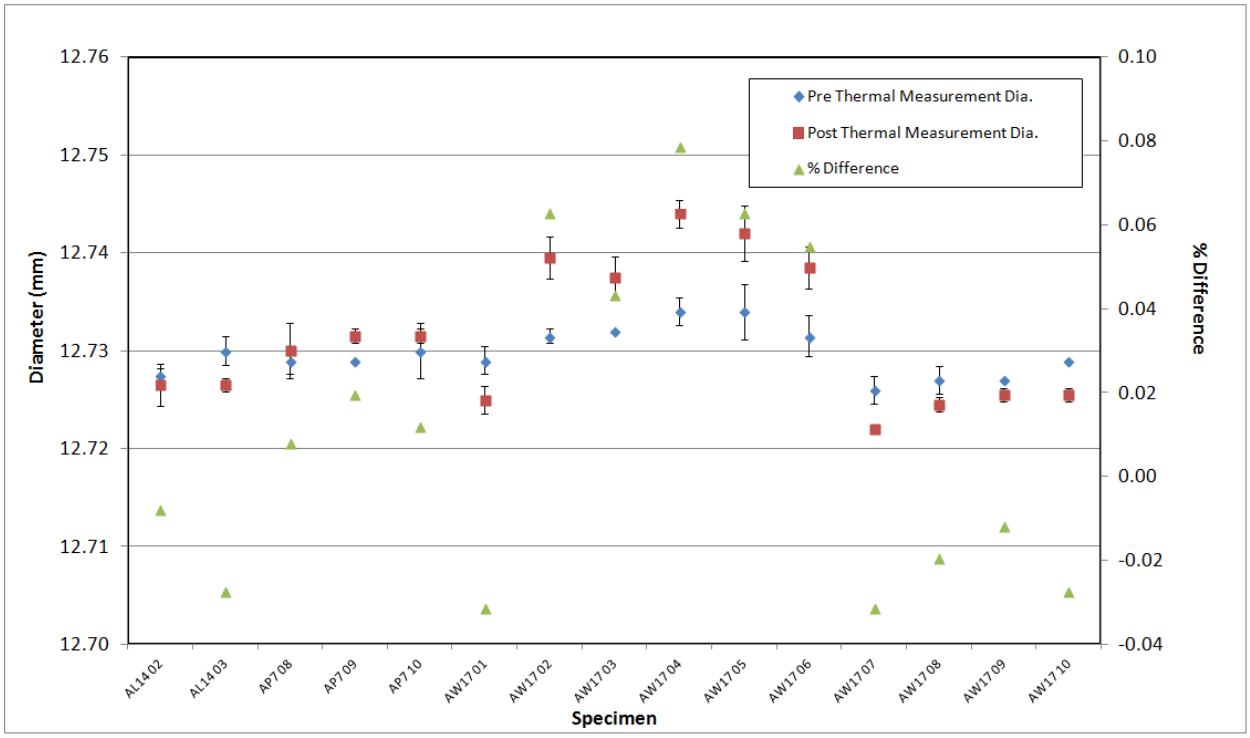

Figure A-173. NBG-17 Piggyback Pre vs. Post Thermal Measurement Diameter Comparison.

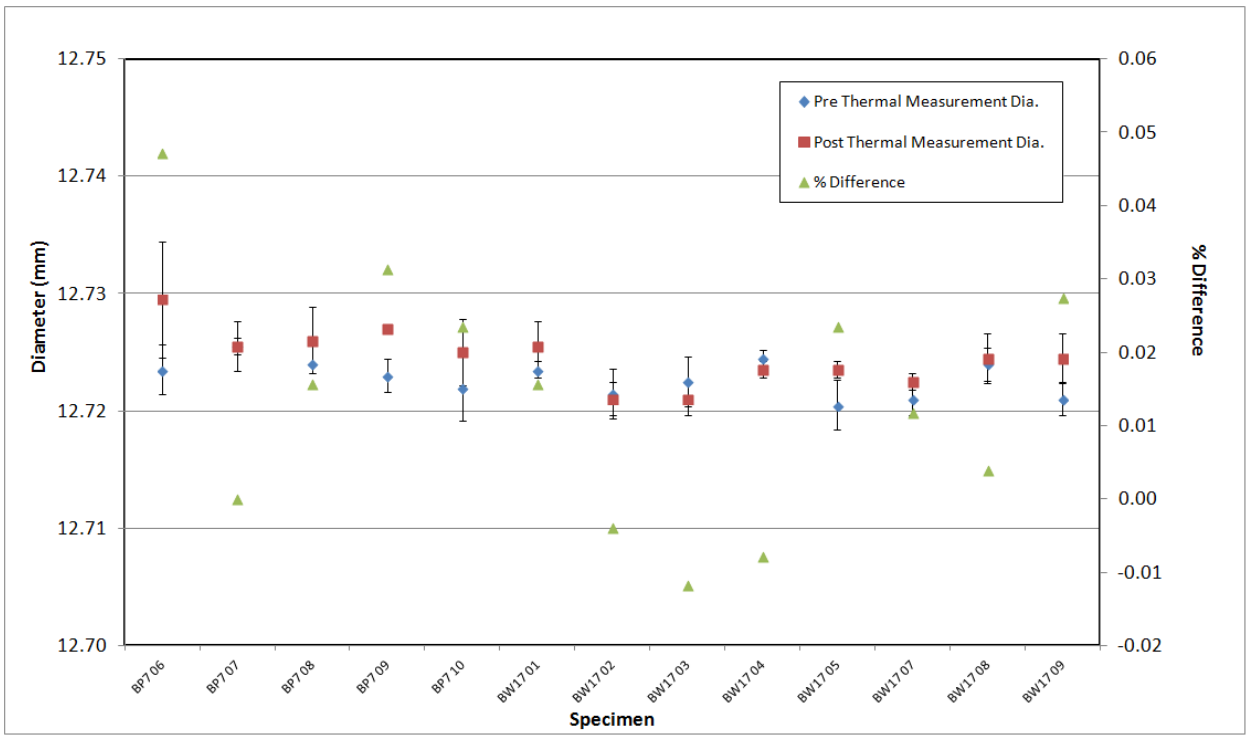

Figure A-174. NBG-18 Piggyback Pre vs. Post Thermal Measurement Diameter Comparison.

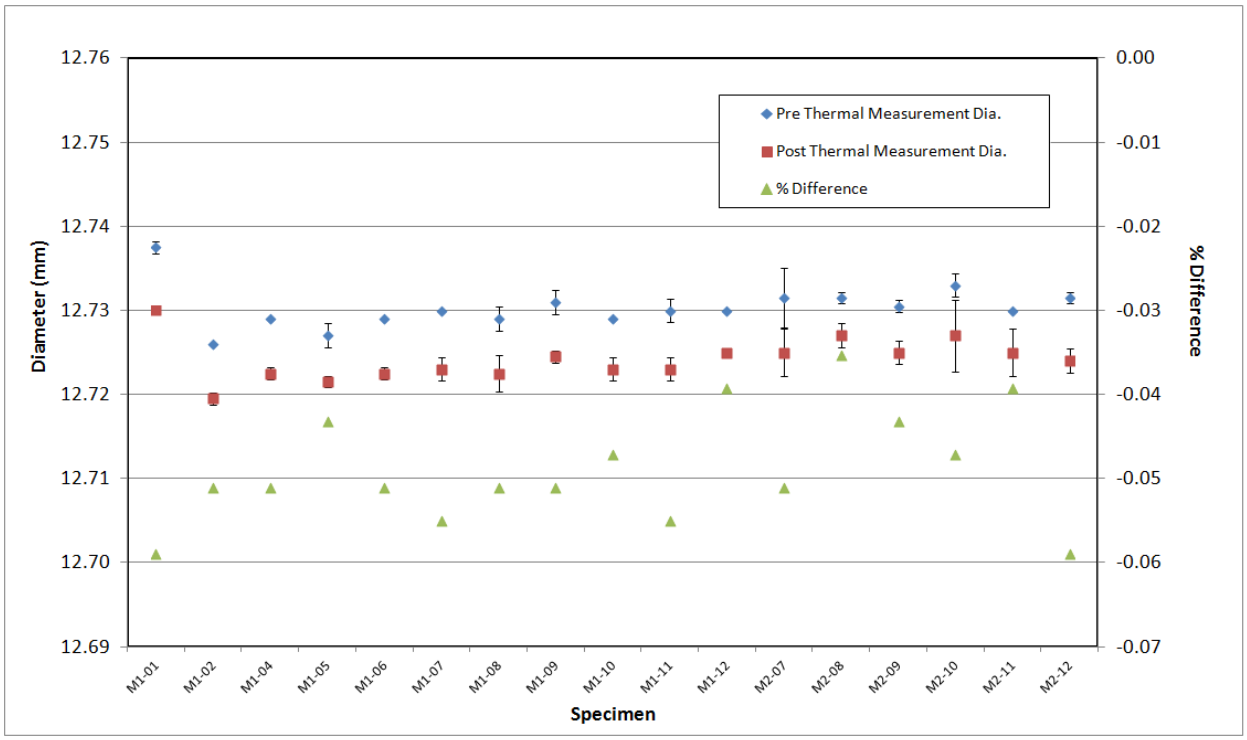

Figure A-175. NBG-25 Piggyback Pre vs. Post Thermal Measurement Diameter Comparison.

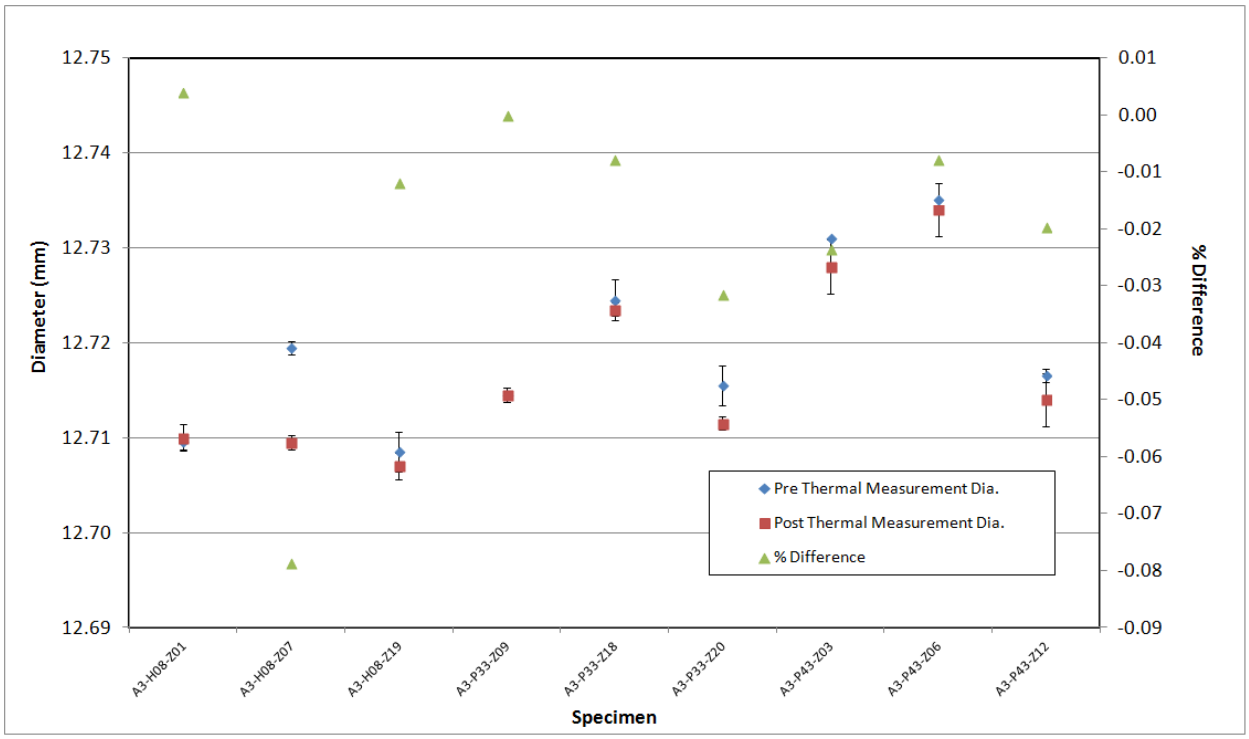

Figure A-176. New Matrix Piggyback Pre vs. Post Thermal Measurement Diameter Comparison.

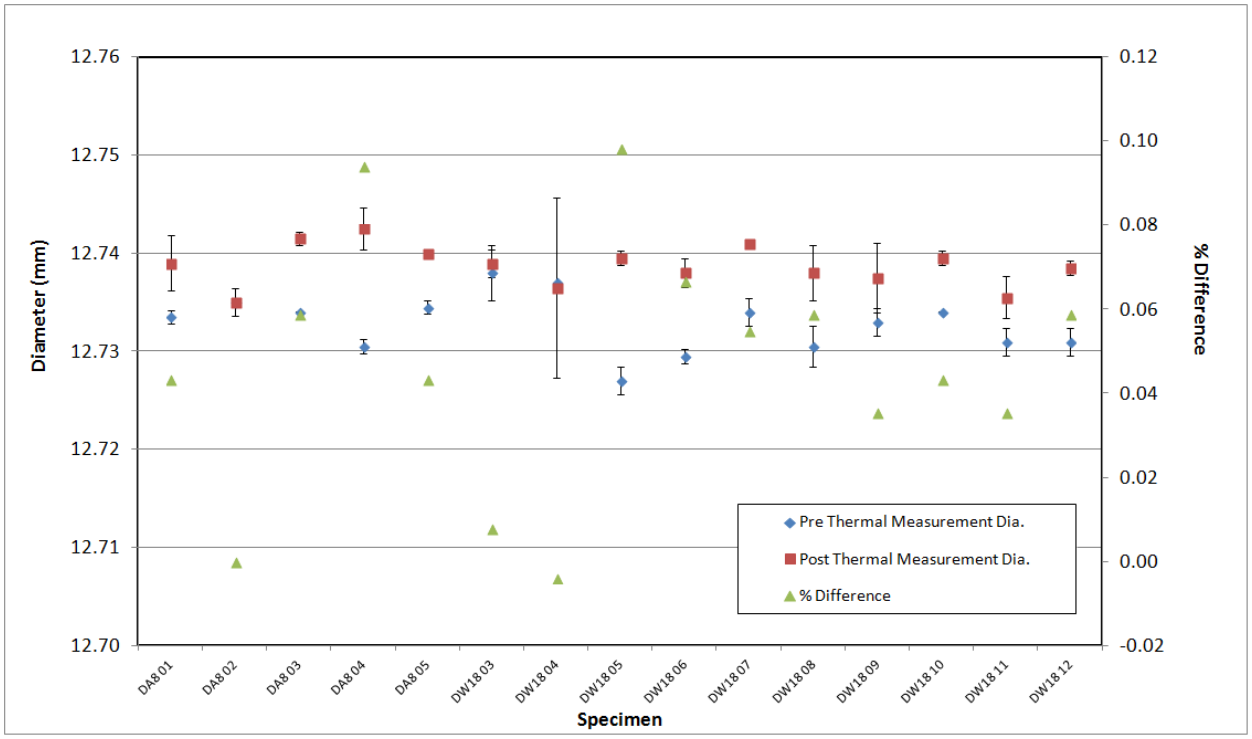

Figure A-177. PCEA Piggyback Pre vs. Post Thermal Measurement Diameter Comparison.

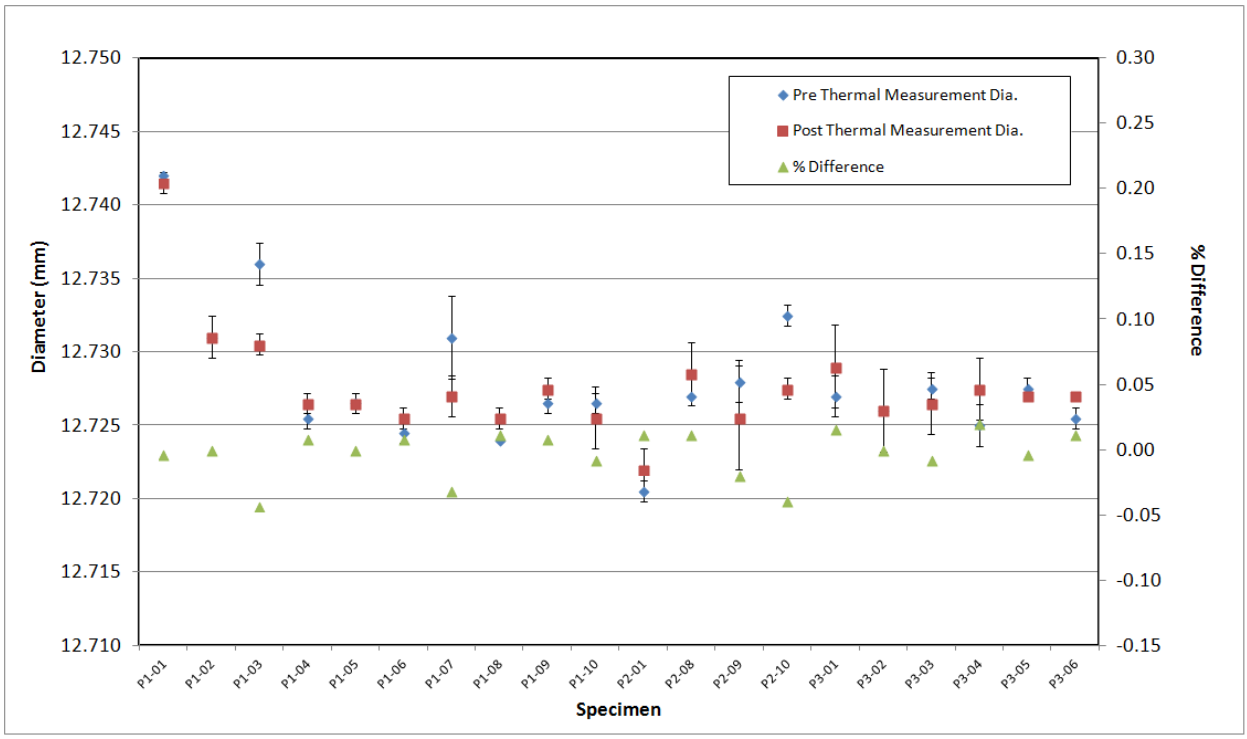

Figure A-178. PCIB Piggyback Pre vs. Post Thermal Measurement Diameter Comparison.

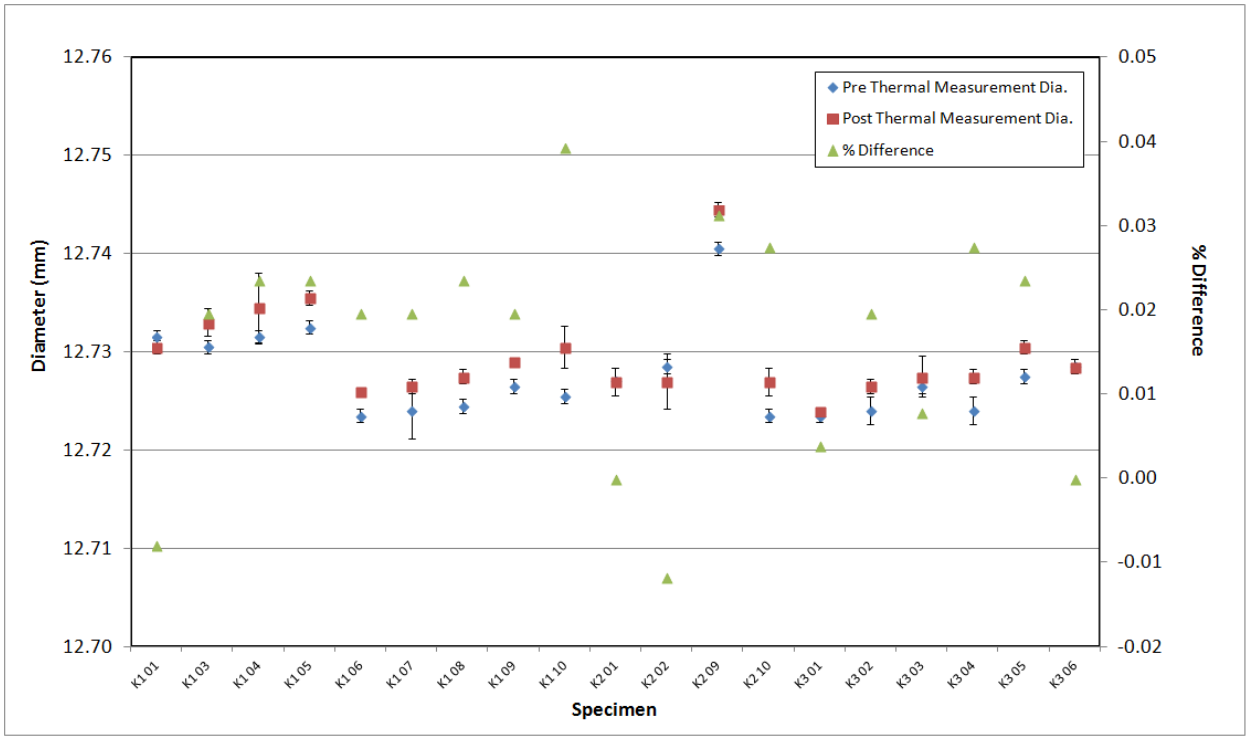

Figure A-179. PGX Piggyback Pre vs. Post Thermal Measurement Diameter Comparison.

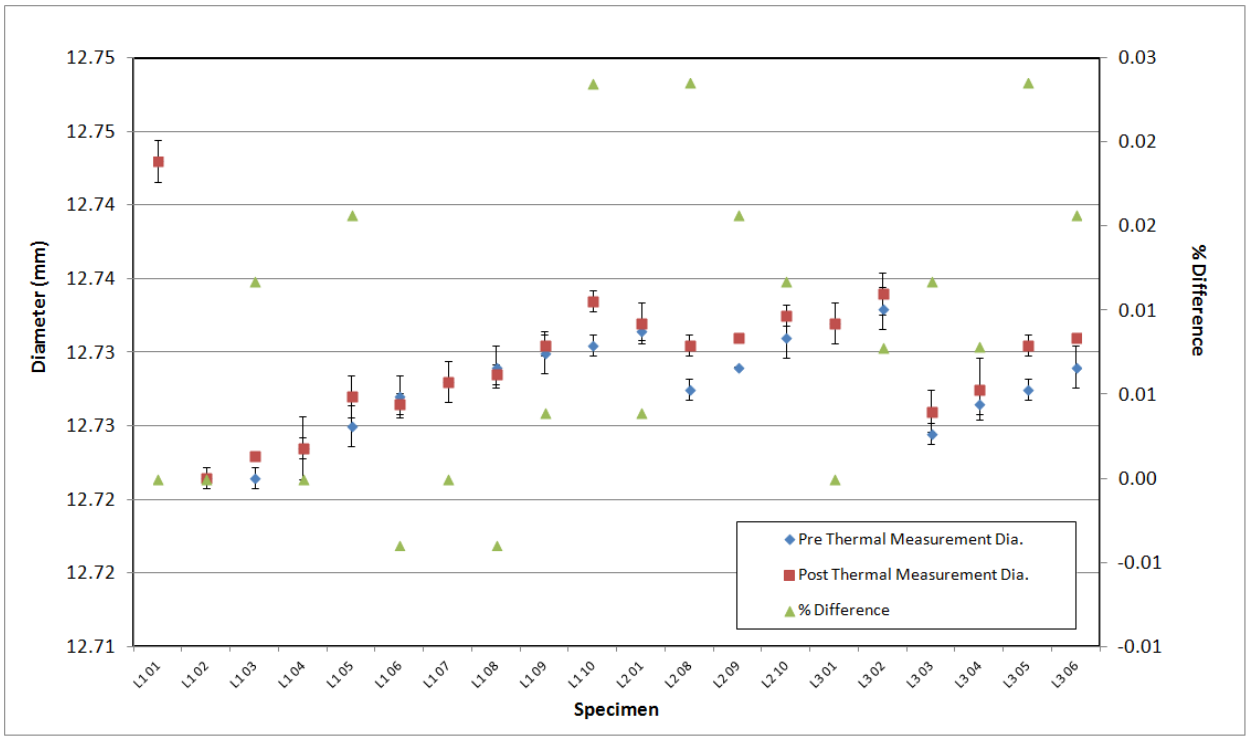

Figure A-180. PPEA Piggyback Pre vs. Post Thermal Measurement Diameter Comparison.

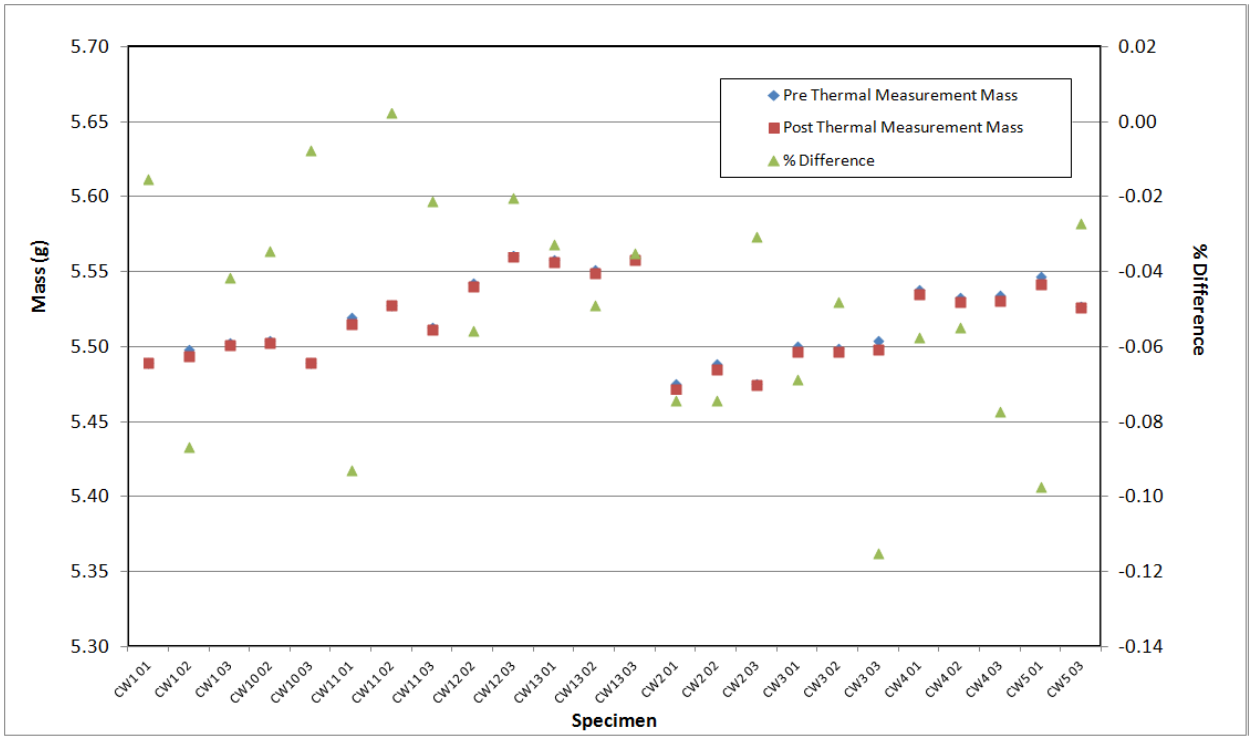

Figure A-181. H-451 Creep Pre vs. Post Thermal Measurement Mass Comparison.

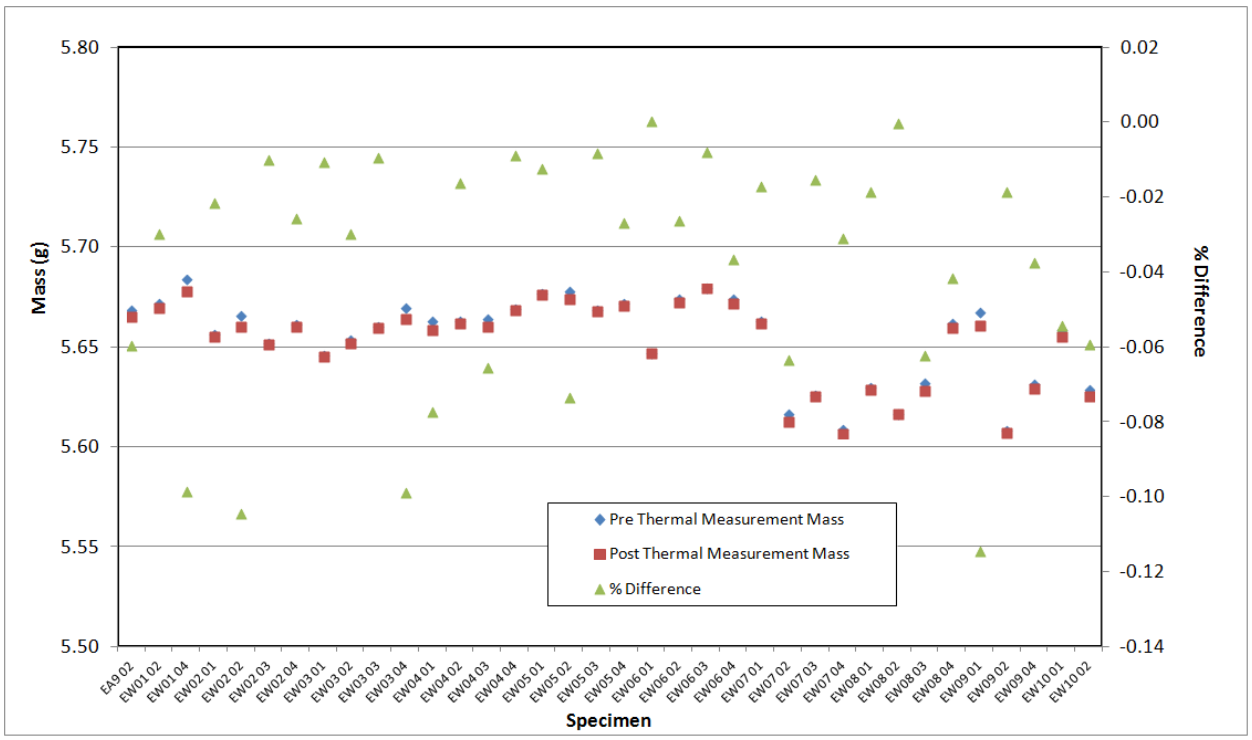

Figure A-182. IG-110 Creep Pre vs. Post Thermal Measurement Mass Comparison.

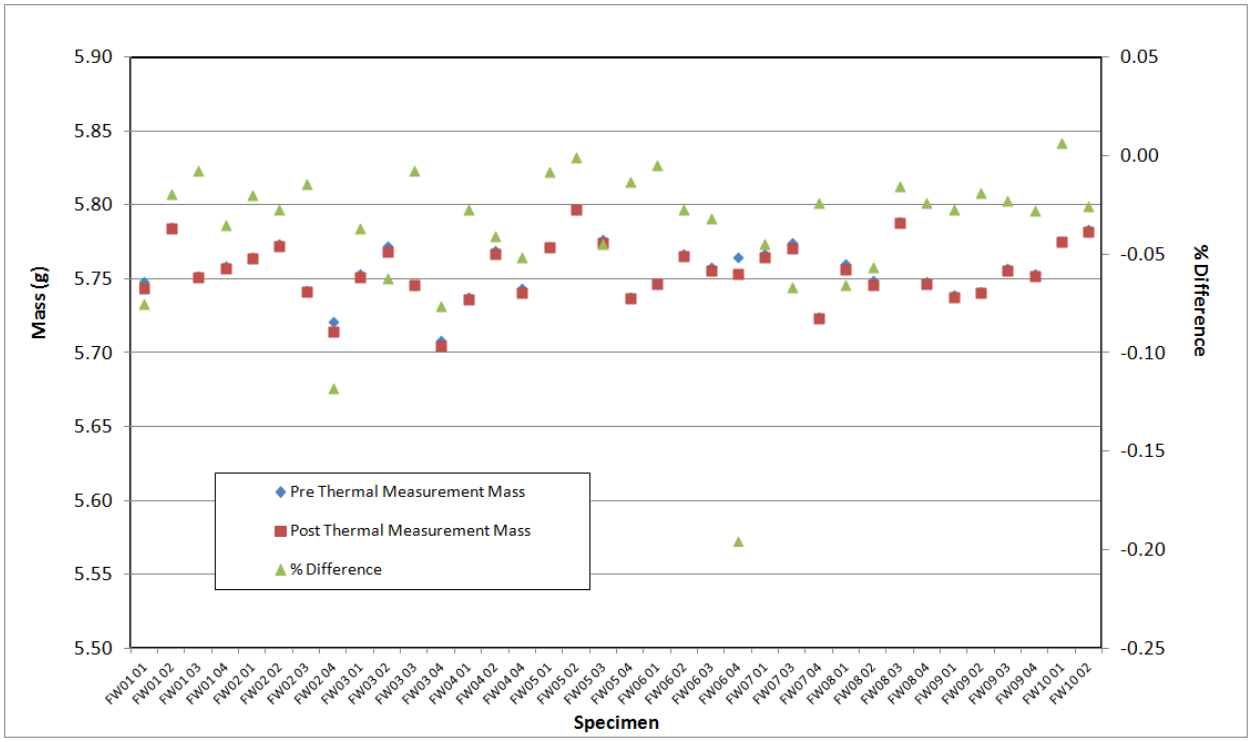

Figure A-183. IG-430 Creep Pre vs. Post Thermal Measurement Mass Comparison.

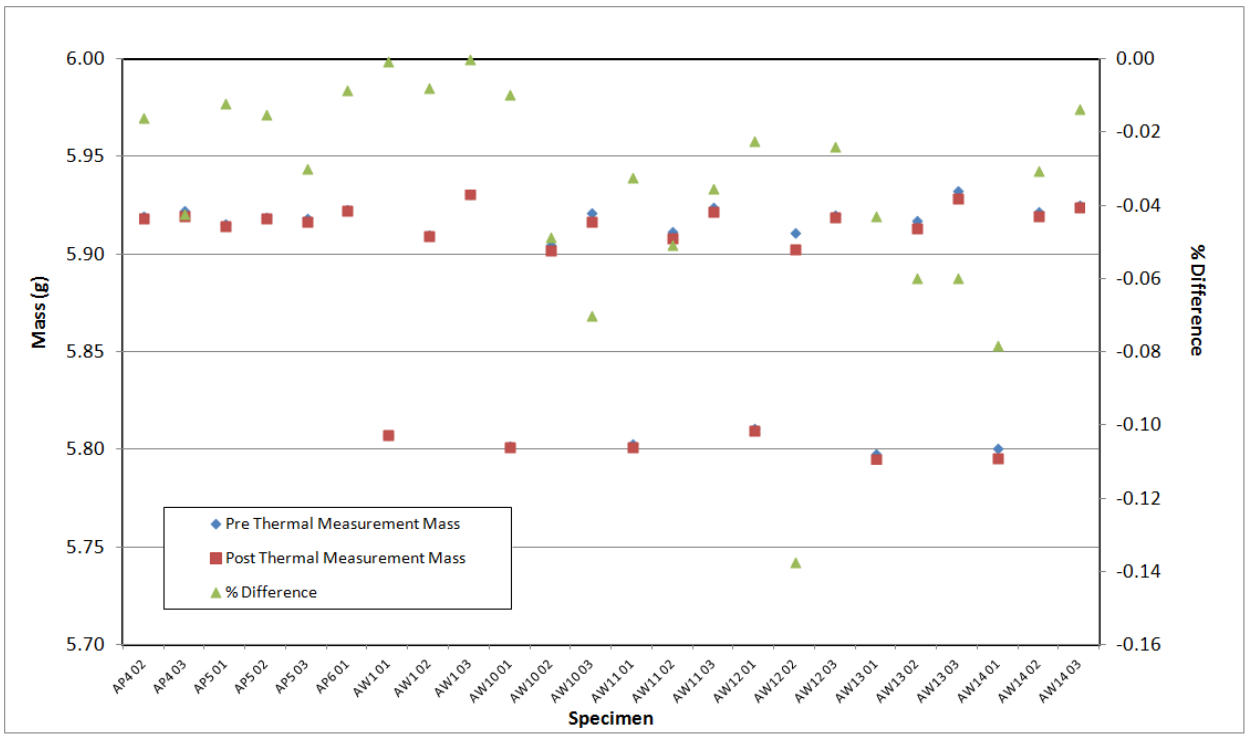

Figure A-184. NBG-17 Creep Pre vs. Post Thermal Measurement Mass Comparison.

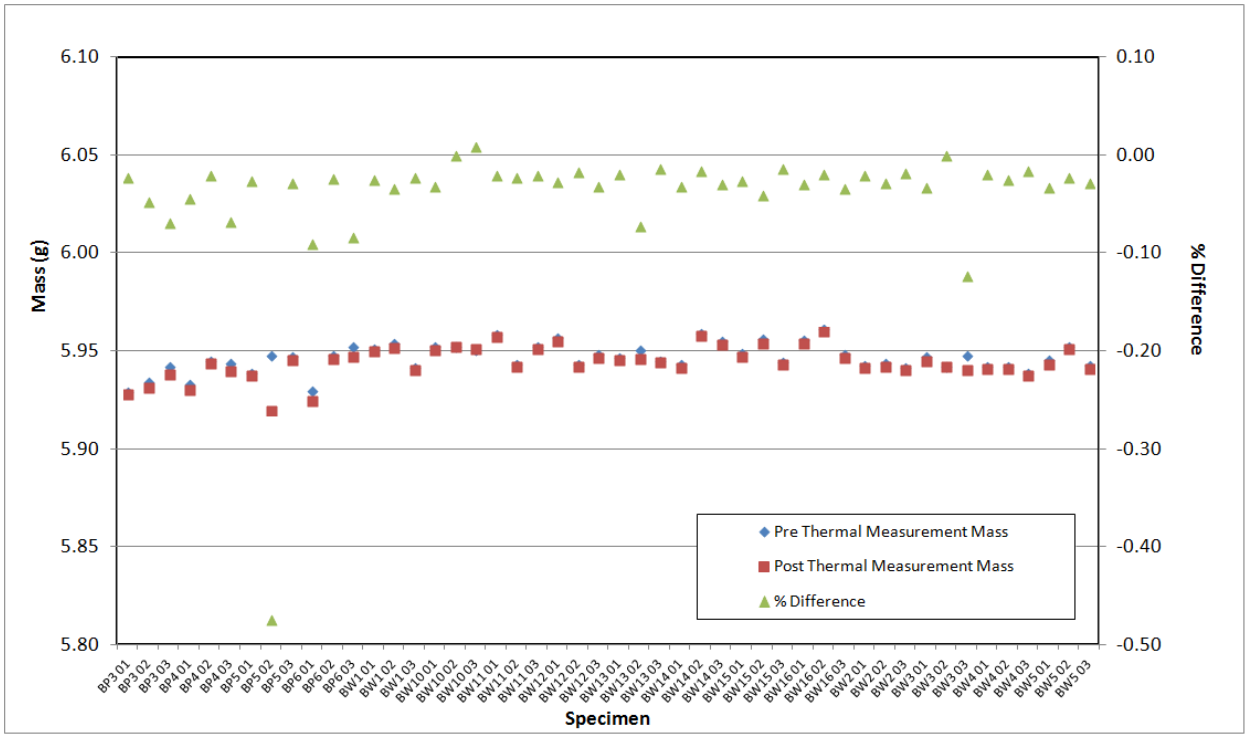

Figure A-185. NBG-18 Creep Pre vs. Post Thermal Measurement Mass Comparison.

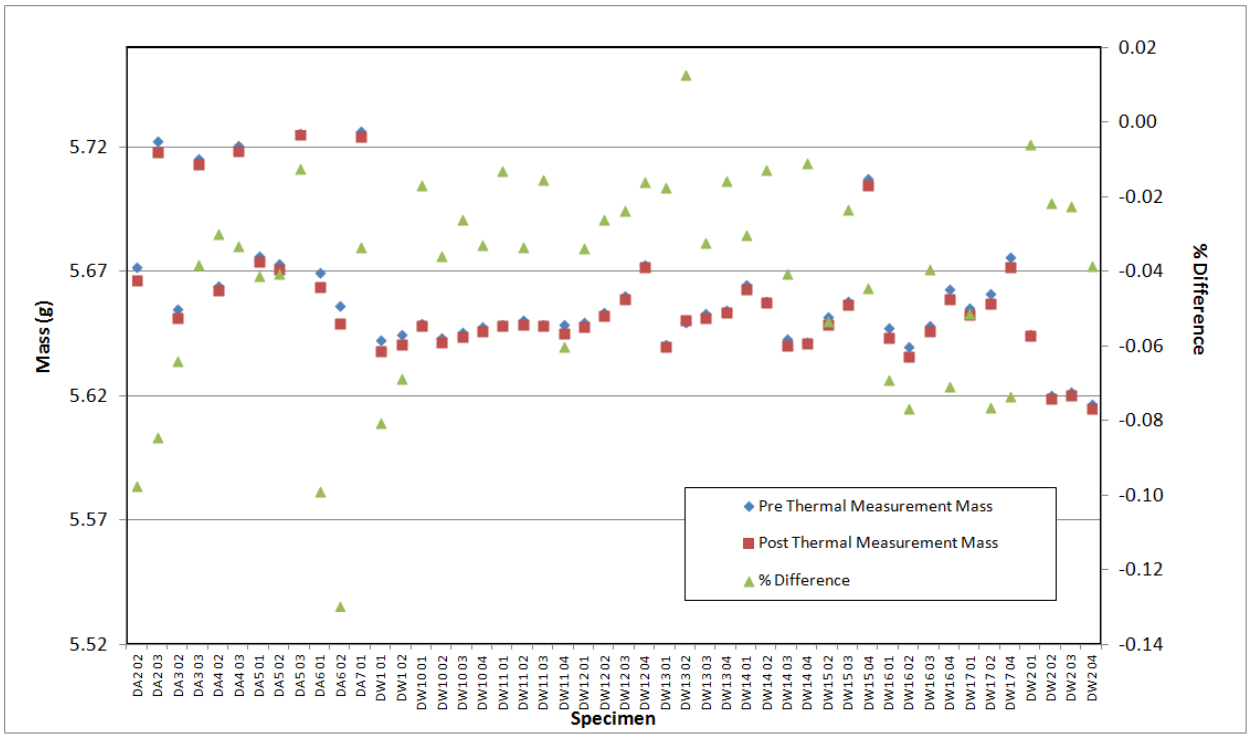

Figure A-186. PCEA Creep Pre vs. Post Thermal Measurement Mass Comparison.

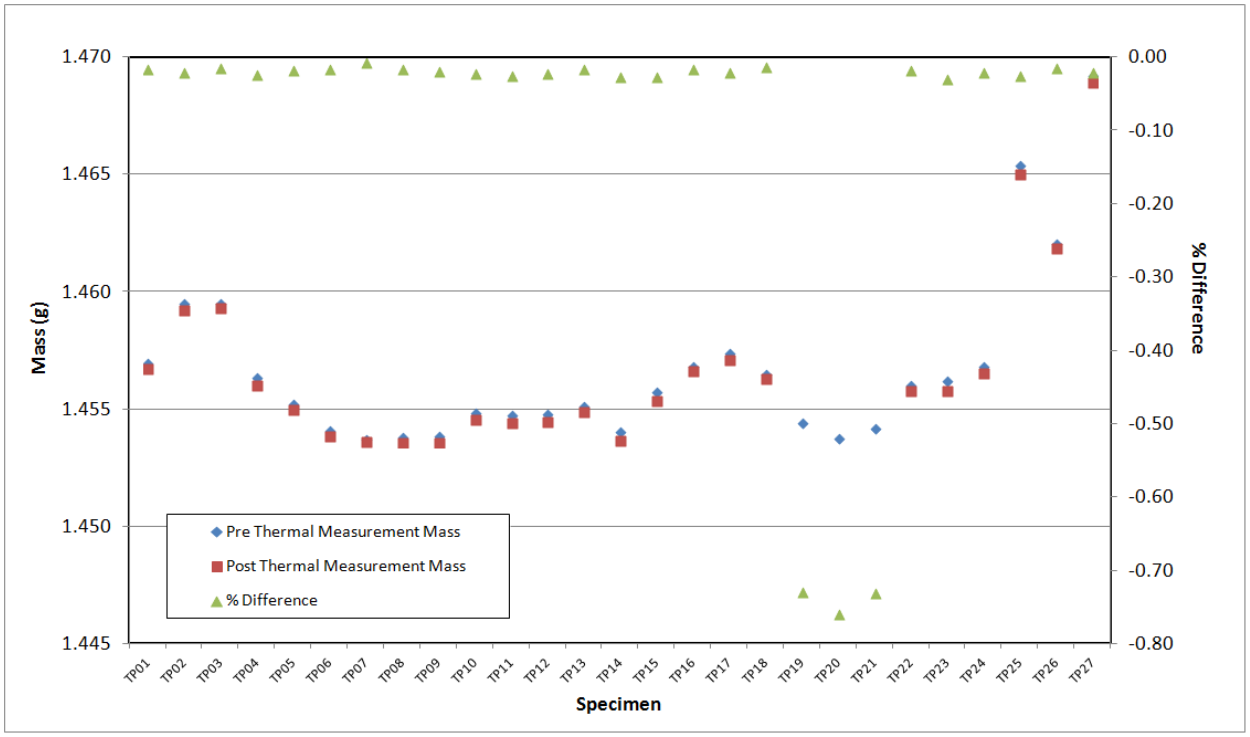

Figure A-187. 2114 Piggyback Pre vs. Post Thermal Measurement Mass Comparison.

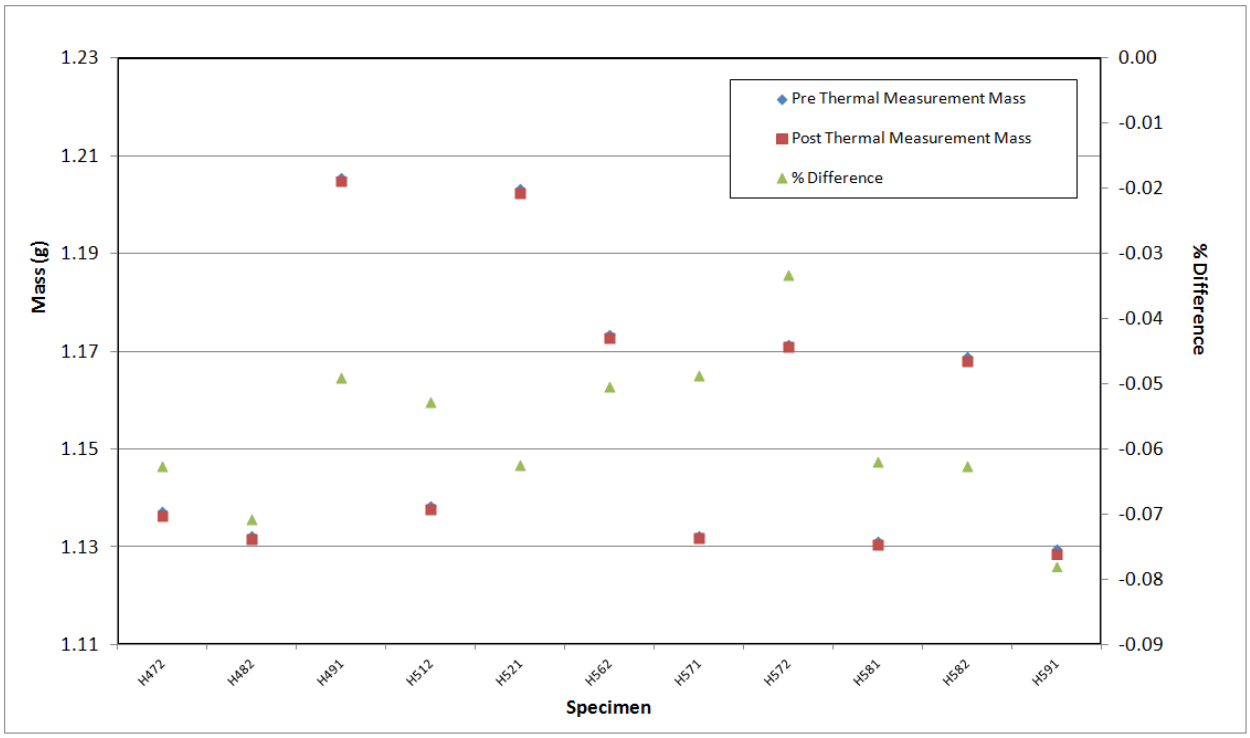

Figure A-188. A3 Matrix Piggyback Pre vs. Post Thermal Measurement Mass Comparison.

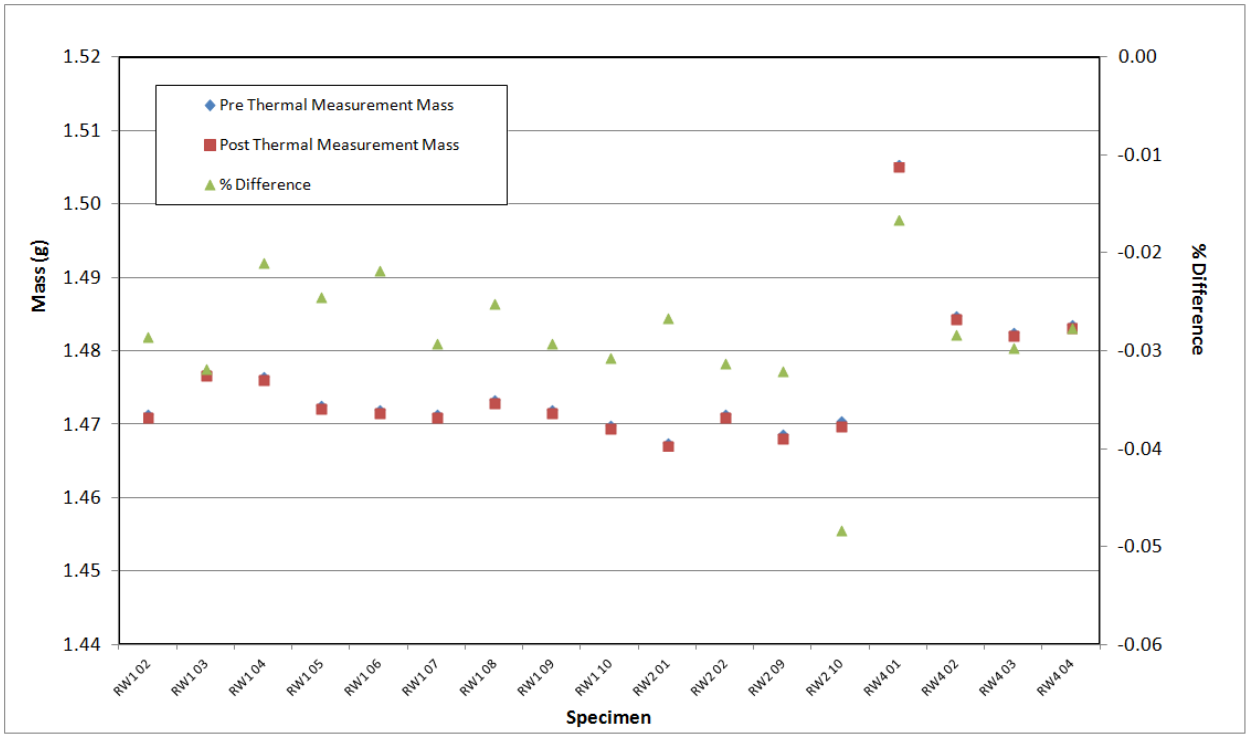

Figure A-189. BAN Piggyback Pre vs. Post Thermal Measurement Mass Comparison.

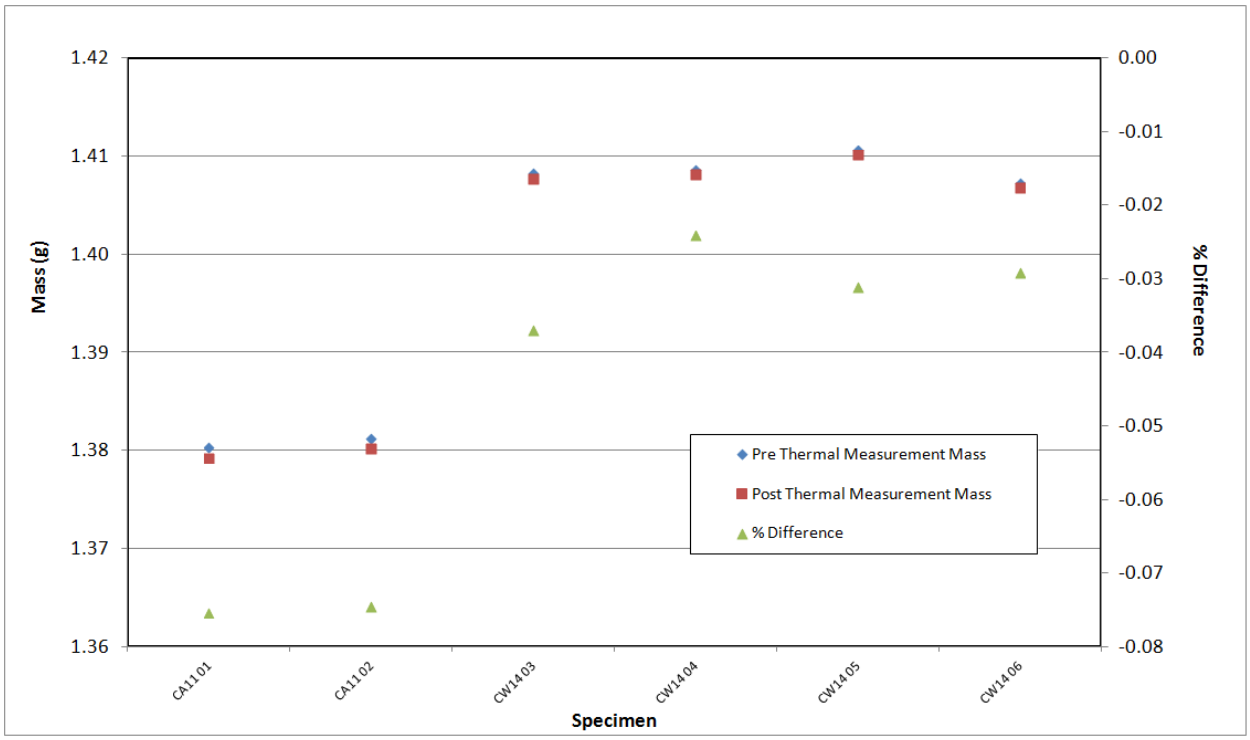

Figure A-190. H-451 Piggyback Pre vs. Post Thermal Measurement Mass Comparison.

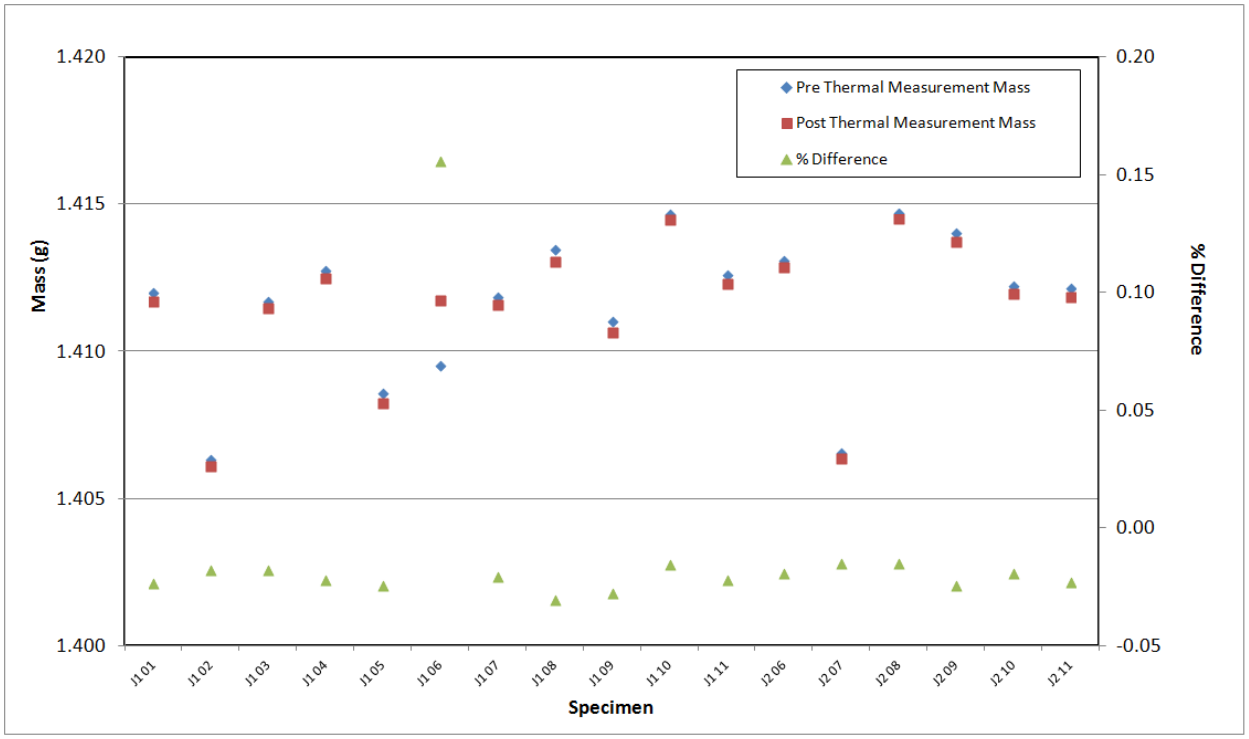

Figure A-191. HLM Piggyback Pre vs. Post Thermal Measurement Mass Comparison.

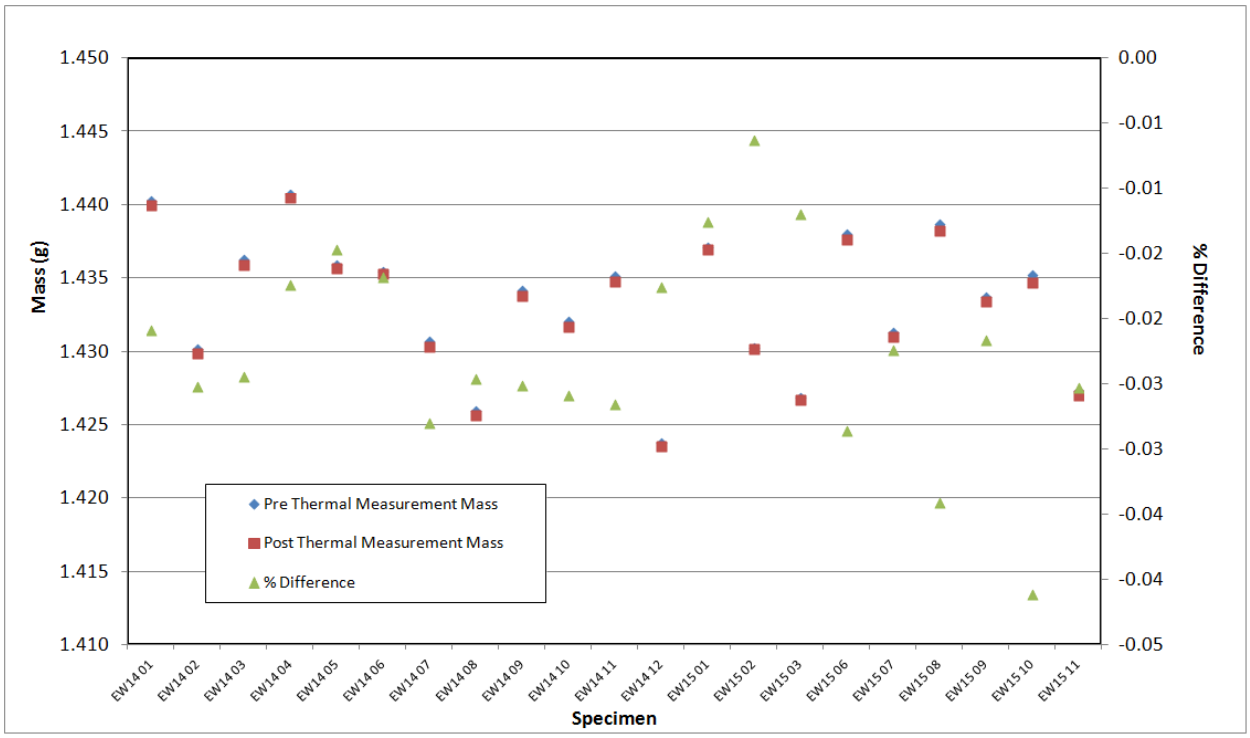

Figure A-192. IG-110 Piggyback Pre vs. Post Thermal Measurement Mass Comparison.

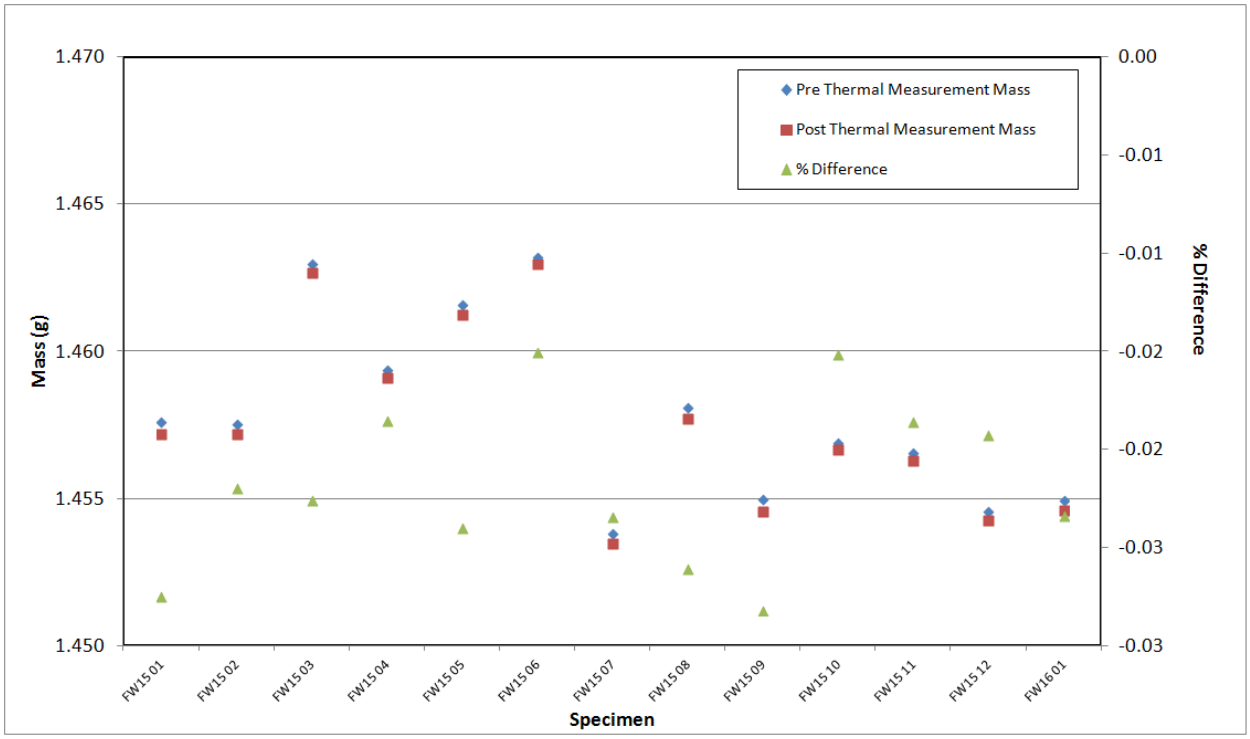

Figure A-193. IG-430 Piggyback Pre vs. Post Thermal Measurement Mass Comparison.

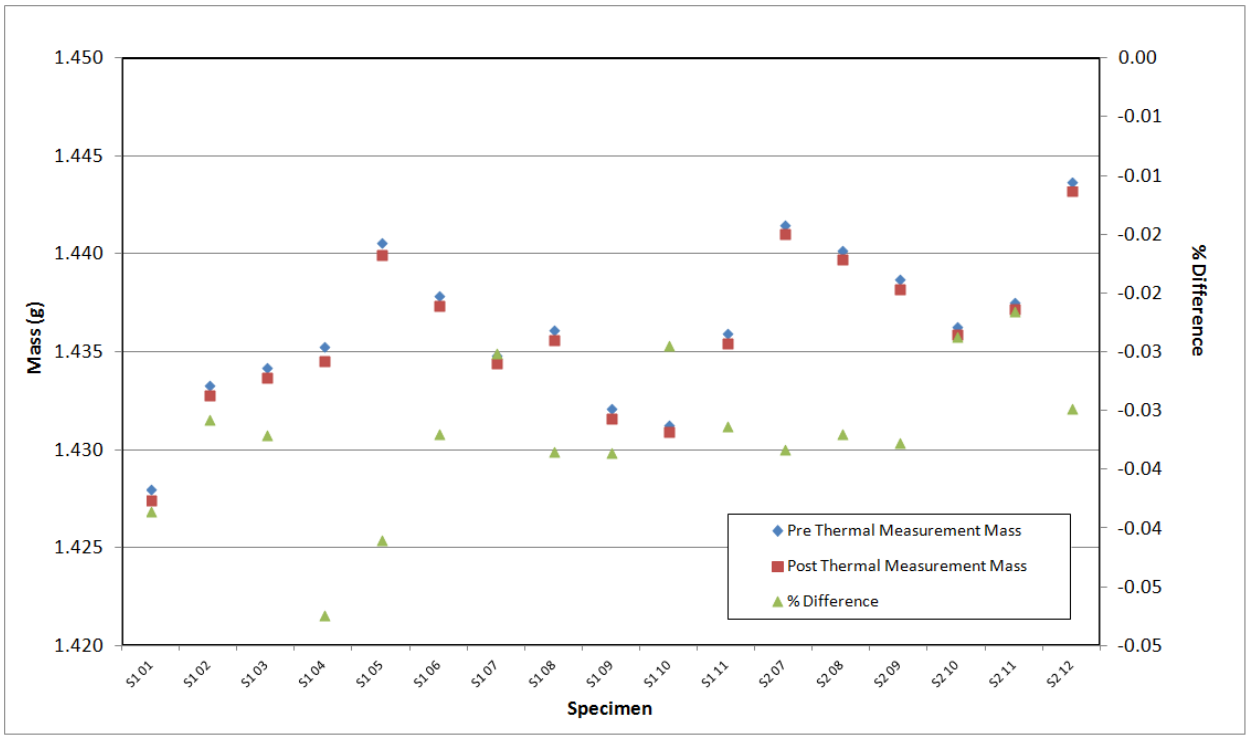

Figure A-194. NBG-10 Piggyback Pre vs. Post Thermal Measurement Mass Comparison.

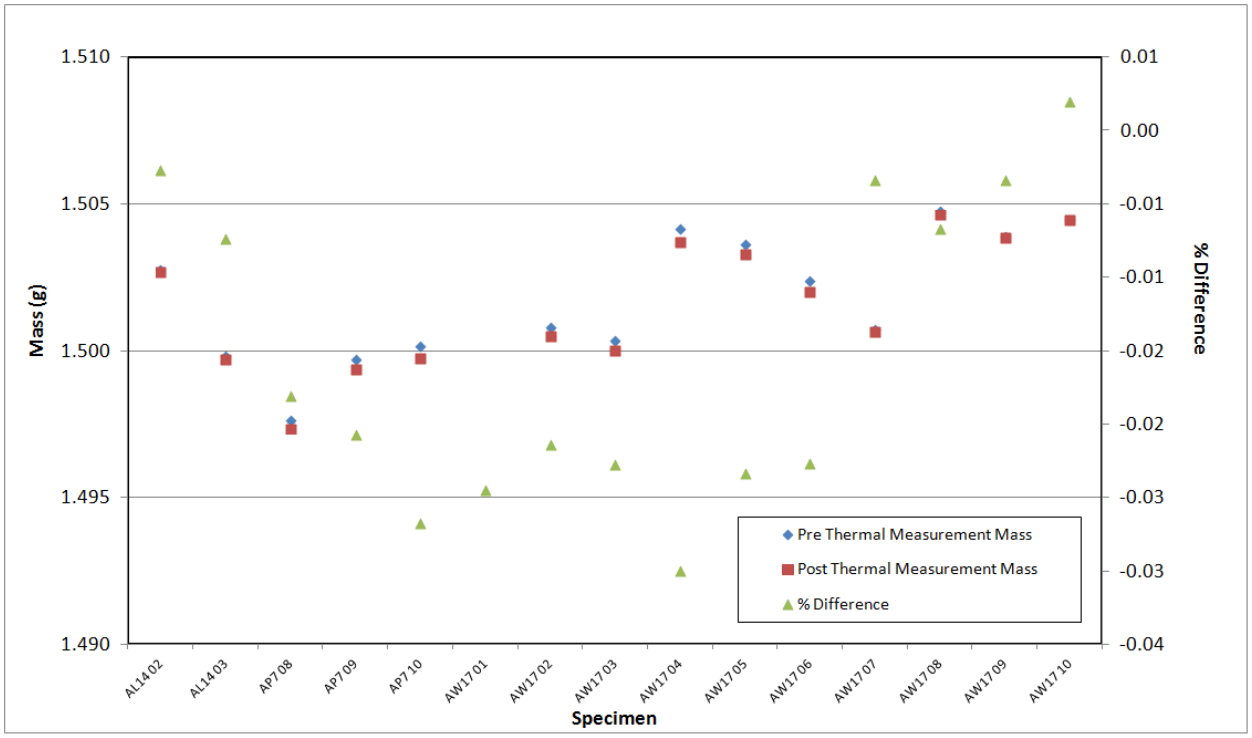

Figure A-195. NBG-17 Piggyback Pre vs. Post Thermal Measurement Mass Comparison.

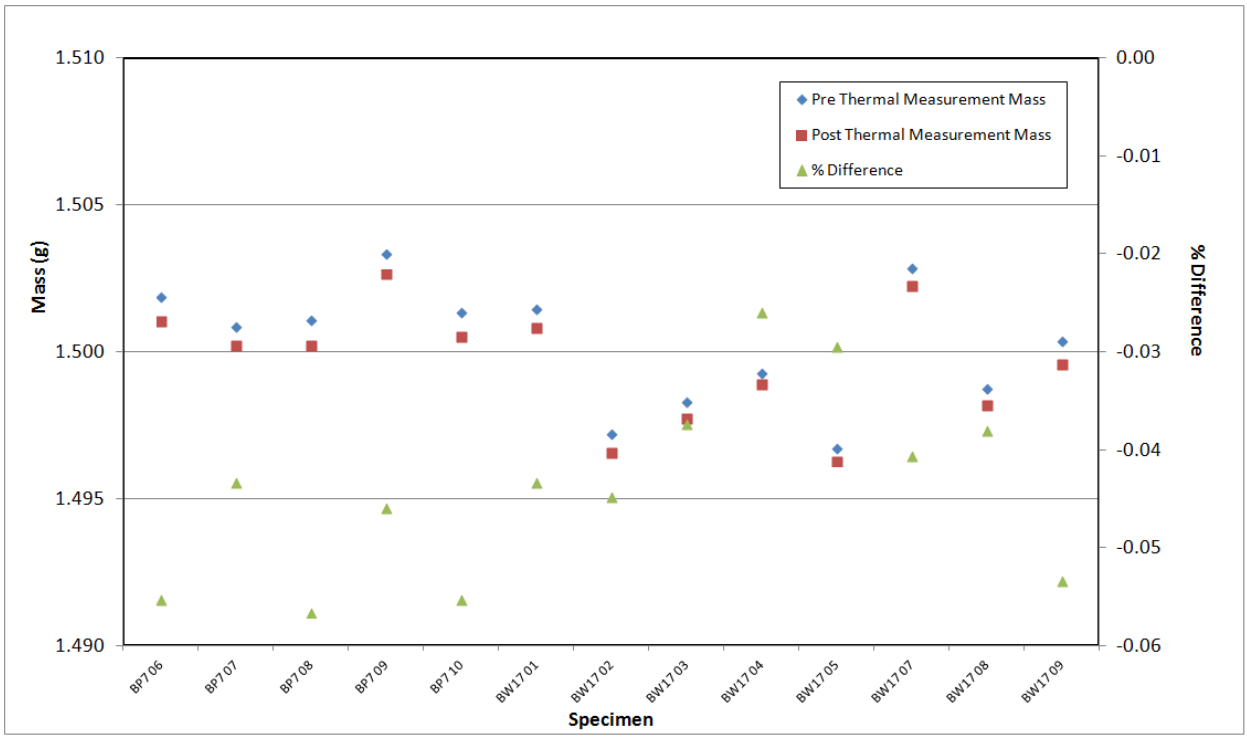

Figure A-196. NBG-18 Piggyback Pre vs. Post Thermal Measurement Mass Comparison.

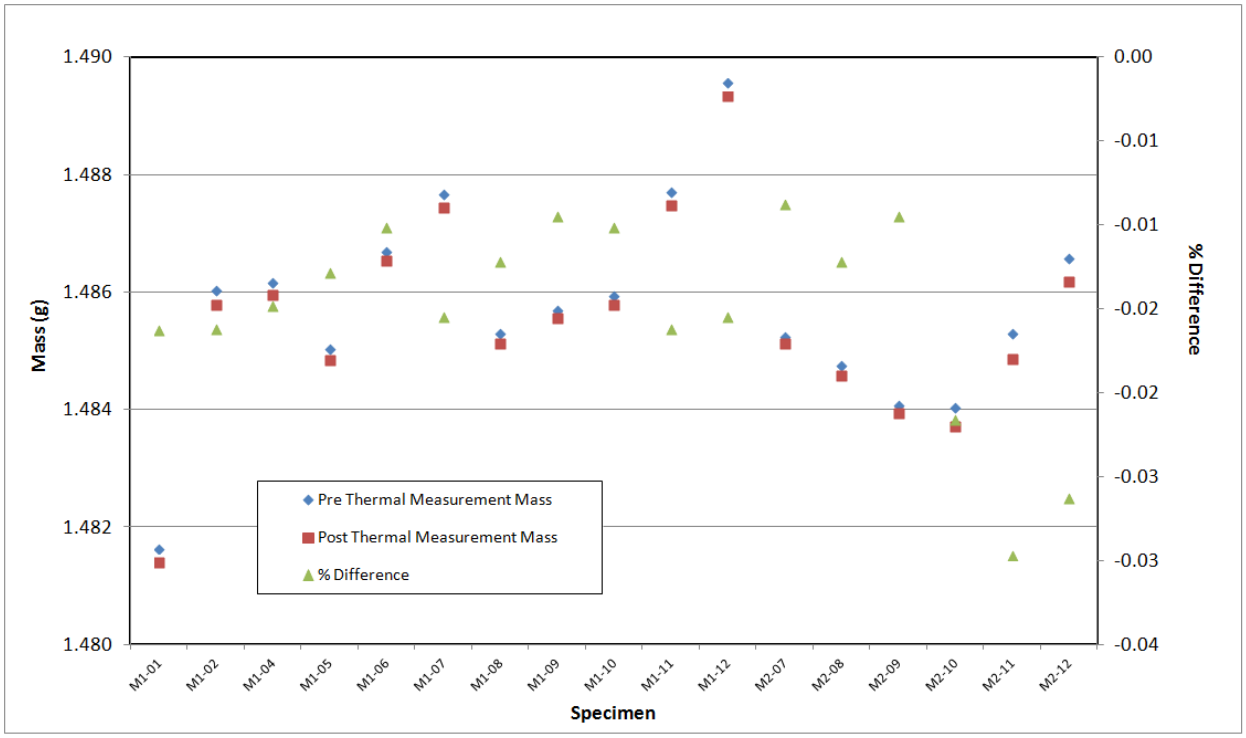

Figure A-197. NBG-25 Piggyback Pre vs. Post Thermal Measurement Mass Comparison.

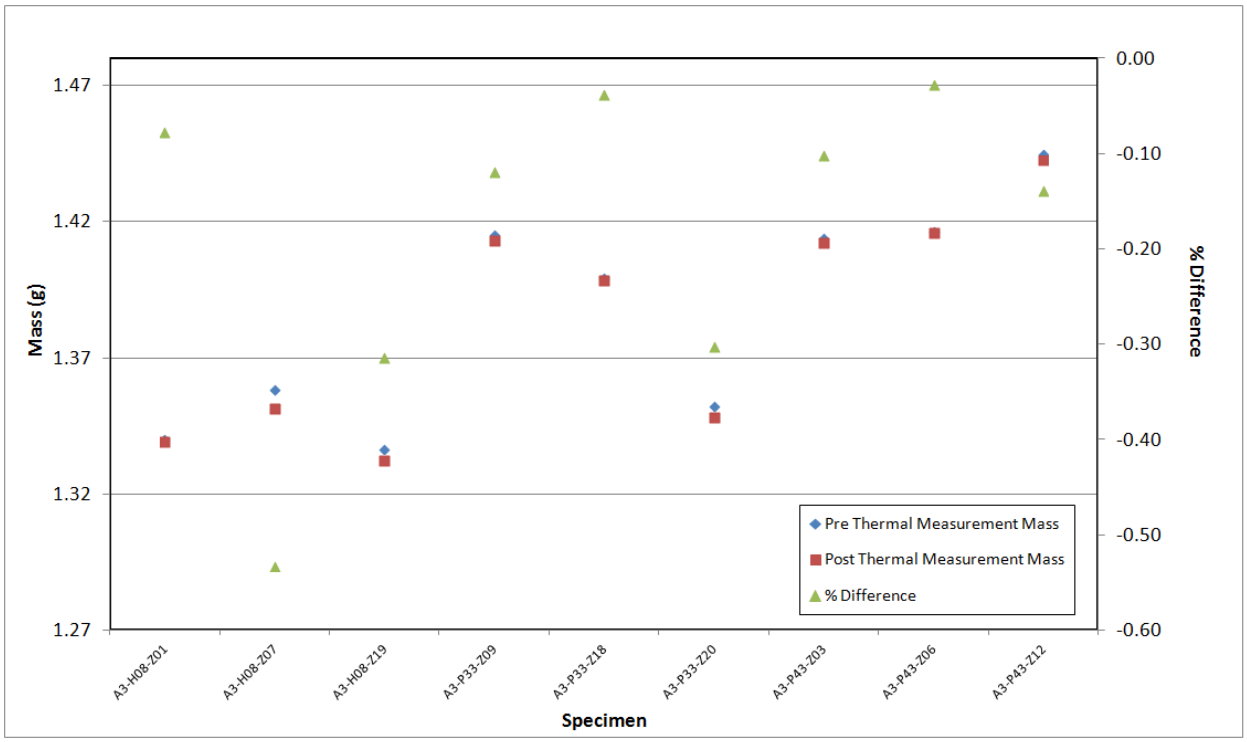

Figure A-198. New Matrix Piggyback Pre vs. Post Thermal Measurement Mass Comparison.

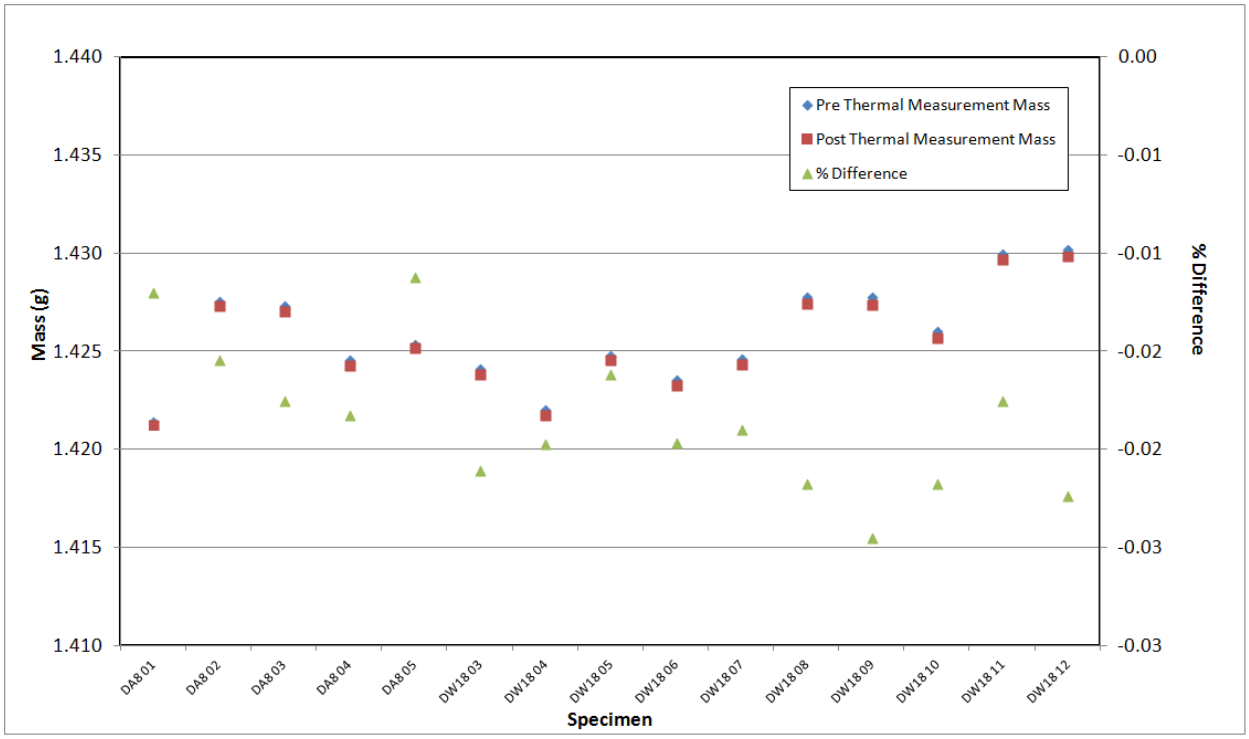

Figure A-199. PCEA Piggyback Pre vs. Post Thermal Measurement Mass Comparison.

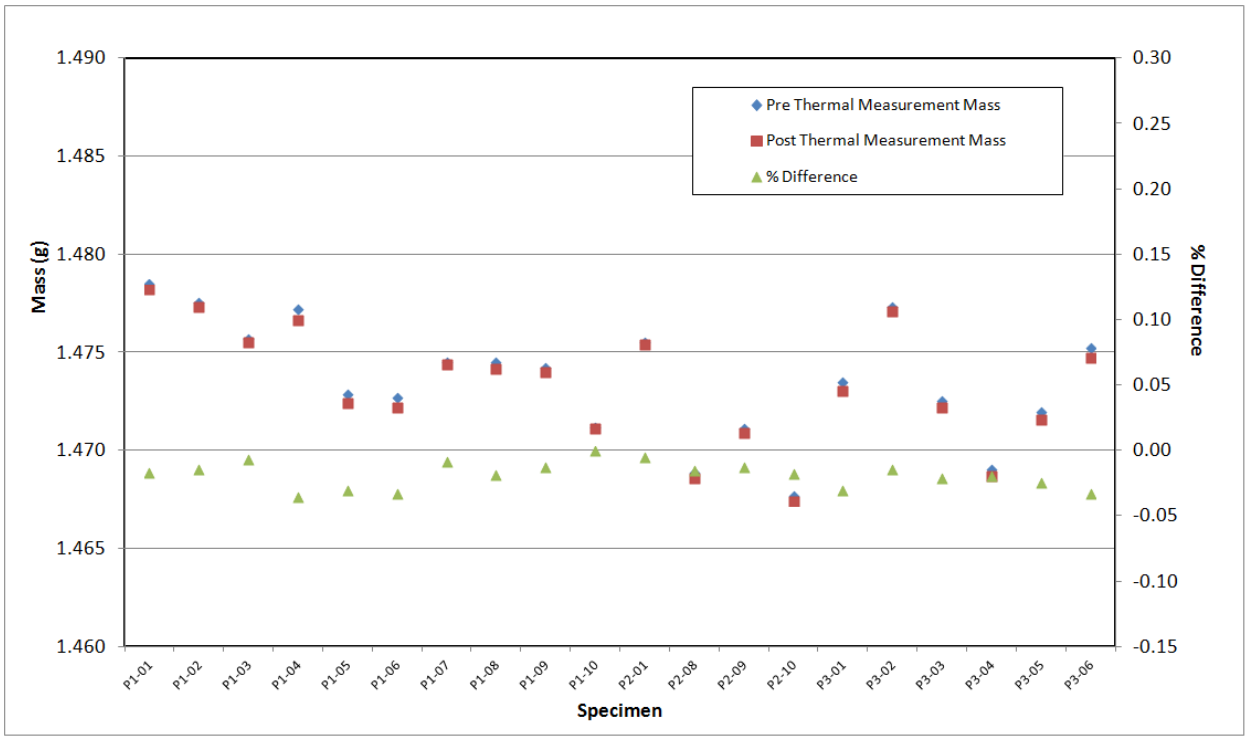

Figure A-200. PCIB Piggyback Pre vs. Post Thermal Measurement Mass Comparison.

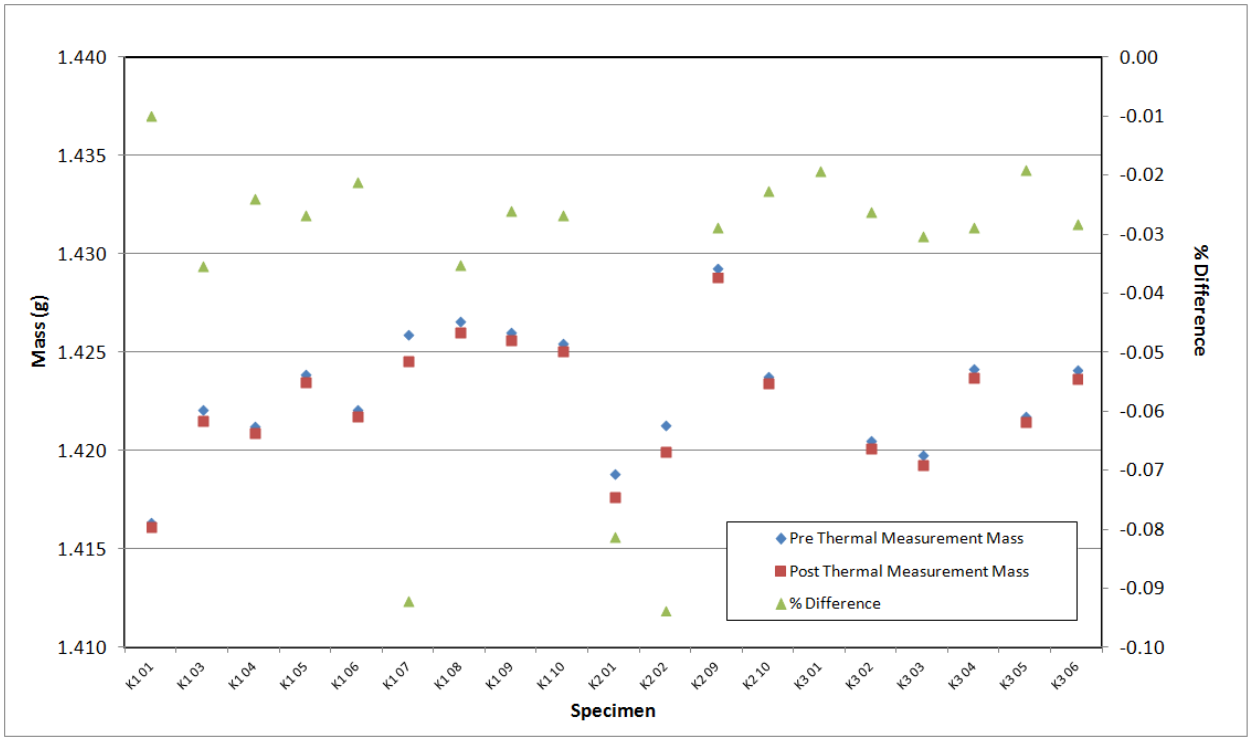

Figure A-201. PGX Piggyback Pre vs. Post Thermal Measurement Mass Comparison.

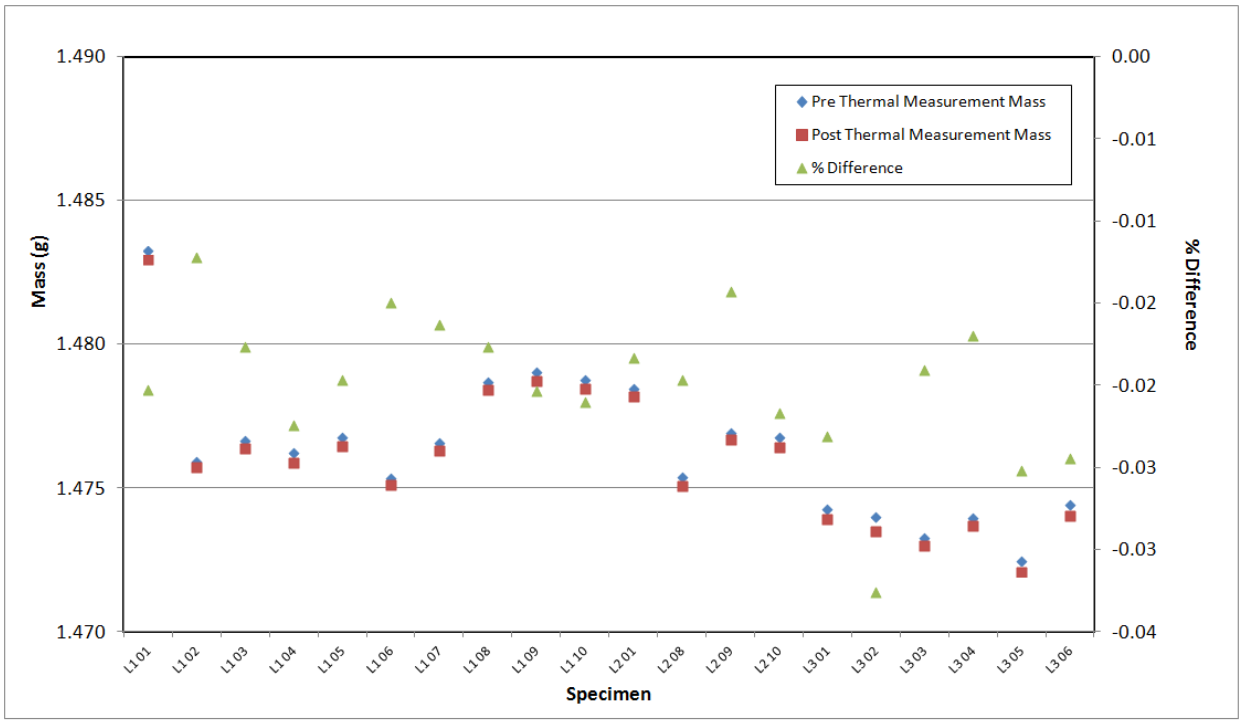

Figure A-202. PPEA Piggyback Pre vs. Post Thermal Measurement Mass Comparison.

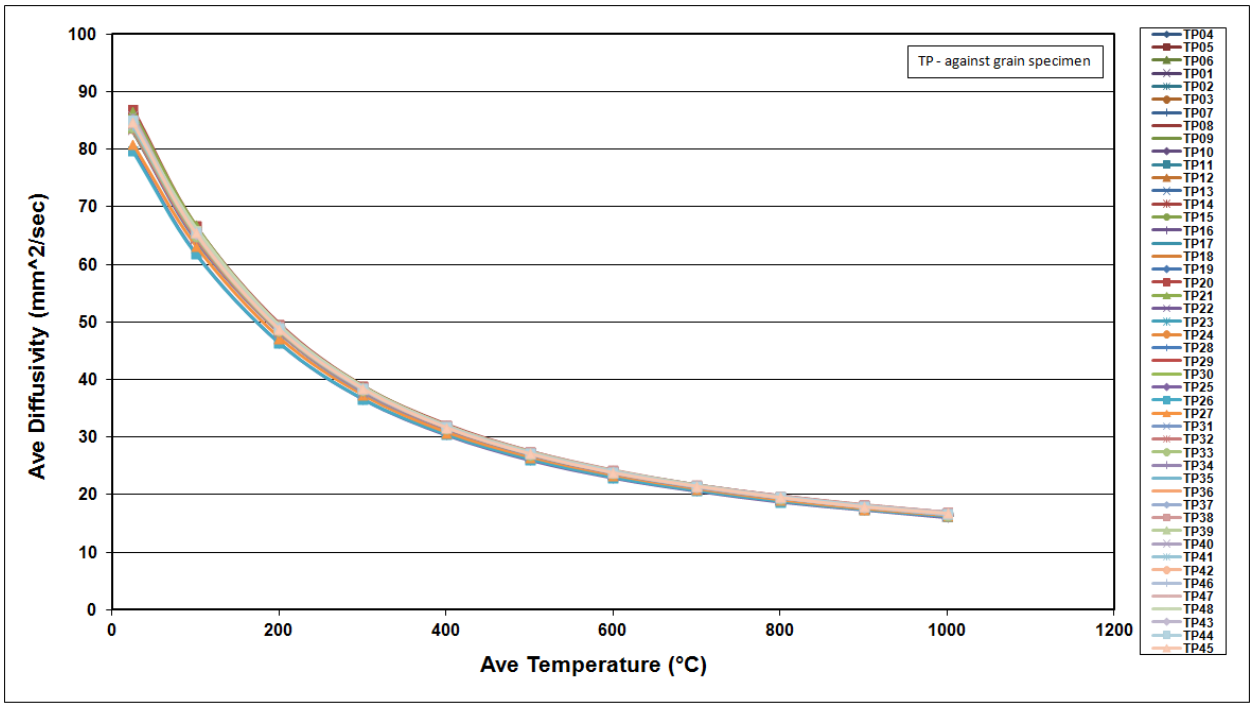

Figure A-203. 2114 Piggyback Diffusivity.

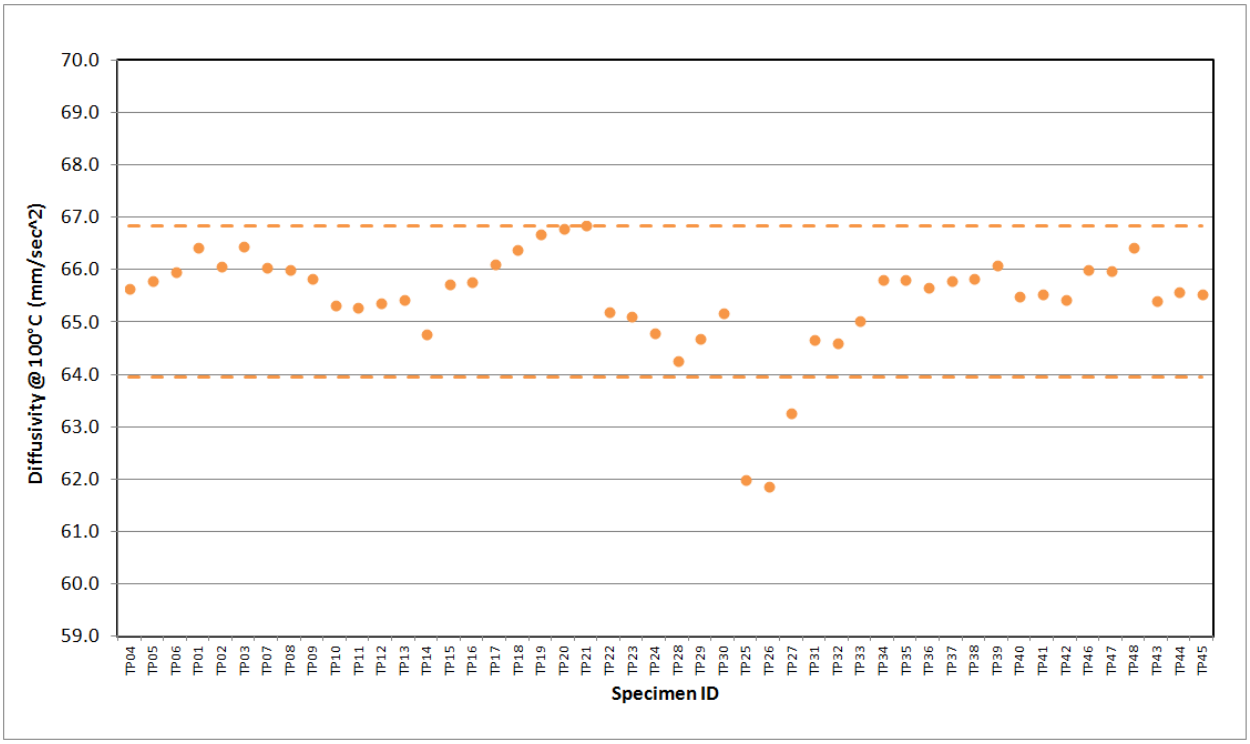

Figure A-204. 2114 Piggyback Diffusivity @ 100°C.

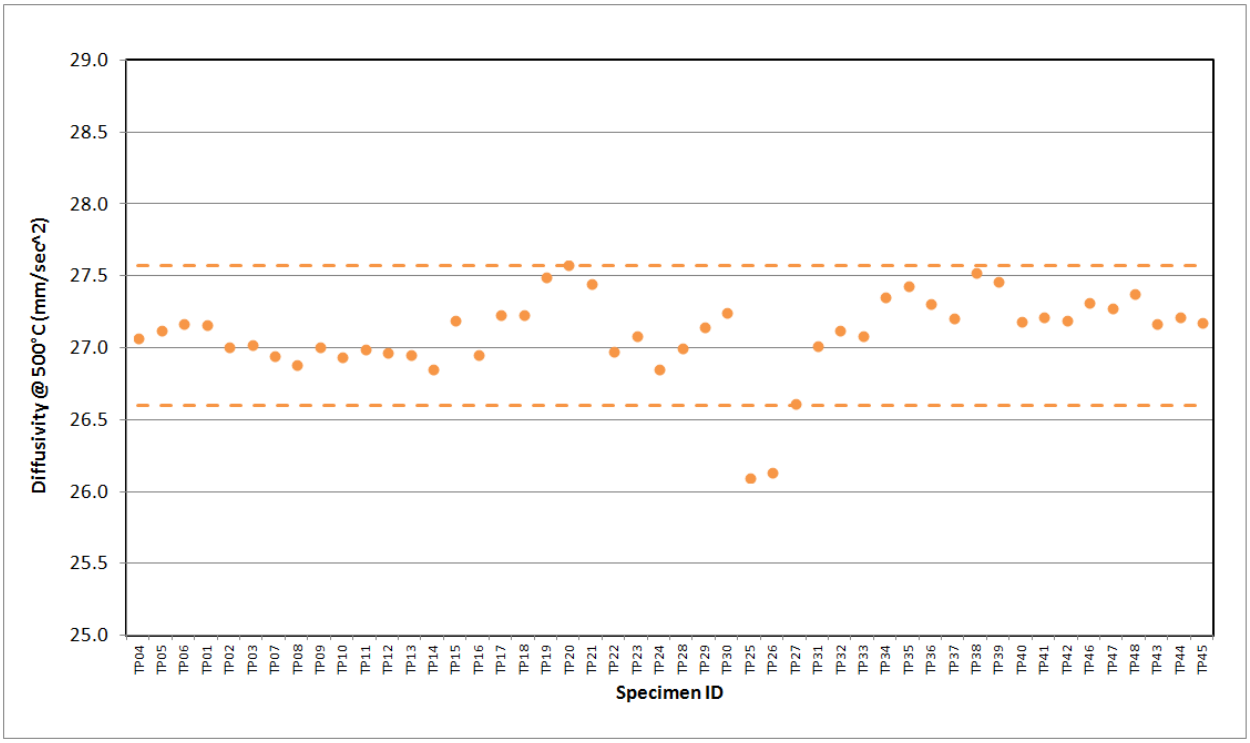

Figure A-205. 2114 Piggyback Diffusivity @ 500°C.

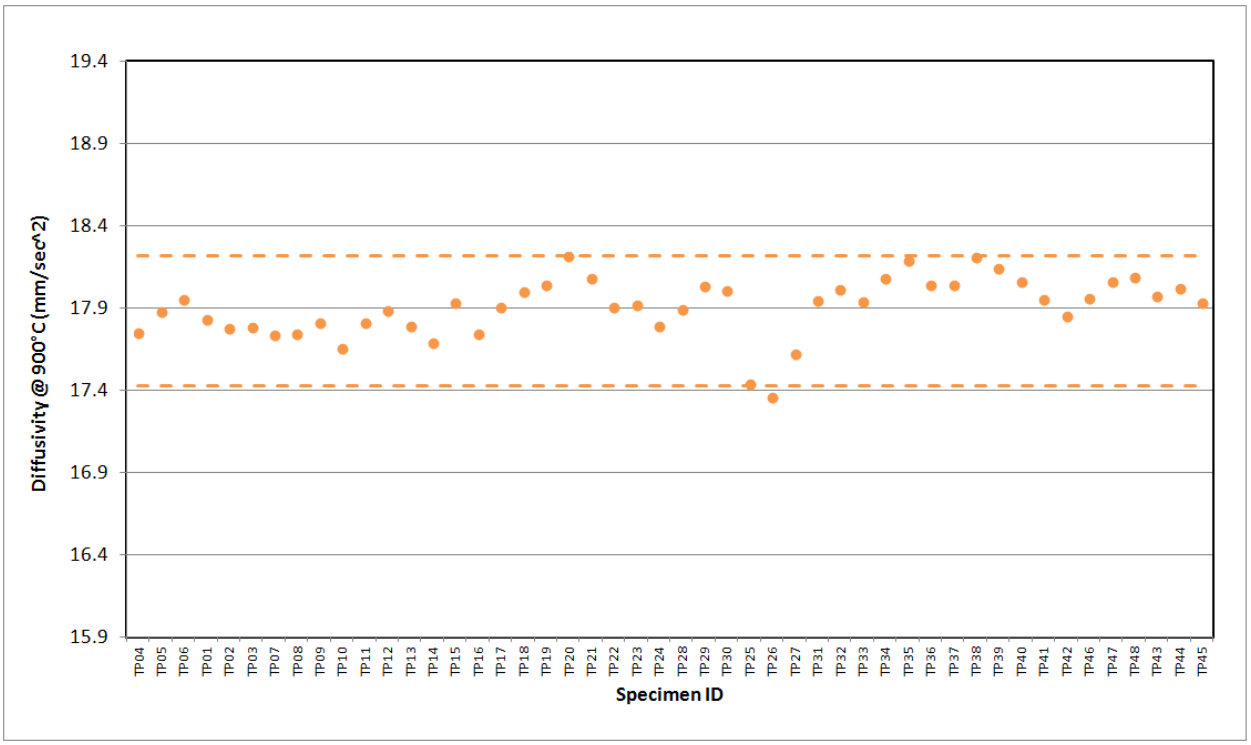

Figure A-206. 2114 Piggyback Diffusivity @ 900°C.

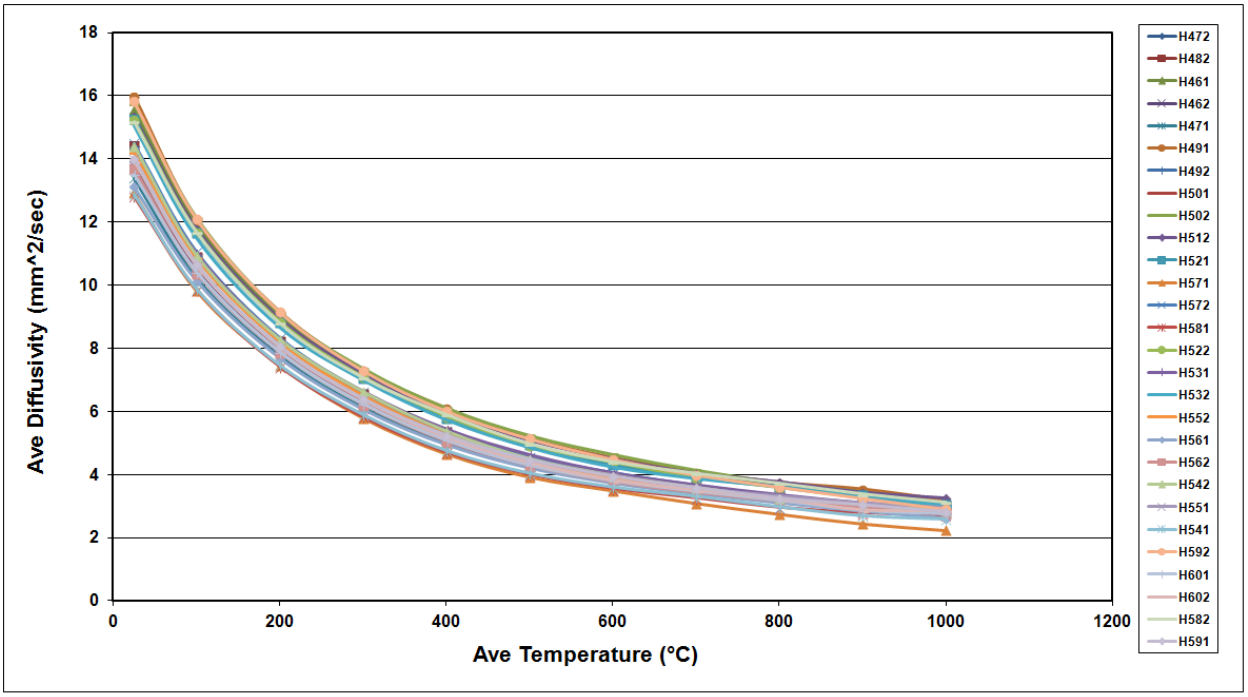

Figure A-207. A3 Matrix Piggyback Diffusivity.

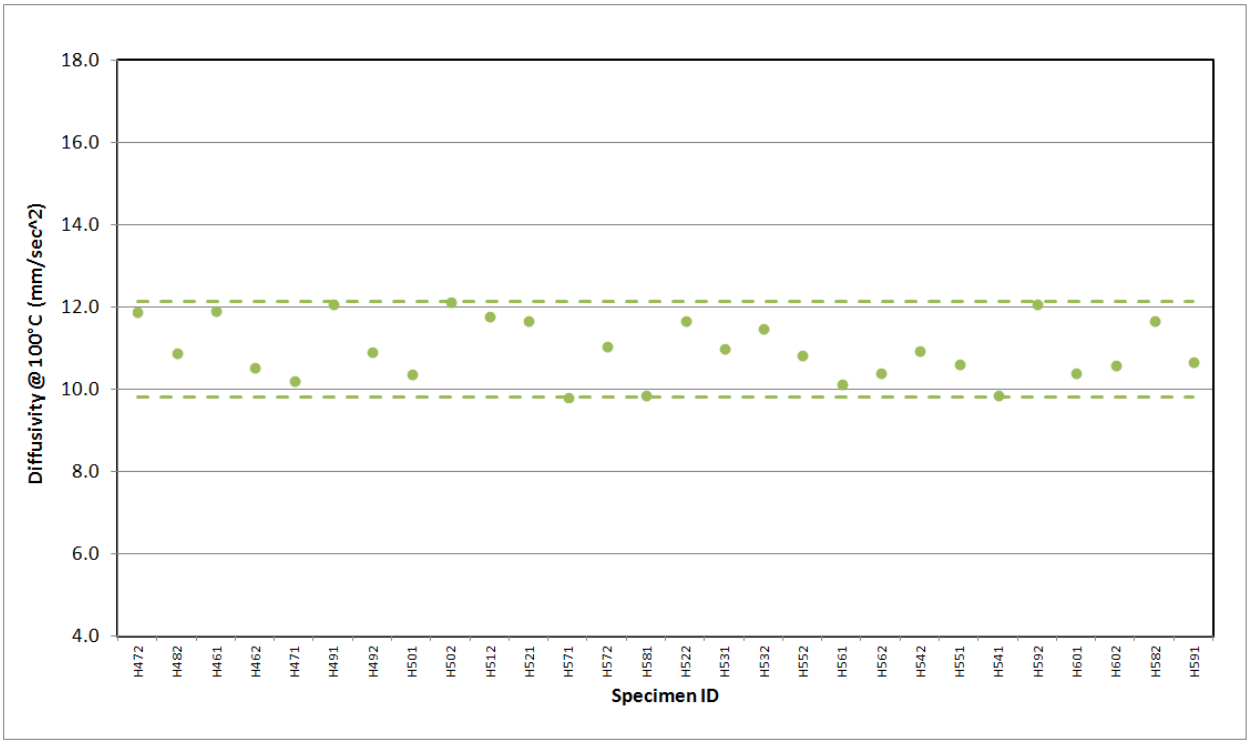

Figure A-208. A3 Matrix Piggyback Diffusivity @ 100°C.

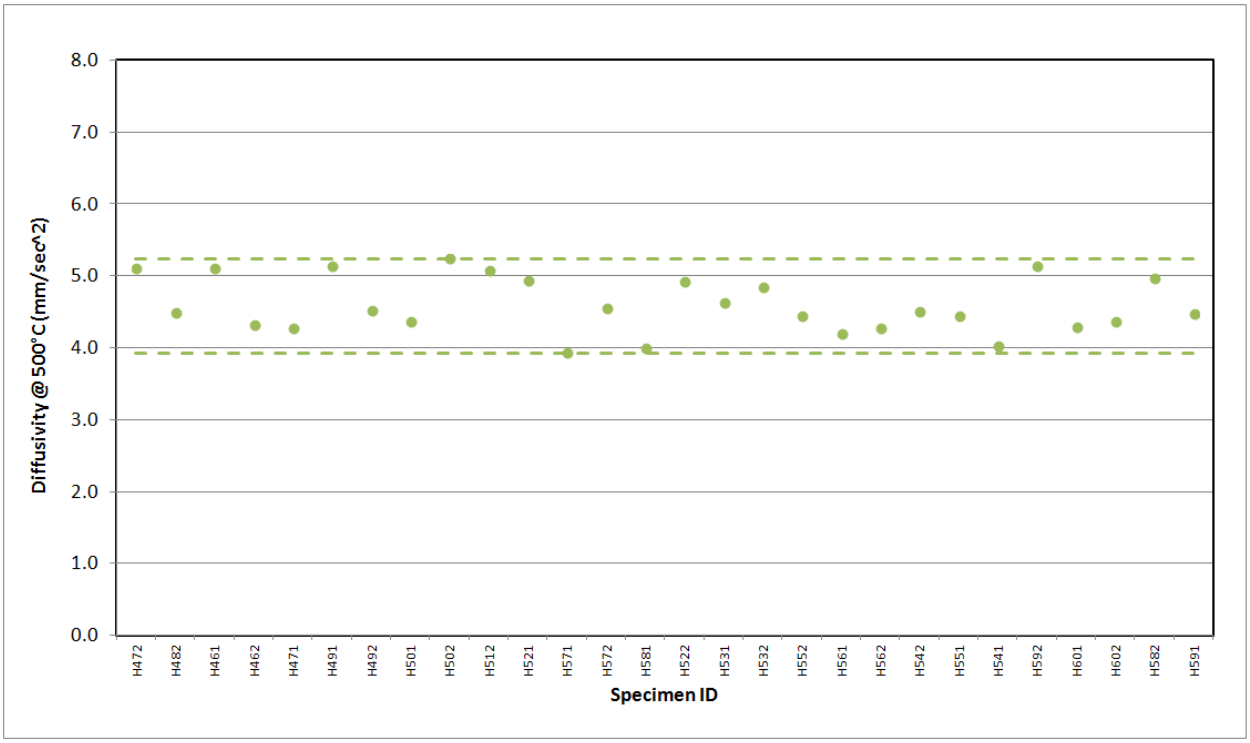

Figure A-209. A3 Matrix Piggyback Diffusivity @ 500°C.

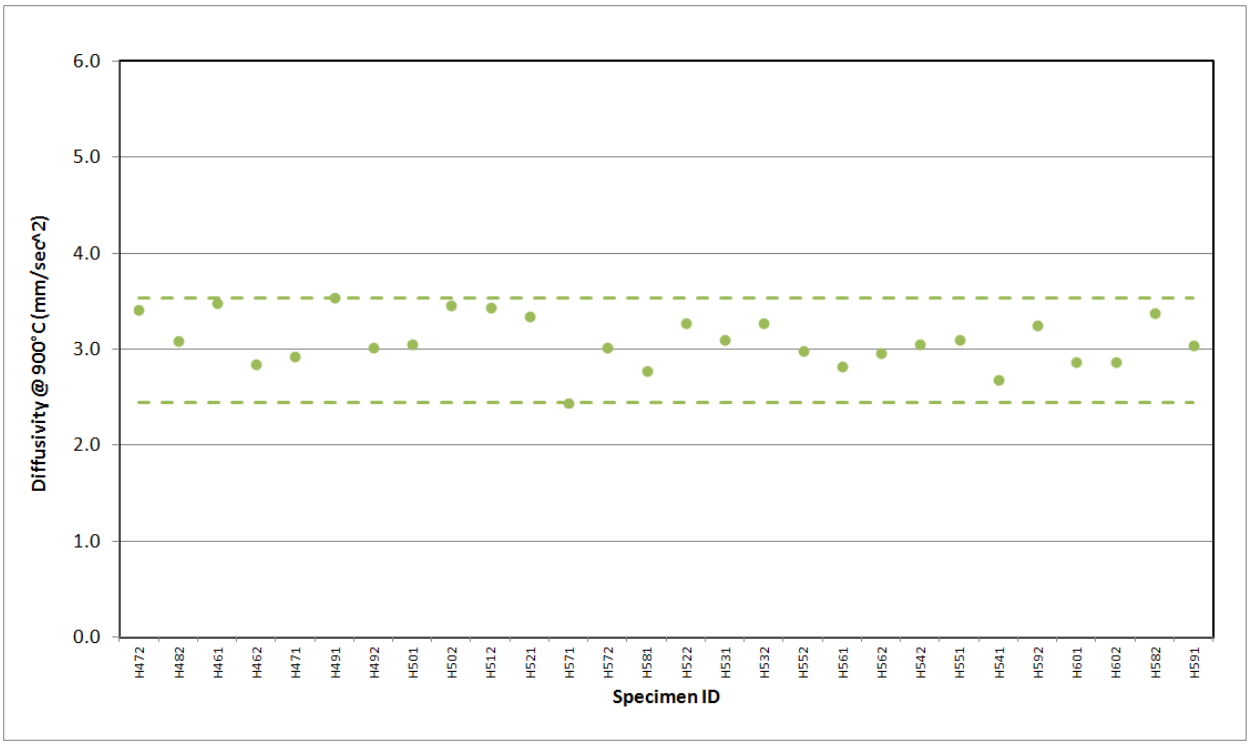

Figure A-210. A3 Matrix Piggyback Diffusivity @ 900°C.

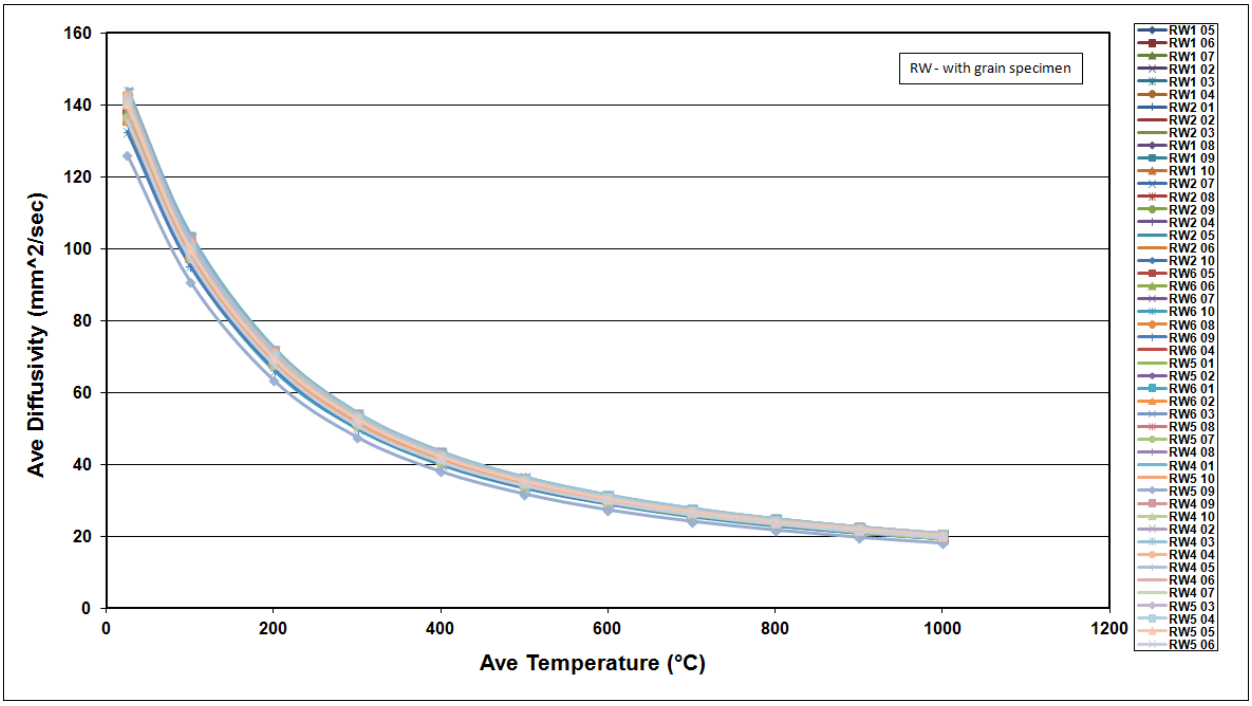

Figure A-211. BAN Piggyback Diffusivity.

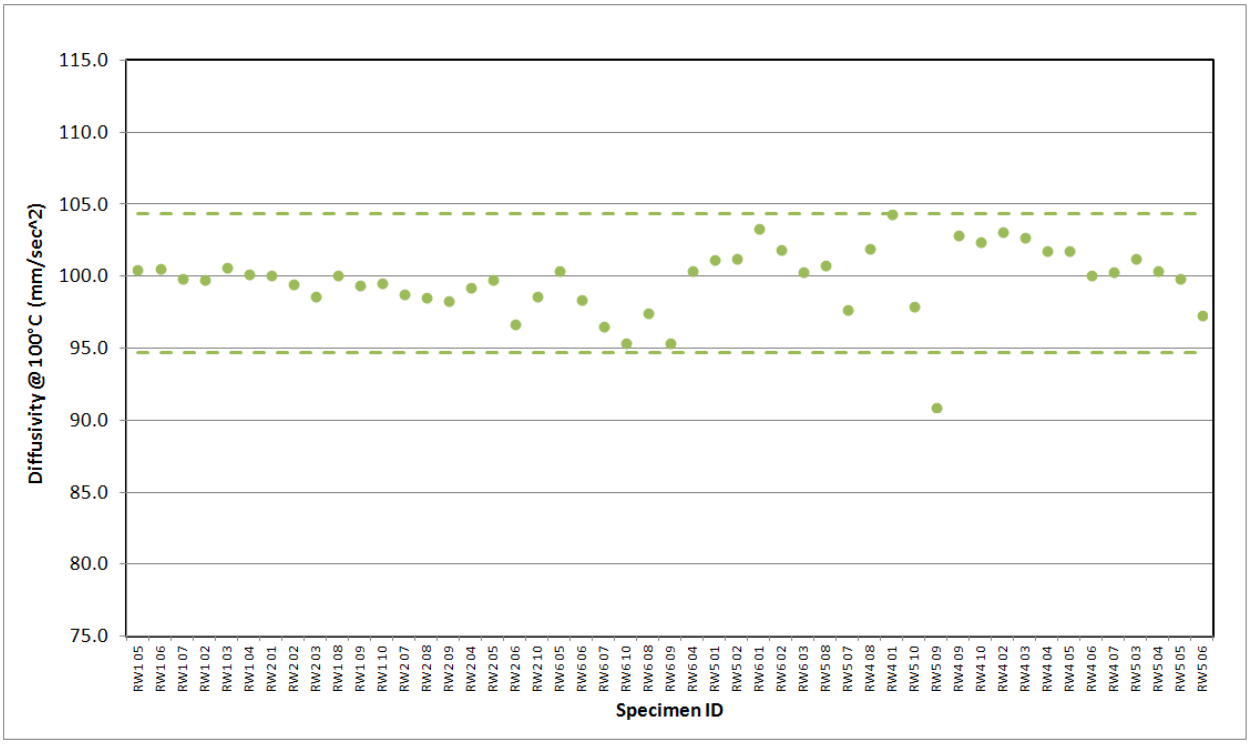

Figure A-212. BAN Piggyback Diffusivity @ 100°C.

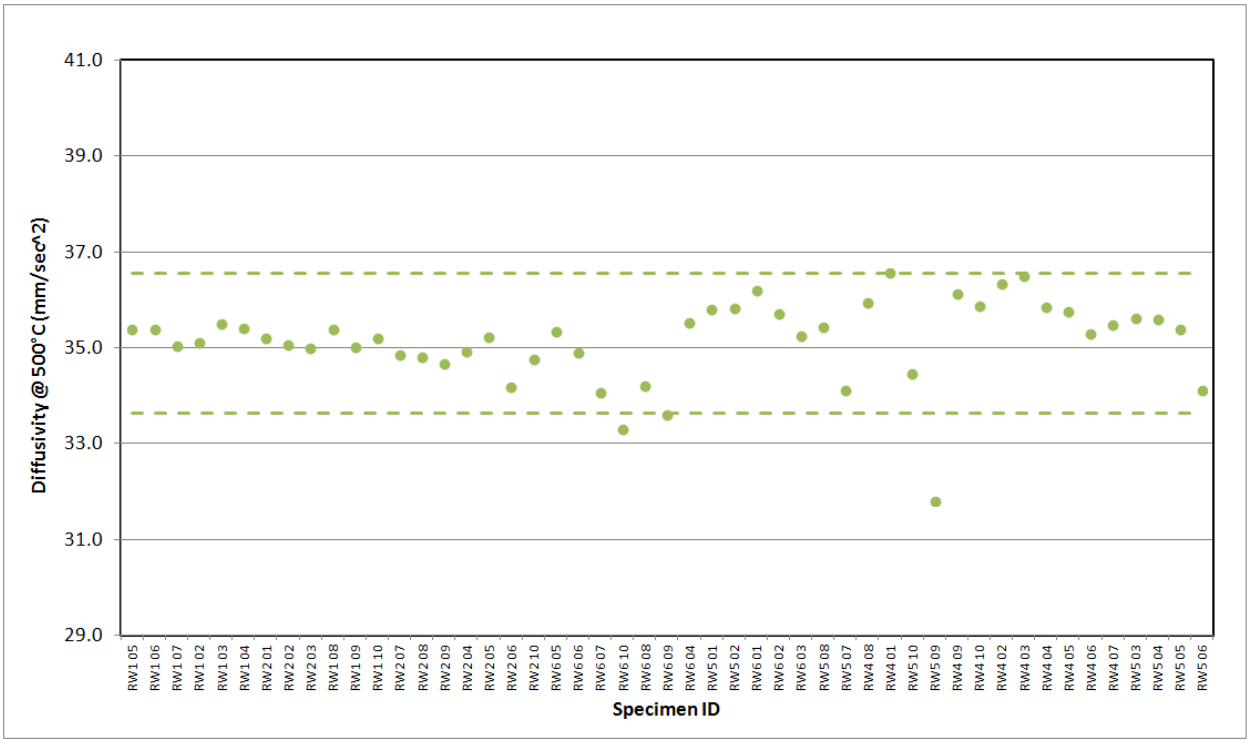

Figure A-213. BAN Piggyback Diffusivity @ 500°C.

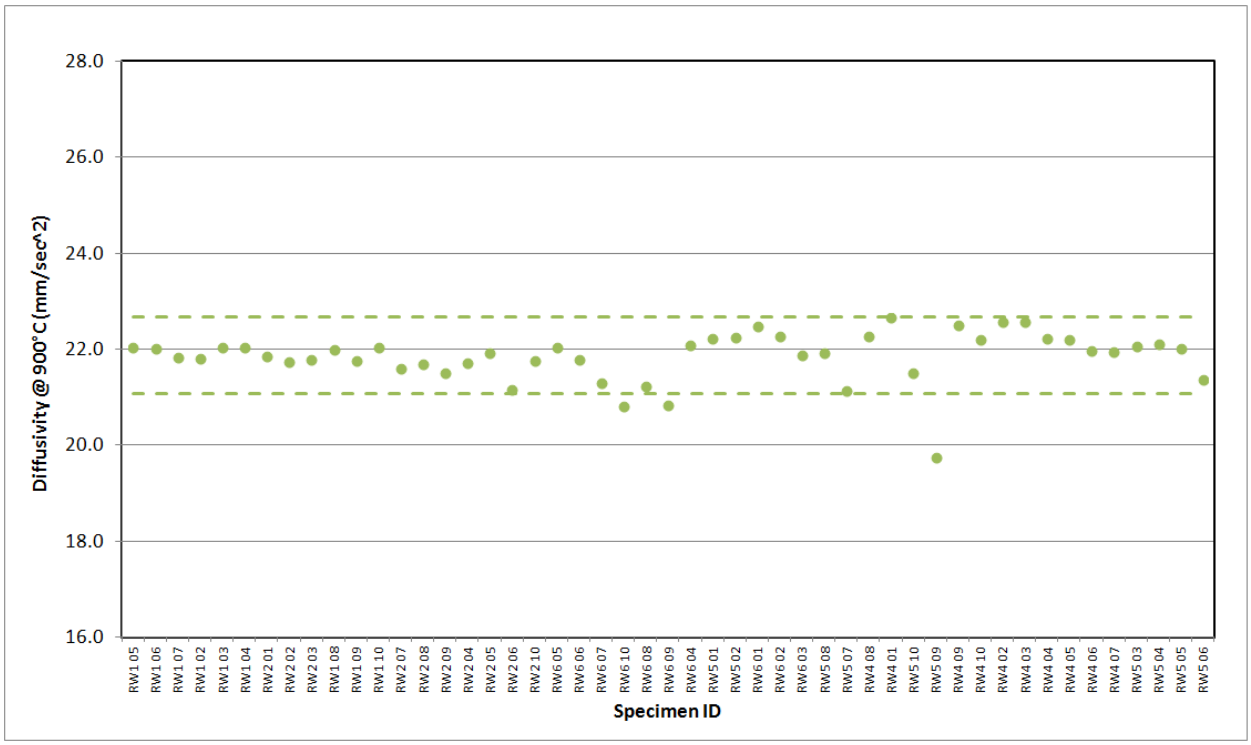

Figure A-214. BAN Piggyback Diffusivity @ 900°C.

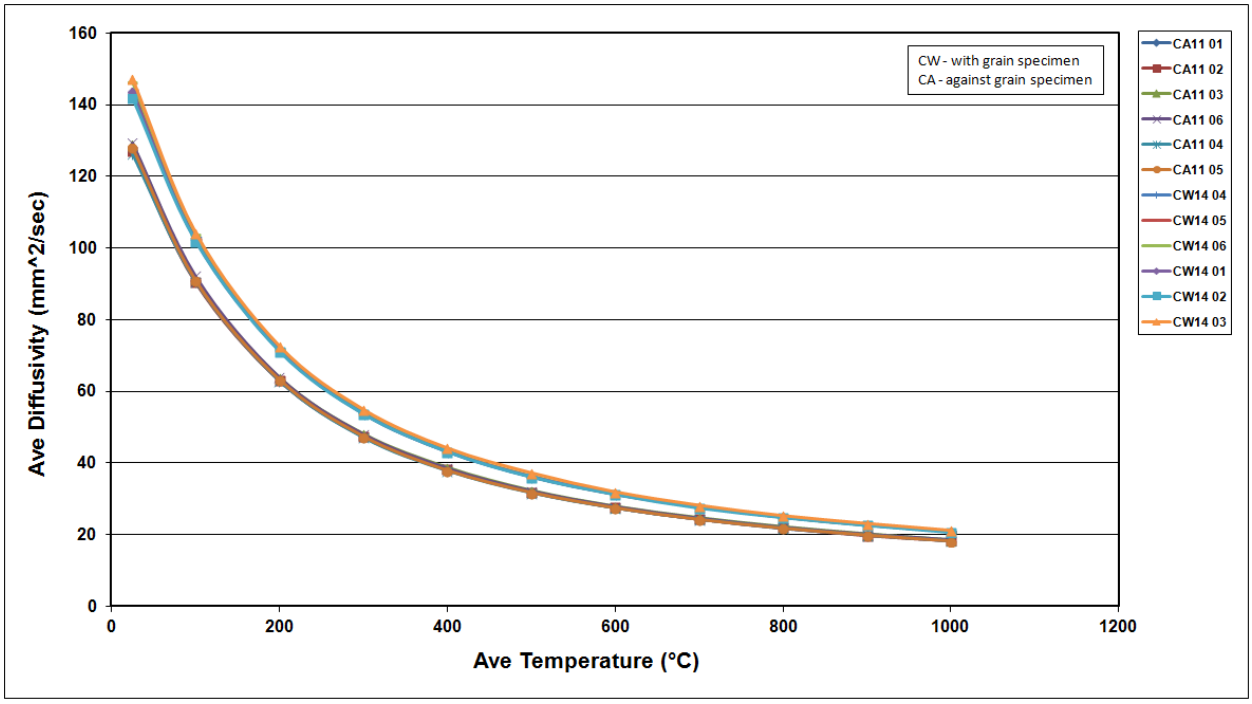

Figure A-215. H-451 Piggyback Diffusivity.

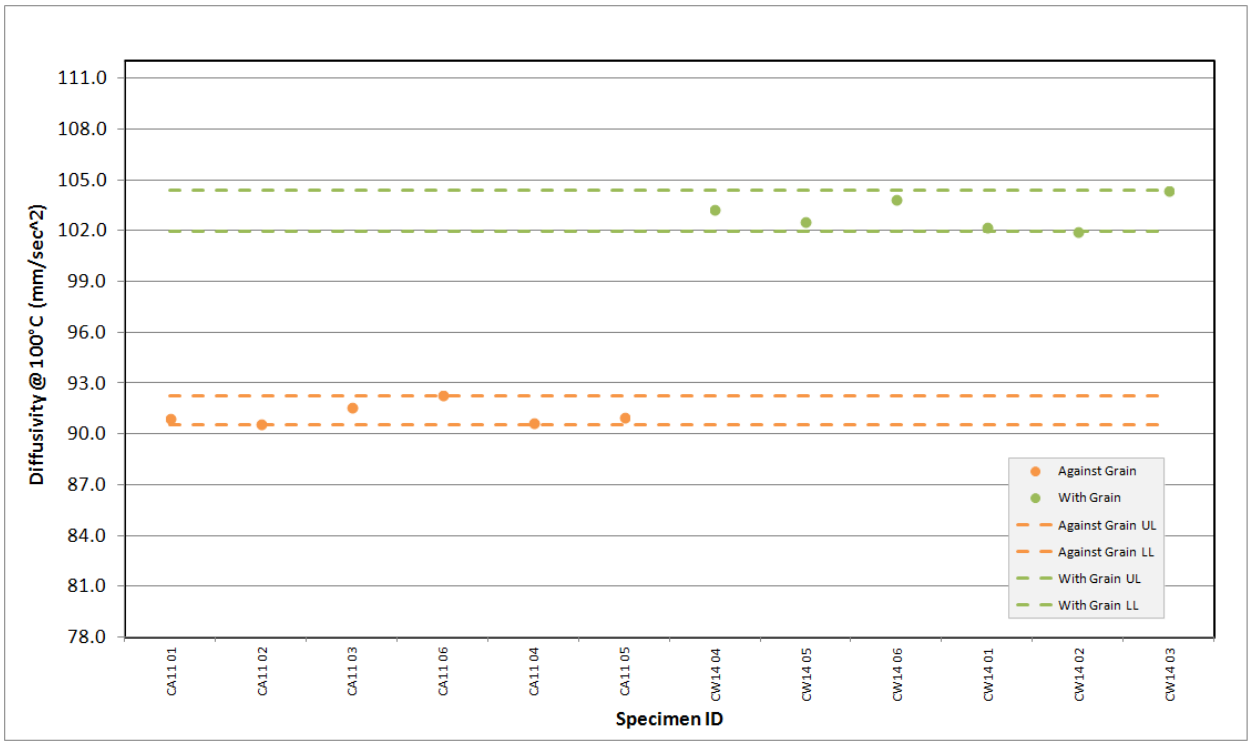

Figure A-216. H-451 Piggyback Diffusivity @ 100°C.

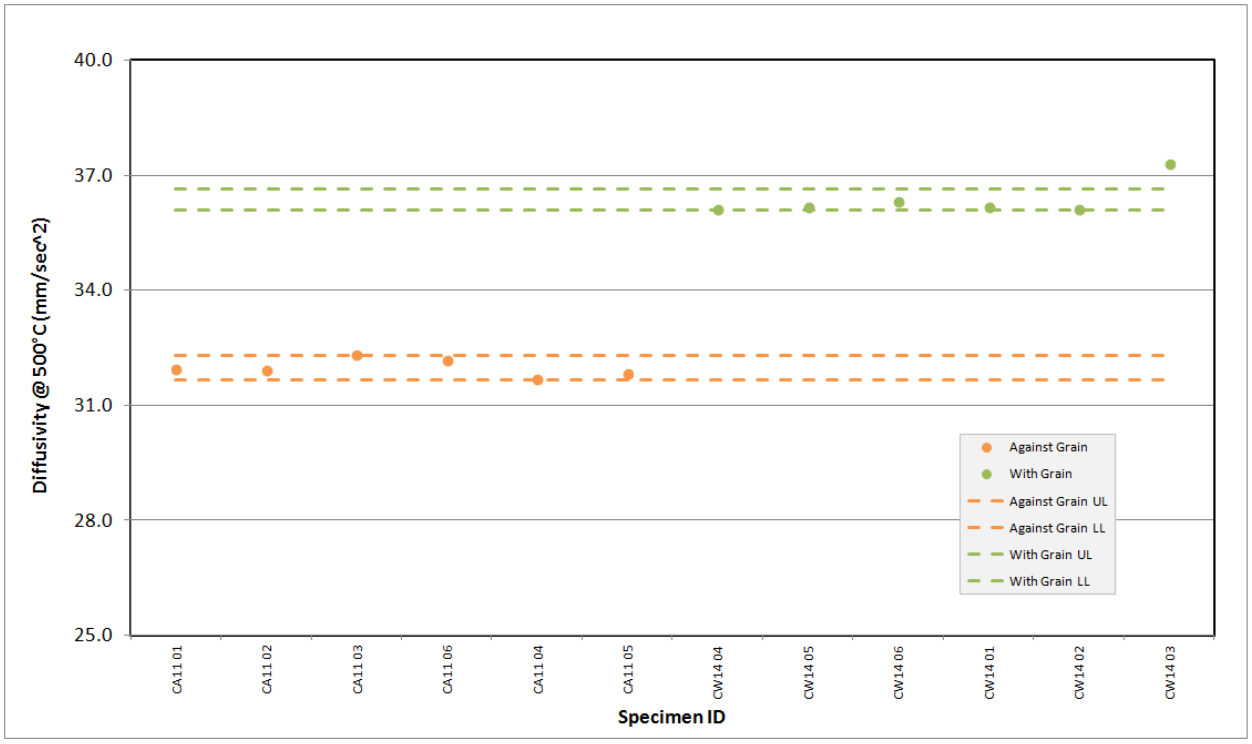

Figure A-217. H-451 Piggyback Diffusivity @ 500°C.

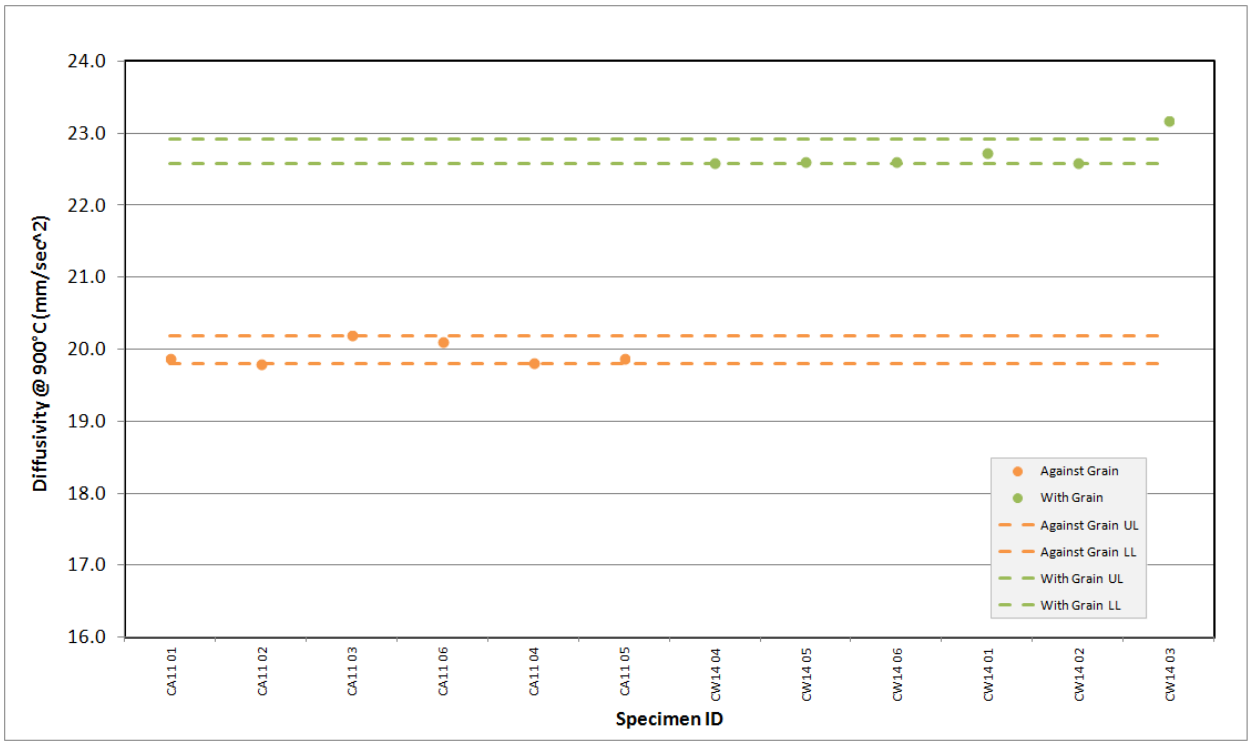

Figure A-218. H-451 Piggyback Diffusivity @ 900°C.

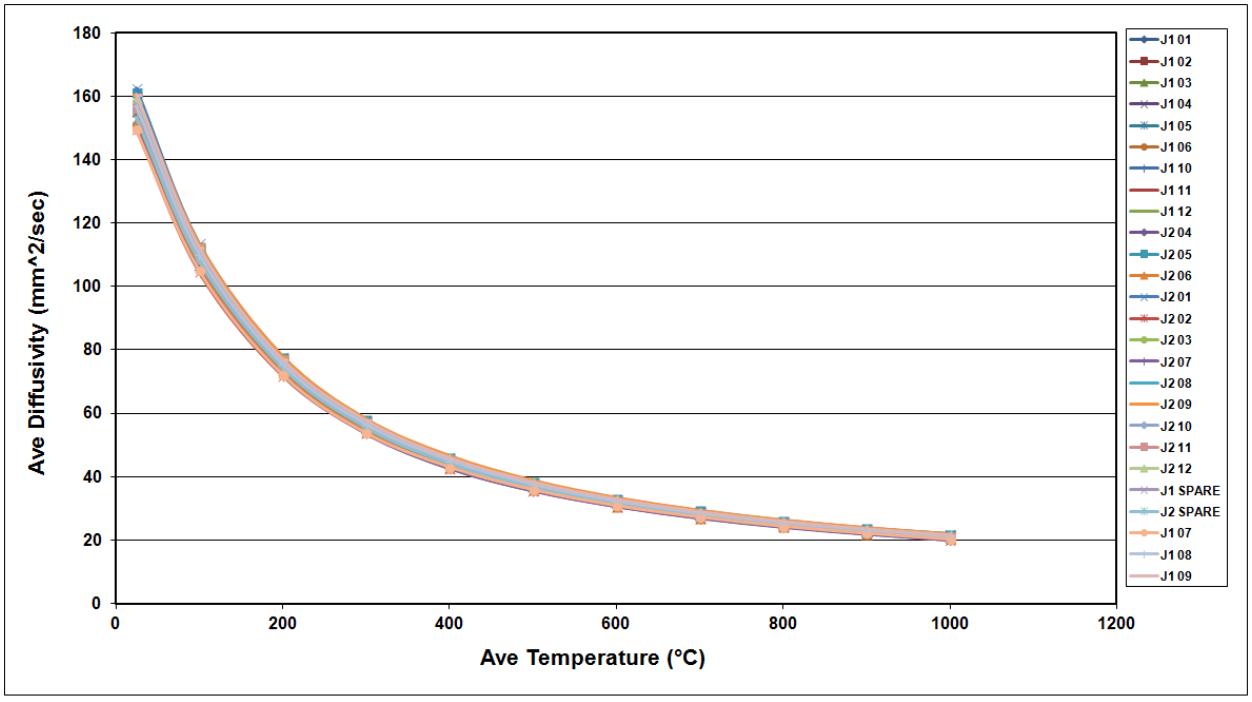

Figure A-219. HLM Piggyback Diffusivity.

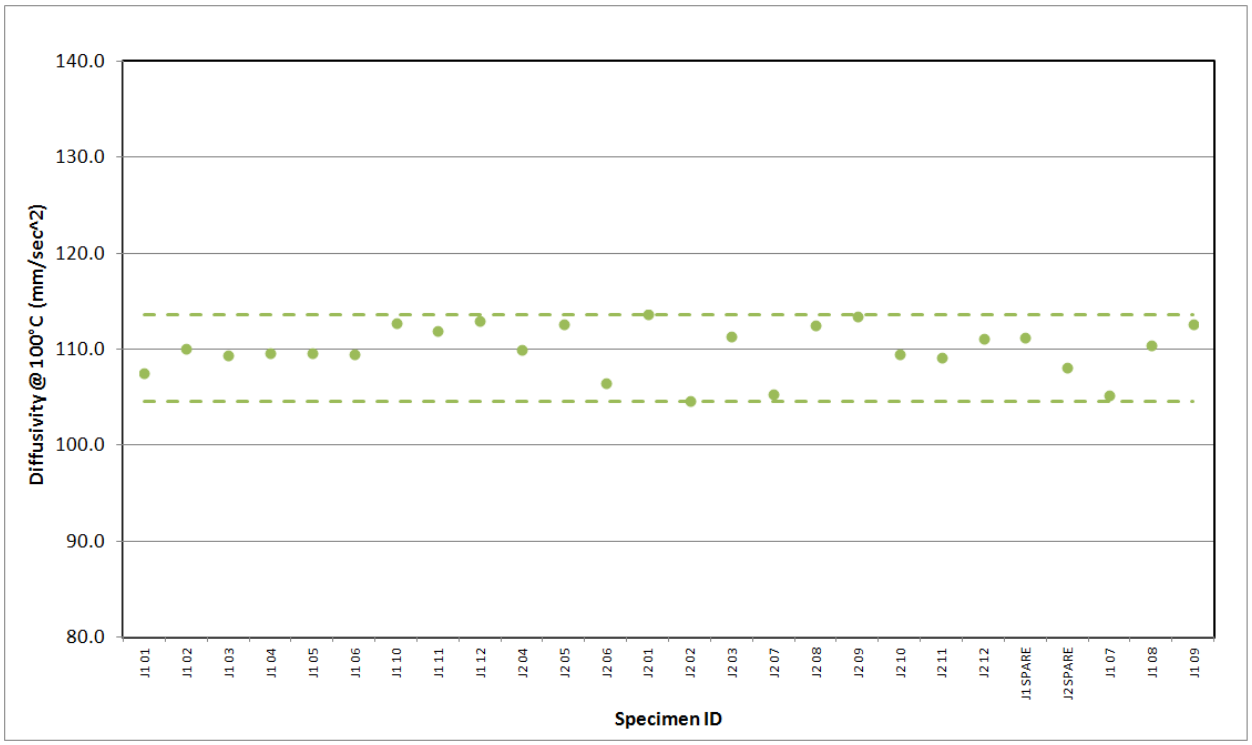

Figure A-220. HLM Piggyback Diffusivity @ 100°C.

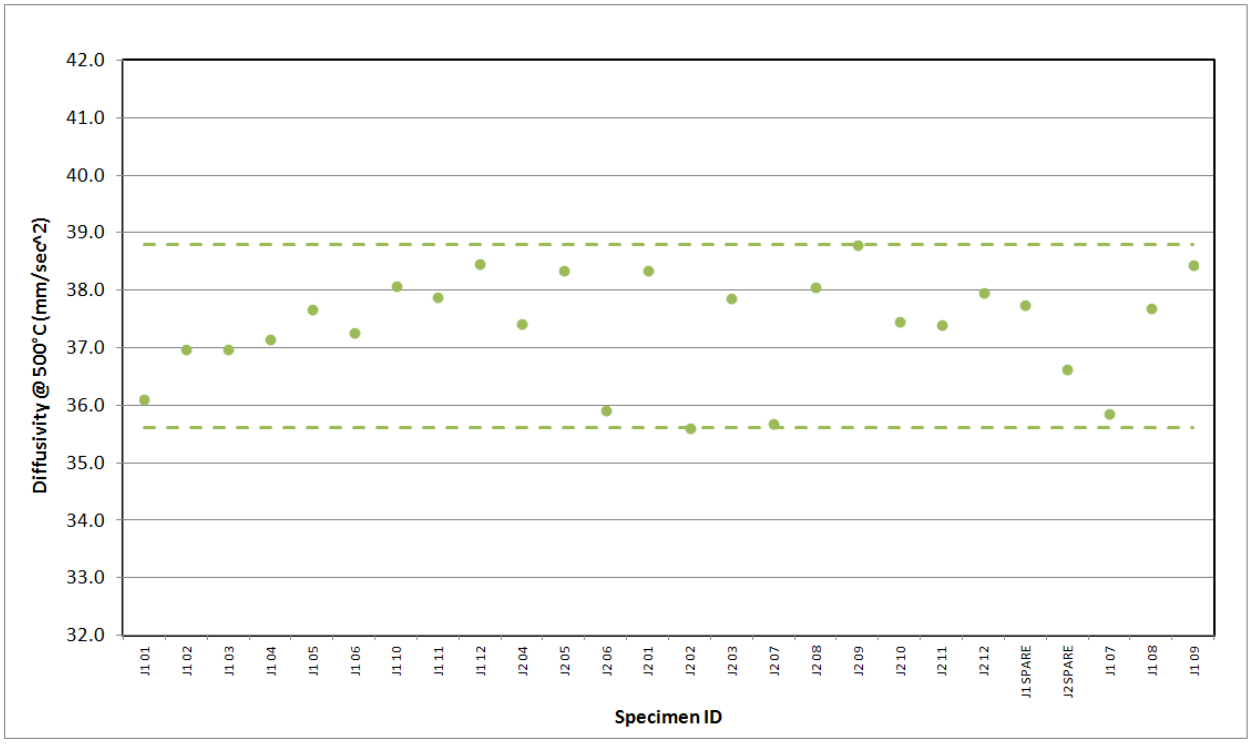

Figure A-221. HLM Piggyback Diffusivity @ 500°C.

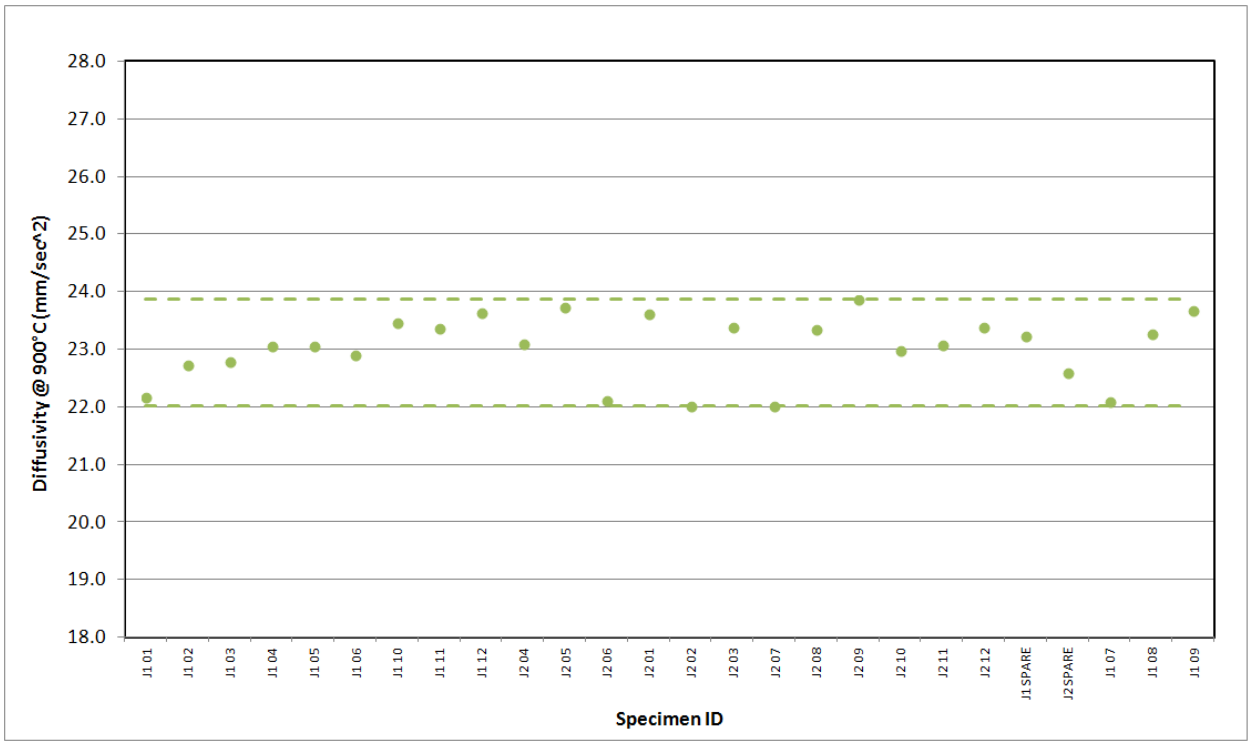

Figure A-222. HLM Piggyback Diffusivity @ 900°C.

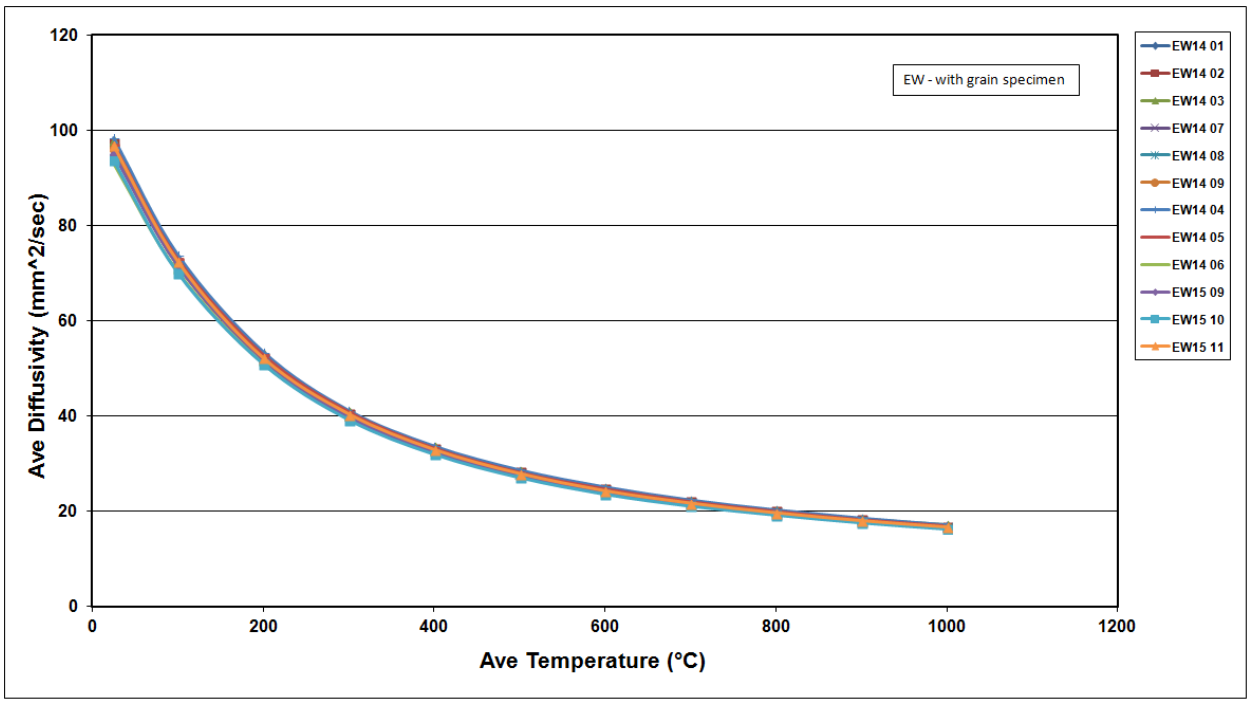

Figure A-223. IG-110 Piggyback Diffusivity.

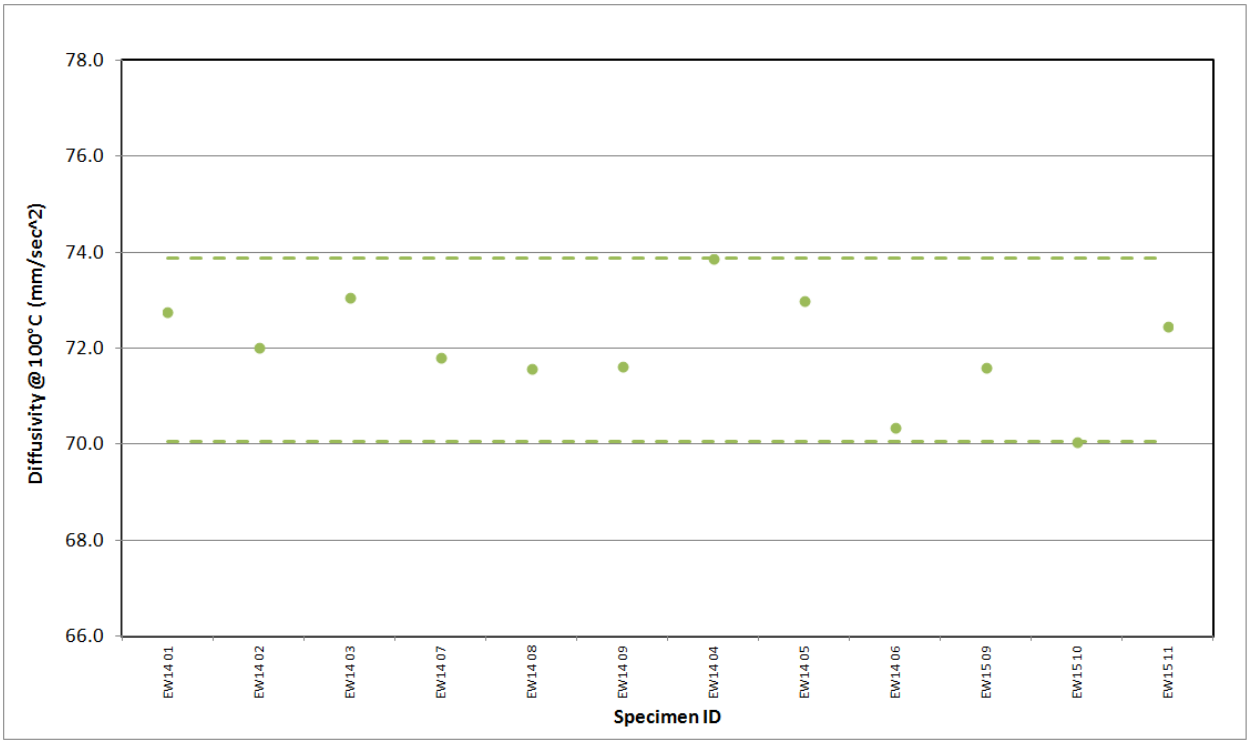

Figure A-224. IG-110 Piggyback Diffusivity @ 100°C.

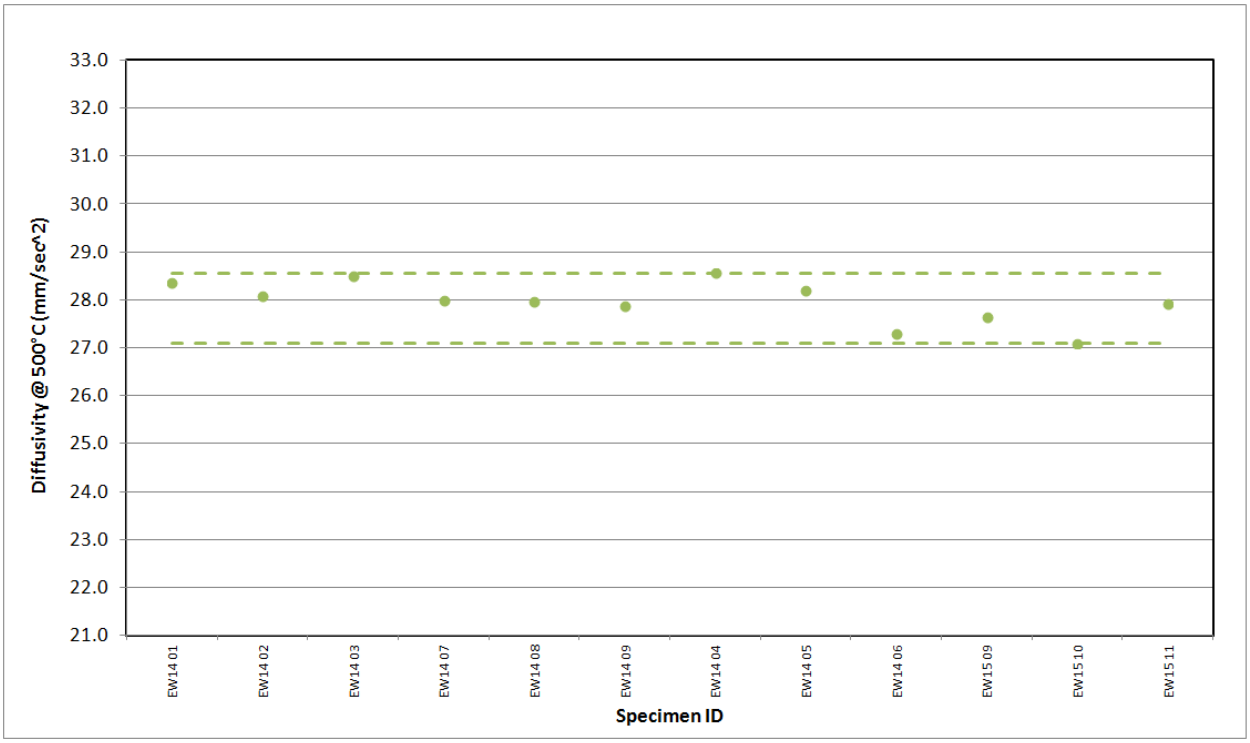

Figure A-225. IG-110 Piggyback Diffusivity @ 500°C.

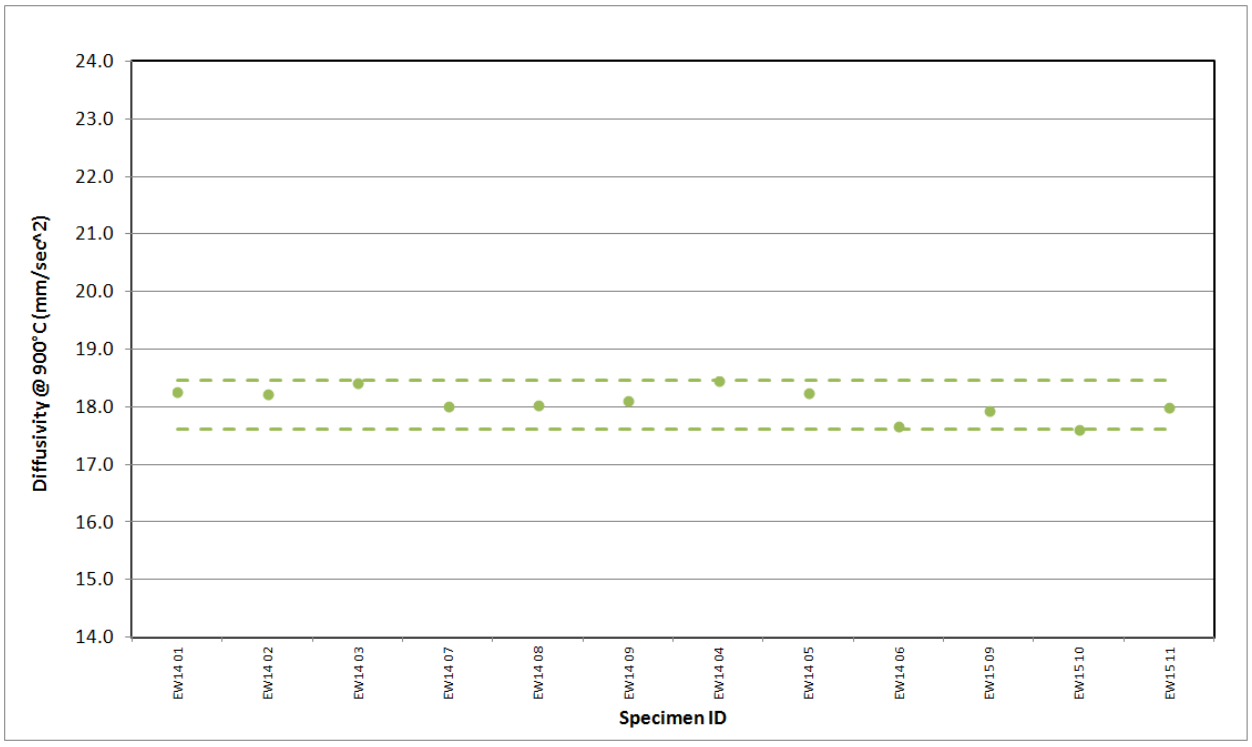

Figure A-226. IG-110 Piggyback Diffusivity @ 900°C.

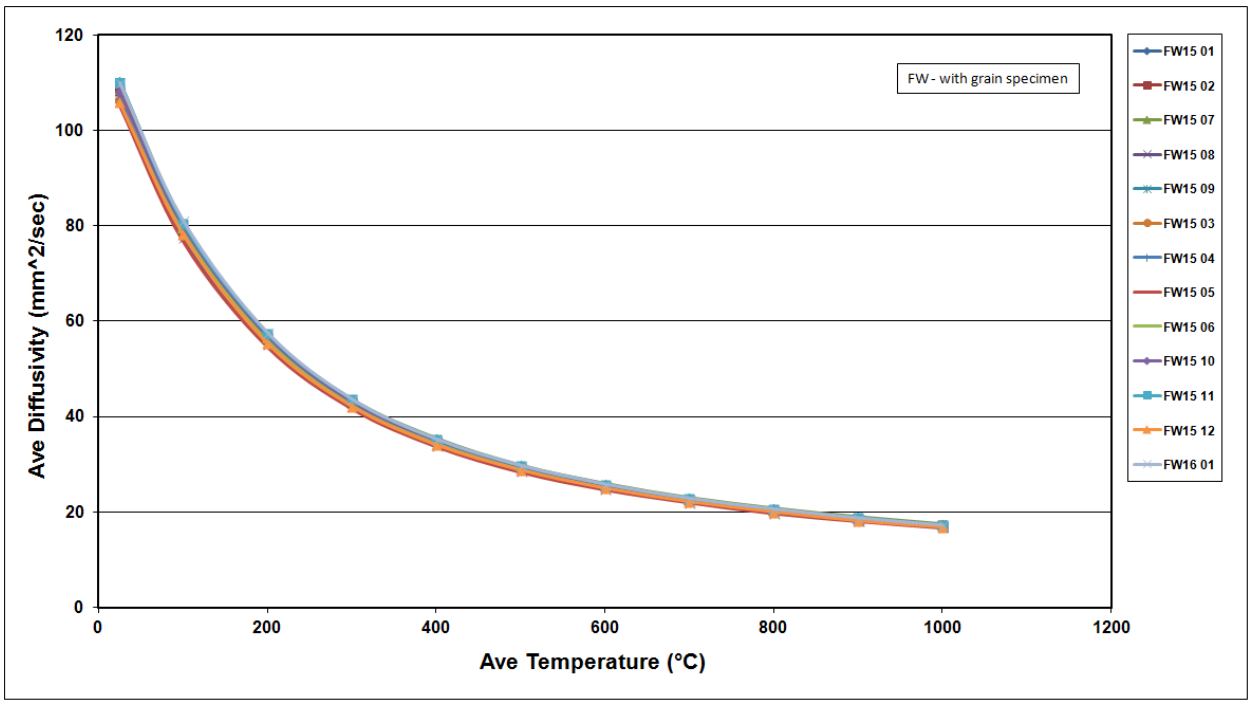

Figure A-227. IG-430 Piggyback Diffusivity.

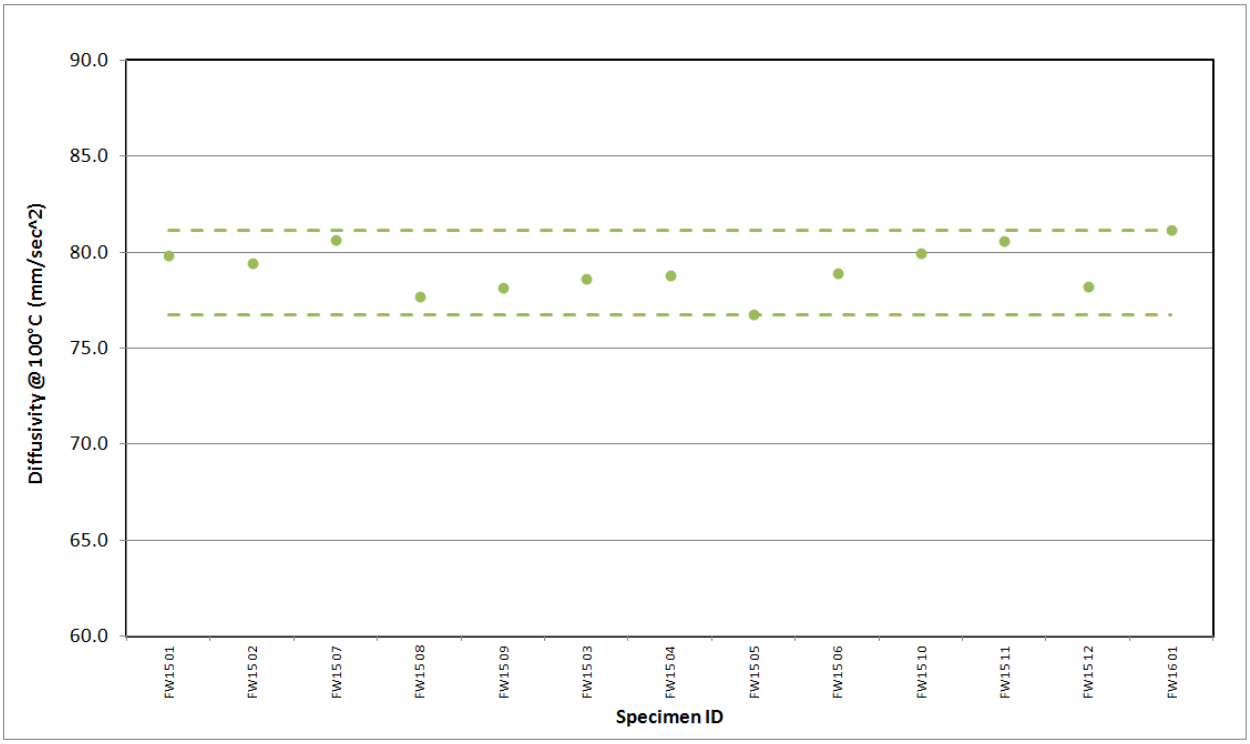

Figure A-228. IG-430 Piggyback Diffusivity @ 100°C.

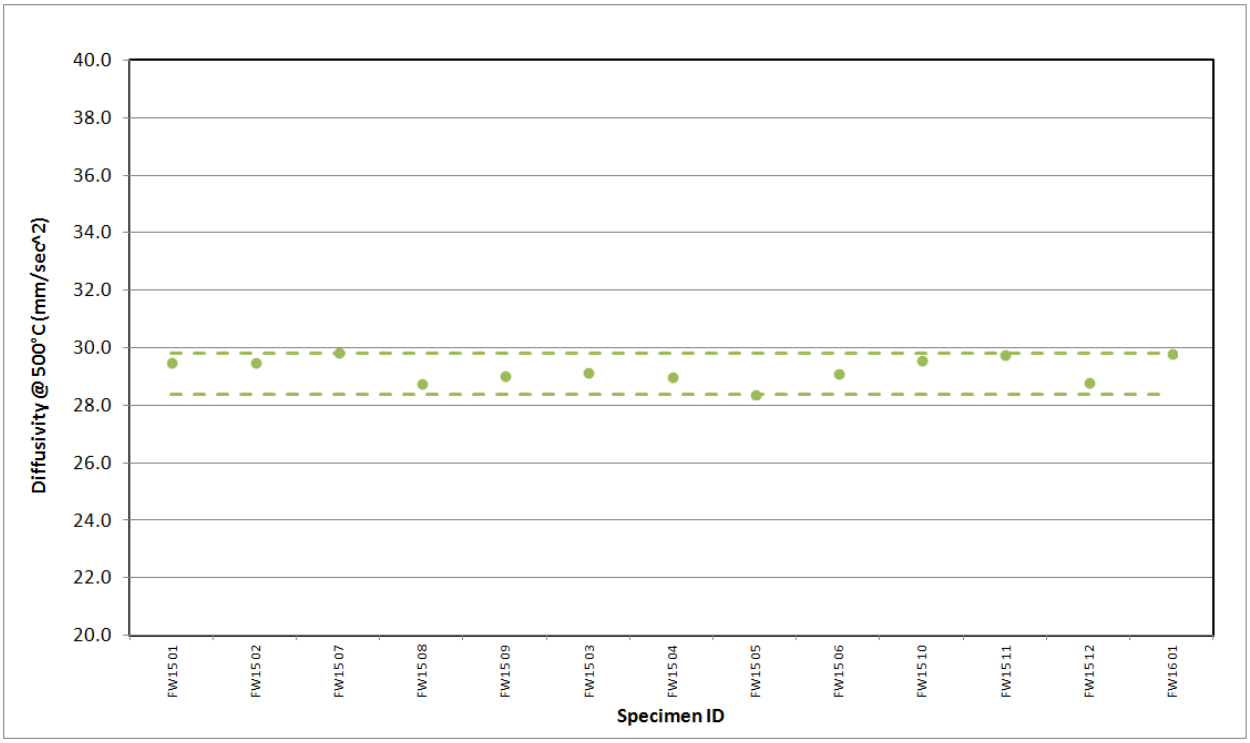

Figure A-229. IG-430 Piggyback Diffusivity @ 500°C.

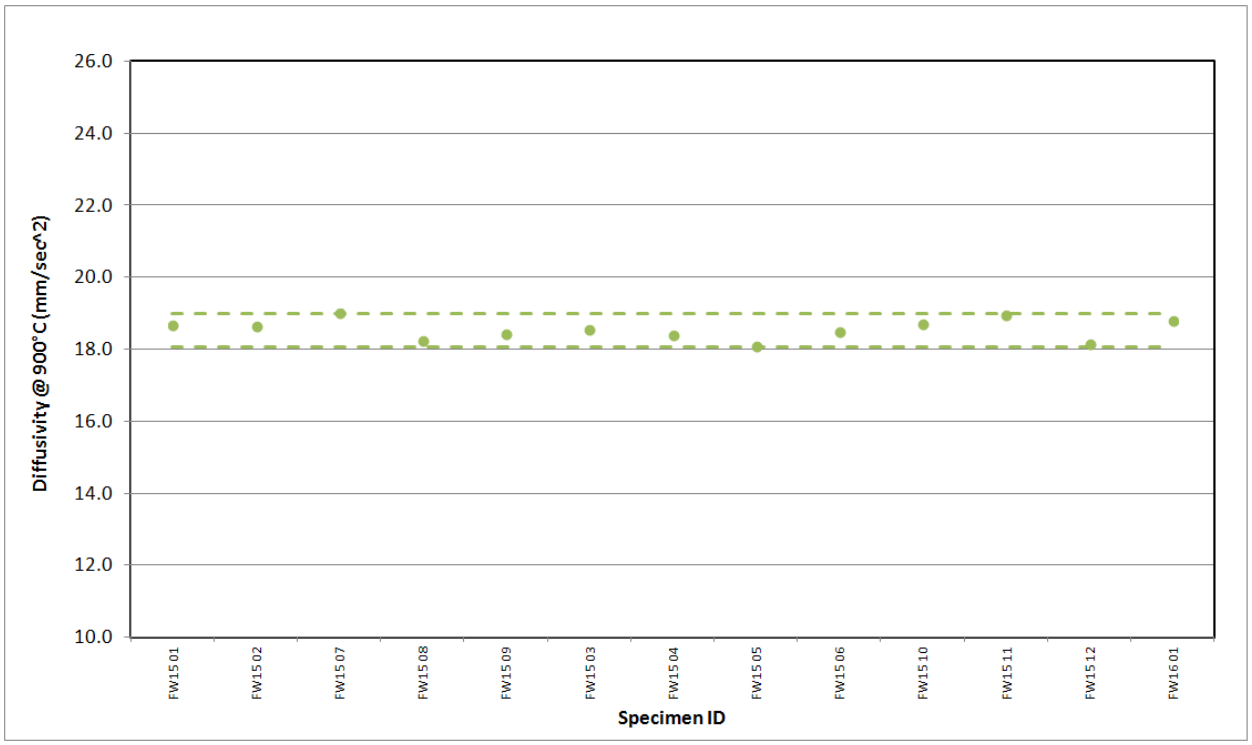

Figure A-230. IG-430 Piggyback Diffusivity @ 900°C.

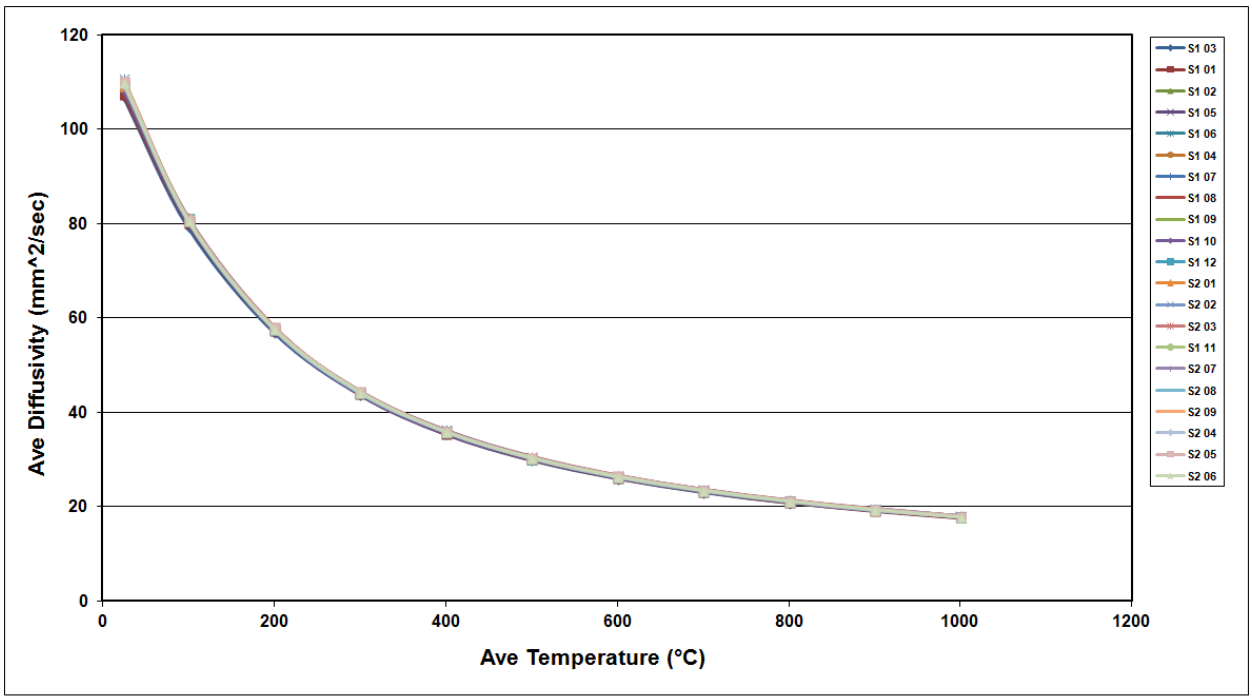

Figure A-231. NBG-10 Piggyback Diffusivity.

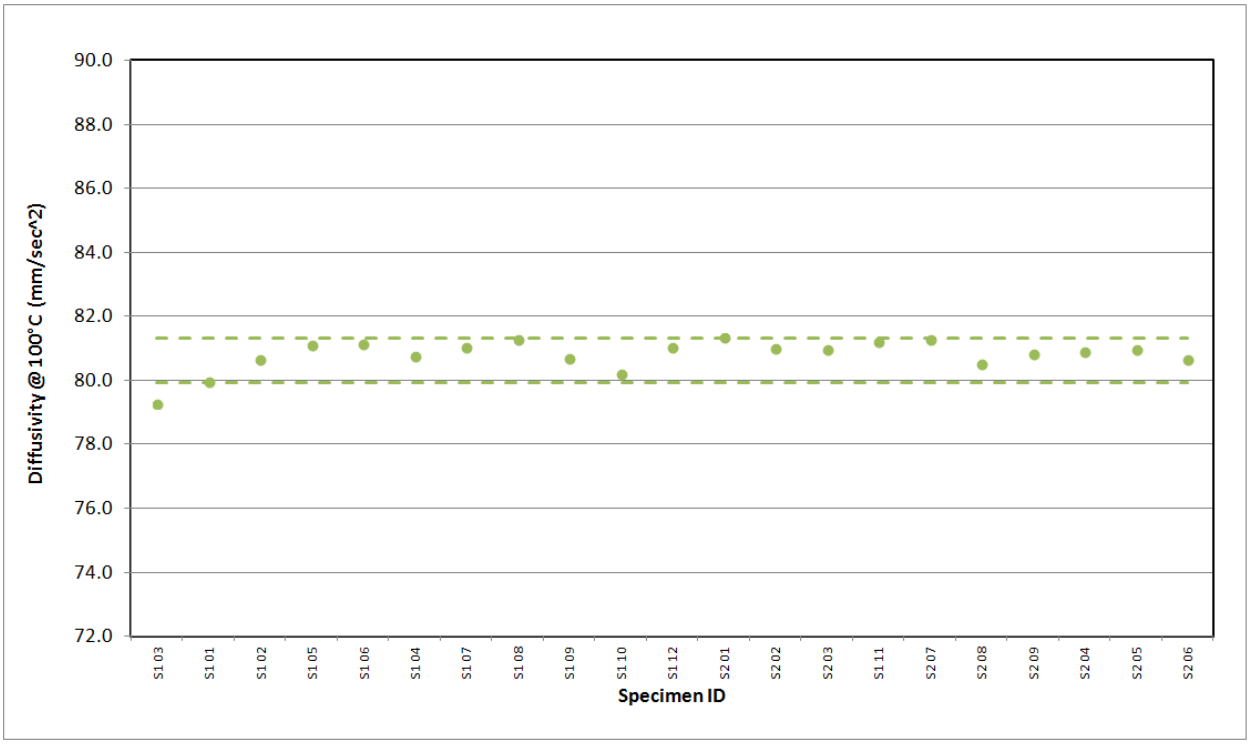

Figure A-232. NBG-10 Piggyback Diffusivity @ 100°C.

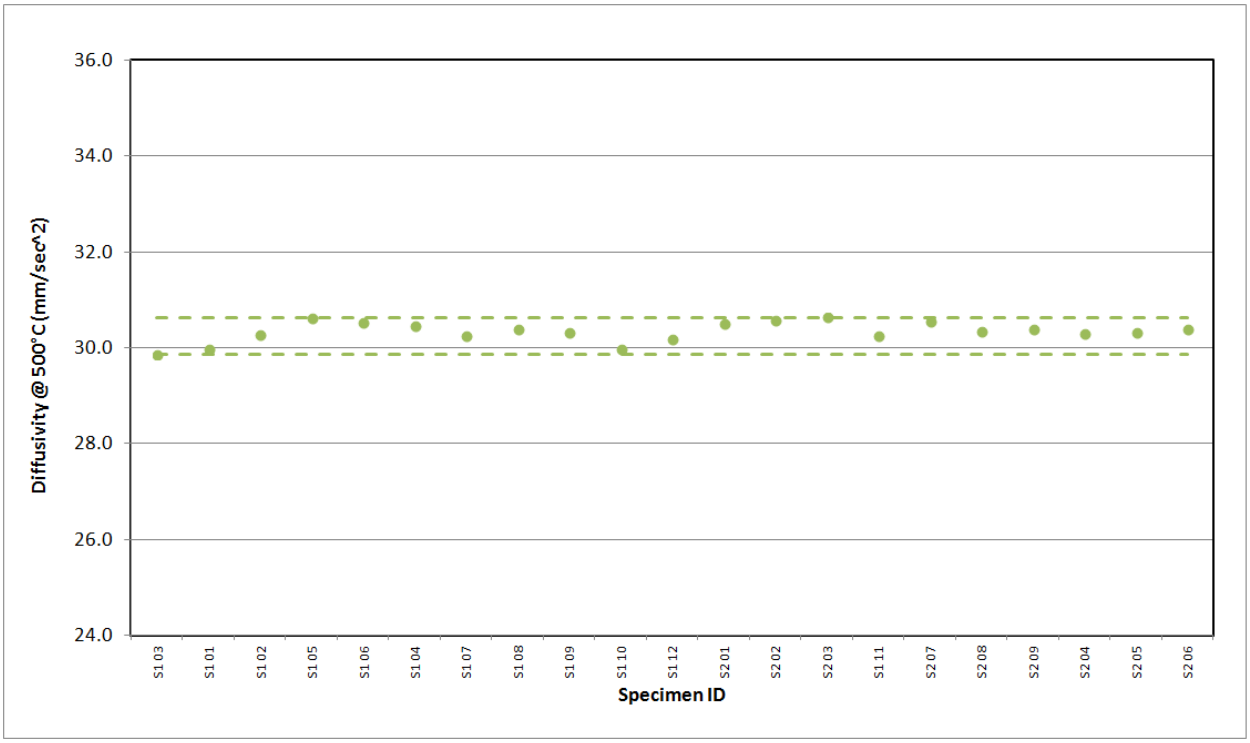

Figure A-233. NBG-10 Piggyback Diffusivity @ 500°C.

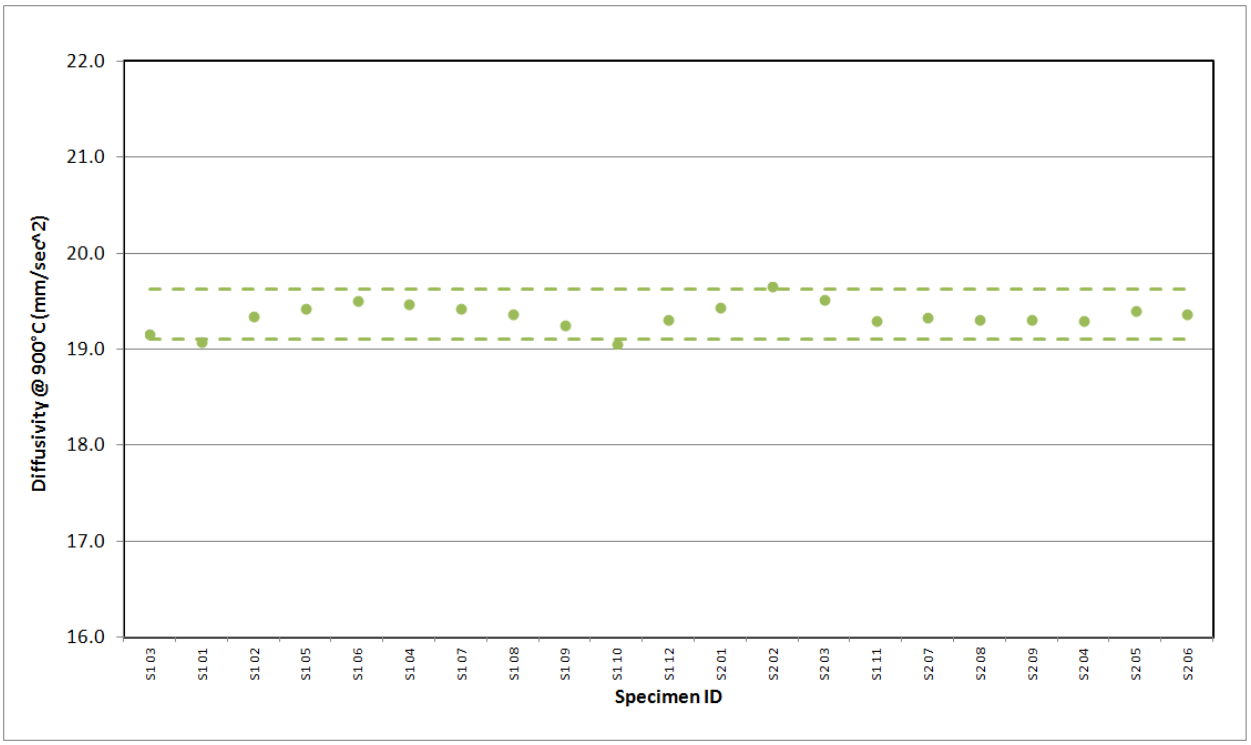

Figure A-234. NBG-10 Piggyback Diffusivity @ 900°C.

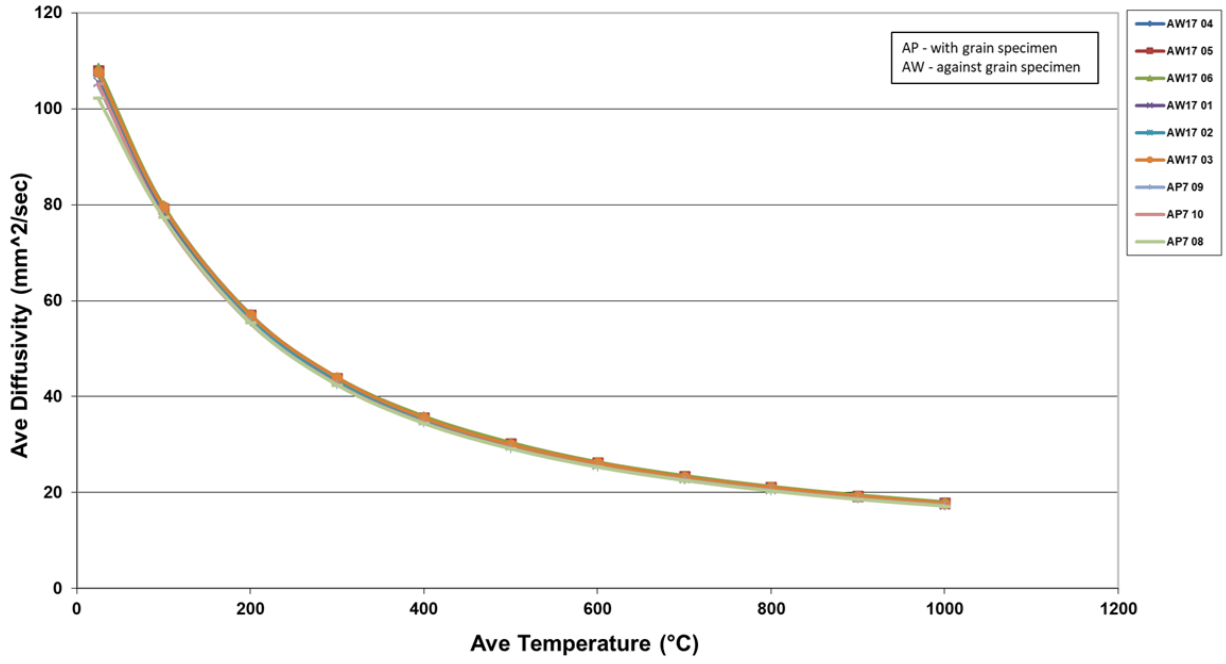

Figure A-235. NBG-17 Piggyback Diffusivity.

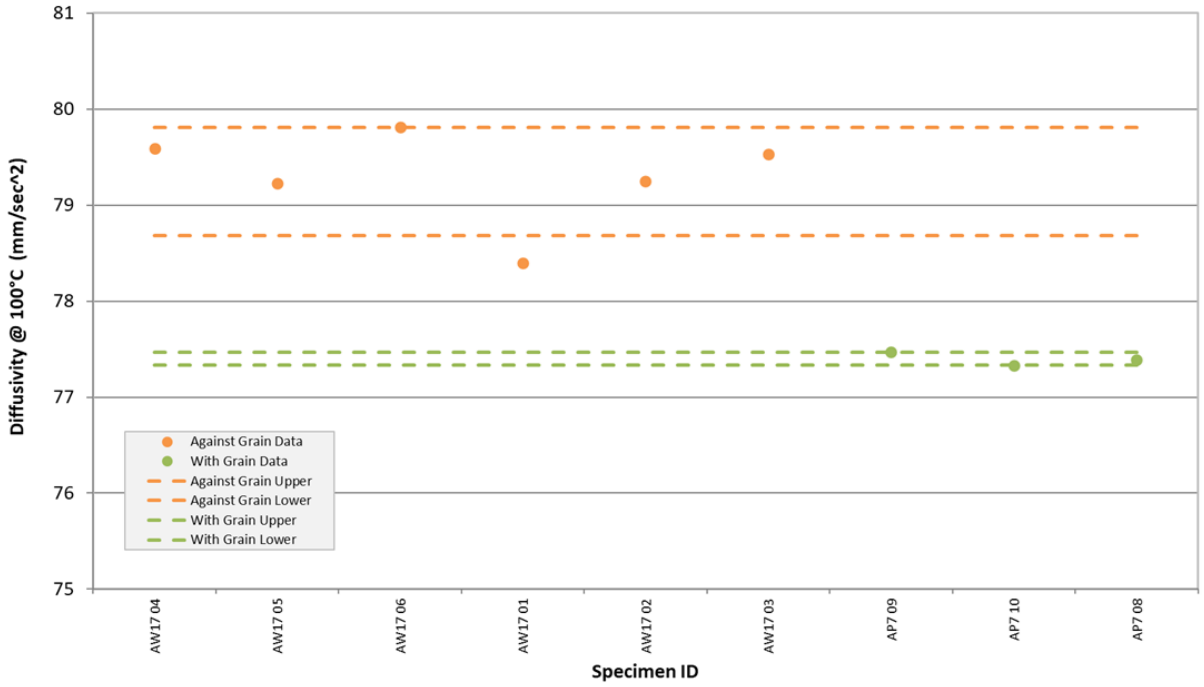

Figure A-236. NBG-17 Piggyback Diffusivity @ 100°C.

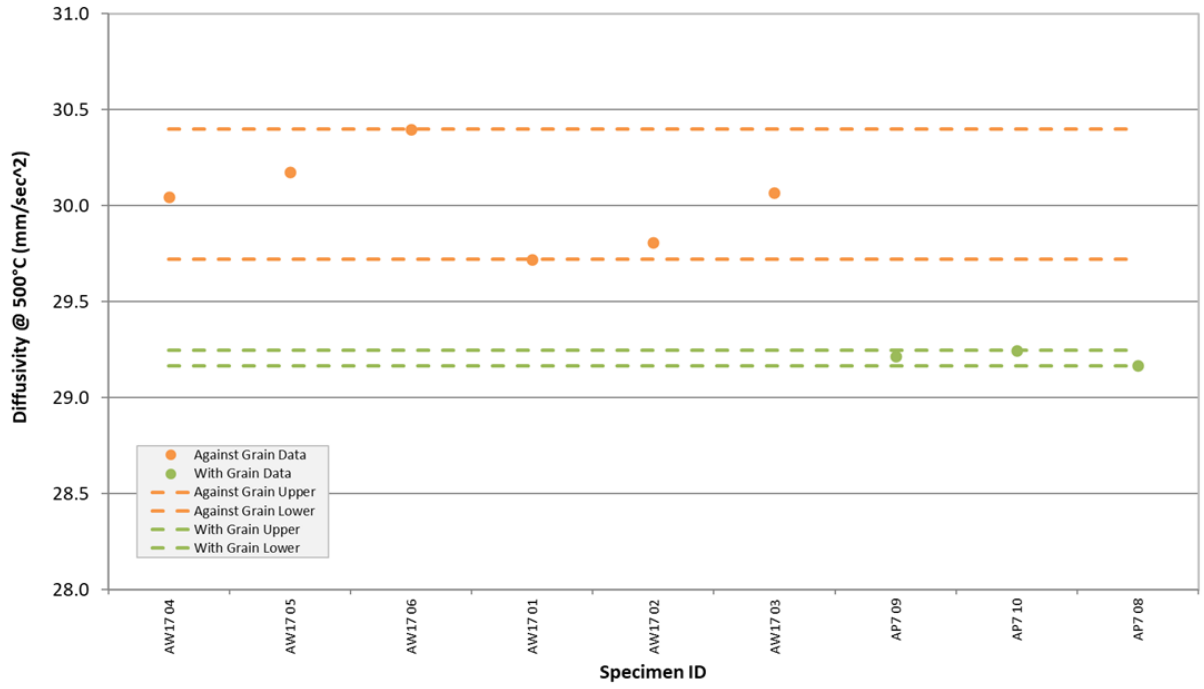

Figure A-237. NBG-17 Piggyback Diffusivity @ 500°C.

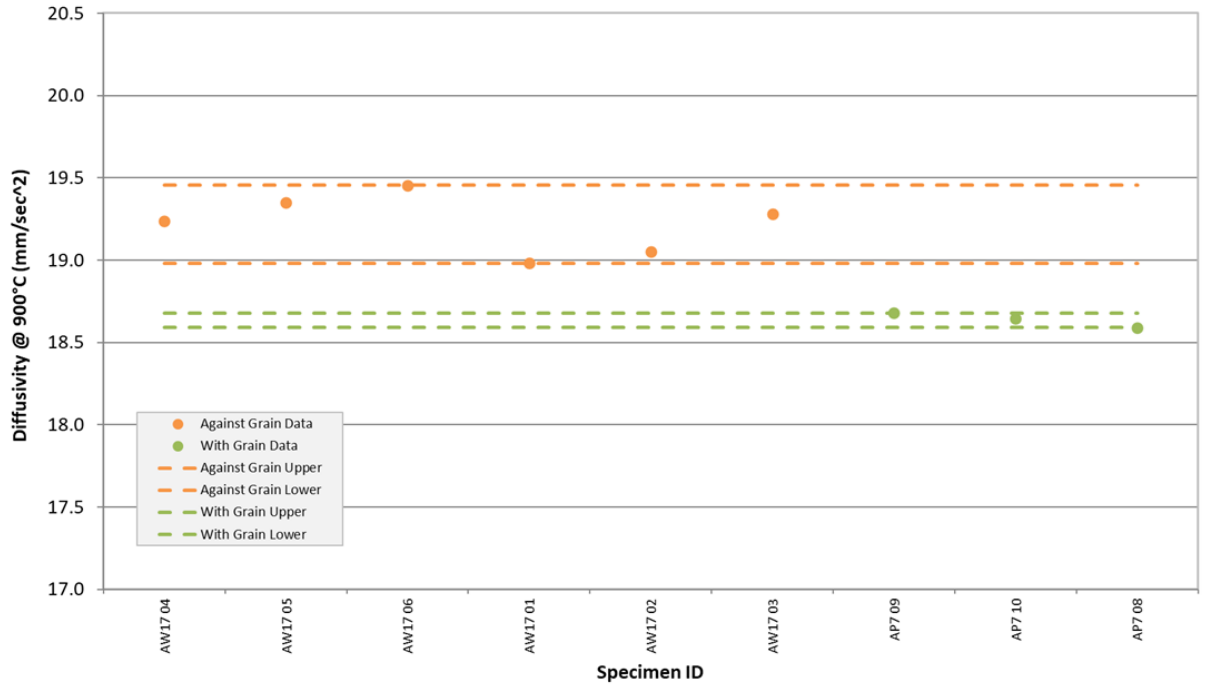

Figure A-238. NBG-17 Piggyback Diffusivity @ 900°C.

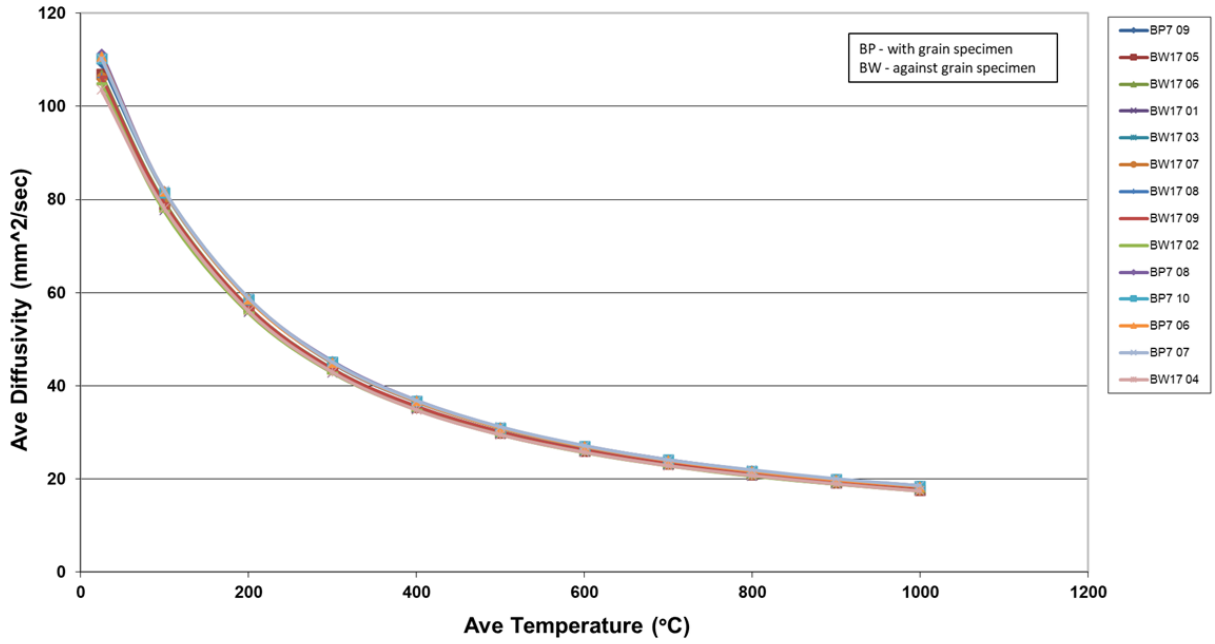

Figure A-239. NBG-18 Piggyback Diffusivity.

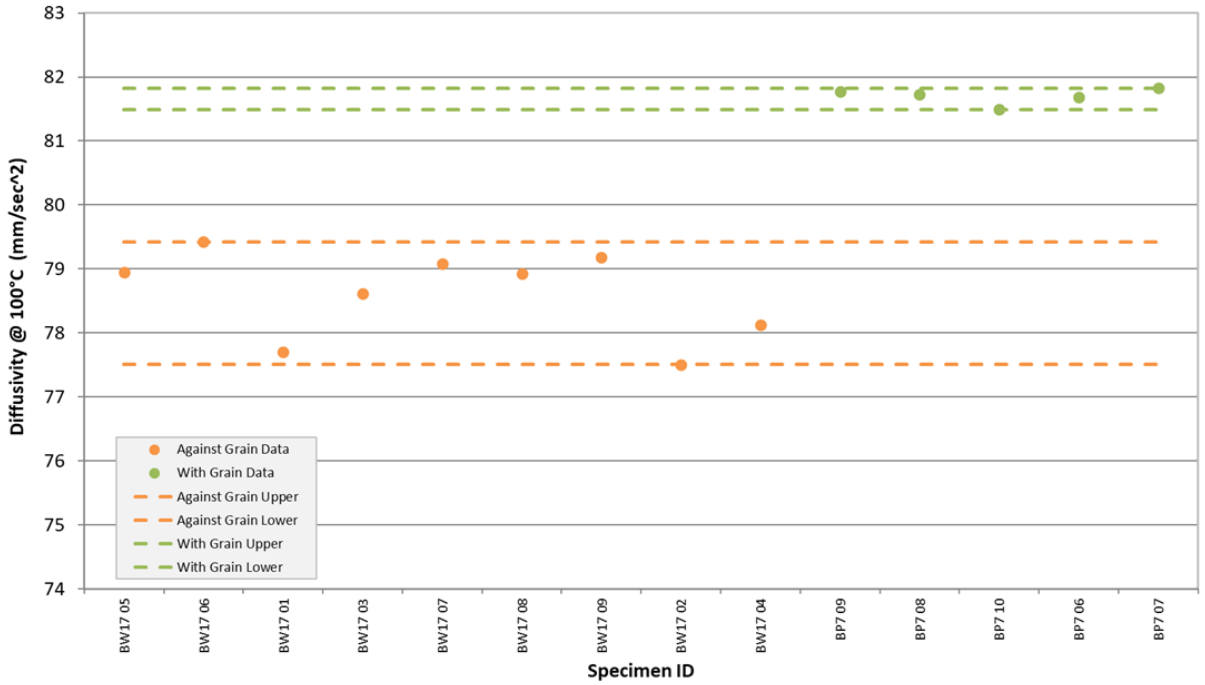

Figure A-240. NBG-18 Piggyback Diffusivity @ 100°C.

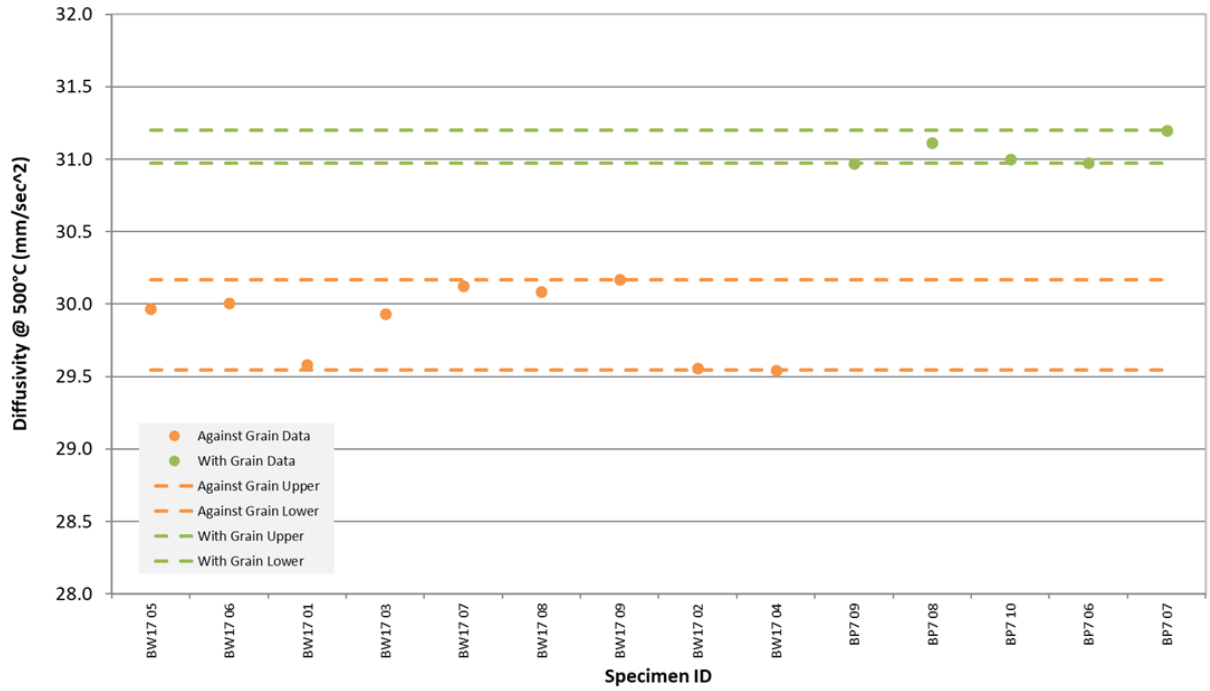

Figure A-241. NBG-18 Piggyback Diffusivity @ 500°C.

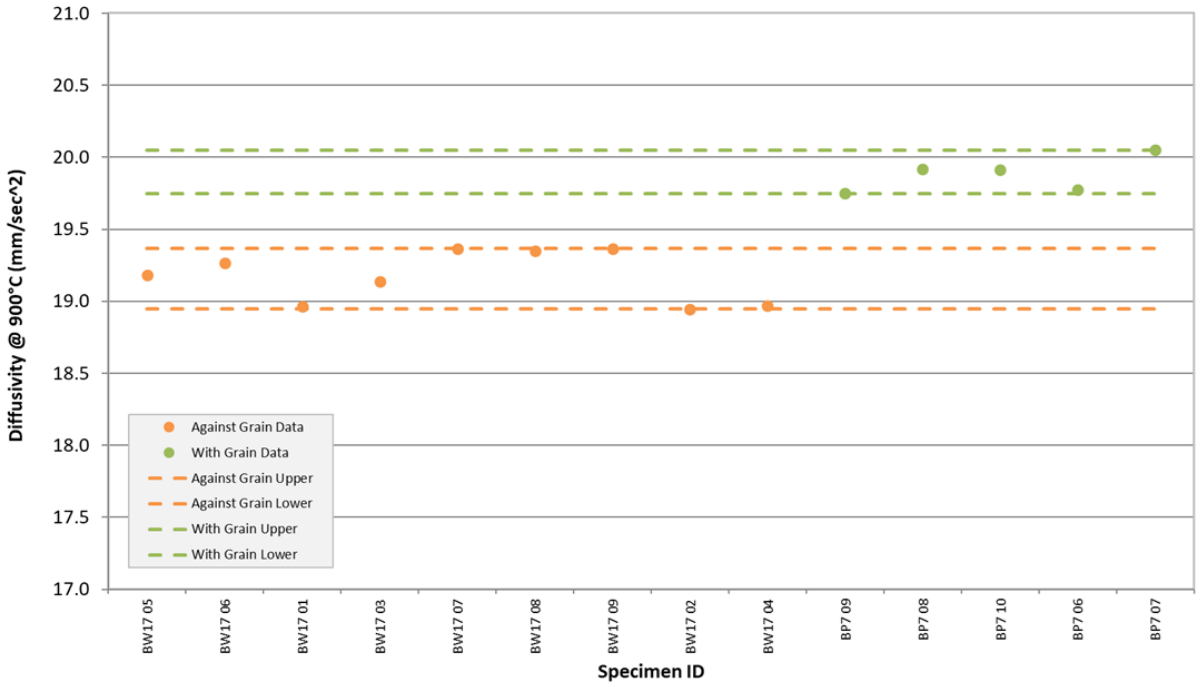

Figure A-242. NBG-18 Diffusivity @ 900°C.

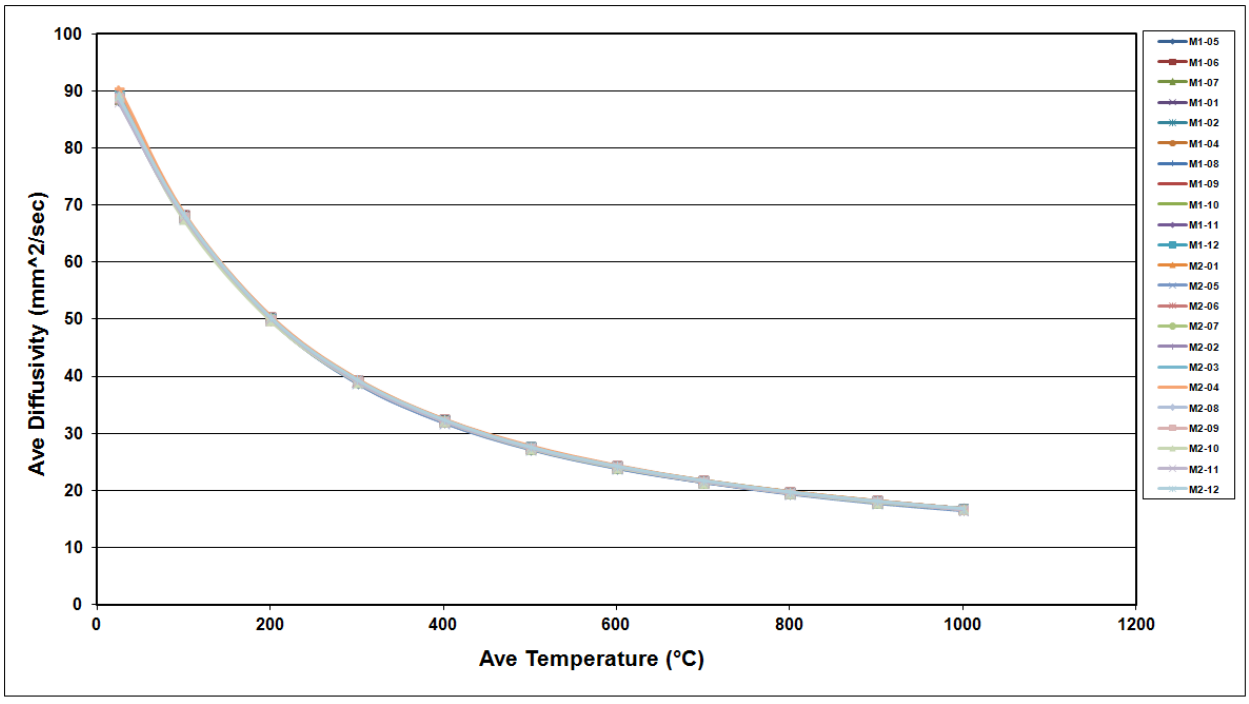

Figure A-243. NBG-25 Piggyback Diffusivity.

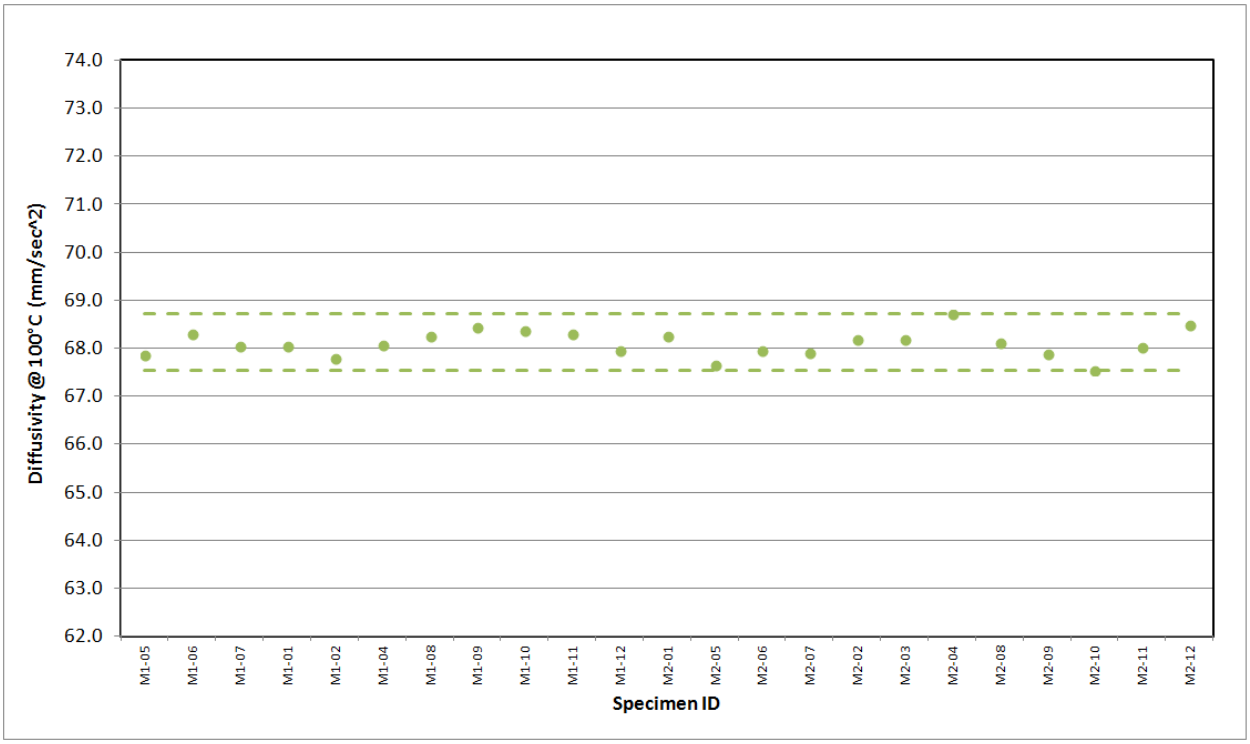

Figure A-244. NBG-25 Piggyback Diffusivity @ 100°C.

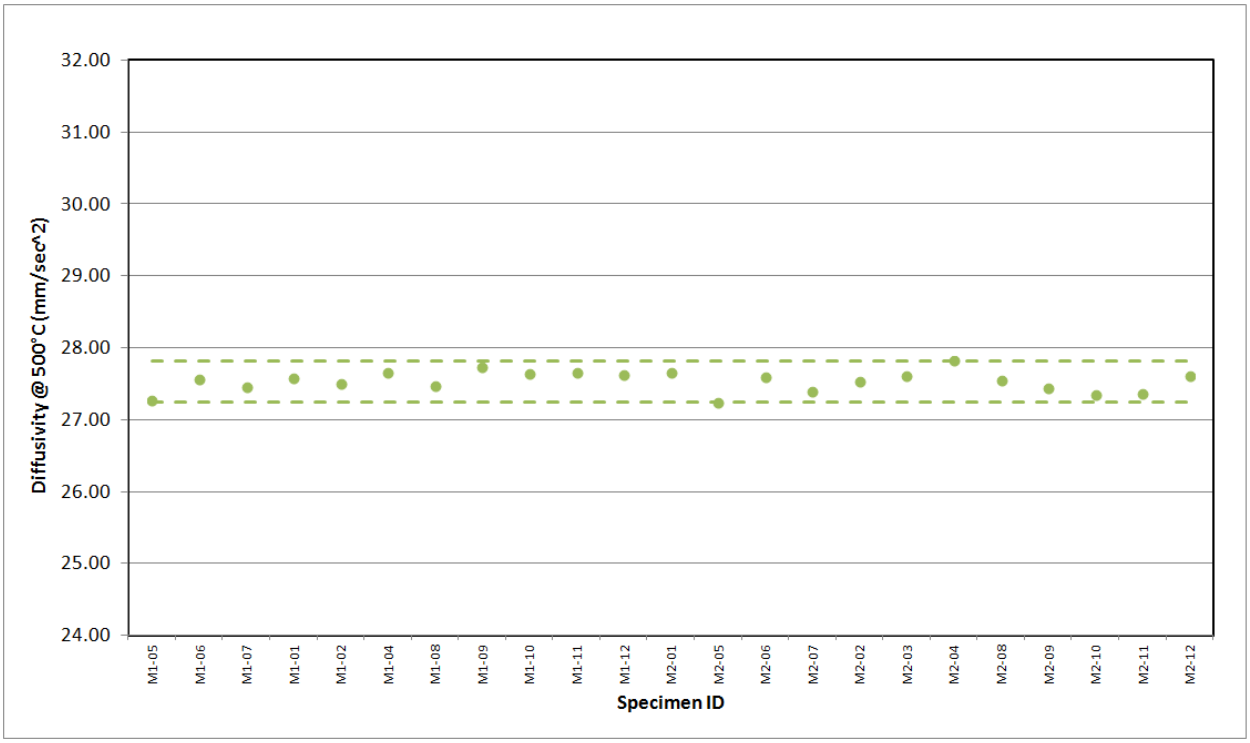

Figure A-245. NBG-25 Piggyback Diffusivity @ 500°C.

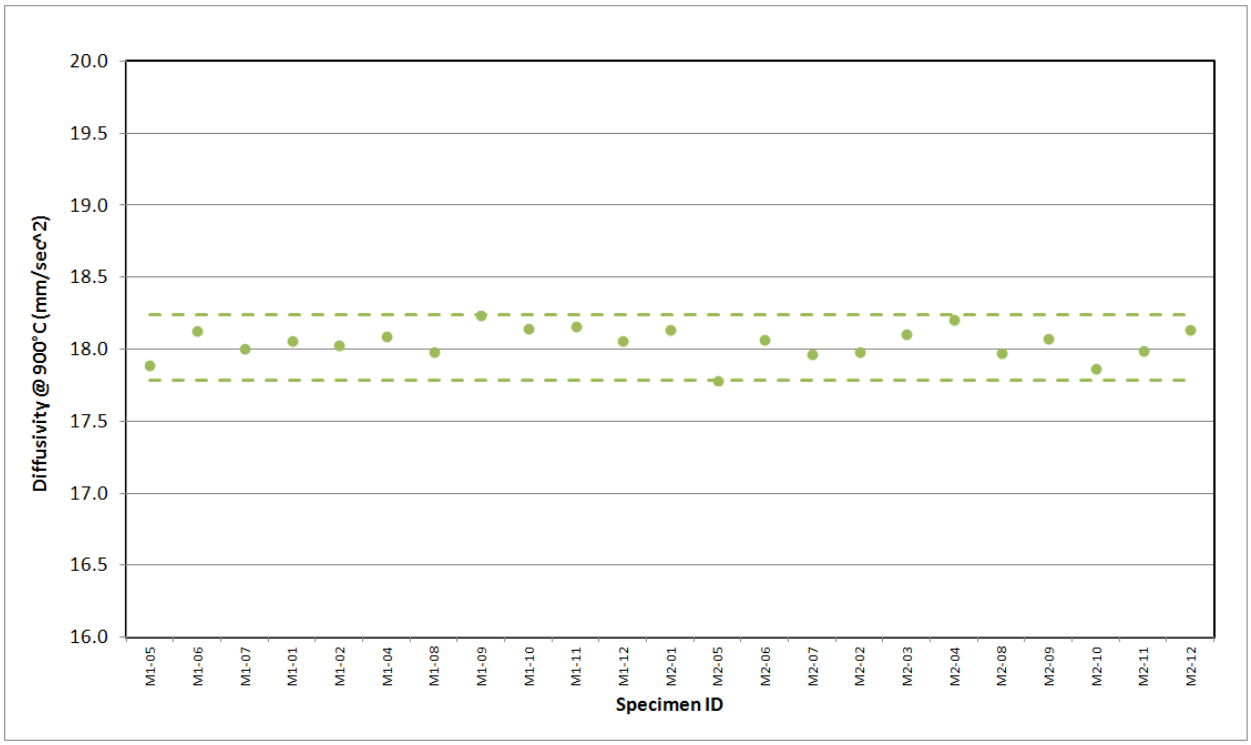

Figure A-246. NBG-25 Piggyback Diffusivity @ 900°C.

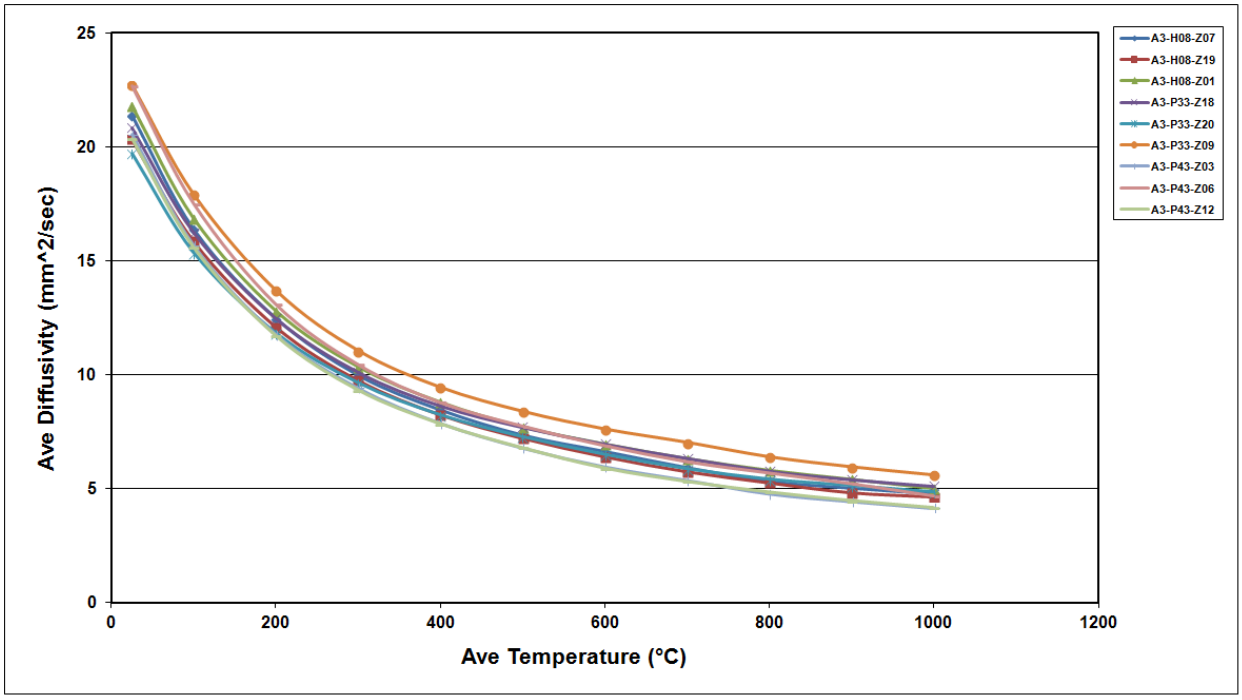

Figure A-247. New Matrix Piggyback Diffusivity.

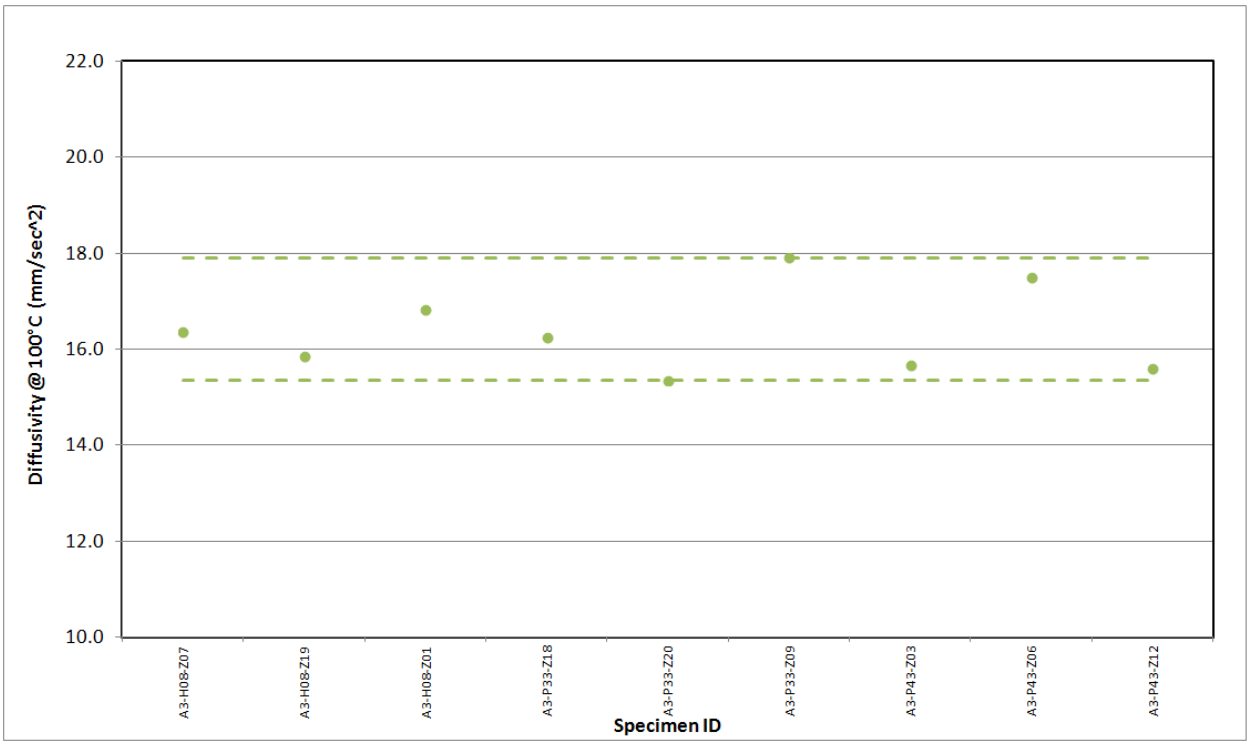

Figure A-248. New Matrix Piggyback Diffusivity @ 100°C.

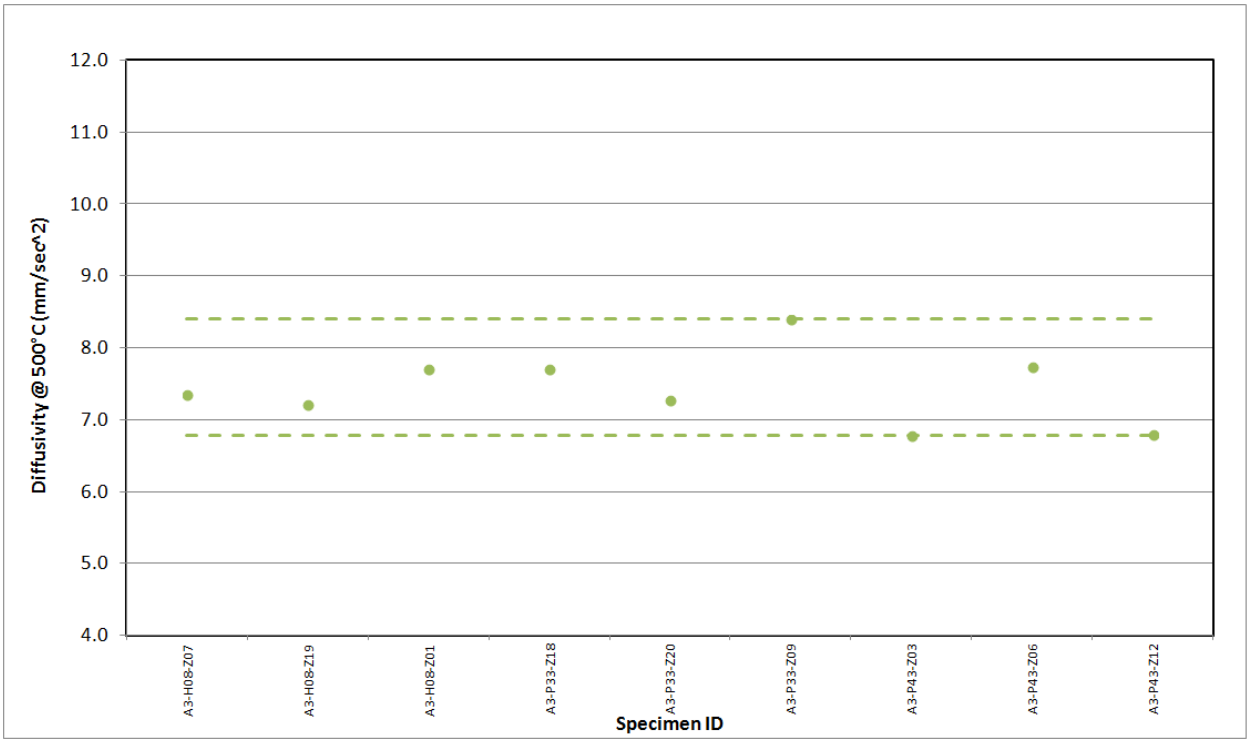

Figure A-249. New Matrix Piggyback Diffusivity @ 500°C.

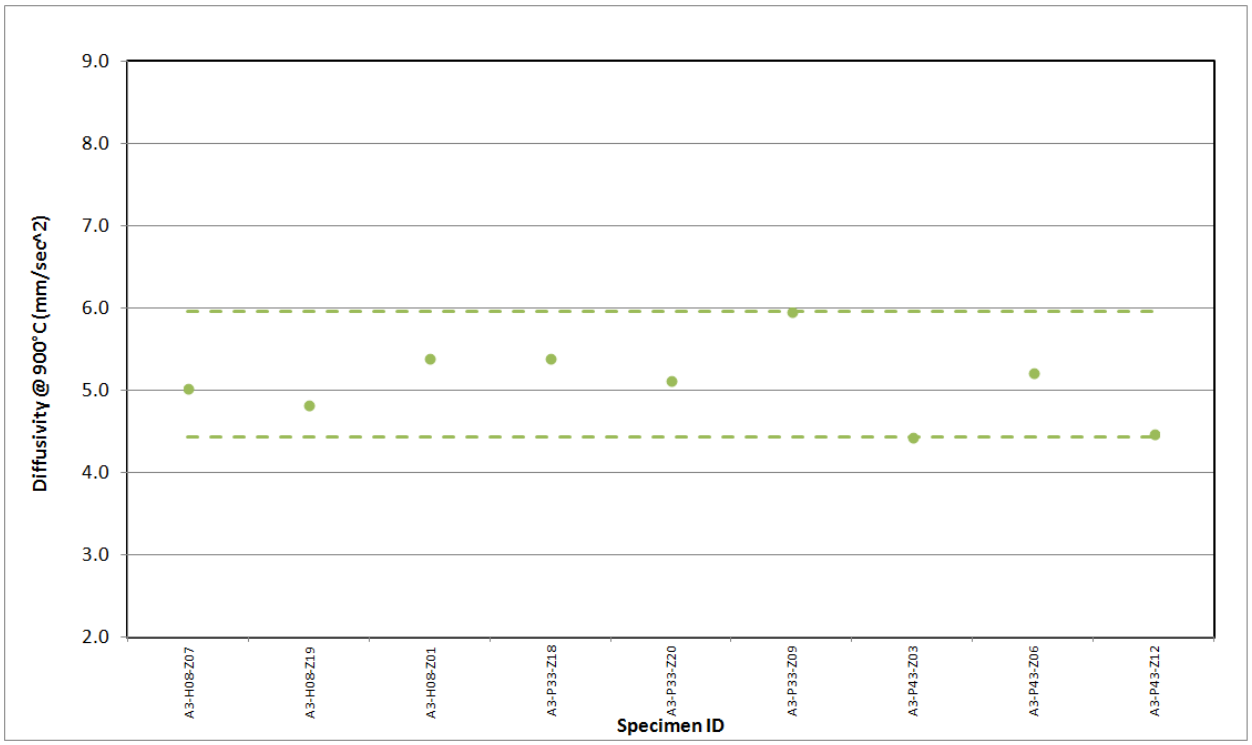

Figure A-250. New Matrix Piggyback Diffusivity @ 900°C.

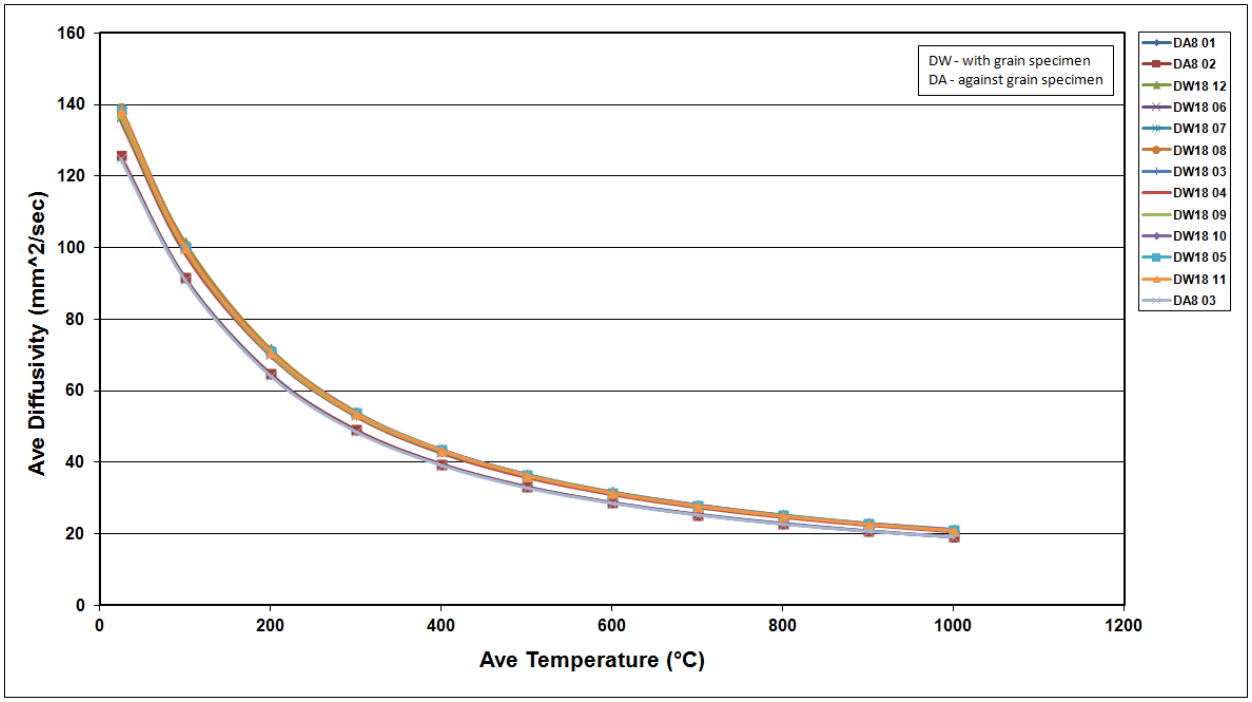

Figure A-251. PCEA Piggyback Diffusivity.

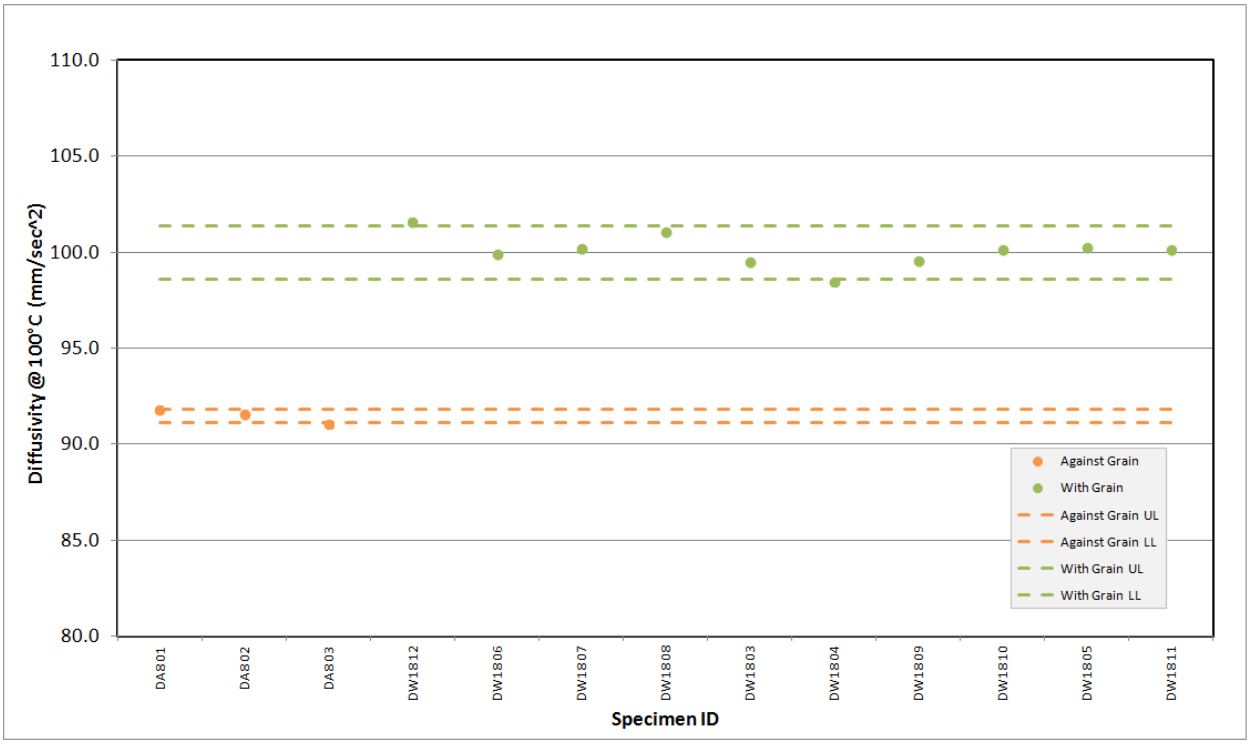

Figure A-252. PCEA Piggyback Diffusivity @ 100°C.

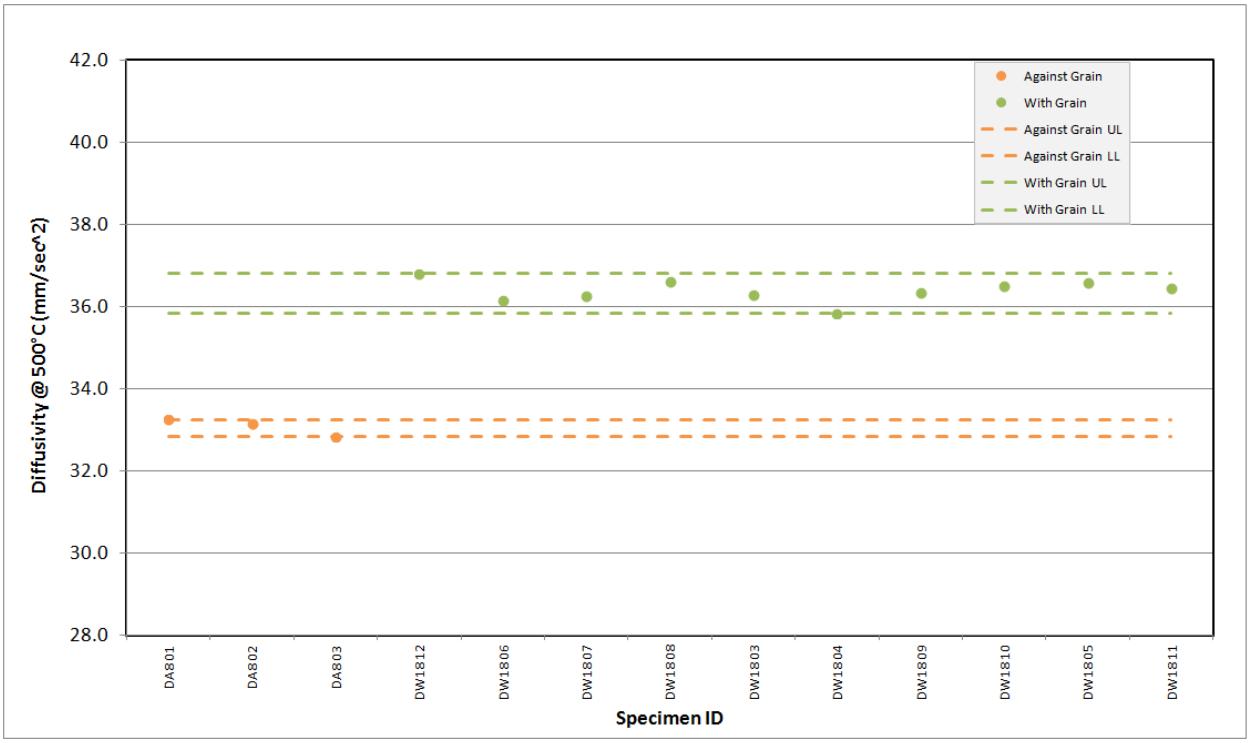

Figure A-253. PCEA Piggyback Diffusivity @ 500°C.

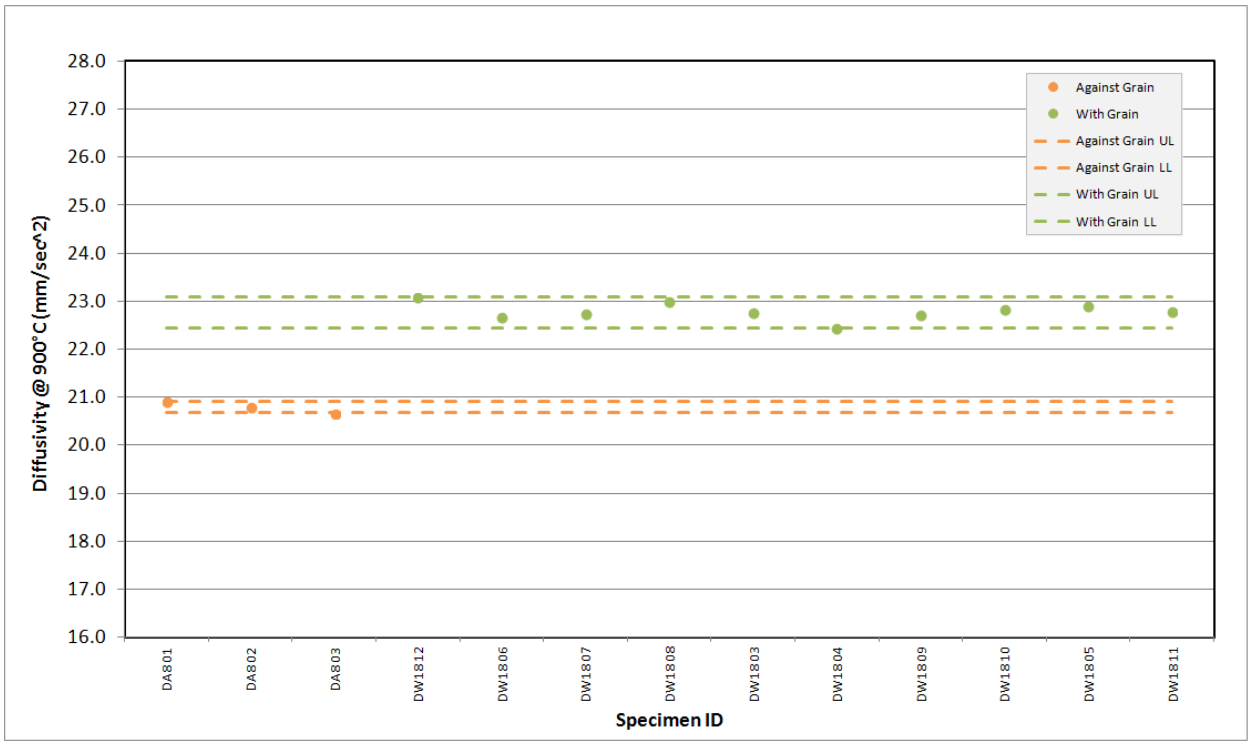

Figure A-254. PCEA Piggyback Diffusivity @ 900°C.

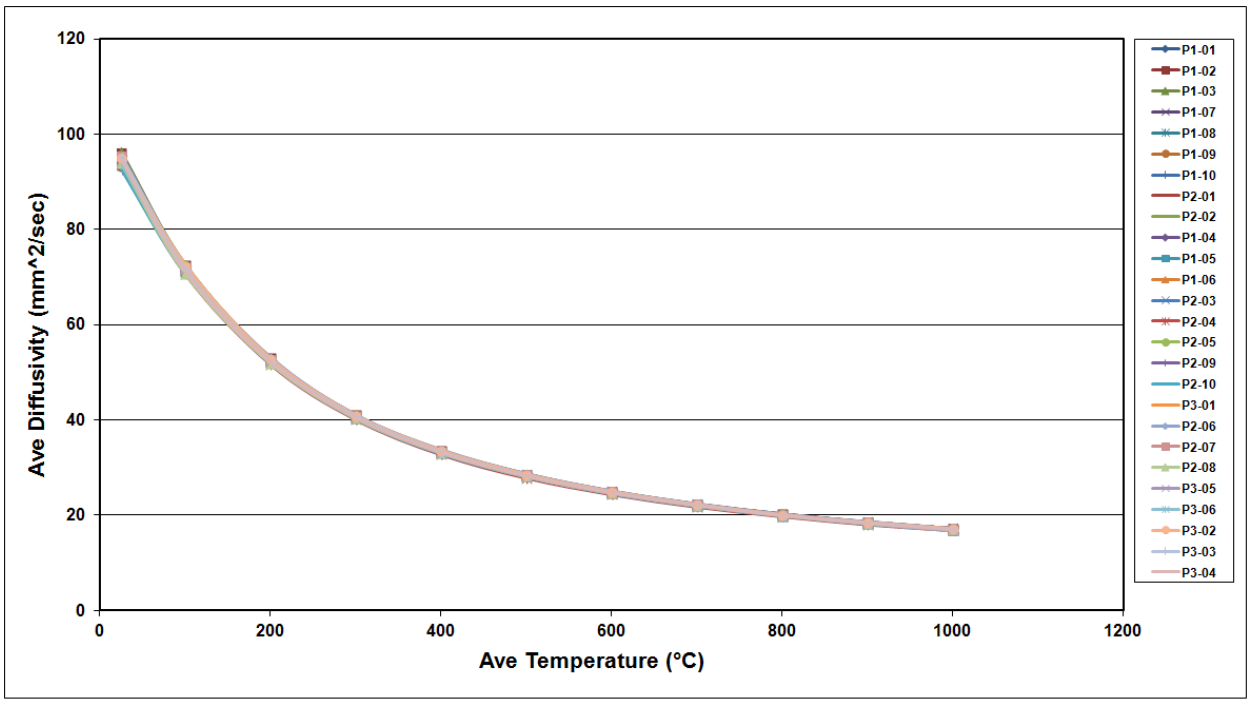

Figure A-255. PCIB Piggyback Diffusivity.

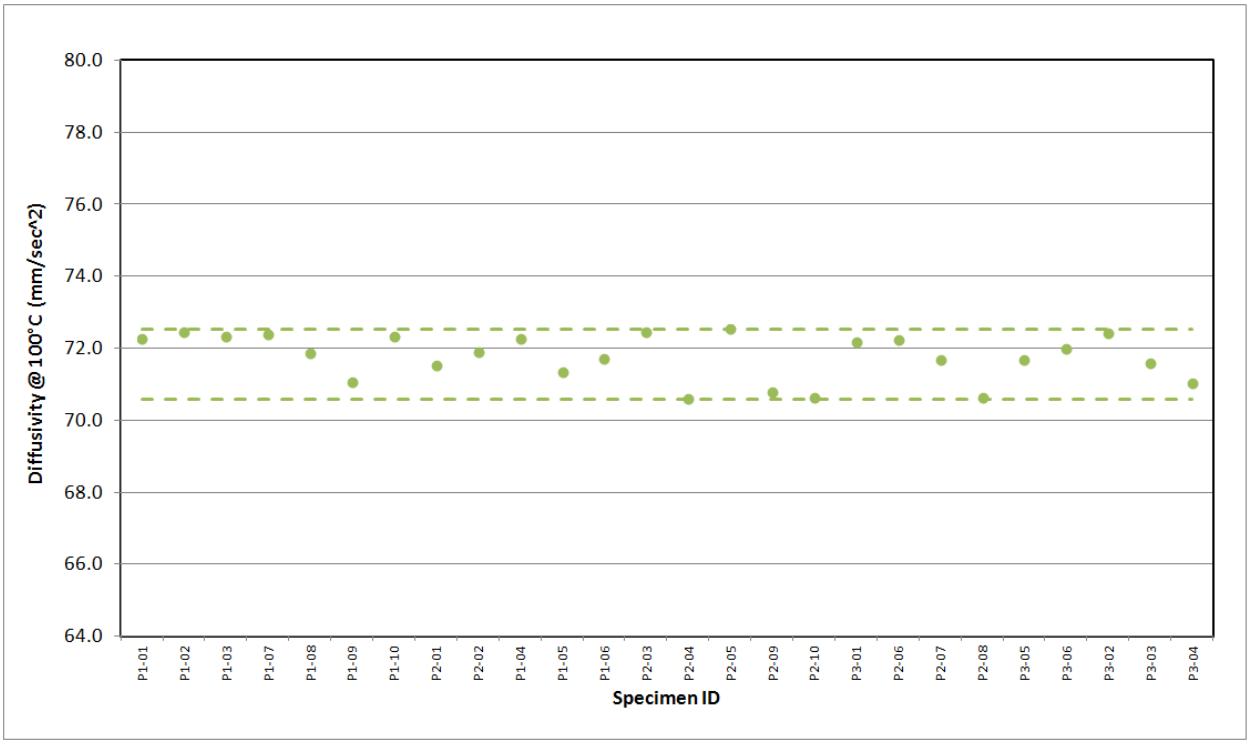

Figure A-256. PCIB Piggyback Diffusivity @ 100°C.

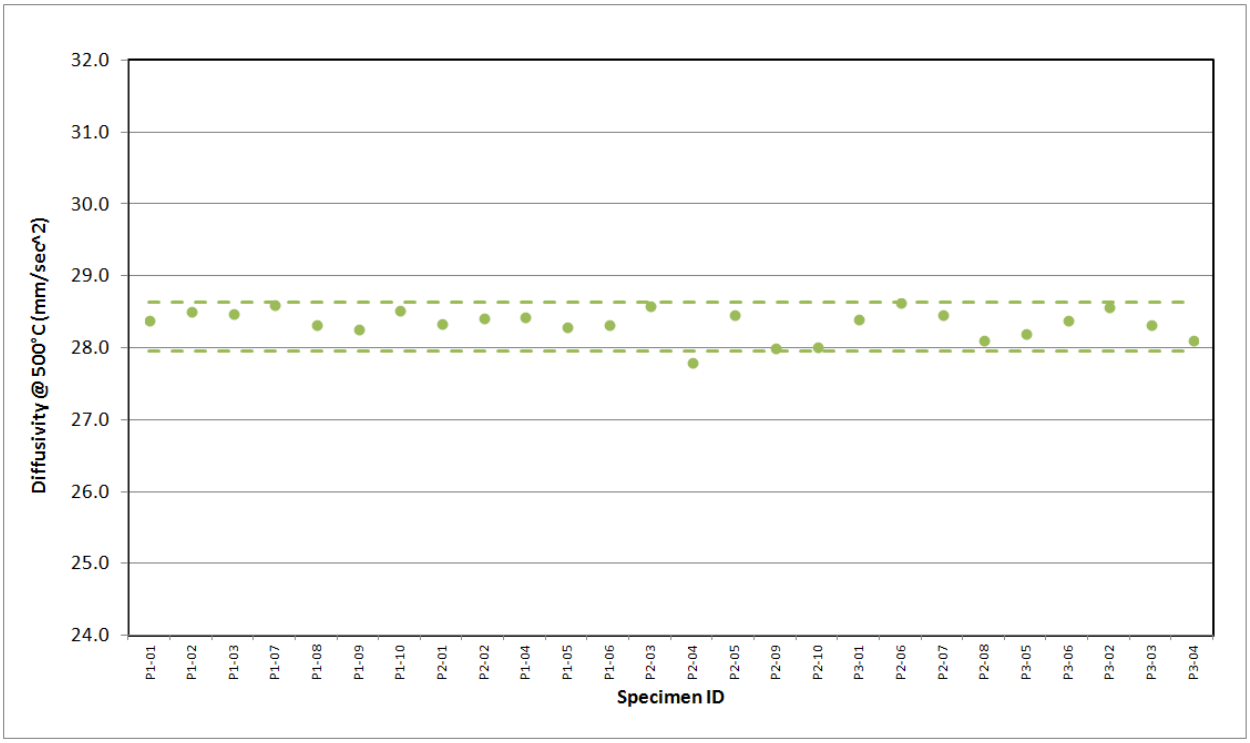

Figure A-257. PCIB Piggyback Diffusivity @ 500°C.

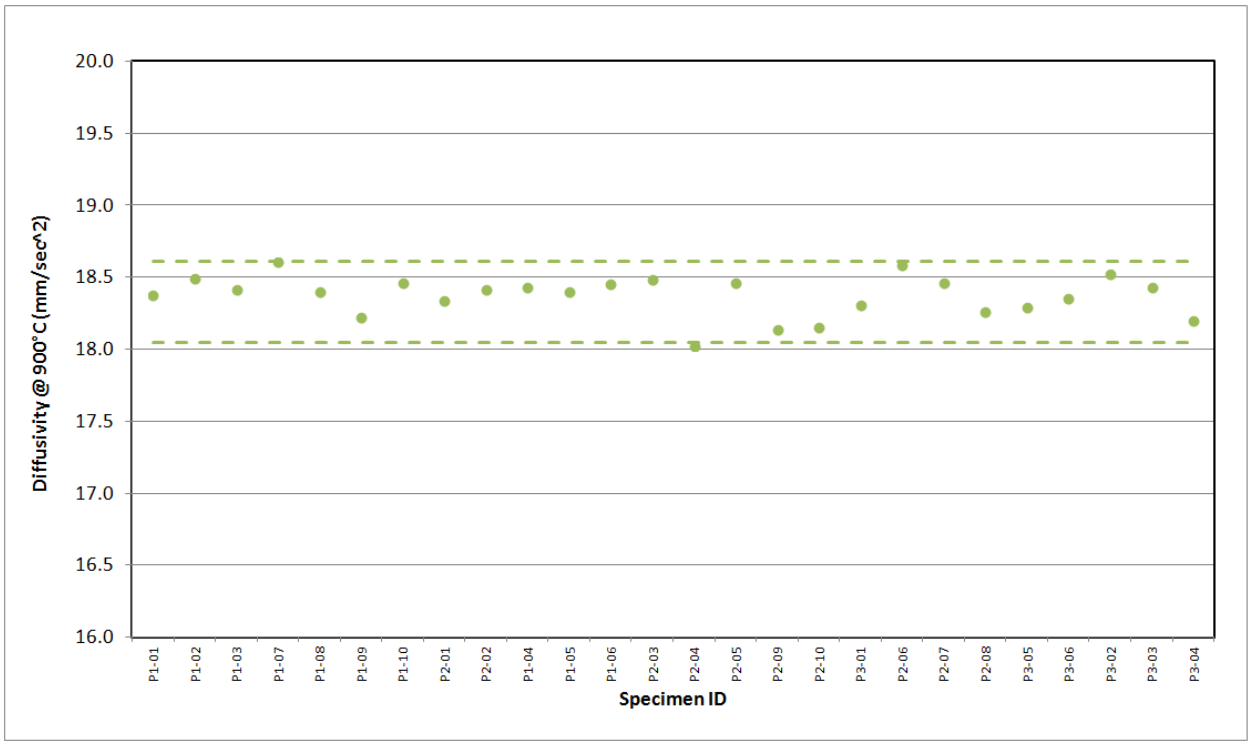

Figure A-258. PCIB Piggyback Diffusivity @ 900°C.

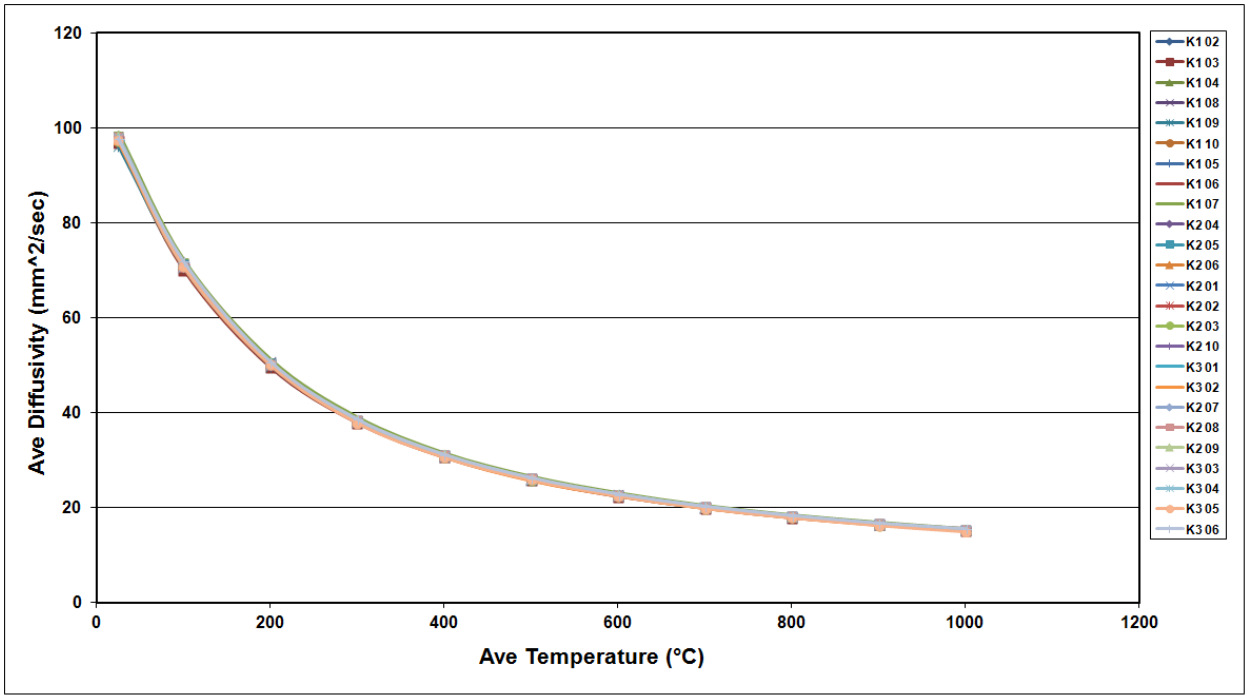

Figure A-259. PGX Piggyback Diffusivity.

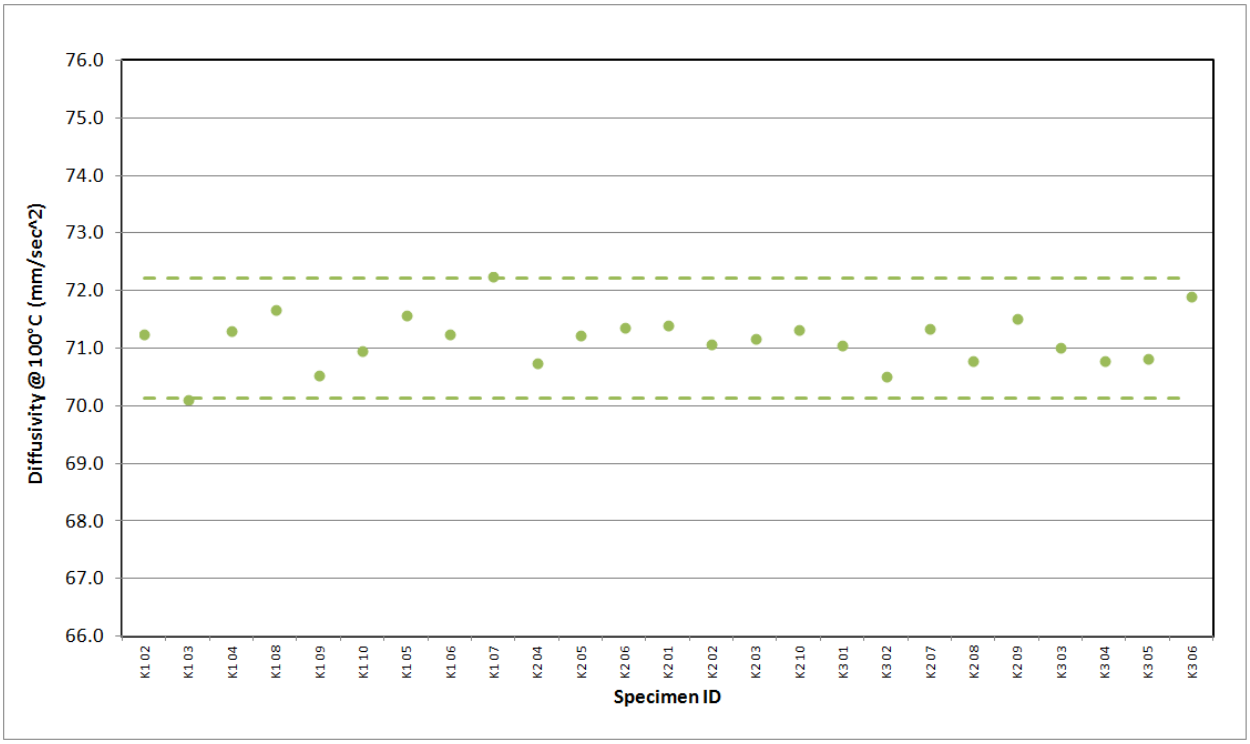

Figure A-260. PGX Piggyback Diffusivity @ 100°C.

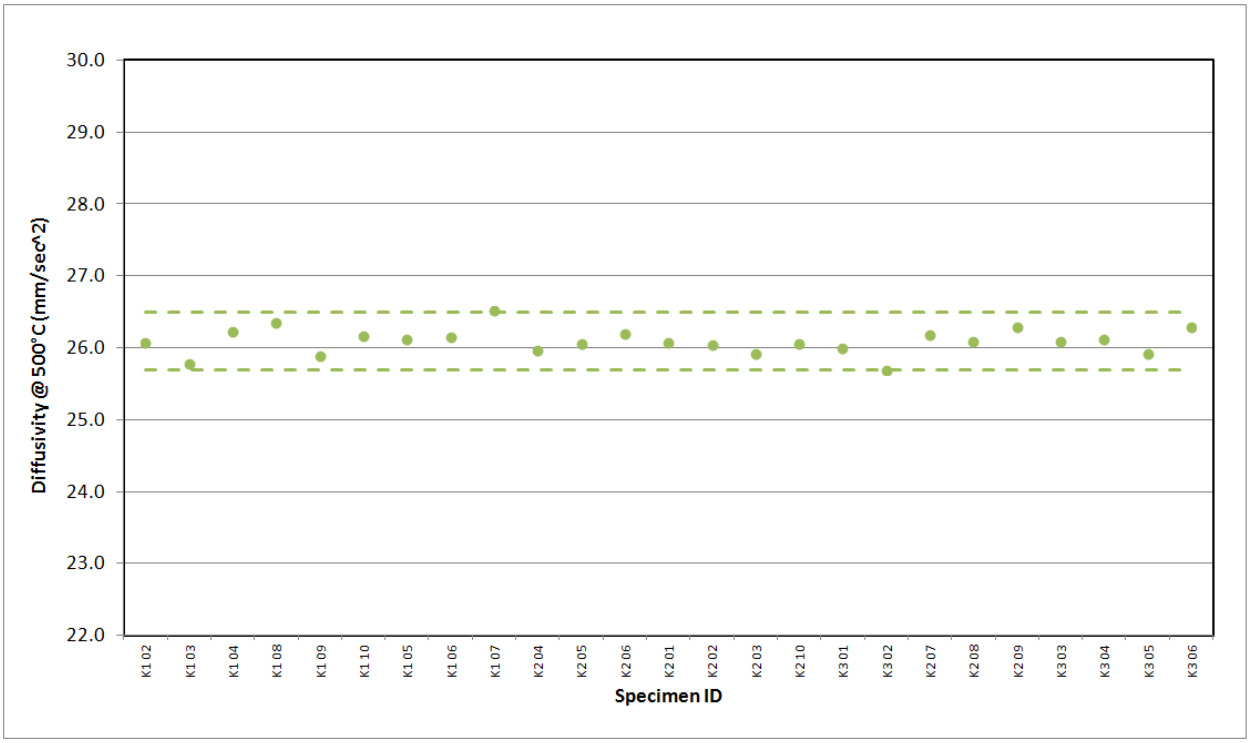

Figure A-261. PGX Piggyback Diffusivity @ 500°C.

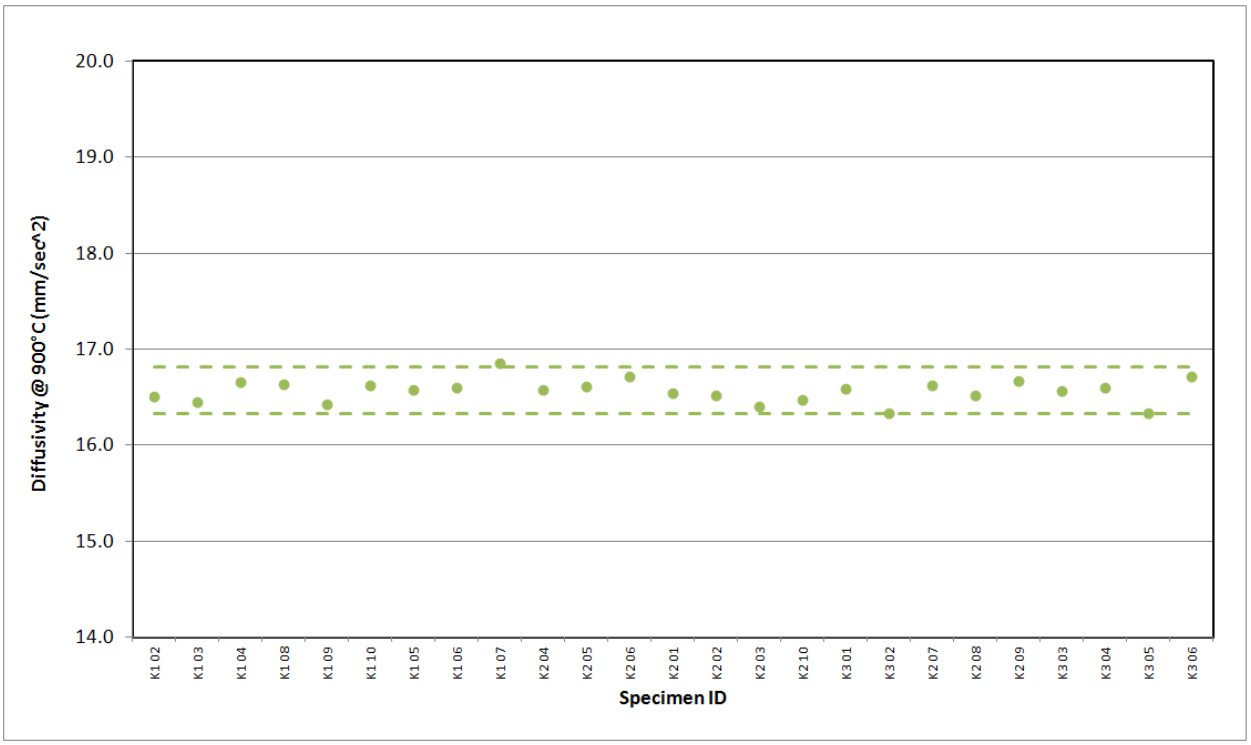

Figure A-262. PGX Piggyback Diffusivity @ 900°C.

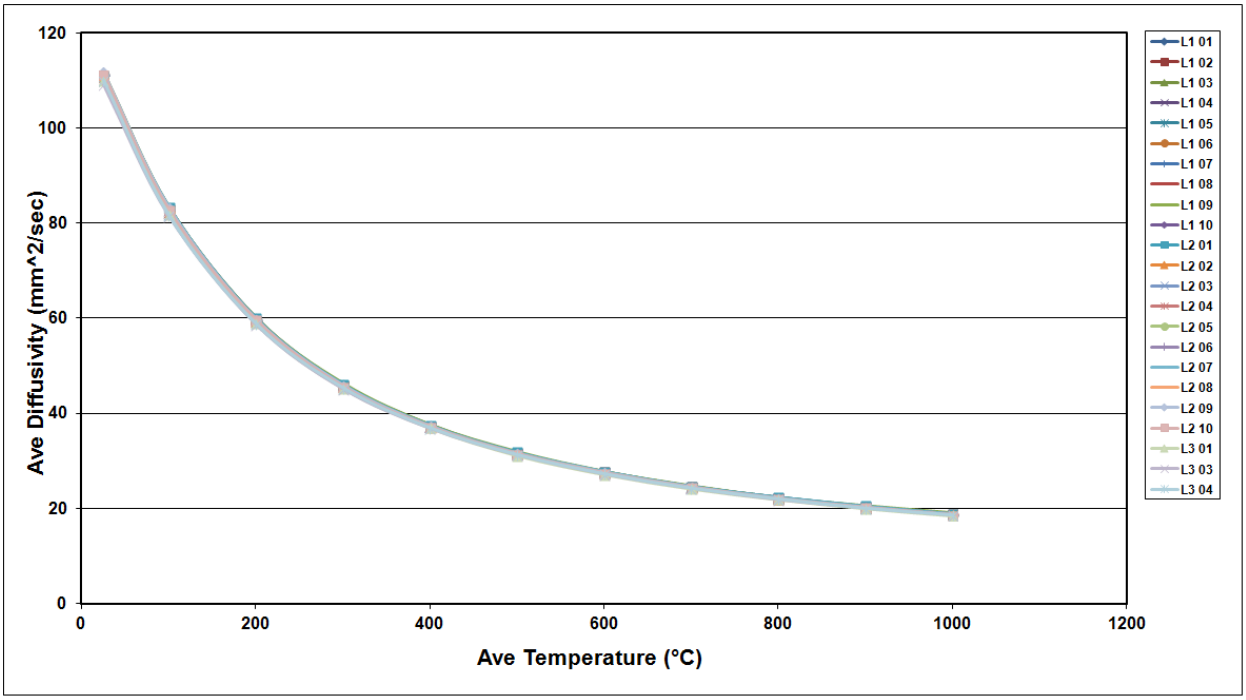

Figure A-263. PPEA Piggyback Diffusivity.

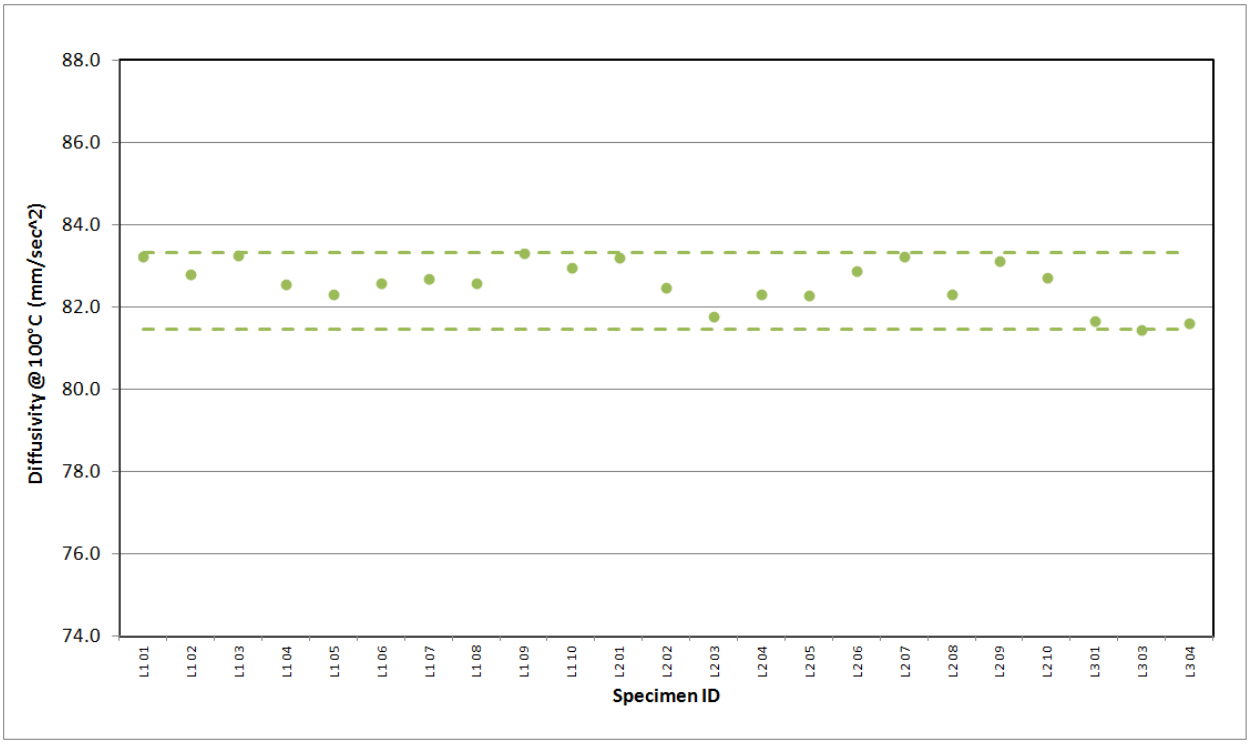

Figure A-264. PPEA Piggyback Diffusivity @ 100°C.

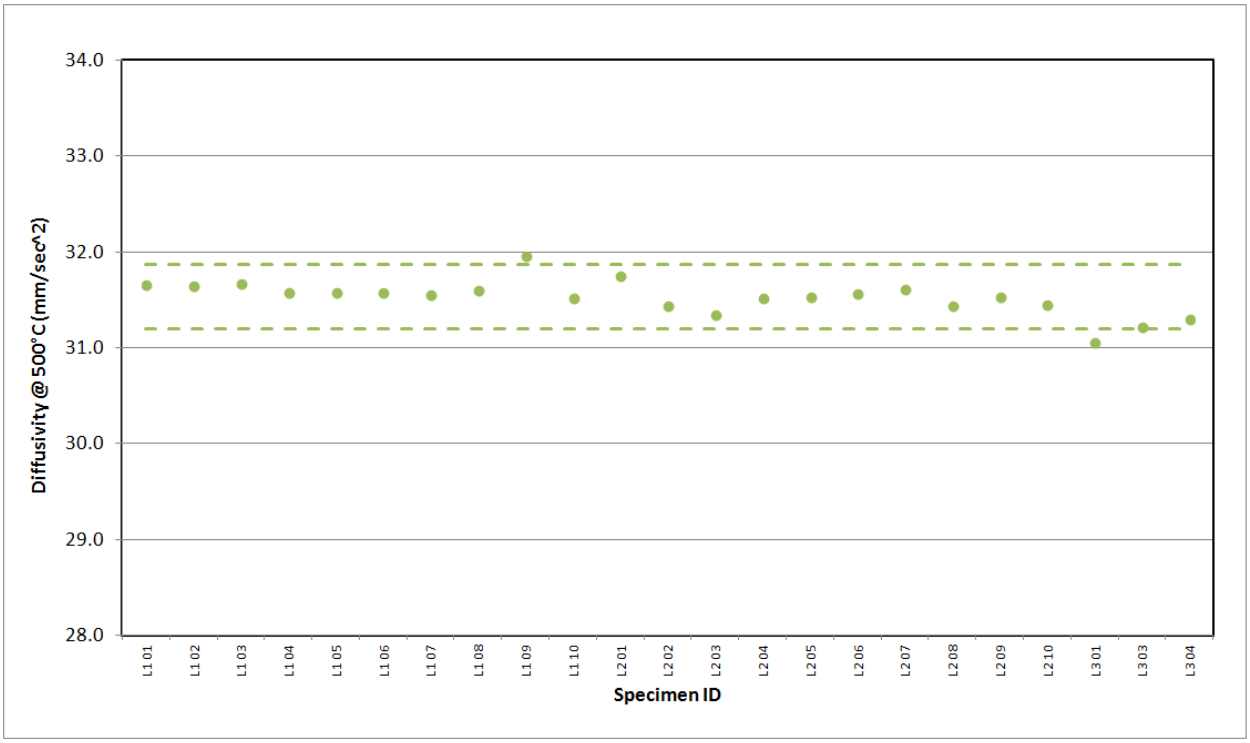

Figure A-265. PPEA Piggyback Diffusivity @ 500°C.

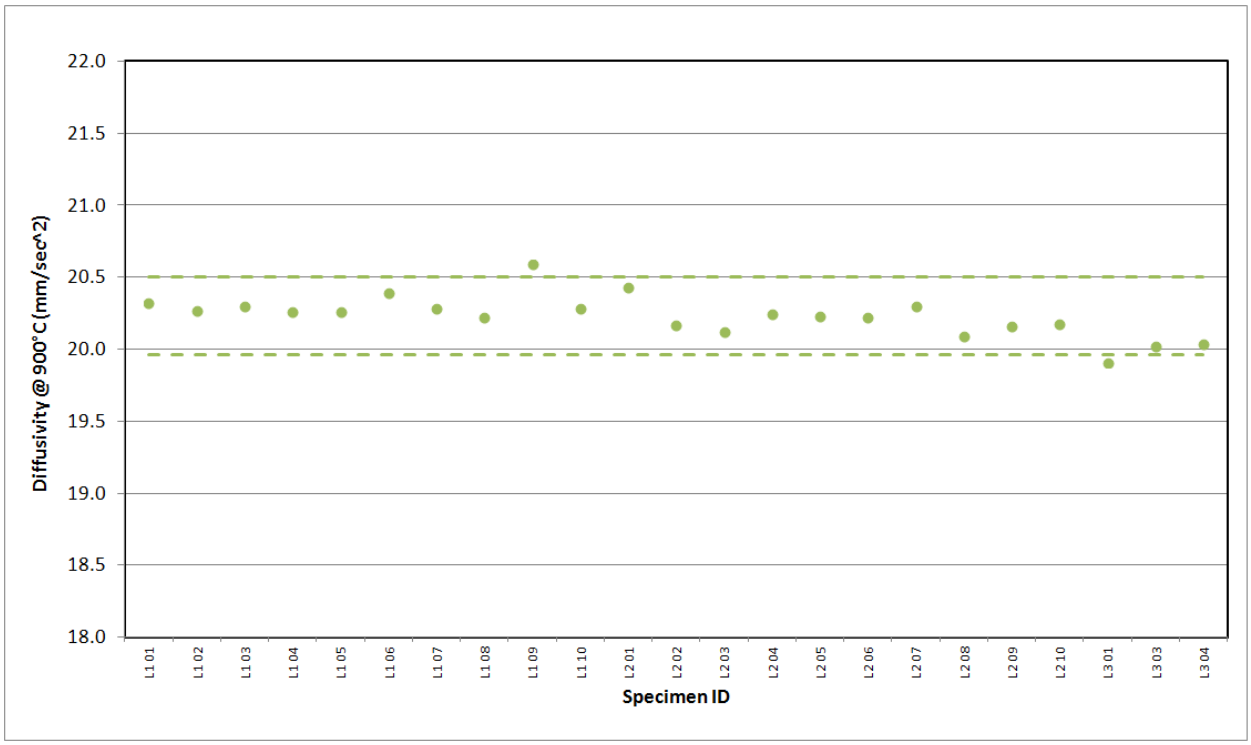

Figure A-266. PPEA Piggyback Diffusivity @ 900°C.

Appendix B

Statistical Tables

Table B-1. Creep Pre Thermal Measurement Length (mm) Summary Statistics.

Combined Specimens	Mean	Std Dev	CoV (%)	Median	Upper Limit	Lower Limit
H451	25.387	0.0083	0.03	25.389	25.397	25.377
IG-110	25.379	0.0087	0.03	25.381	25.399	25.363
IG-430	25.382	0.0037	0.01	25.382	25.386	25.378
NBG-17	25.377	0.0052	0.02	25.378	25.390	25.364
NBG-18	25.365	0.0053	0.02	25.365	25.377	25.355
PCEA	25.379	0.0124	0.05	25.373	25.405	25.343
Against Grain Specimens	**Mean**	**Std Dev**	**CoV (%)**	**Median**	**Upper Limit**	**Lower Limit**
H451	25.391	0.0032	0.01	25.391	25.396	25.386
IG-110	25.383	0.0064	0.03	25.385	25.388	25.375
IG-430	25.384	0.0010	0.00	25.384	25.386	25.383
NBG-17	25.377	0.0045	0.02	25.377	25.387	25.365
NBG-18	25.367	0.0020	0.01	25.368	25.371	25.362
PCEA	25.392	0.0070	0.03	25.396	25.403	25.374
With Grain Specimens	**Mean**	**Std Dev**	**CoV (%)**	**Median**	**Upper Limit**	**Lower Limit**
H451	25.382	0.0095	0.04	25.386	25.397	25.357
IG-110	25.376	0.0089	0.04	25.378	25.389	25.367
IG-430	25.381	0.0039	0.02	25.382	25.384	25.378
NBG-17	25.377	0.0057	0.02	25.378	25.390	25.365
NBG-18	25.364	0.0066	0.03	25.363	25.374	25.355
PCEA	25.375	0.0105	0.04	25.371	25.381	25.362

Table B-2. Creep Pre Thermal Measurement Diameter (mm) Summary Statistics.

Combined Specimens	Mean	Std Dev	CoV (%)	Median	Upper Limit	Lower Limit
H451	12.740	0.0041	0.03	12.740	12.748	12.731
IG-110	12.734	0.0028	0.02	12.735	12.740	12.728
IG-430	12.731	0.0042	0.03	12.732	12.739	12.723
NBG-17	12.731	0.0043	0.03	12.730	12.740	12.721
NBG-18	12.730	0.0047	0.04	12.730	12.743	12.719
PCEA	12.737	0.0078	0.06	12.737	12.759	12.719
Against Grain Specimens	**Mean**	**Std Dev**	**CoV (%)**	**Median**	**Upper Limit**	**Lower Limit**
H451	12.739	0.0044	0.03	12.738	12.748	12.733
IG-110	12.735	0.0030	0.02	12.735	12.740	12.730
IG-430	12.732	0.0022	0.02	12.732	12.735	12.729
NBG-17	12.729	0.0037	0.03	12.729	12.736	12.721
NBG-18	12.729	0.0028	0.02	12.729	12.736	12.725
PCEA	12.746	0.0031	0.02	12.746	12.751	12.739
With Grain Specimens	**Mean**	**Std Dev**	**CoV (%)**	**Median**	**Upper Limit**	**Lower Limit**
H451	12.740	0.0037	0.03	12.741	12.747	12.731
IG-110	12.734	0.0027	0.02	12.734	12.739	12.728
IG-430	12.731	0.0045	0.04	12.732	12.739	12.722
NBG-17	12.732	0.0043	0.03	12.732	12.741	12.723
NBG-18	12.731	0.0058	0.05	12.731	12.741	12.719
PCEA	12.734	0.0065	0.05	12.734	12.750	12.719

Table B-3. Creep Pre Thermal Measurement Mass (g) Summary Statistics.

Combined Specimens	Mean	Std Dev	CoV (%)	Median	Upper Limit	Lower Limit
H451	5.485	0.0360	0.66	5.473	5.561	5.424
IG-110	5.654	0.0225	0.40	5.661	5.701	5.597
IG-430	5.764	0.0205	0.36	5.767	5.809	5.711
NBG-17	5.867	0.0694	1.18	5.909	5.935	5.740
NBG-18	5.948	0.0075	0.13	5.948	5.965	5.929
PCEA	5.657	0.0234	0.41	5.653	5.691	5.617
Against Grain Specimens	**Mean**	**Std Dev**	**CoV (%)**	**Median**	**Upper Limit**	**Lower Limit**
H451	5.465	0.0117	0.21	5.466	5.491	5.444
IG-110	5.656	0.0234	0.41	5.662	5.701	5.602
IG-430	5.770	0.0101	0.17	5.773	5.785	5.750
NBG-17	5.879	0.0575	0.98	5.911	5.935	5.788
NBG-18	5.949	0.0056	0.09	5.948	5.961	5.939
PCEA	5.683	0.0282	0.50	5.671	5.727	5.652
With Grain Specimens	**Mean**	**Std Dev**	**CoV (%)**	**Median**	**Upper Limit**	**Lower Limit**
H451	5.505	0.0408	0.74	5.505	5.561	5.424
IG-110	5.652	0.0220	0.39	5.659	5.686	5.604
IG-430	5.762	0.0222	0.39	5.765	5.809	5.709
NBG-17	5.857	0.0077	1.32	5.904	5.934	5.740
NBG-18	5.948	0.0088	0.15	5.949	5.965	5.929
PCEA	5.649	0.0147	0.26	5.649	5.678	5.621

Table B-4 Creep Pre Thermal Measurement Density (g/cm^3, Summary Statistics.

Combined Specimens	Mean	Std Dev	CoV (%)	Median	Upper Limit	Lower Limit
H451	1.7217	0.0110	0.64	1.7180	1.7457	1.7041
IG-110	1.7779	0.0069	0.39	1.7802	1.7918	1.7591
IG-430	1.8132	0.0062	0.34	1.8141	1.8264	1.7974
NBG-17	1.8468	0.0216	1.17	1.8601	1.8675	1.8053
NBG-18	1.8720	0.0020	0.11	1.8720	1.8761	1.8673
PCEA	1.7769	0.0060	0.34	1.7758	1.7869	1.7665
Against Grain Specimens	**Mean**	**Std Dev**	**CoV (%)**	**Median**	**Upper Limit**	**Lower Limit**
H451	1.7153	0.0038	0.22	1.7156	1.7248	1.7082
IG-110	1.7784	0.0072	0.41	1.7804	1.7918	1.7633
IG-430	1.8148	0.0031	0.17	1.8157	1.8197	1.8087
NBG-17	1.8509	0.0181	0.98	1.8610	1.8675	1.8220
NBG-18	1.8719	0.0016	0.09	1.8718	1.8759	1.8686
PCEA	1.7812	0.0091	0.51	1.7773	1.7954	1.7720
With Grain Specimens	**Mean**	**Std Dev**	**CoV (%)**	**Median**	**Upper Limit**	**Lower Limit**
H451	1.7283	0.0121	0.70	1.7292	1.7457	1.7041
IG-110	1.7775	0.0068	0.38	1.7801	1.7875	1.7629
IG-430	1.8127	0.0067	0.37	1.8133	1.8264	1.7974
NBG-17	1.8433	0.0237	1.28	1.8579	1.8661	1.8053
NBG-18	1.8722	0.0024	0.13	1.8725	1.8761	1.8656
PCEA	1.7756	0.0040	0.22	1.7755	1.7848	1.7669

Table B-5. Creep Coefficient of Thermal Expansion (1/K) at 100°C Summary Statistics.

Combined Specimens	Mean	Std Dev	CoV (%)	Median	Upper Limit	Lower Limit
H451	3.18E-06	2.40E-07	7.54	3.12E-06	3.44E-06	2.90E-06
IG-110	3.87E-06	9.32E-08	2.41	3.84E-06	4.09E-06	3.70E-06
IG-430	4.16E-06	2.60E-07	6.26	4.24E-06	4.48E-06	3.74E-06
NBG-17	4.50E-06	l.36E-07	3.02	4.45E-06	4.86E-06	4.32E-06
NBG-18	4.85E-06	l.33E-07	2.75	4.85E-06	5.12E-06	4.55E-06
PCEA	3.92E-06	l.53E-07	3.89	3.89E-06	4.34E-06	3.69E-06
Against Grain Specimens	**Mean**	**Std Dev**	**CoV (%)**	**Median**	**Upper Limit**	**Lower Limit**
H451	3.71E-06	l.26E-07	3.41	3.71E-06	3.86E-06	3.57E-06
IG-110	3.82E-06	6.0lE-08	1.57	3.81E-06	3.90E-06	3.76E-06
IG-430	3.63E-06	l.45E-07	4.00	3.63E-06	3.89E-06	3.49E-06
NBG-17	4.45E-06	9.95E-08	2.23	4.42E-06	4.71E-06	4.32E-06
NBG-18	4.88E-06	l.14E-07	2.35	4.88E-06	5.12E-06	4.70E-06
PCEA	4.05E-06	2.09E-07	5.17	4.09E-06	4.35E-06	3.69E-06
With Grain Specimens	**Mean**	**Std Dev**	**CoV (%)**	**Median**	**Upper Limit**	**Lower Limit**
H451	3.09E-06	9.90E-08	3.20	3.12E-06	3.22E-06	2.90E-06
IG-110	3.88E-06	9.49E-08	2.45	3.86E-06	4.09E-06	3.70E-06
IG-430	4.25E-06	l.23E-07	2.90	4.28E-06	4.48E-06	3.97E-06
NBG-17	4.70E-06	1.01E-07	2.15	4.67E-06	4.86E-06	4.56E-06
NBG-18	4.76E-06	l.49E-07	3.12	4.74E-06	5.02E-06	4.55E-06
PCEA	3.87E-06	9.52E-08	2.46	3.87E-06	4.1 lE-06	3.74E-06

Table B-6. Creep Coefficient of Thermal Expansion (1/K) at 500°C Summary Statistics.

Combined Specimens	Mean	Std Dev	CoV (%)	Median	Upper Limit	Lower Limit
H451	3.72E-06	2.30E-07	6.17	3.66E-06	3.86E-06	3.46E-06
IG-110	4.45E-06	8.61E-08	1.94	4.44E-06	4.64E-06	4.28E-06
IG-430	4.73E-06	2.25E-07	4.76	4.80E-06	5.0lE-06	4.39E-06
NBG-17	5.06E-06	l.66E-07	3.27	5.09E-06	5.46E-06	4.78E-06
NBG-18	5.43E-06	8.72E-08	1.61	5.45E-06	5.58E-06	5.25E-06
PCEA	4.54E-06	l.39E-07	3.06	4.51E-06	4.77E-06	4.37E-06
Against Grain Specimens	**Mean**	**Std Dev**	**CoV (%)**	**Median**	**Upper Limit**	**Lower Limit**
H451	4.25E-06	7.61E-08	1.79	4.23E-06	4.36E-06	4.19E-06
IG-110	4.38E-06	7.61E-08	1.74	4.38E-06	4.47E-06	4.29E-06
IG-430	4.27E-06	l.17E-07	2.74	4.25E-06	4.42E-06	4.1 lE-06
NBG-17	5.02E-06	l.41E-07	2.81	5.05E-06	5.21E-06	4.78E-06
NBG-18	5.45E-06	7.97E-08	1.46	5.48E-06	5.58E-06	5.25E-06
PCEA	4.69E-06	l.68E-07	3.57	4.77E-06	4.88E-06	4.42E-06
With Grain Specimens	**Mean**	**Std Dev**	**CoV (%)**	**Median**	**Upper Limit**	**Lower Limit**
H451	3.63E-06	7.18E-08	1.98	3.65E-06	3.77E-06	3.46E-06
IG-110	4.45E-06	8.46E-08	1.90	4.44E-06	4.64E-06	4.28E-06
IG-430	4.82E-06	9.88E-08	2.05	4.81E-06	5.0lE-06	4.62E-06
NBG-17	5.25E-06	l.51E-07	2.88	5.21E-06	5.46E-06	5.08E-06
NBG-18	5.36E-06	7.79E-08	1.45	5.36E-06	5.49E-06	5.26E-06
PCEA	4.49E-06	7.97E-08	1.77	4.50E-06	4.67E-06	4.37E-06

Table B-7. Creep Coefficient of Thermal Expansion (1/K) at 900°C Summary Statistics.

Combined Specimens	Mean	Std Dev	CoV (%)	Median	Upper Limit	Lower Limit
H451	4.20E-06	2.27E-07	5.40	4.12E-06	4.37E-06	4.02E-06
IG-110	4.88E-06	8.59E-08	1.76	4.87E-06	5.04E-06	4.69E-06
IG-430	5.17E-06	2.28E-07	4.42	5.24E-06	5.50E-06	4.86E-06
NBG-17	5.53E-06	1.55E-07	2.80	5.58E-06	5.89E-06	5.26E-06
NBG-18	5.89E-06	7.29E-08	1.24	5.91E-06	6.03E-06	5.72E-06
PCEA	5.03E-06	1.31E-07	2.60	5.00E-06	5.23E-06	4.87E-06
Against Grain Specimens	**Mean**	**Std Dev**	**CoV (%)**	**Median**	**Upper Limit**	**Lower Limit**
H451	4.74E-06	6.13E-08	1.29	4.72E-06	4.82E-06	4.68E-06
IG-110	4.81E-06	5.88E-08	1.22	4.81E-06	4.87E-06	4.74E-06
IG-430	4.70E-06	1.03E-07	2.18	4.69E-06	4.86E-06	4.56E-06
NBG-17	5.49E-06	1.32E-07	2.41	5.54E-06	5.67E-06	5.26E-06
NBG-18	5.91E-06	6.16E-08	1.04	5.93E-06	6.03E-06	5.75E-06
PCEA	5.17E-06	1.68E-07	3.26	5.23E-06	5.40E-06	4.91E-06
With Grain Specimens	**Mean**	**Std Dev**	**CoV (%)**	**Median**	**Upper Limit**	**Lower Limit**
H451	4.11E-06	5.95E-08	1.45	4.11E-06	4.26E-06	4.02E-06
IG-110	4.88E-06	8.54E-08	1.75	4.88E-06	5.04E-06	4.69E-06
IG-430	5.26E-06	1.02E-07	1.93	5.26E-06	5.47E-06	5.06E-06
NBG-17	5.71E-06	1.32E-07	2.32	5.65E-06	5.89E-06	5.57E-06
NBG-18	5.82E-06	6.06E-08	1.04	5.83E-06	5.89E-06	5.72E-06
PCEA	4.99E-06	7.08E-08	1.42	4.98E-06	5.16E-06	4.87E-06

Table B-8. Creep Modulus (GPa) by Sonic Resonance Summary Statistics.

Combined Specimens	Mean	Std Dev	CoV (%)	Median	Upper Limit	Lower Limit
H451	9.66	0.76	7.83	9.83	10.46	8.74
IG-110	9.71	0.33	3.38	9.75	10.29	9.00
IG-430	9.59	0.52	5.43	9.50	10.31	8.98
NBG-17	11.26	0.46	4.11	11.52	11.82	10.46
NBG-18	12.09	0.25	2.10	12.13	12.63	11.53
PCEA	9.65	1.08	11.23	9.93	10.62	9.19
Against Grain Specimens	**Mean**	**Std Dev**	**CoV (%)**	**Median**	**Upper Limit**	**Lower Limit**
H451	8.01	0.13	1.64	8.03	8.15	7.83
IG-110	9.99	0.29	2.92	10.10	10.29	9.55
IG-430	10.64	0.22	2.07	10.69	10.89	10.38
NBG-17	11.28	0.51	4.51	11.56	11.82	10.46
NBG-18	11.99	0.19	1.59	12.02	12.35	11.53
PCEA	8.73	2.04	23.35	8.76	10.63	5.00
With Grain Specimens	**Mean**	**Std Dev**	**CoV (%)**	**Median**	**Upper Limit**	**Lower Limit**
H451	9.94	0.30	3.07	9.87	10.46	9.49
IG-110	9.65	0.30	3.16	9.74	10.09	8.93
IG-430	9.39	0.23	2.43	9.39	9.80	8.98
NBG-17	11.16	0.03	0.29	11.16	11.20	11.12
NBG-18	12.42	0.10	0.84	12.43	12.63	12.25
PCEA	9.92	0.24	2.38	9.94	10.41	9.43

Table B-9. Creep Resistivity (Lt0-m) Summary Statistics.

Combined Specimens	Mean	Std Dev	CoV (%)	Median	Upper Limit	Lower Limit
H451	7.75	0.38	4.86	7.65	8.27	7.39
IG-110	11.21	0.40	3.60	11.08	12.33	10.61
IG-430	9.60	0.50	5.19	9.66	10.25	8.74
NBG-17	9.59	0.23	2.43	9.51	9.90	9.18
NBG-18	9.48	0.18	1.90	9.56	9.69	9.21
PCEA	7.62	0.34	4.45	7.51	7.79	7.34
Against Grain Specimens	**Mean**	**Std Dev**	**CoV (%)**	**Median**	**Upper Limit**	**Lower Limit**
H451	8.57	0.11	1.30	8.56	8.71	8.47
IG-110	10.98	0.32	2.88	11.09	11.43	10.61
IG-430	8.63	0.17	1.92	8.58	8.87	8.43
NBG-17	9.51	0.21	2.22	9.46	9.90	9.18
NBG-18	9.58	0.06	0.60	9.58	9.69	9.45
PCEA	8.02	0.51	6.39	8.29	8.59	7.38
With Grain Specimens	**Mean**	**Std Dev**	**CoV (%)**	**Median**	**Upper Limit**	**Lower Limit**
H451	7.61	0.15	1.94	7.62	7.90	7.39
IG-110	11.25	0.41	3.63	11.07	12.35	10.71
IG-430	9.79	0.25	2.56	9.78	10.25	9.29
NBG-17	9.85	0.03	0.28	9.84	9.90	9.81
NBG-18	9.17	0.05	0.53	9.15	9.25	9.10
PCEA	7.50	0.07	1.00	7.51	7.64	7.34

Table B-10. Creep Young's Modulus (GPa) by Sonic Velocity.

Combined Specimens	Mean	Std Dev	CoV (%)	Median	Upper Limit	Lower Limit
H451	11.80	0.72	6.10	11.94	12.74	10.50
IG-110	10.87	0.38	3.46	10.91	11.83	10.13
IG-430	10.72	0.64	5.97	10.56	11.46	9.96
NBG-17	14.29	0.61	4.28	14.42	15.06	13.00
NBG-18	15.61	0.37	2.34	15.59	16.46	14.70
PCEA	12.30	0.58	4.70	12.47	12.96	11.68
Against Grain Specimens	**Mean**	**Std Dev**	**CoV (%)**	**Median**	**Upper Limit**	**Lower Limit**
H451	10.29	0.10	0.94	10.32	10.38	10.16
IG-110	11.20	0.45	3.97	11.19	11.95	10.58
IG-430	12.01	0.23	1.94	12.04	12.37	11.70
NBG-17	14.31	0.70	4.86	14.64	15.06	13.00
NBG-18	15.46	0.26	1.70	15.48	16.09	14.88
PCEA	11.76	0.97	8.24	11.19	12.96	10.65
With Grain Specimens	**Mean**	**Std Dev**	**CoV (%)**	**Median**	**Upper Limit**	**Lower Limit**
H451	12.06	0.36	2.94	12.04	12.74	11.52
IG-110	10.81	0.33	3.08	10.83	11.29	10.13
IG-430	10.46	0.27	2.54	10.48	10.95	9.96
NBG-17	14.23	0.10	0.72	14.23	14.42	14.05
NBG-18	16.11	0.17	1.08	16.10	16.46	15.86
PCEA	12.47	0.17	1.40	12.50	12.85	12.10

Table B-11. Creep Shear Modulus (GPa) by Sonic Velocity.

Combined Specimens	Mean	Std Dev	CoV (%)	Median	Upper Limit	Lower Limit
H451	4.41	0.15	3.36	4.43	4.62	4.10
IG-110	4.35	0.14	3.32	4.37	4.53	4.06
IG-430	4.36	0.12	2.72	4.34	4.62	4.20
NBG-17	4.83	0.17	3.43	4.88	5.11	4.51
NBG-18	5.25	0.05	1.03	5.24	5.35	5.15
PCEA	4.53	0.13	2.95	4.57	4.78	4.26
Against Grain Specimens	**Mean**	**Std Dev**	**CoV (%)**	**Median**	**Upper Limit**	**Lower Limit**
H451	4.13	0.09	2.14	4.15	4.22	4.01
IG-110	4.39	0.14	3.19	4.38	4.52	4.12
IG-430	4.54	0.14	2.99	4.52	4.78	4.36
NBG-17	4.81	0.19	3.87	4.89	5.11	4.51
NBG-18	5.23	0.03	0.67	5.23	5.32	5.15
PCEA	4.47	0.20	4.43	4.38	4.78	4.26
With Grain Specimens	**Mean**	**Std Dev**	**CoV (%)**	**Median**	**Upper Limit**	**Lower Limit**
H451	4.46	0.09	2.01	4.47	4.62	4.29
IG-110	4.34	0.15	3.35	4.37	4.53	4.06
IG-430	4.33	0.08	1.76	4.32	4.50	4.20
NBG-17	4.87	0.02	0.40	4.88	4.90	4.83
NBG-18	5.32	0.05	0.92	5.33	5.38	5.24
PCEA	4.55	0.10	2.24	4.57	4.68	4.31

Table B-12a. Piggyback Pre Thermal Measurement Length (mm) Summary Statistics.

Combined Specimens	Mean	Std Dev	CoV (%)	Median	Upper Limit	Lower Limit
2114	6.330	0.007	0.11	6.330	6.341	6.314
A3 Matrix	6.325	0.009	0.14	6.323	6.331	6.317
BAN	6.329	0.007	0.11	6.330	6.338	6.323
H451	6.330	0.006	0.10	6.329	6.336	6.321
HLM	6.329	0.003	0.05	6.330	6.335	6.322
IG-110	6.347	0.004	0.06	6.346	6.353	6.340
IG-430	6.331	0.005	0.08	6.330	6.333	6.328
NBG-10	6.326	0.003	0.04	6.326	6.330	6.322
NBG-17	6.325	0.010	0.16	6.325	6.350	6.308
NBG-18	6.321	0.008	0.12	6.319	6.337	6.305
NBG-25	6.333	0.007	0.11	6.333	6.342	6.326
New Matrix	6.322	0.016	0.26	6.320	6.347	6.296
PCEA	6.340	0.012	0.20	6.339	6.349	6.330
PCIB	6.328	0.003	0.05	6.328	6.337	6.324
PGX	6.327	0.008	0.13	6.329	6.339	6.316
PPEA	6.328	0.004	0.06	6.328	6.334	6.321

Table B-12b. Piggyback Pre Thermal Measurement Length I mm) Summary Statistics.

Against Grain Specimens	Mean	Std Dev	CoV (%)	Median	Upper Limit	Lower Limit
2114	6.330	0.007	0.11	6.330	6.341	6.314
A3 Matrix						
BAN						
H451	6.330	0.005	0.08	6.329	6.332	6.327
HLM						
IG-110						
IG-430						
NBG-10						
NBG-17	6.329	0.010	0.16	6.330	6.345	6.315
NBG-18	6.324	0.005	0.07	6.325	6.330	6.315
NBG-25						
New Matrix						
PCEA	6.346	0.010	0.15	6.340	6.363	6.335
PCIB						
PGX						
PPEA						

Table B-12c. Piggyback Pre Thermal Measurement Length (mm) Summary Statistics.

With Grain Specimens	Mean	Std Dev	CoV (%)	Median	Upper Limit	Lower Limit
2114						
A3 Matrix						
BAN	6.329	0.007	0.11	6.330	6.338	6.323
H451	6.330	0.007	0.12	6.329	6.340	6.317
HLM						
IG-110	6.347	0.004	0.06	6.346	6.353	6.340
IG-430	6.331	0.005	0.08	6.330	6.333	6.328
NBG-10						
NBG-17	6.322	0.010	0.15	6.321	6.342	6.311
NBG-18	6.320	0.009	0.14	6.318	6.332	6.308
NBG-25						
New Matrix						
PCEA	6.335	0.013	0.20	6.337	6.340	6.336
PCIB						
PGX	6.327	0.008	0.13	6.329	6.339	6.316
PPEA						

Table B-13a. Piggyback Pre Thermal Measurement Diameter (mm) Summary Statistics.

Combined Specimens	Mean	Std Dev	CoV (%)	Median	Upper Limit	Lower Limit
2114	12.726	0.005	0.04	12.726	12.735	12.713
A3 Matrix	12.720	0.006	0.05	12.719	12.729	12.713
BAN	12.721	0.005	0.04	12.722	12.734	12.710
H451	12.733	0.002	0.02	12.733	12.737	12.730
HLM	12.726	0.007	0.05	12.727	12.737	12.717
IG-110	12.734	0.002	0.01	12.735	12.738	12.731
IG-430	12.729	0.005	0.04	12.728	12.733	12.726
NBG-10	12.720	0.005	0.04	12.719	12.727	12.711
NBG-17	12.731	0.002	0.02	12.730	12.735	12.726
NBG-18	12.724	0.004	0.04	12.723	12.727	12.720
NBG-25	12.730	0.002	0.02	12.730	12.735	12.726
New Matrix	12.719	0.009	0.07	12.717	12.735	12.709
PCEA	12.733	0.005	0.04	12.733	12.744	12.726
PCIB	12.728	0.004	0.03	12.727	12.738	12.721
PGX	12.729	0.004	0.04	12.728	12.738	12.724
PPEA	12.728	0.005	0.04	12.729	12.741	12.721

Table B-13b. Piggyback Pre Thermal Measurement Diameter (mm) Summary Statistics.

Against Grain Specimens	Mean	Std Dev	CoV (%)	Median	Upper Limit	Lower Limit
2114	12.726	0.005	0.04	12.726	12.735	12.713
A3 Matrix						
BAN						
H451	12.733	0.002	0.02	12.733	12.737	12.730
HLM						
IG-110						
IG-430						
NBG-10						
NBG-17	12.730	0.003	0.02	12.730	12.734	12.726
NBG-18	12.722	0.001	0.01	12.722	12.725	12.721
NBG-25						
New Matrix						
PCEA	12.733	0.005	0.04	12.734	12.742	12.726
PCIB						
PGX						
PPEA						

Table B-13c Piggyback Pre Thermal Measurement Diameter (mm) Summary Statistics.

With Grain Specimens	Mean	Std Dev	CoV (%)	Median	Upper Limit	Lower Limit
2114						
A3 Matrix						
BAN	12.721	0.005	0.04	12.722	12.734	12.710
H451	12.733	0.001	0.01	12.732	12.735	12.731
HLM						
IG-110	12.734	0.002	0.01	12.735	12.738	12.731
IG-430	12.729	0.005	0.04	12.728	12.733	12.726
NBG-10						
NBG-17	12.731	0.002	0.02	12.730	12.735	12.728
NBG-18	12.722	0.001	0.04	12.724	12.728	12.720
NBG-25						
New Matrix						
PCEA	12.733	0.005	0.04	12.732	12.744	12.727
PCIB						
PGX	12.729	0.004	0.04	12.728	12.738	12.724
PPEA						

Table B-14a. Piggyback Pre Thermal Measurement Mass (g) Summary Statistics.

Combined Specimens	Mean	Std Dev	CoV (%)	Median	Upper Limit	Lower Limit
2114	1.462	0.01	0.49	1.461	1.472	1.454
A3 Matrix	1.143	0.03	2.74	1.135	1.205	1.090
BAN	1.475	0.01	0.61	1.473	1.498	1.460
H451	1.395	0.01	0.96	1.392	1.413	1.375
HLM	1.411	0.00	0.19	1.412	1.416	1.406
IG-110	1.433	0.00	0.32	1.433	1.441	1.424
IG-430	1.460	0.00	0.29	1.459	1.467	1.454
NBG-10	1.438	0.00	0.29	1.438	1.444	1.428
NBG-17	1.500	0.01	0.39	1.501	1.505	1.494
NBG-18	1.502	0.00	0.18	1.501	1.508	1.497
NBG-25	1.486	0.00	0.15	1.485	1.489	1.482
New Matrix	1.386	0.04	2.86	1.399	1.445	1.337
PCEA	1.427	0.00	0.30	1.426	1.436	1.418
PCIB	1.474	0.00	0.24	1.474	1.479	1.465
PGX	1.423	0.00	0.24	1.424	1.430	1.414
PPEA	1.476	0.00	0.15	1.476	1.482	1.472

Table B-14b. Piggyback Pre Thermal Measurement Mass (g) Summary Statistics.

Against Grain Specimens	Mean	Std Dev	CoV (%)	Median	Upper Limit	Lower Limit
2114	1.462	0.01	0.49	1.461	1.472	1.454
A3 Matrix						
BAN						
H451	1.384	0.01	0.39	1.383	1.392	1.375
HLM						
IG-110						
IG-430						
NBG-10						
NBG-17	1.500	0.001	0.63	1.503	1.505	1.496
NBG-18	1.500	0.002	0.15	1.500	1.504	1.497
NBG-25						
New Matrix						
PCEA	1.428	0.00	0.32	1.427	1.436	1.421
PCIB						
PGX						
PPEA						

Table B-14c. Piggyback Pre Thermal Measurement Mass (g) Summary Statistics.

With Grain Specimens	Mean	Std Dev	CoV (%)	Median	Upper Limit	Lower Limit
2114						
A3 Matrix						
BAN	1.475	0.01	0.61	1.473	1.498	1.460
H451	1.408	0.00	0.18	1.408	1.413	1.405
HLM						
IG-110	1.433	0.00	0.32	1.433	1.441	1.424
IG-430	1.460	0.00	0.29	1.459	1.467	1.454
NBG-10						
NBG-17	1.500	0.003	0.20	1.500	1.504	1.493
NBG-18	1.502	0.003	0.17	1.502	1.508	1.498
NBG-25						
New Matrix						
PCEA	1.425	0.00	0.24	1.425	1.430	1.418
PCIB						
PGX	1.423	0.00	0.24	1.424	1.430	1.414
PPEA						

Table B-15a. Piggyback Pre Thermal Measurement Density (g/cm^3) Summary Statistics.

Combined Specimens	Mean	Std Dev	CoV (%)	Median	Upper Limit	Lower Limit
2114	1.8164	0.0076	0.42	1.8168	1.8273	1.8062
A3 Matrix	1.4224	0.0384	2.70	1.4115	1.5000	1.3567
BAN	1.8341	0.0110	0.60	1.8313	1.8612	1.8127
H451	1.7307	0.0167	0.96	1.7260	1.7534	1.7060
HLM	1.7531	0.0037	0.21	1.7530	1.7591	1.7443
IG-110	1.7729	0.0057	0.32	1.7726	1.7827	1.7617
IG-430	1.8117	0.0062	0.34	1.8101	1.8237	1.8038
NBG-10	1.7884	0.0043	0.24	1.7877	1.7952	1.7810
NBG-17	1.8629	0.0063	0.34	1.8643	1.8705	1.8527
NBG-18	1.8683	0.0029	0.16	1.8685	1.8728	1.8619
NBG-25	1.8433	0.0023	0.12	1.8432	1.8481	1.8391
New Matrix	1.7255	0.0449	2.60	1.7370	1.7972	1.6736
PCEA	1.7673	0.0046	0.26	1.7670	1.7752	1.7584
PCIB	1.8302	0.0046	0.25	1.8300	1.8390	1.8207
PGX	1.7680	0.0032	0.18	1.7678	1.7732	1.7623
PPEA	1.8335	0.0033	0.18	1.8336	1.8395	1.8277

Table B-15b. Piggyback Pre Thermal Measurement Density (g/cm^3) Summary Statistics.

Against Grain Specimens	Mean	Std Dev	CoV (%)	Median	Upper Limit	Lower Limit
2114	1.8164	0.0076	0.42	1.8168	1.8273	1.8062
A3 Matrix						
BAN						
H451	1.7165	0.0068	0.40	1.7166	1.7262	1.7060
HLM						
IG-110						
IG-430						
NBG-10						
NBG-17	1.8619	0.0100	0.54	1.8643	1.8705	1.8556
NBG-18	1.8659	0.0027	0.14	1.8657	1.8694	1.8619
NBG-25						
New Matrix						
PCEA	1.7678	0.0055	0.31	1.7682	1.7752	1.7584
PCIB						
PGX						
PPEA						

Table B-15c. Piggyback Pre Thermal Measurement Density (g/cm3) Summary Statistics.

With Grain Specimens	Mean	Std Dev	CoV (%)	Median	Upper Limit	Lower Limit
2114						
A3 Matrix						
BAN	1.8341	0.0110	0.60	1.8313	1.8612	1.8127
H451	1.7476	0.0029	0.17	1.7472	1.7504	1.7447
HLM						
IG-110	1.7729	0.0057	0.32	1.7726	1.7827	1.7617
IG-430	1.8117	0.0062	0.34	1.8101	1.8237	1.8038
NBG-10						
NBG-17	1.8634	0.0035	0.19	1.8641	1.8684	1.8569
NBG-18	1.8694	0.0023	0.12	1.8699	1.8728	1.8641
NBG-25						
New Matrix						
PCEA	1.7668	0.0036	0.20	1.7663	1.7722	1.7611
PCIB						
PGX	1.7680	0.0032	0.18	1.7678	1.7732	1.7623
PPEA						

Table B-16a. Piggyback Diffusivity (mm^2/sec) at 100°C Summary Statistics.

Combined Specimens	Mean	Std Dev	CoV (%)	Median	Upper Limit	Lower Limit
2114	65.45	1.00	1.53	65.65	66.84	63.95
A3 Matrix	10.99	0.73	6.68	10.91	12.13	9.82
BAN	99.77	2.35	2.35	100.09	104.32	94.70
H451	97.10	6.25	6.44	97.10	104.36	90.57
HLM	110.02	2.60	2.36	110.01	113.60	104.61
IG-110	72.02	1.10	1.53	71.93	73.87	70.06
IG-430	79.15	1.28	1.62	78.93	81.15	76.75
NBG-10	80.79	0.50	0.61	80.95	81.32	79.94
NBG-17	78.67	1.03	1.31	79.23	79.81	77.33
NBG-18	79.72	1.63	2.04	79.13	81.82	77.50
NBG-25	68.11	0.28	0.40	68.08	68.71	67.54
New Matrix	16.37	0.89	5.41	16.25	17.91	15.36
PCEA	98.13	3.85	3.92	99.92	101.60	91.75
PCIB	71.77	0.64	0.89	71.88	72.53	70.59
PGX	71.17	0.46	0.64	71.25	72.22	70.13
PPEA	82.60	0.56	0.68	82.62	83.32	81.46

Table B-16b. Piggyback Diffusivity (mm^2/sec) at 100°C Summary Statistics.

Against Grain Specimens	Mean	Std Dev	CoV (%)	Median	Upper Limit	Lower Limit
2114	65.45	1.00	1.53	65.65	66.84	63.95
A3 Matrix						
BAN						
H451	91.17	0.65	0.71	90.95	92.26	90.57
HLM						
IG-110						
IG-430						
NBG-10						
NBG-17	79.30	0.49	0.62	79.39	79.81	78.69
NBG-18	78.61	0.68	0.87	78.93	79.43	77.50
NBG-25						
New Matrix						
PCEA	91.51	0.36	0.39	91.60	91.81	91.11
PCIB						
PGX						
PPEA						

Table B-16c. Piggyback Diffusivity (mm^2/sec) at 100°C Summary Statistics.

With Grain Specimens	Mean	Std Dev	CoV (%)	Median	Upper Limit	Lower Limit
2114						
A3 Matrix						
BAN	99.77	2.35	2.35	100.09	104.32	94.70
H451	103.04	0.96	0.94	102.91	104.36	101.94
HLM						
IG-110	72.02	1.10	1.53	71.93	73.87	70.06
IG-430	79.15	1.28	1.62	78.93	81.15	76.75
NBG-10						
NBG-17	77.40	0.07	0.09	77.39	77.47	77.33
NBG-18	81.70	0.13	0.16	81.73	81.82	81.49
NBG-25						
New Matrix						
PCEA	100.12	0.84	0.84	100.16	101.36	98.58
PCIB						
PGX	71.17	0.46	0.64	71.25	72.22	70.13
PPEA						

Table B-17a. Piggyback Diffusivity (mm^2/sec) at 500°C Summary Statistics.

Combined Specimens	Mean	Std Dev	CoV (%)	Median	Upper Limit	Lower Limit
2114	27.10	0.29	1.06	27.15	27.57	26.60
A3 Matrix	4.59	0.39	8.44	4.50	5.24	3.93
BAN	35.15	0.85	2.43	35.29	36.56	33.64
H451	34.16	2.32	6.79	34.20	37.28	31.68
HLM	37.39	0.92	2.47	37.57	38.79	35.61
IG-110	27.96	0.44	1.58	27.97	28.56	27.10
IG-430	29.25	0.45	1.55	29.16	29.83	28.39
NBG-10	30.33	0.21	0.70	30.34	30.63	29.86
NBG-17	29.76	0.46	1.54	29.81	30.40	29.17
NBG-18	30.30	0.62	2.03	30.11	31.20	29.54
NBG-25	27.54	0.15	0.53	27.58	27.82	27.24
New Matrix	7.44	0.51	6.84	7.36	8.40	6.78
PCEA	35.63	1.48	4.14	36.31	36.80	33.18
PCIB	28.35	0.20	0.72	28.39	28.63	27.95
PGX	26.09	0.18	0.68	26.08	26.49	25.69
PPEA	31.53	0.18	0.58	31.56	31.87	31.19

Table B-17b. Piggyback Diffusivity (mm^2/sec) at 500°C Summary Statistics.

Against Grain Specimens	Mean	Std Dev	CoV (%)	Median	Upper Limit	Lower Limit
2114	27.10	0.29	1.06	27.15	27.57	26.60
A3 Matrix						
BAN						
H451	31.97	0.23	0.72	31.92	32.30	31.68
HLM						
IG-110						
IG-430						
NBG-10						
NBG-17	30.04	0.25	0.82	30.06	30.40	29.72
NBG-18	29.88	0.26	0.85	29.97	30.17	29.54
NBG-25						
New Matrix						
PCEA	33.08	0.22	0.66	33.15	33.25	32.84
PCIB						
PGX						
PPEA						

Table B-17c Piggyback Diffusivity (mm^2/sec) at 500°C Summary Statistics

With Grain Specimens	Mean	Std Dev	CoV (%)	Median	Upper Limit	Lower Limit
2114						
A3 Matrix						
BAN	35.15	0.85	2.43	35.29	36.56	33.64
H451	36.36	0.46	1.26	36.17	36.63	36.10
HLM						
IG-110	27.96	0.44	1.58	27.97	28.56	27.10
IG-430	29.25	0.45	1.55	29.16	29.83	28.39
NBG-10						
NBG-17	29.21	0.04	0.14	29.22	29.25	29.17
NBG-18	31.05	0.10	0.33	30.00	31.20	30.97
NBG-25						
New Matrix						
PCEA	36.40	0.27	0.74	36.41	36.80	35.84
PCIB						
PGX	26.09	0.18	0.68	26.08	26.49	25.69
PPEA						

Table B-18a. Piggyback Diffusivity (mm^2/sec) at 900°C Summary Statistics.

Combined Specimens	Mean	Std Dev	CoV (%)	Median	Upper Limit	Lower Limit
2114	17.91	0.18	1.00	17.93	18.22	17.43
A3 Matrix	3.09	0.27	8.63	3.06	3.53	2.45
BAN	21.86	0.52	2.37	21.97	22.67	21.07
H451	21.33	1.46	6.85	21.39	23.17	19.79
HLM	23.03	0.56	2.45	23.09	23.86	22.02
IG-110	18.08	0.26	1.44	18.08	18.45	17.61
IG-430	18.54	0.29	1.55	18.54	18.99	18.08
NBG-10	19.35	0.14	0.74	19.35	19.63	19.11
NBG-17	19.03	0.33	1.72	19.05	19.46	18.59
NBG-18	19.42	0.38	1.98	19.36	20.05	18.95
NBG-25	18.05	0.11	0.60	18.07	18.24	17.79
New Matrix	5.10	0.48	9.40	5.13	5.96	4.44
PCEA	22.34	0.90	4.01	22.75	23.09	20.86
PCIB	18.38	0.14	0.76	18.41	18.61	18.05
PGX	16.57	0.12	0.72	16.58	16.82	16.33
PPEA	20.24	0.14	0.71	20.25	20.50	19.96

Table B-18b. Piggyback Diffusivity (mm^2/sec) at 900°C Summary Statistics.

Against Grain Specimens	Mean	Std Dev	CoV (%)	Median	Upper Limit	Lower Limit
2114	17.91	0.18	1.00	17.93	18.22	17.43
A3 Matrix						
BAN						
H451	19.94	0.16	0.82	19.87	20.19	19.79
HLM						
IG-110						
IG-430						
NBG-10						
NBG-17	19.23	0.18	0.94	19.26	19.46	18.98
NBG-18	19.17	0.18	0.92	19.18	19.37	18.95
NBG-25						
New Matrix						
PCEA	20.79	0.12	0.56	20.80	20.91	20.68
PCIB						
PGX						
PPEA						

Table B-18c. Piggyback Diffusivity (mm^2/sec) at 900°C Summary Statistics.

With Grain Specimens	Mean	Std Dev	CoV (%)	Median	Upper Limit	Lower Limit
2114						
A3 Matrix						
BAN	21.86	0.52	2.37	21.97	22.67	21.07
H451	22.71	0.23	1.01	22.61	22.91	22.58
HLM						
IG-110	18.08	0.26	1.44	18.08	18.45	17.61
IG-430	18.54	0.29	1.55	18.54	18.99	18.08
NBG-10						
NBG-17	18.64	0.05	0.24	18.65	18.68	18.59
NBG-18	19.88	0.12	0.62	19.92	20.05	19.75
NBG-25						
New Matrix						
PCEA	22.80	0.18	0.79	22.79	23.09	22.44
PCIB						
PGX	16.57	0.12	0.72	16.58	16.82	16.33
PPEA						